

**Regulating Reactivity and Selectivity of a Dehydro-Diels–Alder Reaction of
Vinyl Heteroarenes Informed by Mechanism and Application towards the Synthesis of
Photovoltaic Materials**

by

Joseph A. Winkelbauer

B.S. Chemistry, Grove City College, 2015

Submitted to the Graduate Faculty of the
Dietrich School of Arts and Sciences in partial fulfillment
of the requirements for the degree of
Doctor of Philosophy

University of Pittsburgh

2021

UNIVERSITY OF PITTSBURGH
DIETRICH SCHOOL OF ARTS AND SCIENCES

This dissertation was presented

by

Joseph A. Winkelbauer

It was defended on

May 5, 2021

and approved by

Paul Floreancig, Professor, Department of Chemistry

Seth Horne, Associate Professor, Department of Chemistry

Stefan Bernhard, Professor, Department of Chemistry, Carnegie Mellon University

Dissertation Director: Kay M. Brummond, Professor, Department of Chemistry

Copyright © by Joseph A. Winkelbauer

2021

**Regulating Reactivity and Selectivity of a Dehydro-Diels–Alder Reaction of
Vinyl Heteroarenes Informed by Mechanism and Application towards the Synthesis of
Photovoltaic Materials**

Joseph A. Winkelbauer, PhD

University of Pittsburgh, 2021

Ring-fused heteroarenes are present in numerous natural products, FDA approved drugs, agrochemicals, and recently, organic solar cells able to achieve record breaking power conversion efficiencies. Access to these valuable compounds relies primarily on synthesis with dearomative cycloadditions of heteroarenes emerging as an efficient strategy. Many of these reactions require forceful conditions that utilize catalysts, acids and bases, or high temperatures to effect dearomatization. We have developed an intramolecular dearomative didehydro-Diels–Alder (DDDA) reaction which proceeds at temperatures as low as 60 °C with mild conditions, free of additives or catalysts. The adduct of the dearomative cycloaddition, which has been isolated and characterized, readily rearomatizes to either an isomerization product by way of a hydrogen migration or an oxidation product by way of a dehydrogenation.

To determine the substrate dependent factors that control the dearomative cycloaddition, kinetic studies were conducted with in situ reaction monitoring by ReactIR and afforded experimental Gibbs free energies of activation which correlated well with DFT calculations to reveal a highly asynchronous, concerted transition state. Aromaticity of the heteroarene, tether composition, and dispersion interactions were identified as substrate dependent factors that affect reactivity, establishing DFT calculations as a predictive tool in determining reactivity.

For the first time, the 1,4-cyclohexadienyl DA adduct was isolated, characterized, and confirmed as the product of the dearomative cycloaddition with divergent reactivity from the adduct leading to formation of either oxidation or isomerization products. These divergent mechanisms were investigated, and product selectivity was enhanced with control over the reaction parameters. Experiments utilizing deuterium oxide or increased exposure to air revealed the isomerization products were formed by an intermolecular, ionic proton transfer, while oxidation products were formed by an oxygen promoted dehydrogenation. Selectivity for either product was enhanced through reaction parameters such as temperature, solvent polarity, concentration, atmosphere, and additives.

Insight into the mechanisms of dearomatization and product formation allowed us to enhance the reactivity and product selectivity of the dearomative DDDA reaction for vinyl heteroarenes which was then applied towards the synthesis of ladder-type heteroarenes for organic photovoltaic materials. We expect these mechanistic findings to lend insight into other dearomative processes in the future.

Table of Contents

Acknowledgments	xxviii
1.0 Dearomative Cycloadditions of Vinylogous Heteroarenes.....	1
1.1 Valuable Synthetic Targets Containing Polycyclic Heteroarene Frameworks	1
1.2 Forcing Conditions Required in Dearomative Cycloaddition Processes.....	3
1.2.1 Acid Catalyzed Dearomative [4 +2] Cycloadditions of Vinyl Heteroarenes...	4
1.2.2 Base Mediated Dearomative Cycloadditions of Vinyl Heteroarenes	7
1.2.3 Transition-Metal Catalyzed Dearomative Cycloadditions of Vinyl Heteroarenes	8
1.2.4 Organocatalyzed Dearomative Cycloadditions of Vinyl Heteroarenes.....	10
1.2.5 Photoredox Catalyzed Dearomative Cycloadditions of Heteroarenes	11
1.2.6 Electrochemical Dearomative Cycloadditions of Heteroarenes	12
1.2.7 Thermal Dearomative Cycloadditions of Heteroarenes	13
1.2.8 Conclusions	15
1.3 Dearomative Didehydro-Diels–Alder Reaction for Vinyl Heteroarenes	16
1.3.1 Dearomative Didehydro-Diels–Alder Reaction for Vinyl Heteroarenes.....	16
1.3.2 Analogous Mechanistic Insight from Styryl Dearomative DDDA Reactions	19
1.4 Conclusions	23
2.0 Synthesis, Isolation and Characterization of the DA Adduct	24
2.1 Synthesis and NMR Characterization of the DA Adduct	24
2.2 Synthesis and Characterization of the Deuterated DA Adduct XX.....	30

2.6.6.4 Assignment of Spartan Calculated and Experimental ^1H and ^{13}C NMR Resonances.....	73
2.6.7 Heating of 2.6 in DMF to Afford 2.8, 2.7, and 2.23	76
2.6.8 Under Aerobic Conditions, 2.6 Affords 2.8 at Room Temperature	76
2.6.9 Stability of 2.7 under Thermal and Aerobic Conditions	77
2.6.10 Heating of 2.5 in Acetonitrile to Afford 2.6, 2.23, 2.8, and 2.7	78
2.6.11 Synthesis of Cis-Diene.....	79
2.6.12 Conversion of 2.23 to 2.8, 2.7, and Unknown at Room Temperature in CDCl_3	80
3.0 Factors that Determine Reactivity for the Dearomative DA Cycloaddition	81
3.1 Determination of Reaction Rates and Half-Lives for Dearomative DDDA Precursors by In Situ Reaction Monitoring with ReactIR.....	81
3.2 Determination of Activation Energy and Pre-Exponential Factor via the Arrhenius Equation	85
3.3 Determination of Gibbs Free Energy of Activation, Enthalpy, and Entropy via the Eyring Equation	89
3.4 Analysis of Reactivity in Collaboration with DFT Computational Calculations ...	93
3.4.1 Determination of the Dearomative Cycloaddition Mechanism	93
3.4.2 Gibbs Free Energies of Activation at the M06-2X/6-311+G(d,p)//M06-2X/6-31+G(d) Level of Theory as the Most Accurate to Experimental Energies	101
3.4.3 The Effect of Ground State Conformations on the Reactivity of the Dearomative Cycloaddition Step.....	102

3.4.4 Stabilizing Dispersion Interactions in the Dearomative Cycloaddition Transition States	103
3.4.5 Effect of Heteroarene Aromaticity on Reactivity of the Dearomative Cycloaddition	106
3.5 Conclusions	111
3.6 Experimental.....	112
3.6.1 General Methods	112
3.6.2 Experimental Procedures for ReactIR.....	113
3.6.3 ReactIR Data Output and Rate Calculations with GraphPad	114
3.6.4 Specifications for Measuring Half-Lives for DDDA Precursor	115
3.6.5 Arrhenius Plots.....	117
3.6.6 Eyring Plots	119
3.6.7 Correlation Plots between DFT Computational and Experimentally Derived Gibbs Free Energies of Activation	121
4.0 Divergent Reactivity of the DA Adduct and Regulating the Selectivity for Oxidation or Isomerization Products.....	124
4.1 Reaction Conditions that Affect Product Selectivity	124
4.1.1 Temperature Effect on the Dearomative DDDA Reaction Product Selectivity	125
4.1.2 Concentration Effect on the Dearomative DDDA Reaction Product Selectivity	126
4.1.3 Solvent Effect on the Dearomative DDDA Reaction Product Selectivity ...	126

4.1.4 Water Additive Effect on the Dearomative DDDA Reaction Product Selectivity.....	127
4.1.5 BHT Additive Effect on the Dearomative DDDA Reaction Product Selectivity	128
4.1.6 Atmosphere Effect on the Dearomative DDDA Reaction Product Selectivity	131
4.2 Substrate Identity Effect on the Dearomative DDDA Reaction Product Selectivity	132
4.3 Evidence for Oxidation Product Formation via Dehydrogenation of Diels-Alder Adduct with Oxygen.....	134
4.4 Evidence for Isomerization Product Formation via Proton Transfer of Diels-Alder Adduct	137
4.5 Conclusions	140
4.6 Experimental.....	141
4.6.1 General Methods	141
4.6.2 General Procedures for Dearomative DDDA Reactions	142
4.6.2.1 General Procedure D: Dearomative DDDA Reaction – Conventional Heating.....	142
4.6.2.2 General Procedure E: Dearomative DDDA Reaction – Microwave Heating.....	142
4.6.3 Experiments Showing the Effect of Temperature.....	143
4.6.4 Experiments Showing the Effect of Concentration.....	145
4.6.5 Experiments Showing the Effect of Solvent Polarity	145

4.6.6 Experiments Showing the Effect of Water Additive.....	146
4.6.7 Experiments Showing the Effect of BHT Additive	147
4.6.8 Experiments Showing the Effect of Atmosphere.....	152
4.6.9 Experiments as Evidence for Oxygen Mediated Dehydrogenation to Oxidation Product	153
4.6.10 Experiments as Evidence for Ionic Isomerization to Isomerization Product	155
5.0 Application of the Dearomative DDDA Reaction Towards the Synthesis of Organic Solar Cell Materials.....	157
5.1 Synthesis of Dearomative DDDA Reaction Oxidation Product via Ketone-Tethered Precursors	157
5.2 Progress Towards the Synthesis of Ladder-Type Arene Materials for Organic Solar Cells	160
5.3 Conclusions	163
5.4 Experimental.....	163
5.4.1 General Methods	163
5.4.2 Synthesis of a Multi-Ring Ladder-Type Heteroarene	164
5.4.3 Reaction of the Minor Diastereomer of 5.15 with Lawesson's Reagent	179
Appendix A Compound Characterization Checklist.....	181
Appendix B ^1H and ^{13}C NMR Spectra of Synthetically Prepared Molecules.....	183
Appendix C ReactIR Data Output	337
Bibliography	395

List of Tables

Table 2.1. ^1H NMR characterization of the DA adducts in <i>o</i> -DCB by analogy to 2.6	29
Table 2.2. Computational and experimental ^{13}C NMR resonances of the 2.6, 2.22, 2.23, 2.24, and 2.7	62
Table 2.3. Computational and experimental ^1H NMR resonances of the 2.6, 2.22, 2.23, 2.24, and 2.7	63
Table 2.4. Resonances for 2.6	73
Table 2.5. Resonances for 2.23	73
Table 2.6. Resonances for 2.7	74
Table 2.7. Resonances for 2.22	74
Table 2.8. Resonances for 2.24	75
Table 3.1. Measured half-lives and rate constants for the dearomative DDDA reaction of the thiophene and benzothiophene precursors	84
Table 3.2. Arrhenius trendline components as derived from the LINEST function and the kinetic results derived from the trendline for each substrate	88
Table 3.3. Eyring trendline slope, y-intercept, and R^2 as derived from the LINEST function and the ΔH^\ddagger , ΔS^\ddagger , and ΔG^\ddagger values with their corresponding error	92
Table 3.4. DFT computationally derived Gibbs free energies of activation for the s-cis closed- shell and s-trans open-shell transition states	97
Table 3.5. Newly forming bond lengths in the asynchronous, concerted transition state of the dearomative cycloaddition step	100

Table 3.6. NICS(1)zz aromaticity of the heteroarene for the dearomative cycloaddition precursors and transition states	107
Table 4.1. Dearomative DDDA reaction of precursors with added BHT and affected product ratios.....	130
Table 4.2. Ratio of compounds in 4.6.3 – Rxn 1	143
Table 4.3. Ratio of compounds in 4.6.7 – Rxn 1	147
Table 4.4. Ratio of compounds in 4.6.7 – Rxn 2	148
Table 4.5. Ratio of compounds in 4.6.7 – Rxn 3	148
Table 4.6. Ratio of compounds in 4.6.7 – Rxn 4	149
Table 4.7. Ratio of compounds in 4.6.7 – Rxn 5	149
Table 4.8. Ratio of compounds in 4.6.7 – Rxn 6	150
Table 4.9. Ratio of compounds in 4.6.7 – Rxn 7	150
Table 4.10. Ratio of compounds in 4.6.7 – Rxn 8	151
Table 4.11. Ratio of compounds in 4.6.7 – Rxn 9	151
Table 4.12. Ratio of compounds in 4.6.7 – Rxn 10	152
Table 4.13. Ratio of compounds in 4.6.9 – Rxn 1	154

List of Figures

Figure 1.1. Marketed drugs containing heterocyclic frameworks of benzothiophenes or indoles.....	2
Figure 1.2. Ladder-type conjugated polycyclic structure utilized in OPV solar-cells achieving record-breaking PCE's of greater than 17%	3
Figure 1.3. Synthetic toolbox of forcing conditions for dearomative cycloaddition processes	4
Figure 2.1. Boat-like conformation of the DA adduct 2.6 with bis-allylic hydrogens in flagpole positions	26
Figure 2.2. Possible regio- and stereoisomers of the DA adduct analyzed by the DP4 probability method.....	33
Figure 3.1. 1 st order exponential decay of 2.5 at 90 °C	84
Figure 3.2. Representative Arrhenius plot and its relation to the Arrhenius equation.....	85
Figure 3.3. Representative Eyring plot and its relation to the Eyring equation	89
Figure 3.4. Proposed concerted and stepwise transition states as possible mechanisms for the dearomative cycloaddition step	93
Figure 3.5. Structures of 1.59, the concerted transition state, and the stepwise transition state for the cycloaddition step of the dearomative DDDA reaction with structures optimized by M06-2X/6-31+G(d) and B3LYP/6-31+G(d). Bond distances shown in angstroms.....	95

Figure 3.6. Average deviation of computational Gibbs free energies of activation from experimental energies for both the concerted and stepwise reaction pathways at the M06-2X/6-311+G(d,p)//B3LYP/6-31+G(d) level of theory	98
Figure 3.7. Comparison of different levels of theories used to calculate $\Delta G^{\ddagger}_{\text{comp}}$ and their accuracy to $\Delta G^{\ddagger}_{\text{exp}}$	102
Figure 3.8. Dispersion effect on the stabilization of the concerted cycloaddition transition state.....	105
Figure 3.9. Correlation between $\Delta G^{\ddagger}_{\text{exp(s-cis)}}$, and both precursor and transition state NICS(1) _{zz} aromaticity values for ester-tethered substrates	109
Figure 3.10. Correlation between the $\Delta G^{\ddagger}_{\text{comp(s-cis)}}$ at the M06-2X/M06-2X level of theory and the NICS(1) _{zz} aromaticity calculation	110
Figure 3.11. Eyring plot for the dearomative DDDA reaction of 1.59 using five different reaction temperatures.....	116
Figure 3.12. Eyring plot for the dearomative DDDA reaction of 1.59 using four different reaction temperatures.....	116
Figure 3.13. Arrhenius plot for the dearomative DDDA reaction of 1.50	117
Figure 3.14. Arrhenius plot for the dearomative DDDA reaction of 2.9	117
Figure 3.15. Arrhenius plot for the dearomative DDDA reaction of 1.59	118
Figure 3.16. Arrhenius plot for the dearomative DDDA reaction of 2.5	118
Figure 3.17. Eyring plot for the dearomative DDDA reaction of 1.50	119
Figure 3.18. Eyring plot for the dearomative DDDA reaction of 2.9	119
Figure 3.19. Eyring plot for the dearomative DDDA reaction of 1.59	120
Figure 3.20. Eyring plot for the dearomative DDDA reaction of 2.5	120

Figure 3.21. Correlation between the closed-shell transition state $\Delta G^\ddagger_{\text{comp}}$ with B3LYP/B3LYP level of theory and the $\Delta G^\ddagger_{\text{exp}}$ with 3.5 outlier.....	121
Figure 3.22. Correlation between the closed-shell transition state $\Delta G^\ddagger_{\text{comp}}$ with B3LYP/B3LYP level of theory and the $\Delta G^\ddagger_{\text{exp}}$ without 3.5 outlier	121
Figure 3.23. Correlation between the closed-shell transition state $\Delta G^\ddagger_{\text{comp}}$ with M06-2X/M06-2X level of theory and the $\Delta G^\ddagger_{\text{exp}}$	122
Figure 3.24. Correlation between the closed-shell transition state $\Delta G^\ddagger_{\text{comp}}$ with M06-2X/B3LYP level of theory and the $\Delta G^\ddagger_{\text{exp}}$	122
Figure 3.25. Correlation between the open-shell transition state $\Delta G^\ddagger_{\text{comp}}$ with M06-2X/B3LYP level of theory and the $\Delta G^\ddagger_{\text{exp}}$	123
Figure 4.1. Ratio of oxidation product to isomerization product compared to computationally calculated BDE and acidity of the transferred proton of the Diels-Alder adduct	134
Appendix Figure C.1. 1 st order exponential decay of 1.50 at 77 °C.....	337
Appendix Figure C.2. 1 st order exponential decay of 1.50 at 86 °C.....	343
Appendix Figure C.3. 1 st order exponential decay of 1.50 at 94 °C.....	346
Appendix Figure C.4. 1 st order exponential decay of 1.50 at 108 °C.....	348
Appendix Figure C.5. 1 st order exponential decay of 1.50 at 119 °C.....	350
Appendix Figure C.6. 1 st order exponential decay of 2.7 at 76 °C.....	352
Appendix Figure C.7. 1 st order exponential decay of 2.7 at 85 °C.....	357
Appendix Figure C.8. 1 st order exponential decay of 2.7 at 95 °C.....	360
Appendix Figure C.9. 1 st order exponential decay of 2.7 at 108 °C.....	362
Appendix Figure C.10. 1 st order exponential decay of 2.7 at 113 °C.....	364

Appendix Figure C.11. 1 st order exponential decay of 1.59 at 88 °C.....	366
Appendix Figure C.12. 1 st order exponential decay of 1.59 at 98 °C.....	371
Appendix Figure C.13. 1 st order exponential decay of 1.59 at 109 °C.....	375
Appendix Figure C.14. 1 st order exponential decay of 1.59 at 121 °C.....	377
Appendix Figure C.15. 1 st order exponential decay of 1.59 at 132 °C.....	379
Appendix Figure C.16. 1 st order exponential decay of 2.5 at 73 °C.....	381
Appendix Figure C.17. 1 st order exponential decay of 2.5 at 81 °C.....	386
Appendix Figure C.18. 1 st order exponential decay of 2.5 at 90 °C.....	389
Appendix Figure C.19. 1 st order exponential decay of 2.5 at 96 °C.....	391
Appendix Figure C.20. 1 st order exponential decay of 2.5 at 106 °C.....	393

List of Schemes

Scheme 1.1. Lewis acid catalyzed dearomative [4 +2] cycloaddition of a 2-vinylindole.....	5
Scheme 1.2. Chiral rhodium catalyst utilized as a Lewis acid in a dearomative [4 + 2] cycloaddition.....	6
Scheme 1.3. Chiral holmium catalyst complex utilized as a Lewis acid in dearomative [4 + 2] cycloadditions	7
Scheme 1.4. Base mediated dearomative cycloaddition by sequential amide formation, [4 + 2] cycloaddition, and hydrogen-shift.....	7
Scheme 1.5. Base generated oxyallyl cations as the dienophile for dearomative cycloadditions with vinylindoles.....	8
Scheme 1.6. Gold catalyzed dearomative cycloadditions between allenamides and vinylindoles.	9
Scheme 1.7. Dirhodium chiral catalyst promoted dearomative cycloaddition of vinylindoles with vinyl diazoacetates	9
Scheme 1.8. Synthesis of nitrohydrocarbazoles via organocatalyzed dearomative cycloaddition reaction.....	10
Scheme 1.9. Secondary amine organocatalyst utilized in the dearomative cycloaddition of propynal with 2-vinylindole	11
Scheme 1.10. Photoactivate ruthenium catalyst for dearomative cycloaddition to oxazolo[3,2- α]indolones.....	12
Scheme 1.11. Electrochemical dearomative cycloaddition of phenols and <i>N</i> -acetylindoles to benzofuroindolines.....	13

Scheme 1.12. Thermal dearomative cycloaddition of 2-vinylindoles with highly reactive dienophiles	14
Scheme 1.13. Thermal dearomative cycloaddition of vinylimidazoles with highly reactive <i>N</i> -phenylmaleimide	14
Scheme 1.14. Intramolecular, thermal dearomative cycloaddition of vinylogous furans, pyrroles, and thiophenes	15
Scheme 1.15. Oxidation and isomerization products accessible via the dearomative DDDA reaction.....	16
Scheme 1.16. First report of the dearomative DDDA reaction of vinyl heteroarenes	17
Scheme 1.17. Kanematsu’s reported dearomative DDDA reaction for 2-vinylfurans and 2-vinylpyrroles.....	17
Scheme 1.18. Dearomative DDDA reaction of 3-vinylindoles with improved yields up to 99%	18
Scheme 1.19. Dearomative DDDA reaction of 4-vinylimidazole precursors.....	18
Scheme 1.20. Microwave assisted dearomative DDDA reaction with enhanced product selectivity.....	19
Scheme 1.21. Styryl dearomative DDDA reaction with DFT support for an asynchronous concerted [4 + 2] Diels–Alder cycloaddition.....	20
Scheme 1.22. Styryl dearomative DDDA reaction afforded isomerization product via an intermolecular hydrogen atom abstraction and oxidation product via a concerted intramolecular elimination of hydrogen gas.....	22
Scheme 2.1. Dearomative DDDA reaction of 1.59 to afford mixture of adduct and products	25

Scheme 2.2. Synthesis of dearomative DDDA precursor 2.5 and adduct 2.6	26
Scheme 2.3. Dearomative DDDA reactions with observation and characterization of DA adduct.....	28
Scheme 2.4. Synthesis of dearomative DDDA precursor 2.19 and adduct 2.20	31
Scheme 2.5. Observed deuterium isotope effect from parallel reactions of 2.5 and 2.19	32
Scheme 2.6. Formation of oxidation product, isomerization product, and 1,3-cyclohexadiene product from the DA adduct.....	34
Scheme 2.7. DFT energy diagram for the dearomative DDDA reaction of 2.5 at the M06/6-311+G(d,p)/SMD(DMF)//B3LYP/6-31G(d) level of theory	35
Scheme 2.8. Formation of oxidation product 2.8 from DA adduct 2.6 at rt with bubbling air	36
Scheme 2.9. No conversion of isomerization product 2.7 to oxidation product 2.8 under thermal conditions with bubbling air.....	37
Scheme 2.10. Formation of cis-diene byproduct in acetonitrile with enhanced selectivity in the presence of mole sieves	38
Scheme 2.11. Transformation of cis-diene into oxidation product, isomerization product, and unidentified byproduct	38
Scheme 3.1. Dearomative DDDA precursors selected for the reactivity study and analyzed by in situ ReactIR monitoring of reaction progress	82
Scheme 3.2. Rotational energy barriers required to attain the reactive <i>s</i> -cis conformer for precursors 1.50, 2.9, and 1.59.....	103
Scheme 4.1. Dearomative DDDA reactions of 2.5 with varied temperatures and affected product ratios	125

Scheme 4.2. Dearomative DDDA reaction of 2.5 with varied concentration and affected product ratios	126
Scheme 4.3. Dearomative DDDA reaction of 2.5 with varied solvent and affected product ratios.....	127
Scheme 4.4. Dearomative DDDA reaction of 2.5 with added water and affected product ratios	128
Scheme 4.5. Dearomative DDDA reaction of 2.5 with air exposure and affected product ratios	132
Scheme 4.6. Formation of oxidation product through a oxygen mediated dehydrogenation	135
Scheme 4.7. Dearomative DDDA reaction of 2.5 in tol-d ₈ at 150 °C for 3 h.....	136
Scheme 4.8. Mechanism of deuterium incorporation observed in dearomative Diels-Alder reactions with deuterium oxide present.....	139
Scheme 5.1. Retrosynthetic route for organic solar cell materials via the dearomative DDDA oxidation product	158
Scheme 5.2. Synthesis of dearomative DDDA reaction oxidation product via the ketone-tethered precursors	159
Scheme 5.3. Oxidative coupling of DA oxidation product with dr of 39:61	161
Scheme 5.4. Synthesis of the polycyclic ladder-type arene with Lawesson's reagent.....	162

List of Equations

Equation 3.1. Arrhenius plot line equation	86
Equation 3.2. Linear form of the Arrhenius equation.....	86
Equation 3.3. Activation energy	86
Equation 3.4. Pre-exponential value.....	86
Equation 3.5. Rate of reaction at 363 K	86
Equation 3.6. Error for activation energy	87
Equation 3.7. Error for pre-exponential value.....	87
Equation 3.8. Eyring plot line equation	90
Equation 3.9. Linear form of the Eyring equation	90
Equation 3.10. Enthalpy	90
Equation 3.11. Entropy.....	90
Equation 3.12. Rate of reaction at 363 K	90
Equation 3.13. Error for enthalpy	90
Equation 3.14. Error for entropy	90
Equation 3.15. Gibbs free energy of activation	91
Equation 3.16. Error for Gibbs free energy of activation	91
Equation 3.17. Quadrature to calculate error for Gibbs free energy of activation	91

List of Abbreviations

Δ	heat
ΔG^\ddagger	Gibbs free energy of activation
ΔH^\ddagger	enthalpy of activation
ΔS^\ddagger	entropy of activation
$^1\text{H NMR}$	proton nuclear magnetic resonance
$^{13}\text{C NMR}$	carbon nuclear magnetic resonance
\AA	angstrom
A	pre-exponential factor
a.u.	arbitrary units
Ac_2O	acetic anhydride
AcOH	acetic acid
A-D-A	acceptor-donor-acceptor
Avg	average
B	y-intercept
BDE	bond dissociation energy
BHT	di-t-butylhydroxytoluene
Boc	tert-butoxycarbonyl protecting group
Calc	calculated
Cat	catalyst
CDCl_3	chloroform-d
CFL	compact fluorescent light

Comp	computational
COSY	correlated spectroscopy
D ₂ O	deuterium oxide
DA	Diels–Alder
DBU	1,8-diazabicyclo[5.4.0]undec-7-ene
DCE	dichloroethane
DCM	dichloromethane
DDDA	didehydro-Diels–Alder
DFT	density-functional theory
DI	deionized
DIBAL	diisobutylaluminum hydride
DIPEA	<i>N,N</i> -diisopropylethylamine
Disp.	dispersion
DMAP	4-dimethylaminopyridine
DMF	<i>N,N</i> -dimethylformamide
dr	diastereomeric ratio
E _a	activation energy
EDCI	<i>N</i> -(3-Dimethylaminopropyl)- <i>N'</i> -ethylcarbodiimide hydrochloride
ee	enantiomeric excess
EI	electron ionization
er	enantiomeric ratio
ES	electron spray
ESI	electron spray ionization

Et ₂ O	diethyl ether
EtOAc	ethyl acetate
Exp	experimental
FTMS	Fourier transform ion cyclotron resonance mass spectrometer
<i>h</i>	Planck's constant
h	hours
H ₂	molecular hydrogen
H ₂ O	water
Hex	n-hexane
HFIP	hexafluoroisopropanol
HMBC	heteronuclear multiple bond correlation
HRMS	high resolution mass spectroscopy
HSQC	heteronuclear single quantum correlation
HWE	Horner–Wadsworth–Emmons
IR	infrared
Isom	isomerization product
k	rate constant
k _B	Boltzmann constant
LDA	lithium diisopropylamide
LiAlD ₄	lithium aluminum deuteride
LiAlH ₄	lithium aluminum hydride
m	slope
mA	milliamps

MeCN	acetonitrile
min	minutes
MP	melting point
MS	mass spectroscopy
NICS	nucleus-independent chemical shifts
NMR	nuclear magnetic resonance
O ₂	molecular oxygen
<i>o</i> -DCB	<i>o</i> -dichlorobenzene
OPV	organic photovoltaic
Oxid	oxidation product
PCE	power conversion efficiency
PhNO ₂	nitrobenzene
ppm	parts per million
R	gas constant
R ²	R-squared
R _f	retention factor
rt	room temperature
SMD	solvation model based on density
T	temperature
t _{1/2}	half-life
TBA	tribromoacetic acid
TFE	tetrafluoroethanol
THF	tetrahydrofuran

TLC	thin layer chromatography
TOF	time of flight
tol	toluene
TS	transition state
UV	ultraviolet
μ W	microwave

Acknowledgments

First, I would like to thank my family for their love and support during these past years of graduate school: my best friend and wife Carolyn who has motivated and encouraged me each day of my program, and our son Silas who has brought an incredible amount of joy to my life. My parents Norb and Kim, who raised me in love and wisdom. My father-in-law and mother-in-law Brian and Kelley who have loved me as their own. My sister Michelle as well as my brothers-in-law and sisters-in-law Calvin, Dan, Dave, Tim, Mallory, Caroline, and Audrey who have been my closest friends. Finally, my great-uncle Howard who has always supported me in my pursuit of education and science.

Next, I would like to thank my advisor, Prof. Kay Brummond who helped me to grow as a researcher and inspired me to strive for excellence in my scientific endeavors. Prof. Peng Liu who had patience and helped me to grow as a collaborator. I would also like to thank my committee members, Prof. Paul Floreancig, Prof. Seth Horne, and Prof. Stefan Bernhard for their help and support in my graduate education. I would like to acknowledge all the members of the Brummond research group, past and present, for their help, support, friendship, and comradery during my time at Pitt including Sarah Wells who introduced me to the research group, Paul Jackson, Lauren Burrows, Ashley Bober who mentored me in laboratory techniques and partnered with me on this research project, Humair Omar, Joe Burchick, a fellow nerd and mentor, Tugce Erbay, Dan Dempe, Eric Deihl, Mariah Meehan, Yifan Qi, Fatemeh Haghighi, and Maya Hayden.

I would like to thank our custodians, especially Tracy, not only for keeping our work area clean, but also for always having a kind word and smile every day. I would like to give special thanks to everyone at Grove City College who played a part in providing me with an exceptional

undergraduate education. Particularly Dr. Michael Falcetta and Dr. Charles Kriley who taught and mentored me in my first chemistry courses as well as my first research opportunities. I would also like to thank the church family and friends who have supported and encouraged me in the love of Christ through all of the mountains that I've faced these past years. Most of all, I thank my Lord and Savior Jesus Christ, my source of strength, who has shown me His great love and faithfulness.

1.0 Dearomative Cycloadditions of Vinylogous Heteroarenes

1.1 Valuable Synthetic Targets Containing Polycyclic Heteroarene Frameworks

Heteroarenes represent valuable scaffolds towards the synthesis of natural products, pharmaceuticals, pesticides, and other biologically active compounds.¹⁻⁵ Thiophenes as well as other sulfur based heteroarenes are especially valuable in medicinal chemistry as frameworks that are common in natural products and pharmaceuticals with therapeutic properties.⁶⁻⁹ Marketed drugs with benzothiophene frameworks include the asthma medication Zileuton (**1.1**), osteoporosis treatment Raloxifene (**1.2**), and antifungal Sertaconazole (**1.3**).¹⁰⁻¹² Marketed drugs containing thiophene frameworks include the anti-psychotic Olanzapine (**1.4**), glaucoma treatment Dorzolamide (**1.5**), and antiplatelet Clopidogrel (**1.6**).¹³⁻¹⁵

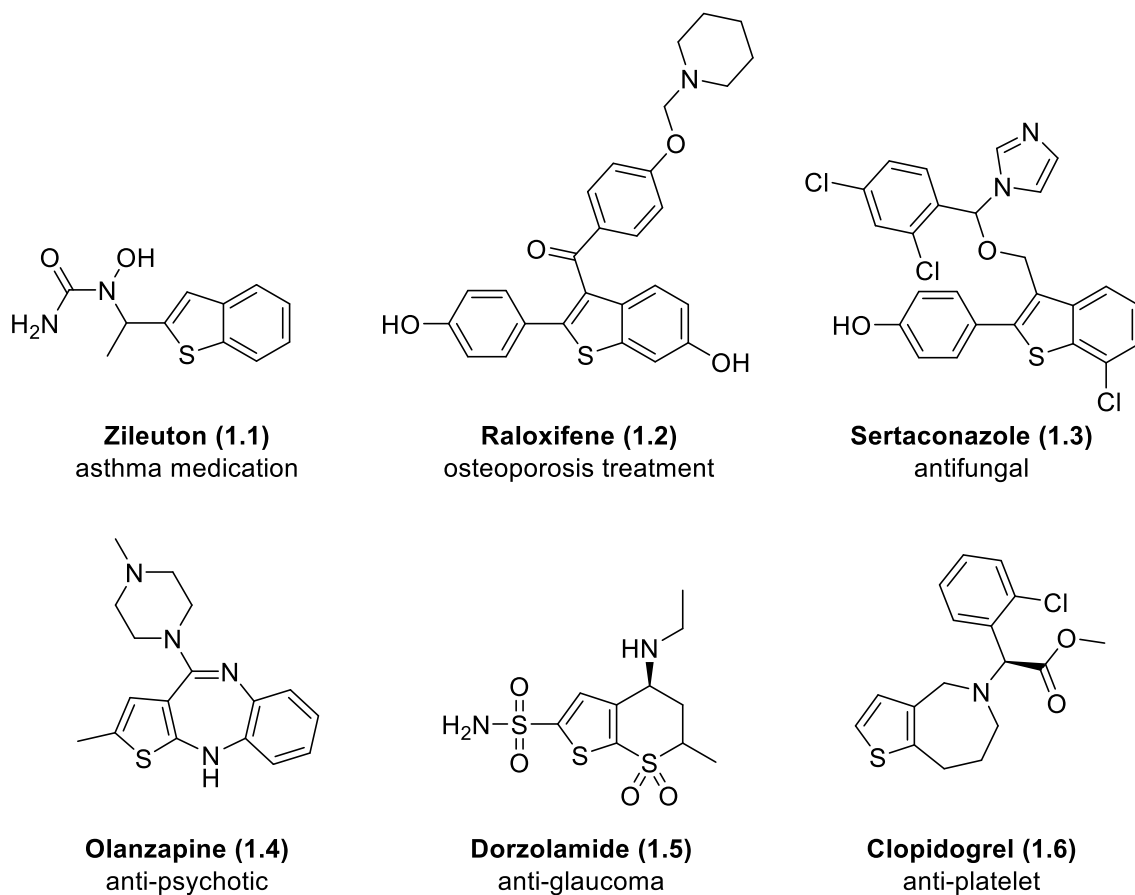
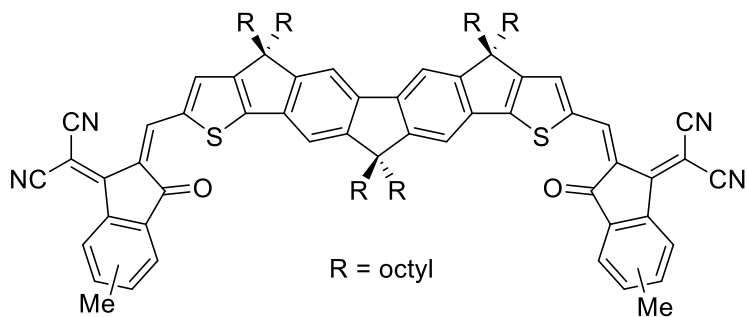
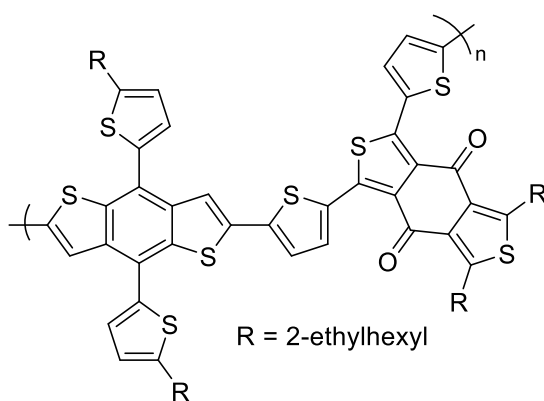


Figure 1.1. Marketed drugs containing heterocyclic frameworks of benzothiophenes or indoles

Recently, interest has grown in the application of heteroarenes towards ladder-type conjugated materials that have shown record breaking power conversion efficiencies (PCE) of greater than 17% in organic photovoltaic (OPV) solar-cells.¹⁶ Sulfur based heteroarenes in particular have found increasing success in the application towards these materials. For example, a record-performing OPV solar-cell was achieved by blending Acceptor-Donor-Acceptor (A-D-A) molecules (**1.7**) and electron donor molecules (**1.8**) with conjugated polymers, incorporated into a tandem cell (Figure 1.2). The value and importance of heteroarenes and their derivatives continues to grow, and access to these compounds relies heavily upon synthesis.¹⁷⁻²⁰



1.7
acceptor-donor-acceptor



1.8
donor

Figure 1.2. Ladder-type conjugated polycyclic structure utilized in OPV solar-cells achieving record-breaking PCE's of greater than 17%

1.2 Forcing Conditions Required in Dearomative Cycloaddition Processes

Dearomative cycloadditions are emerging as a valuable strategy to build complex polycyclic heteroarene compounds.²¹⁻²⁸ Various new approaches have been developed to effect these cycloadditions, affording products in high yields and high stereoselectivity. Still, forcing conditions are required to activate the aromatic π -system of the heteroarene for the dearomative cycloaddition. This synthetic toolbox includes reaction conditions such as acid catalysis, base

mediation, transition-metal catalysis, organocatalysis, photoredox catalysis, electrochemistry, and thermal conditions that utilize either high temperatures or highly reactive dienophiles. In the following section, we discuss recent examples with high yields and stereoselectivity that highlight several of the more prominent dearomative strategies.

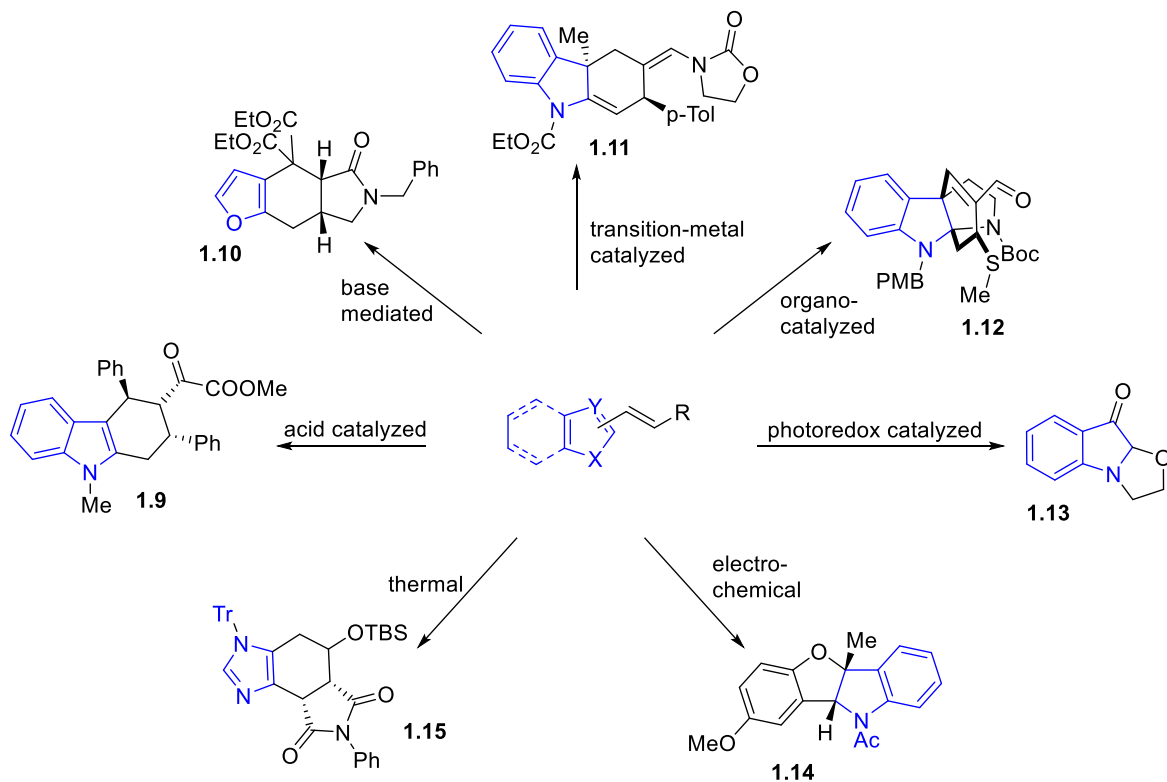
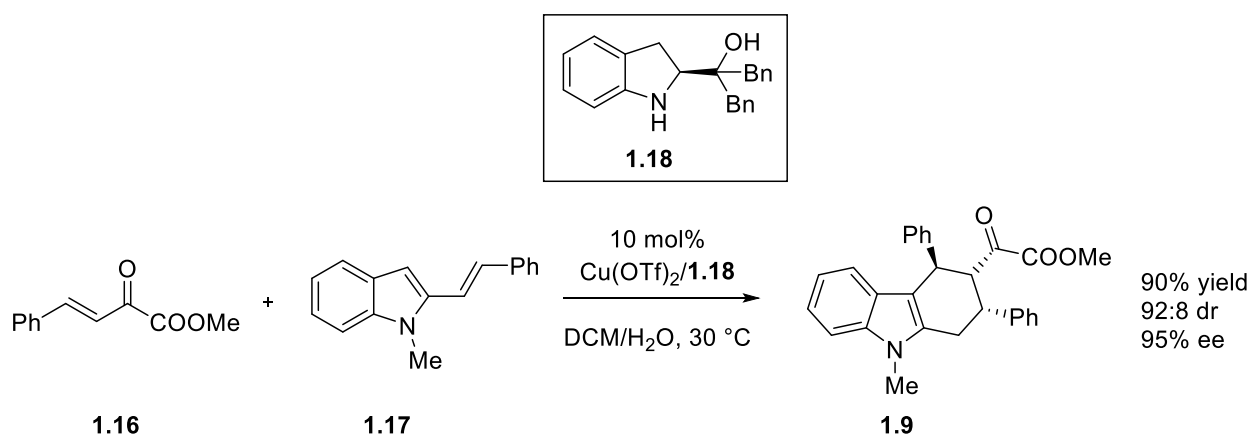


Figure 1.3. Synthetic toolbox of forcing conditions for dearomative cycloaddition processes

1.2.1 Acid Catalyzed Dearomative [4 + 2] Cycloadditions of Vinyl Heteroarenes

Acid catalysis for dearomative cycloadditions of vinyl heteroarenes often utilizes transition-metals that act as a Lewis acid to coordinate with and activate the dienophile in the DA cycloaddition. Transition-metals equipped with chiral ligands control stereoselectivity and impart chirality into the new polycyclic product. Ouyang et al synthesized highly functionalized

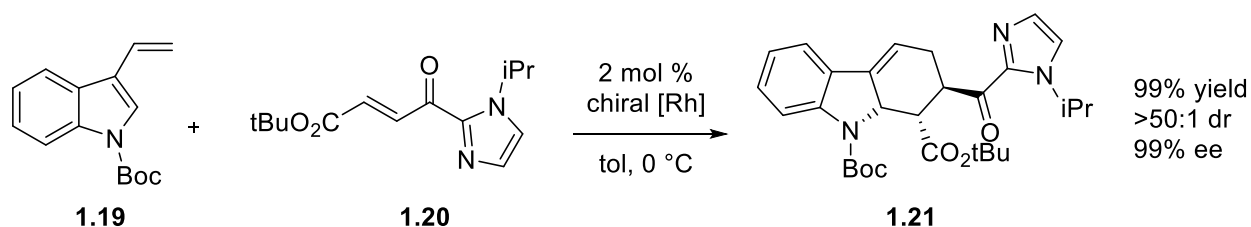
tetrahydrocarbazole **1.9** from 2-viny lindole **1.17** and β,γ -unsaturated α -ketoester **1.16** utilizing copper(II) triflate with chiral indolylmethanol ligand **1.18** as the Lewis acid catalyst (Scheme 1.1).²⁹ Product was afforded in high yield of 90% good stereoselectivities with ee of 95% and dr 92:8. Based on product stereochemistry, the authors propose the reaction mechanism to be a concerted [4 + 2] cycloaddition. Whereas the initial cycloadduct and rearomatization process were not described, stereoselectivity in the product is attributed to a distorted octahedral transition state geometry of the copper complex coordinated to the β,γ -unsaturated α -ketoester **1.16** controlling both the facial and endo approach of 2-viny lindole **1.17**.



Scheme 1.1. Lewis acid catalyzed dearomative [4 + 2] cycloaddition of a 2-viny lindole

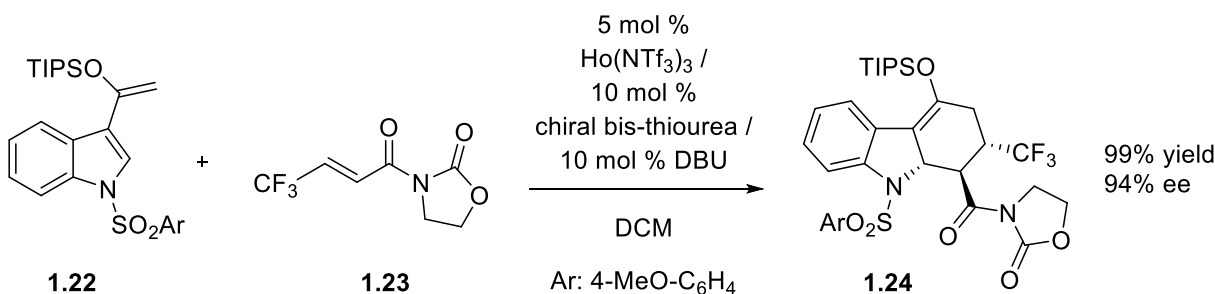
Huang et al demonstrated the use of chiral rhodium(III) as a Lewis acid in the preparation of hydrocarbazole **1.21** from 3-viny lindole **1.19** and α,β -unsaturated 2-acyl imidazole **1.20**.³⁰ The hydrocarbazole **1.21** was afforded in excellent yield (99%), regioselectivity (99:1), diastereoselectivity (>50:1), and enantioselectivity (99%) under optimized conditions. Based on product stereoselectivity, the authors propose that the chiral octahedral rhodium catalyst activates the 2-acyl imidazole dienophile **1.20** via bidentate coordination to the oxygen of the carbonyl and

the unsubstituted nitrogen of the imidazole, increasing reactivity towards the [4 + 2] cycloaddition reaction with the 3-vinylindole **1.19**. Phenylbenzoxazole ligands impart chirality, sterically directing the facial approach of vinylindole **1.19** with an endo attack. Steric clashing between the Boc group on the indole and the isopropyl group on the imidazole effect the observed regioselectivity.



Scheme 1.2. Chiral rhodium catalyst utilized as a Lewis acid in a dearomative [4 + 2] cycloaddition

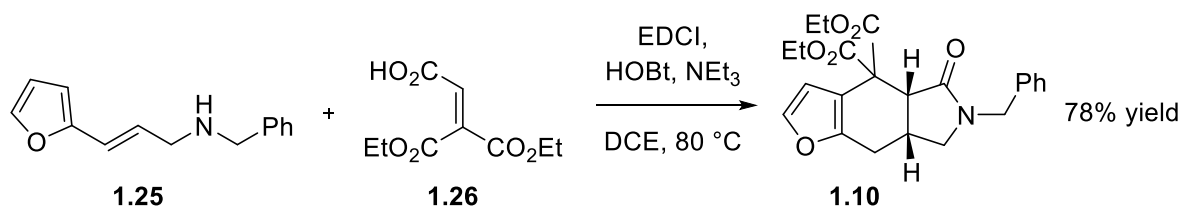
Lanthanide holmium has also been utilized as a chiral Lewis acid in catalytic and asymmetric dearomative cycloadditions. Harada et al synthesized substituted hydrocarbazole **1.24** from 3-vinylindole **1.22** and N-acyloxazolidinone **1.23**.³¹ They were able to synthesize product **1.24** with three chiral stereogenic centers in 99% yield and 94% ee. The authors proposed that the [4 + 2] cycloaddition proceeds through an eight coordinate holmium(III) catalyst complex, a conclusion supported by mass spectroscopy analysis. The complex activates the N-acyloxazolidinone **1.23** by bidentate coordination to both carbonyl oxygens. The thiourea side chain and naphthyl ring of the chiral ligands create a steric barrier which directs a single approach of the 3-vinylindole **1.22** to the dienophile **1.23** to effect the observed regio- and stereochemistry in the product by facial attack of the 3-vinylindole **1.22** with endo approach to the dienophile **1.23**.



Scheme 1.3. Chiral holmium catalyst complex utilized as a Lewis acid in dearomative [4 + 2] cycloadditions

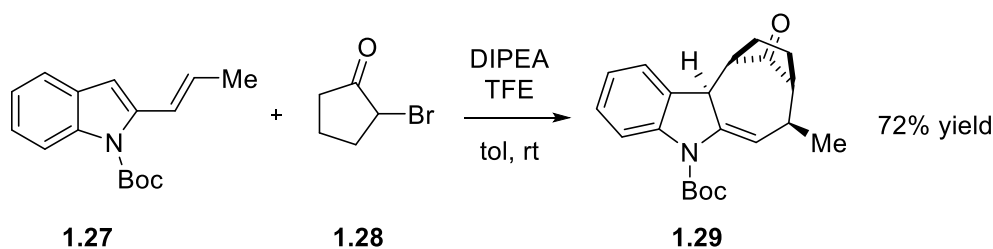
1.2.2 Base Mediated Dearomative Cycloadditions of Vinyl Heteroarenes

Dearomative cycloadditions of vinyl heteroarenes often utilizes basic conditions to initiate formation of a reactive dienophile from starting materials. Sugiura et al demonstrated such a reaction by reaction of 1,1,2-ethenetricarboxylic acid 1,1-diethyl ester **1.26** with E-3-(2-furyl)-2-propenylamine **1.25** under amide condensation conditions to afford cis-fused tricyclic compound **1.10** in moderate yield (78%).³² This reaction proceeds through a sequential amide formation, [4 + 2] cycloaddition, and hydrogen migration. The initial cycloadducts could be isolated and characterized but were found to decompose at room temperature.



Scheme 1.4. Base mediated dearomative cycloaddition by sequential amide formation, [4 + 2] cycloaddition, and hydrogen-shift

Basic conditions were also used to mediate the dearomative [4 + 3] cycloaddition of 2-vinylindole **1.27** with α -bromoketone **1.28** by in situ generation of oxyallyl cations, as performed by Pirovano et al.³³ Cyclohepta[*b*]indole derivative **1.29** was synthesized 72% yield and complete diastereoselectivity. The highly reactive oxyallyl cations are generated from α -bromoketone **1.28** in the presence of *N,N*-diisopropylethylamine (DIPEA) as base and perfluorinated solvent tetrafluoroethanol (TFE). Complete regio- and diastereoselectivity is observed in the product **1.29** which the authors attribute to endo approach in the [4 + 3] cycloaddition which could proceed either by a concerted or fast stepwise process.

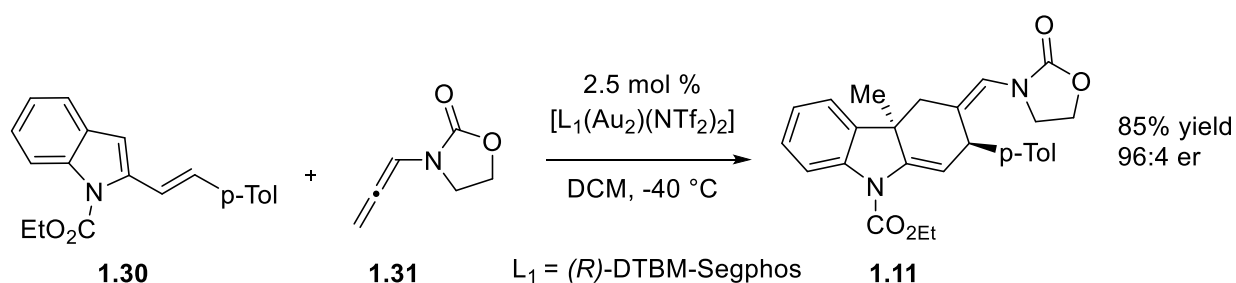


Scheme 1.5. Base generated oxyallyl cations as the dienophile for dearomative cycloadditions with vinylindoles

1.2.3 Transition-Metal Catalyzed Dearomative Cycloadditions of Vinyl Heteroarenes

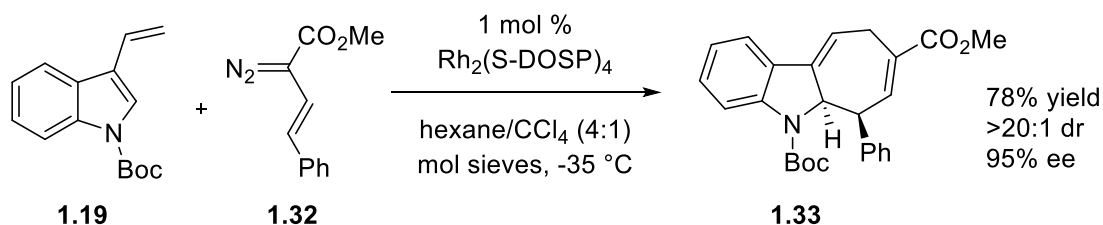
Transition-metals are used to effect dearomative cycloadditions with various types of dienophiles usually through stepwise mechanisms. Stereoselectivity can also be imparted to products with use of chiral ligands on the transition-metal catalysts. Rossi et al demonstrated gold-catalyzed synthesis of tetrahydrocarbazole **1.11** through dearomative [4 + 2] cycloadditions of substituted 2-vinylindole **1.30** with allenamide **1.31** in 85% yield and 96:4 enantiomeric ratio (er) with chiral Seg-Phos derivative ligands effecting stereoselectivity.³⁴ The [4 + 2] cycloaddition

proceeds via a stepwise mechanism as supported by the author's previous reports.³⁵ The chiral gold catalyst coordinates with the allene **1.31** to promote a stepwise cyclization with the 2-vinylindole **1.30** where steric interactions effect the observed stereoselectivity in the product **1.11**.



Scheme 1.6. Gold catalyzed dearomative cycloadditions between allenamides and vinylindoles.

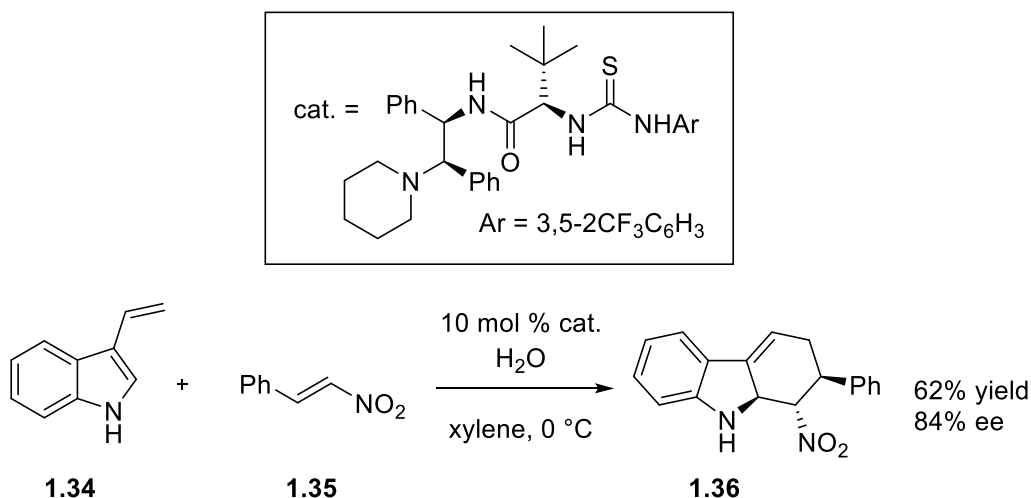
A chiral rhodium catalyst has been demonstrated to effect dearomative cycloadditions by Xu and coworkers.³⁶ Formal [4 + 3] cycloaddition of vinyindole **1.19** with vinyldiazoacetate **1.32** was effected with proline-derived dirhodium tetracarboxylate catalyst to access cyclohepta[*b*]indole **1.33** in 78% yield, >20:1 dr and 95% ee. The mechanism of the formal (4 + 3) cycloaddition proceeds by sequential asymmetric cyclopropanation of **1.32** and Cope rearrangement with the indole **1.19** promoted by the chiral rhodium catalyst which effects the observed enantioselectivity in the products **1.33** through the chiral ligands.



Scheme 1.7. Dirhodium chiral catalyst promoted dearomative cycloaddition of vinyindoles with vinyldiazoacetates

1.2.4 Organocatalyzed Dearomative Cycloadditions of Vinyl Heteroarenes

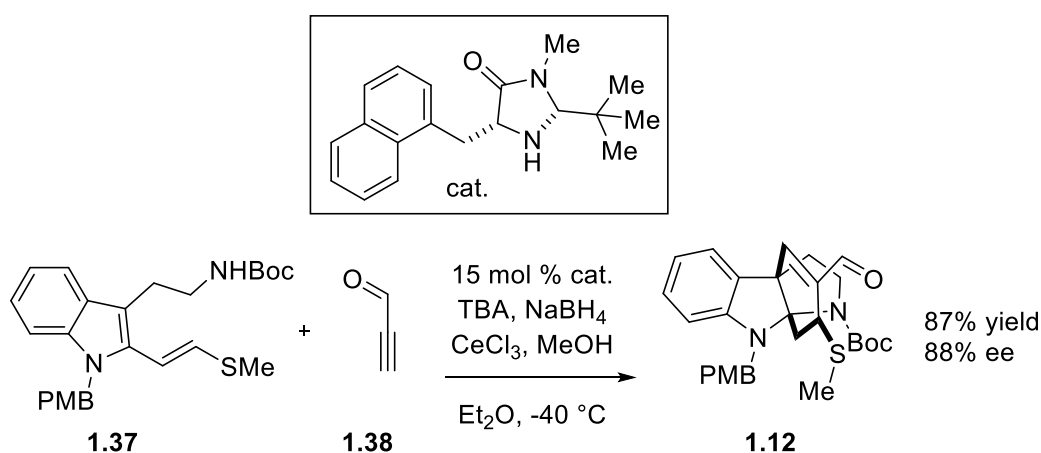
Organocatalyzed dearomative cycloadditions utilize specifically designed organic structures that activate starting materials for cycloaddition by reaction or interaction with Van der Waals forces.³⁷ Yang et al utilize organocatalysis in the synthesis of nitrohydrocarbazole **1.36** from 3-vinylindole **1.34** and nitroolefin **1.35**.³⁸ A chiral tertiary amine thiourea catalyst was used to effect the reaction in high yields (72%) and good ee (84%). Based upon control experiments and DFT calculations, the authors proposed that the thiourea catalyst promotes reactivity of the [4 + 2] cycloaddition via double hydrogen bonding nitroolefin **1.35**. This activates the dienophile for cycloaddition with the vinylindole **1.34** by an *exo* approach, enhancing the enantioselectivity of the reaction.



Scheme 1.8. Synthesis of nitrohydrocarbazoles via organocatalyzed dearomative cycloaddition reaction

Jones et al demonstrated a new organocatalytic DA and sequential amine cyclization affording tetracyclic carbazole frameworks **1.12** from propynal **1.38** and tryptamine derivative

1.37 in 87% yield and 88% ee in .³⁹ A chiral, secondary amine catalyst is utilized for a condensation reaction with the propynal **1.38** to afford an activated iminium ion which proceeds to the [4 + 2] cycloaddition with 2-vinylindole **1.37**. The authors propose, based upon the stereochemistry of the product, that steric interactions with the chiral catalyst increase selectivity for [4 + 2] cycloaddition in a regioselective manner to afford the DA adduct. Protonation of the enamine of the adduct facilitates an amine heterocyclization to deliver the product **1.12** and regenerate the organocatalyst.

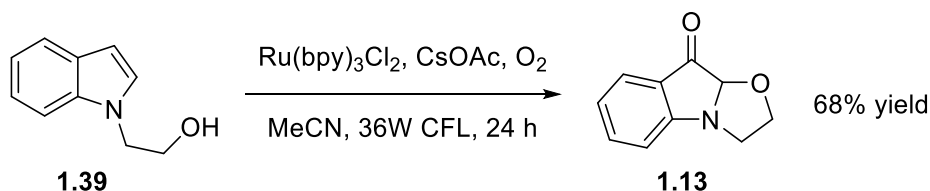


Scheme 1.9. Secondary amine organocatalyst utilized in the dearomative cycloaddition of propynal with 2-vinylindole

1.2.5 Photoredox Catalyzed Dearomative Cycloadditions of Heteroarenes

Reactions of heteroarenes as the two-carbon component of photoredox catalyzed dearomative cycloadditions are well studied and found to be initiated by a variety of means including photoactivated transition-metals, Lewis acids, electron donor-acceptor complexes, arenophiles, or generation of reactive radical intermediates.²⁴ Reactions of vinyl heteroarenes as the four-carbon component of a dearomative cycloaddition have yet to be explored to such an

extent. Zhang et al utilized photoactivated ruthenium catalyst to initiate intramolecular dearomative cycloaddition of indole-tethered alcohol **1.39** to afford oxazolo[3,2- α]indolone **1.13** in good yield (68%) in acetonitrile (MeCN) with light from a 36W compact fluorescent light (CFL) bulb.⁴⁰ Based upon experimental results and literature precedent, the authors propose that the photo-activated ruthenium(II) complex is used to effect a molecular oxygen induced single-electron oxidation of the indole **1.39** which undergoes cyclization via intramolecular nucleophilic attack.

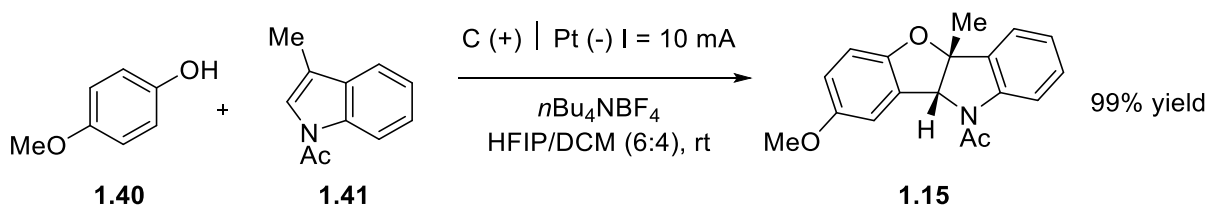


Scheme 1.10. Photoactivate ruthenium catalyst for dearomative cycloaddition to oxazolo[3,2- α]indolones

1.2.6 Electrochemical Dearomative Cycloadditions of Heteroarenes

Heteroarenes, which typically have electron-rich characteristics, are able to be anodically oxidized to the corresponding radical cation which may react by a radical coupling pathway or nucleophilic addition transformation.²⁵ These two reaction pathways are well studied for dearomative reactions of heteroarenes, yet reactions of vinyl heteroarenes as the four-carbon component of a dearomative cycloaddition have yet to be explored to such an extent. Liu et al demonstrated the dearomative, electrooxidative [3 + 2] annulation between phenol **1.40** and *N*-acetylindole (**1.41**) to afford benzofuroindoline **1.15** in up to 99% yield for 23 substrates in hexafluoroisopropanol (HFIP) and dichloromethane (DCM).⁴¹ This [3 + 2] cyclization is accomplished through the single-electron-transfer oxidation of both the *p*-methoxyphenol (**1.40**)

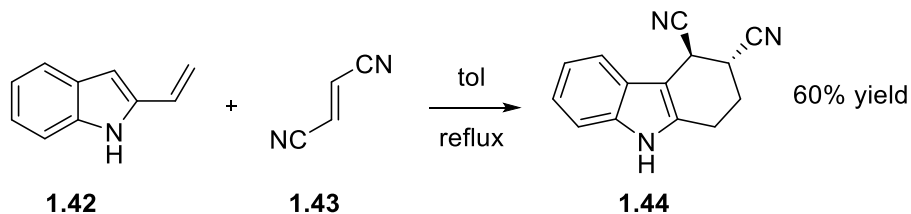
and the *N*-acetylindole (**1.41**) by the anode followed by cross-coupling of the two radical intermediates to generate the final product **1.15**.



Scheme 1.11. Electrochemical dearomative cycloaddition of phenols and *N*-acetylindoles to benzofuroindolines

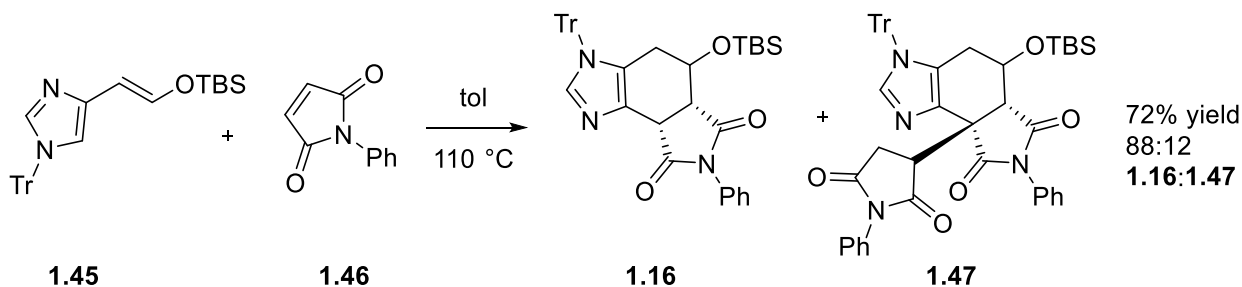
1.2.7 Thermal Dearomative Cycloadditions of Heteroarenes

Due to the lack of a catalyst or reagent to activate substrates for dearomative cycloadditions, thermal dearomative cycloadditions of vinyl heteroarenes typically require either highly reactive dienophiles or elevated temperatures to effect dearomatization. Mohamed et al effected the dearomative cycloaddition of 2-vinylindole **1.42** to carbazole derivative **1.44** with reactive dienophiles such as fumaronitrile **1.43**, dimethyl fumarate, *N*-phenylmaleimide, 1,4-naphthoquinone, and dimethyl acetylenedicarboxylate.⁴² Carbazole derivative **1.44** was afforded under conditions of refluxing toluene in 60% yield. The authors do not report observing the DA adduct, nor do they explain how the isomerization product was formed.



Scheme 1.12. Thermal dearomative cycloaddition of 2-vinylindoles with highly reactive dienophiles

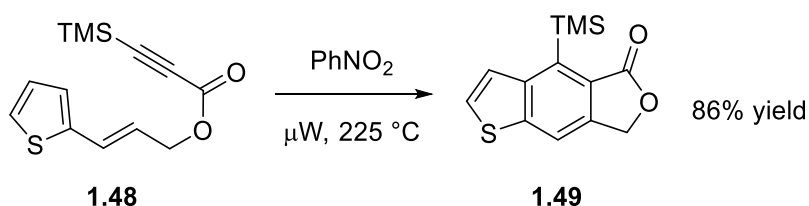
Cotterill et al also utilized a highly reactive dienophile in *N*-phenylmaleimide **1.46** to effect [4 + 2] dearomative cycloaddition with vinylimidazole **1.45** in refluxing toluene.⁴³ The DA adduct of the cycloaddition was observed and reported for several substrates. In most cases, adducts rapidly underwent a [1,3]-hydrogen migration to products **1.16**. A mechanism was not proposed for this migration, yet the product **1.16** was found to proceed into domino reactions affording trityl migration and even Michael addition with *N*-phenylmaleimide leading to formation of complex molecule **1.47**.



Scheme 1.13. Thermal dearomative cycloaddition of vinylimidazoles with highly reactive *N*-phenylmaleimide

Previous researchers from our lab have published dearomative cycloadditions of vinylogous heteroarenes under thermal conditions with elevated reaction temperatures via microwave heating.⁴⁴ Vinylogous furans, pyrroles, and thiophenes underwent intramolecular dearomative cycloadditions to afford either benzofurans, indoles, and benzothiophenes or the

corresponding dihydroaromatic products. Depicted in Scheme 1.14 is 2-vinylthiophene **1.48** reacting to afford benzothiophene **1.49** in 86% yield. In most reactions, temperatures of 225 °C were utilized with select cases proceeding at temperatures as low as 120 °C. Solvent selection afforded affected product selectivity with nitrobenzene increasing selectivity for fully aromatic products and dimethylformamide (DMF) increasing selectivity for dihydroaromatic products.



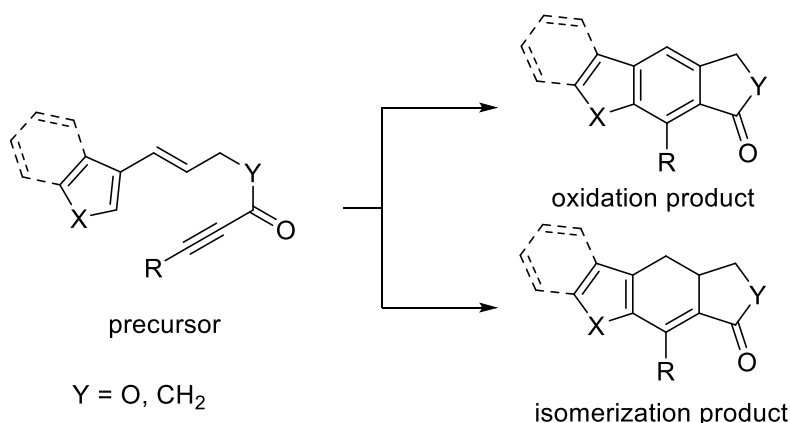
Scheme 1.14. Intramolecular, thermal dearomative cycloaddition of vinylogous furans, pyrroles, and thiophenes

1.2.8 Conclusions

Modern dearomative cycloadditions of vinyl heteroarenes have been employed through a variety of strategies to afford complex products in high yields and high stereoselectivity with efficient methods. The forcing conditions required to effect dearomatization often limit the substrate scope or cost efficiency of these reactions. Acid catalysis or base mediation strategies limit substrate functionality to that which is tolerant of these conditions. Transition-metal catalysis and organocatalysis strategies effect powerful stereochemical control that often require highly expensive catalysts and ligands to do so. Photoredox catalysis and electrochemical strategies are similarly powerful, yet literature examples for vinyl heteroarenes are currently lacking. Finally, thermal strategies often have a substrate scope limited by high temperatures or highly reactive dienophiles. Works utilizing these strategies ordinarily lack mechanistic analysis beyond proposed transition states based upon stereochemical outcomes.

1.3 Dearomative Didehydro-Diels–Alder Reaction for Vinyl Heteroarenes

The dearomative didehydro-Diels–Alder (DDDA) reaction for vinyl heteroarenes precursors affords access to both oxidation and isomerization products. Of all the dearomative cycloaddition strategies, the DDDA reaction is not limited by harsh reagents or expensive catalysts. Historically, the synthetic utility of this reaction has been limited by the low reactivity of the heteroarene precursors, requiring elevated reaction temperatures typically ≥ 130 °C, additives required to access oxidation products, and low afforded yields. Additionally, the mechanisms of the dearomative cycloaddition as well as the product formation mechanisms are not well understood.

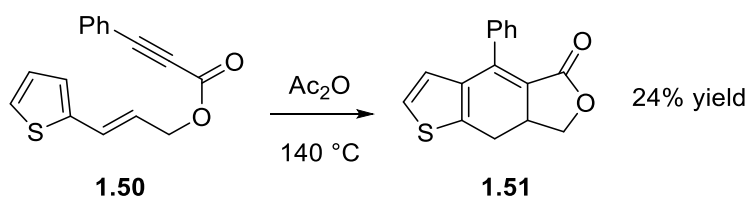


Scheme 1.15. Oxidation and isomerization products accessible via the dearomative DDDA reaction

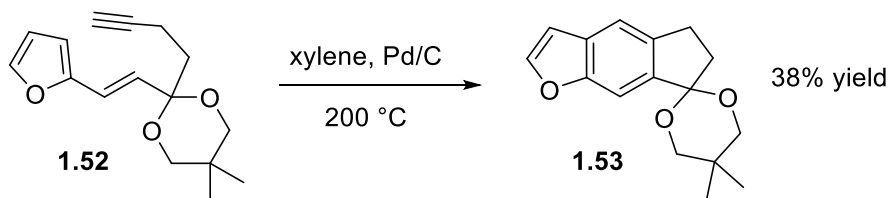
1.3.1 Dearomative Didehydro-Diels–Alder Reaction for Vinyl Heteroarenes

Klemm et al was the first to report the dearomative DDDA reaction for 2- and 3-vinylthiophenes under acidic conditions.⁴⁵ The 2-vinylthiophene **1.50** was refluxed in acetic anhydride to afford exclusively isomerization products **1.51** in relatively poor yield (24%). The

authors do not discuss the mechanisms by which the isomerization products are formed. Kanematsu et al reported dearomative DDDA reactions for 2-vinylfuran **1.52** as well as 2-vinylpyrroles.⁴⁶ Isomerization products were afforded in moderate yield (<59%) but the mechanisms by which they are formed from DA adduct is not discussed. Oxidation product **1.53** was accessed only by utilizing oxidative 2,3-Dichloro-5,6-dicyano-1,4-benzoquinone (DDQ) or Pd/C additives and was afforded in low yield (38%, Scheme 1.53).

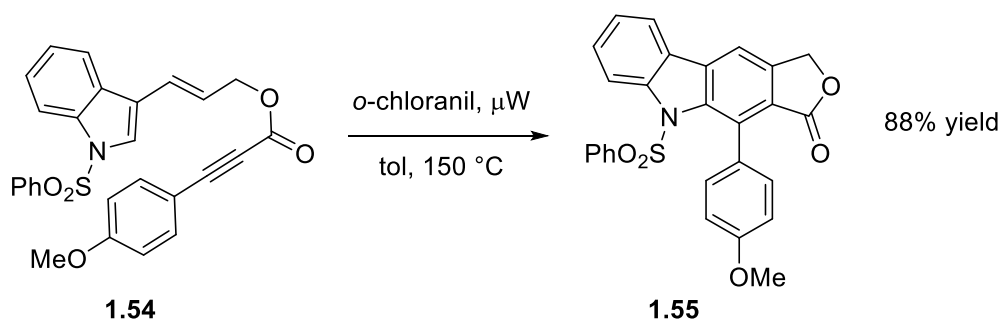


Scheme 1.16. First report of the dearomative DDDA reaction of vinyl heteroarenes



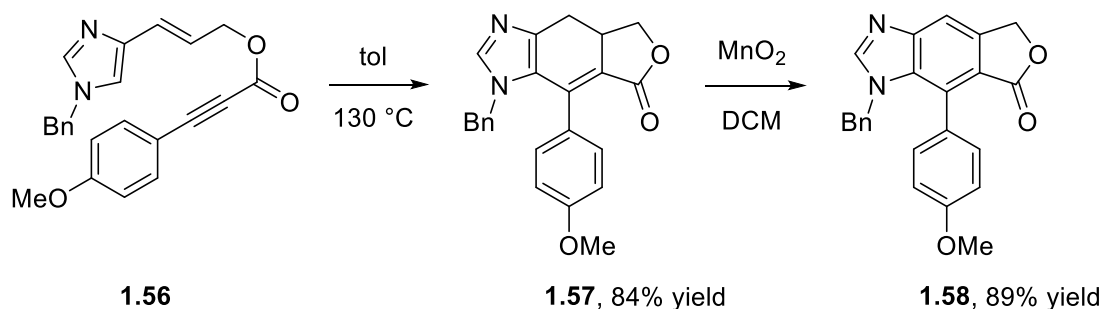
Scheme 1.17. Kanematsu's reported dearomative DDDA reaction for 2-vinylfurans and 2-vinylpyrroles

Hajbi et al effected the dearomative DDDA reaction of 3-vinylindoles **1.54** at 150 °C heated by microwave heating in toluene, protected from light and under inert atmosphere, to afford isomerization products in high yields (up to 99%). Oxidation product **1.55** was accessed only with utilization of *o*-chloranil as an oxidant in up to 88% yields.⁴⁷ Observation of DA adduct was not reported by the authors, nor was a mechanism proposed for formation of products from adduct.



Scheme 1.18. Dearomative DDDA reaction of 3-vinylindoles with improved yields up to 99%

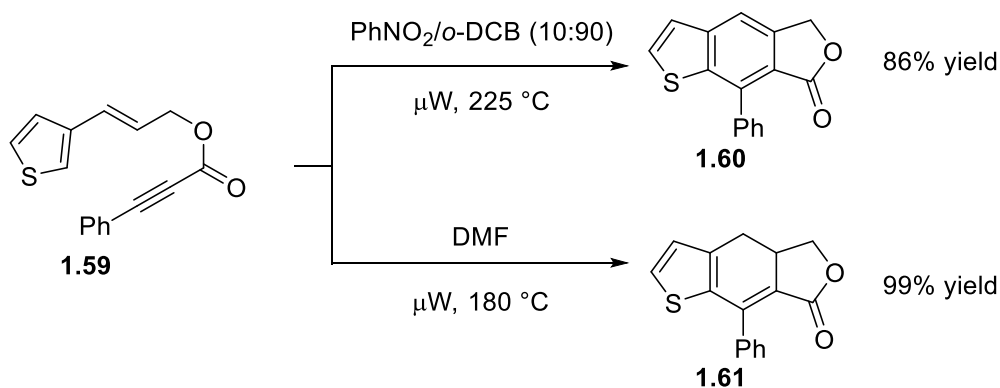
Dearomative DDDA reactions were demonstrated for 4-vinylimidazole **1.56** by Lima et al.⁴⁸ Isomerization product **1.57** was afforded by heating at 130 °C for 48 h in toluene in 84% yield. Oxidation product **1.58** was afforded upon reaction of isomerization product with oxidant manganese oxide in 89% yield. The authors do not report observation of DA adduct and do not discuss mechanisms for product formation.



Scheme 1.19. Dearomative DDDA reaction of 4-vinylimidazole precursors

As previously discussed, our research lab has published dearomative DDDA reactions of vinyl furans, pyrroles, and thiophene **1.59** which proceed under microwave heating temperatures of 225 °C with select cases proceeding at temperatures as low as 120 °C.⁴⁴ Selectivity for oxidation product **1.60** from 2-vinylthiophene **1.59** was enhanced in the presence of oxidant additive

nitrobenzene and afforded in 86% yield while selectivity for isomerization product **1.61** was enhanced by use of more polar solvents such as dimethylformamide (DMF) and afforded in 99% yield.



Scheme 1.20. Microwave assisted dearomative DDDA reaction with enhanced product selectivity

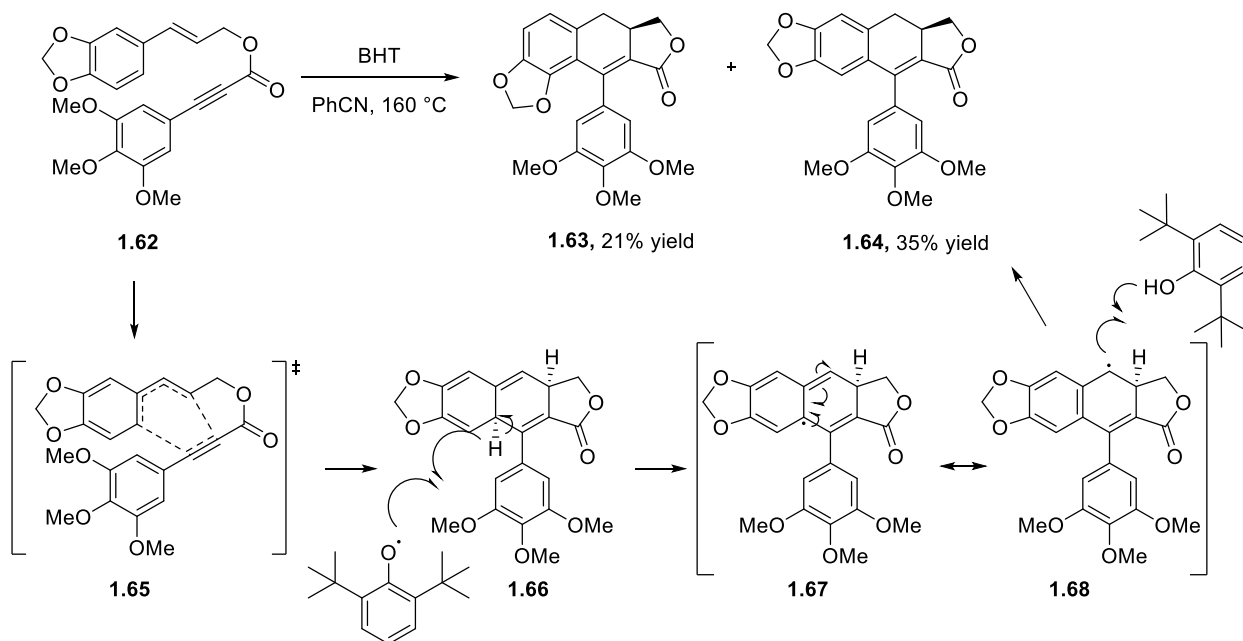
Literature examples have demonstrated use of the dearomative DDDA reaction offer a variety of heteroarenes with varied alkynyl tether compositions. Yet, overall, the utility of the reaction is often hindered by high temperatures above 130 °C, oxidizing additives required to afford oxidation product, and low yields. Furthermore, little is understood for the mechanisms of the dearomative cycloaddition and product formation steps as the DA adduct is rarely observed and has not been fully characterized.

1.3.2 Analogous Mechanistic Insight from Styryl Dearomative DDDA Reactions

There is a lack of literature on mechanistic studies of the dearomative DDDA reaction for vinyl heteroarenes, and as such, the mechanisms for the dearomative cycloaddition as well as

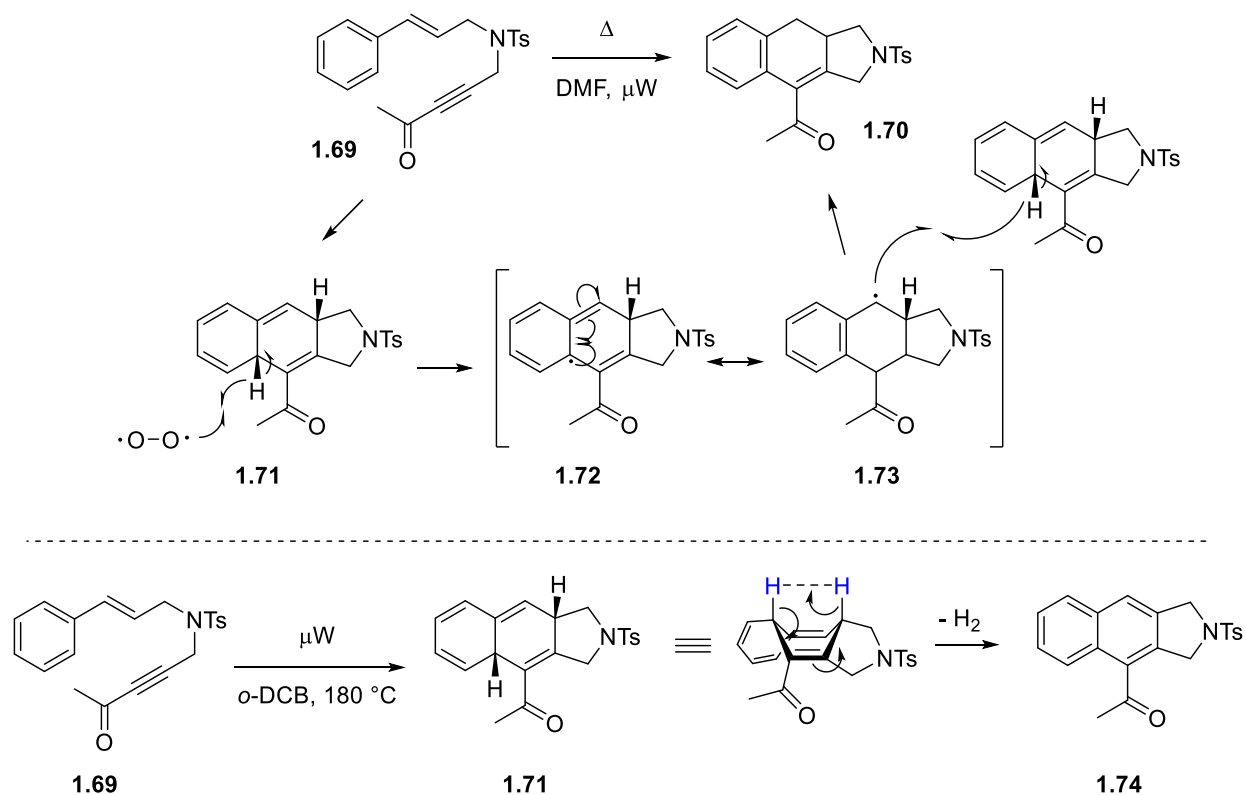
formation of oxidation and isomerization products are not well understood. The closest literature mechanistic studies are for the analogous intramolecular styryl dearomative DDDA reaction.

Andrus et al report the styryl **1.62** dearomative DDDA reaction at 160 °C for 2 h in benzonitrile solvent with 1.5 equivalents of di-*t*-butylhydroxytoluene (BHT) additive to afford isomerization products **1.63** and **1.64** in low yields (<56% combined).⁴⁹ DFT analysis of the dearomative cycloaddition identified an asynchronous concerted [4 + 2] Diels–Alder transition state **1.65** as the lower energy pathway in comparison to singlet-open-shell diradical pathways, and polar pathways. DFT analysis of isomerization product **1.64** formation identified the mechanism to be a BHT assisted [1,3]-formal hydrogen shift, where BHT initiates the hydrogen atom abstraction from the adduct **1.66** and subsequent addition to the newly formed radical **1.68**.



Scheme 1.21. Styryl dearomative DDDA reaction with DFT support for an asynchronous concerted [4 + 2] Diels–Alder cycloaddition

Kocsis et al from our research group also conducted intramolecular styryl **1.69** dearomative DDDA reactions to afford naphthalene (oxidation) **1.74** and dihydronaphthalene (isomerization) **1.70** products under microwave heating.⁵⁰ Deuterium-labeled cross-over experiments supported isomerization product formation occurring via an intermolecular hydrogen atom abstraction and subsequent addition. Triplet oxygen initiates the reaction by hydrogen atom abstraction of the tris-allylic hydrogen in the DA adduct **1.71**. The newly formed radical **1.73** then abstracts the tris-allylic proton of another equivalent of adduct to afford the isomerization product **1.70**. Oxidation product formation **1.74** was proposed to occur by the concerted intramolecular elimination of hydrogen gas, made possible by the close proximity of the flagpole hydrogens in the boat-like conformation of the adduct **1.71**. The elimination of H₂ gas was supported by experiments that quantified the gas by analysis of the reaction headspace with gas chromatography and detection of the resonance for H₂ gas in the reaction solution by ¹H NMR.



Scheme 1.22. Styryl dearomative DDDA reaction afforded isomerization product via an intermolecular hydrogen atom abstraction and oxidation product via a concerted intramolecular elimination of hydrogen gas

Though these works are mechanistic analysis of the dearomative DDDA reaction, it is unclear to what extent these mechanisms are analogous to those for vinyl heteroarenes. Literature examples of the dearomative DDDA reaction for vinyl heteroarenes often afforded variable reactivity and product selectivity with changes in substrate. Further mechanistic studies are required to garner understanding of these reaction processes for vinyl heteroarenes.

1.4 Conclusions

Dearomative cycloadditions are emerging as efficient and effective strategies for accessing valuable, complex polycyclic heteroarene compounds. Yet, most strategies employ forcing conditions such as additives or catalysts to activate the aromatic π -system of the heteroarene for cycloaddition. Therefore, the substrate dependent factors that affect reactivity are often overlooked and understudied in lieu of these conditions. The thermal, intramolecular, dearomative DDDA reaction of vinyl heteroarenes exists as a potential alternative to dearomative reactions with forcing conditions, yet it is also plagued by high temperatures, low yields, and oxidants required to access fully aromatic products. These faults may be attributed to a lack of understanding for these reaction mechanisms as the DA adduct is not observed or fully characterized in literature examples. We propose that a mechanistic analysis of the dearomative DDDA reaction of vinyl heteroarenes would lead to increased synthetic utility and substrate scope for the reaction, as well as inform future dearomative processes.

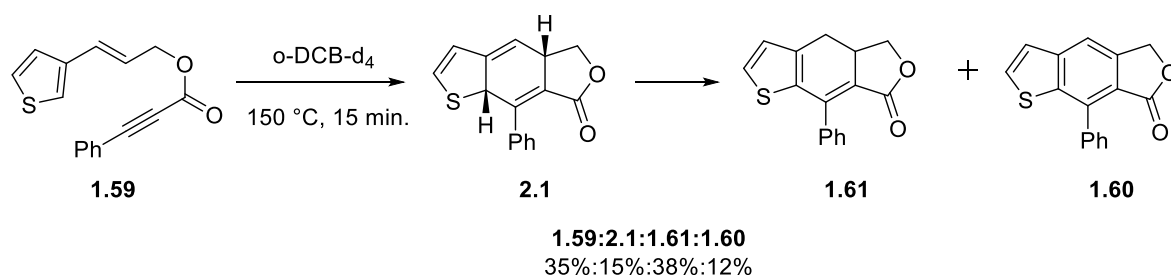
2.0 Synthesis, Isolation and Characterization of the DA Adduct

With changes in substrate affording variable reactivity and product selectivity for the dearomative DDDA reaction of vinylogous heteroarenes, we sought to investigate the mechanisms of the dearomative cycloaddition as well as product formation steps for these substrates. We proposed the DA adduct to be the intermediate between cycloaddition and formation of either oxidation or isomerization products. Isolation and characterization of this adduct provided insight into our mechanism study. Formation of products solely from the adduct was also confirmed.

This chapter is based on results presented in: Winkelbauer J. A.; Bober A. E.; Brummond K. M., Regulating Divergent Product Selectivity of the Dearomative Didehydro-Diels–Alder Reaction through Mechanistic Insight. Manuscript in preparation, submission expected 2021.

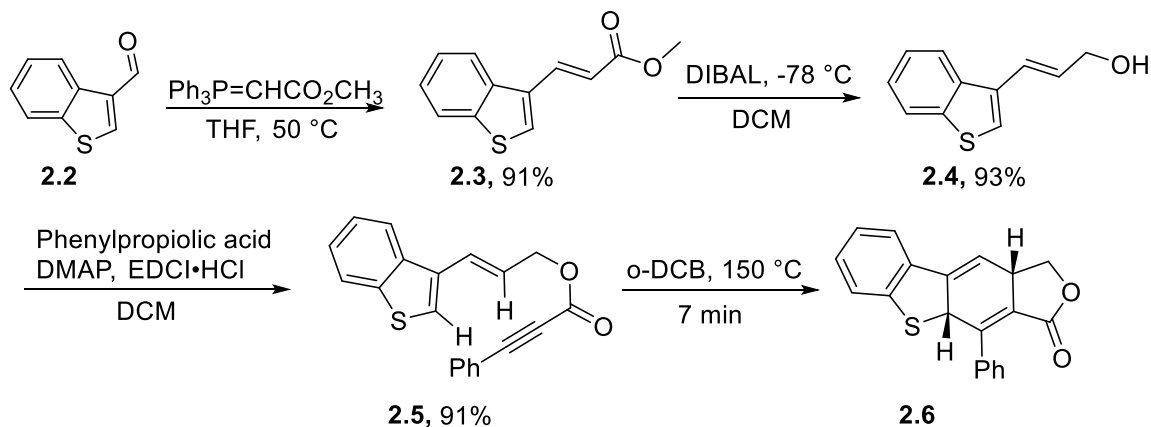
2.1 Synthesis and NMR Characterization of the DA Adduct

The proposed, and later confirmed, DA adduct was first observed in the dearomative DDDA reaction of the ester-tethered 3-thiophene precursor **1.59** when heated for 15 min at 150 °C in deuterated *o*-dichlorobenzene (*o*-DCB- d_4) which afforded a ratio of 35:15:38:12 (precursor **1.59**:adduct **2.1**:isomerization product **1.61**:oxidation product **1.60**) as observed by comparing integrative values of a crude ^1H NMR spectrum.



Scheme 2.1. Dearomative DDDA reaction of **1.59** to afford mixture of adduct and products

We hypothesized that a benzofused heteroarene may lead to a more persistent DA adduct due to stabilization afforded by the intact aromatic benzene. To test this hypothesis, dearomative DDDA precursor **2.5** was prepared. Horner–Wadsworth–Emmons (HWE) reaction of benzo[*b*]thiophene-3-carboxaldehyde **2.2** with methyl-(triphenylphosphoranylidene) acetate afforded (*E*)-3-(benzo[*b*]thiophen-3-yl)acrylate **2.3** in 91% yield. Reduction of the methyl ester **2.3** with diisobutylaluminum hydride (DIBAL) afforded allyl alcohol **2.4** in 93% yield. Alcohol **2.4** was subjected to a Steglich esterification with 4-dimethylaminopyridine (DMAP), *N*-(3-dimethylaminopropyl)-*N'*-ethylcarbodiimide hydrochloride (EDCI•HCl) and phenylpropionic acid to afford the dearomative DDDA precursor **2.5** in 91% yield. Heating the DA precursor **2.5** for 7 min at 150 °C in *o*-DCB-*d*₄ afforded the DA adduct **2.6**. Trace amounts of oxidized product were also present evidenced by ¹H NMR of the crude material. The yield was not determined as adduct **2.6** converted to oxidized product during purification by silica-gel column chromatography.



Scheme 2.2. Synthesis of dearomative DDDA precursor **2.5** and adduct **2.6**

Structural confirmation of adduct **2.6** was accomplished with single (^1H and ^{13}C) and multi-dimensional (COSY, HSQC, and HMBC) NMR techniques. The most diagnostic data related to the two bis-allylic hydrogens (H_A and H_C) identified as the resonances at 5.45 and 3.60 ppm, each showing 5J long-range couplings of 13.5 Hz. Durham and Studebaker have reported these long-range couplings as characteristic of 1,4-cyclohexadiene structures due to an adopted boat-like conformation with the bis-allylic hydrogens in axial positions (Figure 2.1).⁵¹

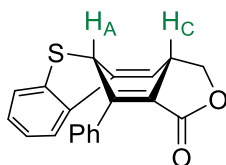
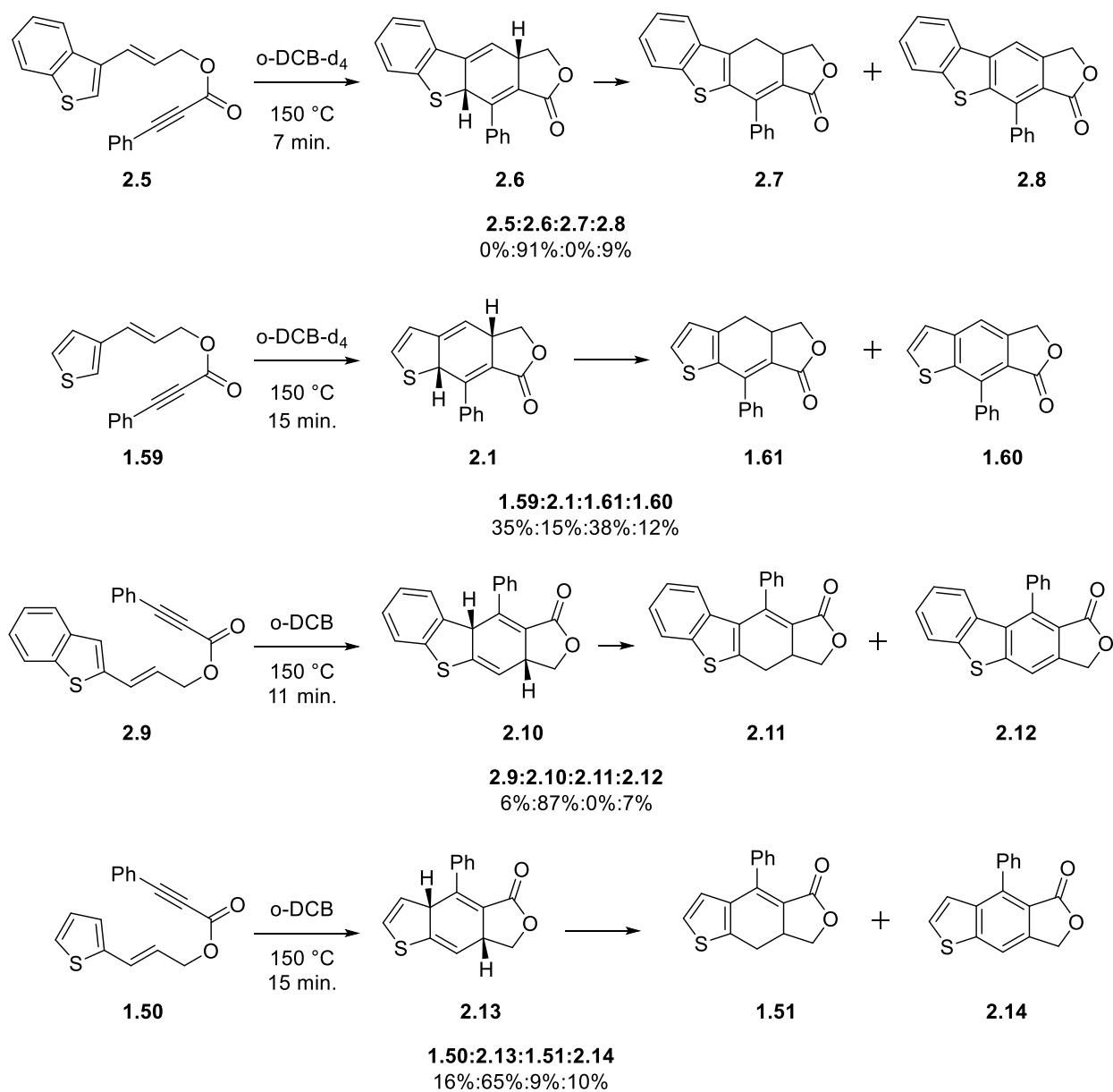


Figure 2.1. Boat-like conformation of the DA adduct **2.6** with bis-allylic hydrogens in flagpole positions

The coupling of the resonances at 5.45 and 3.60 ppm was confirmed by COSY NMR where the correlation was observed (see spectra in appendix B). HSQC NMR gave evidence that the resonances at 3.91 and 4.53 ppm are correlated to the same carbon with resonance at 68.6 ppm, and therefore, can be attributed to the methylene carbon. In HMBC NMR, the bis-allylic carbon

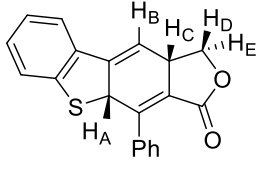
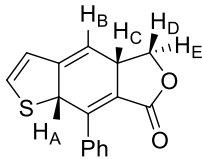
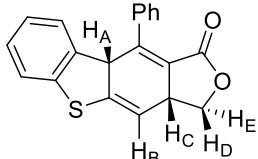
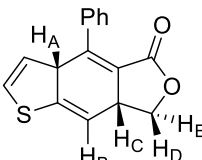
of proton H_A was observed to lack correlation to the methylene protons, indicative of the long spatial distance between these atoms.

DA precursors **1.59**, **2.9**, and **1.50** were synthesized by the same methodology and dearomative DDDA reactions were performed in order to characterize adduct for these substrates. 3-Vinylthiophene **1.59** heated for 15 min at 150 °C in *o*-DCB-d₄ afforded a ratio of 35:15:38:12 (**1.59:2.1:1.61:1.60**). 2-Vinylbenzothiophene **2.9** heated for 11 min at 150 °C in *o*-DCB afforded a ratio of 6:87:0:7 (**2.9:2.10:2.11:2.12**). 2-Vinylthiophene **1.50** heated for 15 min at 150 °C in *o*-DCB afforded a ratio of 16:65:9:10 (**1.50:2.13:1.51:2.14**). These adducts were observed as mixtures with precursor, oxidation product and isomerization products, and therefore, were identified and characterized by analogy to **2.6**.



Scheme 2.3. Dearomative DDDA reactions with observation and characterization of DA adduct

Table 2.1. ^1H NMR characterization of the DA adducts in *o*-DCB by analogy to **2.6**

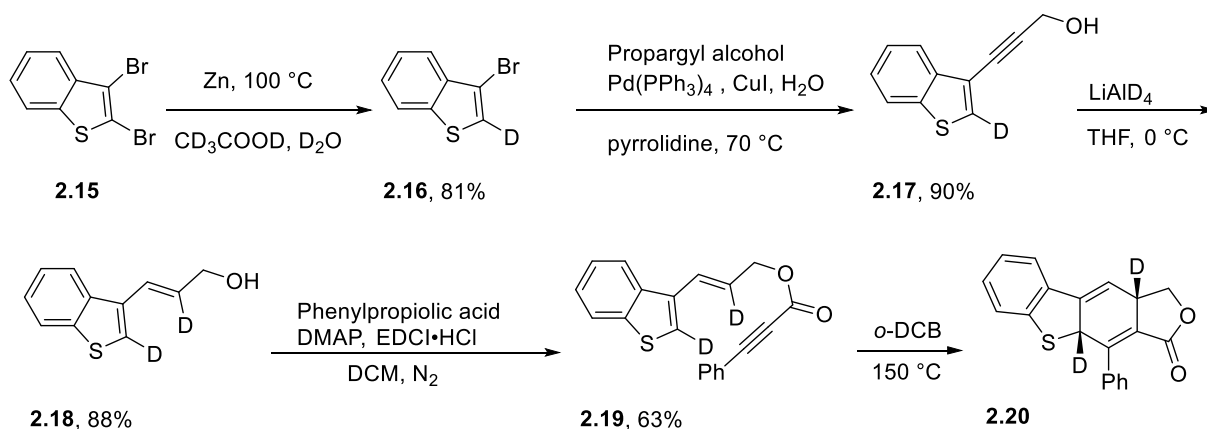
Adduct	Resonances	H_A	H_B	H_C	H_D	H_E
 2.6	δ (ppm)	5.46	5.93	3.64	3.91	4.53
	multiplicity	dd	dd	dddd	dd	dd
	J (Hz)	3.5, 13.5	2.0, 3.5	2.0, 8.6, 10.4, 13.5	8.2, 10.4	8.2, 8.6
 2.1	δ (ppm)	5.30	5.50	3.52	3.82	4.48
	multiplicity	dd	dd	dddd	dd	dd
	J (Hz)	3.8, 14.8	2.1, 3.8	2.1, 8.9, 10.2, 14.8	8.2, 10.2	8.2, 8.9
 2.10	δ (ppm)	4.74	5.59	3.56	3.82	4.50
	multiplicity	dd	dd	dddd	dd	dd
	J (Hz)	3.3, 13.4	1.7, 3.4	1.7, 9.4, 9.4, 13.5	8.6, 9.4	8.6, 9.4
 2.13	δ (ppm)	4.42	5.51	3.45	3.79	4.45
	multiplicity	dd	d	dddd	dd	t
	J (Hz)	3.4, 15.0	3.4	1.9, 8.6, 9.6, 15.0	8.7, 9.7	8.7

Thus, benzofused precursor **2.5** was successfully synthesized, and DA adduct **2.6** was attained and characterized by the heating of **2.5** for 7 min at 150 °C in *o*-DCB- d_4 . Heating of precursors **1.59**, **2.9**, and **1.50** under comparable conditions resulted in mixtures of products and incomplete conversion of starting material as detailed above. Yet, it is still unclear whether this is due to higher stability of **2.6** in comparison to the other adducts or perhaps higher energy barriers for conversion of **2.6** to products.

2.2 Synthesis and Characterization of the Deuterated DA Adduct XX

We postulated that persistence of the DA adduct may be further enhanced with deuteriums at the bis-allylic positions because of the increased bond strength of C-D compared to C-H. And due to the unusual nature of observing a 5J long-range coupling, we saw this as way to further confirm the structural assignment of the DA adduct **2.20** by ^1H NMR. To access this adduct, we first needed to prepare the dearomative DDDA precursor **2.19**.

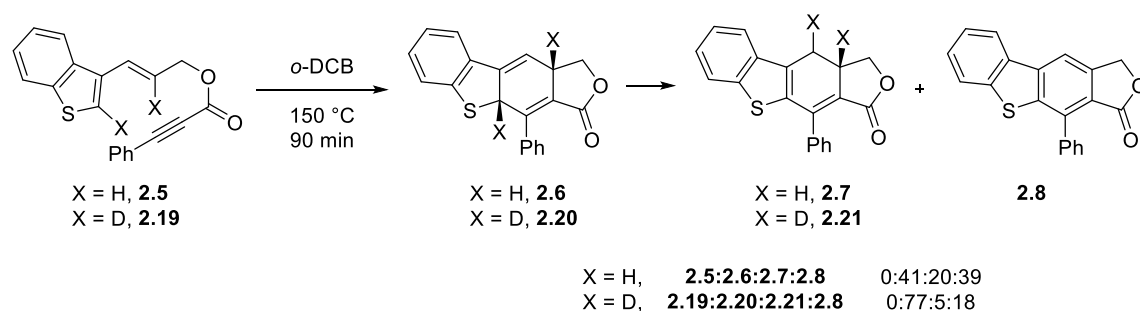
Towards the synthesis of **2.19**, dehalogenation of 2,3-dibromo-benzo[*b*]thiophene **2.15** with zinc powder and acetic acid- d_7 installed the first deuterium with generation of 3-bromobenzo[*b*]thiophene-2- d **2.16** in 81% yield. Sonogashira coupling of **2.16** with propargyl alcohol afforded the corresponding propargyl alcohol **2.17** in 90% yield. **2.17** was reduced by lithium aluminum deuteride (LiAlD_4) to the allyl alcohol **2.18** in 88% yield, installing the second deuterium. Allyl alcohol **2.18** was subjected to a Steglich esterification with DMAP, EDCI•HCl and phenylpropionic acid to afford the dearomative DDDA precursor **2.19** in 63% yield. Finally, the dearomative DDDA reaction of **2.19** for 90 min at 150 °C in *o*-DCB afforded **2.20** with minimal amounts of isomerization and oxidization product present (77%:5%:18%). The yield was not determined as adduct **2.20** converted to oxidized product during purification by silica-gel column chromatography.



Scheme 2.4. Synthesis of dearomative DDDA precursor **2.19** and adduct **2.20**

As expected, the ^1H NMR of **2.20** lacked the corresponding bis-allylic proton resonances that appeared at 5.45 and 3.60 ppm for **2.6**. The appropriate coupling to neighboring protons was also non-existent in the ^1H NMR of **2.20**. This result aided in the confirmation of our NMR characterization.

Parallel dearomative DDDA reaction of **2.5** for 90 min at 150 $^\circ\text{C}$ in *o*-DCB afforded DA adduct **2.6** with a significant increase in the amounts of formed isomerization and oxidation products (41%:20%:39%, Scheme 2.5). Therefore, in parallel reactions, DA adduct **2.20** with deuterium at the bis-allylic positions existed as 77% of the product mixture in comparison to non-deuterated adduct **2.6** which existed as 41% of the product mixture. Deuteriums at the bis-allylic positions in the DA adduct did result in a more persistent adduct, likely due to increased bond strength of C-D compared to C-H. Therefore, the protons or deuteriums at the bis-allylic positions are likely involved in the rate determining step of product formation.



Scheme 2.5. Observed deuterium isotope effect from parallel reactions of **2.5** and **2.19**

2.3 Confirmation of Stereochemistry via the DP4 Probability Method

DFT computations were utilized in the characterization of the DA adduct to confirm the stereochemistry of the synthesized adduct. First, we predicted that the cycloaddition would proceed via a concerted transition state, and therefore, the bis-allylic protons (H_A and H_C) of the 1,4-cyclohexadiene would have cis stereochemistry rather than trans. Trans bis-allylic protons would be indicative of a possible cycloaddition via a stepwise mechanism. Second, we proposed that the isolated and characterized product had the 1,4-cyclohexadiene regiochemistry of the DA adduct, yet 1,3-cyclohexadienes afforded via isomerization of the adduct could have similar ^1H NMR spectra to that of was isolated.

DFT calculations with EDF2/6-31G* geometry optimizations were used to generate predictive ^1H and ^{13}C NMR spectra for the cis and trans 1,4-cyclohexadiene (**2.13** and **2.22**), the cis and trans 1,3-cyclohexadiene β to the ester (**2.23** and **2.24**), and the isomerization product (**2.7**). The DP4 probability method created by the Goodman group allowed us to compare these predictive ^1H and ^{13}C NMR spectra to the experimental spectra of our substrates and calculate the percent probability of a match.⁵²

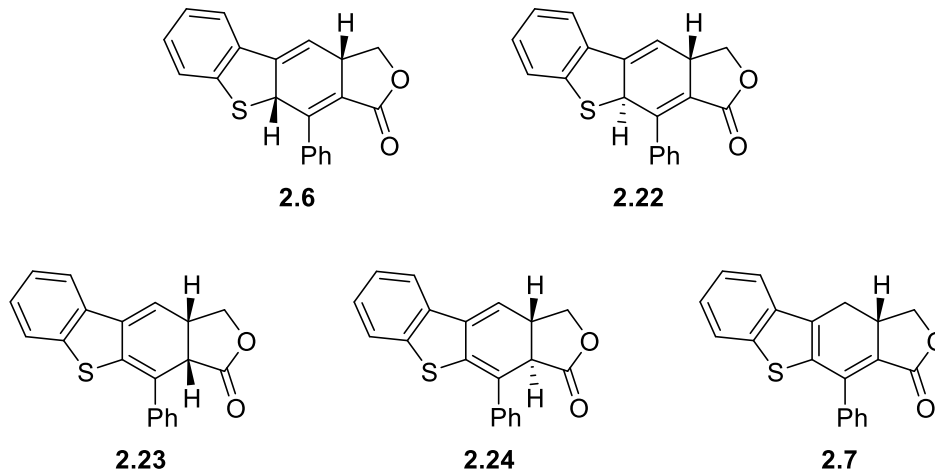


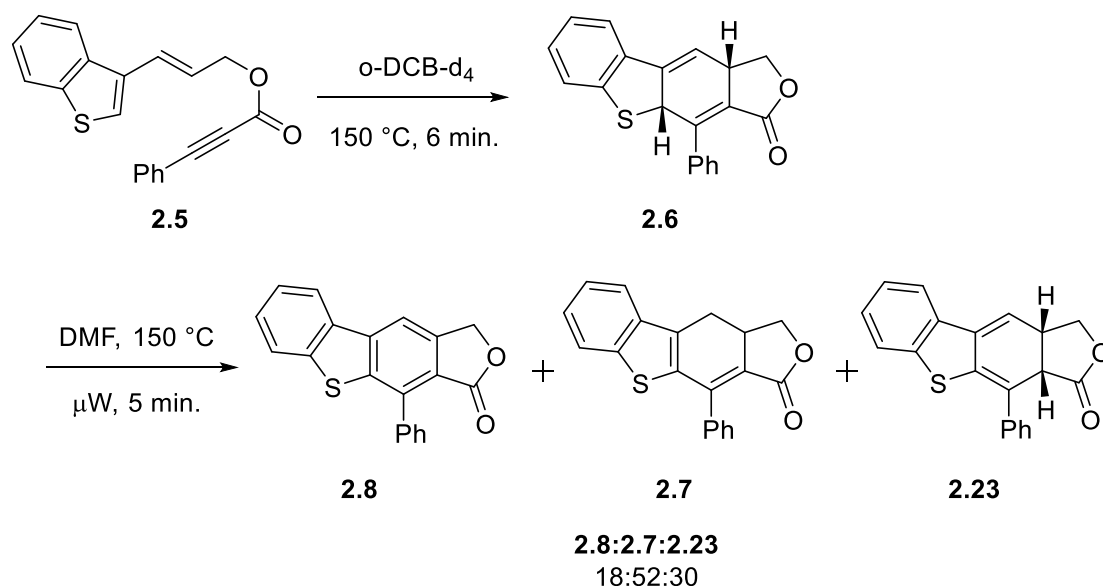
Figure 2.2. Possible regio- and stereoisomers of the DA adduct analyzed by the DP4 probability method

The combined experimental ^1H and ^{13}C NMR's of our proposed cis-1,4-cyclohexadiene DA adduct had a 99.9% match to the Spartan predicted NMR's for **2.13**. This method also gave confirmation of the assignment for two isomerization products from the adduct, **2.23** and **2.7**, whose isolation and characterization are described in section 2.4.2.

2.4 Confirmation of the DA Adduct as the Common Intermediate to Formation of Oxidation Product, Isomerization Product, and Cis-Diene

With isolated DA adduct in hand, we proposed that the adduct was the common intermediate from which oxidation and isomerization products were formed and not just a newly characterized byproduct. To test our hypothesis, isolated DA adduct would be subjected to dearomative DDDA conditions in order to observe if oxidation and isomerization products would be generated from the adduct. **2.5** was heated for 6 min at 150 °C in *o*-DCB to generate **2.6** with

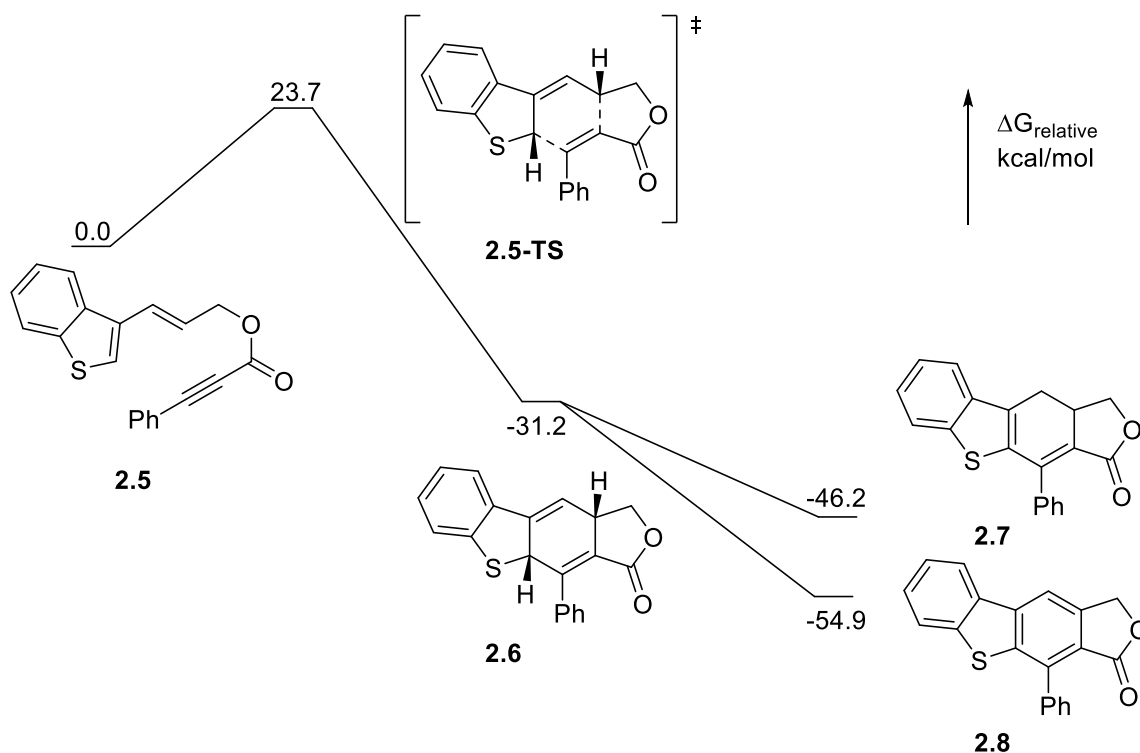
trace formation of **2.8**. The *o*-DCB solvent was removed by high-vacuum, and the adduct was dissolved in DMF before heated for 5 min at 150 °C in the microwave reactor. This reaction of isolated adduct resulted in the formation of **2.8**, **2.7**, and **2.23** in a ratio of 18:52:30 respectively (see ¹H NMR in experimental section). Therefore, the oxidation product, isomerization product, and the cis-diene were all found to be generated directly from isolated DA adduct rather than precursor.



Scheme 2.6. Formation of oxidation product, isomerization product, and 1,3-cyclohexadiene product from the DA adduct

To better understand the product ratios, we investigated the ground state energies for **2.5**, **2.6**, **2.8**, and **2.7** and analyzed the dearomative cycloaddition energy of activation. These calculations were performed by our collaborator Elena Kusevska from the Peng Liu research group. DFT calculations were performed at the M06/6-311+G(d,p)/SMD(DMF)//B3LYP/6-31G(d) level of theory. Results showed a relatively low Gibbs free energy of activation of 23.7

kcal/mol for the dearomative DA cycloaddition step with an exergonic formation of adduct at -31.2 kcal/mol relative to precursor. These ground state energies reveal a thermodynamic driving force towards adduct. Formation of oxidation product (-54.9 kcal/mol) and isomerization product (-46.2 kcal/mol) is also exergonic relative to precursor and suggests that product formation is irreversible.

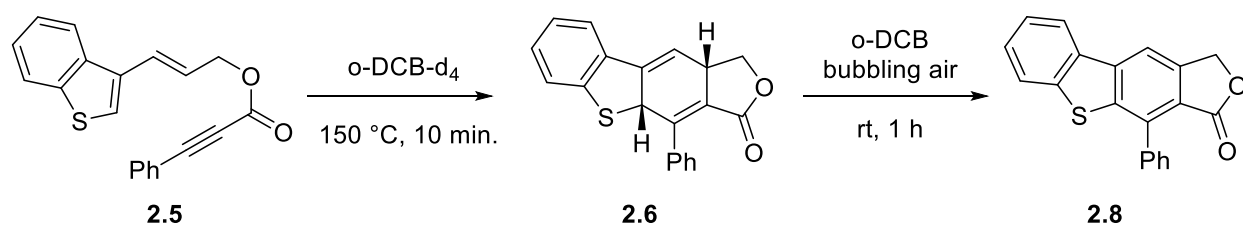


Scheme 2.7. DFT energy diagram for the dearomative DDDA reaction of **2.5** at the M06/6-311+G(d,p)/SMD(DMF)//B3LYP/6-31G(d) level of theory

2.4.1 No Evidence of Oxidation Product Formation from Isomerization Product

We propose that oxidation product forms directly from the DA adduct and is not a product from oxidation of the isomerization product. To test this hypothesis, we sought to effect the

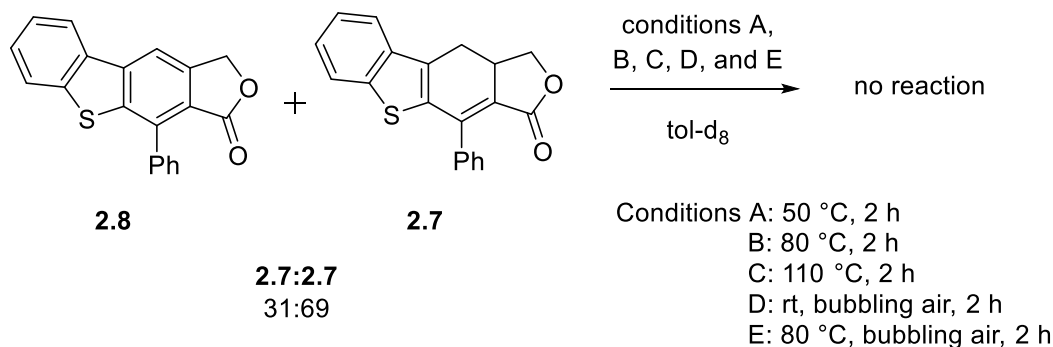
transformation of **2.6** to **2.8** with no formation of **2.7**. Additionally, we sought to subject **2.7** to those same reaction conditions in order to observe if there was any transformation of **2.7** to **2.8**. **2.5** was heated for 10 min at 150 °C in *o*-DCB to afford **2.6** with trace formation of **2.8**. The solution of **2.6** was allowed to cool to room temperature. Then, air was bubbled through the solution over the course of an hour affording **2.8** with trace amounts of **2.6** remaining (see ¹H NMR in experimental section). Thus, oxidation product forms readily from DA adduct at room temperature with an abundance of exposure to air and no evidence of isomerization product formation.



Scheme 2.8. Formation of oxidation product **2.8** from DA adduct **2.6** at rt with bubbling air

Additionally, a mixture of oxidation and isomerization products were subjected to conditions of bubbling air and heat in order to observe any transformation of isomerization product into oxidation product. Toluene-*d*₈ was chosen as a non-polar solvent that afforded trends of increased selectivity for oxidation product formation in dearomative DDDA reactions. A 31:69 mixture of **2.8**:**2.7** was dissolved in toluene-*d*₈ and subjected to heating via an oil bath at 50, 80 and 110 °C for 2 h increments. There was no observed change in the product ratios after any of the 2h increments (see ¹H NMR in experimental section). The solution was then subjected to bubbling air at room temperature for 2h, followed by bubbling air at 80 °C for 2h. There was also no observed change in the product ratios after either of the 2h increments with bubbling air. Therefore,

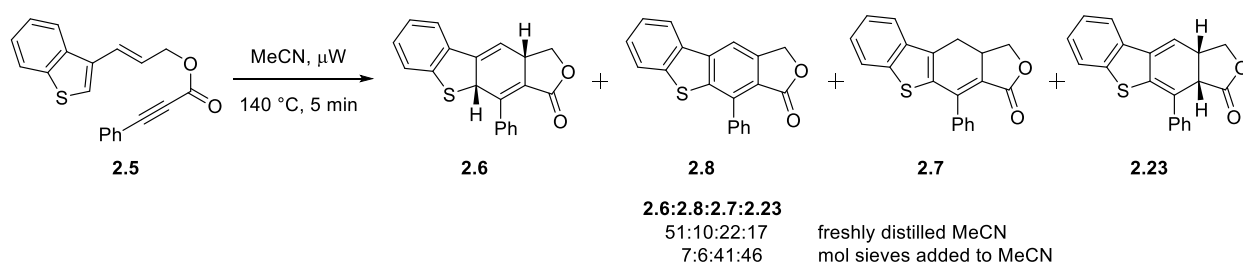
we propose that the isomerization product is a stable product that does not readily oxidize into oxidation product, but rather, oxidation is formed directly from the DA adduct.



Scheme 2.9. No conversion of isomerization product **2.7** to oxidation product **2.8** under thermal conditions with bubbling air

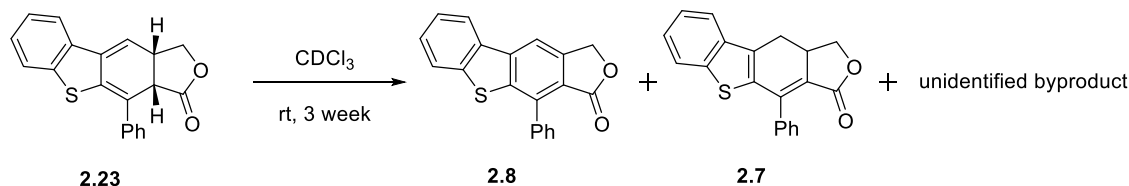
2.4.2 Cis-Diene as a Rarely Observed Byproduct that Converts to Oxidation and Isomerization Products

The cis-diene **2.23** is a byproduct of the dearomative DDDA reaction only found as a mixture with other products when polar solvents such as dimethylformamide or acetonitrile were used. Formation of cis-diene was observed when **2.5** was reacted for 5 min at 140 °C in freshly distilled acetonitrile using microwave heating to afford **2.6:2.8:2.7:2.23** in a ratio of 51:10:22:17 respectively. Repeating the reaction but with distilled acetonitrile solvent mixed with type 4Å mol sieves prior to the reaction afforded **2.6:2.8:2.7:2.23** in a ratio of 7:6:41:46. This enhanced selectivity for cis-diene and isomerization product in the presence of mol sieves suggests that the mol sieves are involved in the isomerization of the adduct to these products.



Scheme 2.10. Formation of cis-diene byproduct in acetonitrile with enhanced selectivity in the presence of mole sieves

Unlike the DA adduct, oxidation product, and isomerization product which have an equivalent R_f and are not separable by column chromatography, the cis-diene has a higher R_f and was isolated from the other products. Isolated cis-diene **2.23** dissolved in chloroform- d_1 at room temperature for 3 weeks afforded a mixture with a ratio of 25:34:29:12 (**2.23**:**2.8**:**2.7**:unidentified byproduct). Therefore, the cis-diene is considered an unstable byproduct of the dearomative DDDA reaction that converts to other products under the reaction conditions. Structural confirmation of the cis-diene was accomplished with single (^1H and ^{13}C) and multi-dimensional (COSY, HSQC, HMBC) NMR techniques as well as comparison to DFT predictive NMR via the DP4 probability method.



Scheme 2.11. Transformation of cis-diene into oxidation product, isomerization product, and unidentified byproduct

The resonances for the allylic protons observed at 3.75 and 3.85 ppm were confirmed by COSY NMR to be correlated to each other (see spectra in appendix B). HSQC NMR gave evidence

that the resonances at 4.63 and 4.54 ppm are correlated to the same carbon with resonance at 72.4 ppm, and therefore, can be attributed to the methylene carbon. In HMBC NMR, the resonance for the allylic proton α to the carbonyl is correlated to the carbonyl carbon, indicative of the short spatial distance between these atoms.

2.5 Conclusions

We established the DA adduct as the product of the dearomative cycloaddition step of the dearomative DDDA reaction and the pivotal intermediate on the reaction pathway to oxidation and isomerization product. This was accomplished by the synthesis and isolation of DA adduct **2.6** with structural confirmation by single and multidimensional NMR analysis, comparison to DFT predictive NMR through the DP4 probability method, and comparison to the synthesized adduct **2.20** with deuterium incorporation at the bis-allylic positions of the 1,4-cyclohexadiene. The DA adducts of precursors **1.59**, **2.9**, and **1.50** were synthesized and characterized by analogy, as the adducts were observed in mixtures of products. The oxidation product, isomerization product, and rarely observed cis-diene byproduct were established to be formed directly from DA adduct with no evidence for interconversion of isomerization product to oxidation product. This mechanistic understanding of the dearomative DDDA reaction is foundational to our efforts to enhance product selectivity and identify factors that control the reactivity of our substrates.

2.6 Experimental

2.6.1 General Methods

Unless otherwise indicated, all reactions were performed in flame-dried glassware under an air atmosphere and stirred with Teflon-coated magnetic stir bars. All commercially available compounds were purchased and used as received unless otherwise specified. Tetrahydrofuran (THF), diethyl ether (Et₂O), and dichloromethane (DCM) were purified by passing through alumina using a Sol-Tek ST-002 solvent purification system. Deuterated chloroform (CDCl₃) was dried over 4Å molecular sieves. Nitrogen gas was purchased from Matheson Tri Gas. Conventional heating was used for reactions that were monitored by ¹H NMR or performed open to the air. All microwave-mediated reactions were carried out using a Biotage Initiator Exp or Anton-Paar Monowave 300 microwave synthesizer. Purification of the compounds by flash column chromatography was performed using silica gel (40-63 μm particle size, 60 Å pore size). TLC analyses were performed on silica gel F₂₅₄ glass plates (250 μm thickness). ¹H NMR and ¹³C NMR spectra were recorded on Bruker Avance 300, 400, or 500 MHz spectrometers. Spectra were referenced to residual chloroform (7.26 ppm, ¹H; 77.16 ppm, ¹³C) or *o*-dichlorobenzene (6.93 ppm, ¹H; 130.04 ¹³C) unless otherwise specified. Chemical shifts are reported in ppm, multiplicities are indicated by s (singlet), d (doublet), t (triplet), q (quartet), p (pentet), m (multiplet), and bs (broad singlet). Coupling constants, *J*, are reported in hertz (Hz). All NMR spectra were obtained at room temperature. IR spectra were obtained using a Nicolet Avatar E.S.P. 360 FT-IR. EI mass spectroscopy was performed on a Waters Micromass GCT high resolution mass spectrometer, while ES mass spectroscopy was performed on a Waters Q-TOF Ultima API, Micromass UK Limited high-resolution mass spectrometer.

2.6.2 Dearomative DDDA Reaction of **1.59** in *o*-DCB

Rxn 1. An oven-dried NMR tube was charged with dearomative DDDA precursor **1.59** (8 mg, 0.03 mmol) dissolved in *o*-DCB- d_4 (0.5 mL, 0.6 M) under an atmosphere of air. The NMR tube was sealed with a polypropylene cap and lowered into an oil bath preheated at 150 °C and heated for 15 min. The NMR tube was removed from the oil bath, rinsed with hexanes, and wiped with a ChemWipe before ^1H NMR was obtained. A 35:15:38:12 ratio of **1.59**:**2.1**:**1.61**:**1.60** was obtained. Ratios were determined by comparing the ^1H NMR resonances at 6.03 ppm (1H) for **1.59**, 5.50 ppm (1H) for **2.1**, 5.14 ppm (2H) for **1.60**, and 2.39 ppm (1H) for **1.61**.

2.6.3 Synthesis of the Dearomative DDDA Precursors

2.6.3.1 General Procedure A: Conversion of Carboxaldehyde to α,β -Unsaturated Ester

Prepared in the manner of Travas-Sejdic, et al.⁵³ A flame-dried, 2-necked, round-bottomed flask equipped with stir bar, condenser, septum, and nitrogen inlet needle, was charged with carboxaldehyde (1.0 equiv), THF (0.17 M), and methyl(triphenylphosphoranylidene) acetate (1.5 equiv), added in single portions by briefly removing the septum. The flask was placed in an oil bath and warmed to 60 °C. After 24 h, the reaction was judged complete evidenced by the disappearance of starting material by TLC. The stir bar was removed and the mixture was concentrated by rotary evaporation. The residue was purified by silica gel flash column chromatography.

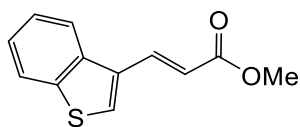
2.6.3.2 General Procedure B: Conversion of α,β -Unsaturated Ester to Allylic Alcohol

Prepared in the manner of Brummond, et al.⁴⁴ A flame-dried, single-necked, round-bottomed flask equipped with stir bar, septum, and nitrogen inlet needle was charged with the α,β -unsaturated ester (1.0 equiv) dissolved in dichloromethane (0.020 M) via syringe. The flask was placed in a dry ice/acetone bath (-78 °C). After 5 min, diisobutylaluminium hydride (DIBAL, 1.0 M in toluene, 3.5 equiv) was added dropwise via syringe, and the reaction mixture was maintained at -78 °C. After 1 h, the reaction was judged complete evidenced by the disappearance of starting material by TLC. Aqueous sodium potassium tartrate (1.2 M) was added and the mixture was vigorously stirred at rt for ca. 16 h. The solution was transferred to a separatory funnel, and the flask was rinsed with dichloromethane and transferred to the separatory funnel. The organic layer was separated, and the aqueous layer was extracted with dichloromethane (3x). The combined organic phase was washed with brine (1x), dried over magnesium sulfate, gravity filtered, and concentrated using rotary evaporation. The residue was purified by silica gel flash column chromatography.

2.6.3.3 General Procedure C: Conversion of Allylic Alcohol to Alkynoate

Prepared in the manner of Brummond, et al.⁴⁴ A flame-dried, single-necked, round-bottomed flask equipped with stir bar, septum, and nitrogen inlet, was charged with *N,N*-dimethylpyridin-4-amine (0.15 equiv) and phenylpropionic acid (1.1 equiv) by briefly removing the septum. Allylic alcohol (1.0 equiv) was dissolved in dichloromethane (0.080 M) and added via syringe. *N*-(3-dimethylaminopropyl)-*N'*-ethylcarbodiimide hydrochloride (1.5 equiv) was added in one portion by briefly removing the septum and the resulting solution was maintained at rt. After 3 h, the reaction was judged complete evidenced by the disappearance of starting material by TLC.

The reaction mixture was transferred to a separatory funnel, and the flask was rinsed with dichloromethane and transferred to the separatory funnel. The solution was washed with deionized water and the aqueous layer was extracted with dichloromethane (3x). The combined organic layers were washed with brine (1x), dried over magnesium sulfate, gravity filtered, and concentrated using rotary evaporation. The residue was purified by silica gel flash column chromatography.

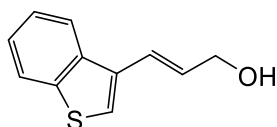


Methyl (E)-3-(benzo[*b*]thiophen-3-yl)acrylate (2.3). Follows General Procedure A. Benzo[*b*]thiophene-3-carboxaldehyde (1.0 g, 6.2 mmol), THF (36 mL), and methyl(triphenylphosphoranylidene) acetate (3.1 g, 9.3 mmol). The crude material was purified by flash column chromatography (20% EtOAc/Hex) to yield the title compound as a yellow solid (1.2 g, 91%). Compound **2.3** was previously prepared by Tay, et al.⁵⁴ Characterization data corresponds to the literature.

Data 2.3 previously characterized

¹H NMR (300 MHz, CDCl₃)
 8.01 (d, *J* = 8.6 Hz, 1H), 7.97 (d, *J* = 16.4 Hz, 1H), 7.87 (d, *J* = 8.5 Hz, 1H), 7.75 (s, 1H), 7.46 (t, *J* = 7.0 Hz, 2H), 6.54 (d, *J* = 16.0 Hz, 1H) 3.84 (s, 3H) ppm. Water impurity at 1.56 ppm.

TLC *R_f* = 0.31 (10% EtOAc/Hex) [silica gel, UV]



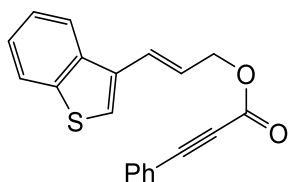
(E)-3-(benzo[*b*]thiophen-3-yl)prop-2-en-1-ol (2.4). Follows General Procedure B. **2.3** (1.2 g, 5.5 mmol), DCM (28 mL), DIBAL (19 mL, 19 mmol), aq sodium potassium tartrate solution (1.2 M, 30 mL). The crude material was purified by flash column chromatography (40% EtOAc/Hex) to yield the title compound as a light-yellow liquid (970 mg, 93%). Compound **2.4** was previously prepared by Wang, et al.⁵⁵ Characterization data corresponds to the literature.

Data **2.4** previously characterized

¹H NMR (300 MHz, CDCl₃)

7.91 (d, *J* = 8.0 Hz, 1H), 7.86 (d, *J* = 8.0 Hz, 1H), 7.44-7.35 (m, 3H), 6.91 (d, *J* = 16.0 Hz, 1H), 6.45 (dt, *J* = 5.7, 15.9 Hz, 1H), 4.37 (d, *J* = 5.2 Hz, 2H), 2.25 (s, 1H) ppm. DCM impurity at 5.30 ppm. EtOAc impurity at 2.05 ppm.

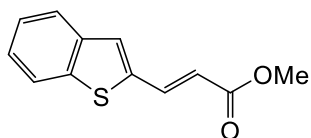
TLC *R_f* = 0.30 (40% EtOAc/Hex) [silica gel, UV]



(E)-3-(benzo[*b*]thiophen-3-yl)allyl 3-phenylpropiolate (2.5). Follows general procedure C: DMAP (13 mg, 0.10 mmol), **2.4** (100 mg, 0.53 mmol), phenylpropionic acid (85 mg, 0.58 mmol), dichloromethane (10 mL), N-(3-dimethylaminopropyl)-N'-ethylcarbodiimide hydrochloride (150 mg, 0.79 mmol). The residue was purified by flash column chromatography (30% EtOAc/Hex) to yield the title compound as a yellow liquid (150 mg, 91%).

Data 2.5

<u>¹H NMR</u>	(400 MHz, CDCl ₃) 7.93 (d, <i>J</i> = 8.1 Hz, 1H), 7.87 (d, <i>J</i> = 8.1, 1H), 7.61 (dd, <i>J</i> = 7.0, 1.5 Hz, 2H), 7.50 (s, 1H), 7.48-7.35 (m, 5H), 7.00 (d, <i>J</i> = 15.9 Hz, 1H), 6.42 (dt, <i>J</i> = 15.8, 6.7 Hz, 1H), 5.0 (d, <i>J</i> = 6.4, 2H) ppm. Water impurity at 1.58 ppm (<0.4%). Grease impurity at 0.10 ppm (<0.1%).
<u>¹³C NMR</u>	(100 MHz, CDCl ₃) 153.9, 140.5, 137.5, 133.1 (2C), 132.8, 130.8, 128.7 (2C), 127.7, 124.7, 124.5, 123.8, 123.6, 123.0, 122.0, 119.6, 86.8, 80.6, 66.8 ppm
<u>IR</u>	(thin film) 3057, 2220, 1709, 1490, 1425, 1379, 1285, 1169, 961 cm ⁻¹
<u>HRMS</u>	(FTMS + p ESI) [M + H] ⁺ calcd for C ₂₀ H ₁₅ O ₂ S: 319.07928, found 319.07969
<u>TLC</u>	<i>R_f</i> = 0.65 (40% EtOAc/Hex) [silica gel, UV]



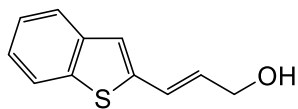
Methyl (E)-3-(benzo[*b*]thiophen-2-yl)acrylate (2.25). Follows General Procedure A. Benzo[*b*]thiophene-2-carboxaldehyde (550 mg, 3.4 mmol), THF (20 mL), and methyl(triphenylphosphoranylidene) acetate (1.7 g, 5.1 mmol). The material was purified by flash column chromatography (20% EtOAc/Hex) to yield the title compound as a yellow solid (720 mg, 97%). Compound **2.25** was previously prepared by Werner, et al.⁵⁶ Characterization data corresponds to the literature.

Data 2.25 previously characterized

¹H NMR (400 MHz, CDCl₃)

7.88 (d, *J* = 15.8 Hz, 1H), 7.81-7.73 (m, 2H), 7.45 (s, 1H), 7.40-7.32 (m, 2H), 6.30 (d, *J* = 15.7 Hz, 1H), 3.82 (s, 3H) ppm

TLC *R_f* = 0.29 (10% EtOAc/Hex) [silica gel, UV]



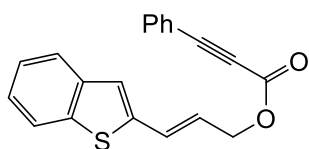
(E)-3-(benzo[*b*]thiophen-2-yl)prop-2-en-1-ol (2.26). Follows General Procedure B. **2.25** (710 mg, 3.3 mmol), DCM (30 mL), DIBAL (11 mL, 11 mmol), aq sodium potassium tartrate solution (1.2 M, 40 mL). The material was purified by flash column chromatography (40% EtOAc/Hex) to yield the title compound as a yellow solid (580 mg, 94%). Compound **2.26** was previously prepared by Shen, et al.⁵⁷ Characterization data corresponds to the literature.

Data 2.26 previously characterized

¹H NMR (400 MHz, CDCl₃)

7.78-7.65 (m, 2H), 7.34-7.27 (m, 2H), 7.14 (s, 1H), 6.85 (d, $J = 15.7$ Hz, 1H), 6.28 (dt, $J = 15.6, 5.5$ Hz, 1H), 4.34 (d, $J = 5.5$ Hz, 2H), 1.74 (s, 1H) ppm. EtOAc impurity at 2.05 ppm. Water impurity at 1.56 ppm.

TLC $R_f = 0.30$ (40% EtOAc/Hex) [silica gel, UV]



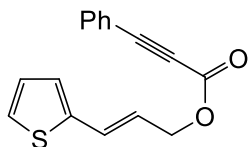
(*E*)-3-(benzo[*b*]thiophen-2-yl)allyl 3-phenylpropiolate (2.9). Follows General Procedure C: DMAP (39 mg, 0.32 mmol), **2.22** (300 mg, 1.6 mmol), phenylpropionic acid (260 mg, 1.8 mmol), dichloromethane (24 mL), N-(3-dimethylaminopropyl)-N'-ethylcarbodiimide hydrochloride (460 mg, 2.4 mmol). The material was purified by flash column chromatography (30% EtOAc/Hex) to yield the title compound as a white solid (400 mg, 79%).

Data 2.9

¹H NMR (400 MHz, CDCl₃)

7.79-7.68 (m, 2H), 7.61 (dd, $J = 8.5, 1.6$ Hz, 2H), 7.45 (t, $J = 7.4$ Hz, 1H), 7.38 (t, $J = 7.9$ Hz, 2H), 7.35-7.29 (m, 2H), 7.22 (s, 1H), 6.95 (d, $J = 15.7$ Hz, 1H), 6.24 (dt, $J = 6.5, 15.6$ Hz, 1H), 4.9 (dd, $J = 6.5, 1.0$ Hz, 2H) ppm. EtOAc impurity at 2.05 ppm (<0.4%). Water impurity at 1.56 ppm (<0.7%). Grease impurity at 1.26 ppm (<2.6%).

<u>¹³C NMR</u>	(100 MHz, CDCl ₃) 153.9, 141.2, 140.0, 139.3, 133.2 (2C), 130.9, 128.9, 128.7 (2C), 125.2, 124.7, 124.3 (2C), 123.8, 122.4, 119.6, 87.0, 80.5, 66.0 ppm
<u>IR</u>	(thin film) 3405, 3063, 2947, 2221, 1696, 1643, 1488, 1444, 1374, 1284, 1171, 1097, 956, 728 cm ⁻¹
<u>HRMS</u>	(FTMS + p ESI) [M + H] ⁺ calcd for C ₂₀ H ₁₅ O ₂ S: 319.0787, found 319.0798
<u>TLC</u>	R _f = 0.66 (40% EtOAc/Hex) [silica gel, UV]
<u>MP</u>	107.0 – 109.3 °C



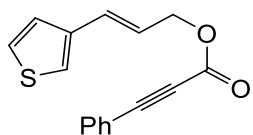
(E)-3-(thiophen-2-yl)allyl 3-phenylpropiolate (1.50). Prepared as described by Brummond, et al.⁴⁴ Follows General Procedure C: DMAP (97 mg, 0.79 mmol), (E)-3-(thiophen-2-yl)prop-2-en-1-ol (555 mg, 3.96 mmol), phenylpropionic acid (636 mg, 4.35 mmol), dichloromethane (66 mL), N-(3-dimethylaminopropyl)-N'-ethylcarbodiimide hydrochloride (1.14 g, 5.94 mmol). The material was purified by flash column chromatography (30% EtOAc/Hex) to yield the title compound as a white solid (798 mg, 75%). Compound **1.50** was previously prepared by Brummond, et al.⁴⁴ Characterization data corresponds to the literature.

Data 1.50 previously characterized

¹H NMR (400 MHz, CDCl₃)

7.60 (d, $J = 7.1$ Hz, 2H), 7.46 (tt, $J = 6.7, 1.4$ Hz, 1H), 7.38 (tt, $J = 6.8, 1.1$ Hz, 2H), 7.21 (d, $J = 4.9$ Hz, 1H), 7.02 (d, $J = 3.5$ Hz, 1H), 6.98 (dd, $J = 5.1, 3.6$, 1H), 6.86 (d, $J = 15.6$ Hz, 1H), 6.16 (dt, $J = 6.6, 15.6$ Hz, 1H), 4.9 (dd, $J = 6.7, 1.1$ Hz, 2H) ppm. DCM impurity at 5.30 ppm (<1.6%). Water impurity at 1.54 ppm (<0.6%).

TLC $R_f = 0.66$ (40% EtOAc/Hex) [silica gel, UV]



(*E*)-3-(thiophen-3-yl)allyl 3-phenylpropiolate (1.59). Prepared as described by Brummond, et al.⁴⁴ Follows General Procedure C: DMAP (11 mg, 0.090 mmol), (*E*)-3-(thiophen-3-yl)prop-2-en-1-ol (85 mg, 0.61 mmol), phenylpropionic acid (100 mg, 0.70 mmol), dichloromethane (5.0 mL), *N*-(3-dimethylaminopropyl)-*N'*-ethylcarbodiimide hydrochloride (170 g, 0.91 mmol). The material was purified by flash column chromatography (30% EtOAc/Hex) to yield the title compound as a clear yellow liquid (130 mg, 82%). Compound **1.59** was previously prepared by Brummond, et al.⁴⁴ Characterization data corresponds to the literature.

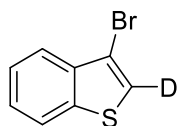
Data 1.59 previously characterized

¹H NMR (400 MHz, CDCl₃)

7.59 (d, $J = 7$ Hz, 2H), 7.45 (tt, $J = 7.5, 1.3$ Hz, 1H), 7.37 (t, $J = 7.8$ Hz, 2H), 7.29 (dd, $J = 3.5, 5.0$ Hz, 1H), 7.23 (d, $J = 4.2$ Hz, 2H), 6.74 (d, $J = 15.7$, 1H), 6.19 (dt, $J = 15.8, 6.7$ Hz, 1H), 4.86 (dd, $J = 6.7, 1.1$ Hz, 2H) ppm. EtOAc impurity at 2.05

ppm (<0.4%). Grease impurity at 1.26 ppm (<0.3%).

TLC R_f = 0.70 (40% EtOAc/Hex) [silica gel, UV]



3-bromobenzo[*b*]thiophene-2-d (2.16). Follows procedure described by Gronowitz.⁵⁸ A 15 mL, two-necked, round-bottomed flask with stir bar, condenser, and septum, was charged with zinc powder (600 mg, 9.3 mmol, 3 equiv), acetic acid-*d*₇ (0.53 mL, 9.3 mmol, 3 equiv), and deionized water (5.0 mL, 0.60 M). The flask was lowered into a preheated oil bath at 100 °C. After 10 min, 2,3-dibromo-benzo[*b*]thiophene (900 mg, 3.1 mmol, 1 equiv) was added in one portion. After 3 h, the reaction showed complete consumption of starting material by GC. 2,3-dibromo-benzo[*b*]thiophene had a retention time of 12 min (185 °C) and product 3-bromobenzo[*b*]thiophene-2-d had a retention time of 9.8 min (150 °C) when the reaction solution is injected at a starting temperature of 80 °C with temperature ramping up to 300 °C at a rate of 15 °C per min. The column used was a Rtx-5 Crossbond (5% diphenyl – 95% dimethyl polysiloxane) 15 m, 0.25 mmID, 0.25 μm df. The solution was allowed to cool to rt and then transferred to a separatory funnel. The aqueous layer was extracted with diethyl ether (3 x 5 mL) and the combined organics were washed with brine, dried over magnesium sulfate, vacuum filtered, and concentrated using rotary evaporation to afford a light orange liquid. The material was purified by silica gel flash column chromatography (100% Hex) to afford the product as a light-yellow liquid (510 mg, 81%).

Data 2.16

¹H NMR (300 MHz, CDCl₃)

8.00 (dd, *J* = 7.8, 0.5 Hz, 1H), 7.93 (dd, *J* = 8.2, 0.6 Hz, 1H), 7.57 (dt, *J* = 7.1, 1.1 Hz, 1H), 7.49 (dt, *J* = 7.6, 1.3 Hz, 1H) ppm. Water impurity at 1.56 ppm.

¹³C NMR (75 MHz, CDCl₃)

138.4, 137.4, 125.2, 124.9, 123.2 (t, *J* = 28.9 Hz), 123.0, 122.6, 107.6 ppm

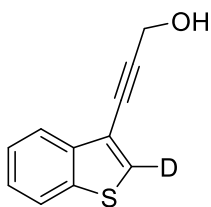
IR (thin film)

3106, 3056, 2924, 2852, 2320, 1557, 1480, 1454, 1419, 1302, 1247, 1162, 1072
cm⁻¹

HRMS (TOF MS ES+)

[M] calcd for C₈H₄D₁SBr: 212.9360, found 212.9230 and 214.9210

TLC *R*_f = 0.53 (100% Hex) [silica gel, UV]



3-(benzo[*b*]thiophen-3-yl-2-d)prop-2-yn-1-ol (2.17). Follows procedure described by Arsenyan, et al.⁵⁹ A flame-dried, 25 mL, two-necked, round-bottomed flask with stir bar, condenser, and septum, was flushed with nitrogen (3x) before charged with **2.16** (409 mg, 1.91 mmol, 1 equiv), propargyl alcohol (167 μL, 2.87 mmol, 1.5 equiv), tetrakis(triphenylphosphine) palladium(0) (22 mg, 0.020 mmol, 0.01 equiv), copper(I) iodide (15 mg, 0.08 mmol, 0.04 equiv), and deionized water (12 mL, 0.16 M) in one portion. The solution was degassed by bubbling N₂ through for 10

min. Pyrrolidine (240 μ L, 2.88 mmol, 2 equiv) was added dropwise via syringe, and the solution was lowered into a preheated oil bath at 75 $^{\circ}$ C. The reaction was maintained overnight before the solution was allowed to cool to rt and transferred to a separatory funnel. The aqueous layer was extracted with diethyl ether (3 x 10 mL) and the combined organics were washed with brine, dried over magnesium sulfate, vacuum filtered, and concentrated using rotary evaporation to afford a dark orange liquid. The oil was purified by silica gel flash column chromatography (30% EtOAc/Hex) to afford the product as a dark yellow, orange oil (325 mg, 90%).

Data 2.17

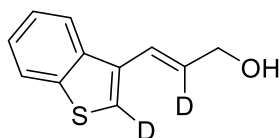
^1H NMR (500 MHz, CDCl_3)
7.97 (d, $J = 7.5$ Hz, 1H), 7.83 (d, $J = 7.5$ Hz, 1H), 7.40 (p, $J = 7.3$ Hz, 2H), 4.62 (s, 2H), 3.11 (s, 1H) ppm. DCM impurity at 5.27 ppm. EtOAc impurity at 4.14, 2.07, and 1.25 ppm.

^{13}C NMR (125 MHz, CDCl_3)
139.1, 138.7, 130.3 (t, $J = 27.9$ Hz), 125.0, 124.7, 122.9, 122.6, 117.5, 90.0, 79.3, 51.5 ppm

IR (thin film)
3943, 3593, 3431, 3054, 2986, 2305, 1631, 1421, 1265, 1016 cm^{-1}

HRMS (FTMS + p ESI)
[M + H] $^{+}$ calcd for $\text{C}_{11}\text{H}_8\text{DOS}$: 190.0431, found 190.0429

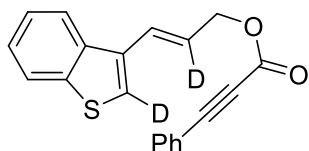
TLC $R_f = 0.27$ (30% EtOAc/Hex) [silica gel, UV]



(E)-3-(benzo[*b*]thiophen-3-yl-2-[²H])prop-2-en-2-[²H]-1-ol (2.18). Follows procedure by Kocsis, et al.⁵⁰ A flame-dried, 25 mL, two-necked, round-bottomed flask with stir bar, condenser, and septum, was charged with lithium aluminum deuteride (LAD, 114 mg, 2.72 mmol, 1.00 equiv). The apparatus was evacuated and filled with nitrogen (3 x). THF (7 mL, 0.370 M) was added via syringe and the solution was cooled in an ice-water bath. A separate flame-dried, 15-mL, round-bottomed flask with septum was charged with 3-(benzo[*b*]thiophen-3-yl-2-[²H])prop-2-yn-1-ol (**3.2.17**, 515 mg, 2.72 mmol, 1.00 equiv) and the flask was evacuated and filled with nitrogen (3 x). THF (4.00 mL, 0.700 M) was added via syringe and the solution was cooled in an ice-water bath. The solution of **2.17** was cannulated dropwise to the lithium aluminum deuteride solution. Additional THF (1 mL) was used to transfer the last traces of **2.17** to the reaction flask. The reaction was maintained at 0 °C in an ice-water bath. After 1 h, the reaction showed no further change as observed by TLC but didn't show complete consumption of starting material. The reaction solution was cannulated dropwise into a separate flask charged with ice-water (10 mL), equipped with a stir bar, and placed in an ice bath. Vigorous bubbling occurred during the transfer process. The solution was allowed to warm to rt after removing from the ice bath. The solution was extracted with diethyl ether (3 x 10 mL) and the combined organics were washed with brine, dried over magnesium sulfate, vacuum filtered, and concentrated using rotary evaporation to afford a yellow liquid. The residue was purified by flash column chromatography (5% ethyl ether/dichloromethane) to afford the product as a yellow liquid (426 mg, 88%) and starting material **2.17** (40 mg).

Data 2.18

<u>¹H NMR</u>	(300 MHz, CDCl ₃) 7.92 – 7.85 (m, 2H), 7.43 – 7.34 (m, 2H), 6.87 (s, 1H), 4.36 (s, 2H), 2.23 (s, 1H) ppm. DCM impurity at 5.30 ppm.
<u>¹³C NMR</u>	(100 MHz, CDCl ₃) 140.3, 137.6, 133.2, 129.9 (t, <i>J</i> = 23.4), 124.5, 124.3, 122.9 (2C), 122.0 (t, <i>J</i> = 27.8), 121.9, 63.5 ppm
<u>IR</u>	(thin film) 3600, 3405, 3054, 2927, 2306, 1423, 1265 cm ⁻¹
<u>HRMS</u>	(FTMS + p ESI) [MH – H ₂ O] ⁺ calcd for C ₁₁ H ₇ D ₂ S: 175.0545, found 175.0542
<u>TLC</u>	<i>R</i> _f = 0.21 (30% EtOAc/Hex) [silica gel, UV]



(*E*)-3-(benzo[*b*]thiophen-3-yl-2-d)allyl-2-d 3-phenylpropiolate (2.19). Follows General Procedure C: DMAP (108 mg, 0.882 mmol), **2.18** (424 mg, 2.21 mmol), phenylpropionic acid (419 mg, 2.87 mmol), dichloromethane (16 mL), N-(3-dimethylaminopropyl)-N'-ethylcarbodiimide hydrochloride (634 mg, 3.31 mmol). The crude material was purified by flash column chromatography (20% EtOAc/Hex) to yield the title compound as a clear yellow liquid (254 mg, 63%).

Data 2.19

¹H NMR (400 MHz, CDCl₃)

7.93 (d, *J* = 7.7 Hz, 1H), 7.87 (d, *J* = 7.7 Hz, 1H), 7.61 (m, 2H), 7.48 – 7.35 (m, 5H), 7.00 (s, 1H), 4.95 (s, 2H) ppm. DCM impurity at 5.30 ppm. EtOAc impurity at 4.14, 2.06, and 1.27 ppm.

¹³C NMR (100 MHz, CDCl₃)

153.9, 140.4, 137.5, 133.1 (2C), 132.7, 130.8, 128.7 (2C), 127.6, 124.7, 124.5, 123.4 (t, *J* = 24.5 Hz), 123.4 (t, *J* = 22.2 Hz), 123.0, 122.0, 119.6, 86.8, 80.6, 66.7 ppm

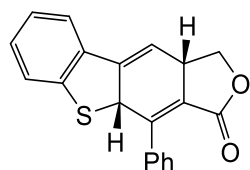
IR (thin film)

3055, 2218, 1704, 1490, 1422, 1375, 1265, 1170, 962 cm⁻¹

HRMS (FTMS + p ESI)

[M+H]⁺ calcd for C₂₀H₁₃D₂O₂S: 321.09183, found 321.09261

TLC *R_f* = 0.65 (40% EtOAc/Hex) [silica gel, UV]



4-phenyl-4a,10a-dihydrobenzo[4,5]thieno[2,3-f]isobenzofuran-3(1H)-one (2.6) (Table 2.1, entry 1). An oven-dried NMR tube was charged with **2.5** (13 mg, 0.04 mmol) dissolved in *o*-dichlorobenzene (0.5 mL, 0.08 M). The NMR tube was sealed with a polypropylene cap and

lowered into a preheated oil bath at 150 °C. After 7 min, the NMR tube was removed from the oil bath, rinsed with hexanes, and wiped with a ChemWipe. A ratio of 91:9 (**2.6:2.8**) was afforded, and thus **2.6** was characterized as a mixture. Attempts to purify **2.6** by column chromatography led to conversion to products. The solution was analyzed by multi-dimensional NMR COSY, HSQC, and HMBC.

Data 2.6

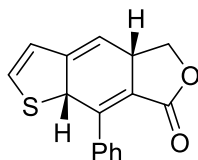
¹H NMR (400 MHz, o-DCB-d₄) ppm
7.34 – 7.25 (m, 5H), 7.19 (d, *J* = 7 Hz, 1H), 7.04 (dt, *J* = 1.3, 7.3 Hz, 1H), 6.98 – 6.91 (m, 2H), 5.93 (dd, *J* = 2.0, 3.5 Hz, 1H), 5.46 (dd, *J* = 3.5, 13.5 Hz, 1H), 4.53 (dd, *J* = 8.6 Hz, 1H), 3.91 (dd, *J* = 8.2, 10.4 Hz, 1H), 3.67 – 3.57 (m, 1H) ppm

¹³C NMR (100 MHz, o-DCB-d₄)
166.2, 146.4, 143.5, 142.9, 136.2, 134.7, 129.5, 129.3, 129.0, 128.9, 128.2, 128.0, 124.8, 123.0, 122.4, 122.2, 114.8, 68.6, 55.5, 41.5 ppm

IR (thin film)
2978, 1756, 1455, 1354, 1223, 1060, 756, 700 cm⁻¹

HRMS (FTMS + p ESI)
[M + H]⁺ calcd for C₂₀H₁₃O₂S: 317.06308, found 317.06243 indicative of formation of oxidation product **2.5** under ionization conditions. 319.07787 was also found in 8% relative abundance, which is the correct mass for **2.6**

TLC *R_f* = 0.44 (40% ethyl acetate/hexanes) [silica gel, UV]

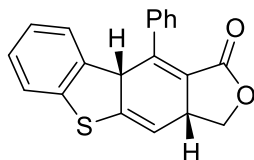


(4a*S*,8a*R*)-8-phenyl-4a,8a-dihydrothieno[2,3-*f*]isobenzofuran-7(5*H*)-one (2.1) (Table 2.1, entry 2). An oven-dried NMR tube was charged with dearomative DDDA precursor **1.59** (8 mg, 0.03 mmol) dissolved in *o*-DCB-*d*₄ (0.5 mL, 0.06 M) under an atmosphere of air. The NMR tube was sealed with a polypropylene cap and lowered into an oil bath preheated at 150 °C and heated for 15 min. The NMR tube was removed from the oil bath, rinsed with hexanes, and wiped with a ChemWipe before ¹H NMR was obtained. A 35:15:38:12 ratio of **1.59**:**2.1**:**1.61**:**1.60** was obtained. Ratios were determined by comparing the ¹H NMR resonances at 6.03 ppm (1H) for **1.59**, 5.50 ppm (1H) for **2.1**, 5.14 ppm (2H) for **1.60**, and 2.39 ppm (1H) for **1.61**. Characterization of **2.1** by analogy to **2.6** can be found in Table 2.1. Attempts to purify **2.1** by column chromatography led to conversion to products.

Data 2.1

¹H NMR (400 MHz, *o*-DCB-*d*₄) ppm

5.50 (dd, *J* = 2.1, 3.8 Hz, 1H), 5.30 (dd, *J* = 3.8, 14.8 Hz, 1H), 4.48 (dd, *J* = 8.2, 8.9 Hz, 1H), 3.82 (dd, *J* = 8.2, 10.2 Hz, 1H), 3.57 – 3.47 (m, 1H) ppm. Resonances for aromatic protons overlapped with other resonances in the mixture and were not characterized.



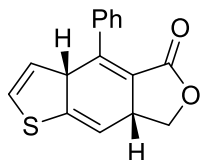
(3aR,9bS)-10-phenyl-3a,9b-dihydrobenzo[4,5]thieno[2,3-f]isobenzofuran-1(3H)-one (2.10)

(Table 2.1, entry 3). An oven-dried NMR tube was charged with dearomative DDDA precursor **2.9** (10 mg, 0.03 mmol) dissolved in *o*-DCB (0.5 mL, 0.06 M) under an atmosphere of air. The NMR tube was sealed with a polypropylene cap and lowered into an oil bath preheated at 150 °C and heated for 11 min. The NMR tube was removed from the oil bath, rinsed with hexanes, and wiped with a ChemWipe before ¹H NMR was obtained. A 6:87:0:7 ratio of **2.9**:**2.10**:**2.11**:**2.12** was obtained. Ratios were determined by comparing the ¹H NMR resonances at 4.81 ppm (2H) for **2.9**, 5.59 ppm (1H) for **2.10**, and 5.12 ppm (2H) for **2.12**. Characterization of **2.10** by analogy to **2.6** can be found in Table 2.1. Attempts to purify **2.10** by column chromatography led to conversion to products.

Data 2.10

¹H NMR (500 MHz, *o*-DCB) ppm

5.59 (dd, *J* = 1.7, 3.4 Hz, 1H), 4.74 (dd, *J* = 3.3, 13.4 Hz, 1H), 4.50 (dd, *J* = 8.6, 9.4 Hz, 1H), 3.82 (dd, *J* = 8.6, 9.4 Hz, 1H), 3.60 – 3.50 (m, 1H) ppm. Resonances for aromatic protons overlapped with other resonances in the mixture and were not characterized.

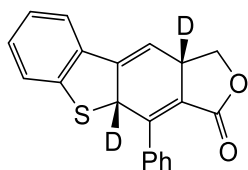


(3aR,7aR)-4-phenyl-7,7a-dihydrothieno[2,3-f]isobenzofuran-5(3aH)-one (2.13) (Table 2.1, entry 4). An oven-dried NMR tube was charged with dearomative DDDA precursor **1.50** (10 mg, 0.04 mmol) dissolved in *o*-DCB (0.5 mL, 0.07 M) under an atmosphere of air. The NMR tube was sealed with a polypropylene cap and lowered into an oil bath preheated at 150 °C and heated for 15 min. The NMR tube was removed from the oil bath, rinsed with hexanes, and wiped with a ChemWipe before ^1H NMR was obtained. A 16:65:9:10 ratio of **1.50:2.13:1.51:2.14** was obtained. Ratios were determined by comparing the ^1H NMR resonances at 4.74 ppm (2H) for **1.50**, 5.51 ppm (1H) for **2.13**, 5.10 ppm (2H) for **2.14**, and 2.51 ppm (1H) for **1.51**. Characterization of **2.13** by analogy to **2.6** can be found in Table 2.1. Attempts to purify **2.13** by column chromatography led to conversion to products.

Data 2.13

^1H NMR (500 MHz, *o*-DCB) ppm

5.51 (dd, $J = 3.4$ Hz, 1H), 4.42 (dd, $J = 3.4, 15.0$ Hz, 1H), 4.45 (dd, $J = 8.7$ Hz, 1H), 3.79 (dd, $J = 8.7, 8.9$ Hz, 1H), 3.51 – 3.39 (m, 1H) ppm. Resonances for aromatic protons overlapped with other resonances in the mixture and were not characterized.



(4aR,10aS)-4-phenyl-4a,10a-dihydrobenzo[4,5]thieno[2,3-f]isobenzofuran-3(1H)-one-

4a,10a-d2 (2.20). A 1-mL, flame-dried, microwave vial with stir bar was charged with precursor **2.19** (24 mg, 0.075 mmol) dissolved in o-DCB (0.50 mL, 0.15 M). The vial was sealed with a crimp cap with Teflon-lined septum, wrapped in parafilm at the top, and lowered into a pre-heated oil bath at 150 °C. After 90 min, the solution was allowed to cool to room temperature before transferred to an NMR tube for NMR analysis. Product ratios were determined by comparing the resonance integrations for starting material, adduct, oxidized product, and isomerized product from the ¹H NMR of the crude reaction solution using No-D spectroscopy. A 0:77:18:5 ratio of **2.19:2.20:2.8:2.21** was obtained. Ratios were determined by comparing the ¹H NMR resonances at 4.54 ppm (1H) for **2.20**, 5.21 ppm (2H) for **2.8**, and 3.09 ppm (1H) for **2.21**.

Data 2.20

¹H NMR (500 MHz, o-DCB) ppm

5.95 (s, 1H), 4.54 (d, *J* = 8.9 Hz, 1H), 3.90 (d, *J* = 9.0 Hz, 1H) ppm. Resonances for aromatic protons overlapped with other resonances in the mixture and were not characterized.

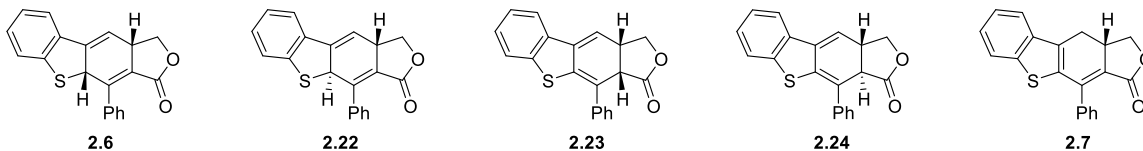
2.6.5 Deuterium Isotope Effect Observed in Parallel Reactions of **2.5** and **2.19**

Rxn 1. A 1-mL, flame-dried, microwave vial with stir bar was charged with precursor **2.5** (20 mg, 0.063 mmol) dissolved in o-dichlorobenzene (0.50 mL, 0.13 M). The vial was sealed with a crimp cap with Teflon-lined septum, wrapped in parafilm at the top, and lowered into a pre-heated oil bath at 150 °C. After 90 min, the solution was allowed to cool to room temperature before transferred to an NMR tube for NMR analysis. Product ratios were determined by comparing the resonance integrations for starting material, adduct, oxidized product, and isomerized product from the ¹H NMR of the crude reaction solution using No-D spectroscopy. A 0:41:39:20 ratio of **2.5**, **2.6**, **2.8**, and **2.7** was obtained. Ratios were determined by comparing the ¹H NMR resonances at 5.45 ppm (1H) for **2.6**, 5.21 ppm (2H) for **2.8**, and 2.79 ppm (1H) for **2.7**.

Rxn 2. A 1-mL, flame-dried, microwave vial with stir bar was charged with precursor **2.19** (24 mg, 0.075 mmol) dissolved in o-dichlorobenzene (0.50 mL, 0.15 M). The vial was sealed with a crimp cap with Teflon-lined septum, wrapped in parafilm at the top, and lowered into a pre-heated oil bath at 150 °C. After 90 min, the solution was allowed to cool to room temperature before transferred to an NMR tube for NMR analysis. Product ratios were determined by comparing the resonance integrations for starting material, adduct, oxidized product, and isomerized product from the ¹H NMR of the crude reaction solution using No-D spectroscopy. A 0:77:18:5 ratio of **2.19**, **2.20**, **2.8**, and **2.21** was obtained. Ratios were determined by comparing the ¹H NMR resonances at 4.53 ppm (1H) for **2.20**, 5.21 ppm (2H) for **2.8**, and 3.09 ppm (1H) for **2.21**.

2.6.6 DP4 Probability Measure Results and Analysis

Table 2.2. Computational and experimental ^{13}C NMR resonances of the **2.6**, **2.22**, **2.23**, **2.24**, and **2.7**



Entry	Computational					Experimental		
	2.13	2.22	2.23	2.24	2.7	2.13	2.23	2.7
1	42.70	44.52	39.88	41.50	27.09	41.59	39.00	26.57
2	56.64	54.86	45.92	42.12	37.81	55.64	45.32	37.06
3	67.37	69.00	72.08	66.73	70.29	68.69	72.35	71.27
4	113.59	115.86	116.46	113.91	119.71	114.87	116.22	119.51
5	121.73	121.28	121.52	121.36	122.34	122.32	121.16	122.53
6	122.04	123.61	122.65	122.73	123.25	122.51	121.81	123.05
7	122.78	124.65	124.31	124.79	125.33	123.16	122.43	125.03
8	124.69	125.03	124.84	127.85	125.41	124.88	125.05	125.99
9	127.91	127.72	127.80	127.85	127.53	128.10	127.74	128.10
10	127.91	127.72	127.80	128.30	127.53	128.32	127.74	128.10
11	128.58	129.84	127.86	128.93	130.01	129.03	127.99	129.35
12	128.58	130.27	128.89	128.93	131.37	129.15	128.77	129.35
13	129.66	130.27	128.89	129.04	131.37	129.41	128.77	129.58
14	129.70	130.86	129.37	131.63	131.63	129.66	129.84	132.94
15	134.02	132.26	133.05	132.48	133.75	134.80	133.73	134.27
16	135.58	135.61	134.77	135.74	136.35	136.34	133.78	137.75
17	143.33	141.15	141.24	138.71	140.68	142.97	139.33	139.05
18	145.85	144.65	141.42	141.78	141.71	143.62	140.68	142.12
19	148.06	145.79	142.73	144.24	145.74	146.50	140.94	143.51
20	165.94	166.14	175.88	169.31	166.30	166.28	176.68	167.95

Table 2.3. Computational and experimental ¹H NMR resonances of the **2.6**, **2.22**, **2.23**, **2.24**, and **2.7**

Entry	Calculated					Experimental		
	2.13	2.22	2.23	2.24	2.7	2.13	2.23	2.7
1	3.92	3.83	3.40	3.40	2.78	3.38	3.75	2.80
2	3.92	4.40	3.66	3.46	3.04	3.66	3.85	3.43
3	4.44	4.41	4.47	4.02	3.55	4.28	4.54	3.68
4	6.15	6.01	4.59	4.29	3.91	5.21	4.62	4.15
5	6.17	6.30	6.13	6.44	4.58	5.69	6.19	4.80
6	7.06	7.10	7.11	7.12	7.39	6.68	7.14	7.38
7	7.11	7.19	7.22	7.21	7.41	6.71	7.25	7.43
8	7.21	7.26	7.25	7.25	7.44	6.79	7.26	7.45
9	7.35	7.37	7.30	7.35	7.44	6.94	7.32	7.46
10	7.41	7.42	7.40	7.40	7.47	7.02	7.43	7.47
11	7.41	7.42	7.40	7.40	7.63	7.04	7.44	7.48
12	7.42	7.46	7.42	7.46	7.64	7.06	7.50	7.49
13	7.48	7.79	7.90	7.54	7.71	7.07	7.69	7.77
14	7.48	7.79	7.90	7.54	7.71	7.08	7.69	7.77

2.6.6.1 DP4 Analysis of the Experimental 2.6 NMR

Assignment of experimental NMR resonances of proposed **2.6** isomer to calculated NMR resonances of each considered isomer.

2.6 (atom, calc, exp):

C1 42.7 41.59
 C10 127.91 128.1
 C11 128.58 129.15
 C12 128.58 129.03
 C13 129.66 129.41
 C14 129.7 129.66
 C15 134.02 134.8
 C16 135.58 136.34
 C17 143.33 142.97
 C18 145.85 143.62
 C19 148.06 146.5
 C2 56.64 55.64
 C20 165.94 166.28
 C3 67.37 68.69
 C4 113.59 114.87
 C5 121.73 122.32
 C6 122.04 122.51
 C7 122.78 123.16
 C8 124.69 124.88

C9 127.91 128.32
 H1 3.92 3.66
 H10 7.41 7.04
 H11 7.41 7.02
 H12 7.42 7.06
 H13 7.48 7.08
 H14 7.48 7.07
 H2 3.92 3.38
 H3 4.44 4.28
 H4 6.15 5.21
 H5 6.17 5.69
 H6 7.06 6.68
 H7 7.11 6.71
 H8 7.21 6.79
 H9 7.35 6.94

2.22 (atom, calc, exp):

C1	44.52	41.59
C10	127.72	128.1
C11	129.84	129.03
C12	130.27	129.41
C13	130.27	129.15
C14	130.86	129.66
C15	132.26	134.8
C16	135.61	136.34
C17	141.15	142.97
C18	144.65	143.62
C19	145.79	146.5
C2	54.86	55.64
C20	166.14	166.28
C3	69.0	68.69
C4	115.86	114.87
C5	121.28	122.32
C6	123.61	122.51
C7	124.65	123.16
C8	125.03	124.88
C9	127.72	128.32
H1	3.83	3.38
H10	7.42	7.04
H11	7.42	7.02
H12	7.46	7.06
H13	7.79	7.08
H14	7.79	7.07
H2	4.4	3.66
H3	4.41	4.28
H4	6.01	5.21
H5	6.3	5.69
H6	7.1	6.68
H7	7.19	6.71
H8	7.26	6.79
H9	7.37	6.94

2.23 (atom, calc, exp):

C1	41.59	41.59
C10	122.78	129.66
C11	121.02	128.1
C12	122.75	129.41
C13	121.09	128.32
C14	122.63	129.15
C15	126.96	134.8
C16	135.31	142.97
C17	141.35	146.5

C18	134.69	136.34
C19	136.94	143.62
C2	47.55	55.64
C20	166.82	166.28
C3	70.96	68.69
C4	112.84	114.87
C5	115.31	122.32
C6	116.26	122.51
C7	120.4	124.88
C8	117.92	123.16
C9	121.41	129.03
H1	3.4	3.38
H10	7.4	7.04
H11	7.4	7.02
H12	7.42	7.06
H13	7.9	7.08
H14	7.9	7.07
H2	3.66	3.66
H3	4.47	4.28
H4	4.59	5.21
H5	6.13	5.69
H6	7.11	6.68
H7	7.22	6.71
H8	7.25	6.79
H9	7.3	6.94

2.24 (atom, calc, exp):

C1	41.5	41.59
C10	128.3	128.32
C11	128.93	129.15
C12	128.93	129.03
C13	129.04	129.41
C14	131.63	129.66
C15	132.48	134.8
C16	135.74	136.34
C17	138.71	142.97
C18	141.78	143.62
C19	144.24	146.5
C2	42.12	55.64
C20	169.31	166.28
C3	66.73	68.69
C4	113.91	114.87
C5	121.36	122.32
C6	122.73	122.51
C7	124.79	123.16
C8	127.85	128.1

C9	127.85	124.88
H1	3.4	3.38
H10	7.4	7.04
H11	7.4	7.02
H12	7.46	7.06
H13	7.54	7.08
H14	7.54	7.07
H2	3.46	3.66
H3	4.02	4.28
H4	4.29	5.21
H5	6.44	5.69
H6	7.12	6.68
H7	7.21	6.71
H8	7.25	6.79
H9	7.35	6.94

H3	3.55	4.28
H4	3.91	5.21
H5	4.58	5.69
H6	7.39	6.68
H7	7.41	6.71
H8	7.44	6.94
H9	7.44	6.79

2.7

(atom, calc, exp):

C1	27.09	41.59
C10	127.53	128.1
C11	130.01	129.03
C12	131.37	129.41
C13	131.37	129.15
C14	131.63	129.66
C15	133.75	134.8
C16	136.35	136.34
C17	140.68	142.97
C18	141.71	143.62
C19	145.74	146.5
C2	37.81	55.64

Warning: Error = 17.8 ppm

C20	166.3	166.28
C3	70.29	68.69
C4	119.71	114.87
C5	122.34	122.32
C6	123.25	122.51
C7	125.33	123.16
C8	125.41	124.88
C9	127.53	128.32
H1	2.78	3.38
H10	7.47	7.02
H11	7.63	7.04
H12	7.64	7.06
H13	7.71	7.08
H14	7.71	7.07
H2	3.04	3.66

The results show the probability that the experimental NMR spectrum corresponds to the indicated calculated NMR spectrum. The DP4 probability calculation uses the DP4-database2 version of the database and uses the t distribution.

Results of DP4 using both carbon and proton data:

2.6: 99.9%
2.22: 0.1%
2.23: 0.0%
2.24: 0.0%
2.7: 0.0%

Results of DP4 using the carbon data only:

2.6: 95.4%
2.22: 4.6%
2.23: 0.0%
2.24: 0.0%
2.7: 0.0%

Results of DP4 using the proton data only:

2.6: 97.1%
2.22: 2.6%
2.23: 0.3%
2.24: 0.1%
2.7: 0.0%

2.6.6.2 DP4 Analysis of the Experimental 2.23 NMR

Assignment of experimental NMR resonances of proposed **2.23** isomer to calculated NMR resonances of each considered isomer.

2.6 (atom, calc, exp):

C1 42.7 39.0
 C10 127.91 127.74
 C11 128.58 128.77
 C12 128.58 127.99
 C13 129.66 128.77
 C14 129.7 129.84
 C15 134.02 133.73
 C16 135.58 133.78
 C17 143.33 139.33
 C18 145.85 140.68
 C19 148.06 140.94

C2 56.64 45.32
 C20 165.94 176.68
 C3 67.37 72.35
 C4 113.59 116.22
 C5 121.73 121.16
 C6 122.04 121.81
 C7 122.78 122.43
 C8 124.69 125.05
 C9 127.91 127.74
 H1 3.92 3.85
 H10 7.41 7.44
 H11 7.41 7.43

H12 7.42 7.5
H13 7.48 7.69
H14 7.48 7.69
H2 3.92 3.75
H3 4.44 4.54
H4 6.15 4.62
H5 6.17 6.19
H6 7.06 7.14
H7 7.11 7.25
H8 7.21 7.26
H9 7.35 7.32

2.22 (atom, calc, exp):

C1 44.52 39.0
C10 127.72 127.74
C11 129.84 127.99
C12 130.27 128.77
C13 130.27 128.77
C14 130.86 129.84
C15 132.26 133.73
C16 135.61 133.78
C17 141.15 139.33
C18 144.65 140.68
C19 145.79 140.94
C2 54.86 45.32
C20 166.14 176.68
C3 69.0 72.35
C4 115.86 116.22
C5 121.28 121.16
C6 123.61 121.81
C7 124.65 122.43
C8 125.03 125.05
C9 127.72 127.74
H1 3.83 3.75
H10 7.42 7.44
H11 7.42 7.43
H12 7.46 7.5
H13 7.79 7.69
H14 7.79 7.69
H2 4.4 3.85
H3 4.41 4.54
H4 6.01 4.62
H5 6.3 6.19
H6 7.1 7.14
H7 7.19 7.25
H8 7.26 7.26

H9 7.37 7.32

2.23 (atom, calc, exp):

C1 39.88 39.0
C10 127.8 127.74
C11 127.86 127.99
C12 128.89 128.77
C13 128.89 128.77
C14 129.37 129.84
C15 133.05 133.73
C16 134.77 133.78
C17 141.24 139.33
C18 141.42 140.68
C19 142.73 140.94
C2 45.92 45.32
C20 175.88 176.68
C3 72.08 72.35
C4 116.46 116.22
C5 121.52 121.16
C6 122.65 121.81
C7 124.31 122.43
C8 124.84 125.05
C9 127.8 127.74
H1 3.4 3.75
H10 7.4 7.44
H11 7.4 7.43
H12 7.42 7.5
H13 7.9 7.69
H14 7.9 7.69
H2 3.66 3.85
H3 4.47 4.54
H4 4.59 4.62
H5 6.13 6.19
H6 7.11 7.14
H7 7.22 7.25
H8 7.25 7.26
H9 7.3 7.32

2.24 (atom, calc, exp):

C1 41.5 39.0
C10 128.3 127.74
C11 128.93 128.77
C12 128.93 127.99
C13 129.04 128.77
C14 131.63 129.84
C15 132.48 133.73

C16	135.74	133.78	C12	131.37	128.77
C17	138.71	139.33	C13	131.37	128.77
C18	141.78	140.68	C14	131.63	129.84
C19	144.24	140.94	C15	133.75	133.73
C2	42.12	45.32	C16	136.35	133.78
C20	169.31	176.68	C17	140.68	139.33
C3	66.73	72.35	C18	141.71	140.68
C4	113.91	116.22	C19	145.74	140.94
C5	121.36	121.16	C2	37.81	45.32
C6	122.73	121.81	C20	166.3	176.68
C7	124.79	122.43	C3	70.29	72.35
C8	127.85	127.74	C4	119.71	116.22
C9	127.85	125.05	C5	122.34	121.16
H1	3.4	3.75	C6	123.25	121.81
H10	7.4	7.44	C7	125.33	122.43
H11	7.4	7.43	C8	125.41	125.05
H12	7.46	7.5	C9	127.53	127.74
H13	7.54	7.69	H1	2.78	3.75
H14	7.54	7.69	H10	7.47	7.43
H2	3.46	3.85	H11	7.63	7.44
H3	4.02	4.54	H12	7.64	7.5
H4	4.29	4.62	H13	7.71	7.69
H5	6.44	6.19	H14	7.71	7.69
H6	7.12	7.14	H2	3.04	3.85
H7	7.21	7.25	H3	3.55	4.54
H8	7.25	7.26	H4	3.91	4.62
H9	7.35	7.32	H5	4.58	6.19
2.7 (atom, calc, exp):			H6	7.39	7.14
C1	27.09	39.0	H7	7.41	7.25
C10	127.53	127.74	H8	7.44	7.32
C11	130.01	127.99	H9	7.44	7.26

The results show the probability that the experimental NMR spectrum corresponds to the indicated calculated NMR spectrum. The DP4 probability calculation uses the DP4-database2 version of the database and uses the t distribution.

Results of DP4 using both carbon and proton data:

2.6: 0.0%
2.22: 0.0%
2.23: 100.0%
2.24: 0.0%
2.7: 0.0%

Results of DP4 using the carbon data only:

2.6: 0.0%
2.22: 0.0%
2.23: 100.0%
2.24: 0.0%
2.7: 0.0%

Results of DP4 using the proton data only:

2.6: 0.0%
2.22: 0.0%
2.23: 71.9%
2.24: 28.1%
2.7: 0.0%

2.6.6.3 DP4 Analysis of the Experimental 2.7 NMR

Assignment of experimental NMR resonances of proposed **2.7** to calculated NMR resonances of each considered isomer.

2.6 (atom, calc, exp):

C1 42.7 26.57

Warning: Error = 16.1 ppm

C10 127.91 128.1
C11 128.58 129.35
C12 128.58 129.35
C13 129.66 129.58
C14 129.7 132.94
C15 134.02 134.27
C16 135.58 137.75
C17 143.33 139.05
C18 145.85 142.12
C19 148.06 143.51

C2 56.64 37.06

Warning: Error = 19.6 ppm

C20 165.94 167.95
C3 67.37 71.27
C4 113.59 119.51
C5 121.73 122.53
C6 122.04 123.05
C7 122.78 125.03
C8 124.69 125.99
C9 127.91 128.1
H1 3.92 3.43

H10 7.41 7.48
H11 7.41 7.47
H12 7.42 7.49
H13 7.48 7.77
H14 7.48 7.77
H2 3.92 2.8
H3 4.44 3.68
H4 6.15 4.15
H5 6.17 4.8
H6 7.06 7.38
H7 7.11 7.43
H8 7.21 7.45
H9 7.35 7.46

2.22 (atom, calc, exp):

C1 44.52 26.57

Warning: Error = 18.0 ppm

C10 127.72 128.1
C11 129.84 129.35
C12 130.27 129.58
C13 130.27 129.35
C14 130.86 132.94
C15 132.26 134.27
C16 135.61 137.75

C17 141.15 139.05
 C18 144.65 142.12
 C19 145.79 143.51
 C2 54.86 37.06
 Warning: Error = 17.8 ppm
 C20 166.14 167.95
 C3 69.0 71.27
 C4 115.86 119.51
 C5 121.28 122.53
 C6 123.61 123.05
 C7 124.65 125.03
 C8 125.03 125.99
 C9 127.72 128.1
 H1 3.83 2.8
 H10 7.42 7.48
 H11 7.42 7.47
 H12 7.46 7.49
 H13 7.79 7.77
 H14 7.79 7.77
 H2 4.4 3.43
 H3 4.41 3.68
 H4 6.01 4.15
 H5 6.3 4.8
 H6 7.1 7.38
 H7 7.19 7.43
 H8 7.26 7.45
 H9 7.37 7.46

2.23 (atom, calc, exp):

C1 41.59 26.57
 Warning: Error = 15.0 ppm
 C10 122.78 132.94
 C11 121.02 128.1
 C12 122.75 129.58
 C13 121.09 128.1
 C14 122.63 129.35
 C15 126.96 134.27
 C16 135.31 139.05
 C17 141.35 143.51
 C18 134.69 137.75
 C19 136.94 142.12
 C2 47.55 37.06
 C20 166.82 167.95
 C3 70.96 71.27
 C4 112.84 119.51
 C5 115.31 122.53

C6 116.26 123.05
 C7 120.4 125.99
 C8 117.92 125.03
 C9 121.41 129.35
 H1 3.4 2.8
 H10 7.4 7.48
 H11 7.4 7.47
 H12 7.42 7.49
 H13 7.9 7.77
 H14 7.9 7.77
 H2 3.66 3.43
 H3 4.47 3.68
 H4 4.59 4.15
 H5 6.13 4.8
 H6 7.11 7.38
 H7 7.22 7.43
 H8 7.25 7.45
 H9 7.3 7.46

2.24 (atom, calc, exp):

C1 41.5 26.57
 C10 128.3 128.1
 C11 128.93 129.35
 C12 128.93 129.35
 C13 129.04 129.58
 C14 131.63 132.94
 C15 132.48 134.27
 C16 135.74 137.75
 C17 138.71 139.05
 C18 141.78 142.12
 C19 144.24 143.51
 C2 42.12 37.06
 C20 169.31 167.95
 C3 66.73 71.27
 C4 113.91 119.51
 C5 121.36 122.53
 C6 122.73 123.05
 C7 124.79 125.03
 C8 127.85 128.1
 C9 127.85 125.99
 H1 3.4 2.8
 H10 7.4 7.48
 H11 7.4 7.47
 H12 7.46 7.49
 H13 7.54 7.77
 H14 7.54 7.77
 H2 3.46 3.43

H3	4.02	3.68
H4	4.29	4.15
H5	6.44	4.8
H6	7.12	7.38
H7	7.21	7.43
H8	7.25	7.45
H9	7.35	7.46

2.7

(atom, calc, exp):

C1	27.09	26.57
C10	127.53	128.1
C11	130.01	129.35
C12	131.37	129.58
C13	131.37	129.35
C14	131.63	132.94
C15	133.75	134.27
C16	136.35	137.75
C17	140.68	139.05
C18	141.71	142.12
C19	145.74	143.51
C2	37.81	37.06

C20	166.3	167.95
C3	70.29	71.27
C4	119.71	119.51
C5	122.34	122.53
C6	123.25	123.05
C7	125.33	125.03
C8	125.41	125.99
C9	127.53	128.1
H1	2.78	2.8
H10	7.47	7.47
H11	7.63	7.48
H12	7.64	7.49
H13	7.71	7.77
H14	7.71	7.77
H2	3.04	3.43
H3	3.55	3.68
H4	3.91	4.15
H5	4.58	4.8
H6	7.39	7.38
H7	7.41	7.43
H8	7.44	7.46
H9	7.44	7.45

The results show the probability that the experimental NMR spectrum corresponds to the indicated calculated NMR spectrum. The DP4 probability calculation uses the DP4-database2 version of the database and uses the t distribution.

Results of DP4 using both carbon and proton data:

2.6: 0.0%
2.22: 0.0%
2.23: 0.0%
2.24: 0.0%
2.7: 100.0%

Results of DP4 using the carbon data only:

2.6: 0.0%
2.22: 0.0%
2.23: 0.0%
2.24: 0.0%
2.7: 100.0%

Results of DP4 using the proton data only:

2.6: 0.0%

2.22: 0.0%

2.23: 0.0%

2.24: 0.0%

2.7: 100.0%

2.6.6.4 Assignment of Spartan Calculated and Experimental ^1H and ^{13}C NMR Resonances

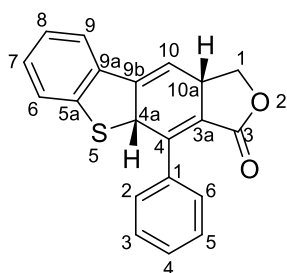


Table 2.4. Resonances for **2.6**

2.6		
	Calculated	Experimental
Carbons		
1	67.37	68.69
3	165.94	166.28
3a	122.04	122.51
4	148.06	146.50
4a	56.64	55.64
5a	143.33	142.97
6	122.78	123.16
7	129.66	129.41
8	124.69	124.88
9	121.73	122.32
9a	134.02	134.80
9b	145.85	143.62
10	113.59	114.87
10a	42.70	41.59
1'	135.58	136.34
2'	128.58	129.15
3'	127.91	128.10
4'	129.70	129.66
5'	127.91	128.32
6'	128.58	129.03
Protons		
6'-H	7.48	7.07
2'-H	7.48	7.08
4'-H	7.42	7.06
3'-H	7.41	7.02
5'-H	7.41	7.04
9-H	7.35	6.94
7-H	7.21	6.79
6-H	7.11	6.71
8-H	7.06	6.68
10-H	6.17	5.69
4a-H	6.15	5.21
1-Ha	4.44	4.28
1-Hb	3.92	3.66
10a-H	3.92	3.38

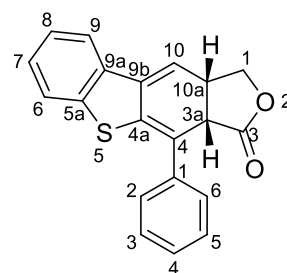


Table 2.5. Resonances for **2.23**

2.23		
	Calculated	Experimental
Carbons		
1	72.08	72.35
3	175.88	176.68
3a	45.92	45.32
4	124.31	122.43
4a	134.77	133.78
5a	141.24	140.94
6	122.65	121.81
7	129.37	129.84
8	124.84	125.05
9	121.52	121.16
9a	133.05	133.73
9b	142.73	140.68
10	116.46	116.22
10a	39.88	39.00
1'	141.42	139.33
2'	127.8	127.74
3'	128.89	128.77
4'	127.86	128.77
5'	128.89	127.99
6'	127.8	127.74
Protons		
2'-H	7.90	7.69
6'-H	7.90	7.69
9-H	7.42	7.50
3'-H	7.40	7.43
5'-H	7.40	7.44
4'-H	7.30	7.32
7-H	7.25	7.26
6-H	7.22	7.25
8-H	7.11	7.14
10-H	6.13	6.19
1-Hb	4.59	4.62
1-Ha	4.47	4.54
10a-H	3.66	3.85
3a-H	3.40	3.75

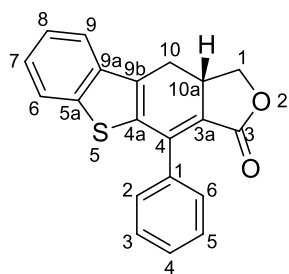


Table 2.6. Resonances for **2.7**

2.7		
	Calculated	Experimental
Carbons		
1	70.29	71.27
3	166.30	167.95
3a	119.71	119.51
4	145.74	143.51
4a	141.71	142.12
5a	140.68	139.05
6	123.25	123.05
7	125.33	125.03
8	125.41	125.99
9	122.34	122.53
9a	136.35	137.75
9b	131.63	132.94
10	27.09	26.57
10a	37.81	37.06
1'	133.75	134.27
2'	131.37	129.35
3'	127.53	128.10
4'	130.01	129.35
5'	127.53	128.10
6'	131.37	129.58
Protons		
6'-H	7.71	7.77
2'-H	7.71	7.77
6-H	7.64	7.49
9-H	7.63	7.48
4'-H	7.47	7.47
5'-H	7.44	7.45
3'-H	7.44	7.46
8-H	7.41	7.43
7-H	7.39	7.38
1-Hb	4.58	4.80
1-Ha	3.91	4.15
10a-H	3.55	3.68
10-Ha	3.04	3.43
10-Hb	2.78	2.80

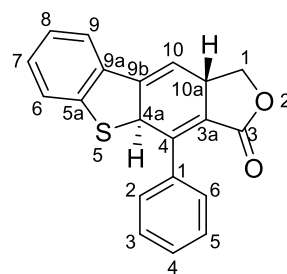


Table 2.7. Resonances for **2.22**

2.22	
	Calculated
Carbons	
1	69.00
3	166.14
3a	124.65
4	145.79
4a	54.86
5a	141.15
6	123.61
7	129.84
8	125.03
9	121.28
9a	135.61
9b	144.65
10	115.86
10a	44.52
1'	132.26
2'	130.27
3'	127.72
4'	130.86
5'	127.72
6'	130.27
Protons	
6'-H	7.79
2'-H	7.79
4'-H	7.46
5'-H	7.42
3'-H	7.42
9-H	7.37
7-H	7.26
6-H	7.19
8-H	7.10
4a-H	6.30
10-H	6.01
1-Hb	4.41
10a-H	4.40
1-Ha	3.83

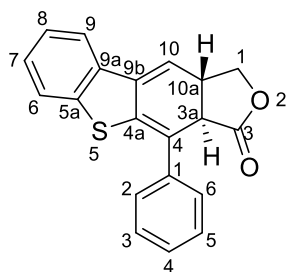


Table 2.8. Resonances for **2.24**

2.24	
	Calculated
Carbons	
1	66.73
3	169.31
3a	41.50
4	131.63
4a	138.71
5a	141.78
6	122.73
7	129.04
8	124.79
9	121.36
9a	132.48
9b	144.24
10	113.91
10a	42.12
1'	135.74
2'	128.93
3'	127.85
4'	128.30
5'	127.85
6'	128.93
Protons	
6'-H	7.54
2'-H	7.54
9-H	7.46
5'-H	7.40
3'-H	7.40
4'-H	7.35
7-H	7.25
6-H	7.21
8-H	7.12
10-H	6.44
1-Hb	4.29
1-Ha	4.02
3a-H	3.46
10a-H	3.40

2.6.7 Heating of 2.6 in DMF to Afford 2.8, 2.7, and 2.23

Rxn 1. An oven-dried NMR tube was charged with **2.5** (11 mg, 0.04 mmol) dissolved in o-DCB (0.5 mL, 0.08 M) under an atmosphere of air. The NMR tube was sealed with a polypropylene cap and lowered into a preheated oil bath at 150 °C. After 6 min, the reaction was paused for ¹H NMR analysis, and the NMR tube was rinsed with hexanes and wiped with a ChemWipe. **2.6** and **2.8** was afforded at a ratio of 95:5 as observed by No-D ¹H NMR. Ratios were determined by comparing the ¹H NMR resonance at 5.94 ppm (1H) for **2.6** to the resonance at 5.21 ppm (2H) for **2.8**. Solvent was removed under reduced pressure, and the crude residue was dissolved in DMF (0.5 mL). The solution was transferred to an oven-dried, 2-mL μW vial and capped with a Teflon-lined septum crimp cap. The vial was irradiated by microwave at 150 °C for 5 min. The solvent was removed by high vacuum and the crude residue was dissolved in chloroform-d. The solution was transferred to an oven-dried NMR tube and analyzed by ¹H NMR. A ratio of 18:52:30 (**2.8:2.7:2.23**) was afforded with residual DMF present. Ratios were determined by comparing the ¹H NMR resonance at 6.20 ppm (1H) for **2.23**, 5.45 ppm (2H) for **2.8**, and 3.40 ppm (1H) for **2.7**.

2.6.8 Under Aerobic Conditions, 2.6 Affords 2.8 at Room Temperature

Rxn 1. An oven-dried NMR tube was charged with **2.5** (20 mg, 0.06 mmol) dissolved in o-DCB (0.5 mL, 0.13 M) under an atmosphere of air. The NMR tube was sealed with a polypropylene cap and lowered into a preheated oil bath at 150 °C. After 10 min, the reaction was paused for ¹H NMR analysis, and the NMR tube was rinsed with hexanes and wiped with a ChemWipe. **2.6** and **2.8** was afforded at a ratio of 96:4 as observed by No-D ¹H NMR. Ratios were determined by comparing the ¹H NMR resonance at 3.90 ppm (1H) for **2.6** to the resonance at 5.21 ppm (2H) for

2.8. The solution was transferred to an oven-dried, 2-mL μ W vial and capped with a Teflon-lined septum crimp cap and needle venting to the air. Air was bubbled through the solution. After 1 h, the solution was transferred to an oven-dried NMR tube for No-D ^1H NMR analysis. **2.8** was afforded exclusively.

2.6.9 Stability of 2.7 under Thermal and Aerobic Conditions

Rxn 1. An oven-dried NMR tube was charged with a mixture of **2.8** and **2.7** at a ratio of 31:69 (7 mg, 0.02 mmol) and mesitylene (1 μL , 0.01 μmol) dissolved in toluene- d_8 (0.5 mL, 0.13 M) under an atmosphere of air. Ratios were determined by comparing the ^1H NMR resonance at 4.51 ppm (2H) for **2.8** and 2.35 ppm (1H) for **2.7** to the resonance at 6.55 ppm (3H) for mesitylene. The NMR tube was sealed with a polypropylene cap and lowered into a preheated oil bath at 50 $^\circ\text{C}$. After 2 h, the reaction was paused for ^1H NMR analysis, and the NMR tube was rinsed with hexanes and wiped with a ChemWipe. A ratio of 32:68 (**2.8:2.7**) was observed by crude ^1H NMR. The solution was lowered into a preheated oil bath at 80 $^\circ\text{C}$. After 2 h, the reaction was paused for ^1H NMR analysis, and the NMR tube was rinsed with hexanes and wiped with a ChemWipe. A ratio of 32:68 (**2.8:2.7**) was observed by crude ^1H NMR. The solution was lowered into a preheated oil bath at 110 $^\circ\text{C}$. After 2 h, the reaction was paused for ^1H NMR analysis, and the NMR tube was rinsed with hexanes and wiped with a ChemWipe. A ratio of 32:68 (**2.8:2.7**) was observed by crude ^1H NMR. The cap was removed, and air was bubbled through the solution at room temperature. After 2 h, the reaction was paused and a ratio of 32:68 (**2.8:2.7**) was observed by crude ^1H NMR analysis. The solution was lowered into a preheated oil bath at 80 $^\circ\text{C}$ and air was bubbled through the solution. After 2 h, the reaction was paused for ^1H NMR analysis, and the

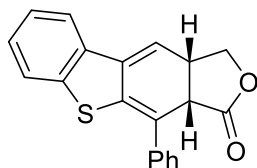
NMR tube was rinsed with hexanes and wiped with a ChemWipe. A ratio of 31:69 (**2.8:2.7**) was observed by crude ^1H NMR.

2.6.10 Heating of 2.5 in Acetonitrile to Afford 2.6, 2.23, 2.8, and 2.7

Rxn 1. An oven-dried, 0.5 mL microwave vial with stir bar was charged with **2.5** (12 mg, 0.04 mmol) dissolved in acetonitrile (0.5 mL 0.08 M). The vial was sealed with a Teflon-lined septum crimp cap and the solution was irradiated by microwave to 140 °C for 5 min. The solution was then transferred to a 25 mL round-bottom flask, and the solvent removed under reduced pressure to afford a yellow residue which was dissolved in chloroform-d under nitrogen. ^1H NMR in CDCl_3 showed a mixture of **2.8**, **2.7**, **2.6**, and **2.23** (10:22:51:17, respectively). Ratios were determined by comparing the ^1H NMR resonance at 6.28 ppm (1H) for **2.6**, 6.20 ppm (1H) for **2.23**, 5.45 ppm (2H) for **2.8**, and 3.44 ppm (1H) for **2.7**.

Rxn 2. An oven-dried, 0.5 mL microwave vial with stir bar was charged with **2.5** (11 mg, 0.03 mmol) dissolved in distilled acetonitrile that was stored over molecular sieves (type 4Å, 8-12 mesh beads, grade 514) which contained pulverized mole sieves that gave the solution a slight cloudy appearance. The vial was sealed with a Teflon-lined septum crimp cap and the solution was irradiated by microwave to 140 °C for 5 min. The solution was then transferred to a 25 mL round-bottom flask, and the solvent removed under reduced pressure to afford a yellow residue which was dissolved in chloroform-d under nitrogen. ^1H NMR in CDCl_3 showed a mixture of **2.8**, **2.7**, **2.6**, and **2.23** (6:41:7:46, respectively). Ratios were determined by comparing the ^1H NMR resonance at 6.28 ppm (1H) for **2.6**, 6.20 ppm (1H) for **2.23**, 5.45 ppm (2H) for **2.8**, and 3.44 ppm (1H) for **2.7**.

2.6.11 Synthesis of Cis-Diene



(3aS,10aS)-4-phenyl-3a,10a-dihydrobenzo[4,5]thieno[2,3-f]isobenzofuran-3(1H)-one (2.23).

An oven-dried, 0.5 mL microwave vial with stir bar was charged with **2.5** (11 mg, 0.03 mmol) dissolved in distilled acetonitrile that was stored over molecular sieves (type 4Å, 8-12 mesh beads, grade 514) which contained pulverized mole sieves that gave the solution a slight cloudy appearance. The vial was sealed with a Teflon-lined septum crimp cap and the solution was irradiated by microwave to 140 °C for 5 min. The solution was then transferred to a 25 mL round-bottom flask, and the solvent removed under reduced pressure to afford a yellow residue. The residue was purified by silica gel flash column chromatography (100% DCM) to afford the product as a light-yellow solid (5 mg, 42%).

Data 2.23

¹H NMR (600 MHz, CDCl₃)

7.69 (d, *J* = 7.8 Hz, 2H), 7.50 (d, *J* = 7.8 Hz, 1H), 7.43 (t, *J* = 7.8 Hz, 2H), 7.31 (t, *J* = 7.4 Hz, 1H), 7.25 (q, *J* = 8.0, 14.3 Hz, 2H), 7.14 (dt, *J* = 1.9, 8.4 Hz, 1H), 6.19 (d, *J* = 3.7 Hz, 1H), 4.63 (dd, *J* = 5.7, 8.9 Hz, 1H), 4.54 (dd, *J* = 2.3, 9.1 Hz, 1H), 3.85 (m, 1H), 3.75 (d, *J* = 9.7 Hz, 1H) ppm. DCM impurity at 5.30 ppm. Water impurity at 1.56 ppm.

<u>¹³C NMR</u>	(125 MHz, CDCl ₃) 176.7, 140.9, 140.7, 139.3, 133.8, 133.7, 129.8, 128.8 (2C), 128.0, 127.7 (2C), 125.1, 122.4, 121.8, 121.2, 116.2, 72.4, 45.3, 39.0 ppm
<u>IR</u>	(thin film) 3482, 3060, 2908, 2252, 1765, 1589, 1494, 1449, 1372, 1197, 1151, 1090, 1028, 988, 909, 830, 764, 732, 697 cm ⁻¹
<u>HRMS</u>	(FTMS + p ESI) [M + H] ⁺ calcd for C ₂₀ H ₁₅ O ₂ S: 319.07873, found 319.07817 317.06281 was also found in 50% relative abundance, indicative of formation of oxidation product 2.5 under ionization conditions
TLC	R _f = 0.37 (100% DCM) [silica gel, UV]

2.6.12 Conversion of **2.23** to **2.8**, **2.7**, and Unknown at Room Temperature in CDCl₃

Rxn 1. An oven-dried NMR tube was charged with **2.23** (7 mg, 0.02 mmol) dissolved in CDCl₃ (0.5 mL, 0.04 M). The NMR tube was sealed with a polypropylene cap kept at room temperature for 3 weeks. The crude solution afforded a ratio of 25:34:29:12 (**2.23**:**2.8**:**2.7**:unknown). Ratios were determined by comparing the ¹H NMR resonance at 6.20 ppm (1H) for **2.23**, 5.45 ppm (2H) for **2.8**, 2.81 ppm (1H) for **2.7**, and 5.29 ppm for the unknown.

3.0 Factors that Determine Reactivity for the Dearomative DA Cycloaddition

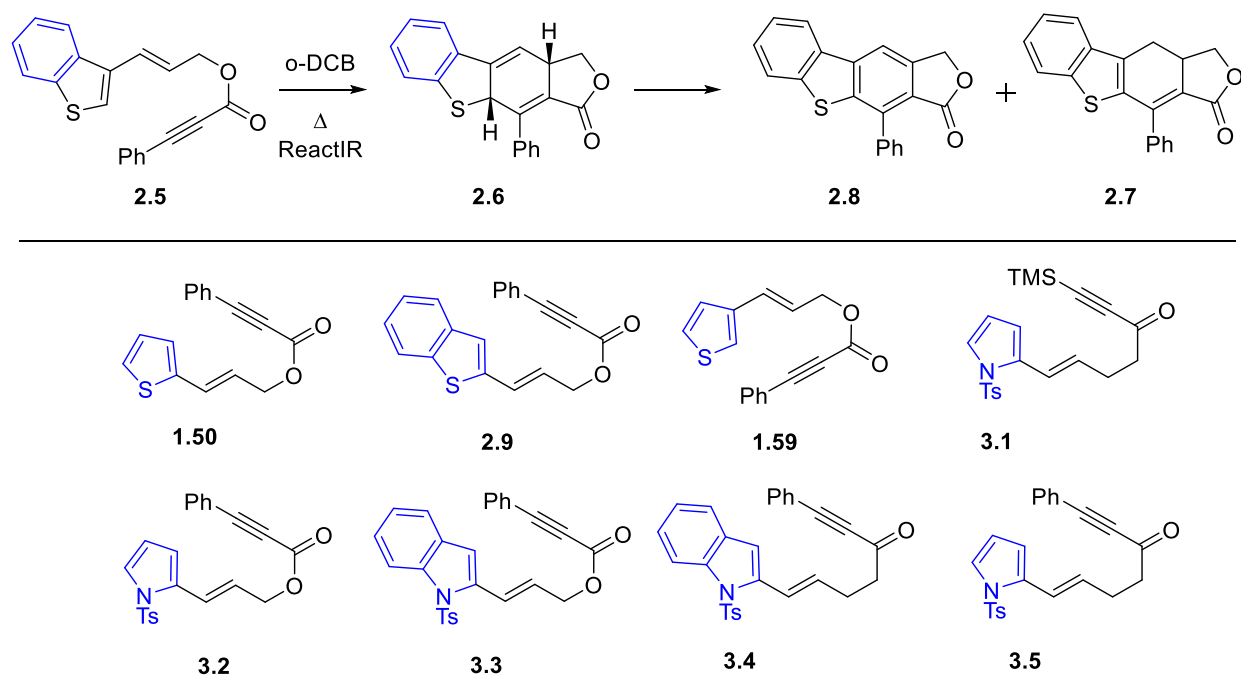
Having established the DA adduct as the result of the dearomative cycloaddition step and the intermediate to the oxidation and isomerization products, we were poised to investigate the substrate dependent factors that determine reactivity for the cycloaddition step. We launched a cooperative investigation utilizing reactivity data from experimental rate studies and computationally calculated energies from our collaboration with Professor Peng Liu's research group of the University of Pittsburgh. Correlation of our experimentally derived Gibbs free energies of activation with density functional theory (DFT) calculations provided insight into the mechanistic pathway of Dearomatization and the substrate dependent factors that determine reactivity.

This chapter is based on results presented in: Winkelbauer J. A.; Bober A. E.; Qi X.; Kusevska E.; Liu P.; Brummond K. M., Mechanisms and origin of reactivity of dearomative didehydro-Diels–Alder reactions of heteroarenes. Manuscript in preparation, submission expected 2021.

3.1 Determination of Reaction Rates and Half-Lives for Dearomative DDDA Precursors by In Situ Reaction Monitoring with ReactIR

To derive experimental reactivity data for the dearomative DDDA reaction, rate experiments monitored in situ by ReactIR were performed and the resulting data was evaluated to determine activation energy (E_a) and Gibbs free energies of activation ($\Delta G^\ddagger_{\text{exp}}$). Nine precursors

(**1.59**, **2.5**, **1.50**, **2.9**, **3.2**, **3.3**, **3.5**, **3.4**, and **3.1**) were selected based on results showing dearomative DDDA reactions that occurred in high yield and at a range of reaction temperatures. These precursors were selected to evaluate the impact of the heteroarene identity, tether functionality and position on the heteroarene, and group on the alkyne terminus on reactivity. Synthesis, ReactIR experiments, and determination of reaction rate constant and half-lives for the pyrrole and indole precursors were performed by Brummond Lab member Ashley Bober and are not described herein. Synthesis of the thiophene and benzothiophene precursors was performed by the same method as **2.5** described previously in chapter 2.1.



Scheme 3.1. Dearomative DDDA precursors selected for the reactivity study and analyzed by in situ ReactIR monitoring of reaction progress

A minimum of five separate experiments were conducted for each dearomative DDDA precursor with each experiment having a unique reaction temperature. The recorded temperature

is the internal temperature of the solution as measured by the ReactIR probe. For each series of reactions, the oil bath temperature was increased by an increment of 10 °C; however, the increase in the oil bath temperature did not translate to the internal reaction temperature. Thus, the actual temperature difference between each experiment in the series is between 5–15 °C. The consumption of starting material was measured by the disappearance of the absorption at ~1280 cm^{-1} which we propose may be the C-O bond stretching of the ester. Formation of oxidation and isomerization products was evidenced by the development of overlapping carbonyl absorptions at a higher frequency (~1760 cm^{-1}). The reaction was judged complete when the absorption at ~1280 cm^{-1} showed no change in intensity for at least 30 min. Complete disappearance of starting material was confirmed by TLC. A trend for the consumption of starting material was extracted using the iC IR 7.0 software and measured using peak height with a two-point baseline after solvent subtraction was applied. The trend data were exported to iC Kinetics 5.0 software, and the consumption of starting material vs. time data was plotted using GraphPad Prism 7.0. The half-lives and rate constants for each of the reactions were determined with GraphPad from a best-fit curve by plotting absorption intensity in arbitrary units relative to time in minutes (Figure 3.1). The data included by the best-fit curve contained 4-5 half-lives for each reaction. The selected reaction rate was first-order in substrate and an exponential one-phase decay nonlinear regression was applied to the data set, using a least square fit analysis. The half-lives and reaction rate constants for each experiment are reported in Table 3.1.

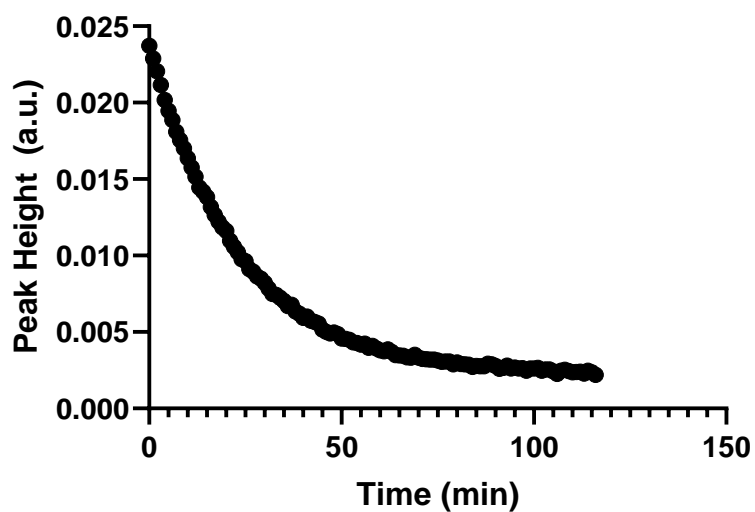
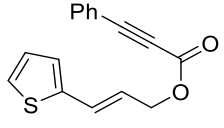
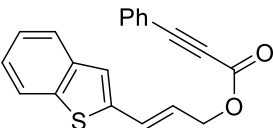
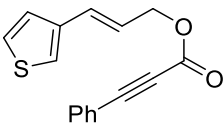
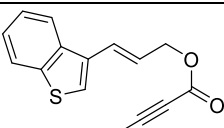


Figure 3.1. 1st order exponential decay of **2.5** at 90 °C

Table 3.1. Measured half-lives and rate constants for the dearomative DDDA reaction of the thiophene and benzothiophene precursors

Precursor	Entry	T (°C)	t _{1/2} (min)	k (s ⁻¹)
 1.50	1	77	154	7.49E-05
	2	86	47	2.44E-04
	3	94	28	4.16E-04
	4	108	12	9.31E-04
	5	119	6	2.06E-03
 2.9	6	76	140	8.23E-05
	7	85	63	1.83E-04
	8	95	23	5.06E-04
	9	108	13	9.04E-04
	10	113	8	1.36E-03
 1.59	11	88	91	1.27E-04
	12	98	43	2.68E-04
	13	109	16	7.41E-04
	14	121	7	1.63E-03
	15	132	4	3.20E-03
 2.5	16	73	58	1.98E-04
	17	81	28	4.09E-04
	18	90	16	7.18E-04
	19	96	9	1.28E-03
	20	106	5	2.40E-03

T – temperature
 $t_{1/2}$ – half-life
 k – rate constant

3.2 Determination of Activation Energy and Pre-Exponential Factor via the Arrhenius Equation

To determine the DDDA activation energy (E_a) and pre-exponential factor (A) for each precursor, an Arrhenius plot was generated by plotting $\ln(k)$ against $1/T$ where k is the reaction rate constant in inverse seconds and T is the temperature in Kelvin.

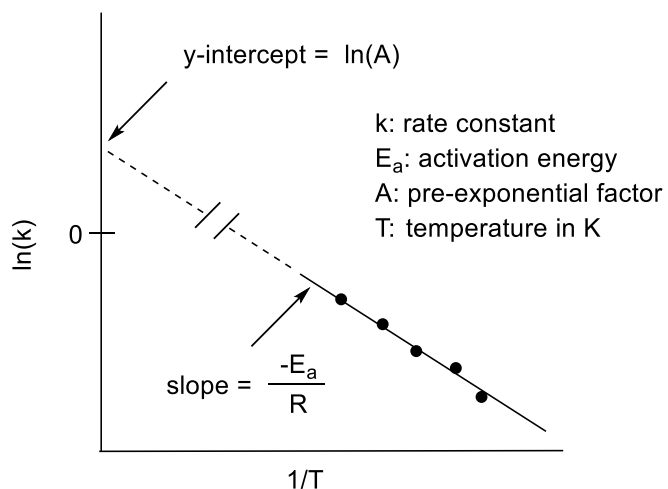


Figure 3.2. Representative Arrhenius plot and its relation to the Arrhenius equation

The Arrhenius plot afforded a trendline for the data with equation $y = m \cdot x + b$ (eq 3.1) where m is the slope of the line and b is the y-intercept. The trendline for the Arrhenius plot was generated by a linear regression analysis using the LINEST function in Microsoft Excel. The

LINEST function calculates a straight line that best fits our data by using the least squares method. The *const* value was set to TRUE so that the y-intercept would not be forced to equal zero. The *stats* value was set to TRUE so that the function output would include the linear regression statistics. The components of the trendline generated through the LINEST function include the slope, standard error for the slope, y-intercept, standard error for the y-intercept, R^2 , and the y estimate standard error.

Equation 3.1. Arrhenius plot line equation

$$y = m \cdot x + b$$

where: $y = \ln(k)$; $m = \text{slope} = -E_a/R$; $x = 1/T$; $b = \text{y-intercept} = \ln(A)$

We related eq 3.1 to the linear form of the Arrhenius equation $\ln(k) = -E_a/(R \cdot T) + \ln(A)$ (eq 3.2) where E_a is the activation energy in kcal/mol, R is the gas constant 0.001987 kcal/(mol•K), and A is the pre-exponential factor for the reaction in inverse seconds.

Equation 3.2. Linear form of the Arrhenius equation

$$\ln(k) = -E_a/(R \cdot T) + \ln(A)$$

Equation 3.3. Activation energy

$$E_a = -m \cdot R$$

Equation 3.4. Pre-exponential value

$$A = e^b$$

Equation 3.5. Rate of reaction at 363 K

$$k_{363} = e^{(m \cdot (1/363) + b)}$$

The error for E_a was calculated by substituting the slope with the slope error value, and the error for A was calculated by substituting the y-intercept with the y-intercept error value.

Equation 3.6. Error for activation energy

$$E_{a \text{ error}} = -m_{\text{error}} \cdot R$$

Equation 3.7. Error for pre-exponential value

$$A_{\text{error}} = e^{b \text{ error}}$$

The activation energy, pre-exponential value, and the error for both were determined by these same methods for each dearomative DDDA precursor. Rate constants at 363 K were derived from the trendline as a means to compare rate constants across substrates. 363 K was chosen as a median temperature across all reaction temperatures.

Table 3.2. Arrhenius trendline components as derived from the LINEST function and the kinetic results derived from the trendline for each substrate

	1.50	2.9	1.59	2.5	3.2	3.3	3.5	3.4	3.1
Slope	-10229	-10016	-10881	-9886	-13397	-11653	-12837	-9248	-10028
Slope Standard Error	844	715	329	333	757	517	912	1025	837
Y-Intercept	20.0	19.4	21.2	20.1	31.0	26.4	28.0	18.1	18.2
Y-Intercept Standard Error	2.3	1.9	0.9	0.9	2.2	1.5	2.5	2.8	2.3
R ²	0.980	0.985	0.997	0.997	0.987	0.994	0.980	0.953	0.980
Y Estimate Standard Error	0.21	0.16	0.08	0.07	0.20	0.11	0.17	0.20	0.15
k ₃₆₃ (s ⁻¹)	2.68E-04	2.73E-04	1.51E-04	7.74E-04	2.70E-03	3.46E-03	6.33E-04	6.03E-04	8.39E-05
E _a (kcal/mol)	20.3	19.9	21.6	19.6	26.62	23.16	25.51	18.38	19.93
E _{a error} (kcal/mol)	± 1.7	± 1.4	± 0.7	± 0.7	± 1.5	± 1.0	± 1.8	± 2.0	± 1.7
A (s ⁻¹)	4.63E+08	2.63E+08	1.57E+09	5.20E+08	2.88E+13	3.02E+11	1.44E+12	6.99E+07	8.34E+07
A _{error} (s ⁻¹)	± 9.8	± 7.0	± 2.4	± 2.5	± 9.1	± 4.5	± 12.6	± 17.0	± 10.3

3.3 Determination of Gibbs Free Energy of Activation, Enthalpy, and Entropy via the Eyring Equation

To determine the Gibbs free energy of activation, enthalpy, and entropy for each precursor, an Eyring plot was generated by plotting $\ln(k \cdot h/(k_B \cdot T))$ against $1/T$ where k is the rate of the reaction in inverse seconds, h is Planck's constant = $6.63 \times 10^{-34} \text{ J} \cdot \text{s}$, k_B is Boltzmann's constant = $1.38 \times 10^{-23} \text{ J} \cdot \text{K}^{-1}$ and T is the temperature in Kelvin.

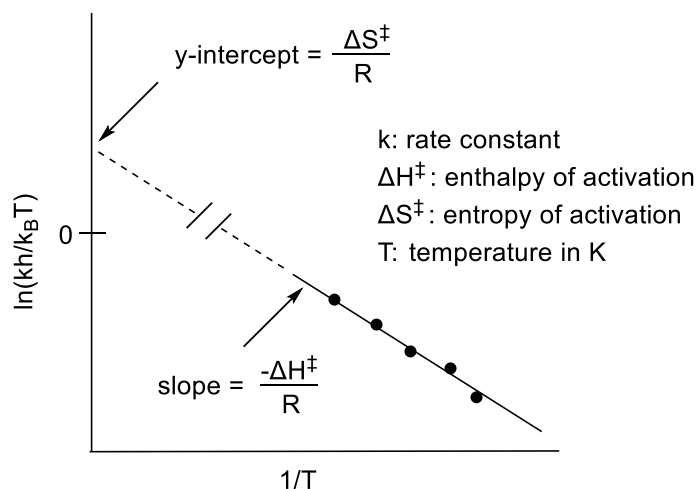


Figure 3.3. Representative Eyring plot and its relation to the Eyring equation

The Eyring plot affords a trendline for the data using the linear equation eq 3.8. Just as performed for the Arrhenius plots, the trendline for the Eyring plot was generated by a linear regression analysis using the LINEST function in Microsoft Excel. The LINEST function was set with the same parameters and output the same components of the trendline.

Equation 3.8. Eyring plot line equation

$$y = m \cdot x + b$$

where: $y = \ln(k \cdot h/(k_B \cdot T))$; $m = \text{slope} = -\Delta H^\ddagger/R$; $x = 1/T$; $b = \text{y-intercept} = \Delta S^\ddagger/R$

We related eq 3.8 to the linear form of the Eyring equation $\ln(k \cdot h/(k_B \cdot T)) = -\Delta H^\ddagger/(R \cdot T) + \Delta S^\ddagger/R$ (eq 3.9) where ΔH^\ddagger is the enthalpy of the reaction in kcal/mol, R is the gas constant 0.001987 kcal/(mol \cdot K), and ΔS^\ddagger is entropy of the reaction in kcal/mol.

Equation 3.9. Linear form of the Eyring equation

$$\ln(k \cdot h/(k_B \cdot T)) = -\Delta H^\ddagger/RT + \Delta S^\ddagger/R$$

Equation 3.10. Enthalpy

$$\Delta H^\ddagger = -m \cdot R$$

Equation 3.11. Entropy

$$\Delta S^\ddagger = b \cdot R$$

Equation 3.12. Rate of reaction at 363 K

$$k_{363} = k_B \cdot T \cdot e^{(m \cdot (1/363) + b)} / h$$

The error for ΔH^\ddagger can be calculated by substituting the slope with the slope error, and the error for ΔS^\ddagger can be calculated by substituting the y-intercept with the y-intercept error.

Equation 3.13. Error for enthalpy

$$\Delta H^\ddagger_{\text{error}} = -m_{\text{error}} \cdot R$$

Equation 3.14. Error for entropy

$$\Delta S^\ddagger_{\text{error}} = b_{\text{error}} \cdot R$$

Gibbs free energy of activation can be calculated with the equation $\Delta G^\ddagger = \Delta H^\ddagger - \Delta S^\ddagger T$ (eq 3.15) at 363 K.

Equation 3.15. Gibbs free energy of activation

$$\Delta G^\ddagger = \Delta H^\ddagger - \Delta S^\ddagger \cdot T$$

The error for ΔG^\ddagger can be calculated by substituting ΔH^\ddagger and ΔS^\ddagger with the error for ΔH^\ddagger and ΔS^\ddagger at 363 K. Propagation of error through the result of a subtraction is done through quadrature.

Equation 3.16. Error for Gibbs free energy of activation

$$\Delta G^\ddagger_{\text{error}} = \Delta H^\ddagger_{\text{error}} - \Delta S^\ddagger_{\text{error}} \cdot T$$

Equation 3.17. Quadrature to calculate error for Gibbs free energy of activation

$$\Delta G^\ddagger_{\text{error}} = \sqrt{(\Delta H^\ddagger_{\text{error}})^2 + (\Delta S^\ddagger_{\text{error}} \cdot T)^2}$$

The Gibbs free energy of activation, enthalpy, entropy, and the error for each were determined by these same methods for each dearomative DDDA precursor. Rate constants at 363 K as derived from the Eyring plot trendline remain unchanged and consistent to those derived from the Arrhenius plot trendline.

Table 3.3. Eyring trendline slope, y-intercept, and R^2 as derived from the LINEST function and the ΔH^\ddagger , ΔS^\ddagger , and ΔG^\ddagger values with their corresponding error

	1.50	2.9	1.59	2.5	3.2	3.3	3.5	3.4	3.1
Slope	-9859	-9649	-10499	-9524	-13053	-11309	-12475	-8882	-9668
Slope Standard Error	846	717	331	333	756	518	911	1027	837
Y-Intercept	-10.7	-11.3	-9.5	-10.6	0.4	-4.2	-2.7	-12.6	-12.4
Y-Intercept Standard Error	2.29	1.95	0.87	0.92	2.21	1.51	2.53	2.84	2.33
R^2	0.978	0.984	0.997	0.996	0.987	0.994	0.979	0.949	0.978
Y Estimate Standard Error	0.21	0.16	0.08	0.07	0.20	0.11	0.17	0.20	0.15
k_{363} (s^{-1})	2.68E-04	2.73E-04	1.51E-04	7.74E-04	1.65E-03	2.70E-03	3.46E-03	6.33E-04	6.03E-04
ΔH^\ddagger (kcal/mol)	19.6	19.2	20.9	18.9	25.9	22.5	24.8	17.7	19.2
$\Delta H^\ddagger_{\text{error}}$ (kcal/mol)	± 1.7	± 1.4	± 0.7	± 0.7	± 1.5	± 1.0	± 1.8	± 2.0	± 1.7
ΔS^\ddagger (kcal/mol)	-2.10E-02	-2.20E-02	-1.90E-02	-2.10E-02	7.75E-04	-8.28E-03	-5.27E-03	-2.50E-02	-2.47E-02
$\Delta S^\ddagger_{\text{error}}$ (kcal/mol)	$\pm 4.60E-03$	$\pm 3.90E-03$	$\pm 1.70E-03$	$\pm 1.80E-03$	$\pm 4.39E-03$	$\pm 3.00E-03$	$\pm 5.04E-03$	$\pm 5.63E-03$	$\pm 4.63E-03$
ΔG^\ddagger (kcal/mol)	27.3	27.3	27.7	26.6	25.7	25.5	26.7	26.7	28.2
$\Delta G^\ddagger_{\text{error}}$ (kcal/mol)	± 2.4	± 2.0	± 0.9	± 0.9	± 2.2	± 1.5	± 2.6	± 2.9	± 2.4

3.4 Analysis of Reactivity in Collaboration with DFT Computational Calculations

With experimental reactivity and rate data in hand, we sought to correlate our data with DFT computational calculations in order to derive the most likely mechanism of the dearomative cycloaddition step of the DDDA reaction, as well as determine which substrate dependent factors affect reactivity. All DFT computational calculations were performed by our collaborators Xiaotian Qi, Elena Kusevska, and Professor Peng Liu of the University of Pittsburgh.

3.4.1 Determination of the Dearomative Cycloaddition Mechanism

The thermal dearomative step of the DDDA reaction between the heterarenyl diene and the alkynyl dienophile is one that involves an initial [4 + 2] cycloaddition step to afford a 1,4-cyclohexadienyl intermediate. Mechanistically, the cycloaddition step may proceed via a concerted pathway with a six-membered, cyclic transition state or a stepwise pathway via a diradical intermediate (Figure 3.4).

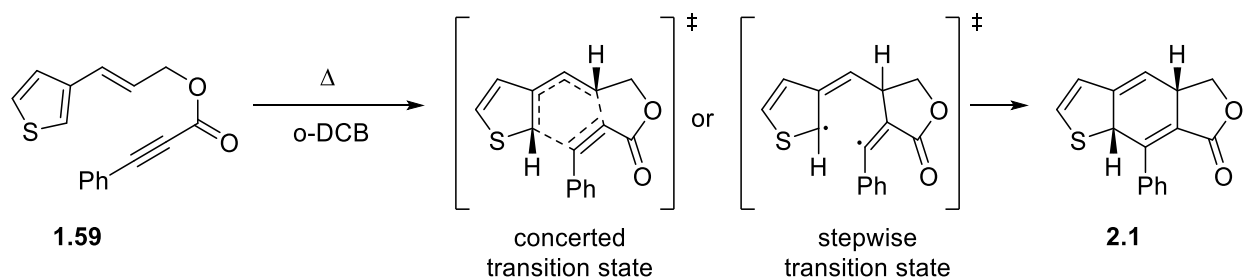


Figure 3.4. Proposed concerted and stepwise transition states as possible mechanisms for the dearomative cycloaddition step

We proposed that correlating the computed Gibbs free energies of activation ($\Delta G^\ddagger_{\text{comp}}$) for the concerted and stepwise transition states with experimentally derived $\Delta G^\ddagger_{\text{exp}}$ would help to elucidate the preferred mechanism. The $\Delta G^\ddagger_{\text{comp}}$ for both the stepwise and concerted reaction pathways were calculated for all nine DDDA precursors. M06-2X/6-311+G(d,p) single point energies were derived with both M06-2X/6-31+G(d) and B3LYP/6-31+G(d) structure optimization, and B3LYP/6-311+G(d,p) single point energies were derived with B3LYP/6-31+G(d) structure optimization. The SMD solvation model with o-DCB as the chosen solvent was used for the geometry optimizations as well as the single point energy calculations to match the experimental solvent. The computational Gibbs free energies of activation also include a thermal correction to 363 K which was the median experimental temperature. Example structure optimizations of **1.59** and the concerted and stepwise transition states with both M06-2X/6-31+G(d) and B3LYP/6-31+G(d) structure optimization are shown (Figure 3.5).

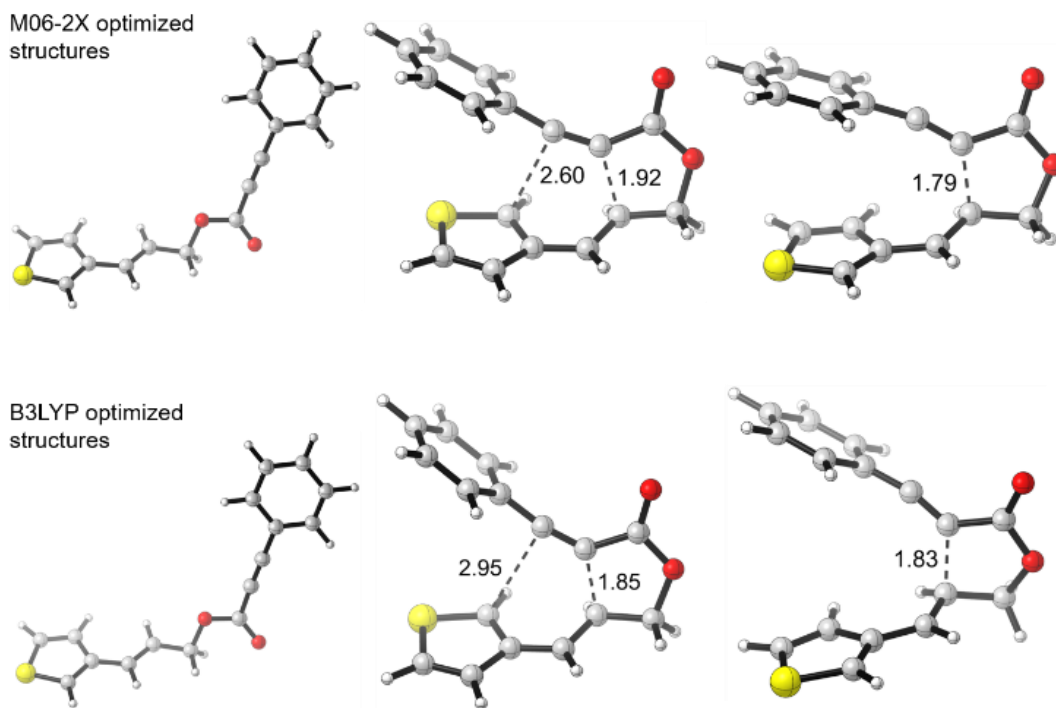


Figure 3.5. Structures of **1.59**, the concerted transition state, and the stepwise transition state for the cycloaddition step of the dearomative DDDA reaction with structures optimized by M06-2X/6-31+G(d) and B3LYP/6-31+G(d).

Bond distances shown in angstroms.

The closed-shell transition state with the s-cis conformer of the vinyl heteroarene, utilized in the concerted pathway, was located for each dearomative DDDA precursor. The open-shell transition state with the s-trans conformer of the vinyl heteroarene, utilized in the stepwise pathway, was not able to be located for **1.50**, **2.9**, **3.5**, or **3.1** for the M06-2X/6-311+G(d,p) single point energies with M06-2X/6-31+G(d) geometry optimizations. The s-trans open-shell transition state was not able to be located for **3.4** at any of the attempted levels of theory. The s-cis open-shell transition state was also considered but could not be located at either level of theory for all precursors. For these cases where the transition states were not able to be located, the geometry would collapse to the s-cis closed-shell transition state, suggesting that they do not exist as

stationary points on the potential energy surfaces for the dearomative DDDA reactions. The Gibbs free energies of activation for all precursors are summarized in Table 3.4.

Table 3.4. DFT computationally derived Gibbs free energies of activation for the s-cis closed-shell and s-trans open-shell transition states

	1.50	2.9	1.59	2.5	3.2	3.3	3.5	3.4	3.1
experimental ΔG^\ddagger (kcal/mol)	27.3	27.3	27.7	26.6	25.7	25.5	26.7	26.7	28.2
ΔG^\ddagger s-cis closed-shell (kcal/mol)									
B3LYP/6-311+G(d,p)//B3LYP/6-31+G(d)	32.4	32.2	33.1	30.6	30.6	30.2	34.7	30.9	34.7
M06-2X/6-311+G(d,p)//M06-2X/6-31+G(d)	30.2	28.8	30.2	28.8	29.2	26.2	28.1	28.3	29.5
M06-2X/6-311+G(d,p)//B3LYP/6-31+G(d)	32.0	31.0	31.2	28.2	29.9	30.2	32.1	29.4	31.4
ΔG^\ddagger s-trans open-shell (kcal/mol)									
B3LYP/6-311+G(d,p)//B3LYP/6-31+G(d)	30.2	30.9	33.0	33.3	36.5	35.8	44.0	-	44.0
M06-2X/6-311+G(d,p)//M06-2X/6-31+G(d)	-	-	33.2	35.3	36.6	33.9	-	-	-
M06-2X/6-311+G(d,p)//B3LYP/6-31+G(d)	32.1	32.9	34.7	35.0	38.6	35.8	40.0	-	44.4

The mechanism of the dearomative cycloaddition was determined to be the concerted pathway due to the s-cis closed-shell transition state being lower in energy than the open-shell transition states for all precursors. Additionally, the concerted pathway had a smaller average deviation of computed activation energies from the experimentally derived activation free energies than the stepwise pathway at the M06-2X/6-311+G(d,p)//B3LYP/6-31+G(d) level of theory. The average deviations were 3.7 and 9.8 kcal/mol for the concerted and stepwise pathways, respectively. The closed-shell and open-shell transition states were compared with the M06-2X/6-311+G(d,p) single point energies and B3LYP/6-31+G(d) geometry optimizations as the M06-2X/6-311+G(d,p) single point energies include dispersion corrections that B3LYP/6-311+G(d,p) lacks, and several open-shell transition states were not able to be located with M06-2X/6-31+G(d) geometry optimizations.

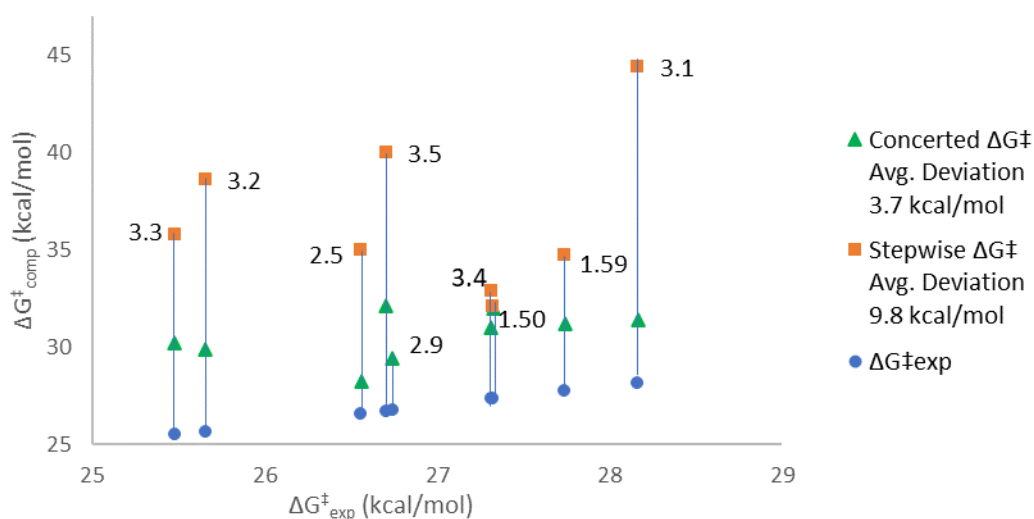


Figure 3.6. Average deviation of computational Gibbs free energies of activation from experimental energies for both the concerted and stepwise reaction pathways at the M06-2X/6-311+G(d,p)//B3LYP/6-31+G(d) level of theory

Analysis of the newly formed bond lengths in the concerted pathway for the dearomative cycloaddition step led to the discovery that the mechanism proceeds through an early and highly asynchronous concerted transition state. The degree of asynchronicity of the transition state was observed by the measurement of the newly forming bond lengths. These lengths were compared for both the M06-2X/6-31+G(d) and B3LYP/6-31+G(d) structure optimizations and are summarized in Table 3.5. Both levels of theory showed that the bond length for lactone formation was significantly shorter than the bond length between the heteroarene and the alkyne, indicative of the highly asynchronous concerted dearomative DDDA transition state (Figure 3.5). Overall, the M06-2X/6-31+G(d) level of theory showed a more synchronous TS structure with a difference in bond lengths of 0.53–0.81 Å compared to the B3LYP/6-31+G(d) level of theory which showed a difference in bond lengths of 0.88–1.32 Å. The B3LYP/6-31+G(d) level of theory lacks an accurate description for dispersion forces which may be responsible for the predicted longer bond forming distances between the heteroarene and the alkyne. The bond length differences found with the M06-2X/6-31+G(d) level of theory are comparable to the differences in bond length of ~0.8 Å found in the concerted asynchronous transitions state for the styryl Diels–Alder reactions.⁴⁹ This early transition state leads to less distortion of the heteroarene and a relatively small decrease of aromaticity from the precursor suggesting that substrate dependent factors such as aromaticity and electronic properties may have a reduced impact on reactivity.

Table 3.5. Newly forming bond lengths in the asynchronous, concerted transition state of the dearomative cycloaddition step

	1.50	2.9	1.59	2.5	3.2	3.3	3.5	3.4	3.1
1st formed bond length M06-2X/6-31+G(d) (Å)	1.88	1.94	1.92	1.94	1.88	1.95	1.92	1.98	1.95
2nd formed bond length M06-2X/6-31+G(d) (Å)	2.65	2.64	2.60	2.62	2.69	2.64	2.56	2.51	2.48
1st formed bond length B3LYP/6-31+G(d) (Å)	1.82	1.85	1.85	1.89	1.83	1.87	1.85	1.89	1.86
2nd formed bond length B3LYP/6-31+G(d) (Å)	3.14	3.14	2.95	2.94	3.15	3.08	2.97	2.93	2.74

3.4.2 Gibbs Free Energies of Activation at the M06-2X/6-311+G(d,p)//M06-2X/6-31+G(d)

Level of Theory as the Most Accurate to Experimental Energies

With the asynchronous, concerted reaction pathway as the proposed mechanism for the dearomative cycloaddition, we then sought to evaluate which level of theory would afford computational Gibbs free energies of activation ($\Delta G_{\text{comp}}^\ddagger$) that would be the most accurate to experimental energies ($\Delta G_{\text{exp}}^\ddagger$) and thus the best predictive tool (Figure 3.7). The M06-2X/6-311+G(d,p)//M06-2X/6-31+G(d) level of theory provided the best agreement to experiments with an average overestimation from $\Delta G_{\text{exp}}^\ddagger$ of 2.0 kcal/mol and had a moderate correlation to $\Delta G_{\text{exp}}^\ddagger$ ($R^2 = 0.48$). The B3LYP/6-311+G(d,p)//B3LYP/6-31+G(d) level of theory provided a worse agreement to experiments with an average overestimation from $\Delta G_{\text{exp}}^\ddagger$ of 5.3 kcal/mol yet had significantly improved correlation to $\Delta G_{\text{exp}}^\ddagger$ ($R^2 = 0.84$) when **3.5** was removed as an outlier. The M06-2X/6-311+G(d,p)//B3LYP/6-31+G(d) level of theory provided an average overestimation from $\Delta G_{\text{exp}}^\ddagger$ of 3.7 kcal/mol and had a poor correlation to $\Delta G_{\text{exp}}^\ddagger$ ($R^2 = 0.23$). Overall, the M06-2X/6-311+G(d,p)//M06-2X/6-31+G(d) level of theory was established to be a more reliable level of theory for prediction of the absolute activation energies of the concerted dearomative cycloaddition. However, the B3LYP/6-311+G(d,p)//B3LYP/6-31+G(d) level of theory can still be used to predict the relative reactivity trend of different precursors.

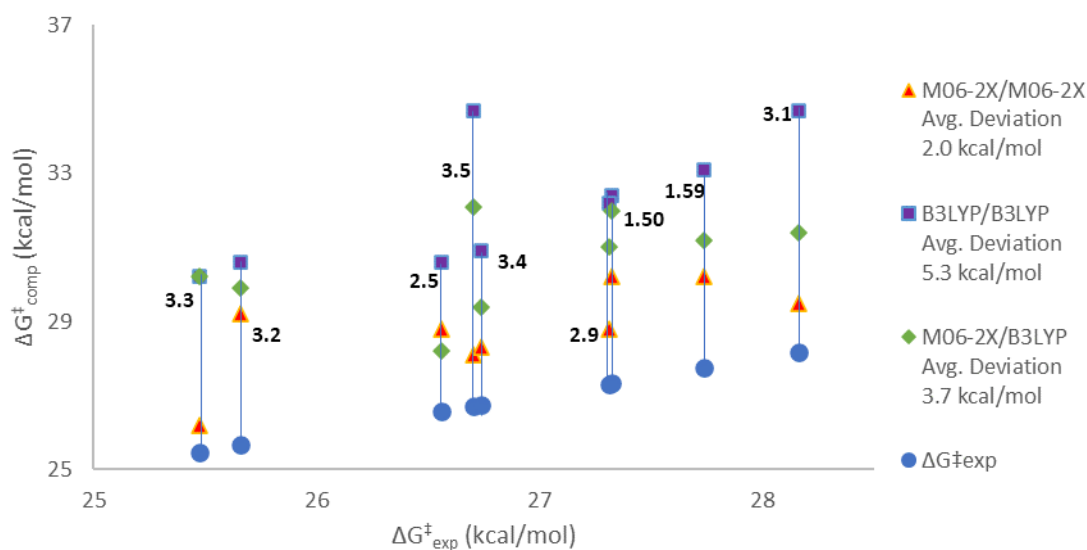
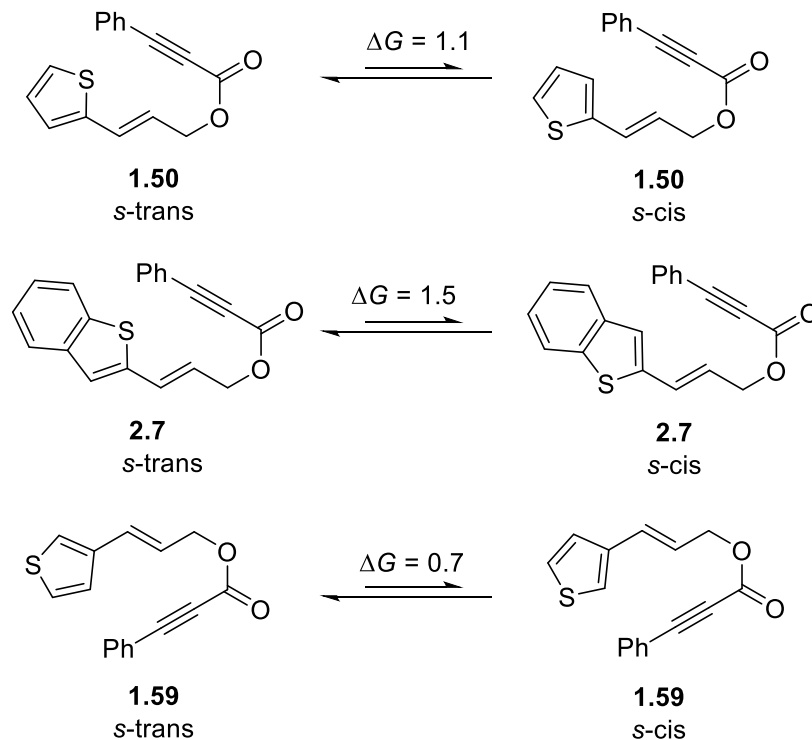


Figure 3.7. Comparison of different levels of theories used to calculate $\Delta G^\ddagger_{\text{comp}}$ and their accuracy to $\Delta G^\ddagger_{\text{exp}}$.

3.4.3 The Effect of Ground State Conformations on the Reactivity of the Dearomative Cycloaddition Step

We next sought to determine the substrate dependent factors that contribute to reactivity. The first to be evaluated was the energy required to access the reactive *s*-cis conformation of the vinyl heteroarene. M06-2X/6-31+G(d) geometry optimizations of the dearomative DDDA precursors were analyzed to determine the lowest energy rotamer for the precursors studied. Most afforded the *s*-cis rotamer as the lowest energy conformer in the ground state. The exceptions being **1.50**, **2.9**, and **1.59** for which the *s*-trans rotamer is 1.1, 1.5, and 0.7 kcal/mol more stable than the corresponding *s*-cis rotamer, respectively (Scheme 3.2). Therefore, the energy required to attain the reactive *s*-cis conformation from the unreactive *s*-trans does contribute to the overall energy barrier of the dearomative cycloaddition. This additional required energy is not present for the other dearomative DDDA precursors, thus **1.50**, **2.9**, and **1.59** have consequentially higher Gibbs free energies of activation than the other substrates.



Scheme 3.2. Rotational energy barriers required to attain the reactive *s-cis* conformer for precursors **1.50**, **2.9**, and

1.59

3.4.4 Stabilizing Dispersion Interactions in the Dearomative Cycloaddition Transition

States

Experimentally, the precursors with phenyl substitution on the terminus of the alkyne are more reactive than **3.1** with TMS substitution on the terminus of the alkyne. This result may be indicative of a π/π -stacking type interaction occurring between the heteroarene and the phenyl on the terminus of the alkyne. The relatively long forming C–C bond distances in the asynchronous, concerted transition state place the arene rings at a distance where the stacking would be possible. Cooperative dispersion interactions between dienes and dienophiles in the transition state have

been shown in previous studies by Houk et al to increase stabilization by up to 10 kcal/mol in Diels–Alder reactions.⁶⁰ To investigate these effects in our dearomative cycloaddition, London dispersion energies (ΔE_{disp}) between the heteroarene and the phenyl group in the transition state were calculated. The dispersion energy in the transition state for **3.1** ($\Delta E_{\text{disp}} = -12.9$ kcal/mol) was found to be less stabilizing than that of **3.5** ($\Delta E_{\text{disp}} = -16.7$ kcal/mol) by 3.8 kcal/mol. Though the calculated dispersion energies follow the reactivity trend, the lower reactivity of **3.1** may also be due to destabilizing steric interactions between the TMS group and the heteroarene rather than a lack of π -stabilizing interactions in the transition state.

Therefore, the dispersion interaction in the transition state of **2.9** was contrasted with an analogous concerted transition state of **2.9** containing a methyl substituted alkyne **2.9-Me** rather than the phenyl substitution (Figure 3.8). ΔE_{disp} between the highlighted heteroarene and phenyl moieties in the transition state of **2.9** was calculated to be -15.2 kcal/mol which was 4.2 kcal/mol higher than that of the analogous transition state with the methyl substituted alkyne ($\Delta E_{\text{disp}} = -11.0$ kcal/mol). These results demonstrate the stabilizing dispersion interactions present between the heteroarene and the phenyl terminus of the alkyne.

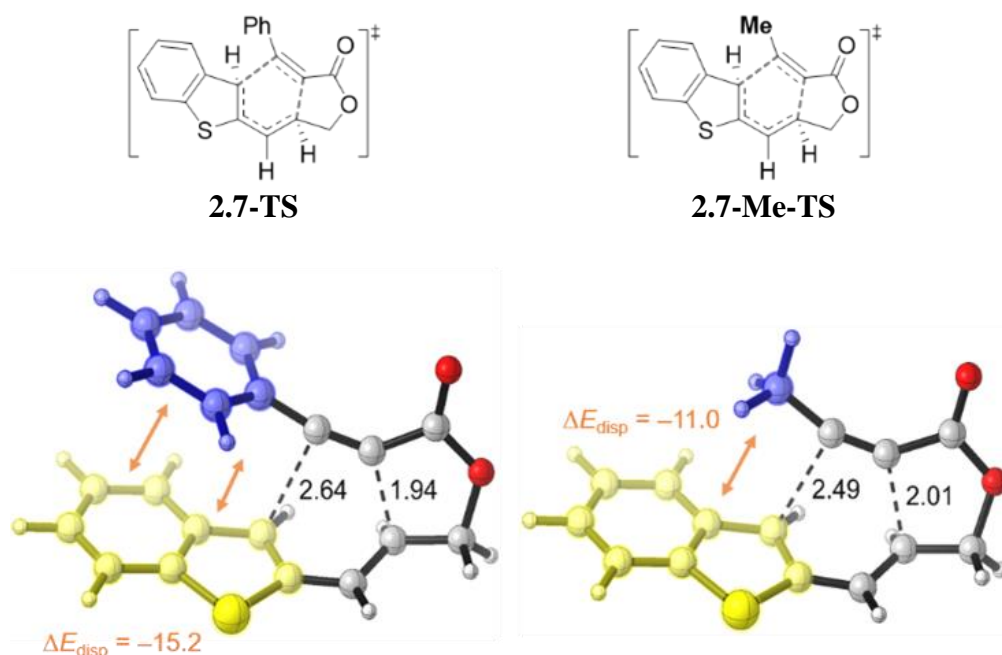


Figure 3.8. Dispersion effect on the stabilization of the concerted cycloaddition transition state

Optimized structures of transition states also show that there is a more favored π - π stacking interaction between the phenyl alkyne terminus and the benzo-fused heteroarenes in comparison to the non-benzo-fused heteroarenes. In each case, the benzo-fused precursors afforded transition states with greater stabilizing dispersion energies than their non-benzo-fused counterparts. **2.9**, **2.5**, **3.3**, and **3.4** (-15.2, -12.0, -21.1, and -21.3 kcal/mol) each had a dispersion stabilization energy that was lower than the non-benzo-fused **1.50**, **1.59**, **3.2**, and **3.5** (-11.0, -11.7, -16.1, and -16.7 kcal/mol) respectively. The presence of the benzene fused to the heteroarene likely affords an increase in the stabilizing π - π stacking interaction.

3.4.5 Effect of Heteroarene Aromaticity on Reactivity of the Dearomative Cycloaddition

To determine the effect that aromaticity of the heteroarene has on the reactivity of the dearomative cycloaddition, experimentally derived Gibbs free energies of activation were compared to the computationally derived aromaticity of the heteroarenes. Aromaticity was calculated using nucleus-independent chemicals shift (NICS) which is the negative of the magnetic shielding at a given point, using the NICS(1)zz method. The NICS(1)zz values were calculated by the placement of a ghost atom 1 Å above the heterocyclic ring for each precursor and their respective concerted transition state. These aromaticity calculations are summarized in Table 3.6. The NICS(1)zz values of the dearomative cycloaddition precursors are close to those of their respective transition states, indicative of a relatively small decrease of aromaticity of the heteroarene in the transition states. This is consistent with the proposed early, asynchronous transition state where the forming C-C bond between the heteroarene and the alkyne is longer than that of the forming lactone C-C bond.

Table 3.6. NICS(1)zz aromaticity of the heteroarene for the dearomative cycloaddition precursors and transition states

	1.50	2.9	1.59	2.5	3.2	3.3	3.5	3.4	3.1
experimental ΔG^\ddagger (kcal/mol)	27.3	27.3	27.7	26.6	25.7	25.5	26.7	26.7	28.2
experimental $\Delta G^\ddagger_{\text{exp(s-cis)}}$ (kcal/mol)	26.2	25.8	27.0	26.6	25.7	25.5	26.7	26.7	28.2
precursor NICS(1)zz (ppm) M06-2X/M06-2X	-27.8	-21.8	-28.8	-25.1	-25.1	-20.7	-25.8	-20.0	-25.5
transition state NICS(1)zz (ppm) M06-2X/M06-2X	-28.0	-20.8	-29.0	-22.8	-24.0	-17.9	-23.2	-16.3	-23.5

We then sought to isolate the contribution that heteroarene aromaticity had on the Gibbs free energy of activation to see the effect of aromaticity on reactivity. Tether composition affects the Gibbs free energy of activation due to the additional conformational mobility of a ketone-tethered precursor over that of an ester-tethered precursor. Therefore, only ester-tethered substrates were considered to eliminate this contribution in our analysis. As described previously, the ground state conformer for the precursors is the reactive s-cis conformation for all substrates except **2.9**, **1.50**, and **1.59** which have the s-trans conformation. Therefore, the $\Delta G^\ddagger_{\text{exp}}$ for **2.9**, **1.50**, and **1.59** was adjusted by subtracting the computed energy difference between the s-trans and s-cis conformers (1.5, 1.1, and 0.7 kcal/mol, respectively). These adjusted Gibbs free energies of activation, denoted as $\Delta G^\ddagger_{\text{exp(s-cis)}}$, are used in our comparison to reflect the reactivities of the reactive s-cis conformer of each precursor.

Therefore, the NICS(1)zz aromaticity of the heteroarene in the ester-tethered precursors and concerted transition states were plotted against the adjusted Gibbs free energies of activation, $\Delta G^\ddagger_{\text{exp(s-cis)}}$. The precursors afforded a correlation with $R^2 = 0.63$ for the trendline, and the transition states afforded a correlation with $R^2 = 0.56$ for the trendline (Figure 3.9). Aromaticity of the heteroarene in the precursor afforded a better correlation to the Gibbs free energy of activation than the aromaticity in the transition state, so that transition state calculations may not be necessary to use aromaticity as a predictive tool for reactivity. The positive correlation between aromaticity of the heteroarene and the Gibbs free energy of activation suggests that aromaticity is one of several influencing factors that control reactivity. For example, C3-substituted **1.59** (-28.8 ppm) and **2.5** (-25.1 ppm) are more aromatic than the corresponding C2-substituted **1.50** (-27.8 ppm) and **2.9** (-21.8 ppm). Consequentially, **1.59** and **2.5** (27.0 and 26.6 kcal/mol) have higher $\Delta G^\ddagger_{\text{exp(s-cis)}}$ than **1.50** and **2.9** (26.2 and 25.8 kcal/mol), respectively.

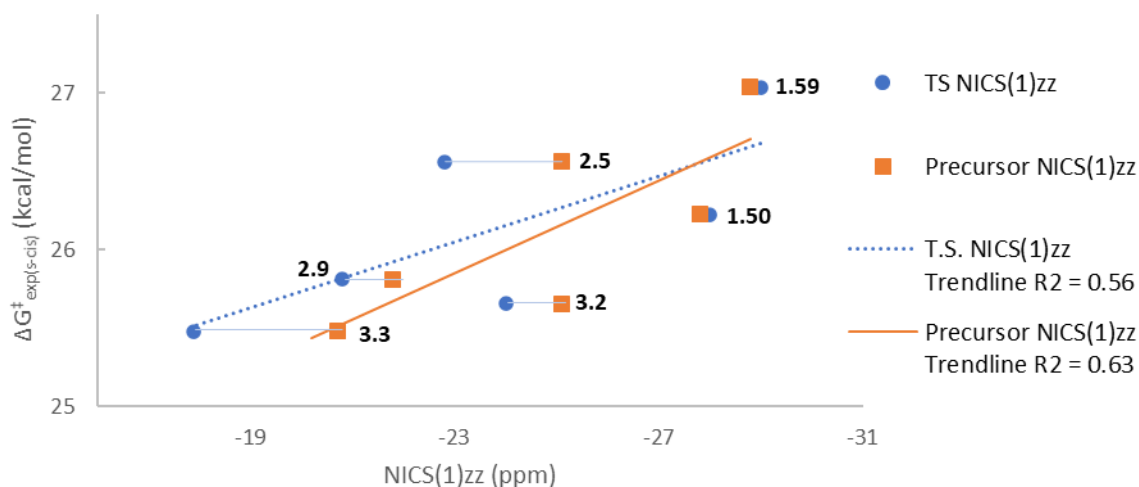


Figure 3.9. Correlation between $\Delta G^\ddagger_{\text{exp}(s\text{-cis})}$, and both precursor and transition state NICS(1)_{zz} aromaticity values for ester-tethered substrates

NICS(1)_{zz} aromaticity of the heteroarene in the ester-tethered precursors and concerted transition states were plotted against the adjusted computational Gibbs free energies of activation, $\Delta G^\ddagger_{\text{comp}(s\text{-cis})}$ as well, and afforded improved correlation. The precursors afforded a correlation with $R^2 = 0.88$ for the trendline, and the transition states afforded a correlation with $R^2 = 0.85$ for the trendline (Figure 3.10). The improved correlation for the computed Gibbs free energies of activation over the experimental energies is attributed to the lack of experimental error. As with experimental energies, aromaticity of the heteroarene in the precursor afforded a better correlation to the Gibbs free energy of activation than the aromaticity in the transition state. The positive correlation between aromaticity of the heteroarene and the computed Gibbs free energy of activation with improved correlation is in agreement with the correlation with experimental energies that aromaticity is one of several influencing factors that affects reactivity.

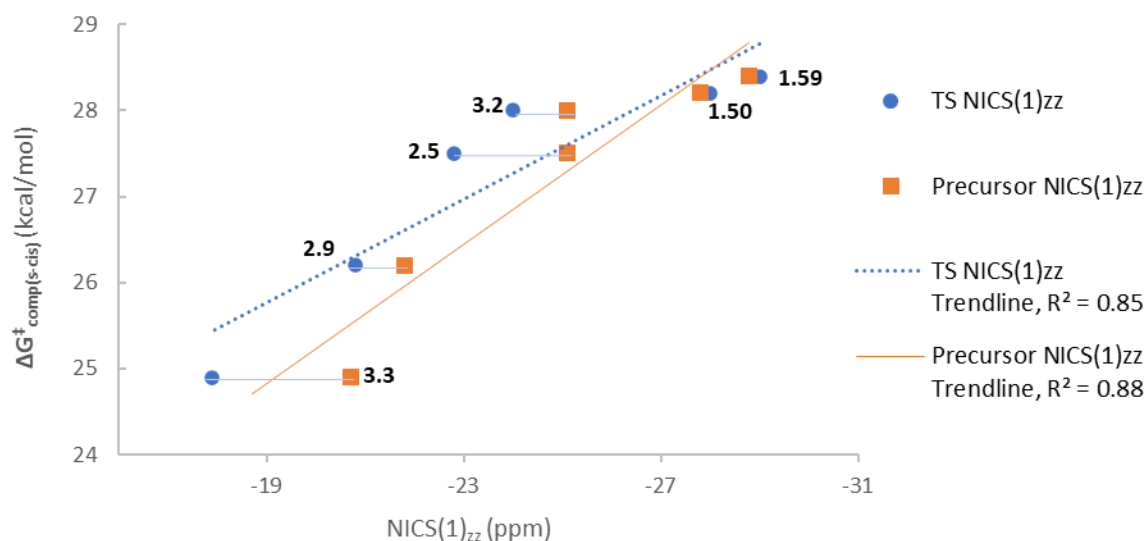


Figure 3.10. Correlation between the $\Delta G^{\ddagger}_{\text{comp(s-cis)}}$ at the M06-2X/M06-2X level of theory and the NICS(1)_{zz} aromaticity calculation

However, the dearomative cycloaddition appears to lack sensitivity to the effect that the fused benzene ring has on the aromaticity of the heteroarene. Benzo-fused heteroarenes **2.9**, **2.5**, and **3.3** are less aromatic than their non-benzo-fused counterparts **1.50**, **1.59**, and **3.2**, yet the reaction rate of the dearomative cycloaddition for the benzo-fused heteroarenes is only accelerated by a factor of 1.02, 5.13, and 1.28-fold, respectively. This rate enhancement is relatively small when compared to the 400,000-fold rate enhancement observed in the Diels-Alder reaction between naphthalene and tetracyanoethylene over that of benzene and tetracyanoethylene.⁶¹ The lack of sensitivity to heteroarene aromaticity is consistent with the proposed early transition state that retains the aromaticity of the heteroarenes. Therefore, a broad range of heteroarenes with varied levels of aromaticity may be used as precursors for the dearomative DDDA reaction.

3.5 Conclusions

We established that the dearomative cycloaddition step of the dearomative DDDA reaction proceeds through a highly asynchronous, closed-shell, concerted transition state where the five-membered ring is formed to a greater degree than the six-membered ring. This was accomplished through a cooperative investigation incorporating experimentally derived kinetic data with computational DFT analysis to afford a deeper mechanistic understanding of the dearomative cycloaddition step and the substrate dependent factors that determine reactivity. Dearomative DDDA reactions were monitored in situ with ReactIR to afford kinetic reactivity data including Gibbs free energies of activation. These experimental energies were correlated with computational DFT calculated Gibbs free energies of activation. M06-2X/6-311+G(d,p)//M06-2X/6-31+G(d) level of theory afforded the most accurate computational energies of those tested while B3LYP/6-311+G(d,p)//B3LYP/6-31+G(d) level of theory had improved correlation to experimental energies and may be useful in the prediction of relative reactivity trends for different precursors. NICS(1)zz aromaticity calculations have a positive correlation with experimental Gibbs free energies of activation, yet the impacts on Gibbs free energies of activation are less than a few kcal/mol which is in agreement with the early transition state. Stabilizing dispersion interactions between the phenyl terminus of the alkyne and the heteroarenes were observed. The energy required to attain the reactive s-cis conformation of the vinyl heteroarene from the unreactive s-trans conformation was also found to contribute to the overall energy barrier of the dearomative cycloaddition. These results serve to benchmark DFT computation as a predictive tool in reactivity determination for the dearomative cycloaddition and to lend insight into the substrate dependent factors that control reactivity for this and other dearomative processes.

3.6 Experimental

3.6.1 General Methods

Unless otherwise indicated, all reactions were performed in flame-dried glassware under an air atmosphere and stirred with Teflon-coated magnetic stir bars. All commercially available compounds were purchased and used as received unless otherwise specified. Tetrahydrofuran (THF) was purified by passing through alumina using the Sol-Tek ST002 solvent purification system. Deuterated chloroform (CDCl_3) was passed over 3 Å molecular sieves. Nitrogen gas was purchased from Matheson Tri Gas. Purification of compounds by flash column chromatography was performed using silica gel (40-63 μm particle size, 60 Å pore size). TLC analyses were performed on silica gel F₂₅₄ glass-backed plates (250 μm thickness). ^1H NMR and ^{13}C NMR spectra were recorded on Bruker Avance 300, 400, or 500 MHz spectrometers. Spectra were referenced to residual chloroform (7.26 ppm, ^1H ; 77.16 ppm, ^{13}C). Chemical shifts (δ) are reported in ppm and multiplicities are indicated by s (singlet), d (doublet), t (triplet), q (quartet), quint (quintet), and m (multiplet). Coupling constants, J, are reported in hertz (Hz). All NMR spectra were obtained at room temperature. Compound characterization IR spectra were obtained using a Nicolet Avatar E.S.P. 360 FT-IR. ReactIR spectra were obtained using a Mettler Toledo ReactIR 45M with a silicone probe (SiComp, 9.5 x 1.5 mm AgX Fiber, Resistive Temperature Device). EI mass spectroscopy was performed on a Waters Micromass GCT high resolution mass spectrometer, while ES mass spectroscopy was performed on a Waters Q-TOF Ultima API, Micromass UK Limited high-resolution mass spectrometer.

3.6.2 Experimental Procedures for ReactIR

The dewar of the ReactIR 45M was filled with liquid nitrogen and the instrument was switched on 2 h prior to experiment. A 10 mL, 2-necked, heart-shaped flask equipped with a stir bar (flea sized) was fitted with the 9.5 mm silicone ReactIR probe via a 14/20 Teflon adapter. The tip of the probe was carefully positioned slightly above the stir bar through the center neck, and a 14/20 glass stopper was inserted into the side neck. The flask was clamped directly above a pre-heated oil-bath, while cautiously moving the fiber arm so as to avoid excessive bending. The iC IR 4.0 was used for data collection. The data collection frequency was set to 30 s, 1 min, or 3 min, depending upon predetermined reaction time and the temperature was monitored via the ReactIR probe. The alignment and clean steps were performed, and if necessary, the probe tip was cleaned by temporarily removing from the flask and gently wiping with an acetone soaked Kimwipe. A background scan in air was collected. The glass stopper was temporarily removed and *o*-dichlorobenzene (*o*-DCB, 1 mL) was added in a single portion via syringe—the probe tip must be immersed in *o*-DCB. The pre-heated oil bath was raised to the flask. Once the internal temperature reached equilibria as evidenced by the readout, the glass stopper was temporarily removed, and a solution of precursor (20 mg) diluted in *o*-DCB (0.5 mL) was added in a single portion via syringe. At this point, the reaction solution contained 20 mg of precursor dissolved in 1.5 mL (2.0 g) *o*-DCB affording a weight percent of 1.0%, well above the 0.1% detection limit of the ReactIR infrared absorber. The reaction progress was monitored by disappearance of starting material as observed by a decreasing peak height for a particular absorption attributed to the starting material—an absorption identified by the iC IR software to afford the best trend. Complete disappearance of starting material was confirmed by TLC. A trend for the consumption of starting material was extracted using the iC IR 7.0 software and measured using peak height with a two-point baseline

after solvent subtraction was applied. The trend data were exported to iC Kinetics 5.0 software, and the consumption of starting material vs. time data was plotted using GraphPad Prism 7.0. The reaction displayed first-order kinetics for the substrate. An exponential one-phase decay nonlinear regression was applied to the data set, using a least squares fit analysis.

3.6.3 ReactIR Data Output and Rate Calculations with GraphPad

As described in the experiment procedure, each ReactIR experiment began with a period where the probe recorded the absorption of background air or solvent during temperature equilibration, before starting material was added to the reaction vessel. All data recorded by the probe before the addition of starting material was considered irrelevant to the experiment. Therefore, the plots of consumption of starting material over time were set so that the introduction of starting material to the reaction has a time point of zero, and the probe recordings before that point were discarded and not displayed. Probe recordings after the point of five half-lives were also discarded and not displayed so as to eliminate error from the decomposition of products after the consumption of starting material was complete.

Plots of consumption of starting material over time are displayed as peak height vs. duration of the experiment. Peak height is recorded by the iC IR software with arbitrary units (a.u.). The GraphPad data output is displayed below the plot of consumption of starting material and represents the statistics for the one phase decay nonlinear regression. Y0 is the Y value when the time is zero. The plateau is the Y value at an infinite time. K is the rate constant expressed in inverse minutes. Tau is the reciprocal of K. The half-life is displayed as determined by $\ln(2)/K$. The span is the difference between Y0 and the plateau. The 95% confidence interval is also displayed for the previous statistics. Statistics related to the goodness of the fit are given, including

the degrees of freedom, R^2 value, sum of squares, and the standard error of estimate ($Sy.x$). The only constraint imposed upon the one phase decay nonlinear regression is that the rate is greater than zero.

The data points for each ReactIR experiment and the corresponding plot and GraphPad output have been recorded and can be found in Appendix C.

3.6.4 Specifications for Measuring Half-Lives for DDDA Precursor

A minimum of five separate experiments were conducted for each DDDA precursor with each experiment having a unique reaction temperature. A significant improvement to the trendline fit was not observed beyond four data points for either the Eyring or Arrhenius plots. For example, Figure 3.11 shows an Eyring plot of **1.59** using five different reactions temperatures with an $R^2 = 0.997$ while Figure 3.12 shows a plot with four reactions with the same fit ($R^2 = 0.997$). The recorded temperature is the internal temperature of the solution as measured by the ReactIR probe. For each series of reactions, the oil bath temperature was increased by an increment of 10 °C; however, the increase in the oil bath temperature did not translate to the internal reaction temperature. Thus, the actual temperature difference between each experiment in the series is between 5–15 °C.

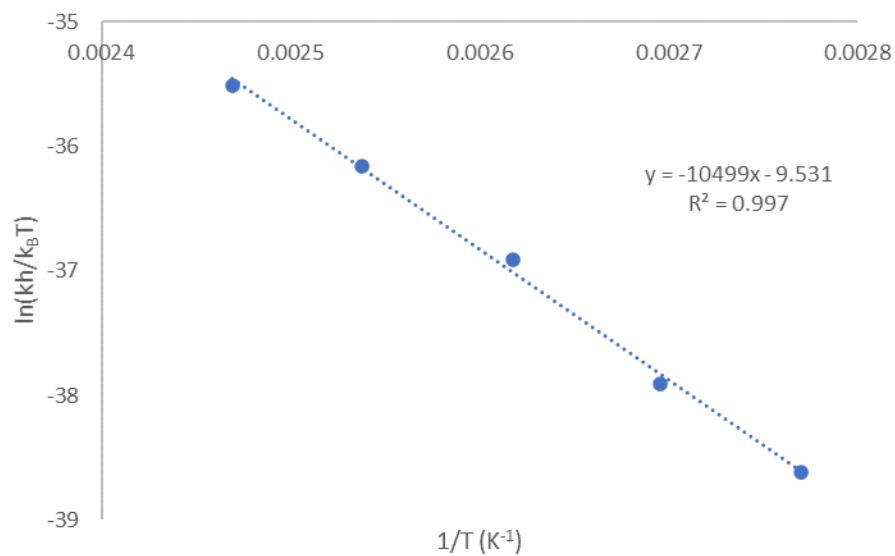


Figure 3.11. Eyring plot for the dearomative DDDA reaction of **1.59** using five different reaction temperatures

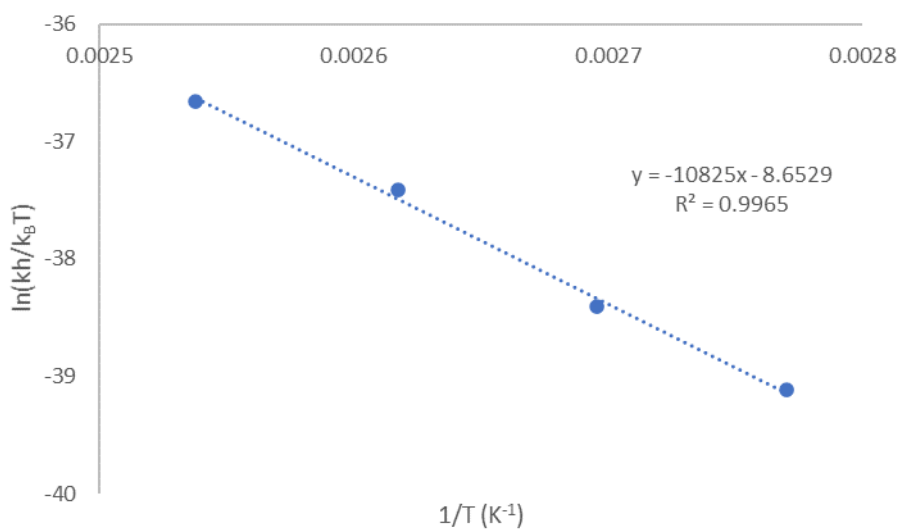


Figure 3.12. Eyring plot for the dearomative DDDA reaction of **1.59** using four different reaction temperatures

3.6.5 Arrhenius Plots

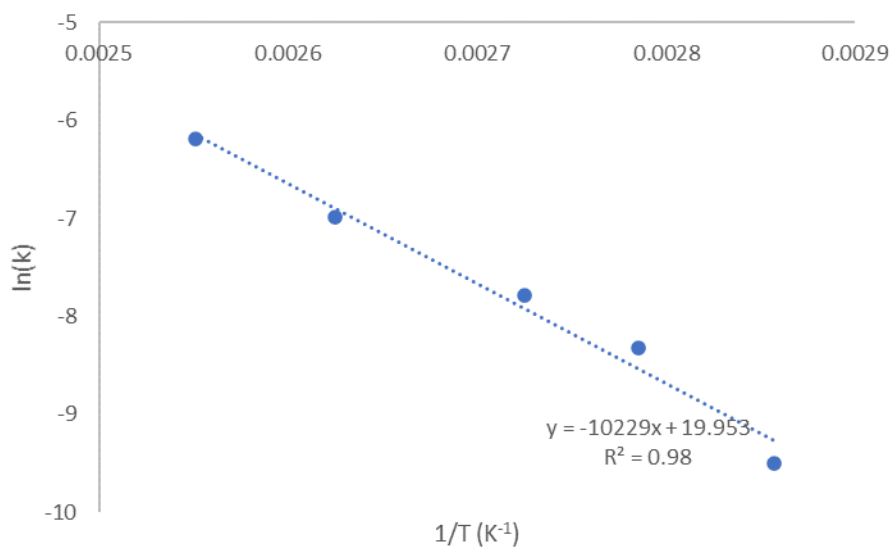


Figure 3.13. Arrhenius plot for the dearomative DDDA reaction of **1.50**

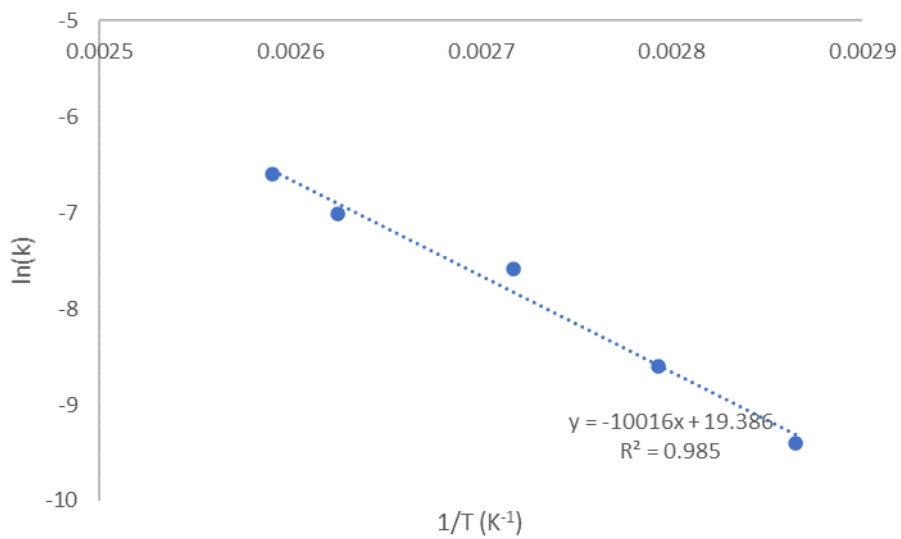


Figure 3.14. Arrhenius plot for the dearomative DDDA reaction of **2.9**

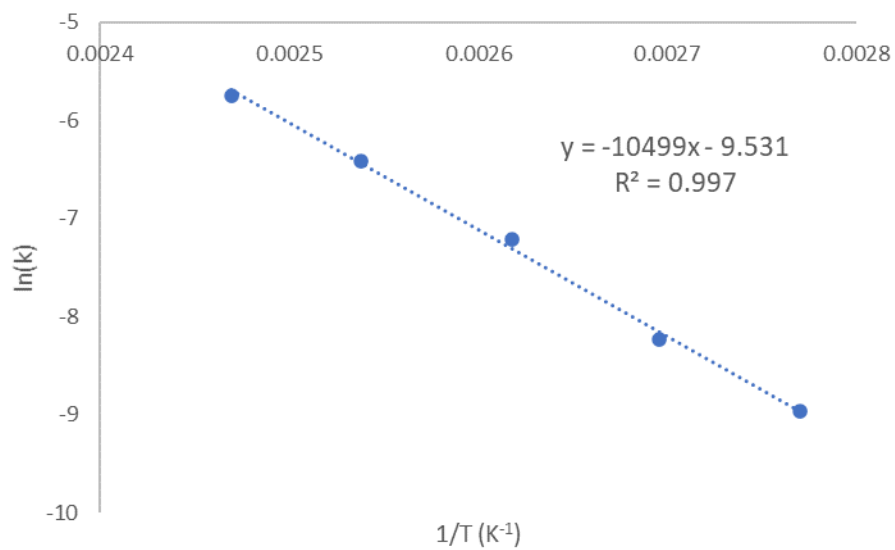


Figure 3.15. Arrhenius plot for the dearomative DDDA reaction of **1.59**

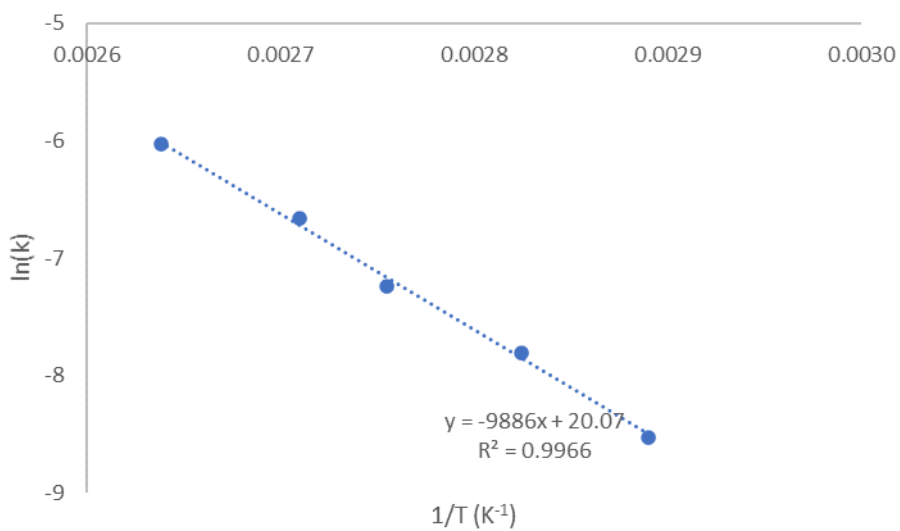


Figure 3.16. Arrhenius plot for the dearomative DDDA reaction of **2.5**

3.6.6 Eyring Plots

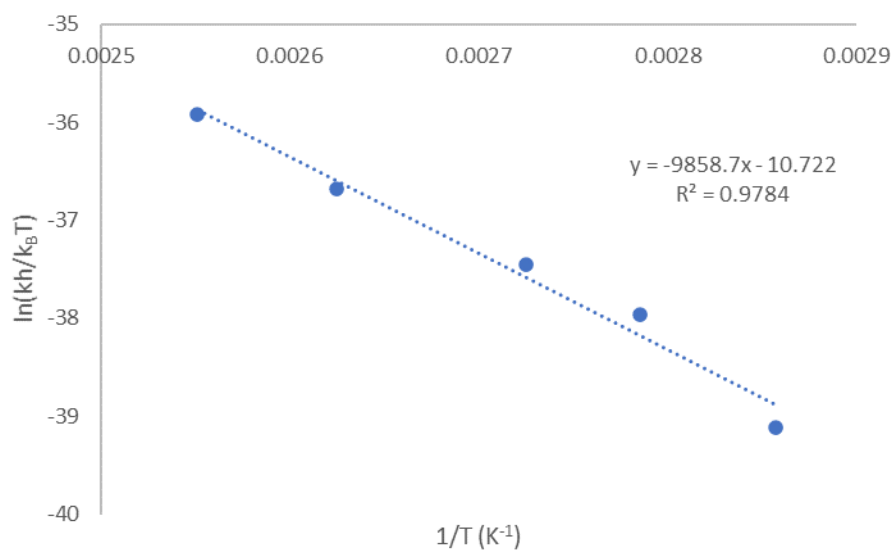


Figure 3.17. Eyring plot for the dearomative DDDA reaction of **1.50**

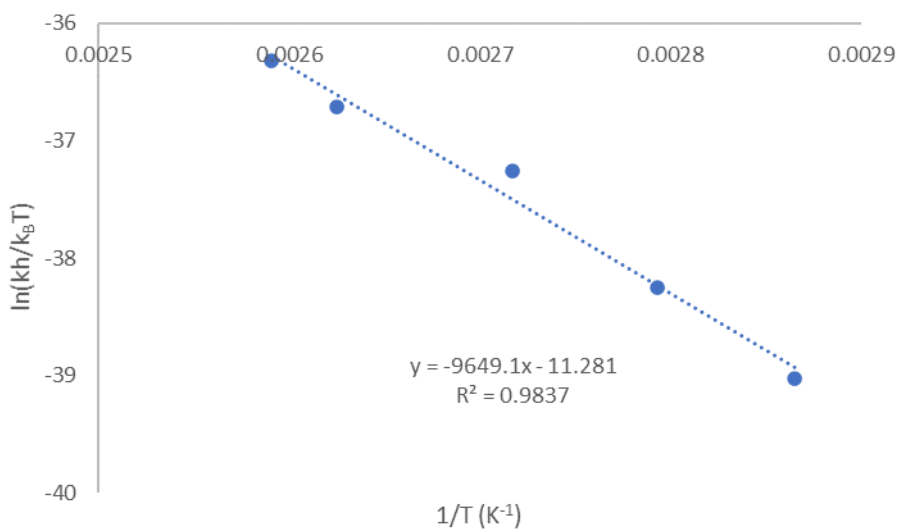


Figure 3.18. Eyring plot for the dearomative DDDA reaction of **2.9**

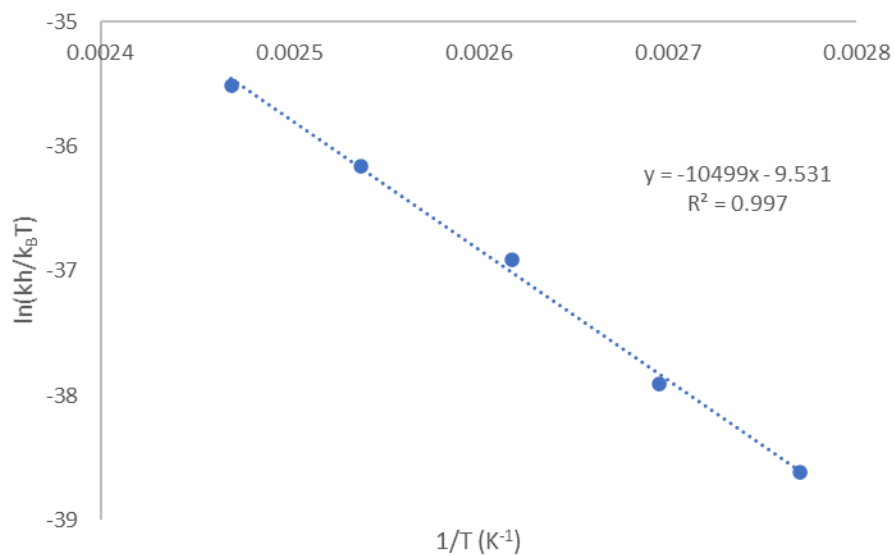


Figure 3.19. Eyring plot for the dearomative DDDA reaction of **1.59**

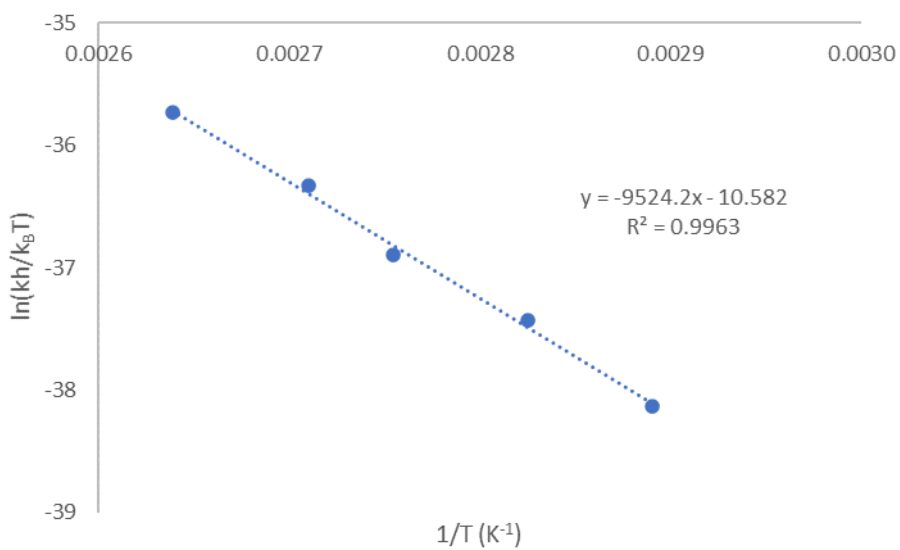


Figure 3.20. Eyring plot for the dearomative DDDA reaction of **2.5**

3.6.7 Correlation Plots between DFT Computational and Experimentally Derived Gibbs Free Energies of Activation

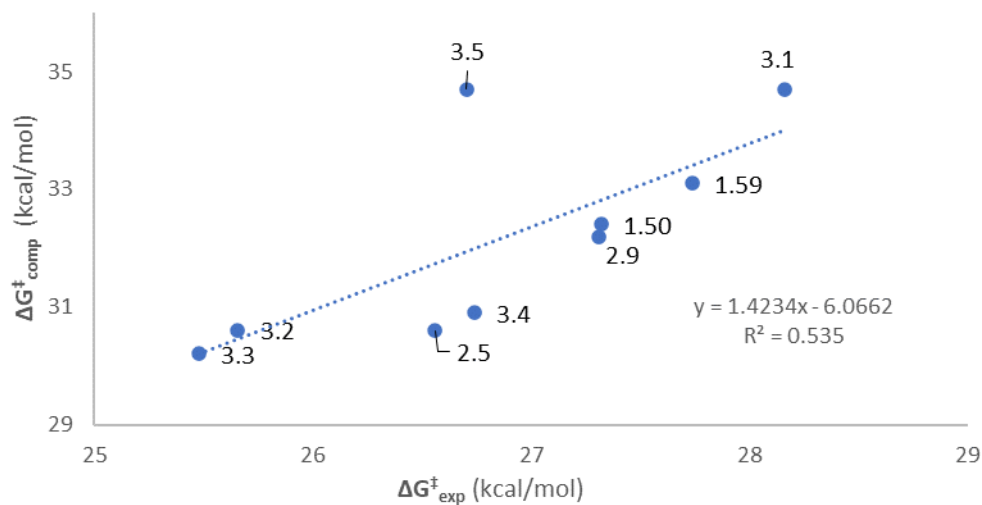


Figure 3.21. Correlation between the closed-shell transition state $\Delta G^\ddagger_{\text{comp}}$ with B3LYP/B3LYP level of theory and the $\Delta G^\ddagger_{\text{exp}}$ with **3.5** outlier

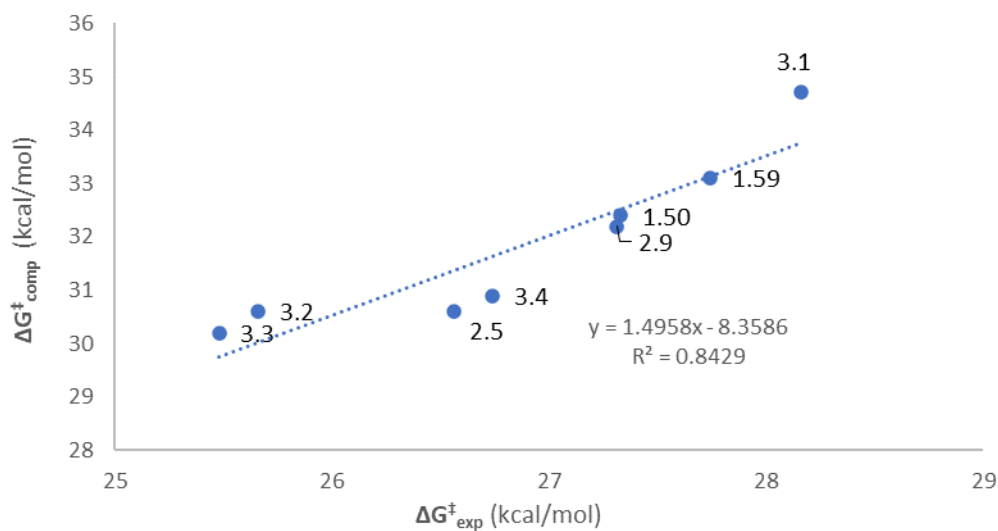


Figure 3.22. Correlation between the closed-shell transition state $\Delta G^\ddagger_{\text{comp}}$ with B3LYP/B3LYP level of theory and the $\Delta G^\ddagger_{\text{exp}}$ without **3.5** outlier

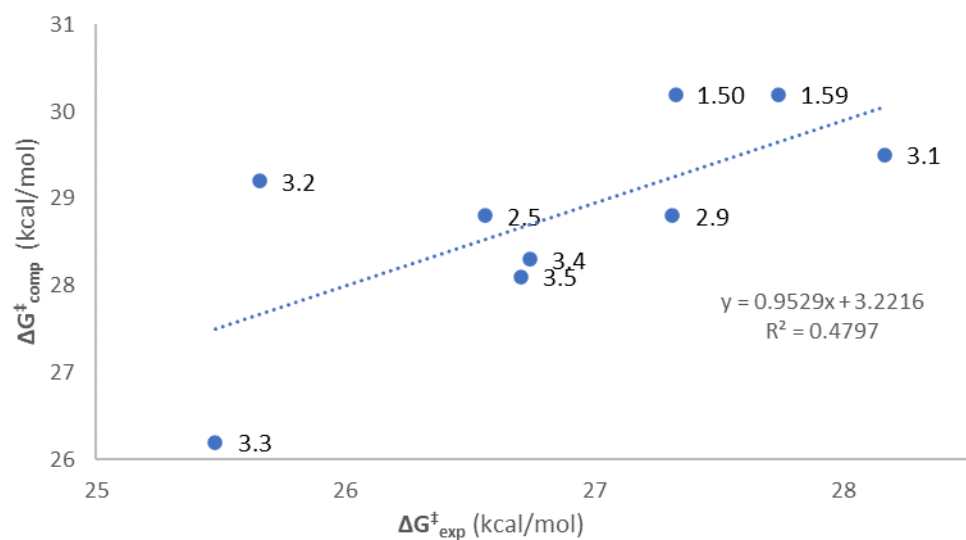


Figure 3.23. Correlation between the closed-shell transition state $\Delta G^\ddagger_{\text{comp}}$ with M06-2X/M06-2X level of theory and the $\Delta G^\ddagger_{\text{exp}}$

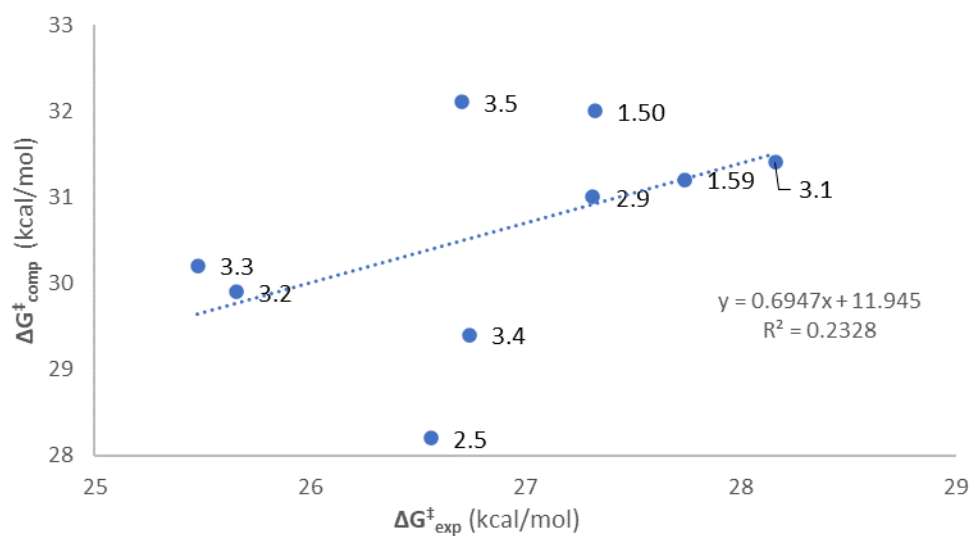


Figure 3.24. Correlation between the closed-shell transition state $\Delta G^\ddagger_{\text{comp}}$ with M06-2X/B3LYP level of theory and the $\Delta G^\ddagger_{\text{exp}}$

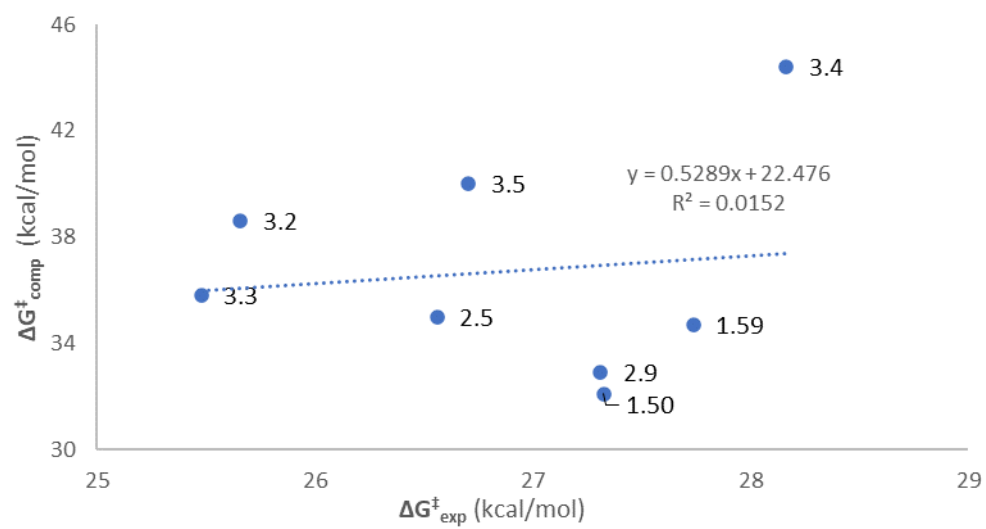


Figure 3.25. Correlation between the open-shell transition state $\Delta G^\ddagger_{\text{comp}}$ with M06-2X/B3LYP level of theory and the $\Delta G^\ddagger_{\text{exp}}$

4.0 Divergent Reactivity of the DA Adduct and Regulating the Selectivity for Oxidation or Isomerization Products

Having established the DA adduct to be on the pathway to both the oxidation and isomerization products, we were poised to investigate the mechanisms for their formation from adduct. We launched an investigation where dearomative DDDA conditions were systematically varied to identify how different reaction parameters affected product selectivity as a way to gain insight into the mechanisms of product formation. In turn, this information is used to regulate the dearomative DDDA reaction selectivity for either the oxidation or isomerization product.

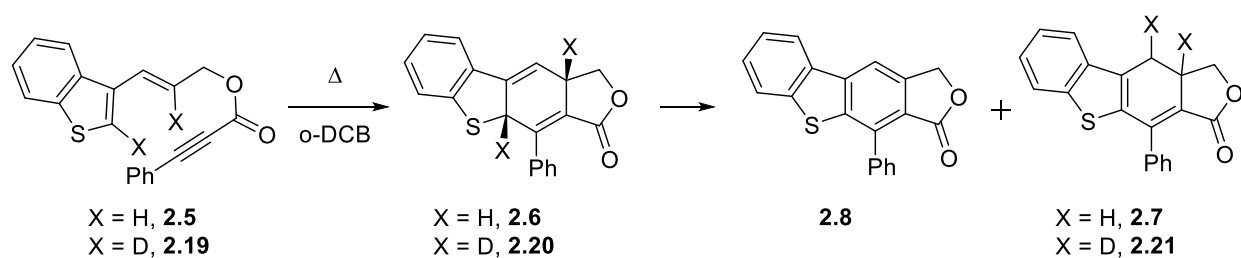
This chapter is based on results presented in: Winkelbauer J. A.; Bober A. E.; Brummond K. M., Regulating Divergent Product Selectivity of the Dearomative Didehydro-Diels–Alder Reaction through Mechanistic Insight. Manuscript in preparation, submission expected 2021.

4.1 Reaction Conditions that Affect Product Selectivity

The following effects of varied reaction conditions on the product selectivity of the dearomative DDDA reaction were observed as trends across multiple experiments and are herein reported with limited examples for direct comparison of the observed effects.

4.1.1 Temperature Effect on the Dearomative DDDA Reaction Product Selectivity

To determine the effect that temperature has on the product selectivity of the dearomative DDDA reaction of **2.5**, reaction temperatures were systematically varied, and product ratios were measured. Benzothiophene precursor **2.5** heated for 3 days at 60 °C in *o*-DCB afforded only **2.8**. The reaction progress and product ratios were monitored by ¹H NMR (see NMR overlay in experimental section). **2.19** for 2 h at 150 °C in *o*-DCB afforded a mixture of products with a 74:26 ratio of **2.8**:**2.21** along with a large quantity of adduct **2.20** remaining. Performing this same reaction at 180 °C resulted in an increased presence of isomerization product. Reaction of **2.19** heated for 2 h at 180 °C in *o*-DCB afforded a 45:55 ratio of products **2.8**:**2.21** with significantly less adduct **2.20** remaining. These three experiments demonstrate that reaction temperature has a significant impact on product ratios. Selectivity for the isomerization product increases at higher temperatures but a mixture of oxidation and isomerization products are afforded. The oxidation product is afforded exclusively at low temperature.

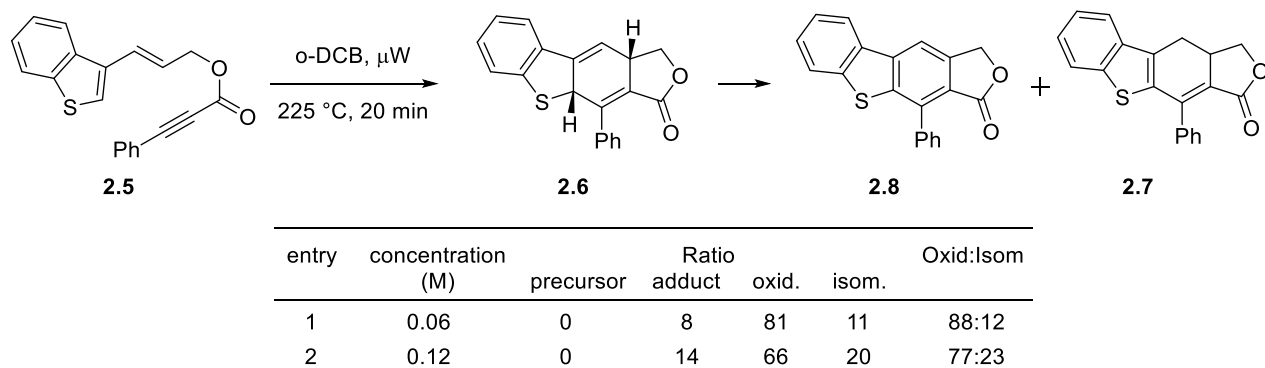


entry	precursor	T (°C)	t (h)	precursor	Ratio adduct	oxid.	isom.	Oxid:Isom
1	2.5	60	72	0	0	100	0	100:0
2	2.19	150	2	0	65	26	9	74:26
3	2.19	180	2	0	33	30	37	45:55

Scheme 4.1. Dearomative DDDA reactions of **2.5** with varied temperatures and affected product ratios

4.1.2 Concentration Effect on the Dearomative DDDA Reaction Product Selectivity

To determine the effect that reaction concentration has on the product selectivity of the dearomative DDDA reaction of **2.5**, reaction concentrations were systematically varied, and product ratios were measured. DDDA precursor **2.5** was heated for 20 min at 225 °C in *o*-DCB via microwave heating at a concentration of 0.06 M affording a mixture of products with a 88:12 ratio of **2.8**:**2.7** and some adduct **2.6** remaining. Reaction of **2.5** heated for 20 min at 225 °C in *o*-DCB via microwave at a concentration of 0.12 M afforded a 77:23 ratio of products **2.8**:**2.7** with some adduct remaining. These two experiments demonstrate that product ratios vary with changes in reaction concentration. A doubling of the reaction concentration resulted in a modest increase in the isomerization product.

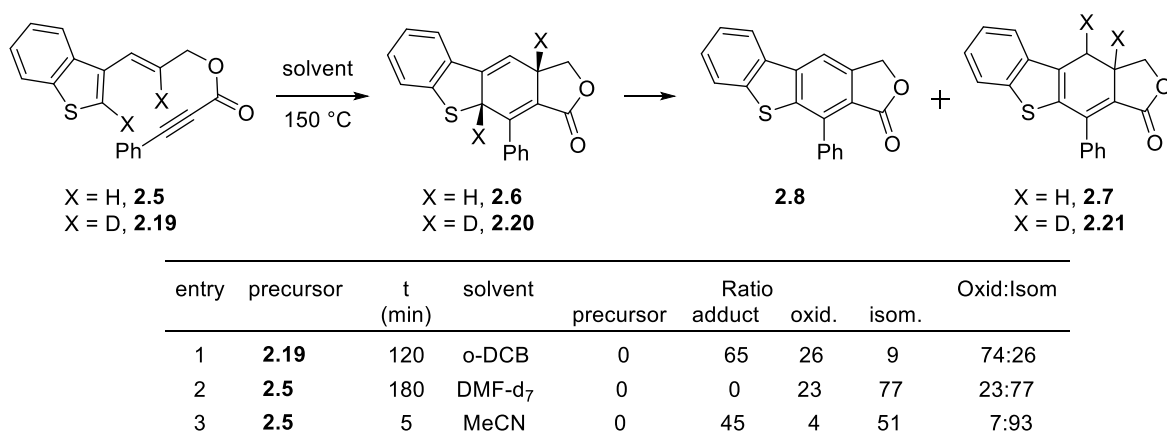


Scheme 4.2. Dearomative DDDA reaction of **2.5** with varied concentration and affected product ratios

4.1.3 Solvent Effect on the Dearomative DDDA Reaction Product Selectivity

To determine the effect that solvent has on the product selectivity of the dearomative DDDA reaction of **2.5**, reaction solvents with different dielectric constants (ϵ) were applied and product ratios were measured. **2.19** was heated for 2 h at 150 °C in *o*-DCB ($\epsilon = 9.9$) and afforded

a mixture of products in a 74:26 ratio of **2.8**:**2.21** with considerable adduct **2.6** remaining. **2.5** heated for 3 h at 150 °C in DMF-d₇ ($\epsilon = 36.7$) afforded a 23:77 ratio of **2.8**:**2.7** with no adduct remaining. Heating **2.5** in acetonitrile ($\epsilon = 37.5$) for 5 min at 150 °C afforded a 7:93 ratio of **2.8**:**2.7** with a considerable amount of adduct remaining. These three experiments demonstrate that product ratios for the dearomative DDDA reaction of **2.5** vary with changes in solvent dielectric constant. Selectivity for the isomerization product shows a modest increase as the solvent dielectric constant is increased.

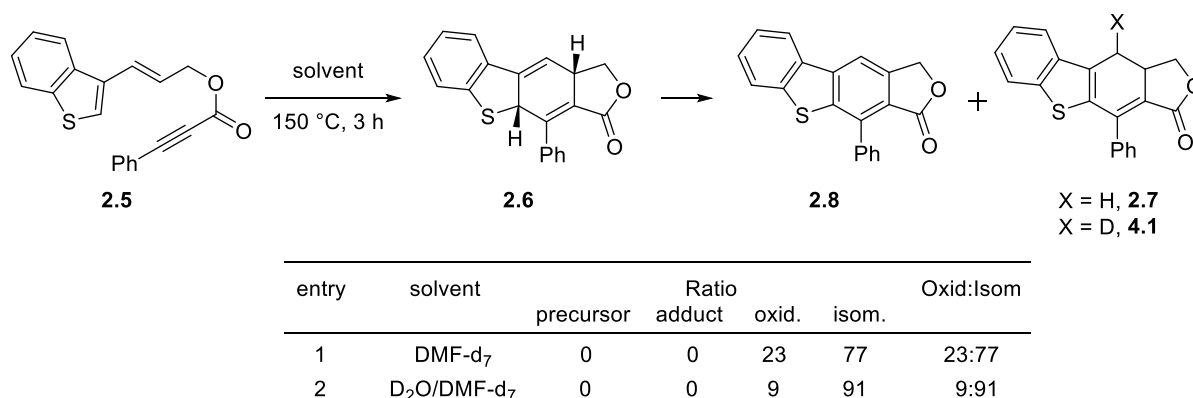


Scheme 4.3. Dearomative DDDA reaction of **2.5** with varied solvent and affected product ratios

4.1.4 Water Additive Effect on the Dearomative DDDA Reaction Product Selectivity

To determine the effect that additives have on the product selectivity of the dearomative DDDA reaction of **2.5**, water was added to increase the dielectric constant of the reaction media and product ratios were measured. **2.5** heated for 3 h at 150 °C in DMF-d₇ afforded a mixture of products with a 23:77 ratio of **2.8**:**2.7**. Reaction of **2.5** heated for 3 h at 150 °C in D₂O/DMF-d₇ (10% v/v) afforded a 9:91 ratio of products **2.8**:**2.21**. These two experiments demonstrate that product ratios for the dearomative DDDA reaction of **2.5** vary with the presence of water.

Selectivity for the isomerization product shows a modest increase in the presence of water. The most striking observation is the isolation of isomerization product **4.1** with deuterium incorporation. This finding is discussed further in section 4.4.



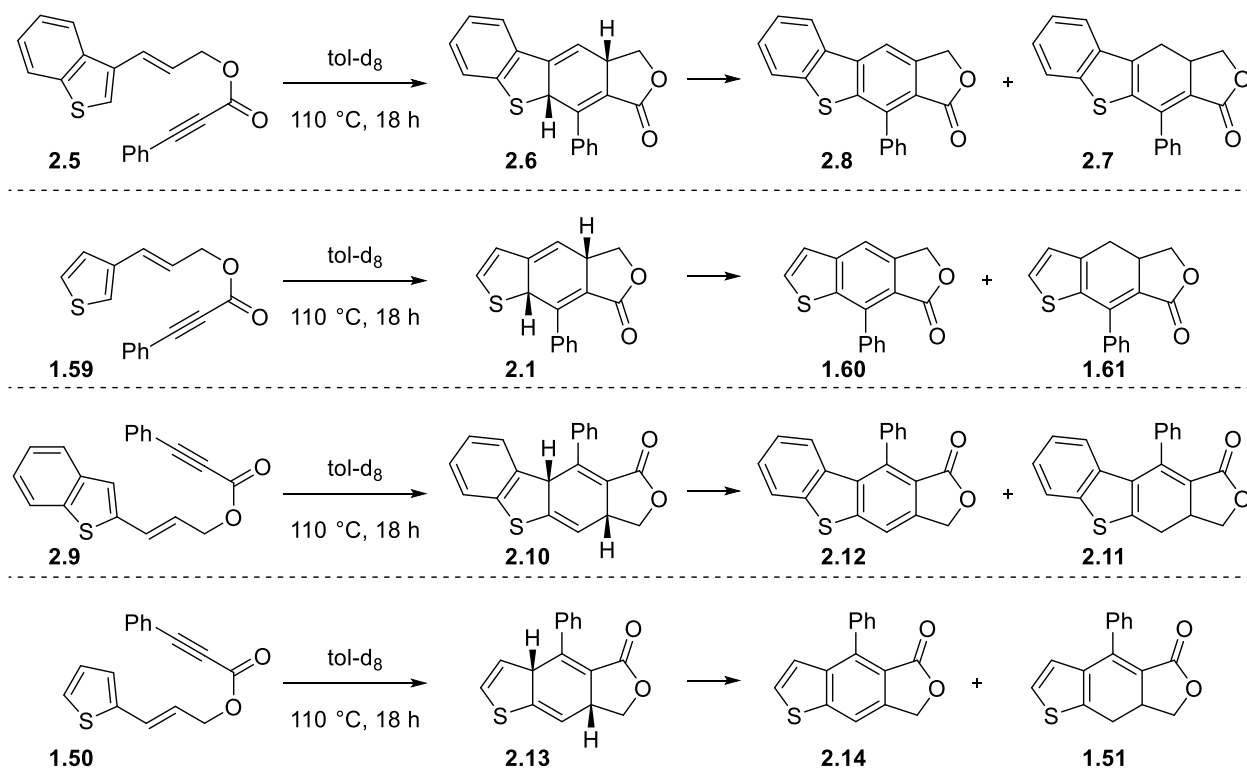
Scheme 4.4. Dearomative DDDA reaction of **2.5** with added water and affected product ratios

4.1.5 BHT Additive Effect on the Dearomative DDDA Reaction Product Selectivity

To determine the effect that a radical inhibitor has on the product selectivity of the dearomative cycloaddition of **2.5**, **1.59**, **2.9**, and **1.50**, 3,5-di-tert-4-butylhydroxytoluene (BHT) was added and product ratios were measured and compared to parallel reactions without BHT. Four separate reactions of precursors **2.5**, **1.59**, **2.9**, and **1.50** were heated for 18 h at 110 °C in toluene-d₈ within an NMR tube (entries 1, 3, 5, and 7, Table 4.1). Reactions were then performed under the same conditions but with 1 equivalent of added BHT (entries 2, 4, 6, and 8). Both sets of reactions were monitored at the 3, 8, and 18 h timepoints by pausing the reaction for ¹H NMR analysis of the crude solution. Yields and ratios were determined by comparing ¹H NMR resonances of substrates to a mesitylene internal standard. **2.5** showed complete selectivity for oxidation product under both sets of conditions (entries 1 and 2). **1.59**, **2.9**, and **1.50** all showed a

marked increase in isomerization product in the presence of BHT (compare entries 3–8). These four sets of experiments demonstrate that product ratios for the dearomative DDDA reaction of vary with the presence of BHT. Selectivity for the isomerization product shows a modest increase in the presence of BHT.

Table 4.1. Dearomative DDDA reaction of precursors with added BHT and affected product ratios



Entry	Precursor	Solvent/ Additive	Oxid:Isom	Yield (%)
1	2.5	Tol- d_8	100:0	94
2	2.5	Tol- d_8 BHT (1 equiv)	100:0	89
3	1.59	Tol- d_8	52:48	72
4	1.59	Tol- d_8 BHT (1 equiv)	29:71	84
5	2.9	Tol- d_8	76:24	97
6	2.9	Tol- d_8 BHT (1 equiv)	67:33	88
7	1.50	Tol- d_8	93:7	90
8	1.50	Tol- d_8 BHT (1 equiv)	67:33	83

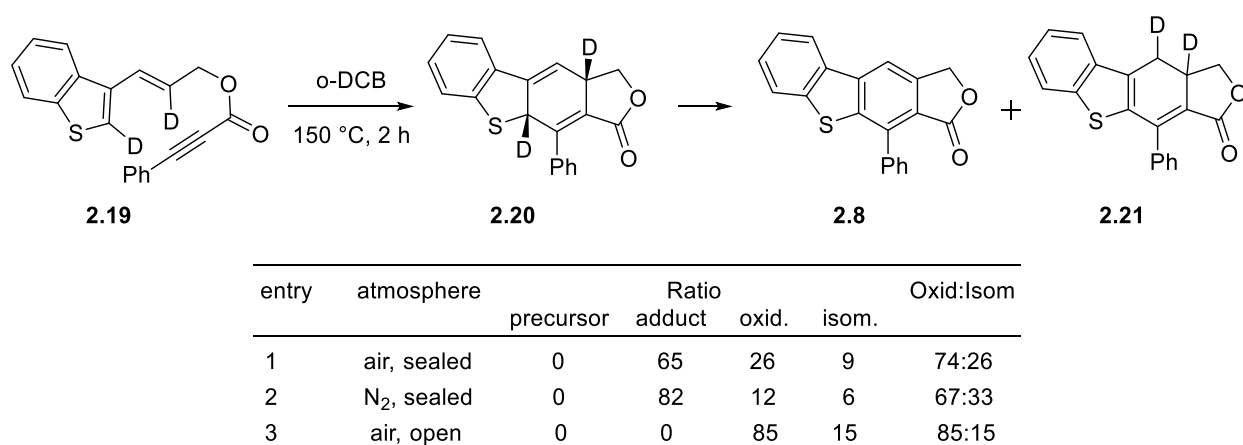
Additionally, the ratio of adduct observed at the 3 h timepoint was significantly increased for reactions that included BHT. Reaction of **2.5** showed an increase of adduct from 43% to 70% at the 3 h timepoint with BHT added (see experimental section 4.6.7). Reaction of **1.59** showed an increase from 5% to 12% with BHT added. Reaction of **2.9** showed an increase of adduct from 3% to 56% at the 3 h timepoint with BHT added, and reaction of **1.50** showed an increase from 2% to 32% with BHT added. These experiments demonstrate that BHT slows conversion of adduct to products as evidenced by an increased ratio of adduct at the 3 h timepoint.

The reactions of **2.5** in toluene- d_8 at 110 °C with and without BHT additive (entries 1 and 2, Table 4.1) afforded exclusively oxidation product **2.8**. To determine the effect of BHT additive on the product selectivity, these two reactions were repeated in *o*-DCB- d_4 at 150 °C. Reaction of **2.5** in *o*-DCB- d_4 at 150 °C without BHT additive afforded a ratio of 82:18 oxidation to isomerization product. Reaction of **2.5** in *o*-DCB- d_4 at 150 °C with 1 equivalent of BHT additive afforded a ratio of 77:23 oxidation to isomerization product. Presence of BHT additive afforded a small increase in formation of isomerization product under these conditions for **2.5** in comparison to the other precursors. It remains unclear as to why the addition of BHT had less of an impact on product selectivity for dearomative DDDA reaction of **2.5**.

4.1.6 Atmosphere Effect on the Dearomative DDDA Reaction Product Selectivity

To determine the effect that atmosphere has on the product selectivity of the dearomative cycloaddition of **2.5**, the reaction atmosphere was varied, and product ratios were measured. **2.19** heated for 2 h at 150 °C in *o*-DCB, sealed via a screw-top vial under air, afforded a mixture of products with a 65:26:9 ratio of **2.20:2.8:2.21**. A repeat of this reaction under an atmosphere of nitrogen afforded a mixture of products with a 82:12:6 ratio of **2.20:2.8:2.21**. Reaction of **2.19**

heated for 2 h at 150 °C in *o*-DCB, open to air via a 16-gauge needle, afforded a mixture of products with a 85:15 ratio of **2.8**:**2.21** and no remaining adduct present. Replacing the air atmosphere with one of nitrogen afforded an increased accumulation of adduct as conversion to oxidation product was slowed. Reaction that was open to air afforded an increase in the conversion of adduct to oxidation product. Selectivity for the oxidation product shows an atmosphere with increased exposure to air.



Scheme 4.5. Dearomative DDDA reaction of **2.5** with air exposure and affected product ratios

4.2 Substrate Identity Effect on the Dearomative DDDA Reaction Product Selectivity

To determine the effect that the tether attachment point has on the product selectivity of the dearomative cycloaddition, substrates **2.5**, **1.59**, **2.9**, and **1.50** were reacted under identical condition and product ratios were measured. In identical reactions, **2.5**, **1.59**, **2.9**, and **1.50** were heated for 18 h at 110 °C in toluene-*d*₈ (Table 4.1, entries 1, 3, 5, and 7). Reaction of **2.5** afforded a higher ratio of oxidation to isomerization products than **2.9**, yet reaction of **1.59** afforded a lower

ratio of oxidation to isomerization products than **1.50**. Tether position did not show a clear effect on product ratios for these precursors.

Comparison of the same set of reactions also showed the effect of heteroarene-fused benzene ring on the product selectivity. Reaction of **2.5** afforded a higher ratio of oxidation to isomerization products than **1.59**, yet reaction of **2.9** afforded a lower ratio of oxidation to isomerization products than **1.50**. The presence of a fused benzene ring did not show a clear effect on product ratios for these precursors.

Relative product selectivity based upon the ratio of oxidation to isomerization products was then compared to computational gas phase bond dissociation energies (BDE's) and acidities for the bisallylic hydrogen nearest the heteroarene in the adduct. These calculations were performed at the (u)M06-2X/6-311+g(d,p)//(u)M06-2X/6-31+g(d) level of theory by our collaborator Elena Kusevska from the Peng Liu research group. No correlation was found between the experimental product ratios and the calculated BDE's or acidities at this level of theory. These preliminary computational analyses are insufficient to predict experimental dearomative DDDA product ratios and therefore suggest that computational transition state analysis for the product formation steps would be necessary in order to use computational calculations as a predictive tool for determination of product selectivity.

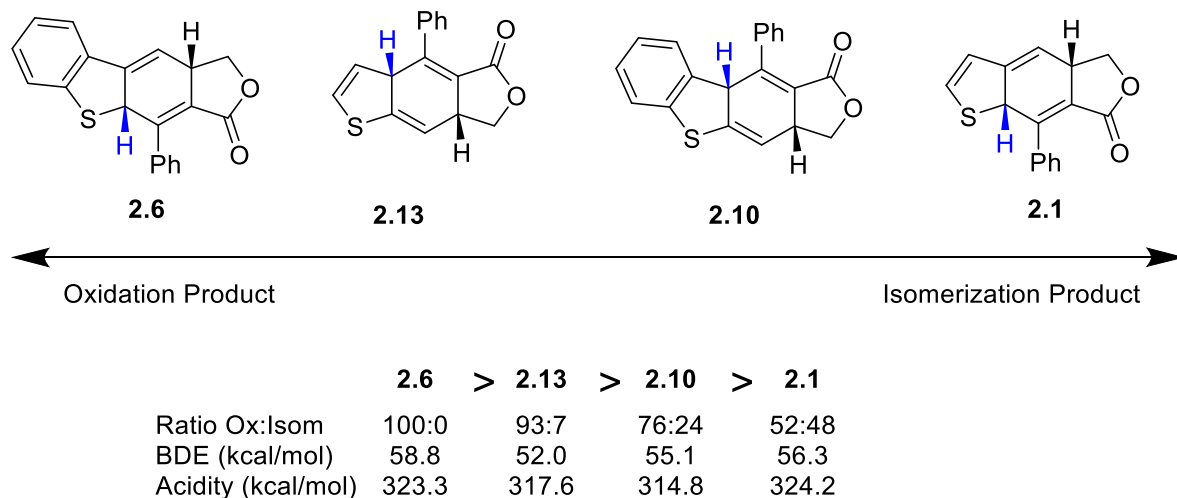
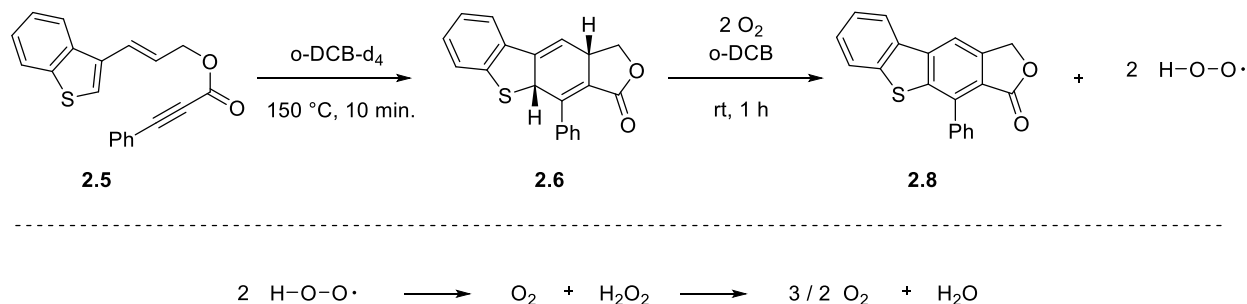


Figure 4.1. Ratio of oxidation product to isomerization product compared to computationally calculated BDE and acidity of the transferred proton of the Diels-Alder adduct

4.3 Evidence for Oxidation Product Formation via Dehydrogenation of Diels-Alder Adduct with Oxygen

As previously discussed, Diels-Alder adduct at room temperature, in *o*-DCB with air bubbled through for 1 h afforded complete selectivity for oxidation product (see section 2.4.1). Also, no evidence was observed for transformation of isomerization product into oxidation product under thermal conditions with or without enhanced exposure to air. These results support the hypothesis that formation of oxidation product is dependent on the presence of molecular oxygen. This is markedly different than the styrenyl dearomative DDDA reaction previously reported by Kocsis which afforded oxidation product and also detected evolved hydrogen gas in both aerobic and anaerobic conditions (see section 1.3.2).⁵⁰ The dearomative DDDA reaction of vinyl heteroarenes does not appear to involve release of hydrogen gas akin to the styrenyl dearomative DDDA reaction but rather produces oxidation product by an atmosphere dependent

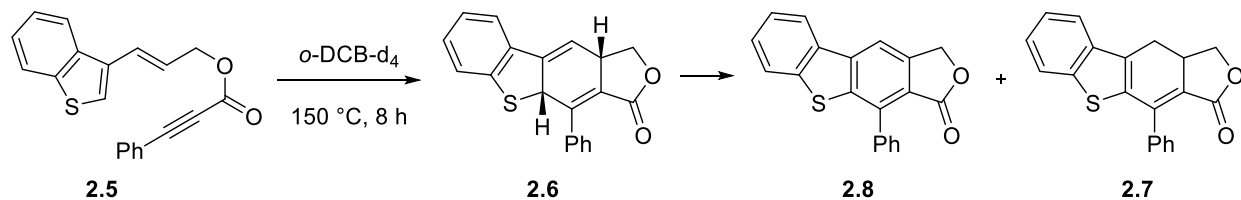
dehydrogenation pathway similar to that described by Hendry for the oxidation of 1,4-cyclohexadiene to benzene.⁶² This pathway may be initiated by triplet molecular oxygen and then propagated by hydroperoxyl radicals which Hoffman and coworkers have found to be far more reactive.⁶³ These formed peroxides may then decompose into water and molecular oxygen.



Scheme 4.6. Formation of oxidation product through an oxygen mediated dehydrogenation

Reactions to monitor for the evolution of hydrogen gas as a product in the formation of oxidation product afforded no detection of H₂ gas. These experiments include seeking a detectable H₂ gas resonance in the ¹H NMR of reactions that afforded oxidation product, as well as seeking a detectable presence of H₂ gas in the headspace of a sealed vial reaction that afforded oxidation product. To check for the evolution of hydrogen gas as a product of oxidation product formation, ¹H NMR was analyzed for the reaction of **2.5** at 150 °C in *o*-DCB-d₄ after 3 and 8 hours (Scheme 4.7). After the reaction was completed, H₂ gas was bubbled through the solution for 2 min. and ¹H NMR was performed to observe the resonance for H₂ gas at 4.53 ppm. The solution was then bubbled through with argon gas for 2 min. and ¹H NMR was performed to observe the disappearance of the resonance for H₂ gas at 4.53 ppm. These experiments confirmed the ¹H NMR chemical shift for H₂ gas in *o*-DCB-d₄ to be 4.53 ppm. A resonance is observed at 4.53 ppm in the ¹H NMR at the 8 h timepoint, but the integration of that resonance remains consistent after

bubbling of argon gas through the solution, confirming the resonance to not be H₂ but rather a decomposition or unknown byproduct. The ¹H NMR for this reaction at the 3 h timepoint afforded a 17:65:18 ratio of **2.6**:**2.8**:**2.7**, but no resonance was observed for H₂ gas. This experiment was performed under the same reaction conditions in which H₂ gas was observed by ¹H NMR in dearomative DDDA reactions of styrene substrates.⁵⁰ The resonance for H₂ gas when bubbled through a solution of toluene-d₈ was observed to appear at 4.51 ppm by ¹H NMR. ¹H NMR was analyzed for the reaction of **2.5** at 110 °C in toluene-d₈ after 3, 8, and 18 hours, as well as the parallel reactions of **1.59**, **2.9**, and **1.50** (Table 4.1, see experimental section for NMR spectra). No H₂ gas was observed in the reaction solution by ¹H NMR for any substrate at any timepoint.



Scheme 4.7. Dearomative DDDA reaction of **2.5** in tol-d₈ at 150 °C for 3 h

To check the reaction headspace for evolved hydrogen gas, two sealed vial reactions were performed. **2.5**, sealed in a vial under air was heated for 90 min at 150 °C in *o*-DCB and afforded a 41:39:20 ratio of **2.6**:**2.8**:**2.7**. The vial was allowed to cool to room temperature and the headspace of the reaction was analyzed with no detection of hydrogen gas. The same experiment was repeated with precursor **2.19** and afforded a 77:18:5 ratio of **2.6**:**2.8**:**2.21**. No deuterium gas was detected in the reaction headspace for this reaction. For both reactions, the detection of evolved gas is inconclusive due to the limited amount of oxidation product that was formed. Yet, the formation of oxidation product was dramatically reduced in the sealed conditions with

comparison to the reaction with air bubbled through, presumably due to the limited amount of air available in the sealed vessel.

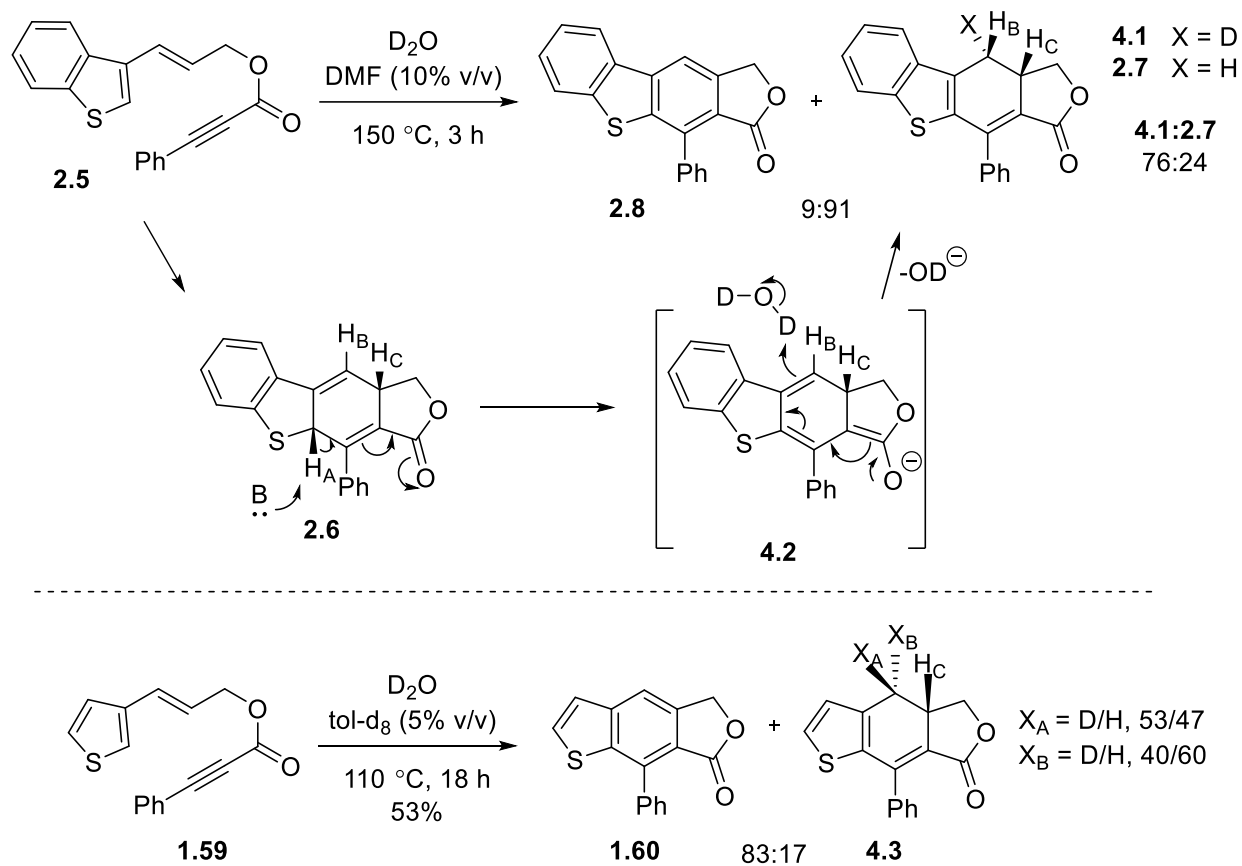
The higher ratio of oxidation product found when the reaction has an increased exposure to air is a result of the increased exposure to oxygen from the air. Likewise, reactions at lower temperatures, concentrations, and longer durations allow for increased exposure to air which affords a higher ratio of oxidation product. This mechanism differs from those of styrenyl precursors, which selectively provided oxidized product at elevated temperatures.⁵⁰ For most cases, the conversion of adduct to oxidation product is slowed in the presence of BHT and the ratio of oxidation product to isomerization product decreases which provides evidence that this transformation of adduct to oxidation product involves a radical process (see section 4.1.5). The presence of BHT in the reaction slows the dehydrogenation of adduct by acting as a radical scavenger for either oxygen in the solution or hydrogen atom abstracted adduct, thus slowing the formation of oxidation product.

4.4 Evidence for Isomerization Product Formation via Proton Transfer of Diels-Alder Adduct

Deuterium incorporation was observed when D₂O was introduced as an additive in dearomative DDDA reaction of **2.5**. Reaction of **2.5** heated for 3 h at 150 °C in D₂O/DMF (10% v/v) afforded predominantly isomerization product **4.1** with 76% deuterium incorporation at the X position as well as some **2.8** (91:9 respectively, Scheme 4.8). Deuterium incorporation was determined by comparing the integral intensities of resonances H_C at 3.70 ppm and H_A at 2.82

ppm. Product **4.1** was afforded as a single diastereomer and the stereochemistry shown was determined by the disappearance of the splitting for H_A ($J^{AC} = 17.3$ Hz).

We proposed that deuterium incorporation into isomerization product in the presence of D₂O would also occur with other precursors and in less nonpolar solvents. Dearomative DDDA reaction of **1.59** was performed in toluene with added D₂O rather than in DMF. Reaction of **1.59** heated for 18 h at 110 °C in D₂O/toluene (5% v/v) afforded a ratio of 83:17 of oxidation product to isomerization product in 53% yield. Deuterium incorporation was observed in the isomerization product and was determined by comparing the integral intensities of resonances X_A at 3.14 ppm, X_B at 2.70 ppm, and a methylene hydrogen of the lactone at 4.72 ppm. Product **4.3** was afforded as a mixture of diastereomers with overall deuterium incorporation of 53% at X_A and 40% at X_B.



Scheme 4.8. Mechanism of deuterium incorporation observed in dearomative Diels-Alder reactions with deuterium oxide present

The deuterium incorporation found in the isomerization product support formation of the product by an intermolecular, ionic proton transfer. Deuterium incorporation via a radical mechanism would be unlikely due to unfavorable generation of a hydroxyl radical. Deprotonation of the bis-allylic C–H_A of **2.6** affords the resonance-stabilized anion **4.2** that reacts with D₂O to afford **4.1**. The orbital alignment of bis-allylic hydrogen H_A with the π-orbitals of the adjacent α,β-unsaturated lactone enhances the acidity of the adduct. Selectivity for deuteration at the concave face is attributed to the steric incumbrance posed by H_C at the ring-fusion.

Enhanced selectivity for isomerization product was found in reactions with elevated temperatures and higher concentrations, likely due to increased intermolecular collisions necessary for the proton transfer. Reactions in solvents of higher polarity also afforded enhanced selectivity for isomerization product, most likely due to improved stabilization of an ionic intermediate. Finally, water, as an additive, acts as a more sterically accessible proton source for protonation of the ionic intermediate to afford enhanced selectivity for isomerization product.

4.5 Conclusions

We established that the dearomative DDDA reaction proceeds to either oxidation or isomerization products from the DA adduct via divergent mechanistic pathways with reaction conditions of temperature, concentration, solvent polarity, atmosphere, and mild additives as factors that control product selectivity. Reaction of DA adduct with bubbling air at room temperature supports the formation of oxidation product by an oxygen effected dehydrogenation of the adduct. Formation of isomerization product by an intermolecular, ionic proton transfer is supported by reactions where deuterium abstraction from D₂O affords deuterium incorporation into the isomerization product. Selectivity for the oxidation product was enhanced with reaction conditions of lower temperatures, non-polar solvents, lower concentrations, and increased exposure to air. Selectivity for the isomerization product was enhanced with conditions of higher temperatures, polar solvents, higher concentrations, water or BHT additives, and decreased exposure to air. Our mechanistic analysis of the dearomative DDDA reaction of heteroarenes has afforded improved understanding of its divergent mechanisms of reactivity and has allowed us to

determine the factors which control product selectivity. These findings enable us to enhance the scope and utility of this reaction for these and future substrates.

4.6 Experimental

4.6.1 General Methods

Unless otherwise indicated, all reactions were performed in flame-dried glassware under an air atmosphere and stirred with Teflon-coated magnetic stir bars. All commercially available compounds were purchased and used as received unless otherwise specified. Tetrahydrofuran (THF), diethyl ether (Et₂O), and dichloromethane (DCM) were purified by passing through alumina using a Sol-Tek ST-002 solvent purification system. Deuterated chloroform (CDCl₃) was dried over 4Å molecular sieves. Nitrogen gas was purchased from Matheson Tri Gas. Conventional heating was used for reactions that were monitored by ¹H NMR or performed open to the air. All microwave-mediated reactions were carried out using a Biotage Initiator Exp or Anton-Paar Monowave 300 microwave synthesizer. Purification of the compounds by flash column chromatography was performed using silica gel (40-63 μm particle size, 60 Å pore size). TLC analyses were performed on silica gel F₂₅₄ glass plates (250 μm thickness). ¹H NMR and ¹³C NMR spectra were recorded on Bruker Avance 300, 400, or 500 MHz spectrometers. Spectra were referenced to residual chloroform (7.26 ppm, ¹H; 77.16 ppm, ¹³C) or *o*-dichlorobenzene (6.93 ppm, ¹H; 130.04 ¹³C) unless otherwise specified. Chemical shifts are reported in ppm, multiplicities are indicated by s (singlet), d (doublet), t (triplet), q (quartet), p (pentet), m (multiplet), and bs (broad singlet). Coupling constants, *J*, are reported in hertz (Hz). All NMR spectra were obtained at room

temperature. IR spectra were obtained using a Nicolet Avatar E.S.P. 360 FT-IR. EI mass spectroscopy was performed on a Waters Micromass GCT high resolution mass spectrometer, while ES mass spectroscopy was performed on a Waters Q-TOF Ultima API, Micromass UK Limited high-resolution mass spectrometer.

4.6.2 General Procedures for Dearomative DDDA Reactions

4.6.2.1 General Procedure D: Dearomative DDDA Reaction – Conventional Heating

An oven-dried NMR tube was charged with dearomative DDDA precursor (1 equiv) dissolved in solvent under an atmosphere of air. In some cases, butylated hydroxytoluene (BHT), deuterium oxide (D_2O), or water was added. In some cases, an internal standard of mesitylene was added to calculate an NMR yield. The NMR tube was sealed with a polypropylene cap and lowered into a preheated oil bath. Reaction progress was monitored by 1H NMR by comparing the resonance integrations for starting material, adduct, oxidized product, and isomerized product at different time points. The reaction was paused for 1H NMR analysis. The NMR tube was removed from the oil bath, rinsed with hexanes, and wiped with a ChemWipe. After obtaining an NMR spectrum, the tube was returned to the oil bath. Reaction time does not include the time required to obtain NMR spectrum at each time point (~15-20 min each). All yields are unoptimized.

4.6.2.2 General Procedure E: Dearomative DDDA Reaction – Microwave Heating

An oven-dried microwave vial equipped with a stir bar was charged with dearomative DDDA precursor (1 equiv) dissolved in solvent under an atmosphere of air. The vial was sealed with a Teflon-lined septum crimp cap and was heated in a Biotage Initiator Exp or Anton-Paar

Monowave 300 microwave synthesizer. The microwave parameters were set to variable power, constant temperature, fixed hold time set to on, and absorption set to “normal” for nonpolar solvents (o-DCB, DCE, CDCl₃) or “high” for polar solvents (acetonitrile, DMF). Product ratios were determined by comparing the resonance integrations for starting material, adduct, oxidized product, and isomerized product from the ¹H NMR of the reaction solution using No-D spectroscopy,⁶⁴ or by removing the solvent and re-dissolving in CDCl₃. Volatile solvents (DCE) were removed by rotary evaporation, o-DCB and PhNO₂ were removed by passing the reaction solution through a plug of silica gel with hexanes as eluent, and DMF was removed through aqueous extraction. All yields are unoptimized.

4.6.3 Experiments Showing the Effect of Temperature

Rxn 1. Follows General Procedure D. Precursor **2.5** (7 mg, 0.02 mmol) and mesitylene (3 μ L, 0.02 mmol) in o-DCB-d₄ (0.5 mL, 0.04M) was heated at 60 °C for 66 h. A 0:0:100:0 ratio of **2.5**, **2.6**, **2.8**, and **2.7** was obtained in 58% NMR yield based upon the mesitylene internal standard. Ratios were determined by comparing the ¹H NMR resonances at 6.63 ppm (1H) for **2.5**, 5.46 ppm (1H) for **2.6**, and 5.21 ppm (2H) for **2.8** to the resonance at 6.64 ppm for mesitylene.

Table 4.2. Ratio of compounds in 4.6.3 – Rxn 1

Time (h)	2.5	2.6	2.8	2.7	Yield (%)
0	100	0	0	0	100
2	89	6	5	0	102
4	86	5	10	0	99
9	69	6	25	0	82
20	41	6	52	0	71
32	21	4	74	0	74
44	9	3	87	0	65
55	0	0	100	0	55

66	0	0	100	0	58
----	---	---	-----	---	----

Rxn 2. A 1-mL screw-top flask with septum lid and stir bar was charged with precursor **2.19** (24 mg, 0.075 mmol) dissolved in o-dichlorobenzene (0.50 mL, 0.15 M) and sealed with a Teflon-lined septum screw cap under air. The solution was lowered into a pre-heated oil bath at 150 °C. After 2 h, the the solution was allowed to cool to room temperature, then transferred to an NMR tube for ¹H NMR analysis. Product ratios were determined by comparing the resonance integrations for starting material, adduct, oxidized product, and isomerized product from the ¹H NMR of the crude reaction solution using No-D spectroscopy. A 0:65:26:9 ratio of **2.19**, **2.20**, **2.8**, and **2.21** was obtained. Ratios were determined by comparing the ¹H NMR resonances at 4.56 ppm (1H) for **2.6**, 5.21 ppm (2H) for **2.8**, and 2.49 ppm (1H) for **2.7**. An unknown impurity identified by the resonance at 5.04 ppm exists in the starting material and persisted through the reaction to completion.

Rxn 3. Follows General Procedure D. Precursor **2.19** (22 mg, 0.069 mmol) in o-DCB (0.50 mL, 0.14 M) was heated at 180 °C for 120 min. A 0:33:30:37 ratio of **2.19**, **2.20**, **2.8**, and **2.21** was obtained. Ratios were determined by comparing the ¹H NMR resonances at 4.56 ppm (1H) for **2.6**, 5.21 ppm (2H) for **2.8**, and 2.49 ppm (1H) for **2.7**. An unknown impurity identified by the resonance at 5.04 ppm exists in the starting material and persisted through the reaction to completion.

4.6.4 Experiments Showing the Effect of Concentration

Rxn 1. Follows General Procedure E. Precursor **2.5** (19 mg, 0.060 mmol) in o-DCB (1.0 mL, 0.060 M) was heated at 225 °C for 20 min. A 0:8:81:11 ratio of **2.5**, **2.6**, **2.8**, and **2.7** was obtained. Ratios were determined by comparing the ¹H NMR resonances at 6.27 ppm (1H) for **2.6**, 5.44 ppm (2H) for **2.8**, and 2.79 ppm (1H) for **2.7**.

Rxn 2. Follows General Procedure E. Precursor **2.5** (39 mg, 0.12 mmol) in o-DCB (1.0 mL, 0.12 M) was heated at 225 °C for 20 min. A 0:14:66:20 ratio of **2.5**, **2.6**, **2.8**, and **2.7** was obtained. Ratios were determined by comparing the ¹H NMR resonances at 6.27 ppm (1H) for **2.6**, 5.44 ppm (2H) for **2.8**, and 2.79 ppm (1H) for **2.7**.

4.6.5 Experiments Showing the Effect of Solvent Polarity

Rxn 1. A 1-mL screw-top flask with septum lid and stir bar was charged with precursor **2.19** (24 mg, 0.075 mmol) dissolved in o-dichlorobenzene (0.50 mL, 0.15 M) and sealed with a Teflon-lined septum screw cap under air. The solution was lowered into a pre-heated oil bath at 150 °C. After 2 h, the the solution was allowed to cool to room temperature, then transferred to an NMR tube for ¹H NMR analysis. Product ratios were determined by comparing the resonance integrations for starting material, adduct, oxidized product, and isomerized product from the ¹H NMR of the crude reaction solution using No-D spectroscopy. A 0:65:26:9 ratio of **2.19**, **2.20**, **2.8**, and **2.21** was obtained. Ratios were determined by comparing the ¹H NMR resonances at 4.56 ppm (1H) for **2.6**, 5.21 ppm (2H) for **2.8**, and 2.49 ppm (1H) for **2.7**. An unknown impurity identified

by the resonance at 5.04 ppm exists in the starting material and persisted through the reaction to completion.

Rxn 2. Follows General Procedure D. Precursor **2.5** (10 mg, 0.031 mmol) in DMF-d₇ (0.50 mL, 0.060 M), sealed under an atmosphere of air, was heated at 150 °C for 180 min. A 0:0:23:77 ratio of **2.5**, **2.6**, **2.8**, and **2.7** was obtained in 60% isolated yield. Ratios were determined by comparing the ¹H NMR resonances at 5.46 ppm (2H) for **2.8**, and 4.84 ppm (1H) for **2.7**.

Rxn 3. Follows General Procedure D. Precursor **2.5** (6 mg, 0.02 mmol) in CH₃CN (0.5 mL, 0.04 M) was heated at 150 °C for 5 min. A 0:45:4:51 ratio of **2.5**, **2.6**, **2.8**, and **2.7** was obtained. Ratios were determined by comparing the ¹H NMR resonances at 6.20 ppm (1H) for **2.6**, 5.46 ppm (2H) for **2.8**, and 2.81 ppm (1H) for **2.7**.

4.6.6 Experiments Showing the Effect of Water Additive

Rxn 1. Follows General Procedure D. Precursor **2.5** (10 mg, 0.031 mmol) in DMF-d₇ (0.50 mL, 0.060 M), sealed under an atmosphere of air, was heated at 150 °C for 180 min. A 0:0:23:77 ratio of **2.5**, **2.6**, **2.8**, and **2.7** was obtained in 60% isolated yield. Ratios were determined by comparing the ¹H NMR resonances at 5.46 ppm (2H) for **2.8**, and 4.84 ppm (1H) for **2.7**.

Rxn 2. Follows General Procedure D. Precursor **2.5** (10 mg, 0.032 mmol) and D₂O (0.050 mL, 2.8 mmol) in DMF (0.45 mL, 0.60 M) was heated at 150 °C for 180 min. A 0:0:9:91 ratio of **2.5**, **2.6**, **2.8** and **4.1** was obtained in 50% yield. The isomerization product was observed to have 76%

deuterium incorporation. Ratios were determined by comparing the ^1H NMR resonances at 5.46 ppm (2H) for **2.8**, and 2.81 ppm (1H) for **2.7**.

4.6.7 Experiments Showing the Effect of BHT Additive

Rxn 1. Follows General Procedure D. Precursor **2.5** (6 mg, 0.02 mmol) and mesitylene (3 μL , 0.02 mmol) in toluene- d_8 (0.5 mL, 0.04M) was heated at 110 $^\circ\text{C}$ for 18 h. The experiment was paused briefly at the 3 h and 8 h time points for ^1H NMR analysis. A final ratio 0:0:100:0 of **2.5**, **2.6**, **2.8**, and **2.7** was obtained in 89% yield based on internal standard. Ratios were determined by comparing the ^1H NMR resonances at 6.07 ppm (1H) for **2.5**, 5.08 ppm (1H) for **2.6**, and 4.63 ppm (2H) for **2.8** to the resonance at 6.67 ppm for mesitylene.

Table 4.3. Ratio of compounds in 4.6.7 – Rxn 1

Time (h)	2.5	2.6	2.8	2.7	Yield (%)
3	0	43	57	0	100
8	0	0	100	0	91
18	0	0	100	0	94

Rxn 2. Follows General Procedure D. Precursor **2.5** (6 mg, 0.02 mmol), BHT (4 mg, 0.02 mmol), and mesitylene (3 μL , 0.02 mmol) in toluene- d_8 (0.5 mL, 0.04M) was heated at 110 $^\circ\text{C}$ for 18 h. The experiment was paused briefly at the 3 h and 8 h time points for ^1H NMR analysis. A final ratio 0:0:100:0 of **2.5**, **2.6**, **2.8**, and **2.7** was obtained in 96% yield based on internal standard. Ratios were determined by comparing the ^1H NMR resonances at 6.07 ppm (1H) for **2.5**, 5.08 ppm (1H) for **2.6**, and 4.63 ppm (2H) for **2.8** to the resonance at 6.67 ppm for mesitylene.

Table 4.4. Ratio of compounds in 4.6.7 – Rxn 2

Time (h)	2.5	2.6	2.8	2.7	Yield (%)
3	0	70	30	0	100
8	0	0	100	0	86
18	0	0	100	0	89

Rxn 3. Follows General Procedure D. Precursor **1.59** (6 mg, 0.02 mmol) and mesitylene (3 μ L, 0.02 mmol) in toluene- d_8 (0.5 mL, 0.04M) was heated at 110 °C for 18 h. The experiment was paused briefly at the 3 h and 8 h time points for ^1H NMR analysis. A final ratio 5:0:49:46 of **1.59**, **2.1**, **1.60**, and **1.61** was obtained in 70% yield based on internal standard. Ratios were determined by comparing the ^1H NMR resonances at 5.84 ppm (1H) for **1.59**, 3.30 ppm (1H) for **2.1**, 4.56 ppm (2H) for **1.60**, and 3.24 ppm (1H) for **1.61** to the resonance at 6.67 ppm for mesitylene.

Table 4.5. Ratio of compounds in 4.6.7 – Rxn 3

Time (h)	1.59	2.1	1.60	1.61	Yield (%)
3	65	5	20	10	93
8	31	0	38	31	81
18	5	0	49	46	72

Rxn 4. Follows General Procedure D. Precursor **1.59** (6 mg, 0.02 mmol), BHT (4 mg, 0.02 mmol), and mesitylene (3 μ L, 0.02 mmol) in toluene- d_8 (0.5 mL, 0.04M) was heated at 110 °C for 18 h. The experiment was paused briefly at the 3 h and 8 h time points for ^1H NMR analysis. A final ratio 0:0:29:71 of **1.59**, **2.1**, **1.60**, and **1.61** was obtained in 85% yield based on internal standard. Ratios were determined by comparing the ^1H NMR resonances at 5.84 ppm (1H) for **1.59**, 3.30 ppm (1H) for **2.1**, 4.56 ppm (2H) for **1.60**, and 3.24 ppm (1H) for **1.61** to the resonance at 6.67 ppm for mesitylene.

Table 4.6. Ratio of compounds in 4.6.7 – Rxn 4

Time (h)	1.59	2.1	1.60	1.61	Yield (%)
3	58	12	7	23	101
8	23	0	17	60	93
18	0	0	29	71	84

Rxn 5. Follows General Procedure D. Precursor **2.9** (6 mg, 0.02 mmol) and mesitylene (3 μ L, 0.02 mmol) in toluene- d_8 (0.5 mL, 0.04M) was heated at 110 °C for 18 h. The experiment was paused briefly at the 3 h and 8 h time points for ^1H NMR analysis. A final ratio 0:0:76:24 of **2.9**, **2.10**, **2.12**, and **2.11** was obtained in 97% yield based on internal standard. Ratios were determined by comparing the ^1H NMR resonances at 6.0 ppm (1H) for **2.9**, 5.08 ppm (1H) for **2.10**, 4.48 ppm (2H) for **2.12**, and 2.74 ppm (1H) for **2.11** to the resonance at 6.67 ppm for mesitylene.

Table 4.7. Ratio of compounds in 4.6.7 – Rxn 5

Time (h)	2.9	2.10	2.12	2.11	Yield (%)
3	14	3	72	11	127
8	0	0	76	24	95
18	0	0	76	24	97

Rxn 6. Follows General Procedure D. Precursor **2.9** (6 mg, 0.02 mmol), BHT (4 mg, 0.02 mmol), and mesitylene (3 μ L, 0.02 mmol) in toluene- d_8 (0.5 mL, 0.04M) was heated at 110 °C for 18 h. The experiment was paused briefly at the 3 h and 8 h time points for ^1H NMR analysis. A final ratio 0:0:67:33 of **2.9**, **2.10**, **2.12**, and **2.11** was obtained in 91% yield based on internal standard. Ratios were determined by comparing the ^1H NMR resonances at 6.0 ppm (1H) for **2.9**, 5.08 ppm (1H) for **2.10**, 4.48 ppm (2H) for **2.12**, and 2.74 ppm (1H) for **2.11** to the resonance at 6.67 ppm for mesitylene.

(1H) for **2.10**, 4.47 ppm (2H) for **2.12**, and 2.90 ppm (1H) for **2.11** to the resonance at 6.67 ppm for mesitylene.

Table 4.8. Ratio of compounds in 4.6.7 – Rxn 6

Time (h)	2.9	2.10	2.12	2.11	Yield (%)
3	13	56	28	2	97
8	0	0	66	34	92
18	0	0	67	33	88

Rxn 7. Follows General Procedure D. Precursor **1.50** (6 mg, 0.02 mmol) and mesitylene (3 μ L, 0.02 mmol) in toluene- d_8 (0.5 mL, 0.04M) was heated at 110 °C for 18 h. The experiment was paused briefly at the 3 h and 8 h time points for ^1H NMR analysis. A final ratio 0:0:93:7 of **1.50**, **2.13**, **2.14**, and **1.51** was obtained in 87% yield based on internal standard. Ratios were determined by comparing the ^1H NMR resonances at 5.93 ppm (1H) for **1.50**, 5.14 ppm (1H) for **2.13**, 4.47 ppm (2H) for **2.14**, and 3.17 ppm (1H) for **1.51** to the resonance at 6.67 ppm for mesitylene.

Table 4.9. Ratio of compounds in 4.6.7 – Rxn 7

Time (h)	1.50	2.13	2.14	1.51	Yield (%)
3	35	2	58	4	118
8	6	0	88	7	101
18	0	0	93	7	90

Rxn 8. Follows General Procedure D. Precursor **1.50** (6 mg, 0.02 mmol), BHT (4 mg, 0.02 mmol), and mesitylene (3 μ L, 0.02 mmol) in toluene- d_8 (0.5 mL, 0.04M) was heated at 110 °C for 18 h. The experiment was paused briefly at the 3 h and 8 h time points for ^1H NMR analysis. A final ratio 0:0:70:30 of **1.50**, **2.13**, **2.14**, and **1.51** was obtained in 91% yield based on internal standard. Ratios were determined by comparing the ^1H NMR resonances at 5.90 ppm (1H) for **1.50**, 6.65

ppm (1H) for **2.13**, 4.48 ppm (2H) for **2.14**, and 3.15 ppm (1H) for **1.51** to the resonance at 6.67 ppm for mesitylene.

Table 4.10. Ratio of compounds in 4.6.7 – Rxn 8

Time (h)	1.50	2.13	2.14	1.51	Yield (%)
3	35	32	22	11	125
8	8	11	54	27	100
18	0	0	70	30	83

Rxn 9. Follows General Procedure D. Precursor **2.5** (10 mg, 0.03 mmol) and mesitylene (3 μ L, 0.02 mmol) in *o*-DCB- d_4 (0.5 mL, 0.06M) was heated at 150 °C for 8 h. The experiment was paused briefly at the 3 h time point for ^1H NMR analysis. A final ratio 0:0:82:18 of **2.5**, **2.6**, **2.8**, and **2.7** was obtained in 93% yield based on internal standard. Ratios were determined by comparing the ^1H NMR resonances at 6.27 ppm (1H) for **2.5**, 5.94 ppm (1H) for **2.6**, 5.22 ppm (2H) for **2.8**, 3.31 ppm (1H) for **2.7** to the resonance at 6.63 ppm for mesitylene.

Table 4.11. Ratio of compounds in 4.6.7 – Rxn 9

Time (h)	2.5	2.6	2.8	2.7	Yield (%)
3	0	17	65	18	93
8	0	0	82	18	93

Rxn 10. Follows General Procedure D. Precursor **2.5** (10 mg, 0.03 mmol), BHT (7 mg, 0.03 mmol), and mesitylene (3 μ L, 0.02 mmol) in *o*-DCB- d_4 (0.5 mL, 0.06M) was heated at 150 °C for 8 h. The experiment was paused briefly at the 3 h time point for ^1H NMR analysis. A final ratio 0:0:77:23 of **2.5**, **2.6**, **2.8**, and **2.7** was obtained in 53% yield based on internal standard. Ratios were determined by comparing the ^1H NMR resonances at 6.27 ppm (1H) for **2.5**, 5.94 ppm (1H) for **2.6**, 5.22 ppm (2H) for **2.8**, 3.31 ppm (1H) for **2.7** to the resonance at 6.63 ppm for mesitylene.

Table 4.12. Ratio of compounds in 4.6.7 – Rxn 10

Time (h)	2.5	2.6	2.8	2.7	Yield (%)
3	0	17	52	31	96
8	0	0	77	23	83

4.6.8 Experiments Showing the Effect of Atmosphere

Rxn 1. A 1-mL screw-top flask with septum lid and stir bar was charged with precursor **2.19** (24 mg, 0.075 mmol) dissolved in o-dichlorobenzene (0.50 mL, 0.15 M) and sealed with a Teflon-lined septum screw cap under air. The solution was lowered into a pre-heated oil bath at 150 °C. After 2 h, the the solution was allowed to cool to room temperature, then transferred to an NMR tube for ¹H NMR analysis. Product ratios were determined by comparing the resonance integrations for starting material, adduct, oxidized product, and isomerized product from the ¹H NMR of the crude reaction solution using No-D spectroscopy. A 0:65:26:9 ratio of **2.19**, **2.20**, **2.8**, and **2.21** was obtained. Ratios were determined by comparing the ¹H NMR resonances at 4.56 ppm (1H) for **2.6**, 5.21 ppm (2H) for **2.8**, and 2.49 ppm (1H) for **2.7**. An unknown impurity identified by the resonance at 5.04 ppm exists in the starting material and persisted through the reaction to completion.

Rxn 2. A 1-mL, screw-top vial with Teflon-lined septum screw cap and stir bar was charged with precursor **2.5** (23 mg, 0.072 mmol) dissolved in o-dichlorobenzene (0.50 mL, 0.14 M). The solution was degassed by bubbling N₂ through a needle into the solution and venting through an outlet needle. The vial was lowered into a preheated oil bath at 150 °C. After 2 h, the solution was

allowed to cool to rt before being transferred to an NMR tube for analysis. Product ratios were determined by comparing the resonance integrations for starting material, adduct, oxidized product, and isomerized product from the ^1H NMR of the reaction solution using No-D spectroscopy. A 0:82:12:6 ratio of **2.5**, **2.6**, **2.8**, and **2.7** was obtained. Ratios were determined by comparing the ^1H NMR resonances at 5.93 ppm (1H) for **2.6**, 5.21 ppm (2H) for **2.8**, and 2.49 ppm (1H) for **2.7**.

Rxn 3. A flame-dried, 5-mL, single-necked, pear-shaped flask equipped with a condenser, septum, and stir bar was charged with precursor **2.5** (23 mg, 0.072 mmol) dissolved in *o*-dichlorobenzene (0.50 mL, 0.14 M). A 16-gauge needle was inserted into the septum and left open to the air. The flask was lowered into a preheated oil bath at 150 °C. After 2 h, the solution was allowed to cool to room temperature before transferred to an NMR tube for NMR analysis. Product ratios were determined by comparing the resonance integrations for starting material, adduct, oxidized product, and isomerized product from the ^1H NMR of the reaction solution using No-D spectroscopy. A 0:0:85:15 ratio of **2.5**, **2.6**, **2.8**, and **2.7** was obtained. Ratios were determined by comparing the ^1H NMR resonances at 5.21 ppm (2H) for **2.8**, and 2.49 ppm (1H) for **2.7**.

4.6.9 Experiments as Evidence for Oxygen Mediated Dehydrogenation to Oxidation

Product

Rxn 1. Follows General Procedure D. Precursor **2.5** (10 mg, 0.03 mmol) and mesitylene (3 μL , 0.02 mmol) in *o*-DCB- d_4 (0.5 mL, 0.06M) was heated at 150 °C for 8 h. The experiment was paused briefly at the 3 h time point for ^1H NMR analysis. A final ratio 0:0:82:18 of **2.5**, **2.6**, **2.8**, and **2.7** was obtained in 53% yield based on internal standard. Ratios were determined by

comparing the ^1H NMR resonances at 6.27 ppm (1H) for **2.5**, 5.94 ppm (1H) for **2.6**, 5.22 ppm (2H) for **2.8**, 3.31 ppm (1H) for **2.7** to the resonance at 6.63 ppm for mesitylene. After the reaction was completed, H_2 gas was bubbled through the solution for 2 min. and ^1H NMR was performed to observe the appearance of the resonance for H_2 gas at 4.53 ppm. The solution was then bubbled through with argon gas for 2 min. and ^1H NMR was performed to observe the disappearance of the resonance for H_2 gas at 4.53 ppm.

Table 4.13. Ratio of compounds in 4.6.9 – Rxn 1

Time (h)	2.5	2.6	2.8	2.7	Yield (%)
3	0	17	65	18	93
8	0	0	82	18	93

Rxn 2. A 1-mL, flame-dried, microwave vial with stir bar was charged with precursor **2.5** (20 mg, 0.063 mmol) dissolved in o-dichlorobenzene (0.50 mL, 0.13 M). The vial was sealed with a crimp cap with Teflon-lined septum, wrapped in parafilm at the top, and lowered into a pre-heated oil bath at 150 °C. After 90 min, the solution was allowed to cool to room temperature before transferred to an NMR tube for NMR analysis. Product ratios were determined by comparing the resonance integrations for starting material, adduct, oxidized product, and isomerized product from the ^1H NMR of the crude reaction solution using No-D spectroscopy. A 0:41:39:20 ratio of **2.5**, **2.6**, **2.8**, and **2.7** was obtained. Ratios were determined by comparing the ^1H NMR resonances at 5.45 ppm (1H) for **2.6**, 5.21 ppm (2H) for **2.8**, and 2.79 ppm (1H) for **2.7**.

Rxn 3. A 1-mL, flame-dried, microwave vial with stir bar was charged with precursor **2.19** (24 mg, 0.075 mmol) dissolved in o-dichlorobenzene (0.50 mL, 0.15 M). The vial was sealed with a

crimp cap with Teflon-lined septum, wrapped in parafilm at the top, and lowered into a pre-heated oil bath at 150 °C. After 90 min, the solution was allowed to cool to room temperature before transferred to an NMR tube for NMR analysis. Product ratios were determined by comparing the resonance integrations for starting material, adduct, oxidized product, and isomerized product from the ¹H NMR of the crude reaction solution using No-D spectroscopy. A 0:77:18:5 ratio of **2.19**, **2.20**, **2.8**, and **2.21** was obtained. Ratios were determined by comparing the ¹H NMR resonances at 4.53 ppm (1H) for **2.20**, 5.21 ppm (2H) for **2.8**, and 3.09 ppm (1H) for **2.21**.

4.6.10 Experiments as Evidence for Ionic Isomerization to Isomerization Product

Rxn 1. Follows General Procedure D. Precursor **2.5** (10 mg, 0.032 mmol) and D₂O (0.050 mL, 2.8 mmol) in DMF (0.45 mL, 0.60 M) was heated at 150 °C for 180 min. A 0:0:9:91 ratio of **2.5**, **2.6**, **2.8** and **4.1** was obtained in 50% yield. Ratios were determined by comparing the ¹H NMR resonances at 5.46 ppm (2H) for **2.8**, and 2.81 ppm (1H) for **2.7**. Deuterium incorporation was determined by comparing the integral intensities of resonances at 3.70 ppm and at 2.82 ppm. The isomerization product was observed to have 76% deuterium incorporation evidenced by the resonance at 2.82 ppm.

Rxn 2. A 2-mL, oven-dried microwave vial with stir bar was charged with **1.59** (15 mg, 0.06 mmol) in toluene (1207 µL) under an atmosphere of air. D₂O (64 µL, 3.2 mmol) was added via syringe to form a biphasic mixture. The vial was sealed with a Teflon-lined septum crimp cap and lowered into an oil bath preheated to 110 °C. After 18 h, the solution was allowed to cool to rt and concentrated by rotary evaporation. The residue was purified by silica gel flash column chromatography (40% EtOAc/Hex) to yield an 83:17 ratio of **1.60** to **4.3** (8 mg, 53%) with

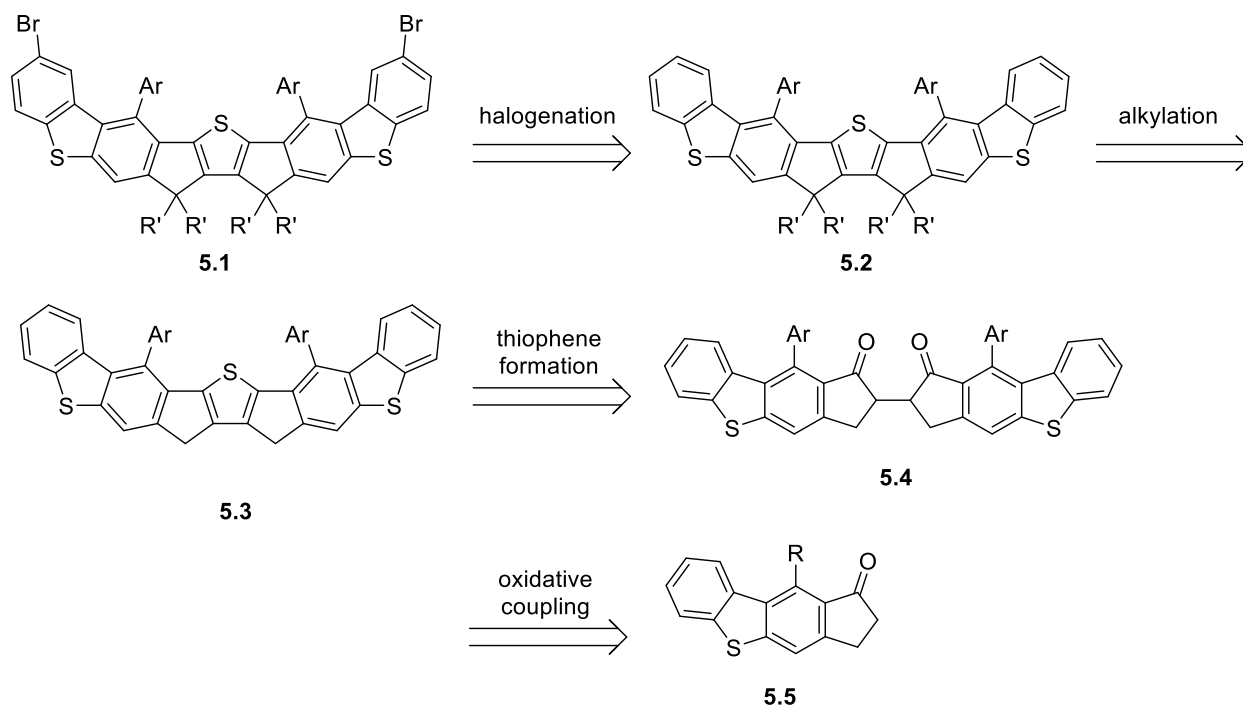
recovered starting material (4 mg, 27%). Deuterium incorporation was determined by comparing the integral intensities of resonances at 3.15 ppm, 2.70 ppm, and 4.72 ppm. The isomerization product was observed to have 53% deuterium incorporation evidenced by the resonance at 3.15 ppm and 40% for the proton at 2.70 ppm.

5.0 Application of the Dearomative DDDA Reaction Towards the Synthesis of Organic Solar Cell Materials

Recently, interest has grown in the application of heteroarenes towards ladder-type conjugated ring systems as materials for organic photovoltaic solar cells. Multi-fused ladder-type arenes have recently reached record-breaking power conversion efficiencies (PCE) in organic photovoltaic solar-cells.¹⁶ We sought to apply our dearomative DDDA reaction to the generation of uniquely substituted ladder-type arenes.

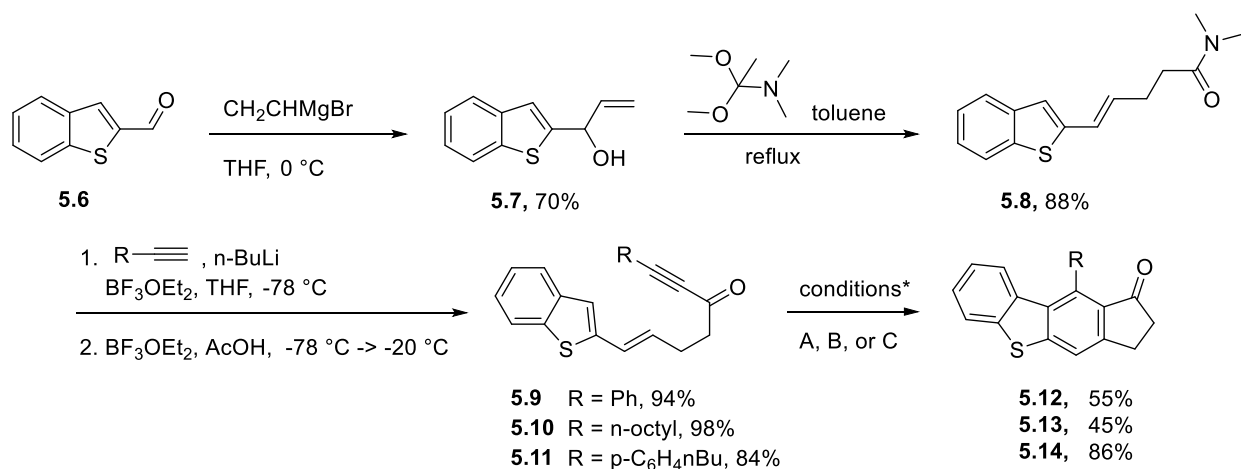
5.1 Synthesis of Dearomative DDDA Reaction Oxidation Product via Ketone-Tethered Precursors

We proposed accessing these ladder-type arenes for organic solar cells via the oxidation product of the dearomative DDDA reaction. Halogenation of the external benzene rings of the ladder-type arene would afford a handle for polymerization or functionalization. Dialkylation of the methylene carbons on the arene would increase solubility while formation of the ladder-type arene would be accomplished by thiophene formation via the 1,4-diketone. Synthesis of the 1,4-diketone would be accomplished by the oxidative coupling of oxidation product from the dearomative DDDA reaction of ketone-tethered precursor affording a 2-cyclopentenone rather than the lactone afforded from ester-tethered precursors.



Scheme 5.1. Retrosynthetic route for organic solar cell materials via the dearomative DDDA oxidation product

To this end, we set out to test the feasibility of the dearomative DDDA reaction as a way to access the oxidation product **5.5**. Benzo[*b*]thiophene-2-carbaldehyde **5.6** was subjected to Grignard reaction with vinyl magnesium bromide to afford allyl alcohol **5.7** in 70% yield. Reaction of allyl alcohol **5.7** to the Eschenmoser-Claisen rearrangement afforded the amide **5.8** in 88% yield. Reaction of amide **5.8** with the appropriate alkyne affords dearomative DDDA precursors **5.9** in 94% yield, **5.10** in 98% yield, and **5.11** in 86% yield.



* A = 1:1 nitrobenzene:*o*-DCB, sealed, under air, 225 °C, 3 min, to afford **5.12**; B = *o*-DCB, open to air, 150 °C, 48h, to afford **5.13**; C = *o*-DCB, open to air, 130 °C, 24h, to afford **5.14**

Scheme 5.2. Synthesis of dearomative DDDA reaction oxidation product via the ketone-tethered precursors

5.9 was heated via microwave irradiation for 3 min at 225 °C in 50% v/v nitrobenzene/*o*-DCB to afford exclusively the oxidation product **5.12** in 55% yield. The nitrobenzene was difficult to separate from **5.12** in the purification step, thus other conditions were employed for formation of **5.13** and **5.14**. Oxidation product **5.12** was extremely insoluble in a number of solvents, i.e., hexanes, acetonitrile, and methanol, thus, was not taken on to the oxidative coupling reaction. To access a more soluble oxidation product from the dearomative DDDA reaction, precursors **5.10** and **5.11** were prepared. **5.10** heated for 48 h at 150 °C in *o*-DCB, open to air, afforded oxidation product **5.13** in 45% yield. The nitrobenzene was difficult to separate from product **5.12** in purification, thus the slower conditions incorporating bubbled air were employed for formation of **5.13**. Precursor **5.11** heated for 24 h at 130 °C in *o*-DCB, open to air, afforded oxidation product **5.14** in 84% yield.

The synthesis of oxidation products **5.13** and **5.14** from the dearomative DDDA reaction was accomplished with complete selectivity. Enhanced selectivity for oxidation product was

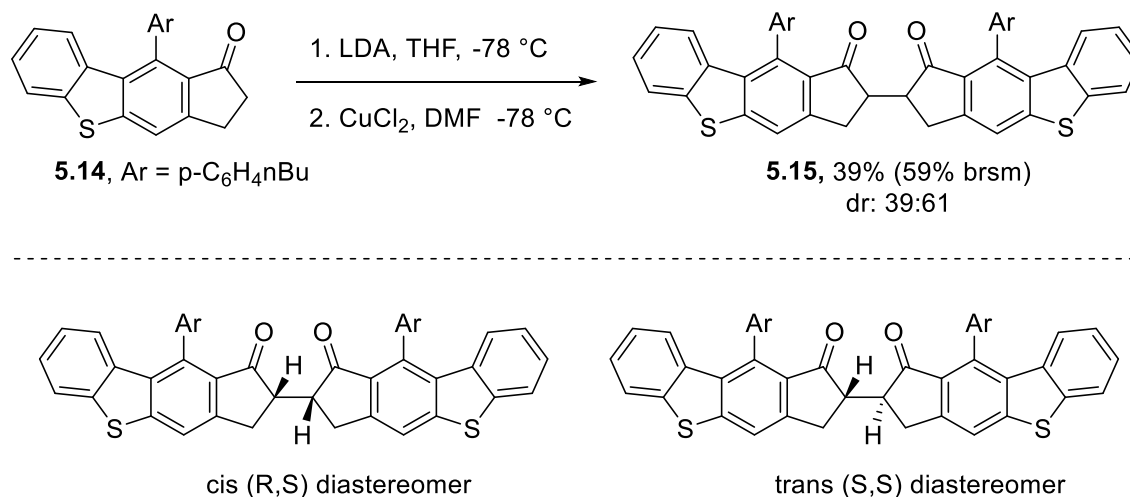
obtained through our new knowledge of the reaction conditions that affect product selectivity. Reaction conditions employed lower temperatures, a relatively non-polar solvent, and increased exposure to air via continuous bubbling through the reaction solution.

5.2 Progress Towards the Synthesis of Ladder-Type Arene Materials for Organic Solar Cells

With oxidation product in hand, our next steps were to apply our product of the dearomative DDDA reaction to the formation of a multi-fused ladder-type arene with conjugation across multiple rings. Oxidative coupling with phenyl substituted **5.12** and alkyl substituted **5.13** was unsuccessful as **5.12** proved insoluble in multiple solvents and reaction of **5.13** led to decomposition and retention of starting material. The insolubility of **5.12** may be due to favorable self-coordination because of strong intermolecular π - π dispersion interactions between aromatic rings. The decomposition of **5.13** under the basic reaction conditions may be due to competing deprotonation at the α position of the alkyl chain rather than desired deprotonation at the alpha position of the cyclopentenone. Evidence for the acidity of the protons at the α position of the alkyl chain can be observed in the ^1H NMR of **5.13** (see appendix B) where the resonance for those protons is shifted downfield to 3.8 ppm due to anisotropy effects from the nearby carbonyl. The resonance is also broadened, potentially due to tautomerization to the enol effecting an exchange broadening.

Oxidative coupling of **5.14** with LDA and CuCl_2 afforded **5.15** in 39% yield (59% based on recovered starting material, Scheme 5.3). Starting material **5.14** was recovered even when 5 equivalents of LDA and CuCl_2 were utilized. Optimization of this step would be vital to the make

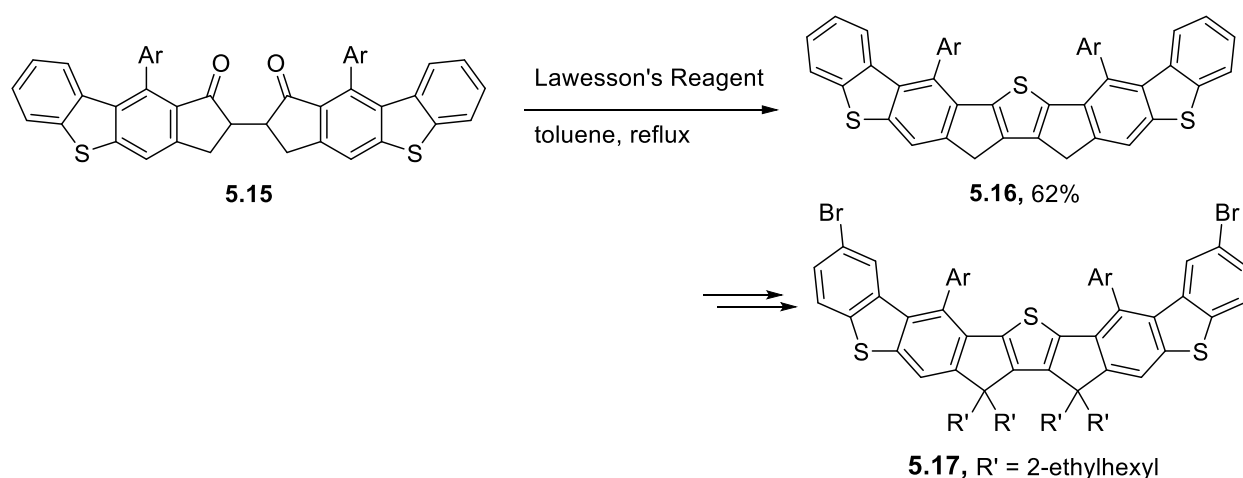
this synthetic route pragmatic. Cis and trans diastereomers of **5.15** for the protons α to the ketones (Scheme 5.3) were isolated and characterized separately as they were separable by flash column chromatography with an afforded diastereomeric ratio (dr) of 39:61. In literature, the diastereomer oxidative coupling products of 1-indanone are identified but not reported as separable, and they are instead characterized as a mixture.^{65, 66} The cis (R,S) and trans (S,S) stereochemistry for the two diastereomers of **5.15** was not determined or assigned between the isolated products. Determination of stereochemistry may be possible in the future as the cis diastereomer is a meso compound, thus optically inactive, and should be distinguishable from the optically active trans diastereomer via polarimetry. Recrystallization of the isolated diastereomers has not been attempted, thus far, but may also possible as both were isolated as solids. Determination of stereochemistry could then be conducted via x-ray crystallography.



Scheme 5.3. Oxidative coupling of DA oxidation product with dr of 39:61

Reaction of **5.15** with Lawesson's reagent to afford the ladder-type arene **5.16** was performed separately for both diastereomers. The major diastereomer of **5.15** when reacted with

Lawesson's reagent in refluxing toluene afforded the ladder-type arene **5.16** in 62% yield (Scheme 5.4). The minor diastereomer of **5.15**, when reacted under the same conditions, did not afford any formation of product **5.16**, but 69% of the starting material **5.15** was recovered. It has yet to be determined as to why the minor diastereomer did not afford product under the same conditions that were successful for the major diastereomer. Recrystallization of **5.16** was attempted by dissolving in a minimal amount of dichloromethane, followed by dilution with n-heptane, and monitoring for crystal formation over the course of days at room temperature and at 0 °C in the laboratory freezer. All recrystallization attempts thus far have been unsuccessful.



Scheme 5.4. Synthesis of the polycyclic ladder-type arene with Lawesson's reagent

Future steps include alkylation of the methylene carbons to increase solubility of the product **5.17** followed by halogenation of the external benzene rings to provide handles for future functionalization or polymerization reactions. Once the feasibility of these future steps is established, Prof. Hutchison from the University of Pittsburgh will assist with a target selection process utilizing computational examination of a wide array of virtual compounds accessible using the proposed dearomative DDDA chemistry.

5.3 Conclusions

We established the dearomative DDDA reaction of vinyl heteroarenes as a key step in the synthesis of novel multi-ring ladder-type arenes which may be used as photovoltaic materials for organic solar cells. The ladder-type arene was successfully synthesized via oxidative coupling and thiophene formation from the oxidation product of the dearomative DDDA reaction. Oxidation product of the ketone-tethered precursor was generated selectively through mild manipulation of the reaction parameters as discovered in our studies. We hope that these novel, linearly fused ladder-type structures will enhance our understanding of photovoltaic materials and lead to improved efficiency in organic solar cells.

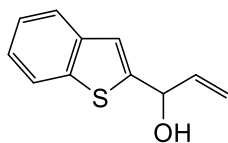
5.4 Experimental

5.4.1 General Methods

Unless otherwise indicated, all reactions were performed in flame-dried glassware under an air atmosphere and stirred with Teflon-coated magnetic stir bars. All commercially available compounds were purchased and used as received unless otherwise specified. Tetrahydrofuran (THF), diethyl ether (Et₂O), and dichloromethane (DCM) were purified by passing through alumina using a Sol-Tek ST-002 solvent purification system. Deuterated chloroform (CDCl₃) was dried over 4Å molecular sieves. Nitrogen gas was purchased from Matheson Tri Gas. Conventional heating was used for reactions that were monitored by ¹H NMR or performed open to the air. All microwave-mediated reactions were carried out using a Biotage Initiator Exp or Anton-Paar

Monowave 300 microwave synthesizer. Purification of the compounds by flash column chromatography was performed using silica gel (40-63 μm particle size, 60 Å pore size). TLC analyses were performed on silica gel F₂₅₄ glass plates (250 μm thickness). ¹H NMR and ¹³C NMR spectra were recorded on Bruker Avance 300, 400, or 500 MHz spectrometers. Spectra were referenced to residual chloroform (7.26 ppm, ¹H; 77.16 ppm, ¹³C) or *o*-dichlorobenzene (6.93 ppm, ¹H; 130.04 ¹³C) unless otherwise specified. Chemical shifts are reported in ppm, multiplicities are indicated by s (singlet), d (doublet), t (triplet), q (quartet), p (pentet), m (multiplet), and bs (broad singlet). Coupling constants, *J*, are reported in hertz (Hz). All NMR spectra were obtained at room temperature. IR spectra were obtained using a Nicolet Avatar E.S.P. 360 FT-IR. EI mass spectroscopy was performed on a Waters Micromass GCT high resolution mass spectrometer, while ES mass spectroscopy was performed on a Waters Q-TOF Ultima API, Micromass UK Limited high-resolution mass spectrometer.

5.4.2 Synthesis of a Multi-Ring Ladder-Type Heteroarene



1-(benzo[b]thiophen-2-yl)prop-2-en-1-ol (5.7). A flame-dried, single-necked, 100-mL, round-bottomed flask equipped with a stir bar, septum, and a nitrogen inlet adaptor was charged with benzo[b]thiophene-2-carboxaldehyde (500 mg, 3.08 mmol) dissolved in THF (37.8 mL, 0.08 M) via syringe. The flask was placed in an ice/water bath (0 °C) and after 5 min, vinyl magnesium bromide (6.2 mL of a 1 M solution in THF, 6.16 mmol) was added dropwise by syringe. The solution was allowed to warm to rt over 1 h. After the complete disappearance of starting material

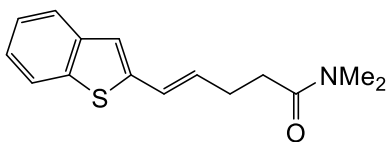
as observed by TLC, sat'd aqueous ammonium chloride (10.0 mL) was added to the flask all at once. The mixture was transferred to a separatory funnel, the layers separated, and the aqueous phase was extracted with ethyl acetate (10 mL x 3). The combined organic phase was washed with brine (10 mL), dried over magnesium sulfate, gravity filtered, and concentrated using rotary evaporation. The resulting brown oil was purified by flash column chromatography (20% ethyl acetate/hexanes) to yield the title compound as a yellow liquid (407 mg, 70%). Compound **5.7** was previously prepared by Wang et al.⁶⁷ Characterization data corresponds to the literature.

Data 5.7

¹H NMR (300 MHz, CDCl₃)

7.82 (dd, $J = 7.4, 1.6$ Hz, 1H), 7.73 (dd, $J = 6.4, 2.0$ Hz, 1H), 7.37-7.27 (m, 2H), 7.21 (s, 1H), 6.23-6.12 (m, 1H), 5.54-5.43 (m, 2H), 5.31 (d, $J = 10.4$, 1H), 2.26 (t, $J = 4.5$ Hz, 1H) ppm. EtOAc impurity at 4.12, 2.05, and 1.25 ppm.

TLC $R_f = 0.57$ (40% ethyl acetate/hexanes) [silica gel, UV]



(E)-5-(benzo[b]thiophen-2-yl)-*N,N*-dimethylpent-4-enamide (5.8). A flame-dried, two-necked, 50-mL, round-bottomed flask equipped with a stir bar, septum, condenser, and a nitrogen inlet adaptor was charged with allyl alcohol **5.7** (780 mg, 4.10 mmol) dissolved in toluene (16.0 mL, 0.26 M) via syringe. *N,N*-dimethylacetamide dimethyl acetal (1.5 mL, 10.26 mmol) was added via syringe in one portion. The flask was placed in an oil bath at 115 °C, and the solution was heated to reflux for 2 h until the complete disappearance of starting material was observed by TLC. The

flask was removed from the oil bath and the solution was allowed to cool to rt. The solution was concentrated under rotary evaporation. The resulting oil was purified by flash column chromatography (80% ethyl acetate/hexanes) to yield the title compound as a light-yellow solid (935 mg, 88%).

Data 5.8

¹H NMR (300 MHz, CDCl₃)
7.76-7.70 (m, 1H), 7.67-7.61 (m, 1H), 7.32-7.22 (m, 2H), 7.06 (s, 1H), 6.66 (d, *J* = 15.4 Hz, 1H), 6.19 (dt, *J* = 15.5, 6.8 Hz, 1H), 2.99 (d, *J* = 13.5 Hz, 6H), 2.63-2.45 (m, 4H) ppm. DCM impurity at 5.30 ppm.

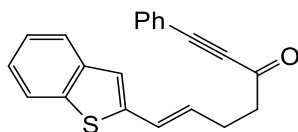
¹³C NMR (75 MHz, CDCl₃)
172.0, 142.9, 140.3, 138.7, 132.4, 124.8, 124.5, 124.4, 123.3, 122.2, 121.7, 37.3, 35.6, 32.9, 28.6 ppm

IR (thin film)
2926, 1777, 1643, 1494, 1401, 1264, 1141, 955, 749 cm⁻¹

HRMS (FTMS + p ESI)
[M + H]⁺ Calcd for C₁₅H₁₈ONS 260.1104; Found 260.1098

TLC *R_f* = 0.30 (80% ethyl acetate/hexanes) [silica gel, UV]

MP 88.0 – 91.6 °C



(E)-7-(benzo[b]thiophen-2-yl)-1-phenylhept-6-en-1-yn-3-one (5.9). A flame-dried, 25-mL, round-bottomed, single-necked flask equipped with stir bar, septum, and a nitrogen inlet adapter was charged with phenylacetylene (0.31 mL, 2.85 mmol) followed by THF (5.0 mL) via syringe. The flask was placed in a dry ice/acetone bath (-78 °C). After 10 min, n-butyllithium (1.58 mL of a 1.6 M solution in hexanes, 2.53 mmol) was added via syringe in one portion. After 5 min, boron trifluoride diethyl etherate (0.33 mL, 2.69 mmol) was added via syringe in one portion. After 15 min, amide **5.8** (410 mg, 1.58 mmol) diluted in THF (5 mL) was added in one portion via syringe. Upon disappearance of starting material as observed by TLC, a second portion of boron trifluoride diethyl etherate (0.33 mL, 2.53 mmol) was added followed by acetic acid (0.15 mL, 2.69 mmol), each were added via syringe in a single portion. The solution was allowed to warm in a brine/ice bath to -20 °C over the course of 1 h. Sat'd. aqueous ammonium chloride (8 mL) was added in one portion and the mixture was transferred to a separatory funnel. The aqueous layer was extracted with ethyl acetate (8 mL x 3). The combined organic layers were dried over magnesium sulfate, gravity filtered, and concentrated under rotary evaporation. The resulting brown oil was purified by flash column chromatography (20% ethyl acetate/hexanes) to yield the title compound as a brown oil (471 mg, 94%).

Data 5.9

¹H NMR (300 MHz, CDCl₃)

7.73 (dd, *J* = 3.0, 6.6 Hz, 1H), 7.66 (dd, *J* = 2.4, 5.8 Hz, 1H), 7.59 (dt, *J* = 1.5, 7.0 Hz, 2H), 7.50-7.35 (m, 3H), 7.33-7.24 (m, 2H), 7.08 (s, 1H), 6.69 (d, *J* = 15.5 Hz, 1H), 6.7 (dt, *J* = 6.9, 15.6 Hz, 1H), 2.89 (t, *J* = 7.2 Hz, 2H), 2.67 (q, *J* = 7.5 Hz, 2H) ppm. Water impurity at 1.57 ppm.

¹³C NMR (75 MHz, CDCl₃)

186.8, 142.6, 140.2, 138.8, 133.2 (2C), 130.9 (2C), 128.8 (2C), 125.3, 124.6, 124.5, 123.4, 122.3, 122.0, 120.0, 91.4, 87.9, 44.8, 27.4 ppm

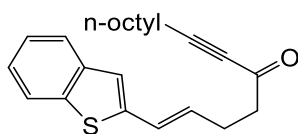
IR (thin film)

3403, 3058, 2925, 2200, 1708, 1671, 1582, 1449, 1320, 1272, 1098, 752, 696 cm⁻¹

HRMS (FTMS + p ESI)

[M + H]⁺ Calcd for C₂₁H₁₇OS 317.0994; Found 317.0986

TLC *R*_f = 0.77 (40% ethyl acetate/hexanes) [silica gel, UV]

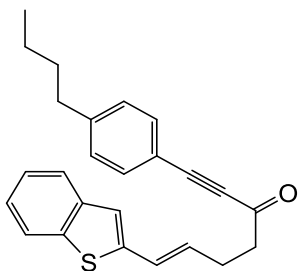


(E)-1-(benzo[b]thiophen-2-yl)pentadec-1-en-6-yn-5-one (5.10). A flame-dried, 25-mL, round-bottomed, single-necked flask equipped with stir bar, septum, and a nitrogen needle inlet was charged with 1-decyne (0.38 mL, 2.03 mmol) followed by THF (3.8 mL) via syringe. The flask was placed in a dry ice/acetone bath (-78 °C). After 10 min, n-butyllithium (1.16 mL of a 1.6 M solution in hexanes, 1.80 mmol) was added via syringe in one portion. After 5 min, boron trifluoride diethyl etherate (0.24 mL, 1.91 mmol) was added via syringe in one portion. After 15 min, amide **5.8** (292 mg, 1.13 mmol) diluted in THF (3.8 mL) was added in one portion via syringe. Upon disappearance of starting material as observed by TLC, a second portion of boron trifluoride diethyl etherate (0.24 mL, 1.91 mmol) was added followed by acetic acid (0.12 mL, 1.91 mmol), each were added via syringe in a single portion. The solution was allowed to warm in a brine/ice bath to -20 °C over the course of 1 h. Sat'd. aqueous ammonium chloride (8 mL) was added in one portion and the mixture was transferred to a separatory funnel. The aqueous layer was extracted

with ethyl acetate (8 mL x 3). The combined organic layers were dried over magnesium sulfate, gravity filtered, and concentrated under rotary evaporation. The resulting oil was purified by flash column chromatography (20% ethyl acetate/hexanes) to yield the title compound as a yellow solid (388 mg, 98%).

Data 5.10

<u>¹H NMR</u>	(500 MHz, CDCl ₃) 7.73 (dd, <i>J</i> = 1.1, 7.4 Hz, 1H), 7.65 (dd, <i>J</i> = 1.7, 6.7 Hz, 1H), 7.31-7.25 (m, 2H), 7.06 (s, 1H), 6.65 (d, <i>J</i> = 15.7 Hz, 1H), 6.13 (dt, <i>J</i> = 6.8, 15.4 Hz, 1H), 2.74 (t, <i>J</i> = 7.3 Hz, 2H), 2.59 (q, <i>J</i> = 6.9 Hz, 2H), 2.37 (t, <i>J</i> = 7.2 Hz, 2H), 1.58 (quint, <i>J</i> = 7.2 Hz, 2H), 1.40 (quint, <i>J</i> = 7.6 Hz, 2H), 1.32-1.25 (m, 9H), 0.89 (t, <i>J</i> = 6.6 Hz, 3H) ppm. EtOAc impurity at 4.12 and 2.05 ppm.
<u>¹³C NMR</u>	(125 MHz, CDCl ₃) 187.0, 142.7, 140.3, 138.8, 131.1, 125.2, 124.6, 124.5, 123.4, 122.3, 121.9, 95.3, 81.0, 44.8, 31.9, 29.2, 29.1, 29.0, 27.9, 27.4, 22.8, 19.1, 14.2 ppm
<u>IR</u>	(thin film) 2924, 2855, 2210, 1671, 1434, 1307, 1238, 1155, 953, 808, 745, 724, 674 cm ⁻¹
<u>HRMS</u>	(FTMS + p ESI) [M + H] ⁺ Calcd for C ₂₃ H ₂₉ OS 353.1934; Found 353.1926
<u>TLC</u>	<i>R_f</i> = 0.72 (40% ethyl acetate/hexanes) [silica gel, UV]
<u>MP</u>	35.9 – 37.1 °C



(E)-7-(benzo[b]thiophen-2-yl)-1-(4-butylphenyl)hept-6-en-1-yn-3-one (5.11). A flame-dried, 25-mL, round-bottomed, single-necked flask equipped with stir bar, septum, and a nitrogen inlet adapter was charged with 1-butyl-4-ethynylbenzene (0.36 mL, 2.08 mmol) followed by THF (4.5 mL) via syringe. The flask was placed in a dry ice/acetone bath (-78 °C). After 10 min, n-butyllithium (1.6 mL of a 1.6 M solution in hexanes, 1.85 mmol) was added via syringe in one portion. After 5 min, boron trifluoride diethyl etherate (0.24 mL, 1.97 mmol) was added via syringe in one portion. After 15 min, amide **5.8** (300 mg, 1.16 mmol) diluted in THF (4.5 mL) was added in one portion via syringe. Upon disappearance of starting material as observed by TLC, a second portion of boron trifluoride diethyl etherate (0.24 mL, 1.97 mmol) was added followed by acetic acid (0.12 mL, 1.97 mmol), each were added via syringe in a single portion. The solution was allowed to warm in a brine/ice bath to -20 °C over the course of 1 h. Sat'd. aqueous ammonium chloride (8 mL) was added in one portion and the mixture was transferred to a separatory funnel. The aqueous layer was extracted with ethyl acetate (8 mL x 3). The combined organic layers were dried over magnesium sulfate, gravity filtered, and concentrated under rotary evaporation. The resulting oil was purified by flash column chromatography (10% ethyl acetate/hexanes) to yield the title compound as a yellow liquid (361 mg, 84%).

Data 5.11

¹H NMR (400 MHz, CDCl₃)

7.74 (dd, $J = 1.7, 7.0$ Hz, 1H), 7.66 (dd, $J = 1.8, 6.4$ Hz, 1H), 7.50 (d, $J = 8.2$ Hz, 2H), 7.32-7.24 (m, 2H), 7.20 (d, $J = 8.1$ Hz, 2H), 7.07 (s, 1H), 6.69 (d, $J = 15.6$ Hz, 1H), 6.17 (dt, $J = 6.8, 15.4$ Hz, 1H), 2.88 (t, $J = 7.3$ Hz, 2H), 2.66 (q, $J = 7.9$ Hz, 4H), 1.64-1.56 (m, 2H), 1.40-1.30 (m, 2H), 0.93 (t, $J = 7.4$ Hz, 3H) ppm

^{13}C NMR (100 MHz, CDCl_3)

186.9, 146.6, 142.7, 140.2, 138.8, 133.3 (2C), 131.0, 128.9 (2C), 125.3, 124.6, 124.5, 123.4, 122.3, 122.0, 117.0, 92.2, 87.7, 44.8, 35.9, 33.3, 27.4, 22.4, 14.0 ppm

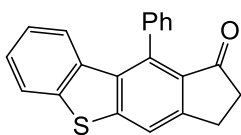
IR (thin film)

3402, 3057, 2926, 2859, 2200, 1709, 1671, 1581, 1449, 1321, 1272, 1099, 753, 695 cm^{-1}

HRMS (TOF MS ES+)

$[\text{M} + \text{H}]^+$ Calcd for $\text{C}_{25}\text{H}_{25}\text{OS}$ 373.1626; Found 373.1630

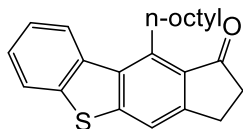
TLC $R_f = 0.37$ (10% ethyl acetate/hexanes) [silica gel, UV]



10-phenyl-2,3-dihydro-1H-benzo[b]indeno[5,6-d]thiophen-1-one (5.12). An oven-dried, 20-mL microwave vial with stir bar was charged with **5.9** (451 mg, 1.43 mmol) dissolved in a 1:1 solution of nitrobenzene : *o*-DCB (20 mL). The vial was sealed with a Teflon-lined septum crimp cap and the solution was heated to 225 °C in a Biotage Initiator microwave reactor for 3 min. The solution was then allowed to cool to room temperature before being transferred directly to a silica gel column for flash column chromatography (100% hexanes, followed by 100% ethyl acetate). The title compound was afforded as a red solid (246 mg, 55%).

Data 5.12

<u>¹H NMR</u>	(300 MHz, CDCl ₃) 7.93 (s, 1H), 7.78 (d, <i>J</i> = 8.0 Hz 1H), 7.57 (t, <i>J</i> = 3.5 Hz, 3H), 7.38-7.31 (m 3H), 7.09-7.02 (m, 1H), 6.74 (d, <i>J</i> = 8.3 Hz, 1H), 3.29-3.22 (m, 2H), 2.76-2.70 (m, 2H) ppm. DCM impurity at 5.30 ppm. Impurities at 2.5 – 0.7 ppm.
<u>¹³C NMR</u>	(75 MHz, CDCl ₃) 205.0, 152.5, 146.9, 139.6, 137.7, 137.3, 135.5, 133.4, 131.4, 129.0 (2C), 128.4 (2C), 128.2, 126.8, 125.4, 124.5, 122.7, 119.6, 37.6, 25.0 ppm
<u>IR</u>	(thin film) 3064, 2859, 1703, 1580, 1494, 1428, 1323, 1237, 1183, 1117, 1032, 851, 739, 695, 520 cm ⁻¹
<u>HRMS</u>	(FTMS + p ESI) [M + H] ⁺ Calcd for C ₂₁ H ₁₅ OS 315.0838; Found 315.0834
<u>TLC</u>	<i>R</i> _f = 0.54 (40% ethyl acetate/hexanes) [silica gel, UV]
<u>MP</u>	Decomposes to black residue 258.2 – 261.3 °C



10-octyl-2,3-dihydro-1H-benzo[b]indeno[5,6-d]thiophen-1-one (5.13). An oven-dried single-necked, 5-mL, round-bottomed flask with stir bar, condenser, and septum was charged with **5.10** (20 mg, 0.06 mmol) dissolved in o-dichlorobenzene (0.5 mL). A 16-gauge needle was inserted into the septum and left open to the air. The flask was lowered into a preheated oil bath at 150 °C.

and stirred for 2 days. Upon disappearance of starting material as observed by TLC, the solution was allowed to cool to room temperature. The crude solution was transferred directly to a silica gel column and purified by flash column chromatography (80% dichloromethane/hexanes) to yield the title compound as an orange solid (9 mg, 45%).

Data 5.13

¹H NMR (400 MHz, CDCl₃)
8.31 (dd, *J* = 1.5, 6.8 Hz, 1H), 7.84 (dd, *J* = 1.9, 6.8 Hz, 1H), 7.71 (s, 1H), 7.52-7.44 (m, 2H), 3.79 (bs, 2H), 3.15 (t, *J* = 6.0 Hz, 2H), 2.76 (t, *J* = 6.7 Hz, 2H), 1.79-1.70 (quint, *J* = 8.0 Hz, 2H), 1.62 (quint, *J* = 7.4 Hz, 2H), 1.45-1.25 (m, 9H), 0.89 (t, *J* = 7.0 Hz, 3H) ppm

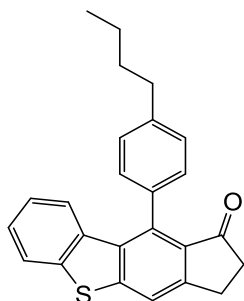
¹³C NMR (125 MHz, CDCl₃)
207.1, 153.1, 147.2, 142.2, 139.6, 135.7, 133.2, 131.1, 126.4, 125.3, 125.0, 123.1, 117.9, 37.9, 32.0, 30.2, 29.6, 29.4, 29.3, 27.8, 24.7, 22.8, 14.3 ppm

IR (thin film)
2923, 2854, 2211, 1699, 1583, 1449, 1325, 1226, 1143, 1081, 1035, 953, 856, 740
506 cm⁻¹

HRMS
(FTMS + p ESI)
[M + H]⁺ Calcd for C₂₃H₂₇OS 351.1777; Found 351.1770

TLC *R_f* = 0.48 (80% dichloromethane/hexanes) [silica gel, UV]

MP 87.5 – 89.5 °C



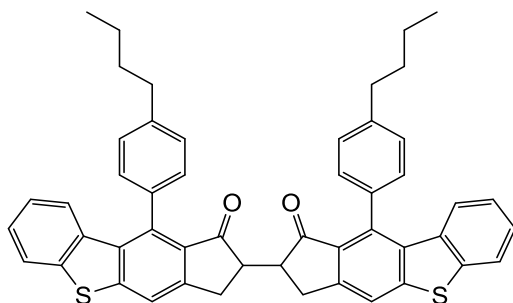
10-(4-butylphenyl)-2,3-dihydro-1H-benzo[b]indeno[5,6-d]thiophen-1-one (5.14). An oven-dried single-necked, 25-mL, round-bottomed flask with stir bar, condenser, and septum was charged with **5.11** (305 mg, 0.82 mmol) dissolved in *o*-dichlorobenzene (18.0 mL). A 16-gauge needle was inserted into the septum and left open to the air. The flask was lowered into a preheated oil bath at 130 °C and heated for 24 h. Upon disappearance of starting material as observed by TLC, the solution was allowed to cool to room temperature. The *o*-DCB solvent was removed by adding the solution to a silica gel plug and flushing the plug with hexanes. The crude product was then removed from the silica plug with ethyl acetate. The crude product dissolved in ethyl acetate was concentrated under rotary evaporation. The resulting crude solid was purified by flash column chromatography (10% ethyl acetate/hexanes) to yield the title compound as a yellow solid (260 mg, 86%).

Data 5.14

¹H NMR (500 MHz, CDCl₃)

7.91 (s, 1H), 7.77 (d, *J* = 8.0 Hz, 1H), 7.37 (d, *J* = 7.9 Hz, 2H), 7.34 (dt, *J* = 0.9, 7.3 Hz, 1H), 7.24 (d, *J* = 8.1 Hz, 2H), 7.04 (dt, *J* = 1.2, 7.8 Hz, 1H), 6.74 (d, *J* = 8.3 Hz, 1H), 3.25 (t, *J* = 6.0 Hz, 2H), 2.79 (t, *J* = 7.6 Hz, 2H), 2.74-2.71 (m, 2H), 1.79-1.72 (m, 2H), 1.50-1.42 (m, 2H), 1.00 (t, *J* = 7.3 Hz, 3H) ppm. Impurities at 2.9, 2.4, and 1.2 ppm.

<u>¹³C NMR</u>	(125 MHz, CDCl ₃) 205.1, 152.5, 146.8, 142.7, 139.6, 138.1, 135.7, 134.5, 133.6, 131.5, 129.1 (2C), 128.1 (2C), 126.7, 125.5, 124.4, 122.7, 119.5, 37.6, 35.7, 33.6, 25.0, 22.5, 14.2 ppm
<u>IR</u>	(thin film) 3055, 2926, 2858, 1709, 1580, 1432, 1321, 1182, 1117, 1030, 857, 774, 743 cm ⁻¹
<u>HRMS</u>	(TOF MS ES+) [M + H] ⁺ Calcd for C ₂₅ H ₂₃ OS 371.1470; Found 371.1448
<u>TLC</u>	R _f = 0.16 (10% ethyl acetate/hexanes) [silica gel, UV]
<u>MP</u>	132.4 – 135.3 °C



10,10'-bis(4-butylphenyl)-2,2',3,3'-tetrahydro-1H,1'H-[2,2'-bibenzo[b]indeno[5,6-d]thiophene]-1,1'-dione (5.15). A flame-dried single-necked, 25-mL, round-bottomed flask with stir bar, septum, and a nitrogen inlet needle was charged with THF (1.7 mL), lowered into a dry ice/acetone bath, and cooled for 5 min. LDA (1.35 mL, 1 M in hexanes/THF) was added to the solution dropwise by syringe. **5.14** (100 mg, 0.27 mmol) dissolved in THF (2.0 mL), in a separate round-bottomed flask under nitrogen, was cannulated to the LDA solution dropwise via syringe. The solution was maintained at -78 °C for 30 min. Copper(II) chloride (182 mg, 1.35 mmol) dissolved in distilled DMF (4.6 mL), in a separate round-bottomed flask under nitrogen, was cannulated to the reaction solution dropwise via syringe. The solution was maintained at -78 °C for

an additional 1 h. The reaction solution was then cannulated to sat. aqueous ammonium chloride (15 mL) at room temperature, in a 50-mL round-bottomed flask, with septum under air. The aqueous layer was extracted with ethyl acetate (10 mL x 3). The combined organic layers were dried over magnesium sulfate, gravity filtered, and concentrated under rotary evaporation. The resulting crude residue was purified by flash column chromatography (60% dichloromethane/hexanes). Cis and trans diastereomers for the protons α to the ketones were isolated and characterized separately as they were separable by flash column chromatography. The afforded a dr of 39:61 (15 mg of the minor diastereomer and 24 mg of the major diastereomer) with both compounds yielded as a yellow solid (39 mg combined, 39% yield, 59% brsm).

Data 5.15 Minor Diastereomer

^1H NMR (400 MHz, CDCl_3)

7.89 (s, 2H), 7.79 (d, $J = 8.3$ Hz, 2H), 7.41-7.34 (m, 6H), 7.29 (dd, $J = 1.6, 7.8$ Hz, 2H), 7.19 (dd, $J = 1.8, 7.6$ Hz, 2H), 7.07 (dt, $J = 0.9, 7.4$ Hz, 2H), 6.81 (d, $J = 8.3$ Hz, 2H), 4.59 (q, $J = 4.8$ Hz, 2H), 3.88 (q, $J = 7.8$ Hz, 2H), 3.44-3.38 (m, 2H), 2.79 (t, $J = 7.8$ Hz, 4H), 1.79-1.71 (m, 4H), 1.51-1.41 (m, 4H), 1.00 (t, $J = 7.3$ Hz, 6H) ppm. Impurity of the major diastereomer present at 3.3 and 3.1 ppm. EtOAc impurity at 4.12 and 2.05 ppm. Water impurity at 1.55 ppm.

^{13}C NMR (100 MHz, CDCl_3)

197.3 (2C), 148.3 (2C), 147.5 (2C), 143.2 (2C), 139.5 (2C), 139.3 (2C), 135.3 (2C), 134.4 (2C), 133.6 (2C), 129.2 (2C), 129.1 (2C), 128.4 (2C), 128.3 (2C), 127.8 (2C), 127.1 (2C), 125.6 (2C), 124.7 (2C), 122.7 (2C), 119.1 (2C), 57.3 (2C), 36.7 (2C), 35.7 (2C), 33.7 (2C), 22.5 (2C), 14.2 (2C) ppm

<u>IR</u>	(thin film) 3334, 3056, 2859, 1667, 1610, 1516, 1433, 1225, 1087, 1005, 954, 838, 743, 565 cm ⁻¹
<u>HRMS</u>	(FTMS + p ESI) [M + H] ⁺ Calcd for C ₅₀ H ₄₃ O ₂ S ₂ 739.2699; Found 739.2674
<u>TLC</u>	<i>R_f</i> = 0.72 (80% dichloromethane/hexanes) [silica gel, UV]
<u>MP</u>	94.2 – 96.0 °C

Data 5.15 Major Diastereomer

¹H NMR (400 MHz, CDCl₃)

7.86 (s, 2H), 7.76 (d, *J* = 8.0 Hz, 2H), 7.36-7.30 (m, 6H), 7.27 (dd, *J* = 2.2, 6.6 Hz, 2H), 7.19 (dd, *J* = 2.2, 8.4 Hz, 2H), 7.02 (dt, *J* = 0.9, 7.2 Hz, 2H), 6.68 (d, *J* = 8.2 Hz, 2H), 3.52 (dd, *J* = 7.5, 16.8 Hz, 2H), 3.27 (dd, *J* = 4.6, 16.9 Hz, 2H), 3.18 (quint, *J* = 6.1 Hz, 2H), 2.76 (t, *J* = 7.7 Hz, 4H), 1.73 (quint, *J* = 7.4 Hz, 4H), 1.50-1.40 (m, 4H), 0.99 (t, *J* = 7.3 Hz, 6H) ppm. DCM impurity at 5.30 ppm. EtOAc impurity at 4.12 and 2.05 ppm.

¹³C NMR (100 MHz, CDCl₃)

204.4 (2C), 150.6 (2C), 146.8 (2C), 142.7 (2C), 139.5 (2C), 138.1 (2C), 135.6 (2C), 134.4 (2C), 133.8 (2C), 131.2 (2C), 129.1 (2C), 129.1 (2C), 128.5 (2C), 128.0 (2C), 126.7 (2C), 125.5 (2C), 124.4 (2C), 122.7 (2C), 119.2 (2C), 49.6 (2C), 35.7 (2C), 33.6 (2C), 30.5 (2C), 22.5 (2C), 14.2 (2C) ppm

IR (thin film)

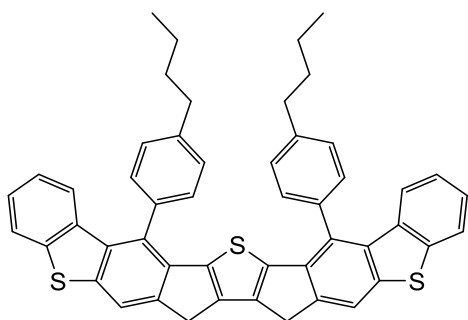
3334, 3056, 2859, 1667, 1610, 1516, 1433, 1225, 1087, 1005, 954, 838, 743, 565
cm⁻¹

HRMS (FTMS + p ESI)

[M + H]⁺ Calcd for C₅₀H₄₃O₂S₂ 739.2699; Found 739.2675

TLC *R_f* = 0.66 (80% dichloromethane/hexanes) [silica gel, UV]

MP 94.0 – 96.6 °C



Tris-thiophene polycyclic ladder-type heteroarene (5.16). A flame-dried single-necked, 5-mL, round-bottomed flask with stir bar, septum, condenser and a nitrogen inlet needle was charged with the isolated major diastereomer of **5.15** (13 mg, 0.02 mmol) dissolved in THF (1.5 mL). Lawesson's reagent (14 mg, 0.04 mmol) was added to the solution all at once. The flask was lowered into a preheated oil bath at 110 °C and refluxed for 24 h. The solution was allowed to cool to room temperature, and the toluene was removed under rotary evaporation. The resulting crude residue was purified by flash column chromatography (20% ethyl acetate/hexanes) to yield the title compound as a brown solid (8 mg, 62% yield).

Data 5.16

¹H NMR (400 MHz, CDCl₃)

7.85 (s, 2H), 7.77 (d, $J = 7.9$ Hz, 2H), 7.33 (d, $J = 7.9$ Hz, 4H), 7.30-7.25 (m, 6H), 7.01 (dt, $J = 0.9, 7.2$ Hz, 2H), 6.81 (d, $J = 8.2$ Hz, 2H), 3.77 (s, 4H), 2.87 (t, $J = 7.6$ Hz, 4H), 1.87-1.80 (m, 4H), 1.61-1.52 (m, 4H), 1.11 (t, $J = 7.4$ Hz, 6H) ppm. Grease impurity at 1.11 and 1.09 ppm.

^{13}C NMR (100 MHz, CDCl_3)
146.6 (2C), 144.4 (2C), 142.9 (2C), 140.8 (2C), 139.8 (2C), 137.3 (2C), 136.7 (2C), 136.1 (2C), 135.8 (2C), 132.5 (2C), 129.9 (2C), 129.4 (4C), 129.2 (4C), 125.7 (2C), 124.8 (2C), 123.8 (2C), 122.7 (2C), 118.3 (2C), 36.0 (2C), 33.9 (2C), 32.9 (2C), 22.7 (2C), 14.3 (2C) ppm

IR (thin film)
3055, 2926, 2857, 1713, 1586, 1510, 1461, 1298, 1260, 1111, 1069, 848, 746, 531 cm^{-1}

HRMS (FTMS + p ESI)
[$\text{M} + \text{H}$] $^{+}$ Calcd for $\text{C}_{50}\text{H}_{40}\text{S}_3$ 736.2287; Found 736.2276

TLC $R_f = 0.52$ (20% ethyl acetate/hexanes) [silica gel, UV]

MP Decomposes to black residue 175.9 – 179.8 $^{\circ}\text{C}$

5.4.3 Reaction of the Minor Diastereomer of **5.15** with Lawesson's Reagent

A flame-dried single-necked, 5-mL, round-bottomed flask with stir bar, septum, condenser and a nitrogen inlet needle was charged with the isolated minor diastereomer of **5.15** (13 mg, 0.02 mmol) dissolved in THF (1.5 mL). Lawesson's reagent (14 mg, 0.04 mmol) was added to the solution all at once. The flask was lowered into a preheated oil bath at 110 $^{\circ}\text{C}$ and refluxed for 24 h. The solution was allowed to cool to room temperature, and the toluene was removed under

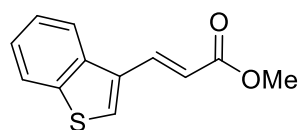
rotary evaporation. The resulting crude residue was purified by flash column chromatography (20% ethyl acetate/hexanes) and 69% of the starting material was recovered (9 mg) with no product formation.

Appendix A Compound Characterization Checklist

COMPOUND	IDENTITY												PURITY				COMPUTATIONAL DATA in SI*				AUTHOR REMARKS
Compound, structure, or table-entry number	Weight and percentage yield												MS Accurate mass (HRMS)				Copy of 1H/13C NMR spectrum in SI*				Total energy
	New	Known	Physical state / mp range if cryst. solid	IR	UV-Vis	1H NMR	13C NMR	MS	Optical rotation/ORD/CD	Enantiomeric/Diastereomeric ratio	X-ray [ORTEP and CIF in SI*]	Rf	Copy of chromatogram in SI*	Quant. GC, HPLC, electrophoresis	Elemental analysis	Cartesian coordinates or Z-matrix	# of imaginary frequencies				
2.3		X	X	X			X						X	X							
2.4		X	X	X			X						X	X							
2.5	X		X	X	X		X	X		X			X	X							
2.25		X	X	X			X						X	X							
2.26		X	X	X			X						X	X							
2.9	X		X	X	X		X	X		X			X	X							
1.50		X	X	X			X						X	X							
1.59		X	X	X			X						X	X							
2.16	X		X	X	X		X	X		X			X	X							
2.17	X		X	X	X		X	X		X			X	X							
2.18	X		X	X	X		X	X		X			X	X							
2.19	X		X	X	X		X	X		X			X	X							
2.6	X		X	X	X		X	X		X			X	X							

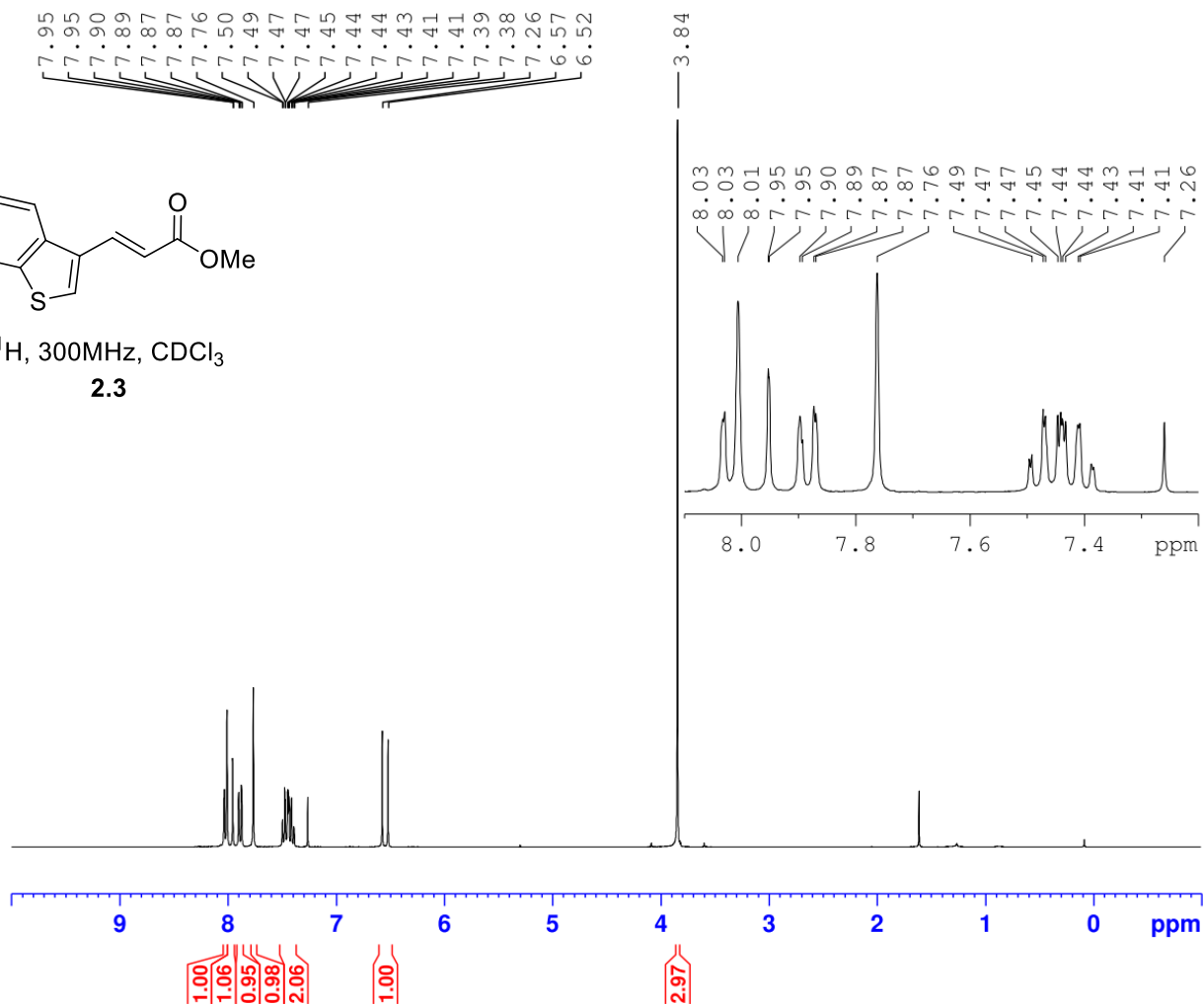
COMPOUND			IDENTITY										PURITY				COMPUTATIONAL DATA in SI*				AUTHOR REMARKS
Compound, structure, or table-entry number			Weight and percentage yield										MS Accurate mass (HRMS)				Copy of 1H/13C NMR spectrum in SI*				
	New	Known	Physical state / mp range if cryst. solid		IR	UV-Vis	1H NMR	13C NMR	MS	Optical rotation/ORD/CD	Enantiomeric/Diastereomeric ratio	X-ray [ORTEP and CIF in SI*]	Rf	Copy of chromatogram in SI*	Quant. GC, HPLC, electrophoresis	Elemental analysis	↔	Cartesian coordinates or Z-matrix	# of imaginary frequencies	Total energy (* SI = Supporting Information)	
2.23	X		X	X	X		X	X		X				X	X						
5.7		X	X	X			X							X	X						
5.8	X		X	X	X		X	X		X				X	X						
5.9	X		X	X	X		X	X		X				X	X						
5.10	X		X	X	X		X	X		X				X	X						
5.11	X		X	X	X		X	X		X				X	X						
5.12	X		X	X	X		X	X		X				X	X						
5.13	X		X	X	X		X	X		X				X	X						
5.14	X		X	X	X		X	X		X				X	X						
5.15	X		X	X	X		X	X		X				X	X						
5.16	X		X	X	X		X	X		X				X	X						

Appendix B ^1H and ^{13}C NMR Spectra of Synthetically Prepared Molecules



¹H, 300MHz, CDCl₃

2.3

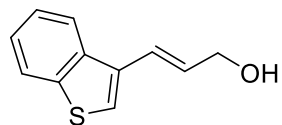


Current Data Parameters
NAME JAW-02-157
EXPNO 1
PROCNO 1

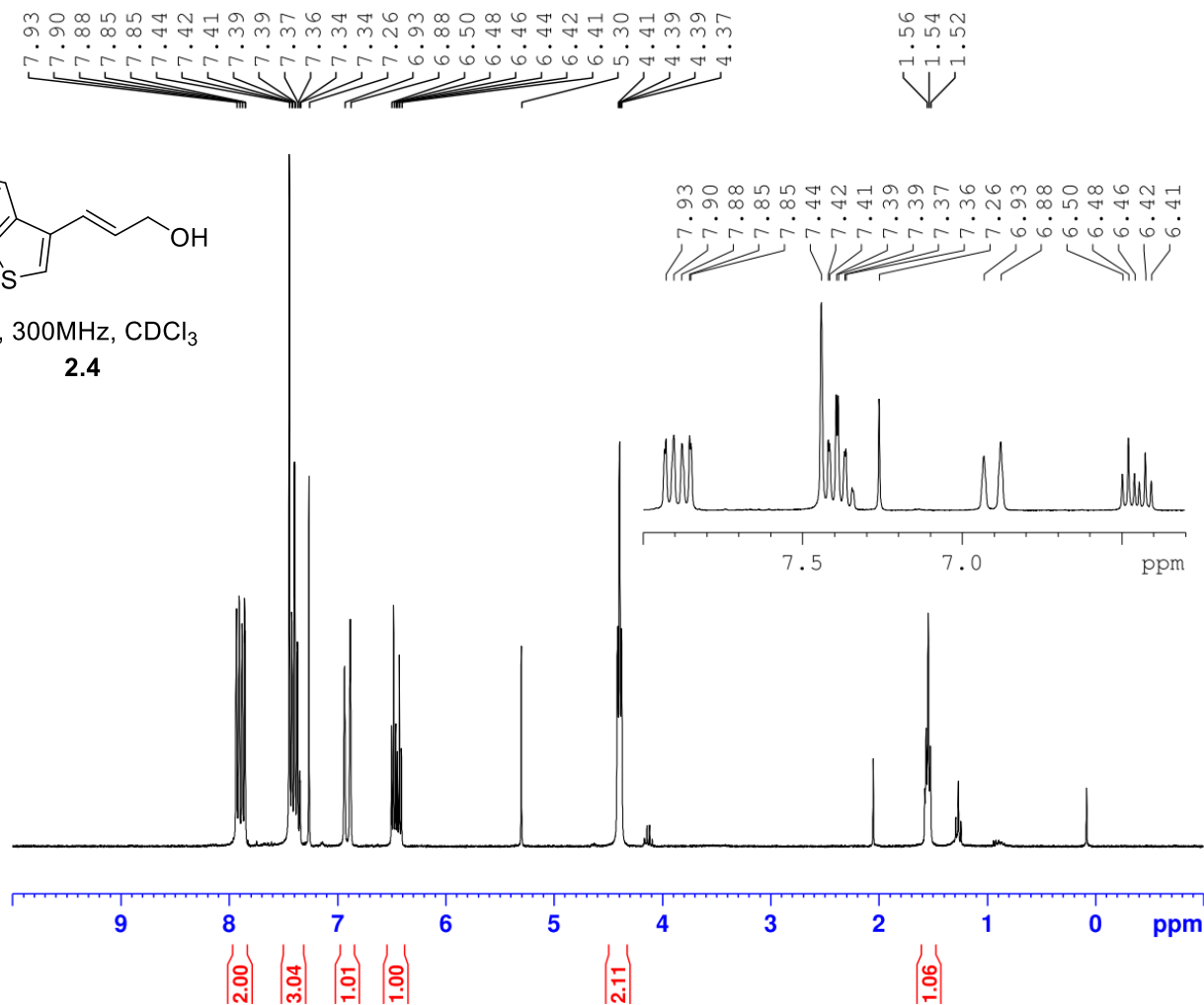
F2 - Acquisition Parameters
Date_ 20181008
Time 10.11
INSTRUM spect
PROBHD 5 mm QNP 1H/1
PULPROG zg30
TD 32768
SOLVENT CDCl₃
NS 16
DS 2
SWH 6188.119 Hz
FIDRES 0.188846 Hz
AQ 2.6476543 sec
RG 128
DW 80.800 usec
DE 6.50 usec
TE -923.4 K
D1 1.00000000 sec
TD0 1

===== CHANNEL f1 =====
SF01 300.2318540 MHz
NUC1 1H
P1 12.71 usec
PLW1 18.19700050 W

F2 - Processing parameters
SI 32768
SF 300.2300089 MHz
WDW EM
SSB 0
LB 0.10 Hz
GB 0
PC 1.00



¹H, 300MHz, CDCl₃
2.4

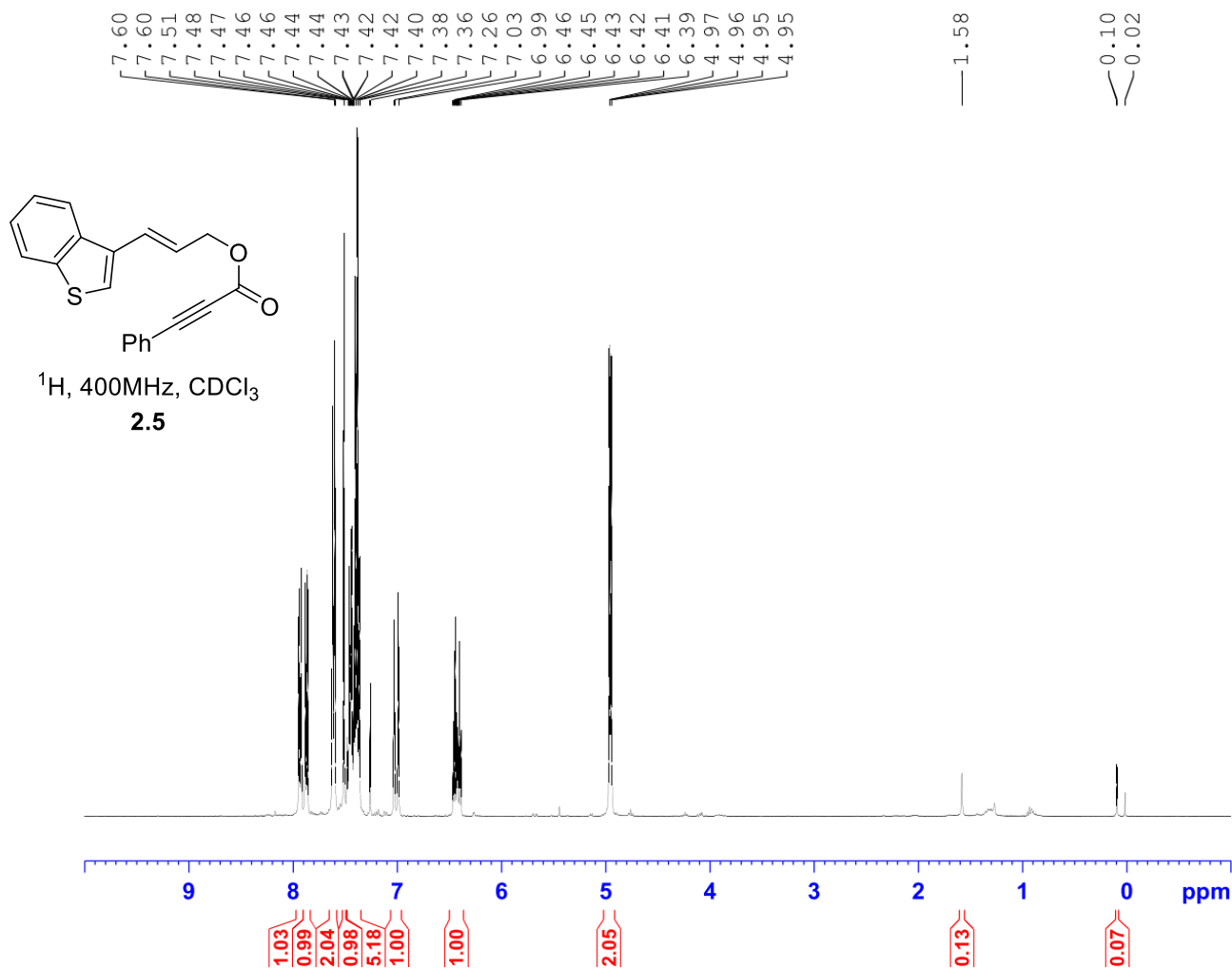


Current Data Parameters
NAME JAW-02-158
EXPNO 1
PROCNO 1

F2 - Acquisition Parameters
Date_ 20181017
Time 11.19
INSTRUM spect
PROBHD 5 mm QNP 1H/1
PULPROG zg30
TD 32768
SOLVENT CDCl₃
NS 16
DS 2
SWH 6188.119 Hz
FIDRES 0.188846 Hz
AQ 2.6476543 sec
RG 322
DW 80.800 usec
DE 6.50 usec
TE -922.3 K
D1 1.00000000 sec
TD0 1

===== CHANNEL f1 =====
SF01 300.2318540 MHz
NUC1 1H
P1 12.71 usec
PLW1 18.19700050 W

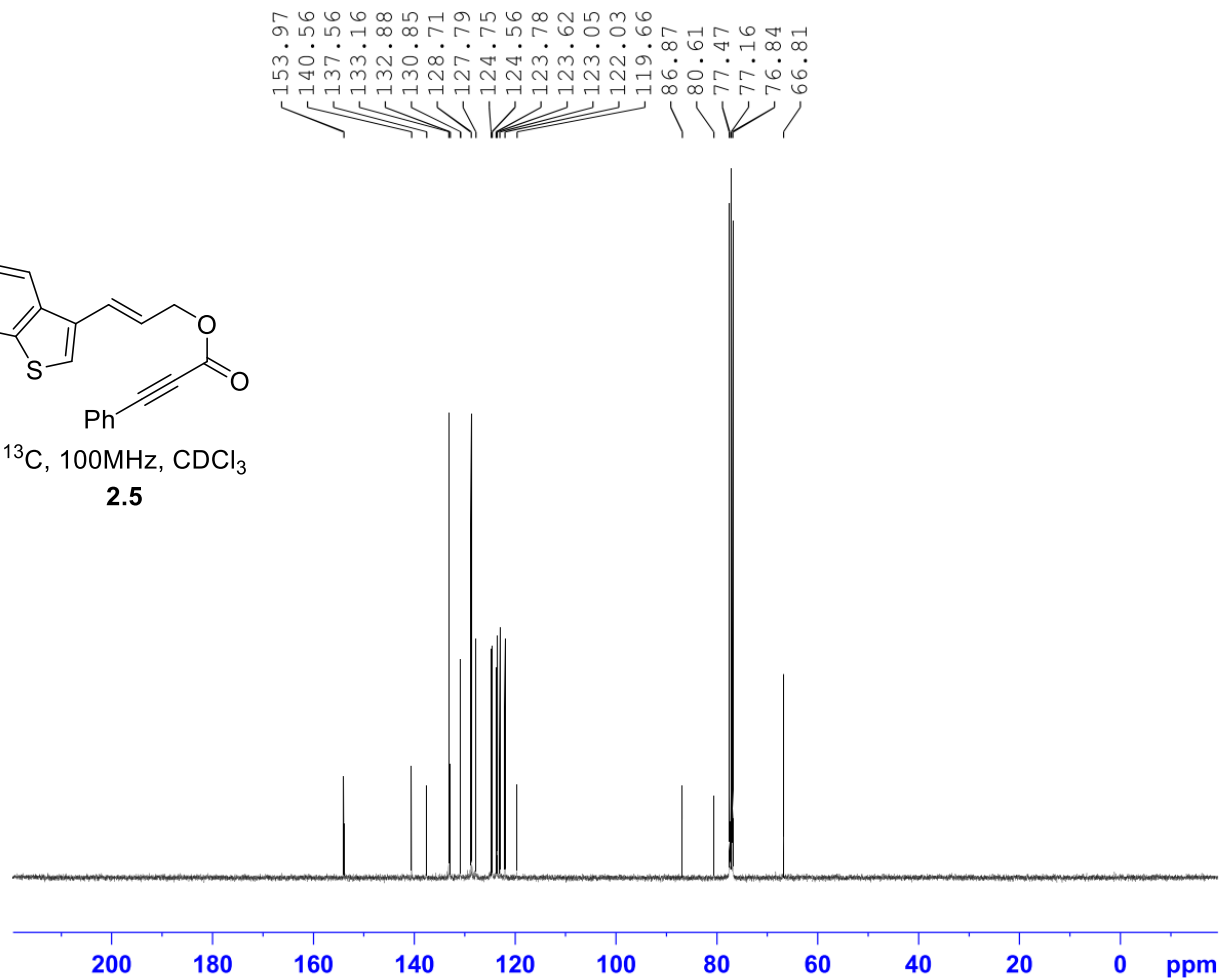
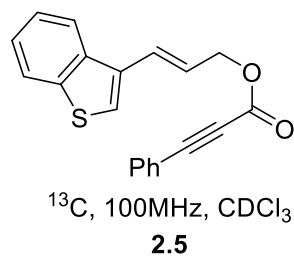
F2 - Processing parameters
SI 32768
SF 300.2300086 MHz
WDW EM
SSB 0
LB 0.10 Hz
GB 0
PC 1.00



Current Data Parameters
NAME JAW-03-107
EXPNO 3
PROCNO 1

F2 - Acquisition Parameters
Date_ 20210419
Time 9.00 h
INSTRUM spect
PROBHD Z108618_0240 (
PULPROG zg30
TD 65536
SOLVENT CDCl3
NS 16
DS 2
SWH 8012.820 Hz
FIDRES 0.244532 Hz
AQ 4.0894465 sec
RG 71.8
DW 62.400 usec
DE 6.50 usec
TE 92.2 K
D1 1.00000000 sec
TD0 1
SF01 400.1324708 MHz
NUC1 1H
P0 4.83 usec
P1 14.50 usec
PLW1 12.00000000 W

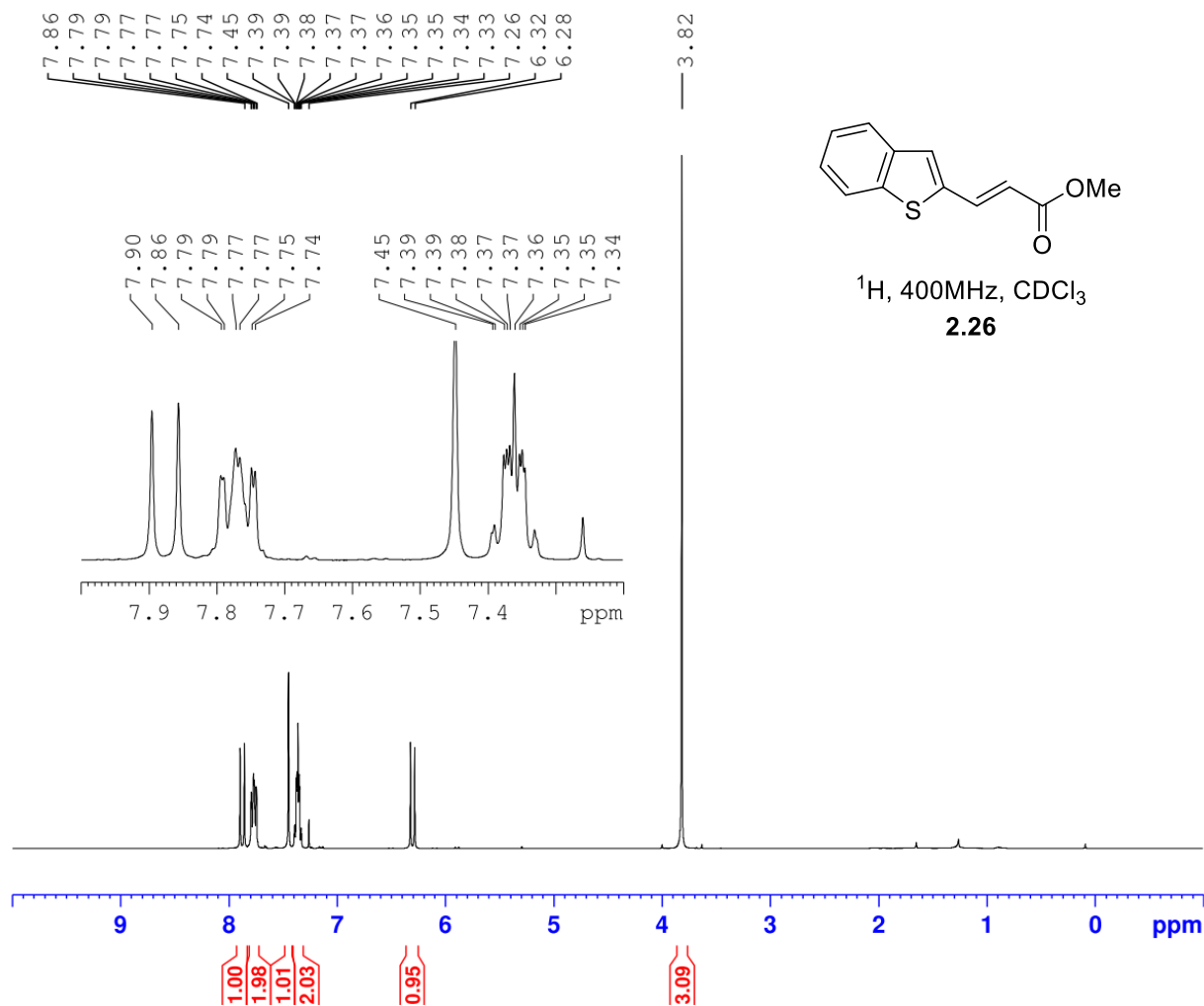
F2 - Processing parameters
SI 65536
SF 400.1300098 MHz
WDW EM
SSB 0
LB 0.30 Hz
GB 0
PC 1.00



Current Data Parameters
 NAME JAW-03-107
 EXPNO 4
 PROCNO 1

F2 - Acquisition Parameters
 Date_ 20210419
 Time_ 21.05 h
 INSTRUM spect
 PROBHD Z108618_0240 (
 PULPROG zgpg30
 TD 65536
 SOLVENT CDCl3
 NS 1024
 DS 4
 SWH 24038.461 Hz
 FIDRES 0.733596 Hz
 AQ 1.3631488 sec
 RG 203
 DW 20.800 usec
 DE 6.50 usec
 TE 91.2 K
 D1 2.00000000 sec
 D11 0.03000000 sec
 TD0 1
 SFO1 100.6228298 MHz
 NUC1 13C
 P0 3.33 usec
 P1 10.00 usec
 PLW1 56.13299942 W
 SFO2 400.1316005 MHz
 NUC2 1H
 CPDPRG[2] waltz65
 PCPD2 90.00 usec
 PLW2 12.00000000 W
 PLW12 0.31147999 W
 PLW13 0.15667000 W

F2 - Processing parameters
 SI 32768
 SF 100.6127586 MHz
 WDW EM
 SSB 0
 LB 1.00 Hz
 GB 0
 PC 1.40

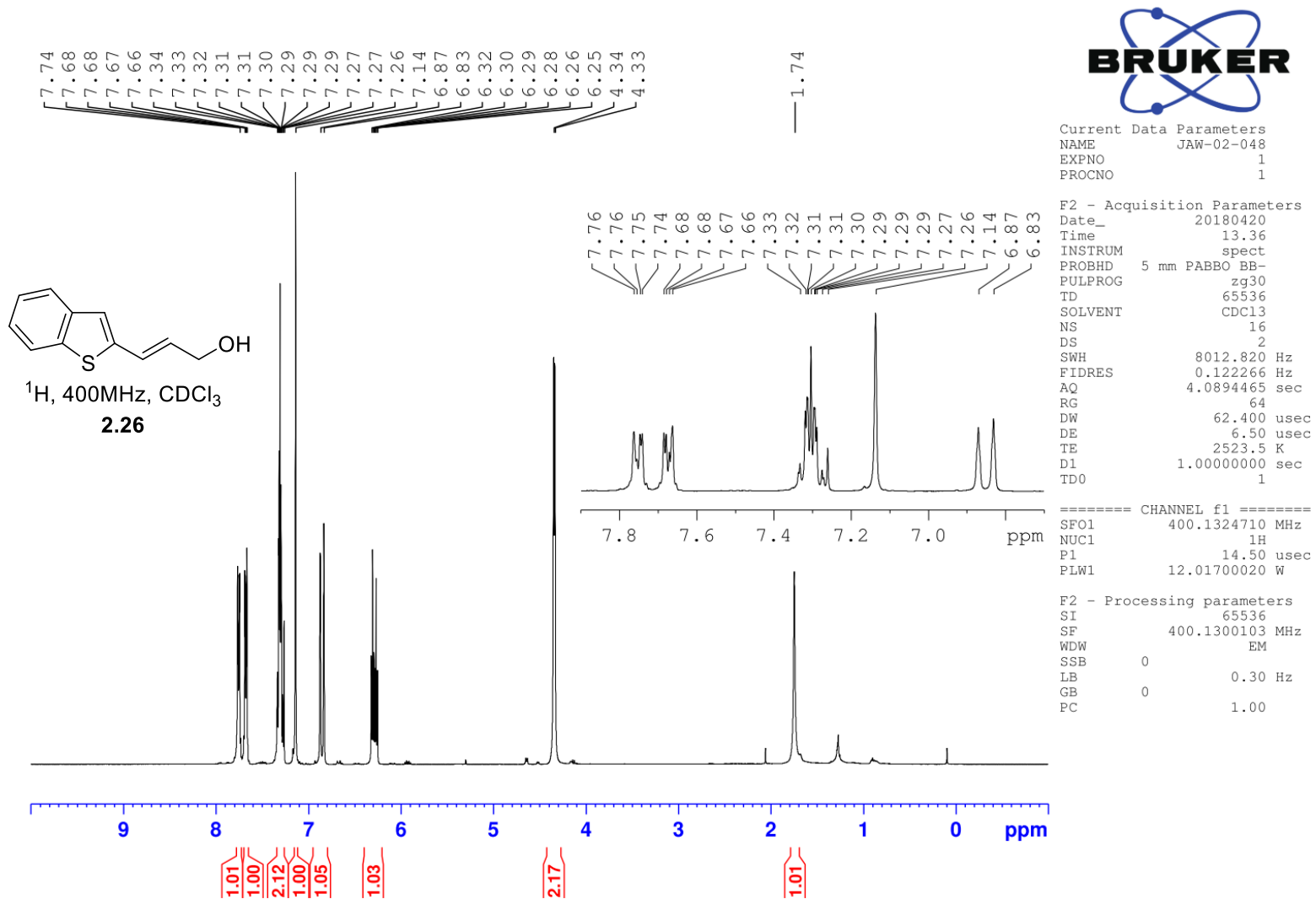


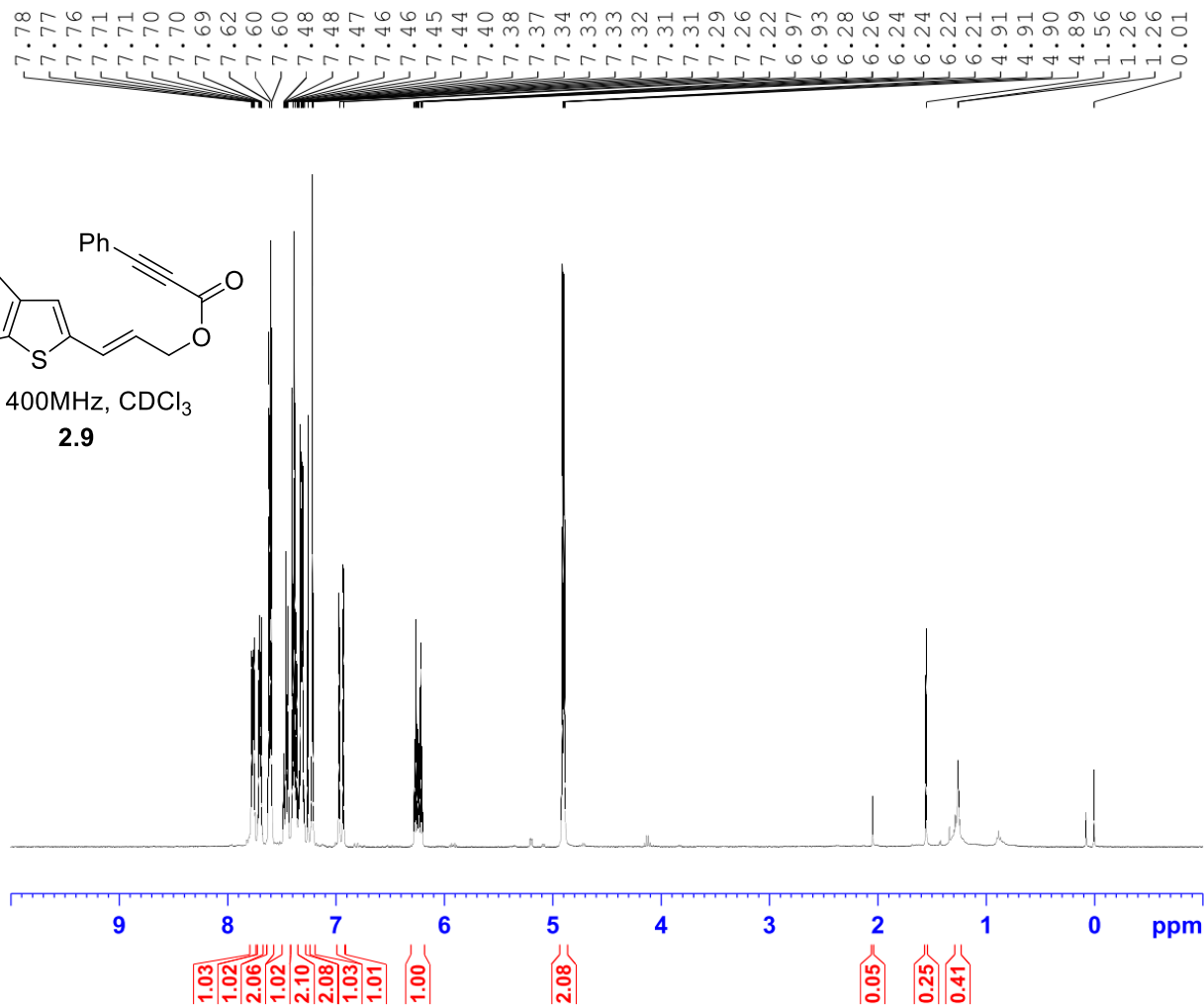
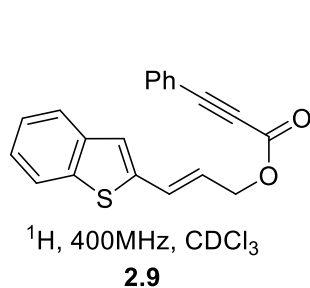
Current Data Parameters
 NAME JAW-02-047
 EXPNO 2
 PROCNO 1

F2 - Acquisition Parameters
 Date_ 20180419
 Time 14.18
 INSTRUM spect
 PROBHD 5 mm PABBO BB-
 PULPROG zg30
 TD 65536
 SOLVENT CDC13
 NS 16
 DS 2
 SWH 8012.820 Hz
 FIDRES 0.122266 Hz
 AQ 4.0894465 sec
 RG 57
 DW 62.400 usec
 DE 6.50 usec
 TE 1994.0 K
 D1 1.00000000 sec
 TD0 1

===== CHANNEL f1 =====
 SF01 400.1324710 MHz
 NUC1 1H
 P1 14.50 usec
 PLW1 12.01700020 W

F2 - Processing parameters
 SI 65536
 SF 400.1300101 MHz
 WDW EM
 SSB 0
 LB 0.30 Hz
 GB 0
 PC 1.00

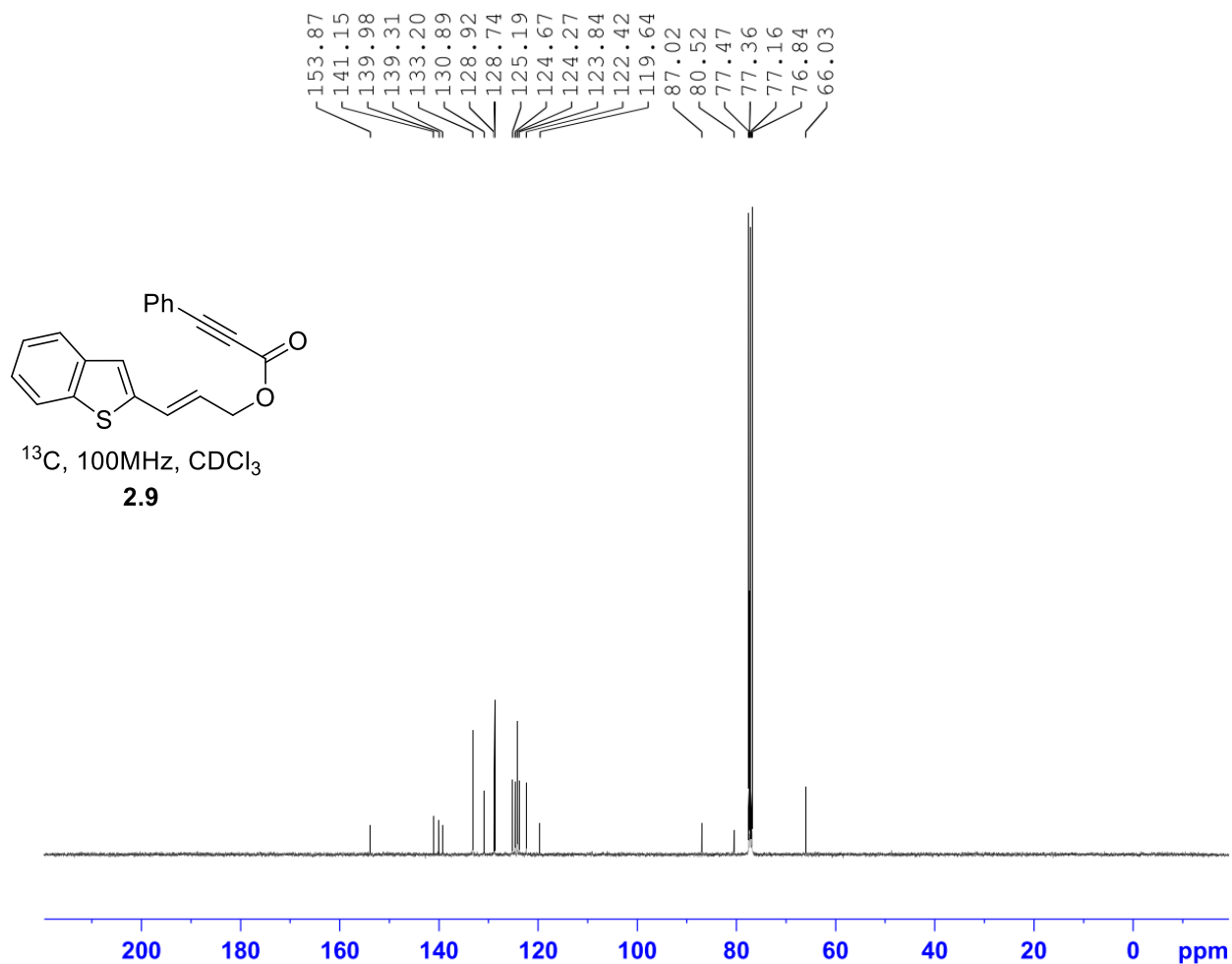




Current Data Parameters
 NAME JAW-03-108
 EXPNO 1
 PROCNO 1

F2 - Acquisition Parameters
 Date_ 20210418
 Time_ 2.20 h
 INSTRUM spect
 PROBHD Z108618_0240 (
 PULPROG zg30
 TD 65536
 SOLVENT CDCl3
 NS 16
 DS 2
 SWH 8012.820 Hz
 FIDRES 0.244532 Hz
 AQ 4.0894465 sec
 RG 101
 DW 62.400 usec
 DE 6.50 usec
 TE 91.1 K
 D1 1.00000000 sec
 TD0 1
 SF01 400.1324708 MHz
 NUC1 1H
 P0 4.83 usec
 P1 14.50 usec
 PLW1 12.00000000 W

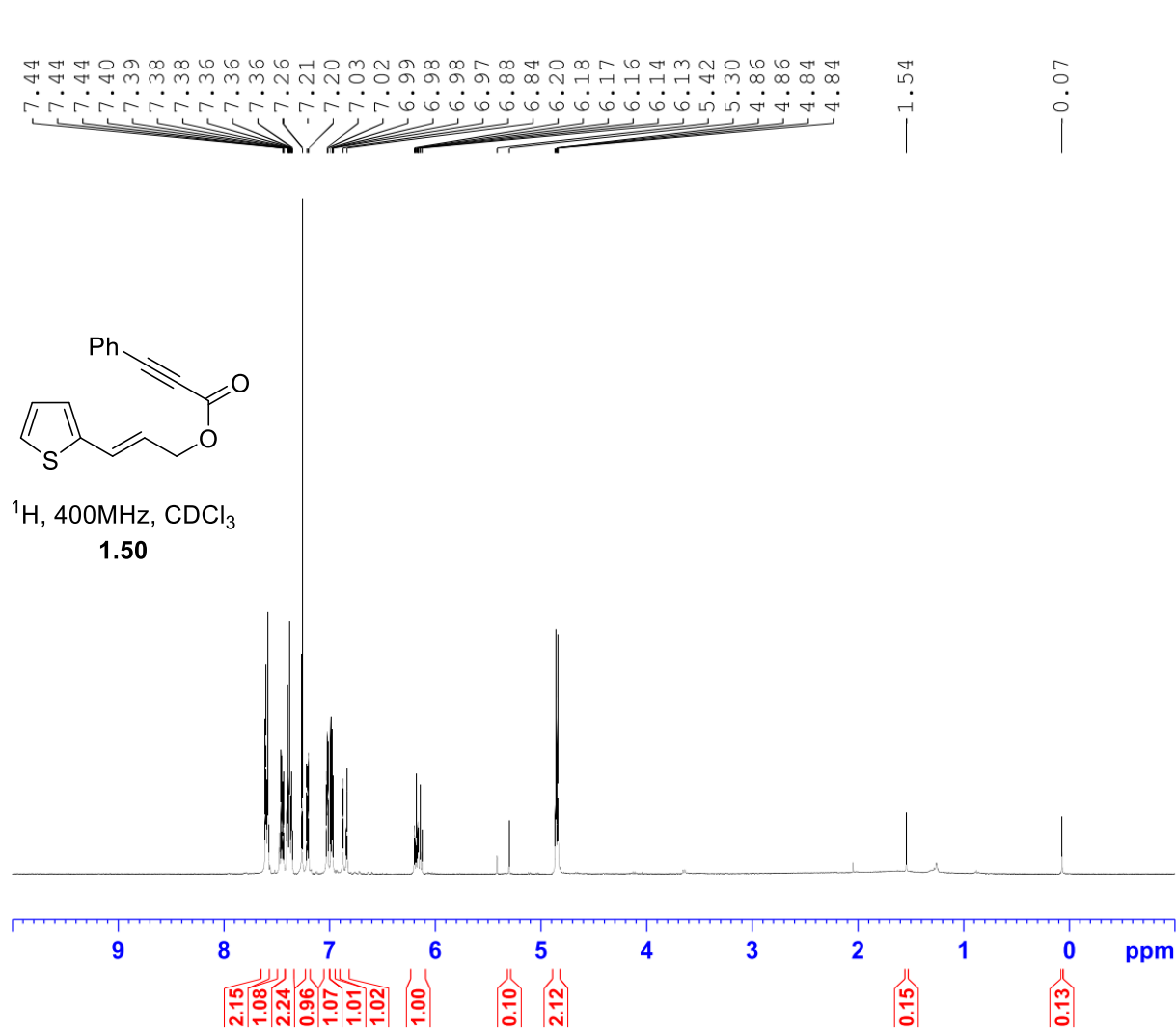
F2 - Processing parameters
 SI 65536
 SF 400.1300099 MHz
 WDW EM
 SSB 0
 LB 0.30 Hz
 GB 0
 PC 1.00



Current Data Parameters
 NAME JAW-03-108
 EXPNO 2
 PROCNO 1

F2 - Acquisition Parameters
 Date_ 20210418
 Time_ 3.20 h
 INSTRUM spect
 PROBHD Z108618_0240 (
 PULPROG zgpg30
 TD 65536
 SOLVENT CDCl3
 NS 1024
 DS 4
 SWH 24038.461 Hz
 FIDRES 0.733596 Hz
 AQ 1.3631488 sec
 RG 203
 DW 20.800 usec
 DE 6.50 usec
 TE 91.1 K
 D1 2.00000000 sec
 D11 0.03000000 sec
 TD0 1
 SFO1 100.6228298 MHz
 NUC1 13C
 P0 3.33 usec
 P1 10.00 usec
 PLW1 56.13299942 W
 SFO2 400.1316005 MHz
 NUC2 1H
 CPDPRG[2] waltz65
 PCPD2 90.00 usec
 PLW2 12.00000000 W
 PLW12 0.31147999 W
 PLW13 0.15667000 W

F2 - Processing parameters
 SI 32768
 SF 100.6127562 MHz
 WDW EM
 SSB 0
 LB 1.00 Hz
 GB 0
 PC 1.40

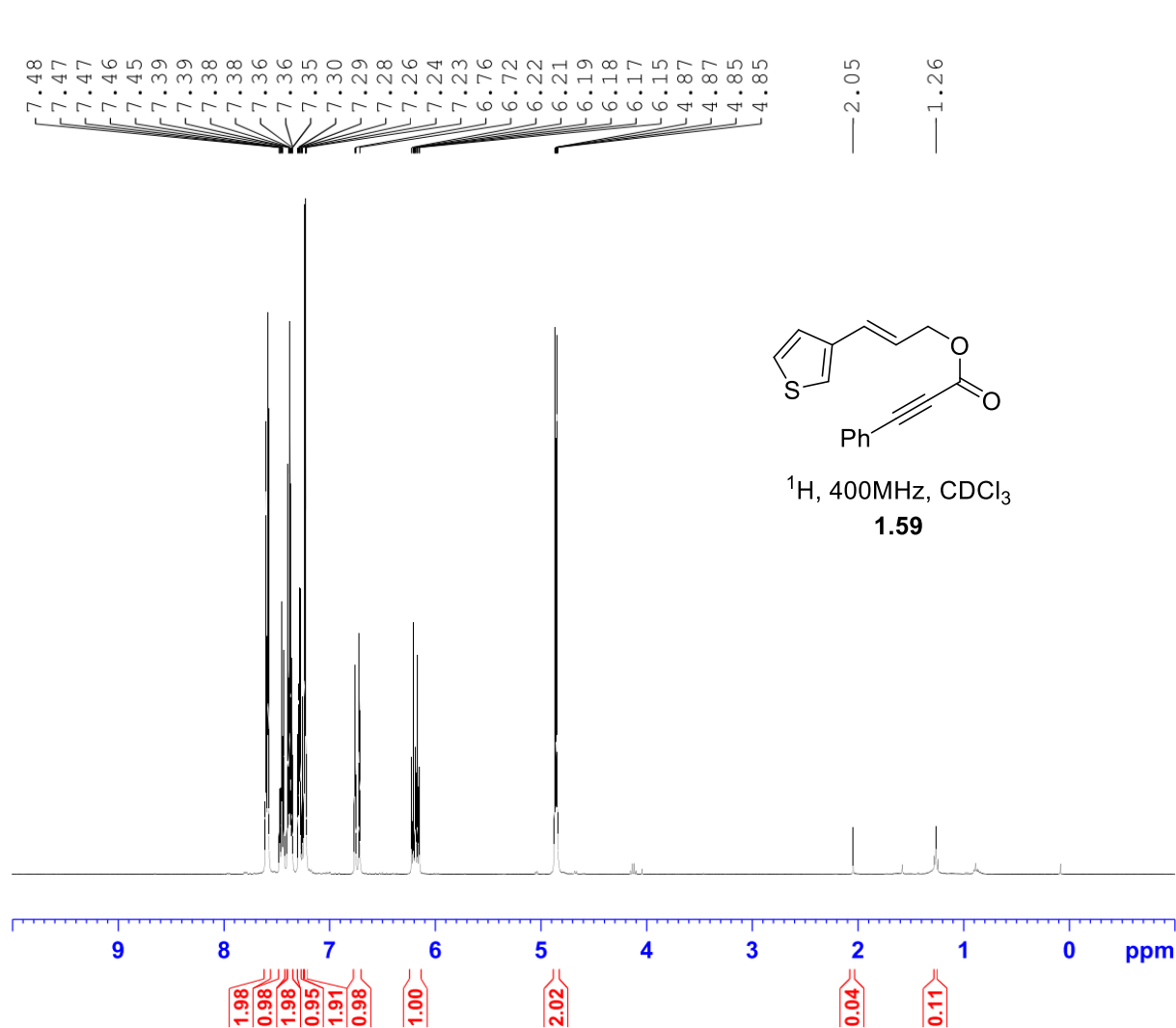


Current Data Parameters
NAME JAW-02-036
EXPNO 1
PROCNO 1

F2 - Acquisition Parameters
Date_ 20180404
Time_ 17.24
INSTRUM spect
PROBHD 5 mm PABBO BB-
PULPROG zg30
TD 65536
SOLVENT CDCl3
NS 16
DS 2
SWH 8012.820 Hz
FIDRES 0.122266 Hz
AQ 4.0894465 sec
RG 128
DW 62.400 usec
DE 6.50 usec
TE 1833.9 K
D1 1.00000000 sec
TD0 1

===== CHANNEL f1 =====
SF01 400.1324710 MHz
NUC1 1H
P1 14.50 usec
PLW1 12.01700020 W

F2 - Processing parameters
SI 65536
SF 400.1300103 MHz
WDW EM
SSB 0
LB 0.30 Hz
GB 0
PC 1.00

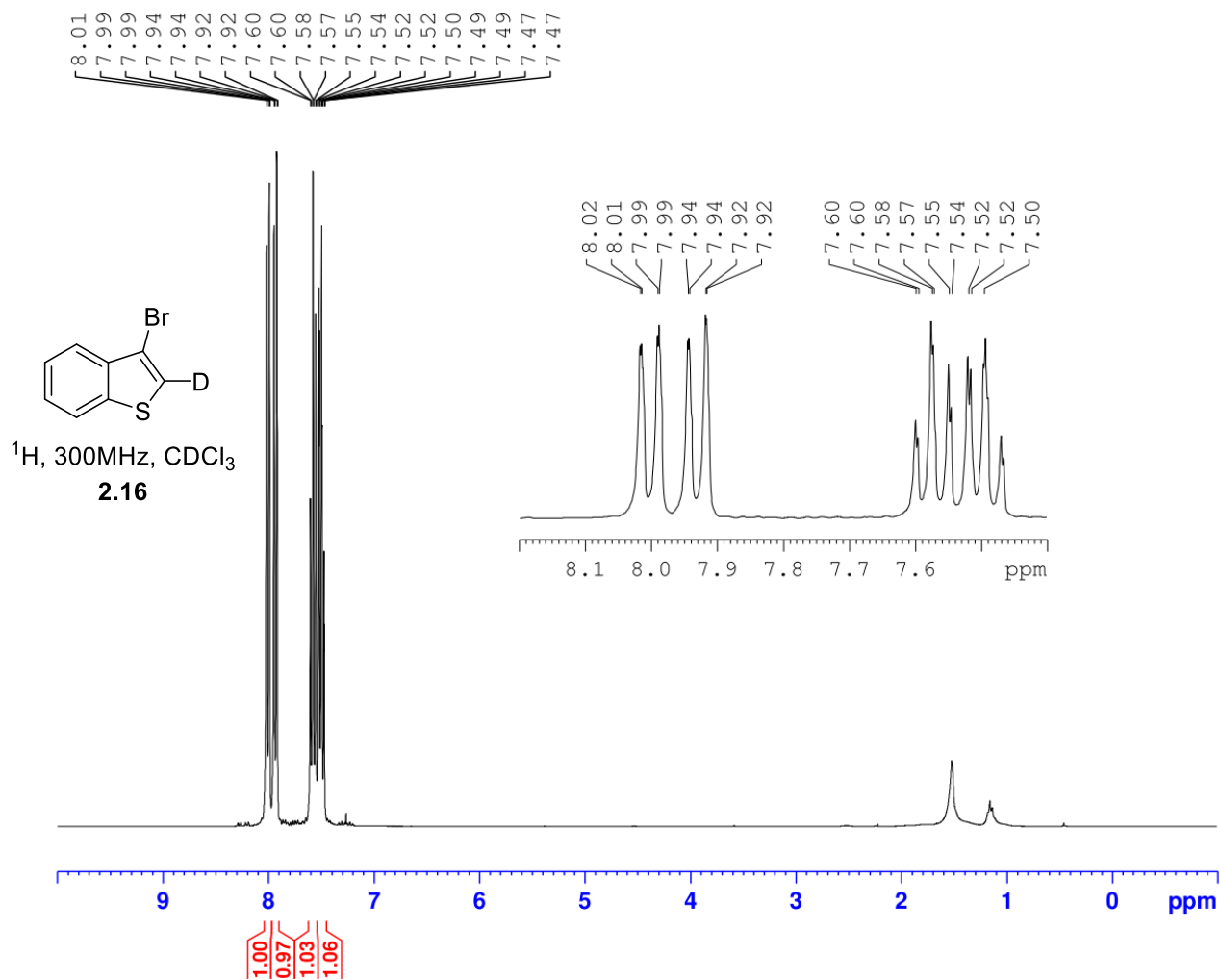


Current Data Parameters
 NAME JAW-01-085
 EXPNO 1
 PROCNO 1

F2 - Acquisition Parameters
 Date_ 20170308
 Time_ 16.17
 INSTRUM spect
 PROBHD 5 mm PABBO BB-
 PULPROG zg30
 TD 65536
 SOLVENT CDCl₃
 NS 16
 DS 2
 SWH 8012.820 Hz
 FIDRES 0.122266 Hz
 AQ 4.0894465 sec
 RG 64
 DW 62.400 usec
 DE 6.50 usec
 TE 884.0 K
 D1 1.00000000 sec
 TD0 1

===== CHANNEL f1 =====
 SF01 400.1324710 MHz
 NUC1 1H
 P1 13.75 usec
 PLW1 12.01700020 W

F2 - Processing parameters
 SI 65536
 SF 400.1300099 MHz
 WDW EM
 SSB 0
 LB 0.30 Hz
 GB 0
 PC 1.00

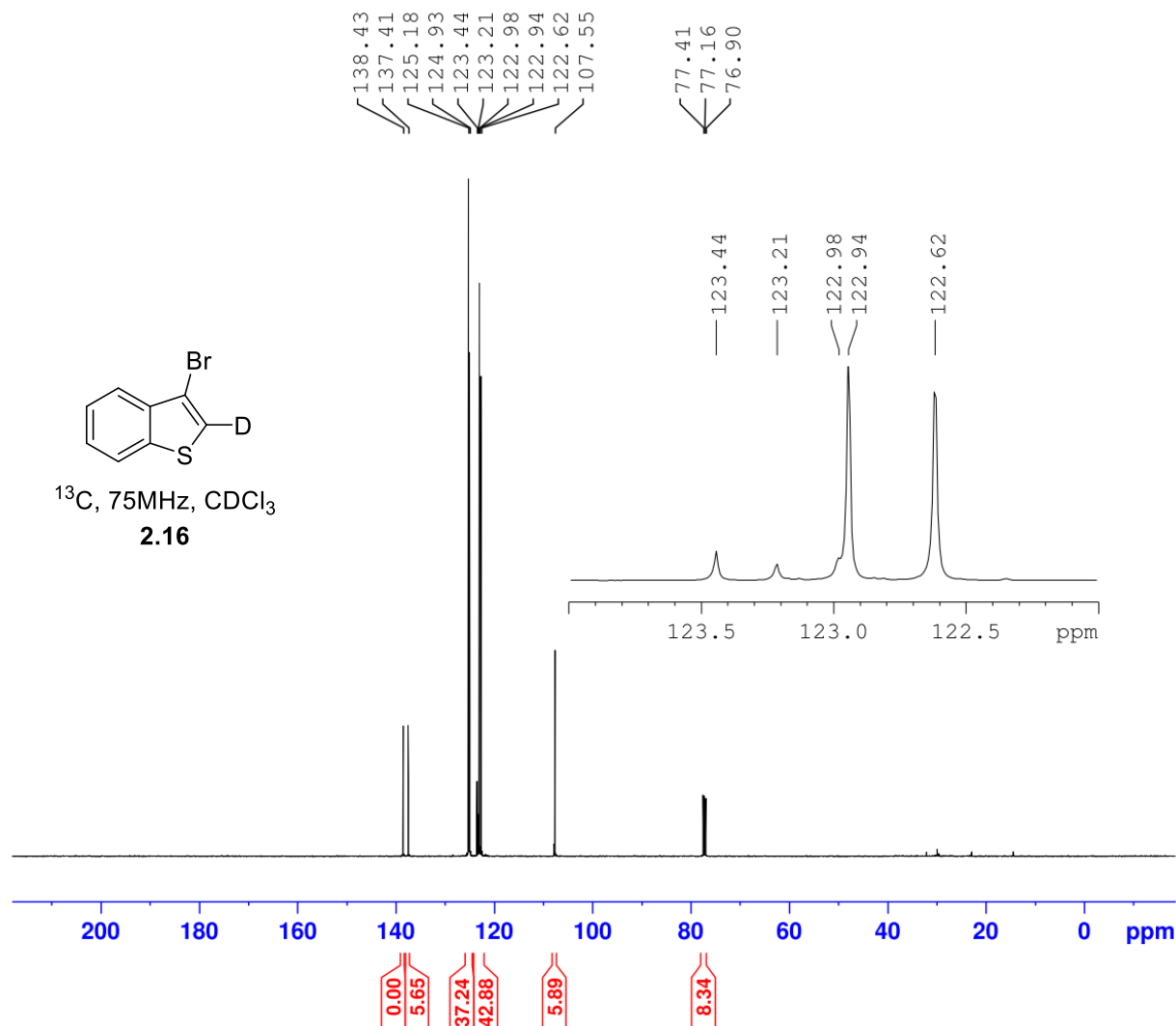
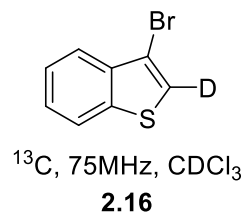


Current Data Parameters
NAME JAW-01-128-A
EXPNO 1
PROCNO 1

F2 - Acquisition Parameters
Date_ 20170717
Time 10.16
INSTRUM spect
PROBHD 5 mm QNP 1H/1
PULPROG zg30
TD 32768
SOLVENT CDCl_3
NS 16
DS 2
SWH 6188.119 Hz
FIDRES 0.188846 Hz
AQ 2.6476543 sec
RG 28.5
DW 80.800 usec
DE 6.50 usec
TE -925.4 K
D1 1.00000000 sec
TD0 1

===== CHANNEL f1 =====
SF01 300.2318540 MHz
NUC1 1H
P1 12.71 usec
PLW1 18.19700050 W

F2 - Processing parameters
SI 32768
SF 300.2300080 MHz
WDW EM
SSB 0
LB 0.10 Hz
GB 0
PC 1.00



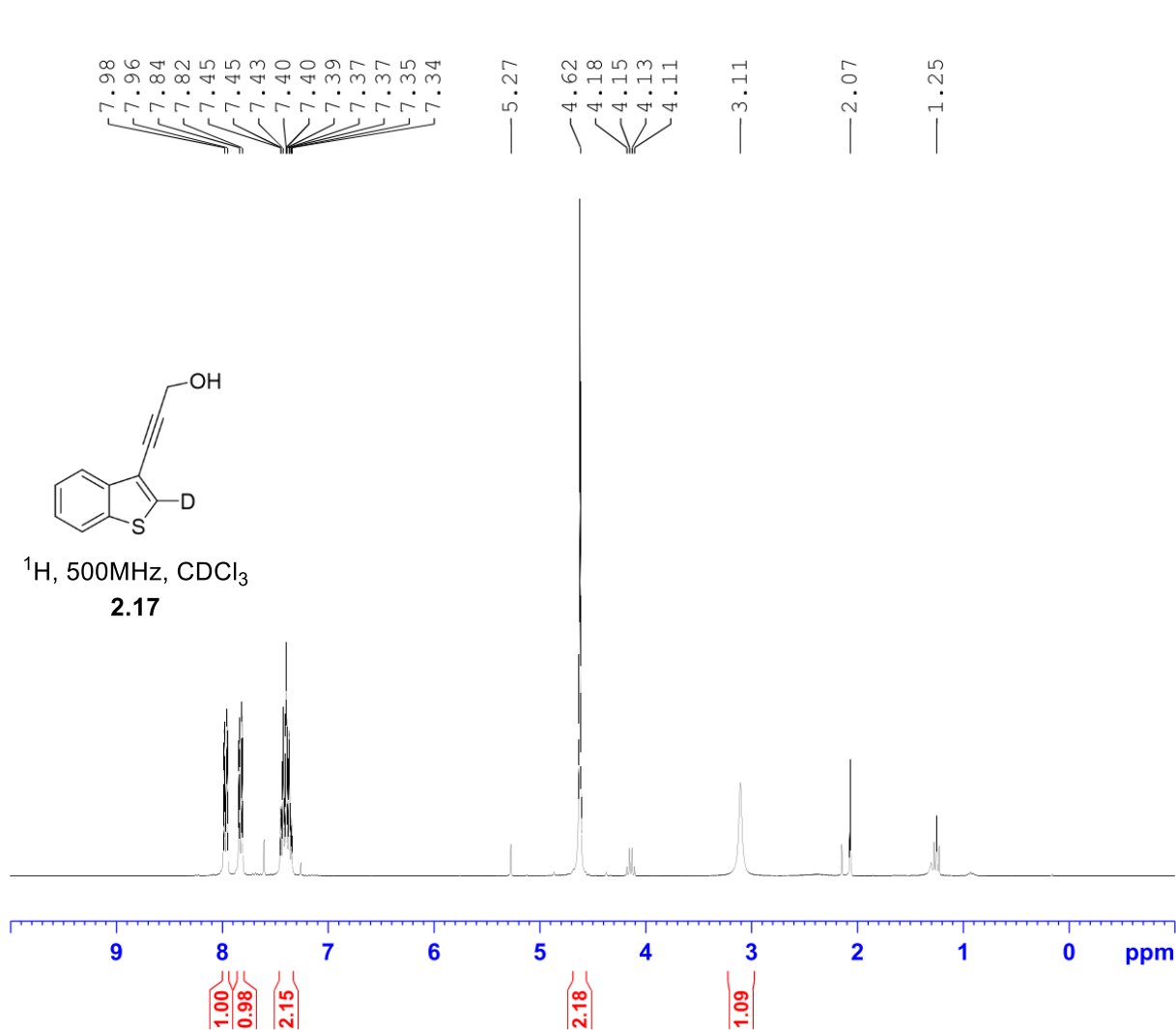
Current Data Parameters
 NAME JAW-01-128-A
 EXPNO 2
 PROCNO 1

F2 - Acquisition Parameters
 Date_ 20170715
 Time 7.08
 INSTRUM spect
 PROBHD 5 mm PABBO BB/
 PULPROG zgpg30
 TD 65536
 SOLVENT CDCl3
 NS 1024
 DS 2
 SWH 29761.904 Hz
 FIDRES 0.454131 Hz
 AQ 1.1010048 sec
 RG 203
 DW 16.800 usec
 DE 6.50 usec
 TE 300.3 K
 D1 2.00000000 sec
 D11 0.03000000 sec
 TD0 1

===== CHANNEL f1 =====
 SFO1 125.7779086 MHz
 NUC1 13C
 P1 10.50 usec
 PLW1 110.00000000 W

===== CHANNEL f2 =====
 SFO2 500.1620006 MHz
 NUC2 1H
 CPDPRG[2] waltz16
 PCPD2 80.00 usec
 PLW2 18.00000000 W
 PLW12 0.37195000 W
 PLW13 0.23805000 W

F2 - Processing parameters
 SI 32768
 SF 125.7653686 MHz
 WDW EM
 SSB 0
 LB 1.00 Hz
 GB 0
 PC 1.40

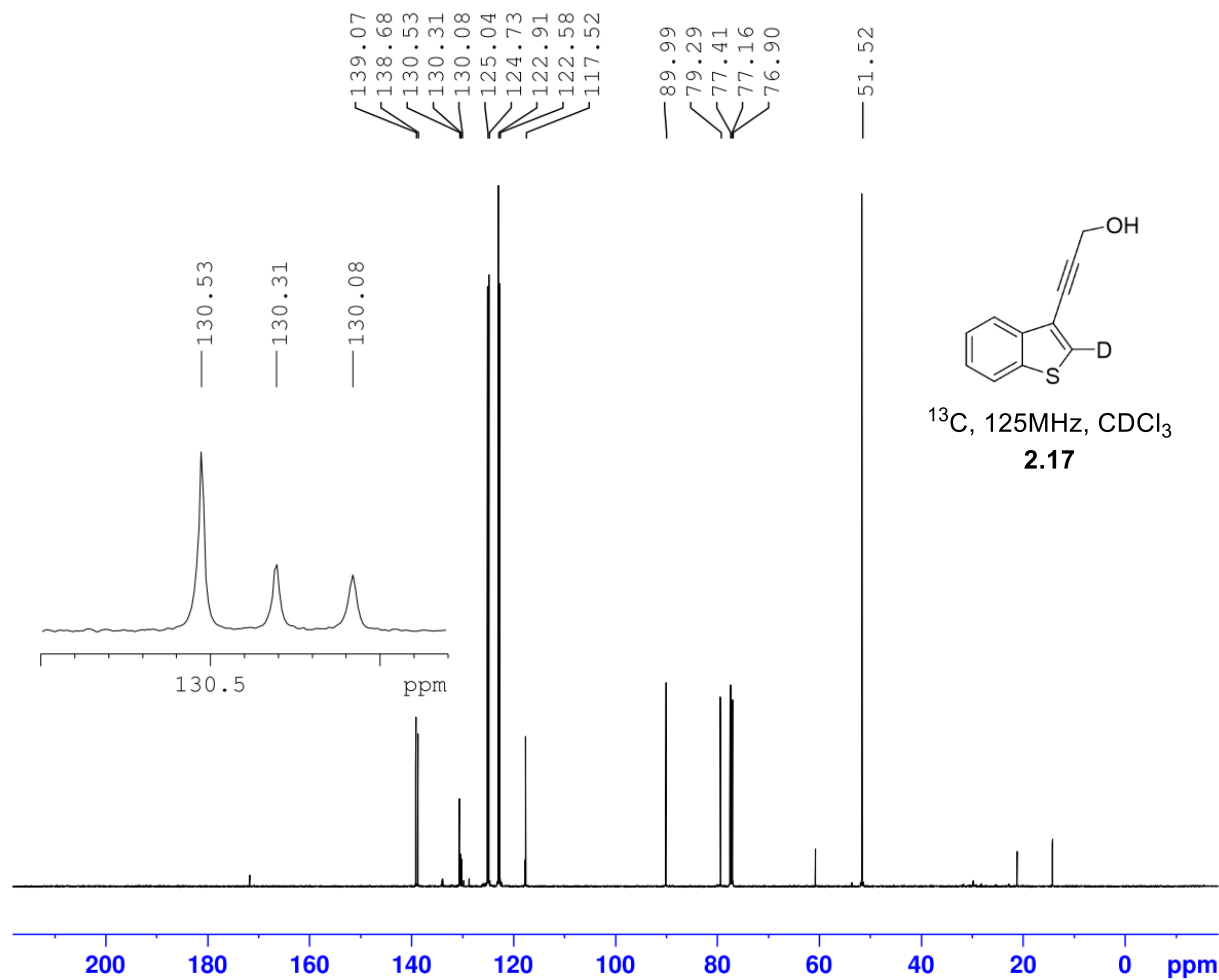


Current Data Parameters
 NAME JAW-01-138
 EXPNO 5
 PROCNO 1

F2 - Acquisition Parameters
 Date_ 20170814
 Time_ 10.04
 INSTRUM spect
 PROBHD 5 mm QNP 1H/1
 PULPROG zg30
 TD 32768
 SOLVENT CDCl3
 NS 16
 DS 2
 SWH 6188.119 Hz
 FIDRES 0.188846 Hz
 AQ 2.6476543 sec
 RG 40.3
 DW 80.800 usec
 DE 6.50 usec
 TE -924.1 K
 D1 1.00000000 sec
 TD0 1

===== CHANNEL f1 =====
 SF01 300.2318540 MHz
 NUC1 1H
 P1 12.71 usec
 PLW1 18.19700050 W

F2 - Processing parameters
 SI 32768
 SF 300.2300082 MHz
 WDW EM
 SSB 0
 LB 0.10 Hz
 GB 0
 PC 1.00



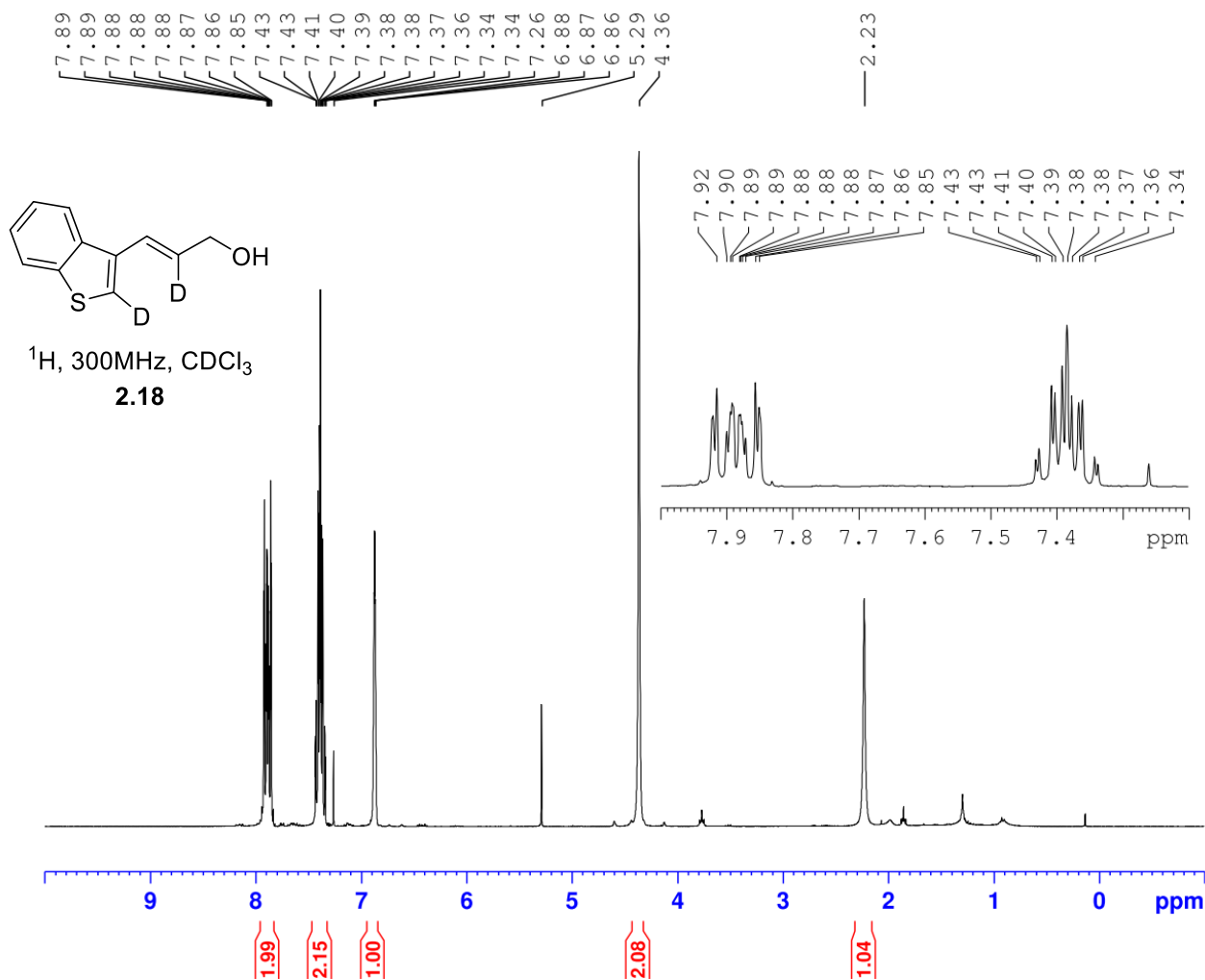
Current Data Parameters
 NAME JAW-01-132
 EXPNO 2
 PROCNO 1

F2 - Acquisition Parameters
 Date_ 20170722
 Time 12.48
 INSTRUM spect
 PROBHD 5 mm PABBO BB/
 PULPROG zgpg30
 TD 65536
 SOLVENT CDC13
 NS 1024
 DS 2
 SWH 29761.904 Hz
 FIDRES 0.454131 Hz
 AQ 1.1010048 sec
 RG 203
 DW 16.800 usec
 DE 6.50 usec
 TE 299.8 K
 D1 2.00000000 sec
 D11 0.03000000 sec
 TD0 1

===== CHANNEL f1 =====
 SFO1 125.7779086 MHz
 NUC1 13C
 P1 10.50 usec
 PLW1 110.0000000 W

===== CHANNEL f2 =====
 SFO2 500.1620006 MHz
 NUC2 1H
 CPDPRG[2] waltz16
 PCPD2 80.00 usec
 PLW2 18.0000000 W
 PLW12 0.37195000 W
 PLW13 0.23805000 W

F2 - Processing parameters
 SI 32768
 SF 125.7653415 MHz
 WDW EM
 SSB 0
 LB 1.00 Hz
 GB 0
 PC 1.40

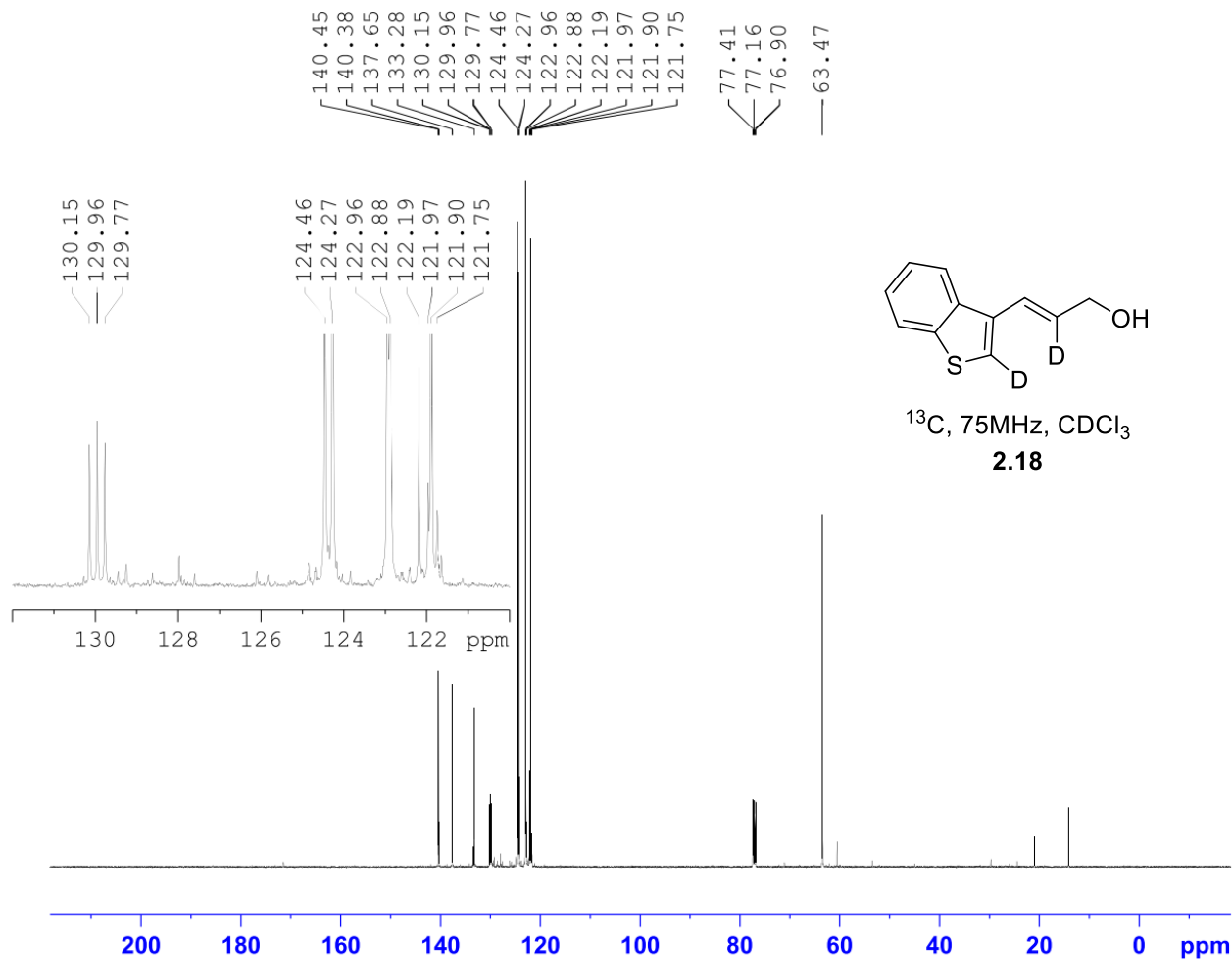


Current Data Parameters
 NAME JAW-01-140
 EXPNO 1
 PROCNO 1

F2 - Acquisition Parameters
 Date_ 20170823
 Time 9.50
 INSTRUM spect
 PROBHD 5 mm QNP 1H/1
 PULPROG zg30
 TD 32768
 SOLVENT CDCl₃
 NS 16
 DS 2
 SWH 6188.119 Hz
 FIDRES 0.188846 Hz
 AQ 2.6476543 sec
 RG 64
 DW 80.800 usec
 DE 6.50 usec
 TE -924.2 K
 D1 1.00000000 sec
 TD0 1

===== CHANNEL f1 =====
 SF01 300.2318540 MHz
 NUC1 1H
 P1 12.71 usec
 PLW1 18.19700050 W

F2 - Processing parameters
 SI 32768
 SF 300.2300083 MHz
 WDW EM
 SSB 0
 LB 0.10 Hz
 GB 0
 PC 1.00



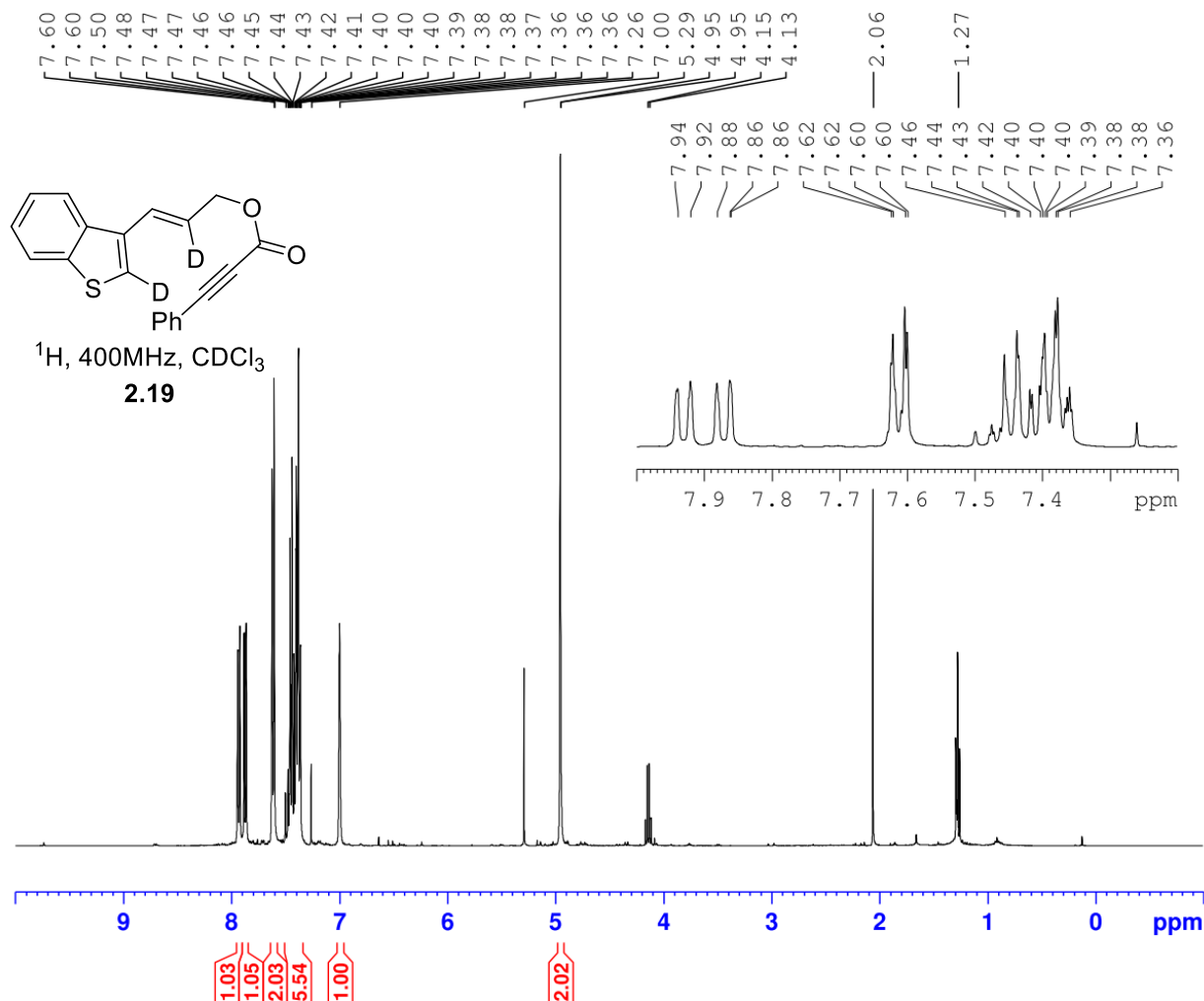
Current Data Parameters
 NAME JAW-01-140
 EXPNO 10
 PROCNO 1

F2 - Acquisition Parameters
 Date_ 20170830
 Time_ 7.15
 INSTRUM spect
 PROBHD 5 mm PABBO BB/
 PULPROG zgpg30
 TD 65536
 SOLVENT CDCl3
 NS 1024
 DS 2
 SWH 29761.904 Hz
 FIDRES 0.454131 Hz
 AQ 1.1010048 sec
 RG 203
 DW 16.800 usec
 DE 6.50 usec
 TE 298.5 K
 D1 2.00000000 sec
 D11 0.03000000 sec
 TD0 1

===== CHANNEL f1 =====
 SFO1 125.7779086 MHz
 NUC1 13C
 P1 10.50 usec
 PLW1 110.00000000 W

===== CHANNEL f2 =====
 SFO2 500.1620006 MHz
 NUC2 1H
 CPDPRG[2] waltz16
 PCPD2 80.00 usec
 PLW2 18.00000000 W
 PLW12 0.37195000 W
 PLW13 0.23805000 W

F2 - Processing parameters
 SI 32768
 SF 125.7653419 MHz
 WDW EM
 SSB 0
 LB 1.00 Hz
 GB 0
 PC 1.40

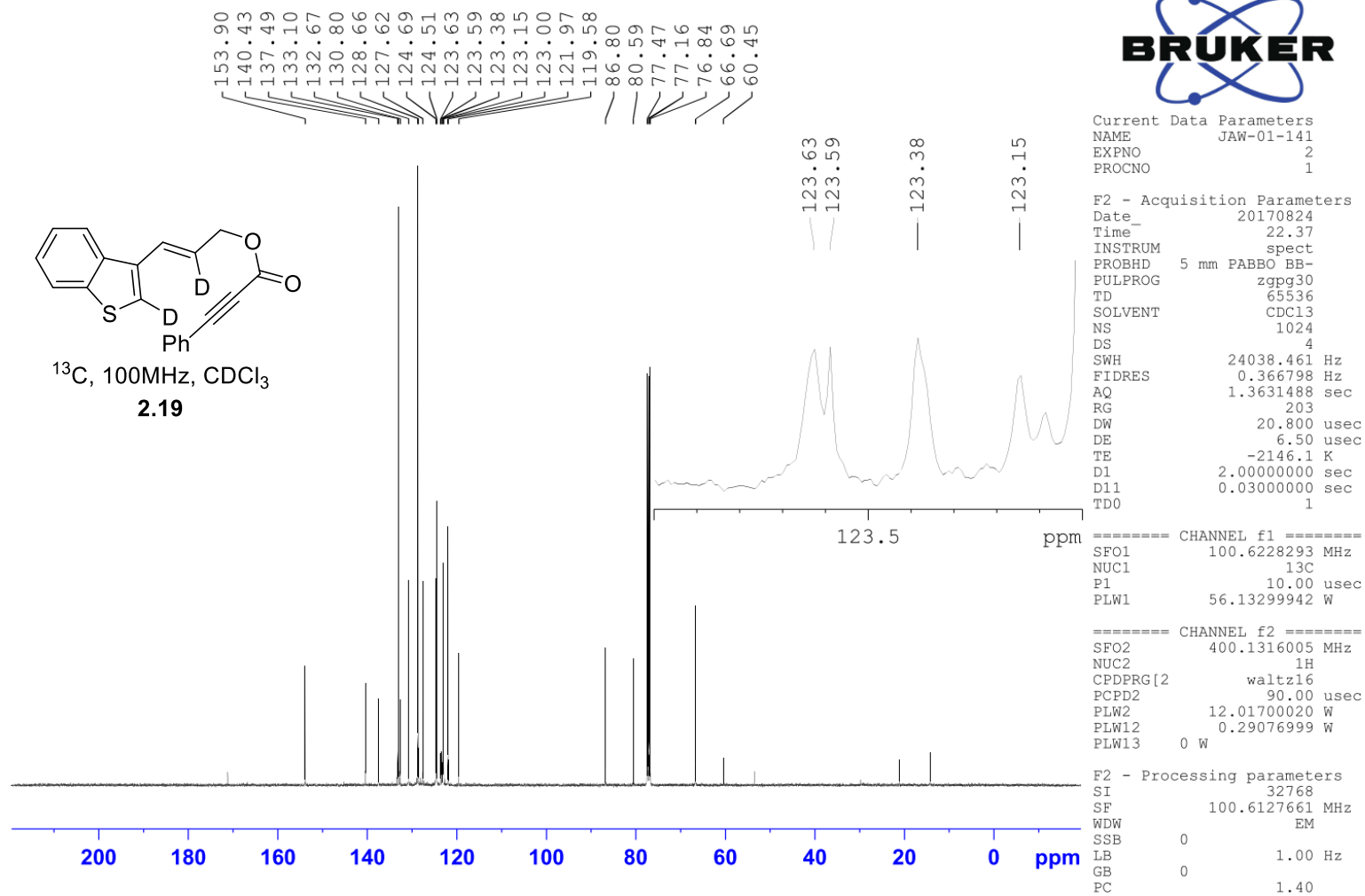


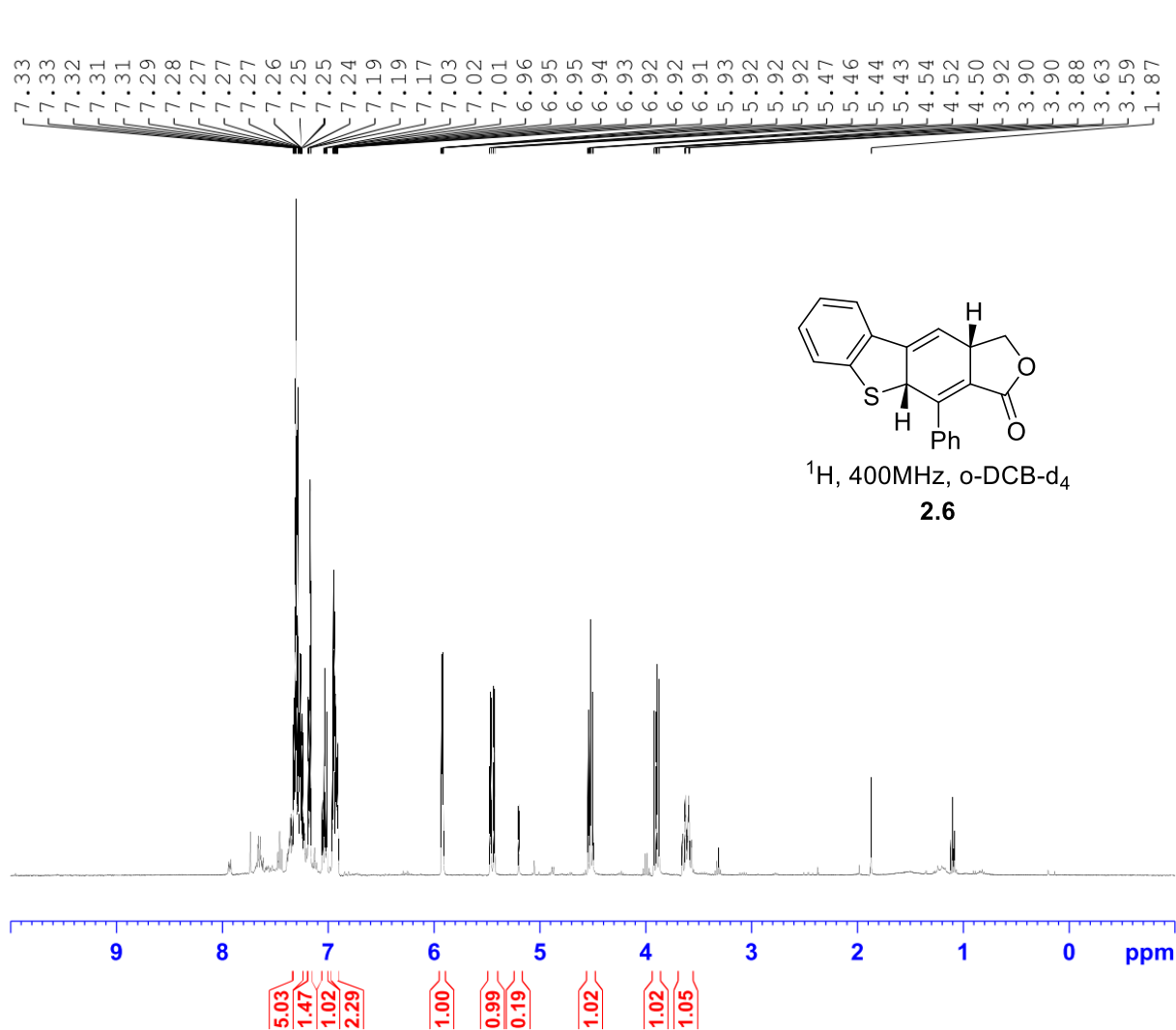
Current Data Parameters
 NAME JAW-01-141
 EXPNO 1
 PROCNO 1

F2 - Acquisition Parameters
 Date_ 20170824
 Time 17.04
 INSTRUM spect
 PROBHD 5 mm PABBO BB-
 PULPROG zg30
 TD 65536
 SOLVENT CDCl3
 NS 16
 DS 2
 SWH 8012.820 Hz
 FIDRES 0.122266 Hz
 AQ 4.0894465 sec
 RG 32
 DW 62.400 usec
 DE 6.50 usec
 TE -1899.1 K
 D1 1.00000000 sec
 TD0 1

===== CHANNEL f1 =====
 SF01 400.1324710 MHz
 NUC1 1H
 P1 13.75 usec
 PLW1 12.01700020 W

F2 - Processing parameters
 SI 65536
 SF 400.1300091 MHz
 WDW EM
 SSB 0
 LB 0.30 Hz
 GB 0
 PC 1.00



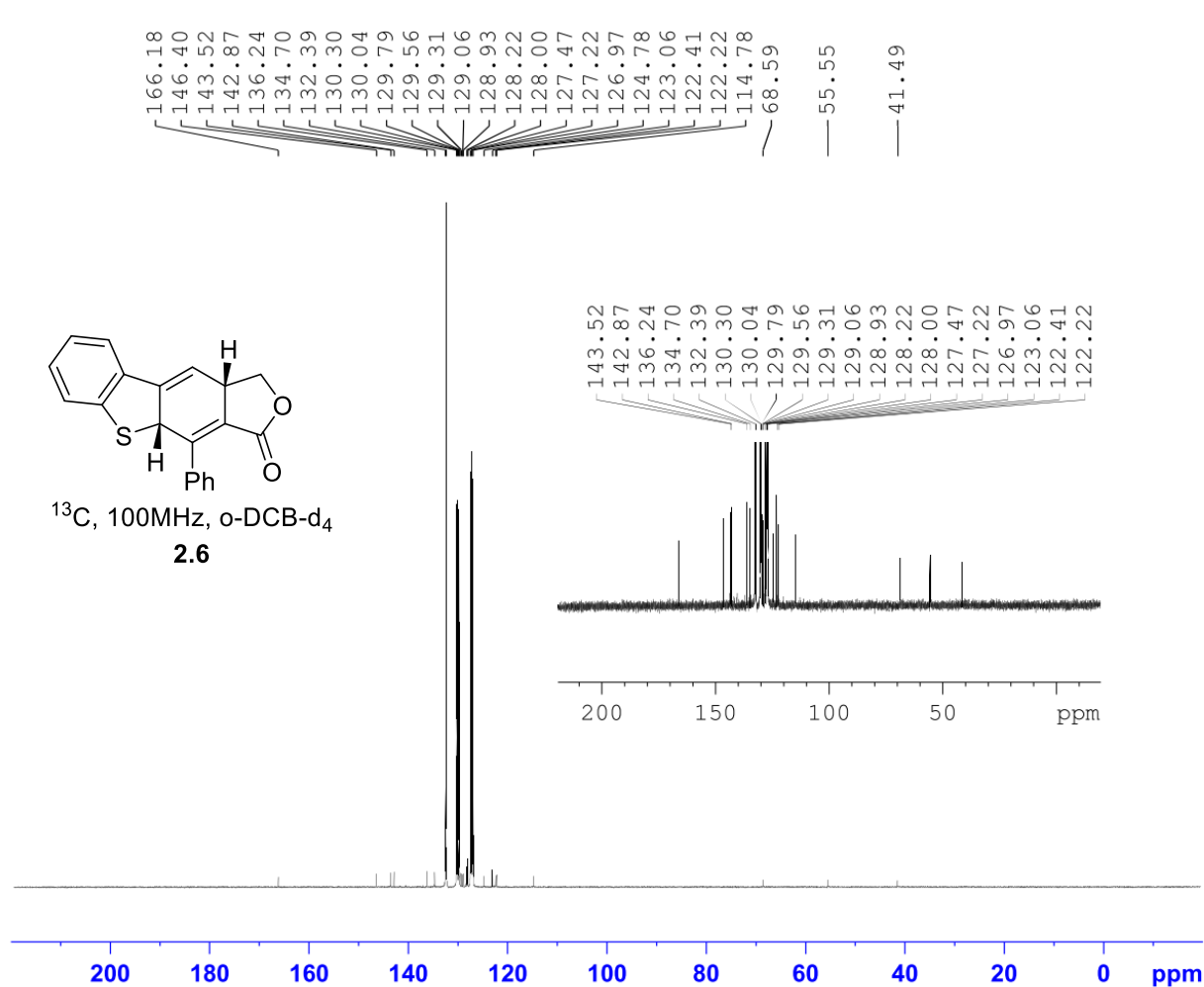


Current Data Parameters
 NAME JAW-01-164
 EXPNO 3
 PROCNO 1

F2 - Acquisition Parameters
 Date_ 20171012
 Time_ 15.39
 INSTRUM spect
 PROBHD 5 mm PADUL 13C
 PULPROG zg30
 TD 65536
 SOLVENT C6D6
 NS 16
 DS 2
 SWH 8223.685 Hz
 FIDRES 0.125483 Hz
 AQ 3.9845889 sec
 RG 114
 DW 60.800 usec
 DE 6.50 usec
 TE 298.1 K
 D1 2.00000000 sec
 TD0 1

===== CHANNEL f1 =====
 NUC1 1H
 P1 9.31 usec
 PL1 -3.90 dB
 PL1W 21.64248466 W
 SFO1 400.2324716 MHz

F2 - Processing parameters
 SI 32768
 SF 400.2300984 MHz
 WDW EM
 SSB 0
 LB 0.30 Hz
 GB 0
 PC 1.00



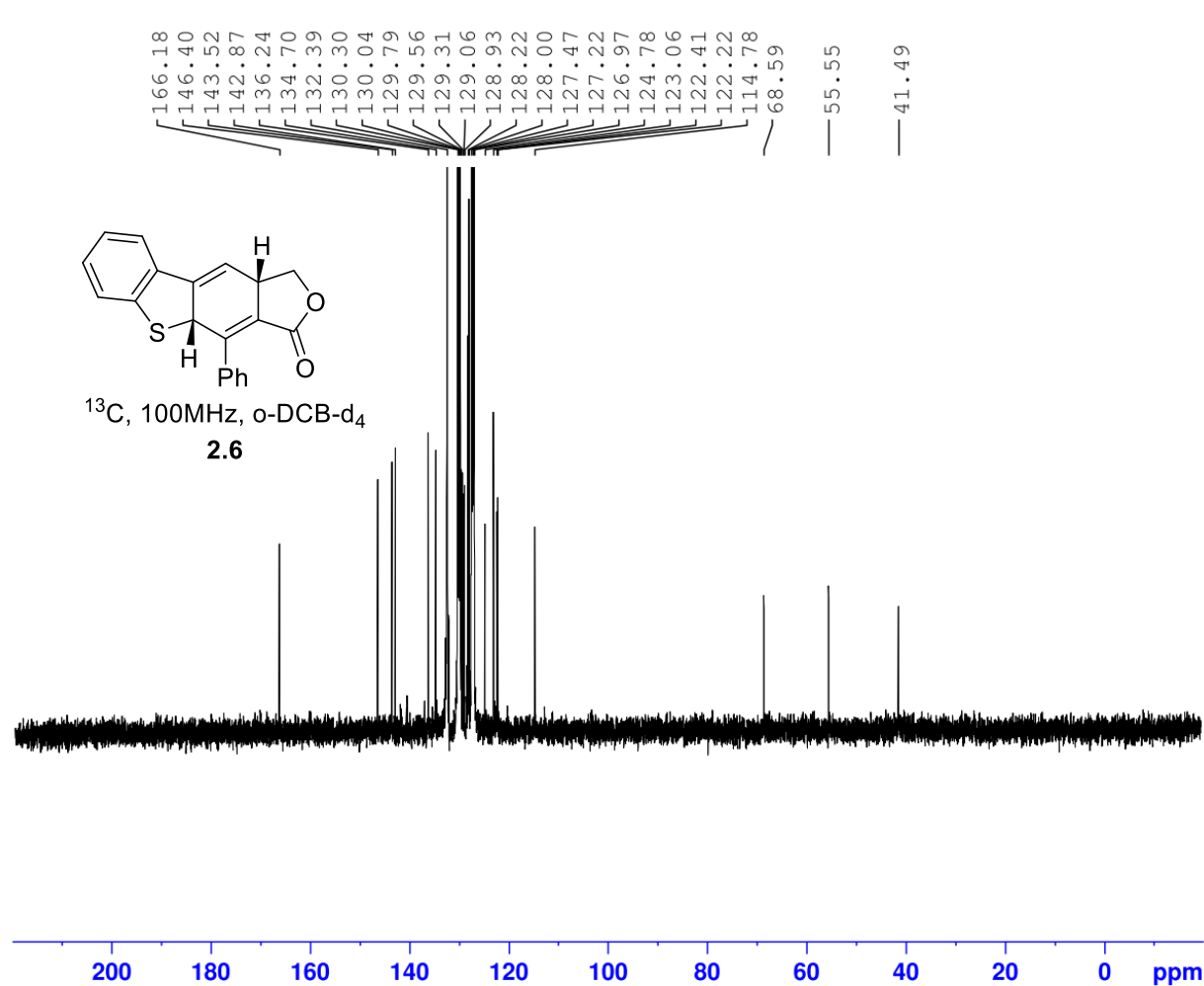
Current Data Parameters
NAME JAW-01-164
EXPNO 4
PROCNO 1

F2 - Acquisition Parameters
Date_ 20171012
Time 16.56
INSTRUM spect
PROBHD 5 mm PADUL 13C
PULPROG zgpg30
TD 65536
SOLVENT C6D6
NS 1024
DS 4
SWH 24038.461 Hz
FIDRES 0.366798 Hz
AQ 1.3631488 sec
RG 203
DW 20.800 usec
DE 6.50 usec
TE 298.2 K
D1 3.00000000 sec
D11 0.03000000 sec
TD0 1

===== CHANNEL f1 =====
NUC1 13C
P1 10.00 usec
PL1 -0.44 dB
PL1W 39.19395828 W
SFO1 100.6479773 MHz

===== CHANNEL f2 =====
CPDPRG[2] waltz16
NUC2 1H
PCPD2 90.00 usec
PL2 -3.90 dB
PL12 15.81 dB
PL13 120.00 dB
PL2W 21.64248466 W
PL12W 0.23137002 W
PL13W 0 W
SFO2 400.2316009 MHz

F2 - Processing parameters
SI 32768
SF 100.6379235 MHz
WDW EM
SSB 0
LB 1.00 Hz
GB 0
PC 1.40



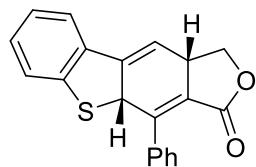
Current Data Parameters
 NAME JAW-01-164
 EXPNO 4
 PROCNO 1

F2 - Acquisition Parameters
 Date_ 20171012
 Time 16.56
 INSTRUM spect
 PROBHD 5 mm PADUL 13C
 PULPROG zgpg30
 TD 65536
 SOLVENT C6D6
 NS 1024
 DS 4
 SWH 24038.461 Hz
 FIDRES 0.366798 Hz
 AQ 1.3631488 sec
 RG 203
 DW 20.800 usec
 DE 6.50 usec
 TE 298.2 K
 D1 3.00000000 sec
 D11 0.03000000 sec
 TD0 1

===== CHANNEL f1 =====
 NUC1 13C
 P1 10.00 usec
 PL1 -0.44 dB
 PL1W 39.19395828 W
 SFO1 100.6479773 MHz

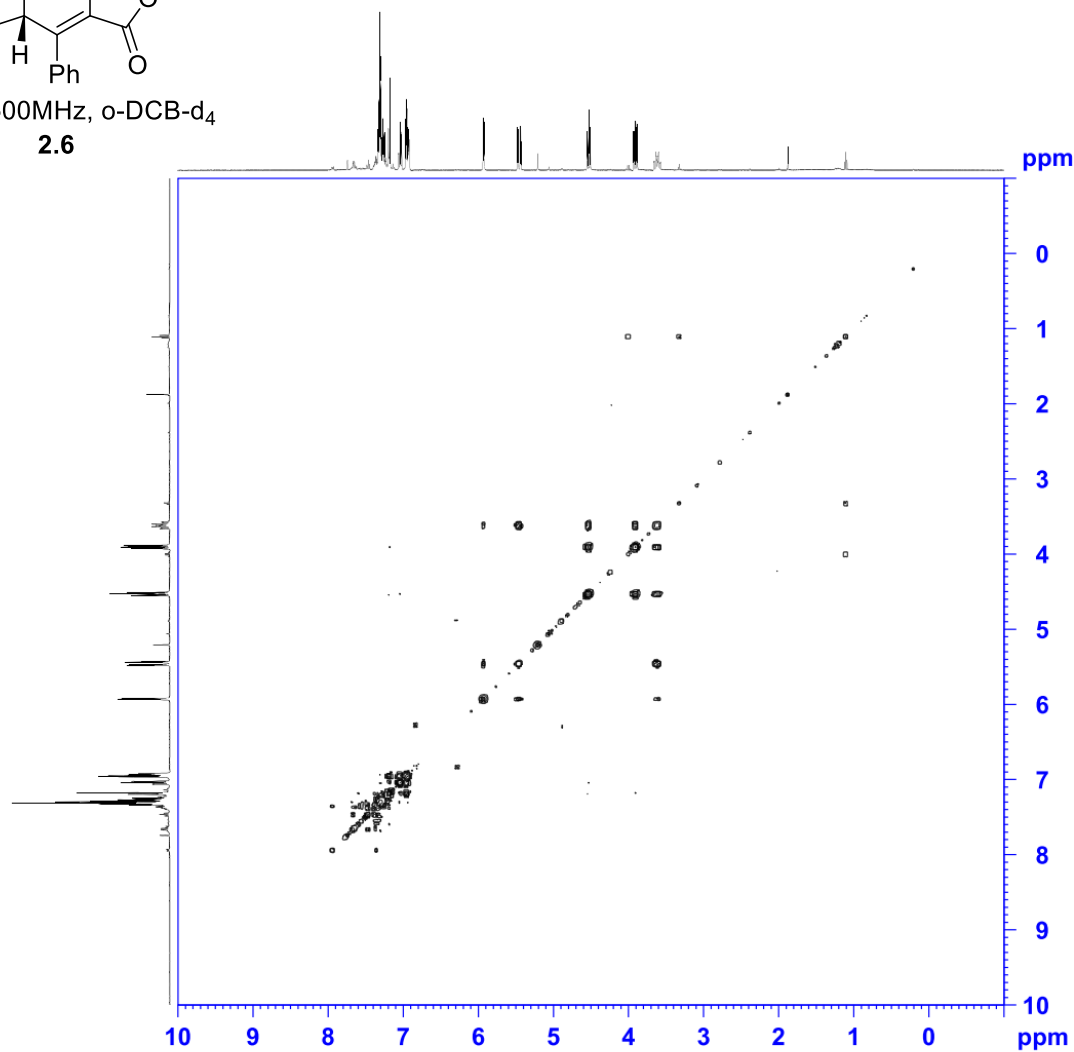
===== CHANNEL f2 =====
 CPDPRG[2] waltz16
 NUC2 1H
 PCPD2 90.00 usec
 PL2 -3.90 dB
 PL12 15.81 dB
 PL13 120.00 dB
 PL2W 21.64248466 W
 PL12W 0.23137002 W
 PL13W 0 W
 SFO2 400.2316009 MHz

F2 - Processing parameters
 SI 32768
 SF 100.6379235 MHz
 WDW EM
 SSB 0
 LB 1.00 Hz
 GB 0
 PC 1.40



COSY, 500MHz, o-DCB-d₄

2.6



```

Current Data Parameters
NAME      JAW-01-164
EXPNO     6
PROCNO    1

F2 - Acquisition Parameters
Date_     20171012
Time      17.07
INSTRUM   spect
PROBHD    5 mm PABBO BB/
PULPROG   cosygpppqf
TD        2048
SOLVENT   C6D6
NS         1
DS         8
SWH        4504.504 Hz
FIDRES     2.199465 Hz
AQ         0.2273280 sec
RG         64
DW         111.000 usec
DE         6.50 usec
TE         296.3 K
DO        0.00000300 sec
D1         1.92586195 sec
D11        0.03000000 sec
D12        0.00002000 sec
D13        0.00000400 sec
D16        0.00020000 sec
INO        0.00022200 sec

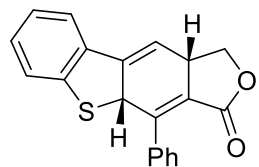
===== CHANNEL f1 =====
SFO1      500.1621512 MHz
NUC1       1H
P0         11.50 usec
P1         11.50 usec
P17        2500.00 usec
PLW1      18.00000000 W
PLW10     3.52139997 W

===== GRADIENT CHANNEL =====
GPNAM[1]  SMSQ10.100
GPZ1      10.00 %
P16       1000.00 usec

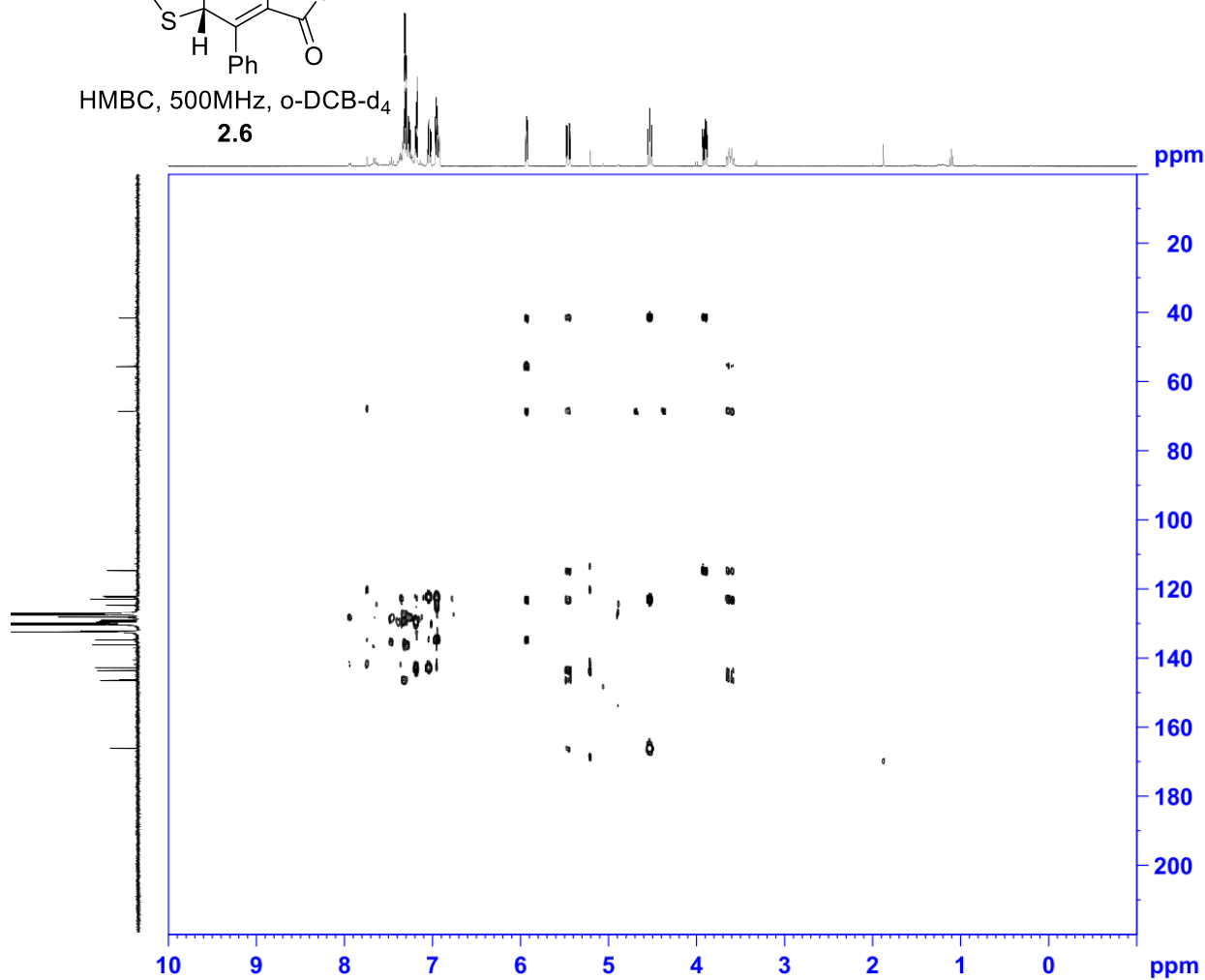
F1 - Acquisition parameters
TD        128
SFO1      500.1622 MHz
FIDRES     70.382881 Hz
SW         9.006 ppm
FnMODE     QF

F2 - Processing parameters
SI         1024
SF         500.1599890 MHz
WDW        QSINE
SSB         0
LB          0 Hz
GB          0
PC          1.40

F1 - Processing parameters
SI         1024
MC2        QF
SF         500.1599889 MHz
WDW        QSINE
SSB         0
LB          0 Hz
GB          0
  
```



HMBC, 500MHz, o-DCB-d₄
2.6



```

Current Data Parameters
NAME      JAW-01-164
EXPNO     8
PROCNO    1

F2 - Acquisition Parameters
Date_     20171012
Time      17.28
INSTRUM   spect
PROBHD    5 mm PABBO BB/
PULPROG   hmbcpglpndqf
TD        2048
SOLVENT   C6D6
NS         4
DS        16
SWH        4504.504 Hz
FIDRES     2.199465 Hz
AQ         0.2273280 sec
RG         203
DW         111.000 usec
DE         6.50 usec
TE         296.9 K
CNST2     145.0000000
CNST13    10.0000000
D0         0.00000300 sec
D1         1.42995799 sec
D2         0.00344828 sec
D6         0.05000000 sec
D16        0.00020000 sec
IN0        0.00001790 sec

===== CHANNEL f1 =====
SFO1      500.1621512 MHz
NUC1       1H
P1         11.50 usec
P2         23.00 usec
PLW1      18.00000000 W

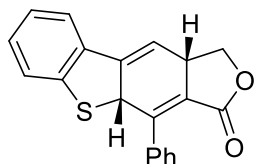
===== CHANNEL f2 =====
SFO2      125.7778879 MHz
NUC2       13C
P3         10.50 usec
PLW2      110.00000000 W

===== GRADIENT CHANNEL =====
GPNAM[1]   SMSQ10.100
GPNAM[2]   SMSQ10.100
GPNAM[3]   SMSQ10.100
GP21       50.00 %
GP22       30.00 %
GP23       40.10 %
P16        1000.00 usec

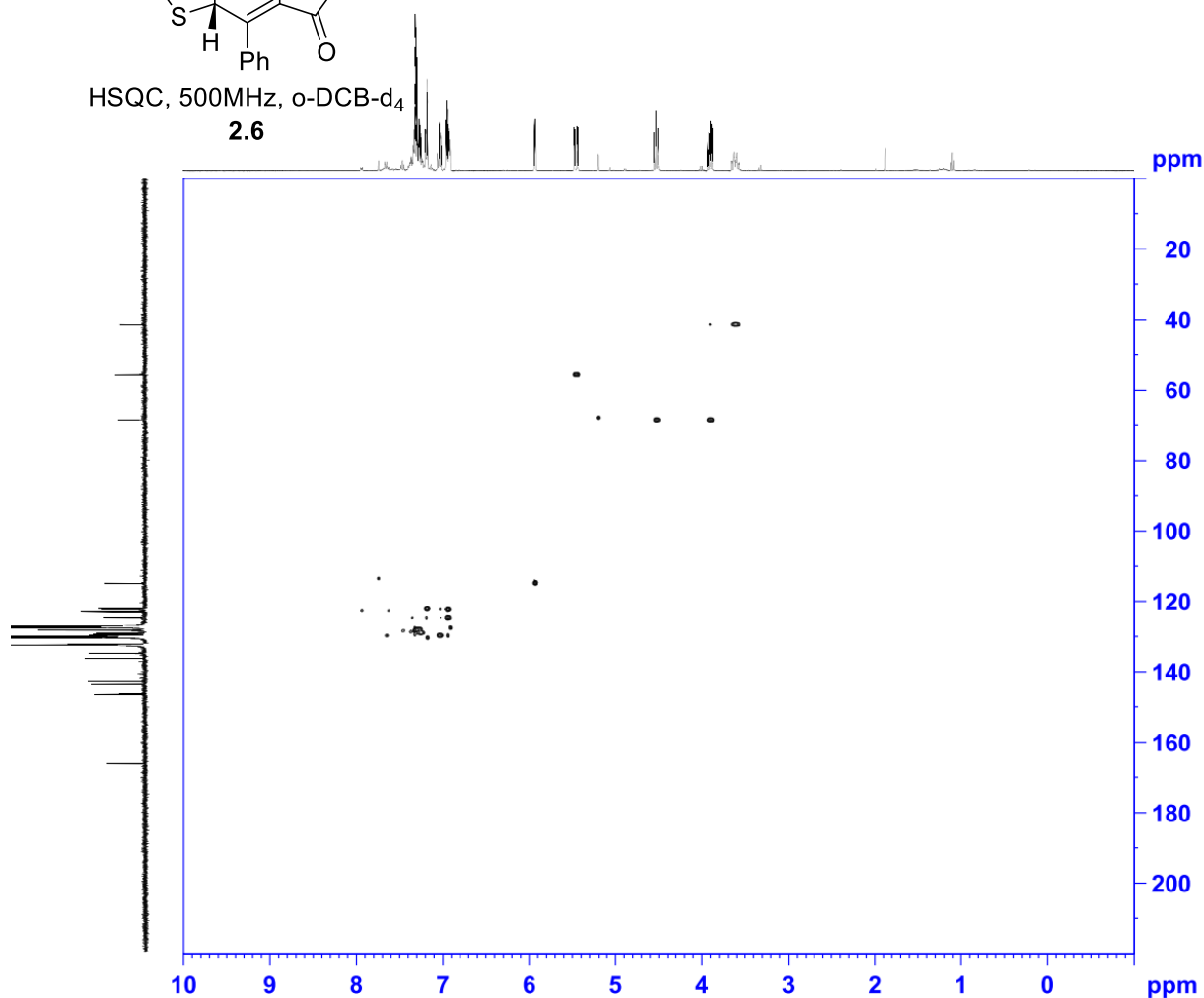
F1 - Acquisition parameters
TD         128
SFO1      125.7779 MHz
FIDRES     436.452515 Hz
SW         222.082 ppm
FnMODE     QF

F2 - Processing parameters
SI         2048
SF         500.1599896 MHz
WDW        SINE
SSB        0
LB         0 Hz
GB         0
PC         1.40

F1 - Processing parameters
SI         1024
MC2        QF
SF         125.7653016 MHz
WDW        SINE
SSB        0
LB         0 Hz
GB         0
  
```



HSQC, 500MHz, o-DCB-d₄
2.6



```
Current Data Parameters
NAME      JAW-01-164
EXPNO     7
PROCNO    1

F2 - Acquisition Parameters
Date_     20171012
Time      17.13
INSTRUM   spect
PROBHD    5 mm PABBO BB/
PULPROG   hsqcetgpa12
TD        1024
SOLVENT   C6D6
NS         2
DS        16
SWH        4504.504 Hz
FIDRES     4.398930 Hz
AQ         0.1136640 sec
RG         203
DW         111.000 usec
DE         6.50 usec
TE         296.3 K
CNST2     145.0000000
DO         0.0000300 sec
D1         1.46313596 sec
D4         0.00172414 sec
D11        0.03000000 sec
D16        0.00020000 sec
D24        0.00086207 sec
IN0        0.00002400 sec
ZGPGTNS

===== CHANNEL f1 =====
SFO1      500.1621512 MHz
NUC1       1H
F1         11.50 usec
P2         23.00 usec
P28        1000.00 usec
PLW1       18.00000000 W

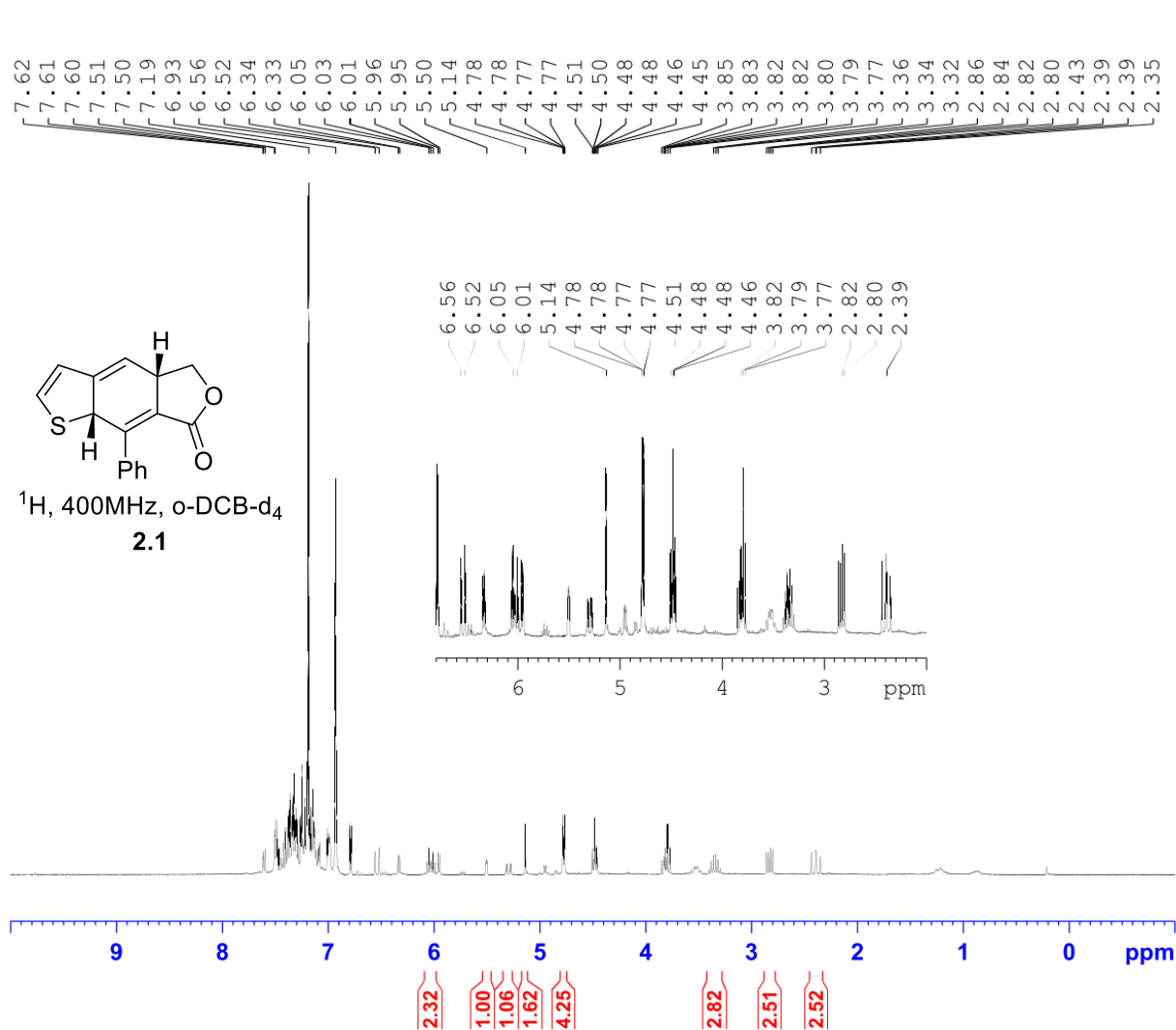
===== CHANNEL f2 =====
SFO2      125.7747618 MHz
NUC2       13C
CPDPRG2   gacp
P3         10.50 usec
P4         21.00 usec
PCPD2     70.00 usec
PLW2      110.00000000 W
PLW12     2.47499990 W

===== GRADIENT CHANNEL =====
GPNAM[1]  SMSQ10.100
GPNAM[2]  SMSQ10.100
GPNAM[3]  SMSQ10.100
GPNAM[4]  SMSQ10.100
GPE1      80.00 %
GPE2      20.10 %
GPE3      11.00 %
GPE4      -5.00 %
P16       1000.00 usec
P19       600.00 usec

F1 - Acquisition parameters
TD         256
SFO1       125.7748 MHz
FIDRES     162.760422 Hz
SW         165.640 ppm
F0MODE     Echo-Antiecho

F2 - Processing parameters
SI         1024
SF         500.1599898 MHz
WDW        QSINE
SSB        2
LB         0 Hz
GB         0
PC         1.40

F1 - Processing parameters
SI         1024
MC2        echo-antiecho
SF         125.7653040 MHz
WDW        QSINE
SSB        2
LB         0 Hz
GB         0
```

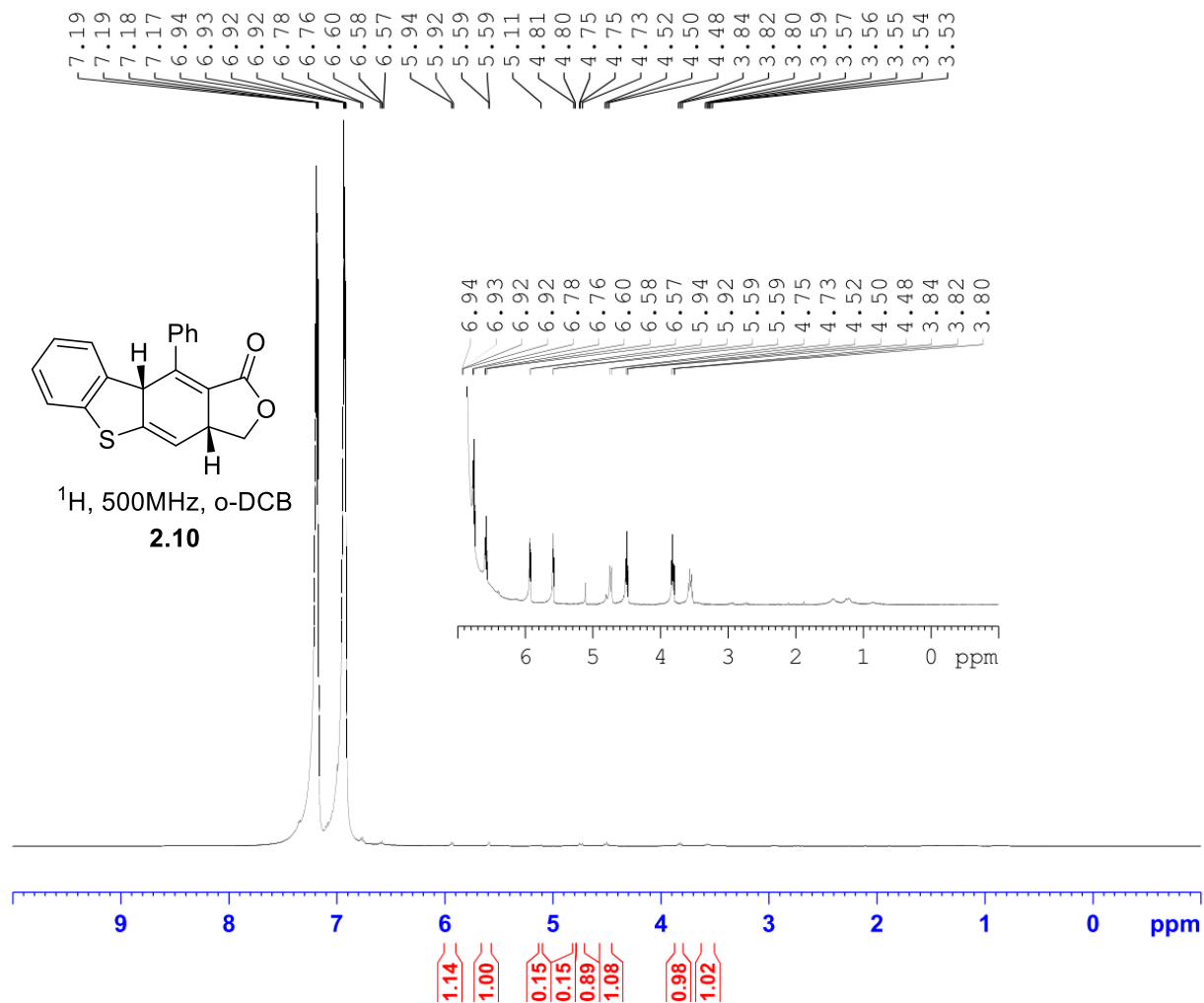


Current Data Parameters
 NAME JAW-01-008
 EXPNO 2
 PROCNO 1

F2 - Acquisition Parameters
 Date_ 20160617
 Time 13.16
 INSTRUM spect
 PROBHD 5 mm PABBO BB-
 PULPROG zg30
 TD 65536
 SOLVENT C6D6
 NS 16
 DS 2
 SWH 8012.820 Hz
 FIDRES 0.122266 Hz
 AQ 4.0894465 sec
 RG 128
 DW 62.400 usec
 DE 6.50 usec
 TE 95.6 K
 D1 1.00000000 sec
 TD0 1

===== CHANNEL f1 =====
 SF01 400.1324710 MHz
 NUC1 1H
 P1 13.75 usec
 PLW1 12.01700020 W

F2 - Processing parameters
 SI 65536
 SF 400.1300900 MHz
 WDW EM
 SSB 0
 LB 0.30 Hz
 GB 0
 PC 1.00

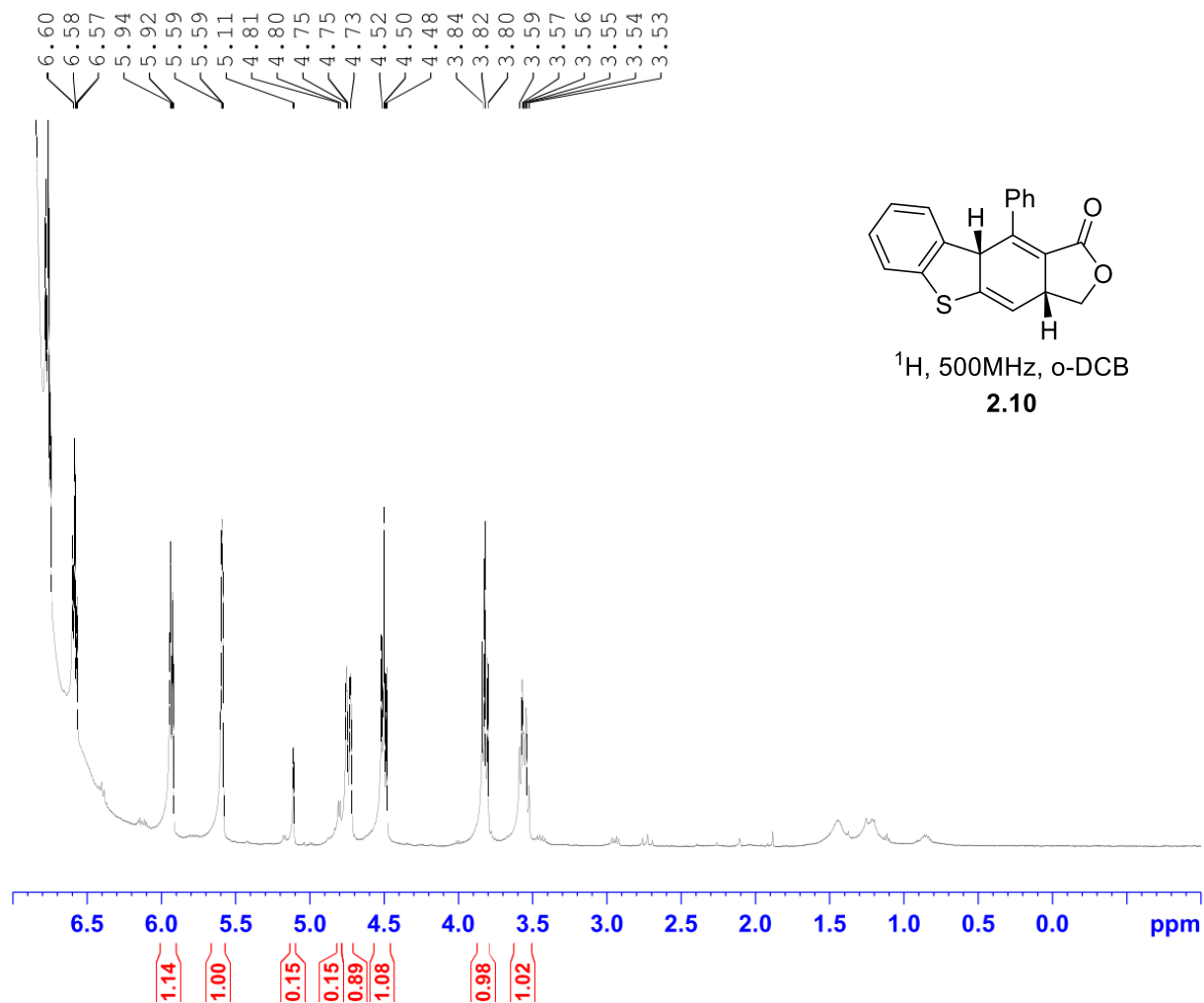


Current Data Parameters
 NAME JAW-02-115
 EXPNO 3
 PROCNO 1

F2 - Acquisition Parameters
 Date_ 20180817
 Time_ 12.53
 INSTRUM spect
 PROBHD 5 mm PABBO BB/
 PULPROG zg30
 TD 65536
 SOLVENT None
 NS 32
 DS 2
 SWH 10000.000 Hz
 FIDRES 0.152588 Hz
 AQ 3.2767999 sec
 RG 5.6
 DW 50.000 usec
 DE 6.50 usec
 TE 296.1 K
 D1 1.00000000 sec
 TD0 1

===== CHANNEL f1 =====
 SFO1 500.1630887 MHz
 NUC1 1H
 P1 11.50 usec
 PLW1 18.00000000 W

F2 - Processing parameters
 SI 65536
 SF 500.1598041 MHz
 WDW EM
 SSB 0
 LB 0.30 Hz
 GB 0
 PC 1.00

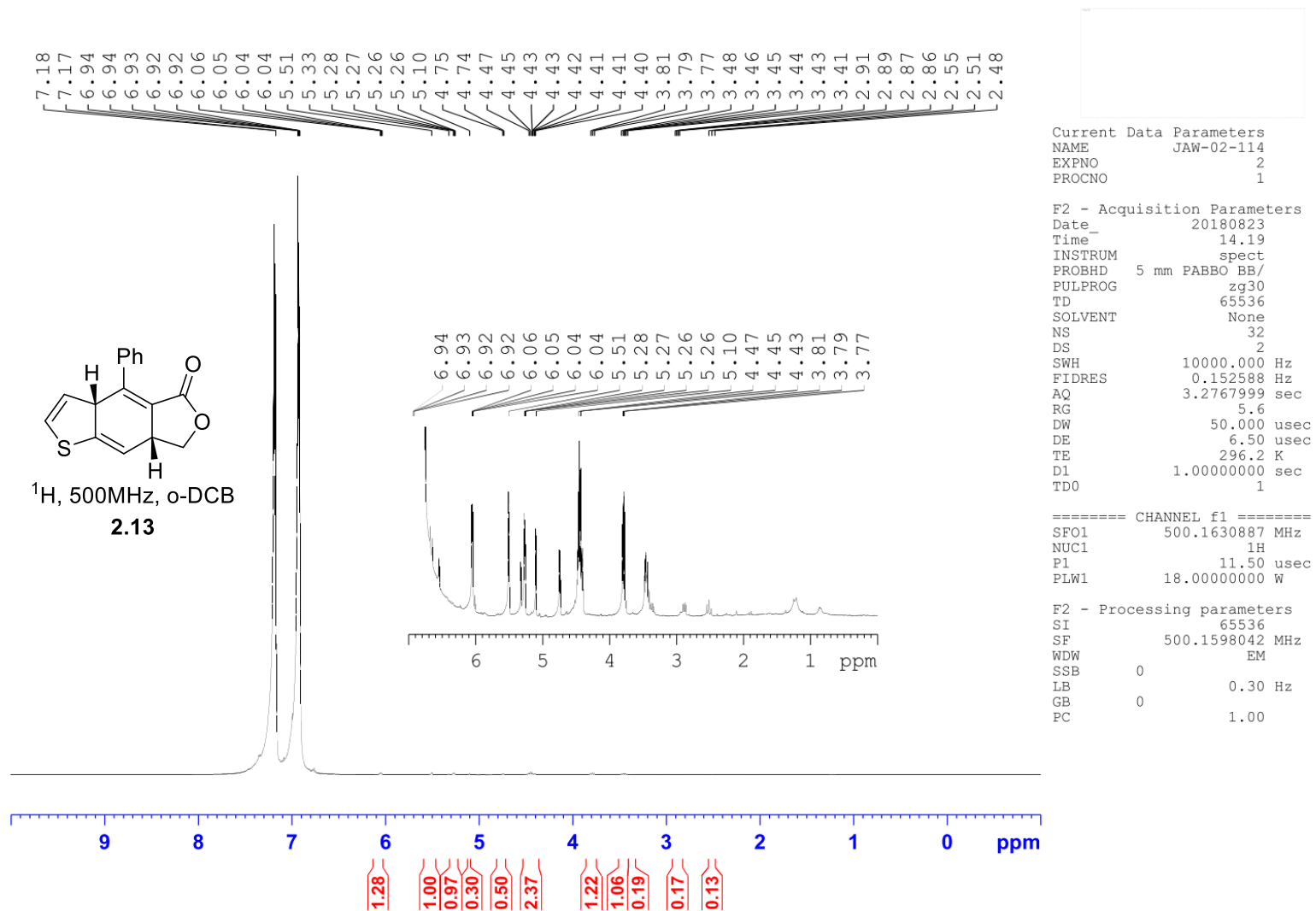


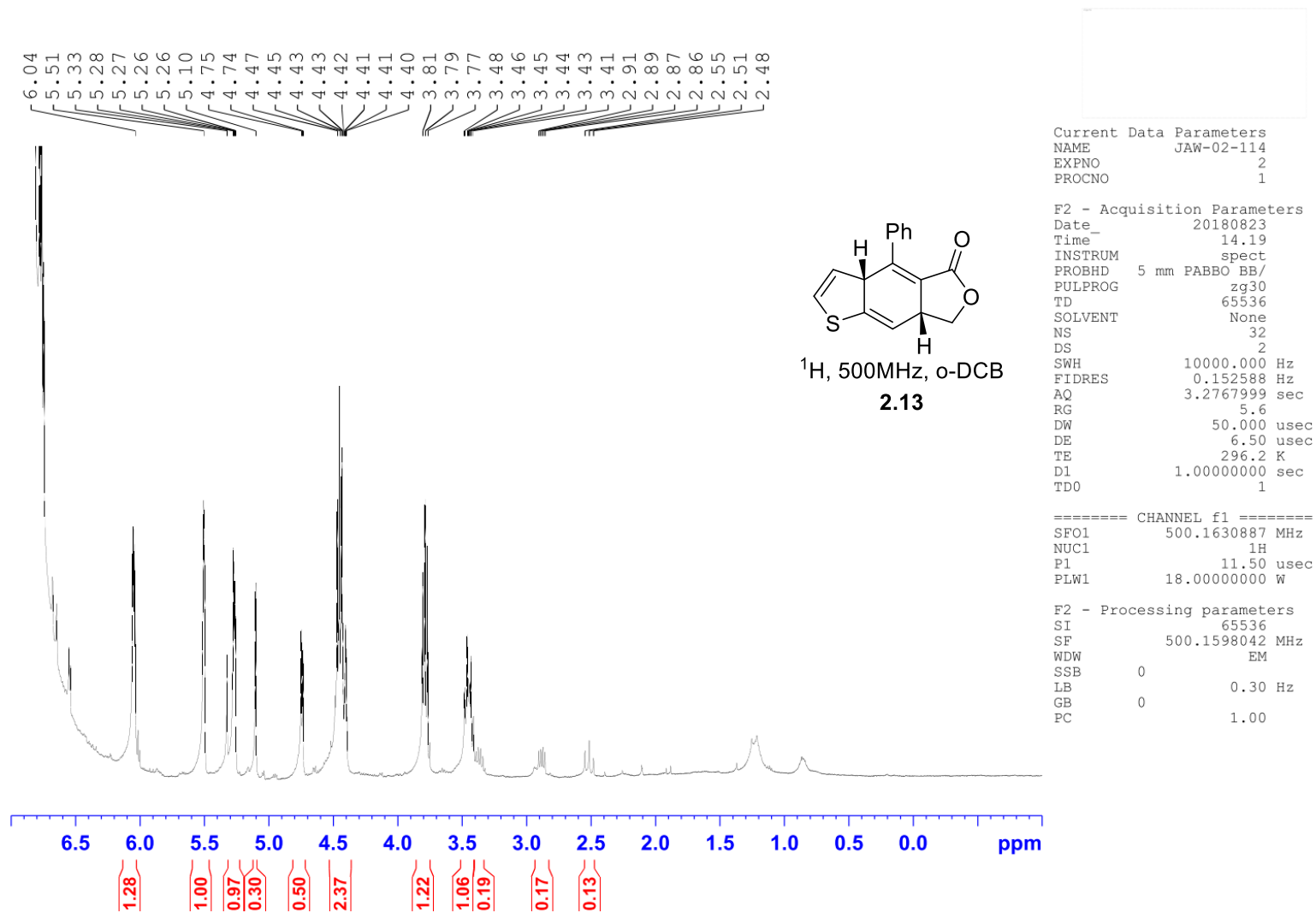
Current Data Parameters
NAME JAW-02-115
EXPNO 3
PROCNO 1

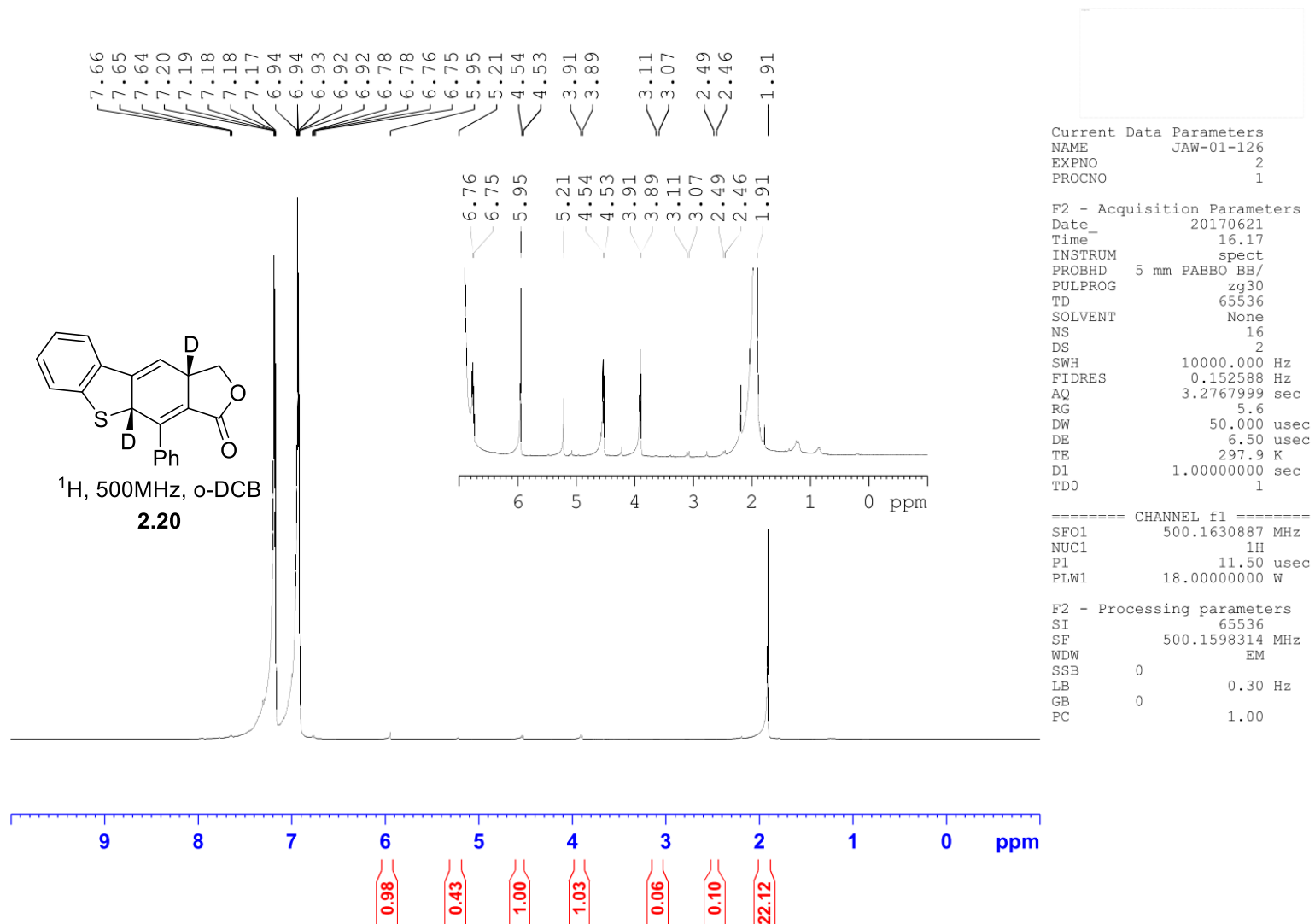
F2 - Acquisition Parameters
Date_ 20180817
Time_ 12.53
INSTRUM spect
PROBHD 5 mm PABBO BB/
PULPROG zg30
TD 65536
SOLVENT None
NS 32
DS 2
SWH 10000.000 Hz
FIDRES 0.152588 Hz
AQ 3.2767999 sec
RG 5.6
DW 50.000 usec
DE 6.50 usec
TE 296.1 K
D1 1.00000000 sec
TD0 1

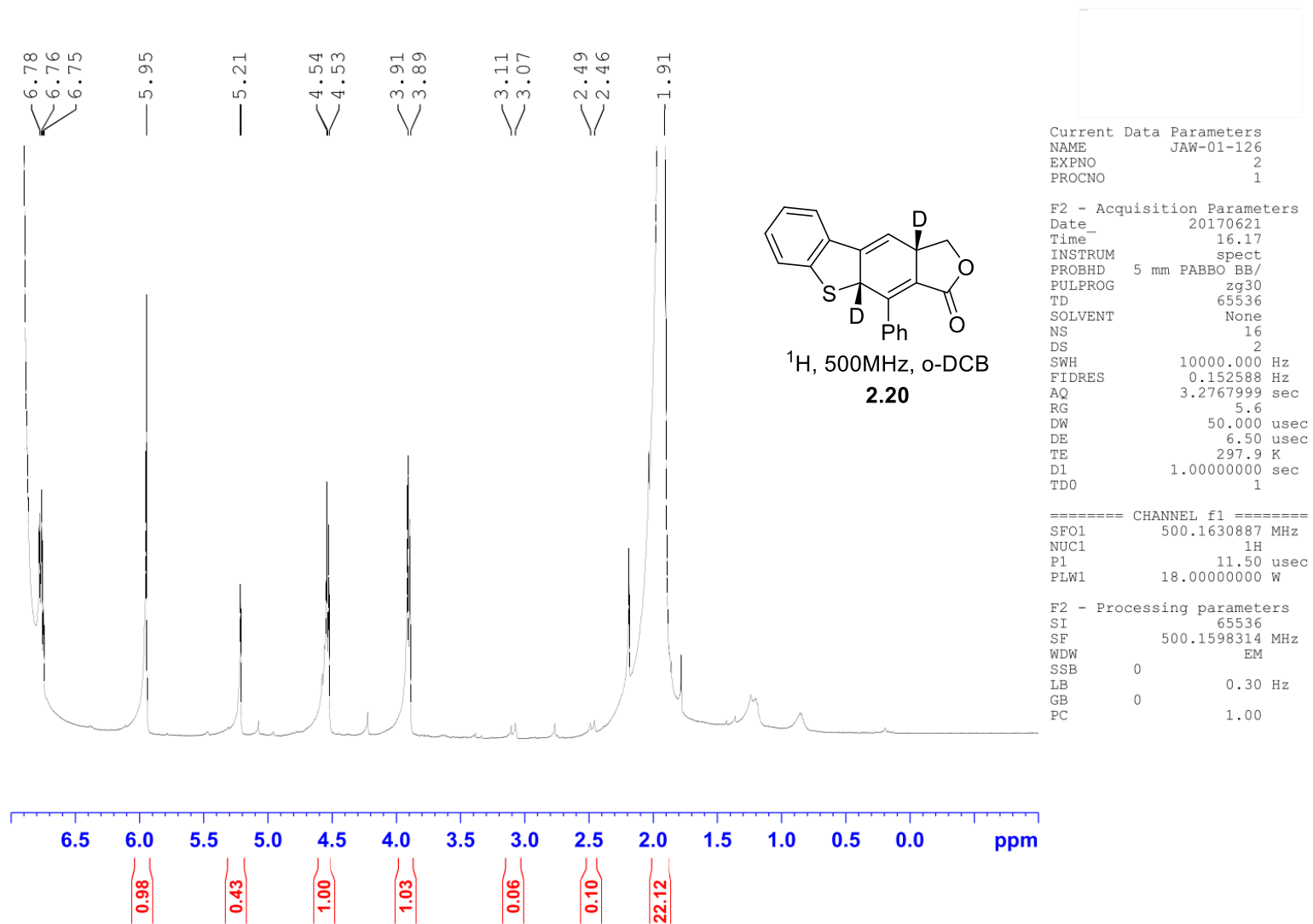
===== CHANNEL f1 =====
SF01 500.1630887 MHz
NUC1 1H
P1 11.50 usec
PLW1 18.00000000 W

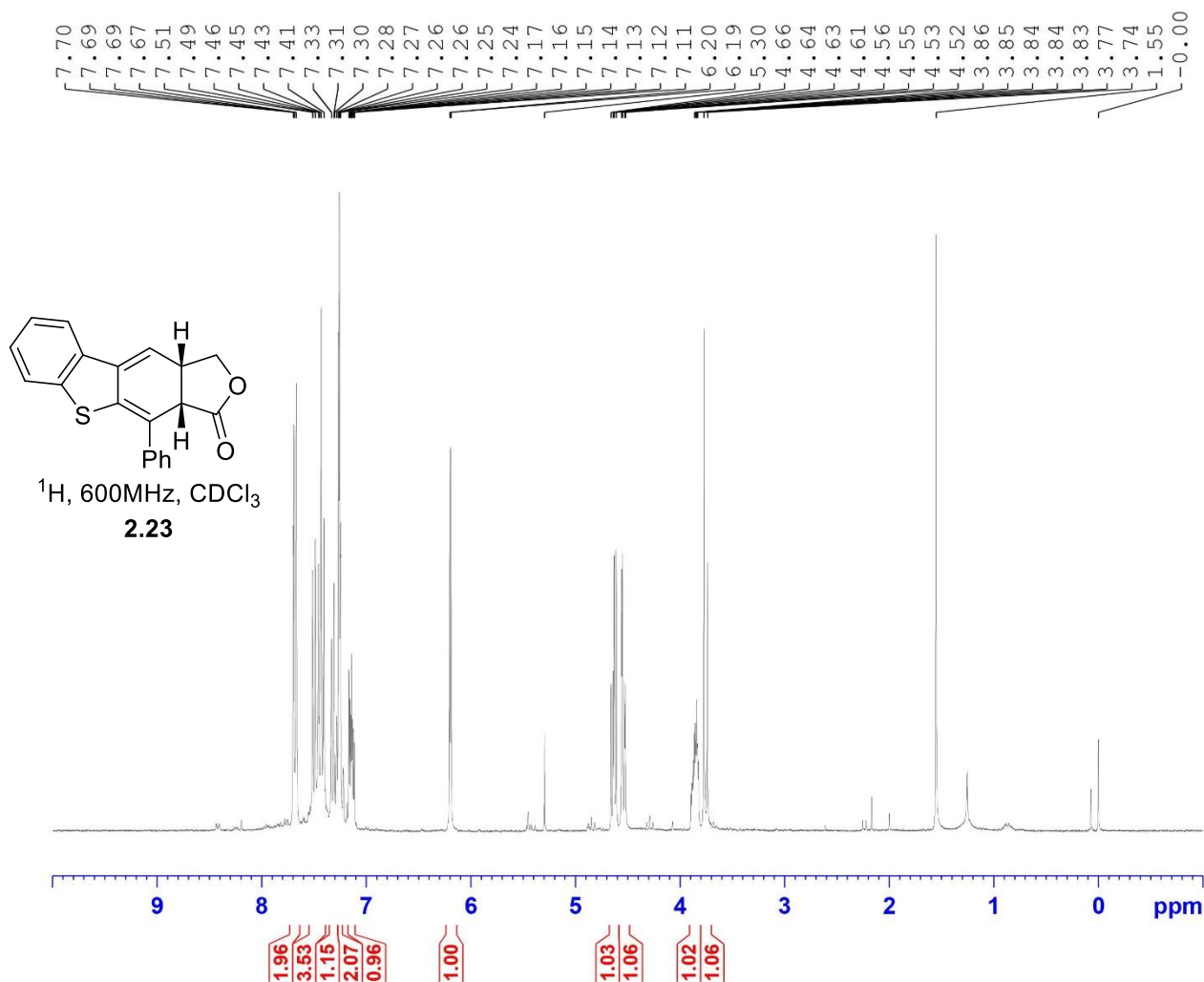
F2 - Processing parameters
SI 65536
SF 500.1598041 MHz
WDW EM
SSB 0
LB 0.30 Hz
GB 0
PC 1.00







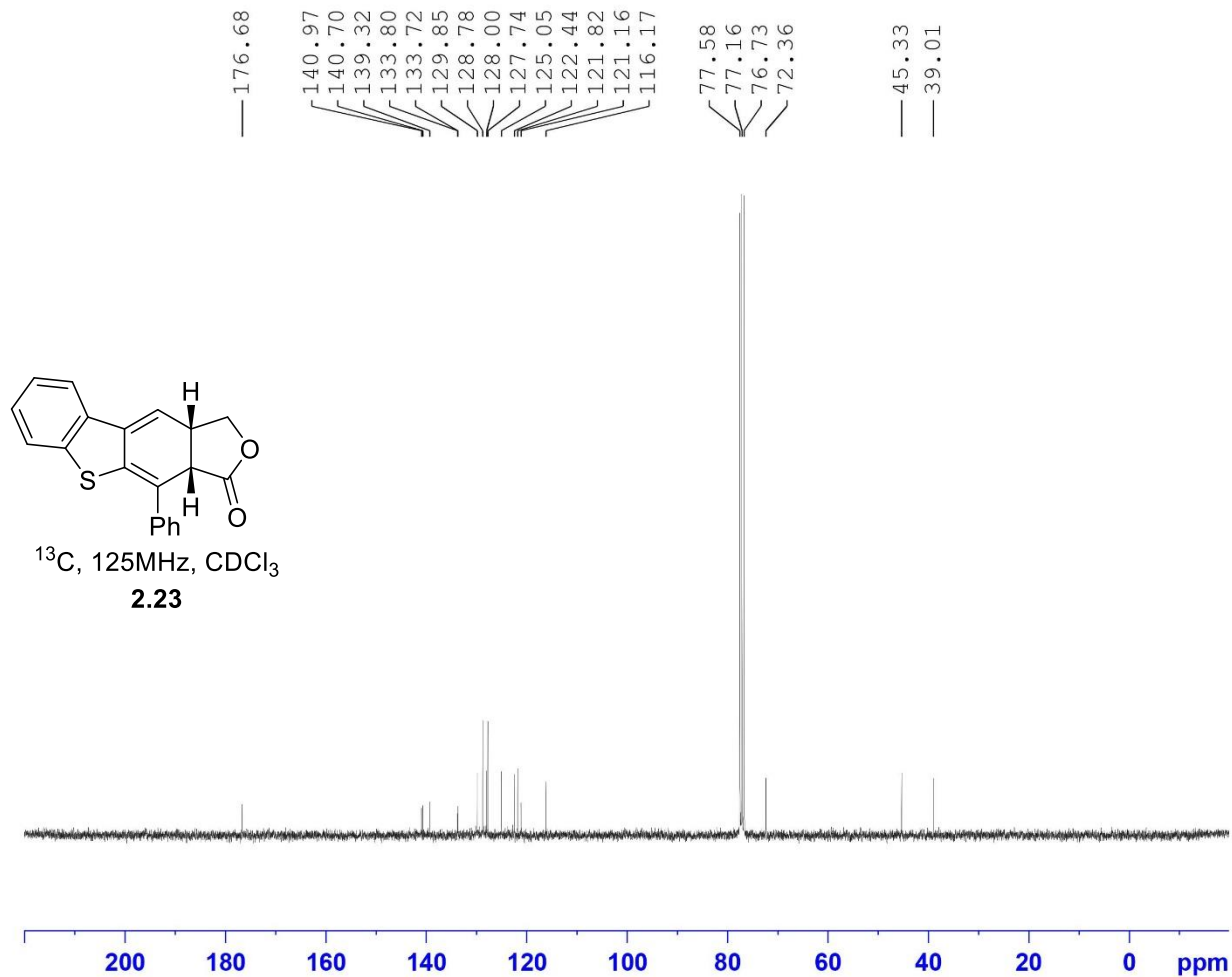




Current Data Parameters
 NAME JAW-03-112
 EXPNO 1
 PROCNO 1

F2 - Acquisition Parameters
 Date_ 20210428
 Time_ 16.09 h
 INSTRUM spect
 PROBHD Z104275_0423 (
 PULPROG zg30
 TD 32768
 SOLVENT CDCl3
 NS 16
 DS 2
 SWH 6009.615 Hz
 FIDRES 0.366798 Hz
 AQ 2.7262976 sec
 RG 181
 DW 83.200 usec
 DE 6.50 usec
 TE 294.5 K
 D1 1.00000000 sec
 TD0 1
 SFO1 300.2318539 MHz
 NUC1 1H
 P0 4.67 usec
 P1 14.00 usec
 PLW1 17.16200066 W

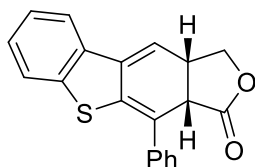
F2 - Processing parameters
 SI 65536
 SF 300.2300080 MHz
 WDW EM
 SSB 0
 LB 0.30 Hz
 GB 0
 PC 1.00



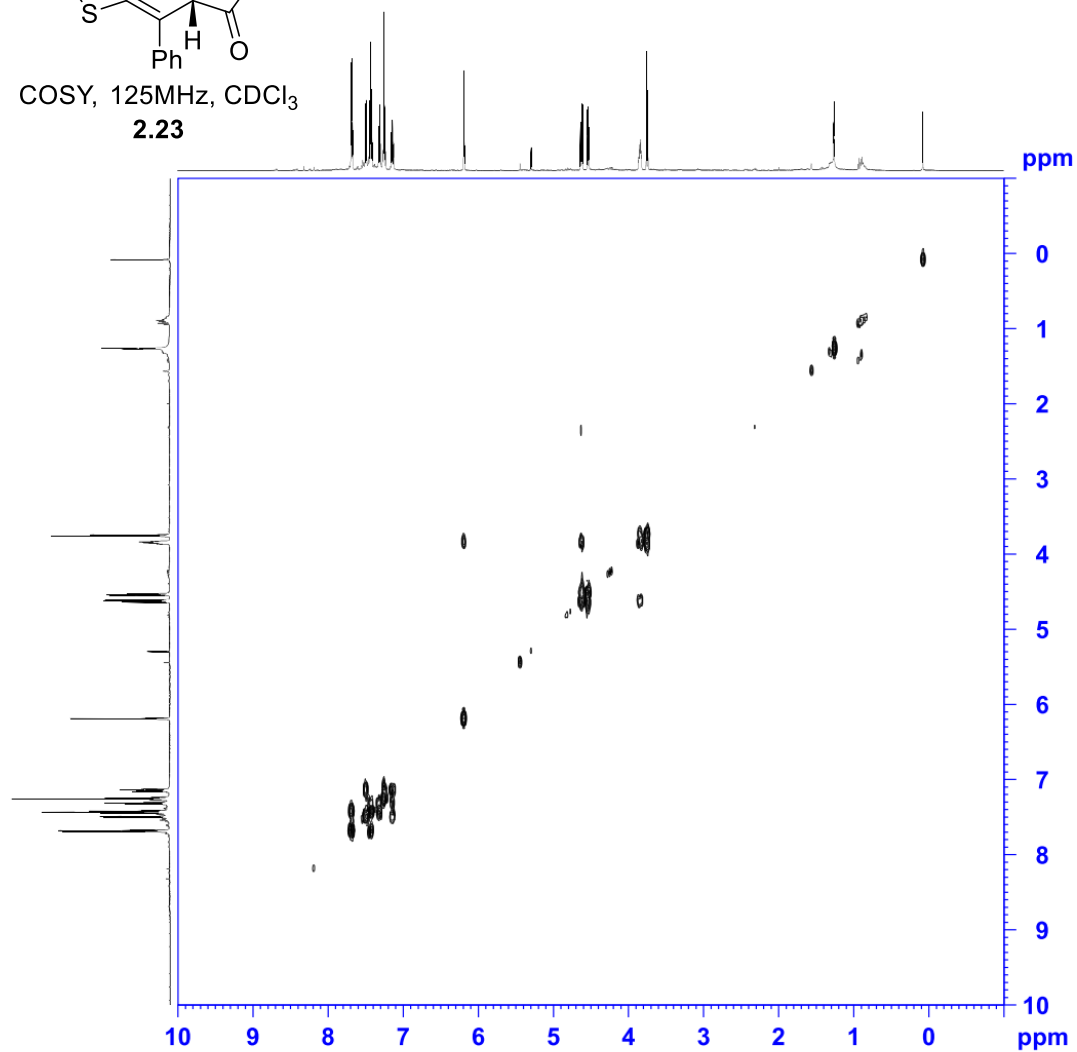
Current Data Parameters
 NAME JAW-03-112
 EXPNO 2
 PROCNO 1

F2 - Acquisition Parameters
 Date_ 20210428
 Time_ 23.12 h
 INSTRUM spect
 PROBHD Z104275_0423 (
 PULPROG zgpg30
 TD 65536
 SOLVENT CDCl3
 NS 1024
 DS 4
 SWH 18115.941 Hz
 FIDRES 0.552855 Hz
 AQ 1.8087935 sec
 RG 1030
 DW 27.600 usec
 DE 6.50 usec
 TE 294.8 K
 D1 2.00000000 sec
 D11 0.03000000 sec
 TD0 1
 SFO1 75.5004428 MHz
 NUC1 13C
 P0 3.33 usec
 P1 10.00 usec
 PLW1 39.28099823 W
 SFO2 300.2312009 MHz
 NUC2 1H
 CPDPRG[2] waltz65
 PCPD2 90.00 usec
 PLW2 17.16200066 W
 PLW12 0.41528001 W
 PLW13 0.20888001 W

F2 - Processing parameters
 SI 32768
 SF 75.4928834 MHz
 WDW EM
 SSB 0
 LB 1.00 Hz
 GB 0
 PC 1.40



COSY, 125MHz, CDCl₃
2.23



Current Data Parameters
NAME JAW-02-179-b
EXPNO 9
PROCNO 1

F2 - Acquisition Parameters
Date_ 20181214
Time 18.11
INSTRUM spect
PROBHD 5 mm PABBO BB/
PULPROG cosygpppqf
TD 2048
SOLVENT CDCl3
NS 6
DS 8
SWH 6684.492 Hz
FIDRES 3.263912 Hz
AQ 0.1531904 sec
RG 203
DW 74.800 usec
DE 6.50 usec
TE 297.4 K
D0 0.00000300 sec
D1 2.00000000 sec
D11 0.03000000 sec
D12 0.00002000 sec
D13 0.00000400 sec
D16 0.00020000 sec
IN0 0.00014960 sec

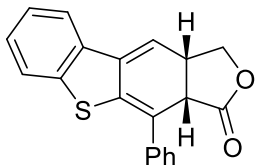
===== CHANNEL f1 =====
SFO1 500.1630071 MHz
NUC1 1H
P0 11.50 usec
P1 11.50 usec
P17 2500.00 usec
PLW1 18.00000000 W
PLW10 3.52139997 W

===== GRADIENT CHANNEL =====
GPNAM[1] SMSQ10.100
GPZ1 10.00 %
P16 1000.00 usec

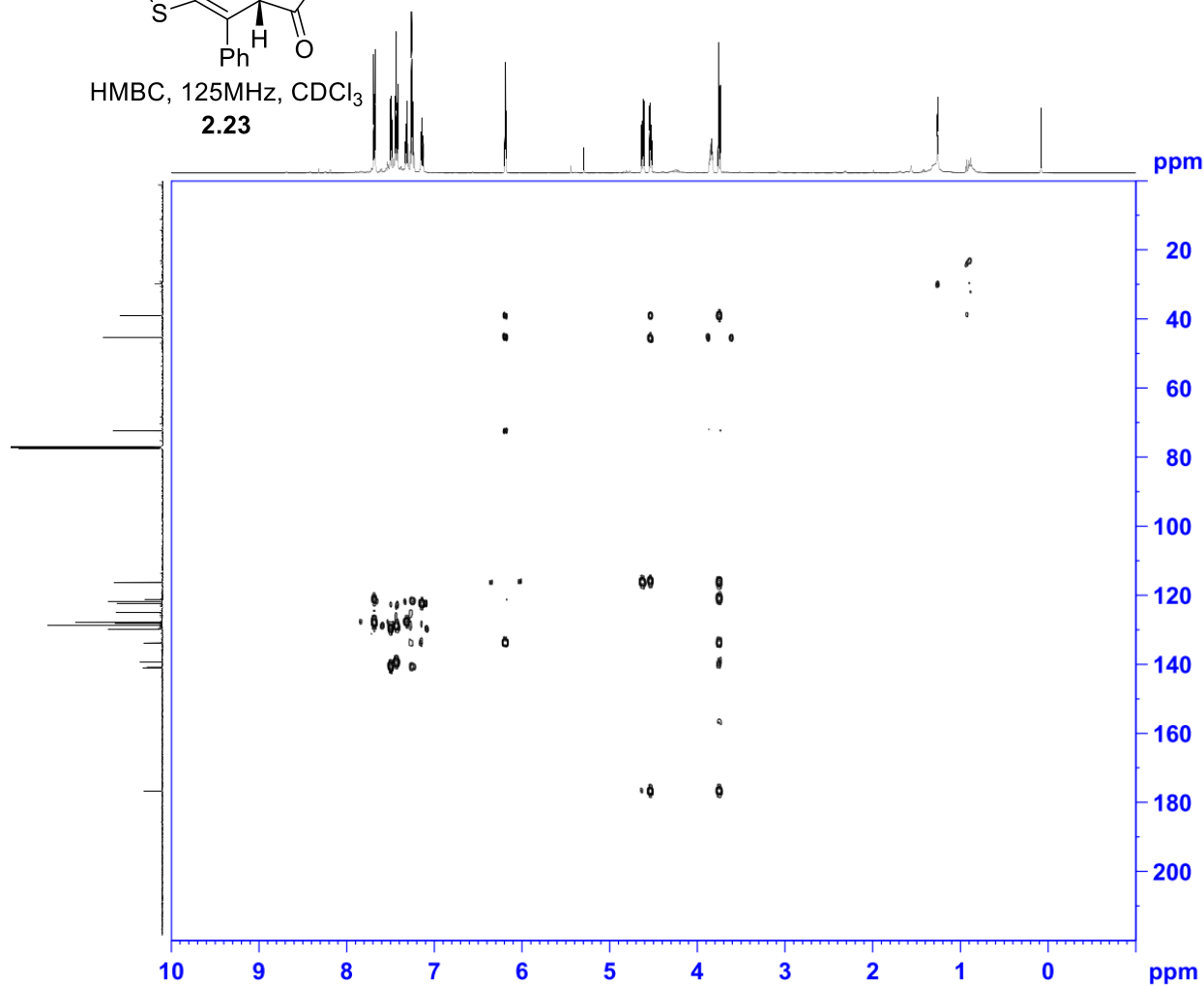
F1 - Acquisition parameters
TD 32
SFO1 500.163 MHz
FIDRES 417.780762 Hz
SW 13.365 ppm
FnMODE QF

F2 - Processing parameters
SI 1024
SF 500.1600127 MHz
WDW QSINE
SSB 0
LB 0 Hz
GB 0
PC 1.40

F1 - Processing parameters
SI 1024
MC2 QF
SF 500.1600139 MHz
WDW QSINE
SSB 0
LB 0 Hz
GB 0



HMBC, 125MHz, CDCl₃
2.23



Current Data Parameters
NAME JAW-02-179-b
EXPNO 7
PROCNO 1

F2 - Acquisition Parameters
Date_ 20181214
Time 17:52
INSTRUM spect
PROBHD 5 mm PABBO BB/
FULPROG hmbcgp1pndqf
TD 2048
SOLVENT CDCl3
NS 8
DS 8
SWH 6510.417 Hz
FIDRES 3.178914 Hz
AQ 0.1572864 sec
RG 203
RW 76.800 usec
DE 6.50 usec
TE 297.3 K
CNST2 145.0000000
CNST13 10.0000000
D0 0.00000300 sec
D1 1.50000000 sec
D2 0.00344828 sec
D6 0.05000000 sec
D16 0.00020000 sec
IN0 0.00001790 sec

----- CHANNEL f1 -----
SFO1 500.1631510 MHz
NUC1 1H
P1 11.50 usec
P2 23.00 usec
PLW1 18.00000000 W

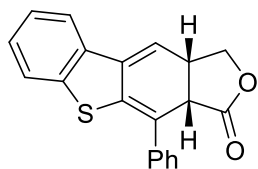
----- CHANNEL f2 -----
SFO2 125.7778879 MHz
NUC2 13C
P3 10.50 usec
PLW2 110.00000000 W

----- GRADIENT CHANNEL -----
GPNAM[1] SMSQ10.100
GPNAM[2] SMSQ10.100
GPNAM[3] SMSQ10.100
GPZ1 50.00 %
GPZ2 30.00 %
GPZ3 40.10 %
P16 1000.00 usec

F1 - Acquisition parameters
TD 32
SFO1 125.7779 MHz
FIDRES 1745.810059 Hz
SW 222.082 ppm
FnMODE QF

F2 - Processing parameters
SI 2048
SF 500.1600127 MHz
WDW SINE
SSB 0
LB 0 Hz
GB 0
PC 1.40

F1 - Processing parameters
SI 1024
MC2 QF
SF 125.7653259 MHz
WDW SINE
SSB 0
LB 0 Hz
GB 0



HSQC, 125MHz, CDCl₃

2.23



Current Data Parameters
NAME JAW-02-179-b
EXPNO 8
PROCNO 1

F2 - Acquisition Parameters
Date_ 20181214
Time_ 18.01
INSTRUM spect
PROBHD 5 mm PABBO BBO
PULPROG haqetgpaap2.2
TD 1024
SOLVENT CDCl₃
NS 4
DS 14
SWH 6009.615 Hz
FIDRES 5.868765 Hz
AQ 0.0851968 sec
RG 203
DW 83.200 usec
DE 6.50 usec
TE 297.4 K
CNS2 145.000000
CNS217 -0.500000
D0 0.0000300 sec
D1 2.0000000 sec
D11 0.00172414 sec
D16 0.0002000 sec
D24 0.0008900 sec
TMS 0.0002410 sec

===== CHANNEL f1 =====
SFO1 500.1623508 MHz
NUC1 1H
P1 11.50 usec
P2 23.00 usec
P28 1000.00 usec
PLM1 18.0000000 W

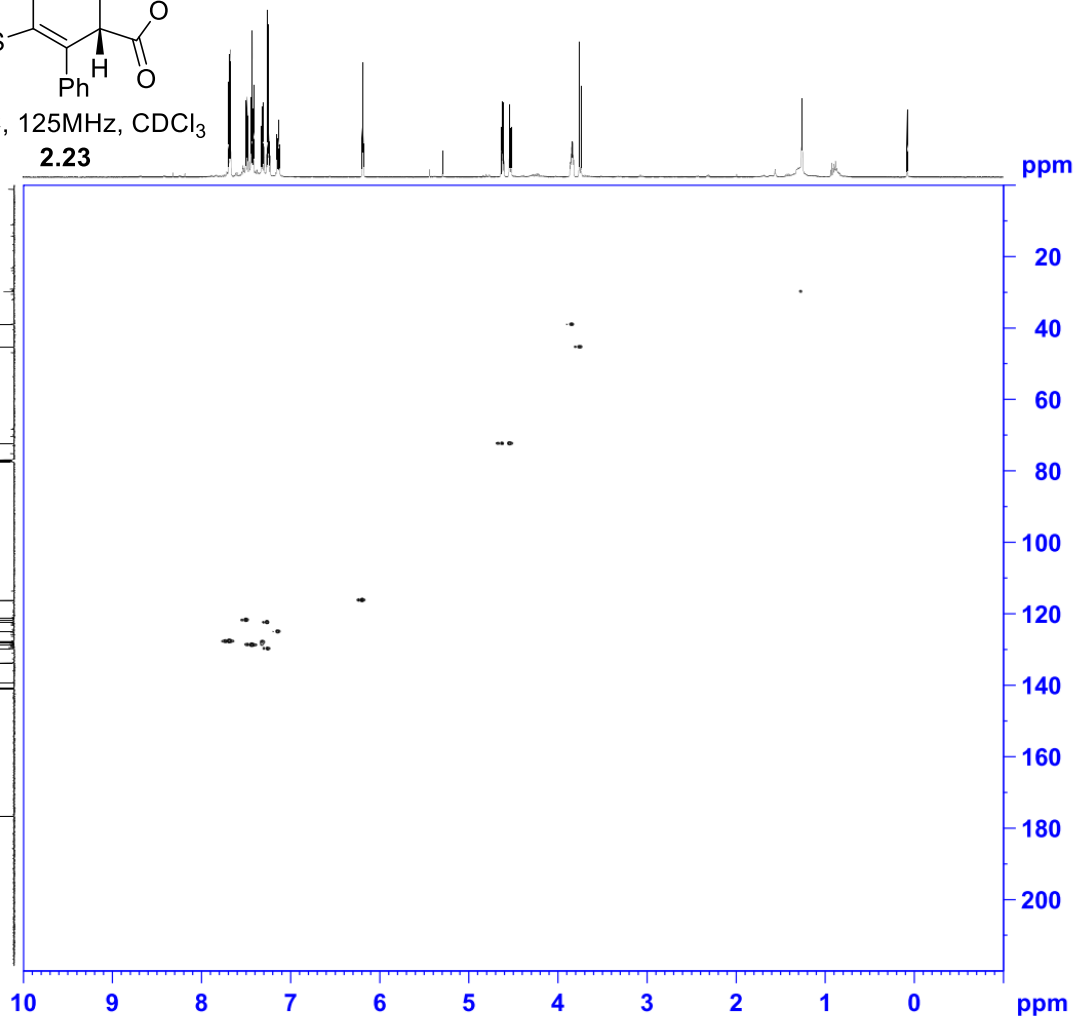
===== CHANNEL f2 =====
SFO2 125.7741354 MHz
NUC2 13C
CPOPRG(2) bl_psm4p 4p.2
P3 10.50 usec
P34 500.00 usec
P24 2000.00 usec
P63 1500.00 usec
PLM0 0 W
PLM2 110.0000000 W
PLM2 2.4749990 W
SFOAL3 Crp60,0.5,20.1
SFOFS3 0 Hz
SFW3 18.52899933 W
SFOAL7 Crp60comp-4
SFOAL7 0 Hz
SFOFS7 0 Hz
SFW7 18.52899933 W
SFOAL14 Crp32,1.5,20.2
SFOAL14 0 Hz
SFW14 7.90590000 W
SFOAL31 Crp32,1.5,20.2
SFOAL31 0 Hz
SFOFS31 0 Hz
SFW31 1.97650003 W

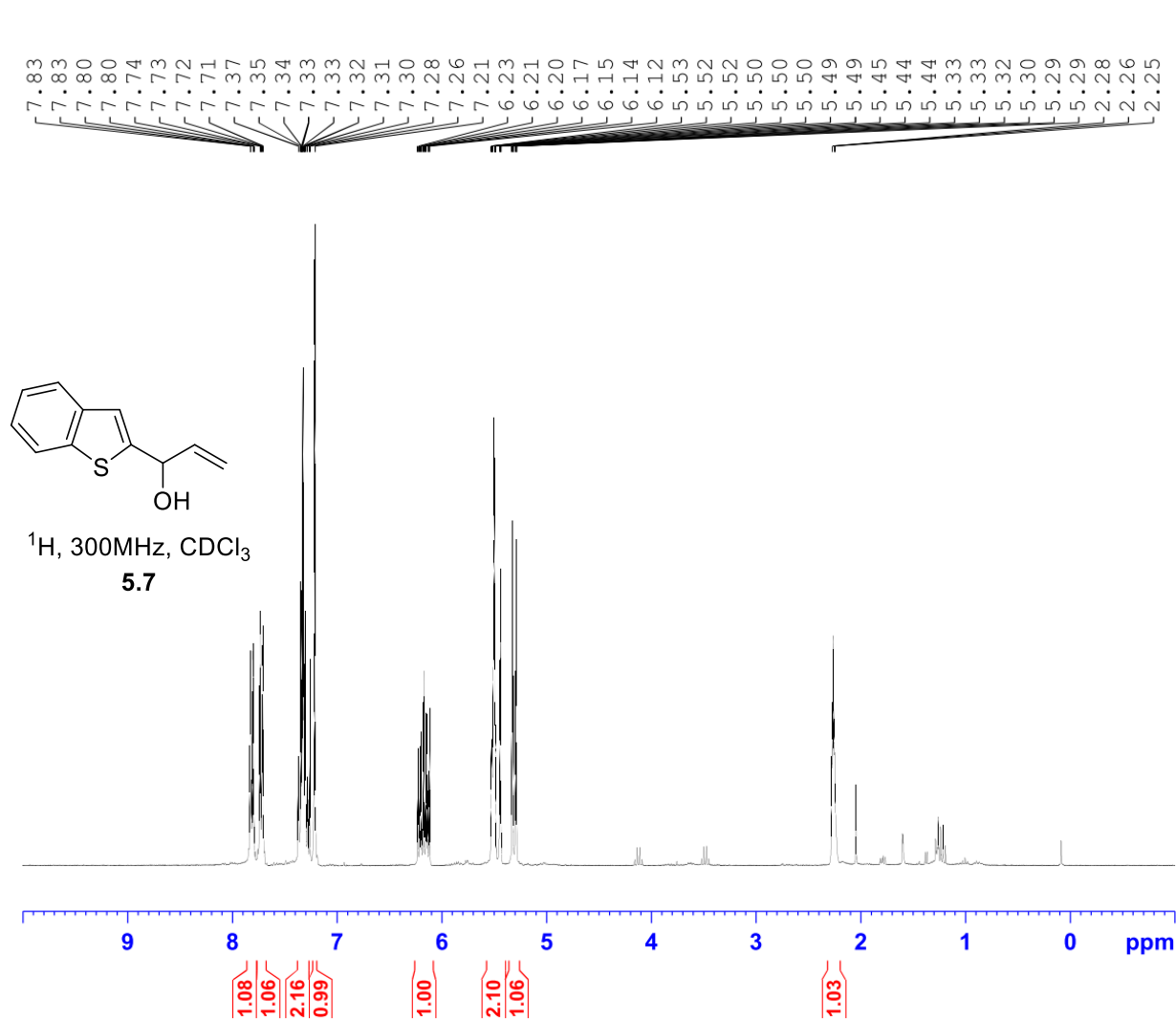
===== GRADIENT CHANNEL =====
GPRAM[1] SMSQ10.100
GPRAM[2] SMSQ10.100
GPRAM[3] SMSQ10.100
GPRAM[4] SMSQ10.100
GPE1 80.00 %
GPE2 20.10 %
GPE3 11.00 %
GPE4 -5.00 %
P16 1000.00 usec
P19 600.00 usec

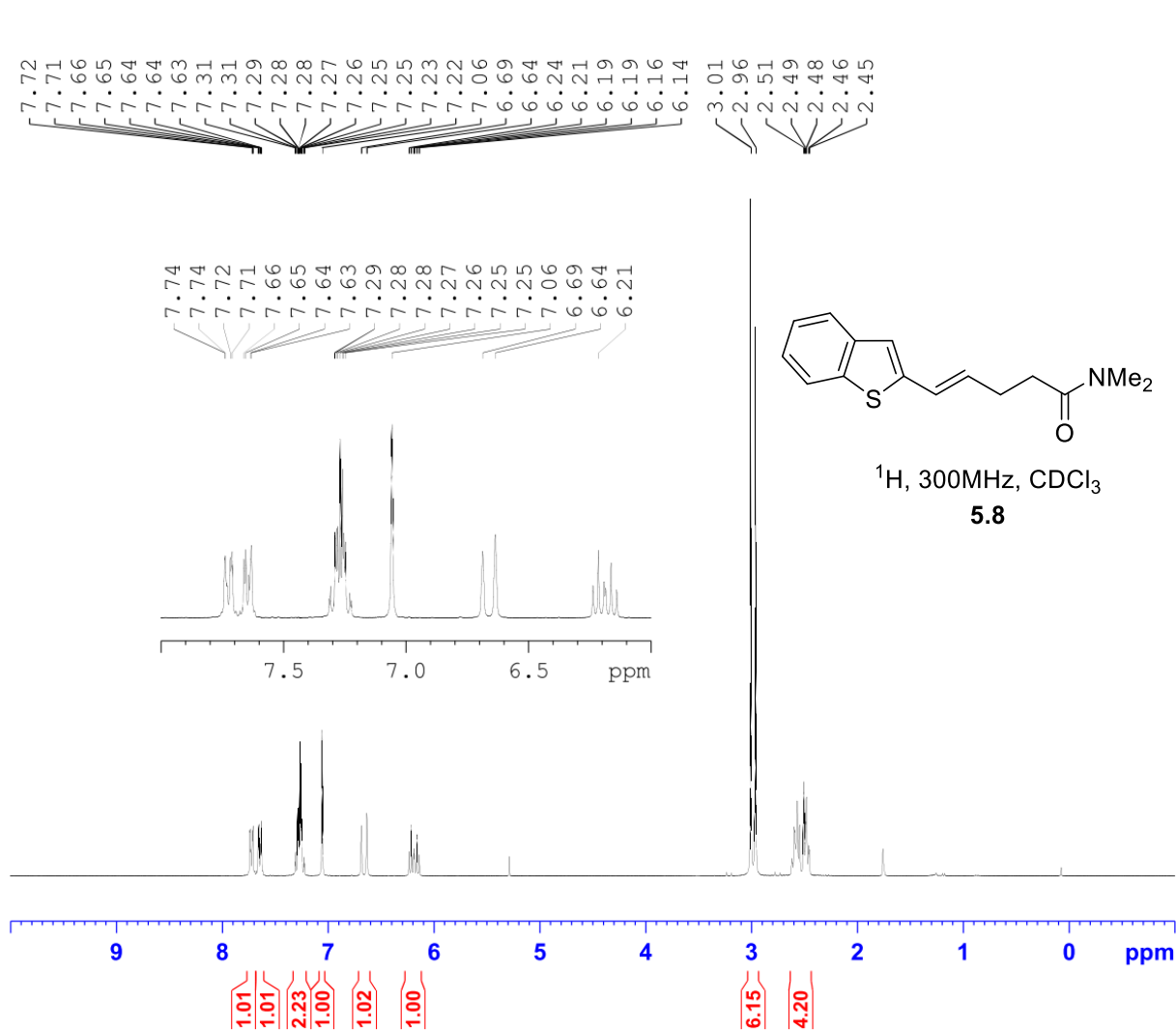
F1 - Acquisition parameters
TD 64
SFO1 125.7741 MHz
FIDRES 648.340271 Hz
SW 164.954 ppm
FNUCDE Echo-Antiecho

F2 - Processing parameters
SI 1024
SF 500.1600000 MHz
NCHW QSIHQ
SSB 2
LB 0 Hz
GB 0
PC 1.40

F1 - Processing parameters
SI 1024
MC2 echo-antiecho
SF 125.7653320 MHz
NCHW QSIHQ
SSB 2
LB 0 Hz
GB 0





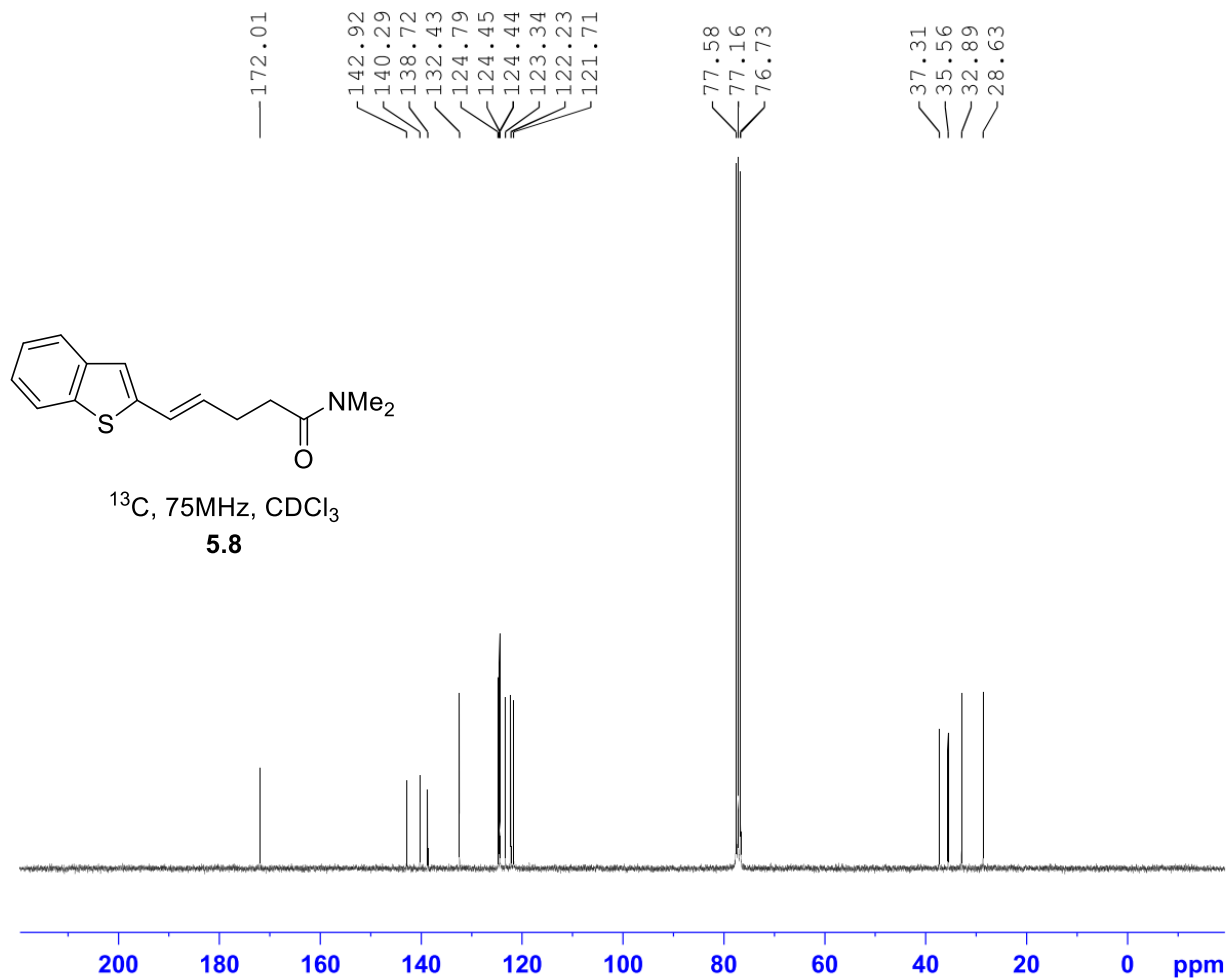


Current Data Parameters
NAME JAW-02-148
EXPNO 1
PROCNO 1

F2 - Acquisition Parameters
Date_ 20180923
Time_ 18.24
INSTRUM spect
PROBHD 5 mm QNP 1H/1
PULPROG zg30
TD 32768
SOLVENT CDCl₃
NS 16
DS 2
SWH 6188.119 Hz
FIDRES 0.188846 Hz
AQ 2.6476543 sec
RG 114
DW 80.800 usec
DE 6.50 usec
TE -923.0 K
D1 1.00000000 sec
TD0 1

===== CHANNEL f1 =====
SF01 300.2318540 MHz
NUC1 1H
P1 12.71 usec
PLW1 18.19700050 W

F2 - Processing parameters
SI 32768
SF 300.2300090 MHz
WDW EM
SSB 0
LB 0.10 Hz
GB 0
PC 1.00



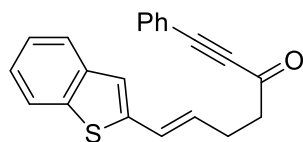
Current Data Parameters
 NAME JAW-02-148
 EXPNO 2
 PROCNO 1

F2 - Acquisition Parameters
 Date_ 20180923
 Time_ 19.31
 INSTRUM spect
 PROBHD 5 mm QNP 1H/1
 PULPROG zgpg30
 TD 65536
 SOLVENT CDCl_3
 NS 1024
 DS 4
 SWH 18028.846 Hz
 FIDRES 0.275098 Hz
 AQ 1.8175317 sec
 RG 406
 DW 27.733 usec
 DE 6.50 usec
 TE -923.2 K
 D1 2.00000000 sec
 D11 0.03000000 sec
 TD0 1

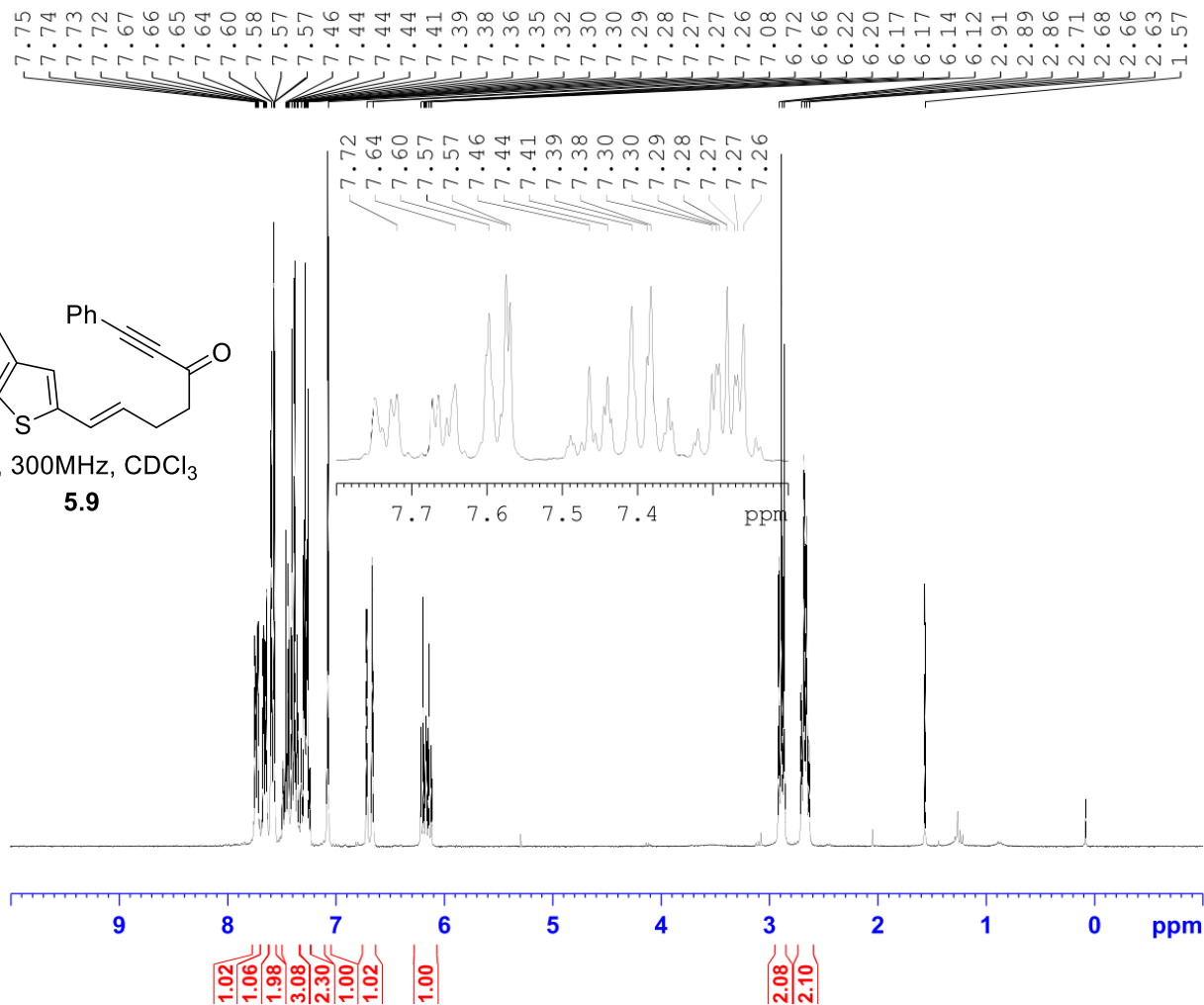
===== CHANNEL f1 =====
 SFO1 75.5004428 MHz
 NUC1 ^{13}C
 P1 12.00 usec
 PLW1 31.62299919 W

===== CHANNEL f2 =====
 SFO2 300.2312009 MHz
 NUC2 ^1H
 CPDPRG[2] waltz16
 PCPD2 90.00 usec
 PLW2 18.19700050 W
 PLW12 0.36291999 W
 PLW13 0.29396001 W

F2 - Processing parameters
 SI 32768
 SF 75.4928860 MHz
 WDW EM
 SSB 0
 LB 1.00 Hz
 GB 0
 PC 1.40



^1H , 300MHz, CDCl_3
5.9

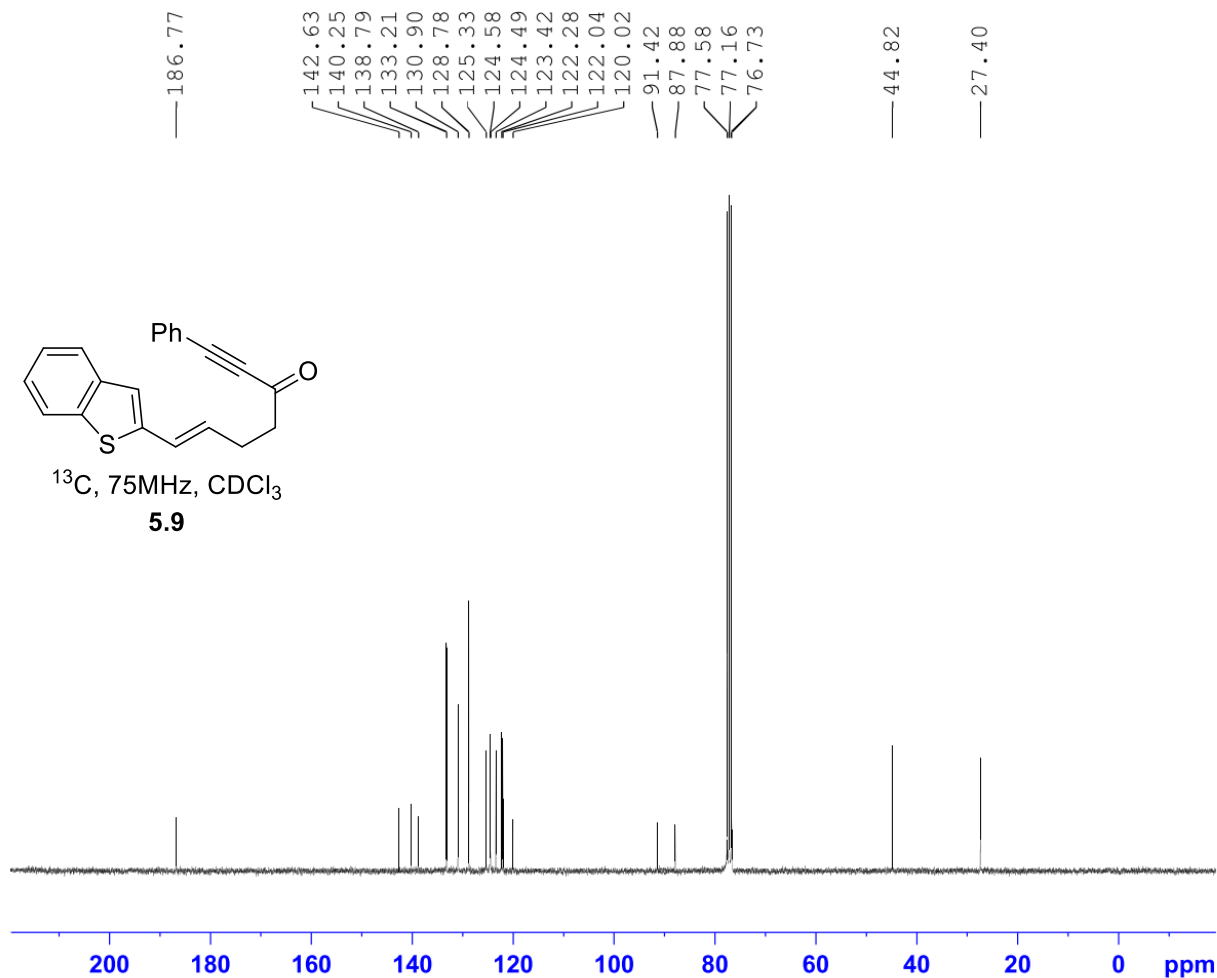


Current Data Parameters
NAME JAW-02-150
EXPNO 1
PROCNO 1

F2 - Acquisition Parameters
Date_ 20180924
Time_ 11.23
INSTRUM spect
PROBHD 5 mm QNP 1H/1
PULPROG zg30
TD 32768
SOLVENT CDCl_3
NS 16
DS 2
SWH 6188.119 Hz
FIDRES 0.188846 Hz
AQ 2.6476543 sec
RG 128
DW 80.800 usec
DE 6.50 usec
TE -923.1 K
D1 1.00000000 sec
TD0 1

===== CHANNEL f1 =====
SFO1 300.2318540 MHz
NUC1 1H
P1 12.71 usec
PLW1 18.19700050 W

F2 - Processing parameters
SI 32768
SF 300.2300091 MHz
WDW EM
SSB 0
LB 0.10 Hz
GB 0
PC 1.00



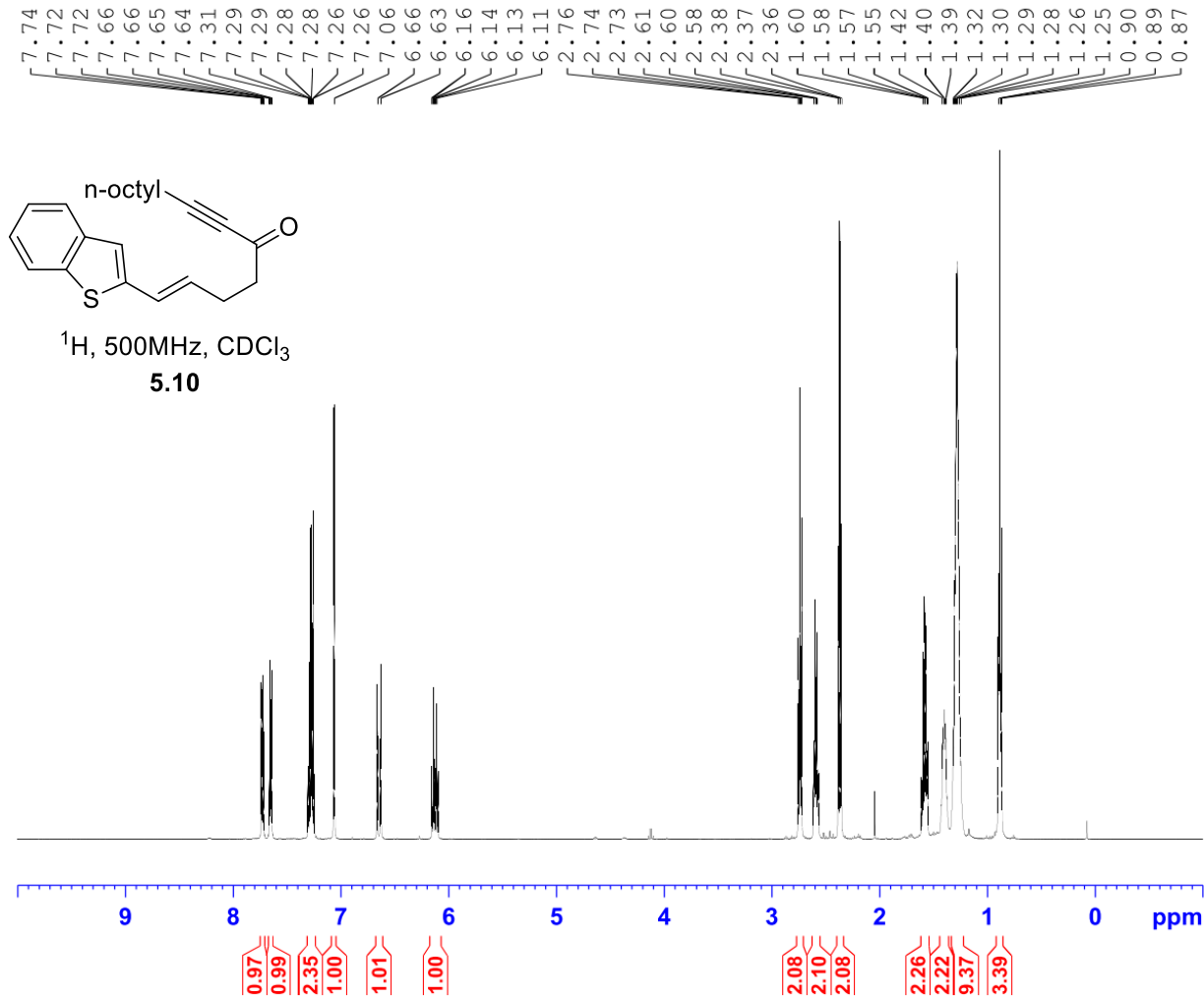
Current Data Parameters
 NAME JAW-02-150
 EXPNO 2
 PROCNO 1

F2 - Acquisition Parameters
 Date_ 20180924
 Time_ 23.12
 INSTRUM spect
 PROBHD 5 mm QNP 1H/1
 PULPROG zgpg30
 TD 65536
 SOLVENT CDCl3
 NS 1024
 DS 4
 SWH 18028.846 Hz
 FIDRES 0.275098 Hz
 AQ 1.8175317 sec
 RG 256
 DW 27.733 usec
 DE 6.50 usec
 TE -923.0 K
 D1 2.00000000 sec
 D11 0.03000000 sec
 TD0 1

===== CHANNEL f1 =====
 SFO1 75.5004428 MHz
 NUC1 13C
 P1 12.00 usec
 PLW1 31.62299919 W

===== CHANNEL f2 =====
 SFO2 300.2312009 MHz
 NUC2 1H
 CPDPRG[2] waltz16
 PCPD2 90.00 usec
 PLW2 18.19700050 W
 PLW12 0.36291999 W
 PLW13 0.29396001 W

F2 - Processing parameters
 SI 32768
 SF 75.4928853 MHz
 WDW EM
 SSB 0
 LB 1.00 Hz
 GB 0
 PC 1.40

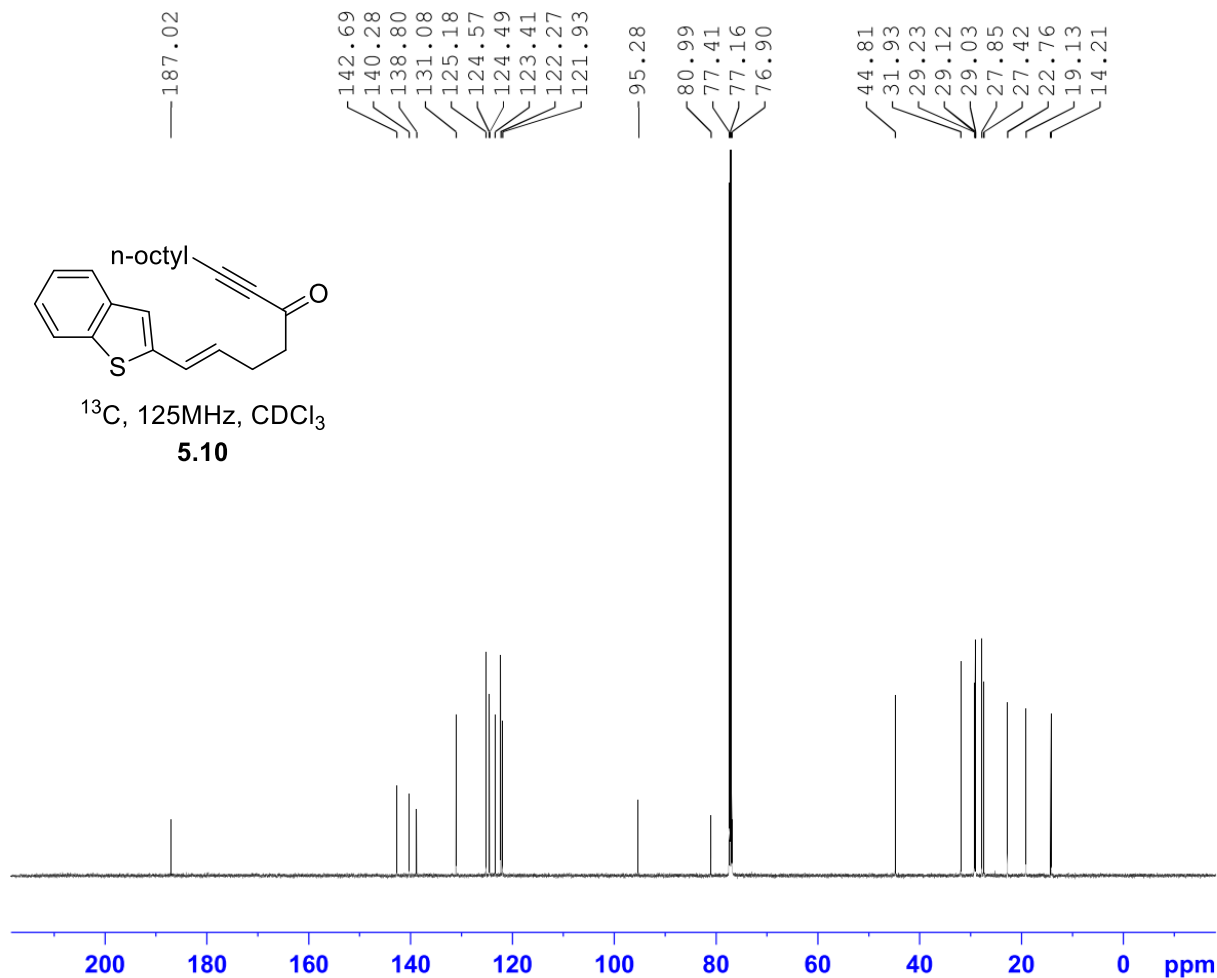


Current Data Parameters
 NAME JAW-02-166
 EXPNO 10
 PROCNO 1

F2 - Acquisition Parameters
 Date_ 20181101
 Time_ 3.10
 INSTRUM spect
 PROBHD 5 mm PABBO BB/
 PULPROG zg30
 TD 65536
 SOLVENT CDCl₃
 NS 16
 DS 2
 SWH 10000.000 Hz
 FIDRES 0.152588 Hz
 AQ 3.2767999 sec
 RG 64
 DW 50.000 usec
 DE 6.50 usec
 TE 298.2 K
 D1 1.00000000 sec
 TD0 1

===== CHANNEL f1 =====
 SF01 500.1630887 MHz
 NUC1 1H
 P1 11.50 usec
 PLW1 18.00000000 W

F2 - Processing parameters
 SI 65536
 SF 500.1600120 MHz
 WDW EM
 SSB 0
 LB 0.30 Hz
 GB 0
 PC 1.00



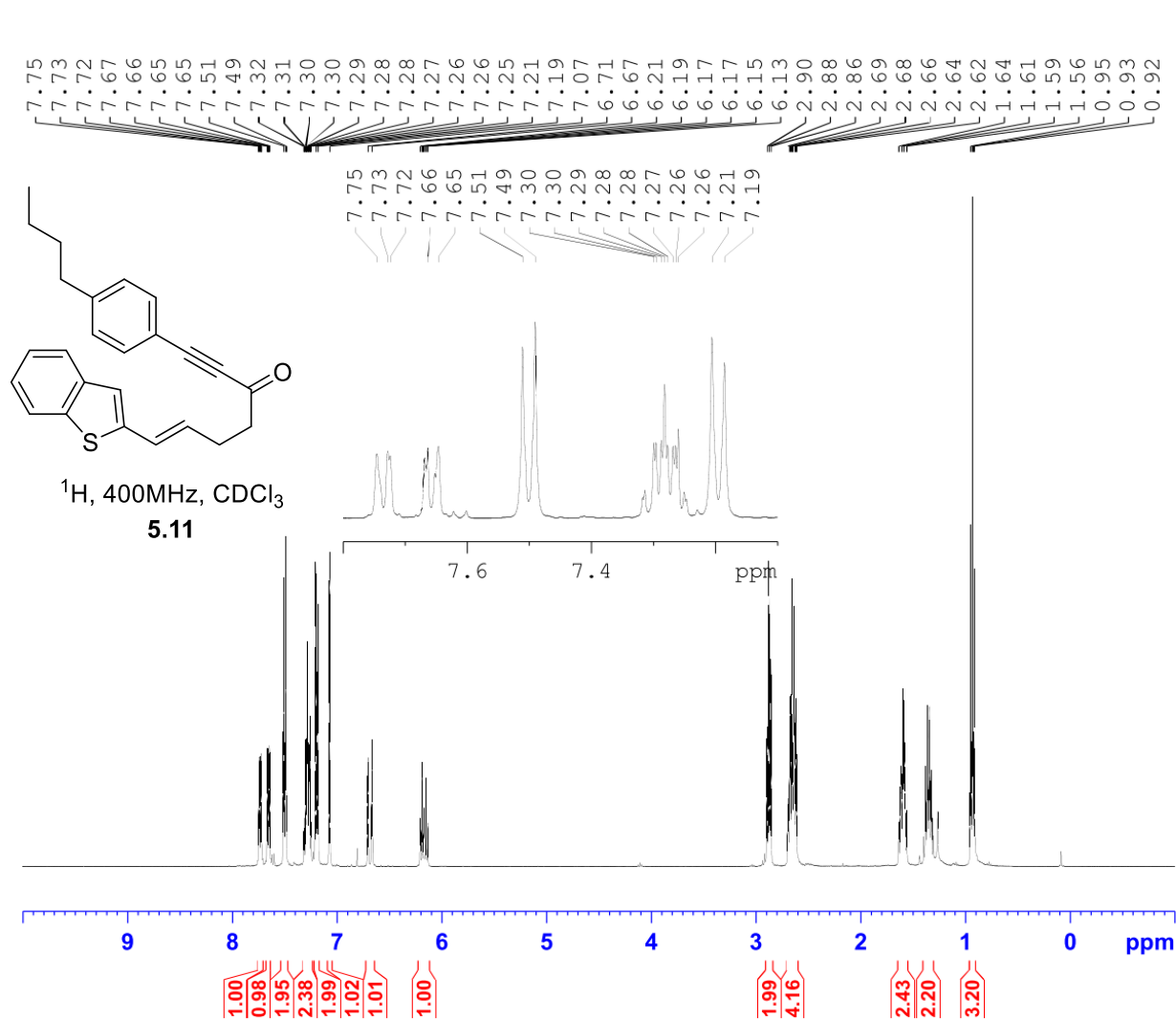
Current Data Parameters
 NAME JAW-02-166
 EXPNO 12
 PROCNO 1

F2 - Acquisition Parameters
 Date_ 20181101
 Time_ 4.20
 INSTRUM spect
 PROBHD 5 mm PABBO BB/
 PULPROG zgpg30
 TD 65536
 SOLVENT CDCl3
 NS 1024
 DS 2
 SWH 29761.904 Hz
 FIDRES 0.454131 Hz
 AQ 1.1010048 sec
 RG 203
 DW 16.800 usec
 DE 6.50 usec
 TE 299.1 K
 D1 2.00000000 sec
 D11 0.03000000 sec
 TD0 1

===== CHANNEL f1 =====
 SFO1 125.7779086 MHz
 NUC1 13C
 P1 10.50 usec
 PLW1 110.00000000 W

===== CHANNEL f2 =====
 SFO2 500.1620006 MHz
 NUC2 1H
 CPDPRG[2] waltz16
 PCPD2 80.00 usec
 PLW2 18.00000000 W
 PLW12 0.37195000 W
 PLW13 0.23805000 W

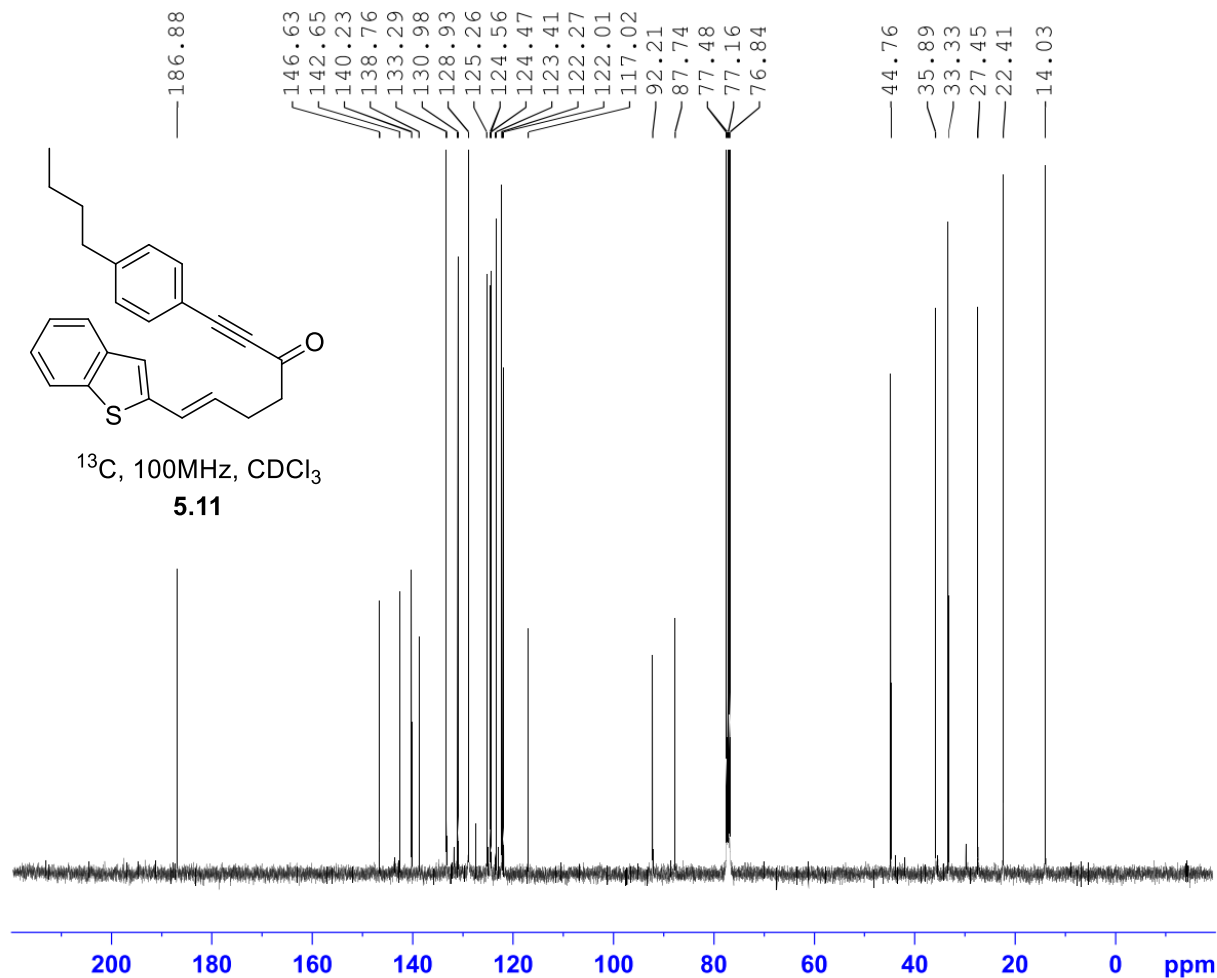
F2 - Processing parameters
 SI 32768
 SF 125.7653145 MHz
 WDW EM
 SSB 0
 LB 1.00 Hz
 GB 0
 PC 1.40



Current Data Parameters
 NAME JAW-03-028
 EXPNO 1
 PROCNO 1

F2 - Acquisition Parameters
 Date_ 20190724
 Time_ 12.58 h
 INSTRUM spect
 PROBHD Z108618_0240 (
 PULPROG zg30
 TD 65536
 SOLVENT CDCl3
 NS 16
 DS 2
 SWH 8012.820 Hz
 FIDRES 0.244532 Hz
 AQ 4.0894465 sec
 RG 57
 DW 62.400 usec
 DE 6.50 usec
 TE 88.6 K
 D1 1.00000000 sec
 TD0 1
 SF01 400.1324708 MHz
 NUC1 1H
 P0 4.83 usec
 P1 14.50 usec
 PLW1 12.00000000 W

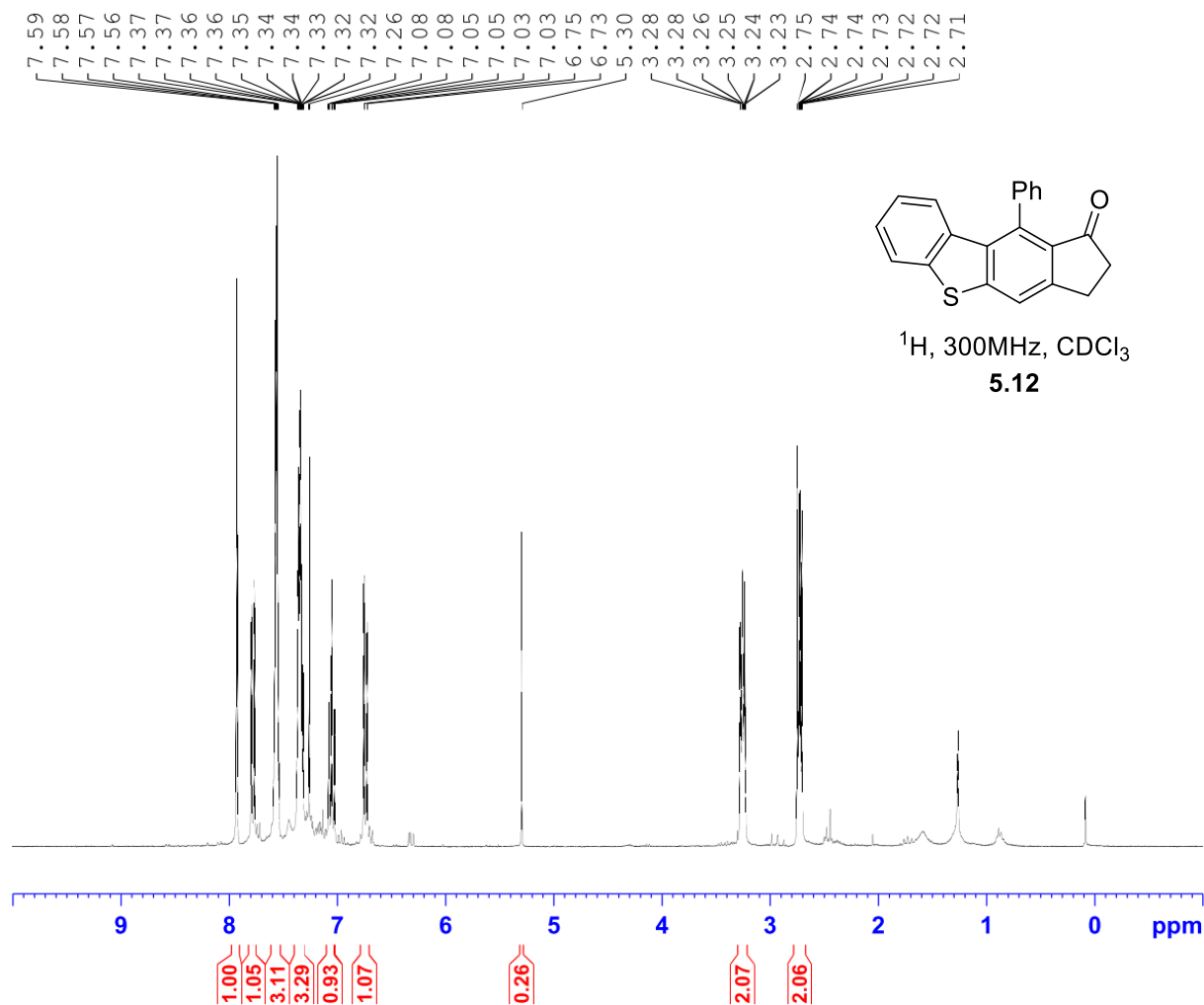
F2 - Processing parameters
 SI 65536
 SF 400.1300097 MHz
 WDW EM
 SSB 0
 LB 0.30 Hz
 GB 0
 PC 1.00



Current Data Parameters
NAME JAW-03-028
EXPNO 2
PROCNO 1

F2 - Acquisition Parameters
Date_ 20190724
Time 22.11 h
INSTRUM spect
PROBHD Z108618_0240 (
PULPROG zgpg30
TD 65536
SOLVENT CDCl3
NS 1024
DS 4
SWH 24038.461 Hz
FIDRES 0.733596 Hz
AQ 1.3631488 sec
RG 203
DW 20.800 usec
DE 6.50 usec
TE 88.9 K
D1 2.00000000 sec
D11 0.03000000 sec
TD0 1
SFO1 100.6228298 MHz
NUC1 13C
P0 3.33 usec
P1 10.00 usec
PLW1 56.13299942 W
SFO2 400.1316005 MHz
NUC2 1H
CPDPRG[2] waltz65
PCPD2 90.00 usec
PLW2 12.00000000 W
PLW12 0.31147999 W
PLW13 0.15667000 W

F2 - Processing parameters
SI 32768
SF 100.6127587 MHz
WDW EM
SSB 0
LB 1.00 Hz
GB 0
PC 1.40

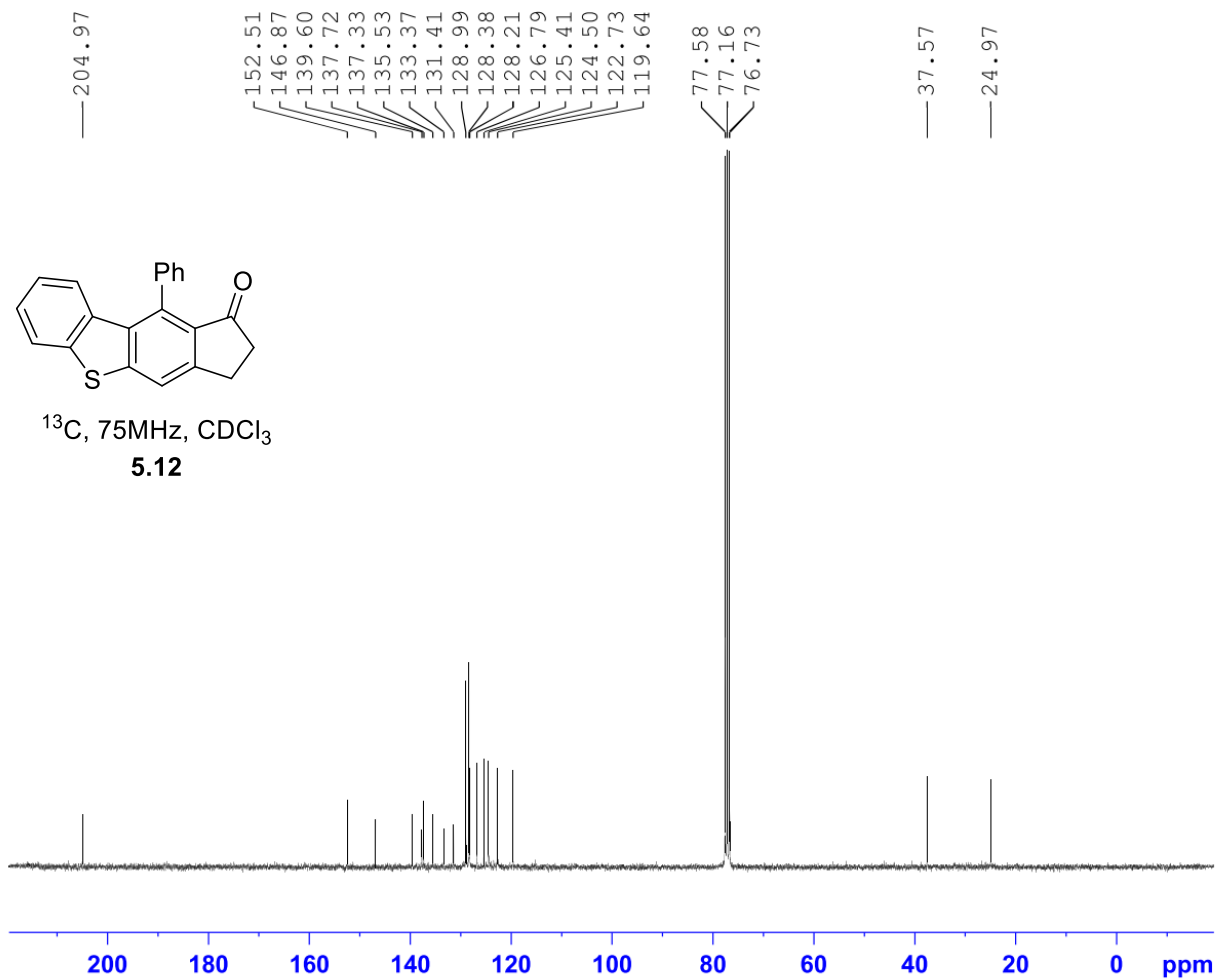


Current Data Parameters
NAME JAW-02-152
EXPNO 2
PROCNO 1

F2 - Acquisition Parameters
Date_ 20180924
Time_ 19.53
INSTRUM spect
PROBHD 5 mm QNP 1H/1
PULPROG zg30
TD 32768
SOLVENT CDCl_3
NS 16
DS 2
SWH 6188.119 Hz
FIDRES 0.188846 Hz
AQ 2.6476543 sec
RG 128
DW 80.800 usec
DE 6.50 usec
TE -923.0 K
D1 1.00000000 sec
TD0 1

===== CHANNEL f1 =====
SF01 300.2318540 MHz
NUC1 1H
P1 12.71 usec
PLW1 18.19700050 W

F2 - Processing parameters
SI 32768
SF 300.2300086 MHz
WDW EM
SSB 0
LB 0.10 Hz
GB 0
PC 1.00



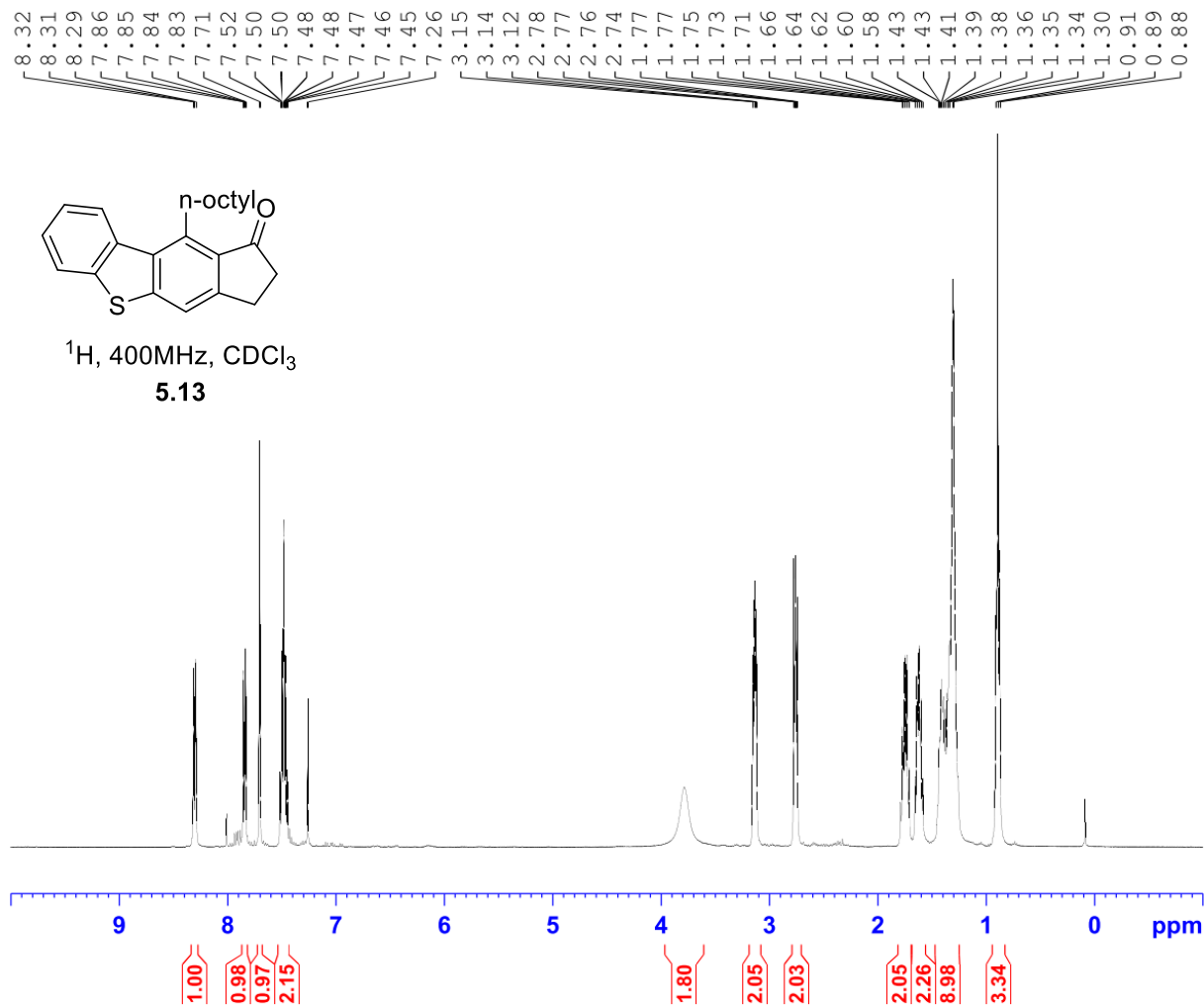
Current Data Parameters
 NAME JAW-02-152
 EXPNO 3
 PROCNO 1

F2 - Acquisition Parameters
 Date_ 20180925
 Time_ 5.39
 INSTRUM spect
 PROBHD 5 mm QNP 1H/1
 PULPROG zgpg30
 TD 65536
 SOLVENT CDCl_3
 NS 1024
 DS 4
 SWH 18028.846 Hz
 FIDRES 0.275098 Hz
 AQ 1.8175317 sec
 RG 256
 DW 27.733 usec
 DE 6.50 usec
 TE -921.5 K
 D1 2.00000000 sec
 D11 0.03000000 sec
 TD0 1

===== CHANNEL f1 =====
 SFO1 75.5004428 MHz
 NUC1 ^{13}C
 P1 12.00 usec
 PLW1 31.62299919 W

===== CHANNEL f2 =====
 SFO2 300.2312009 MHz
 NUC2 ^1H
 CPDPRG[2] waltz16
 PCPD2 90.00 usec
 PLW2 18.19700050 W
 PLW12 0.36291999 W
 PLW13 0.29396001 W

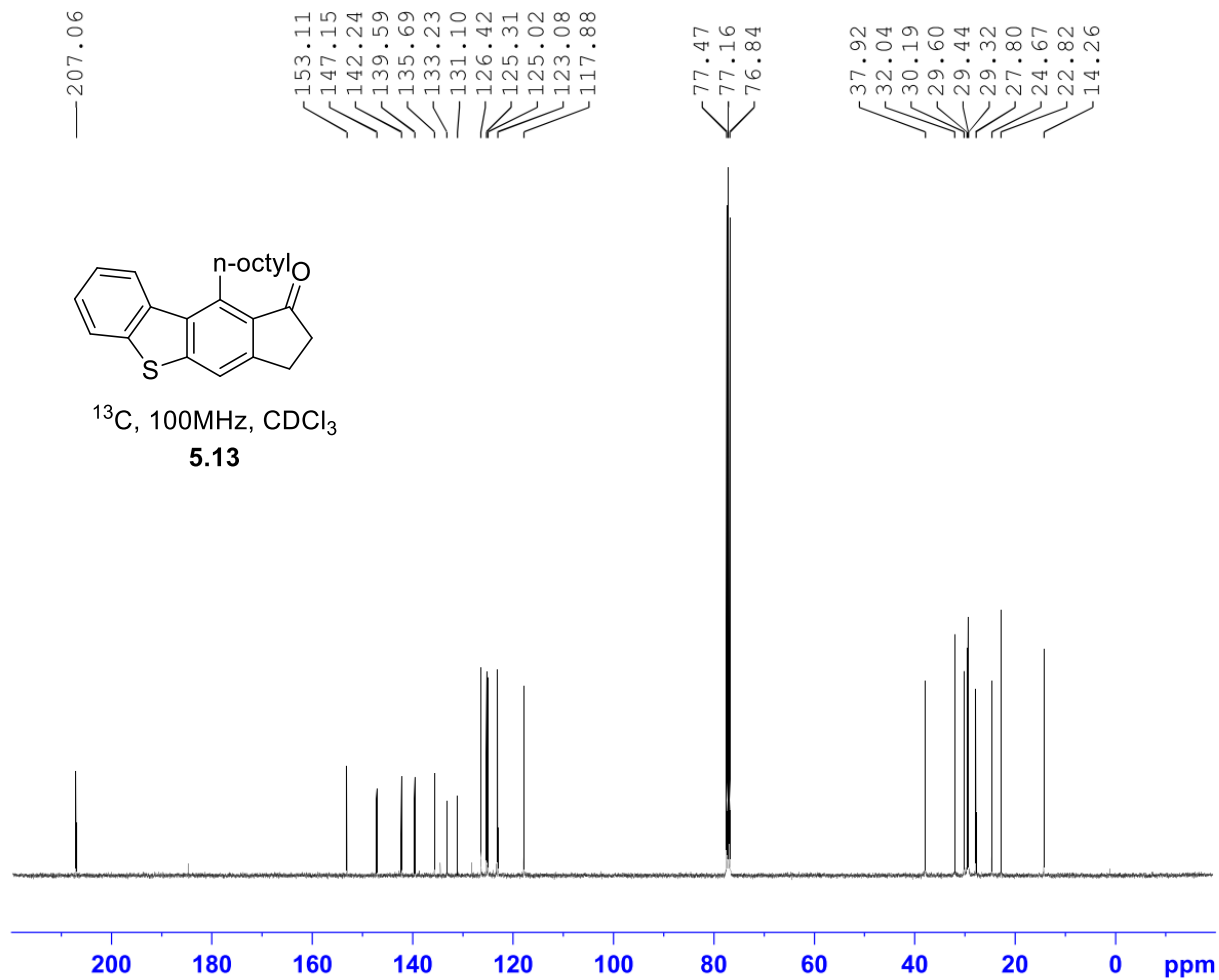
F2 - Processing parameters
 SI 32768
 SF 75.4928853 MHz
 WDW EM
 SSB 0
 LB 1.00 Hz
 GB 0
 PC 1.40



Current Data Parameters
 NAME JAW-02-174
 EXPNO 1
 PROCNO 1

F2 - Acquisition Parameters
 Date_ 20181208
 Time_ 6.52 h
 INSTRUM spect
 PROBHD Z108618_0240 (
 PULPROG zg30
 TD 65536
 SOLVENT CDCl3
 NS 16
 DS 2
 SWH 8012.820 Hz
 FIDRES 0.244532 Hz
 AQ 4.0894465 sec
 RG 32
 DW 62.400 usec
 DE 6.50 usec
 TE 88.3 K
 D1 1.00000000 sec
 TD0 1
 SFO1 400.1324708 MHz
 NUC1 1H
 P0 4.83 usec
 P1 14.50 usec
 PLW1 12.00000000 W

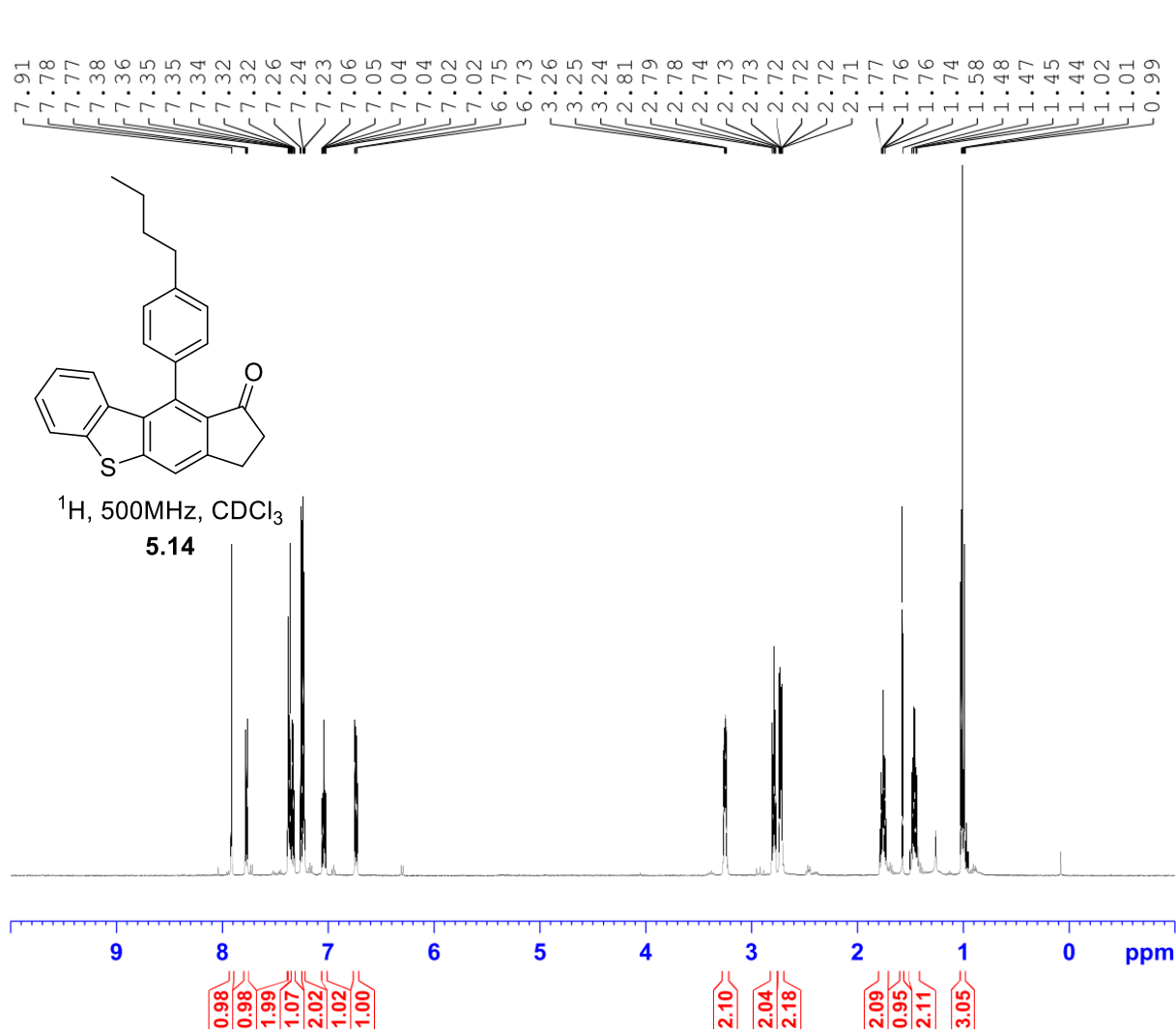
F2 - Processing parameters
 SI 65536
 SF 400.1300099 MHz
 WDW EM
 SSB 0
 LB 0.30 Hz
 GB 0
 PC 1.00



Current Data Parameters
 NAME JAW-02-174
 EXPNO 2
 PROCNO 1

F2 - Acquisition Parameters
 Date_ 20181208
 Time_ 7.52 h
 INSTRUM spect
 PROBHD Z108618_0240 (
 PULPROG zgpg30
 TD 65536
 SOLVENT CDCl3
 NS 1024
 DS 4
 SWH 24038.461 Hz
 FIDRES 0.733596 Hz
 AQ 1.3631488 sec
 RG 203
 DW 20.800 usec
 DE 6.50 usec
 TE 88.3 K
 D1 2.00000000 sec
 D11 0.03000000 sec
 TD0 1
 SFO1 100.6228298 MHz
 NUC1 13C
 P0 3.33 usec
 P1 10.00 usec
 PLW1 56.13299942 W
 SFO2 400.1316005 MHz
 NUC2 1H
 CPDPRG[2] waltz65
 PCPD2 90.00 usec
 PLW2 12.00000000 W
 PLW12 0.31147999 W
 PLW13 0.15667000 W

F2 - Processing parameters
 SI 32768
 SF 100.6127579 MHz
 WDW EM
 SSB 0
 LB 1.00 Hz
 GB 0
 PC 1.40

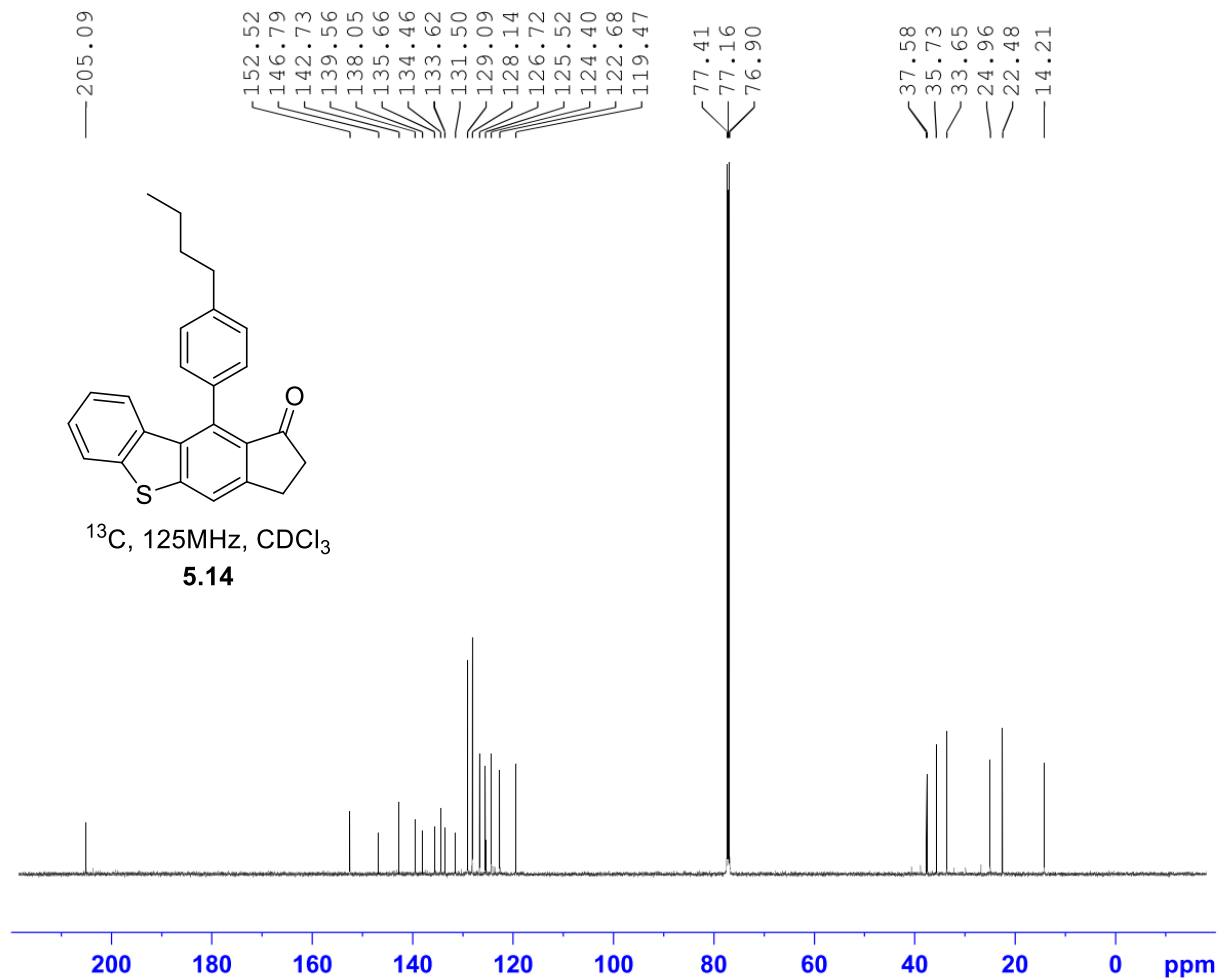


Current Data Parameters
 NAME JAW-03-030
 EXPNO 20
 PROCNO 1

F2 - Acquisition Parameters
 Date_ 20190805
 Time_ 15.48
 INSTRUM spect
 PROBHD 5 mm PABBO BB/
 PULPROG zg30
 TD 65536
 SOLVENT CDCl₃
 NS 16
 DS 2
 SWH 10000.000 Hz
 FIDRES 0.152588 Hz
 AQ 3.2767999 sec
 RG 101
 DW 50.000 usec
 DE 6.50 usec
 TE 295.8 K
 D1 1.00000000 sec
 TD0 1

===== CHANNEL f1 =====
 SF01 500.1630887 MHz
 NUC1 1H
 P1 11.50 usec
 PLW1 18.00000000 W

F2 - Processing parameters
 SI 65536
 SF 500.1600122 MHz
 WDW EM
 SSB 0
 LB 0.30 Hz
 GB 0
 PC 1.00



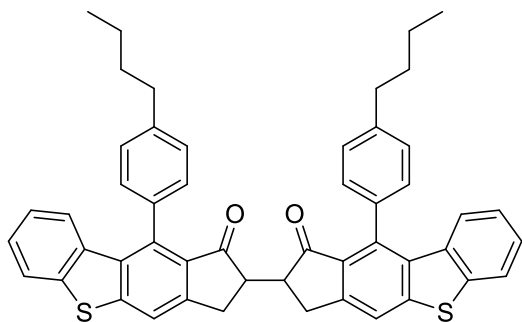
Current Data Parameters
NAME JAW-03-030
EXPNO 21
PROCNO 1

F2 - Acquisition Parameters
Date_ 20190806
Time 7.54
INSTRUM spect
PROBHD 5 mm PABBO BB/
PULPROG zgpg30
TD 65536
SOLVENT CDCl3
NS 1026
DS 2
SWH 29761.904 Hz
FIDRES 0.454131 Hz
AQ 1.1010048 sec
RG 203
DW 16.800 usec
DE 6.50 usec
TE 297.4 K
D1 2.00000000 sec
D11 0.03000000 sec
TD0 1

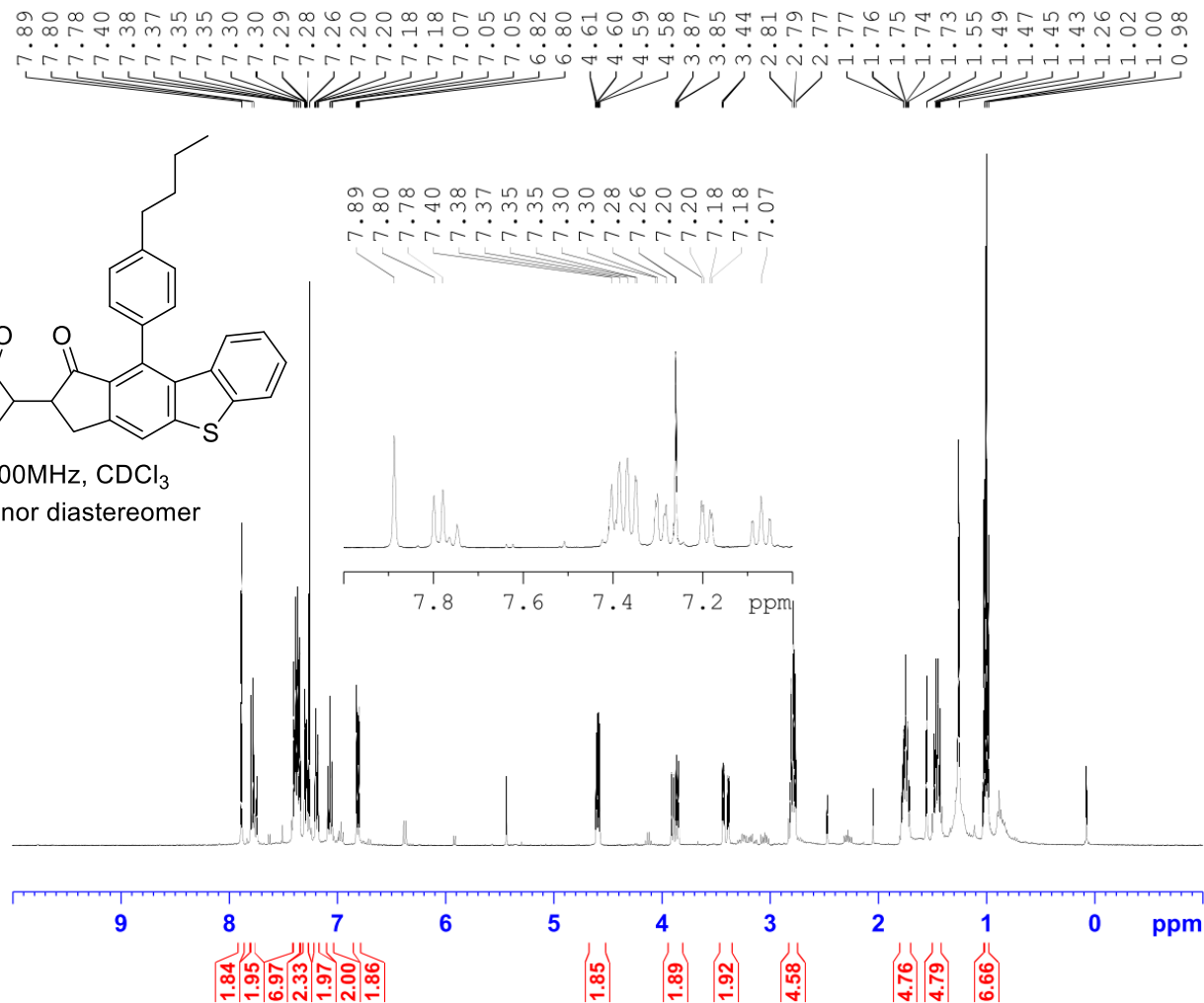
===== CHANNEL f1 =====
SFO1 125.7779086 MHz
NUC1 ^{13}C
P1 10.50 usec
PLW1 110.00000000 W

===== CHANNEL f2 =====
SFO2 500.1620006 MHz
NUC2 ^1H
CPDPRG[2] waltz16
PCPD2 80.00 usec
PLW2 18.00000000 W
PLW12 0.37195000 W
PLW13 0.23805000 W

F2 - Processing parameters
SI 32768
SF 125.7653168 MHz
WDW EM
SSB 0
LB 1.00 Hz
GB 0
PC 1.40



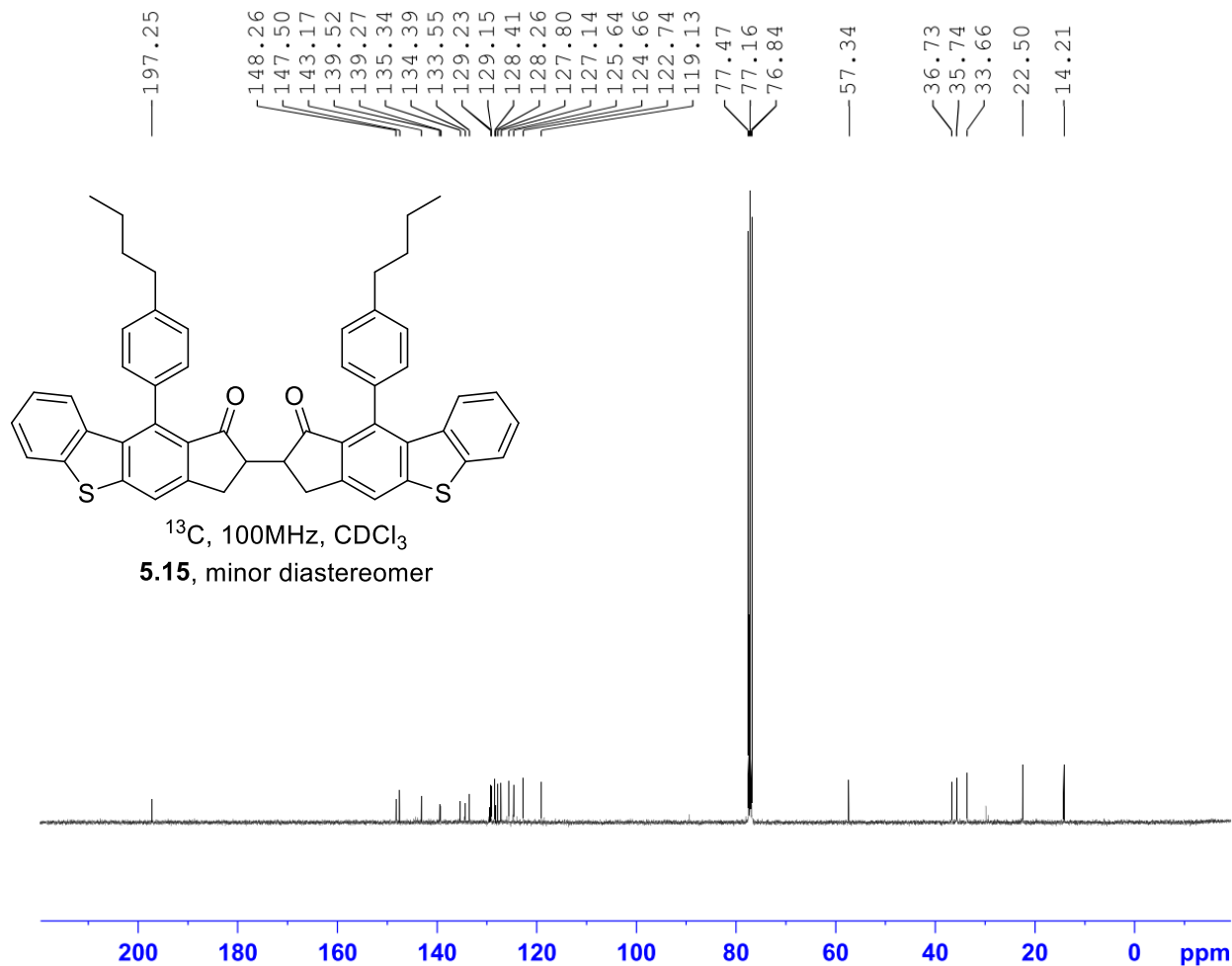
¹H, 400MHz, CDCl₃
5.15, minor diastereomer



Current Data Parameters
NAME JAW-03-061-A
EXPNO 2
PROCNO 1

F2 - Acquisition Parameters
Date_ 20191030
Time_ 14.59 h
INSTRUM spect
PROBHD Z108618_0240 (
PULPROG zg30
TD 65536
SOLVENT CDCl3
NS 16
DS 2
SWH 8012.820 Hz
FIDRES 0.244532 Hz
AQ 4.0894465 sec
RG 101
DW 62.400 usec
DE 6.50 usec
TE 92.0 K
D1 1.00000000 sec
TD0 1
SF01 400.1324708 MHz
NUC1 1H
P0 4.83 usec
P1 14.50 usec
PLW1 12.00000000 W

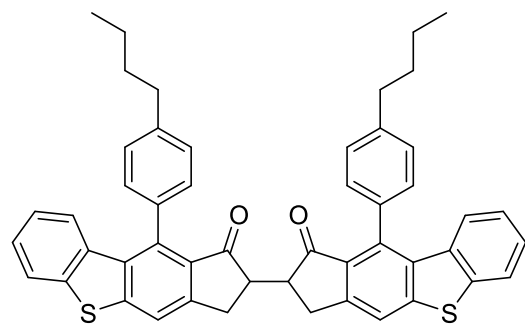
F2 - Processing parameters
SI 65536
SF 400.1300098 MHz
WDW EM
SSB 0
LB 0.30 Hz
GB 0
PC 1.00



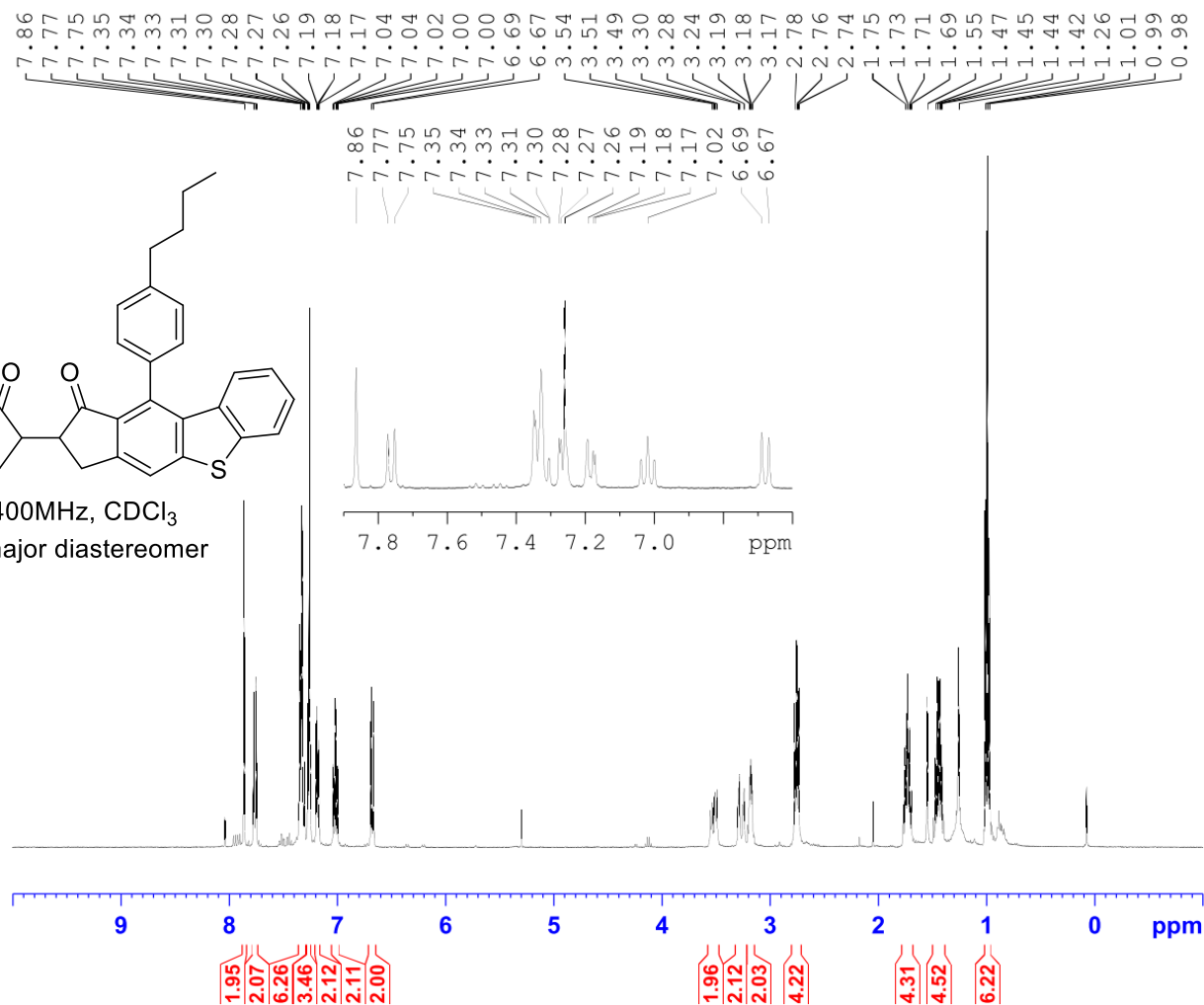
Current Data Parameters
NAME JAW-03-061-A
EXPNO 3
PROCNO 1

F2 - Acquisition Parameters
Date_ 20191031
Time_ 1.42 h
INSTRUM spect
PROBHD Z108618_0240 (
PULPROG zgpg30
TD 65536
SOLVENT CDCl3
NS 1024
DS 4
SWH 24038.461 Hz
FIDRES 0.733596 Hz
AQ 1.3631488 sec
RG 203
DW 20.800 usec
DE 6.50 usec
TE 93.9 K
D1 2.00000000 sec
D11 0.03000000 sec
TD0 1
SFO1 100.6228298 MHz
NUC1 13C
P0 3.33 usec
P1 10.00 usec
PLW1 56.13299942 W
SFO2 400.1316005 MHz
NUC2 1H
CPDPRG[2] waltz65
PCPD2 90.00 usec
PLW2 12.00000000 W
PLW12 0.31147999 W
PLW13 0.15667000 W

F2 - Processing parameters
SI 32768
SF 100.6127564 MHz
WDW EM
SSB 0
LB 1.00 Hz
GB 0
PC 1.40



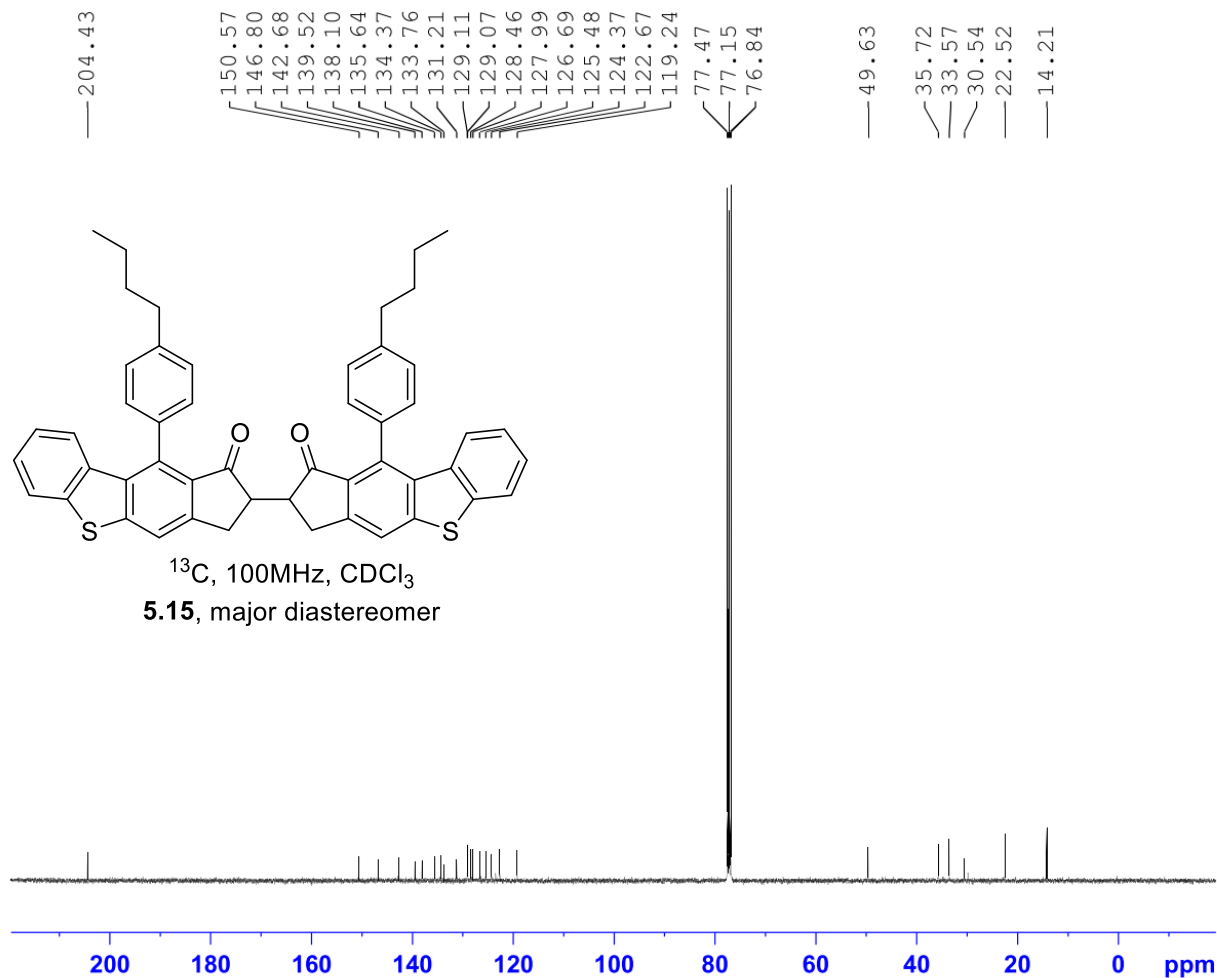
¹H, 400MHz, CDCl₃
5.15, major diastereomer



Current Data Parameters
NAME JAW-03-061-B
EXPNO 2
PROCNO 1

F2 - Acquisition Parameters
Date_ 20191030
Time_ 14.06 h
INSTRUM spect
PROBHD Z108618_0240 (
PULPROG zg30
TD 65536
SOLVENT CDCl3
NS 16
DS 2
SWH 8012.820 Hz
FIDRES 0.244532 Hz
AQ 4.0894465 sec
RG 114
DW 62.400 usec
DE 6.50 usec
TE 93.2 K
D1 1.00000000 sec
TD0 1
SF01 400.1324708 MHz
NUC1 1H
P0 4.83 usec
P1 14.50 usec
PLW1 12.00000000 W

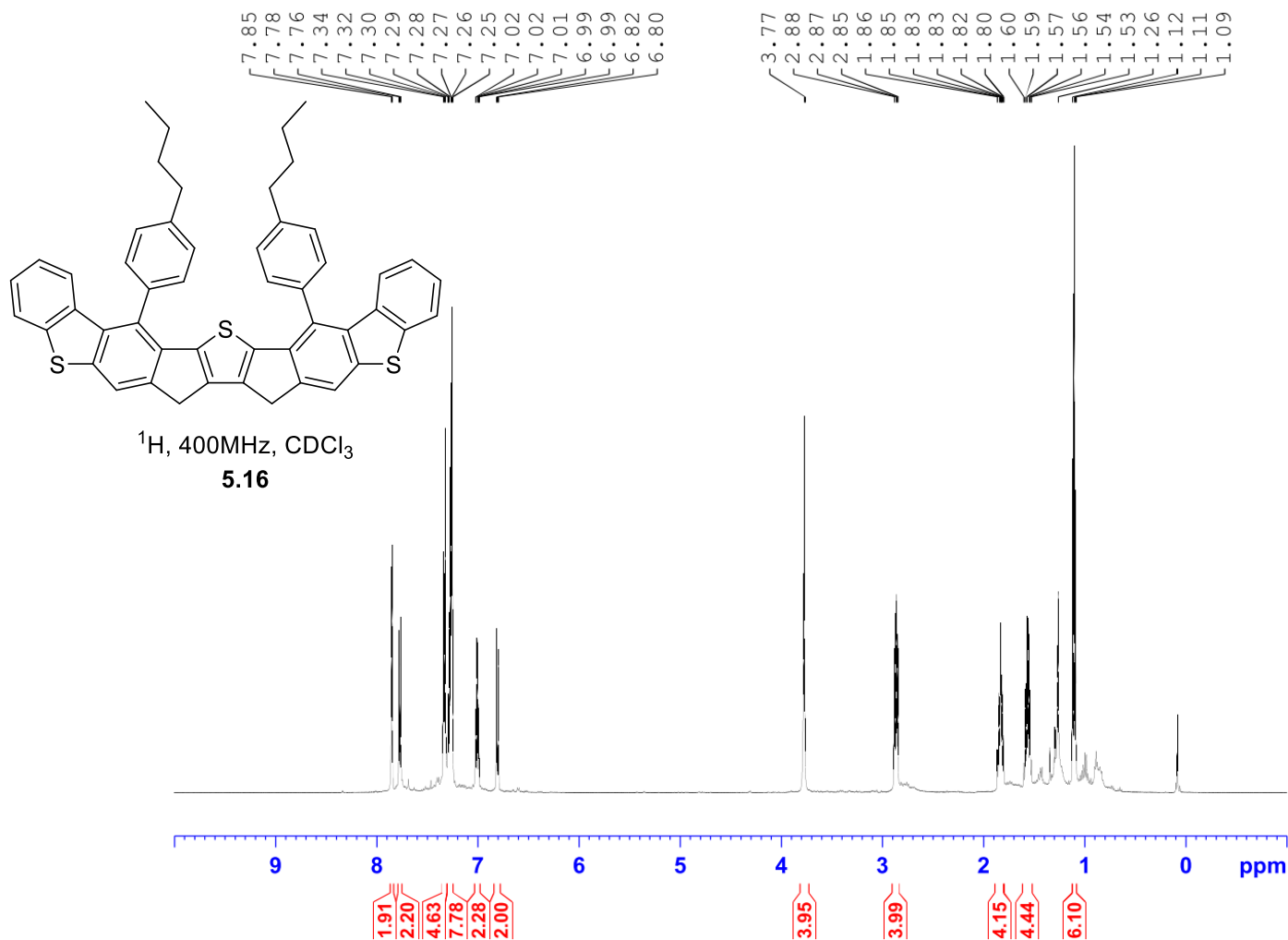
F2 - Processing parameters
SI 65536
SF 400.1300098 MHz
WDW EM
SSB 0
LB 0.30 Hz
GB 0
PC 1.00



Current Data Parameters
 NAME JAW-03-061-B
 EXPNO 3
 PROCNO 1

F2 - Acquisition Parameters
 Date_ 20191030
 Time_ 23.30 h
 INSTRUM spect
 PROBHD Z108618_0240 (
 PULPROG zgpg30
 TD 65536
 SOLVENT CDCl3
 NS 1024
 DS 4
 SWH 24038.461 Hz
 FIDRES 0.733596 Hz
 AQ 1.3631488 sec
 RG 203
 DW 20.800 usec
 DE 6.50 usec
 TE 93.0 K
 D1 2.00000000 sec
 D11 0.03000000 sec
 TD0 1
 SFO1 100.6228298 MHz
 NUC1 13C
 P0 3.33 usec
 P1 10.00 usec
 PLW1 56.13299942 W
 SFO2 400.1316005 MHz
 NUC2 1H
 CPDPRG[2] waltz65
 PCPD2 90.00 usec
 PLW2 12.00000000 W
 PLW12 0.31147999 W
 PLW13 0.15667000 W

F2 - Processing parameters
 SI 32768
 SF 100.6127564 MHz
 WDW EM
 SSB 0
 LB 1.00 Hz
 GB 0
 PC 1.40

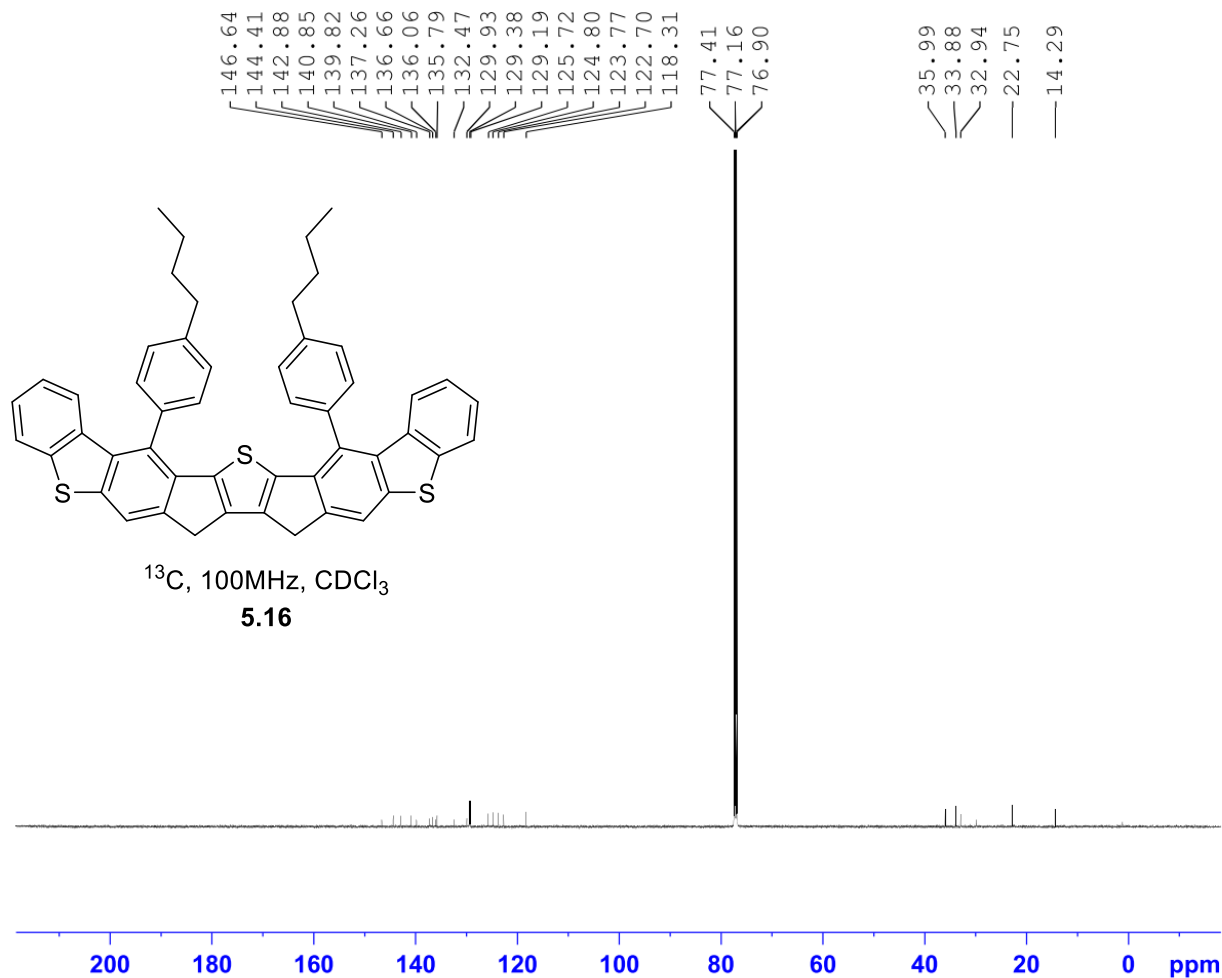


Current Data Parameters
 NAME JAW-03-074
 EXPNO 5
 PROCNO 1

F2 - Acquisition Parameters
 Date_ 20191205
 Time_ 14.23
 INSTRUM spect
 PROBHD 5 mm PABBO BB/
 PULPROG zg30
 TD 65536
 SOLVENT CDCl_3
 NS 16
 DS 2
 SWH 10000.000 Hz
 FIDRES 0.152588 Hz
 AQ 3.2767999 sec
 RG 90.5
 DW 50.000 usec
 DE 6.50 usec
 TE 297.2 K
 D1 1.00000000 sec
 TD0 1

===== CHANNEL f1 =====
 SF01 500.1630887 MHz
 NUC1 ^1H
 P1 11.50 usec
 PLW1 18.00000000 W

F2 - Processing parameters
 SI 65536
 SF 500.1600122 MHz
 WDW EM
 SSB 0
 LB 0.30 Hz
 GB 0
 PC 1.00



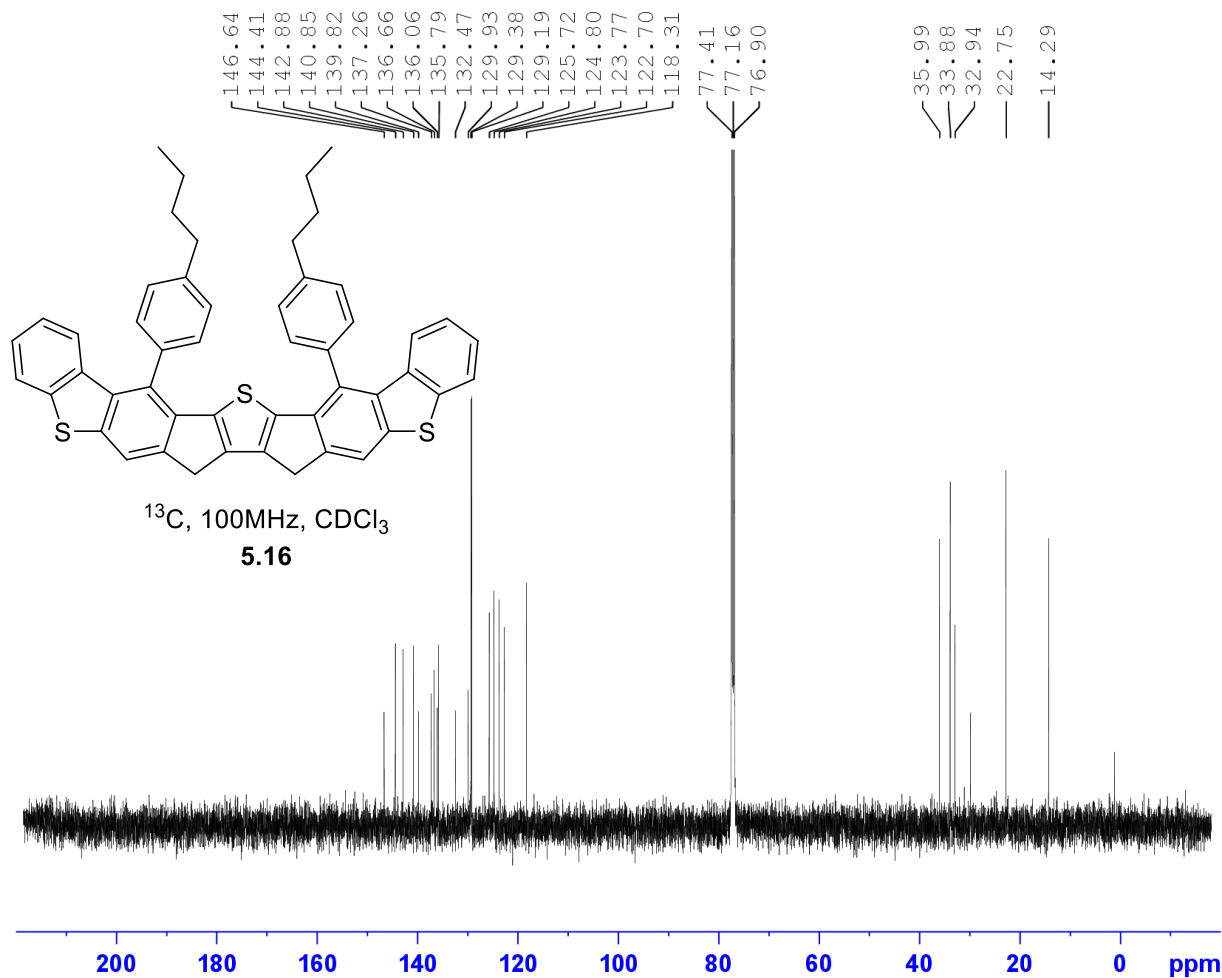
Current Data Parameters
NAME JAW-03-054
EXPNO 3
PROCNO 1

F2 - Acquisition Parameters
Date_ 20191011
Time_ 6.52
INSTRUM spect
PROBHD 5 mm PABBO BB/
PULPROG zgpg30
TD 65536
SOLVENT CDCl₃
NS 2048
DS 2
SWH 29761.904 Hz
FIDRES 0.454131 Hz
AQ 1.1010048 sec
RG 203
DW 16.800 usec
DE 6.50 usec
TE 298.5 K
D1 2.00000000 sec
D11 0.03000000 sec
TD0 1

===== CHANNEL f1 =====
SFO1 125.7779086 MHz
NUC1 13C
P1 10.50 usec
PLW1 110.00000000 W

===== CHANNEL f2 =====
SFO2 500.1620006 MHz
NUC2 1H
CPDPRG[2] waltz16
PCPD2 80.00 usec
PLW2 18.00000000 W
PLW12 0.37195000 W
PLW13 0.23805000 W

F2 - Processing parameters
SI 32768
SF 125.7653135 MHz
WDW EM
SSB 0
LB 1.00 Hz
GB 0
PC 1.40



Current Data Parameters
 NAME JAW-03-054
 EXPNO 3
 PROCNO 1

F2 - Acquisition Parameters
 Date_ 20191011
 Time_ 6.52
 INSTRUM spect
 PROBHD 5 mm PABBO BB/
 PULPROG zgpg30
 TD 65536
 SOLVENT CDCl_3
 NS 2048
 DS 2
 SWH 29761.904 Hz
 FIDRES 0.454131 Hz
 AQ 1.1010048 sec
 RG 203
 DW 16.800 usec
 DE 6.50 usec
 TE 298.5 K
 D1 2.00000000 sec
 D11 0.03000000 sec
 TD0 1

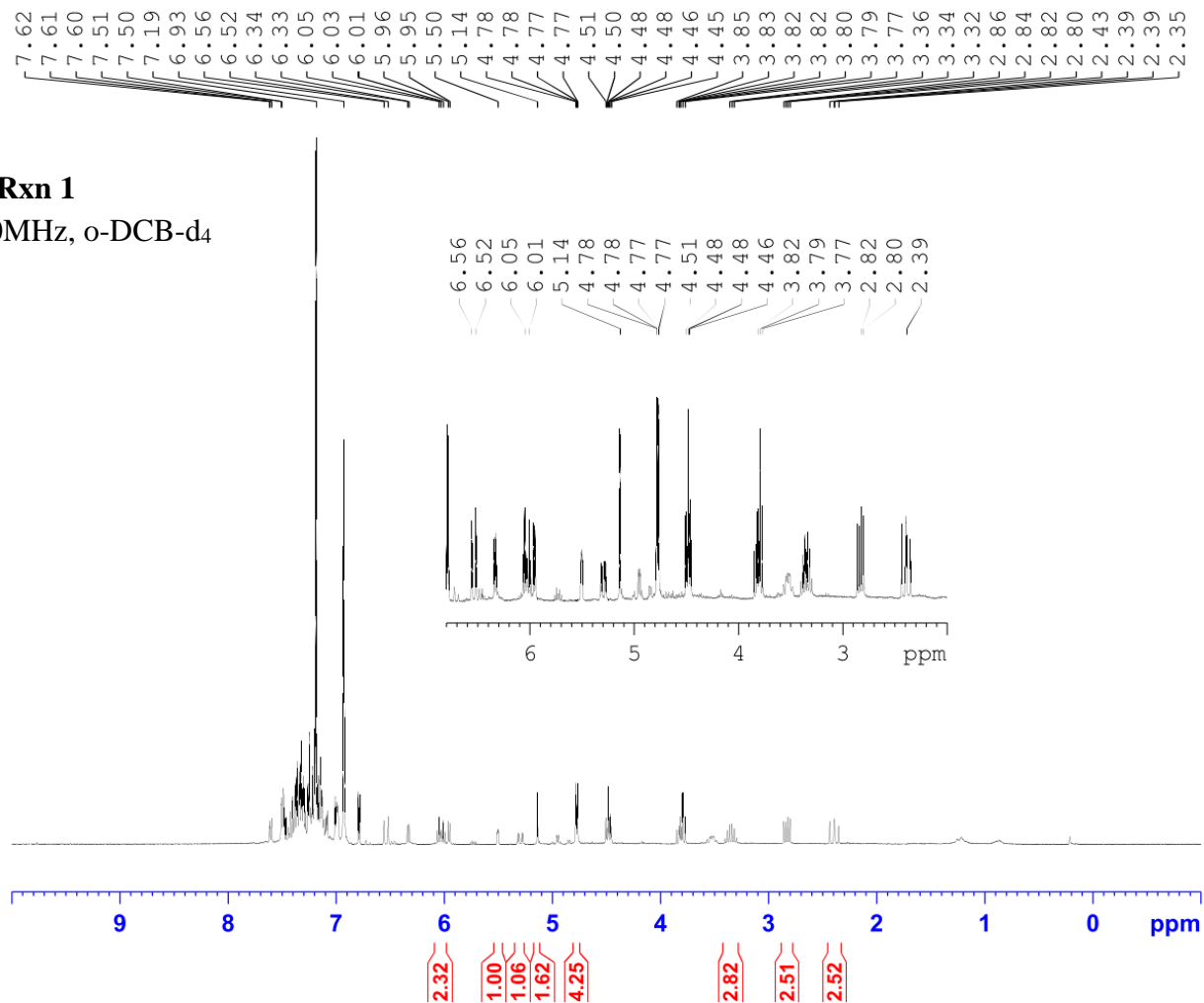
===== CHANNEL f1 =====
 SFO1 125.7779086 MHz
 NUC1 ^{13}C
 P1 10.50 usec
 PLW1 110.00000000 W

===== CHANNEL f2 =====
 SFO2 500.1620006 MHz
 NUC2 ^1H
 CPDPRG[2] waltz16
 PCPD2 80.00 usec
 PLW2 18.00000000 W
 PLW12 0.37195000 W
 PLW13 0.23805000 W

F2 - Processing parameters
 SI 32768
 SF 125.7653135 MHz
 WDW EM
 SSB 0
 LB 1.00 Hz
 GB 0
 PC 1.40

2.6.2 - Rxn 1

^1H , 400MHz, o-DCB-d₄



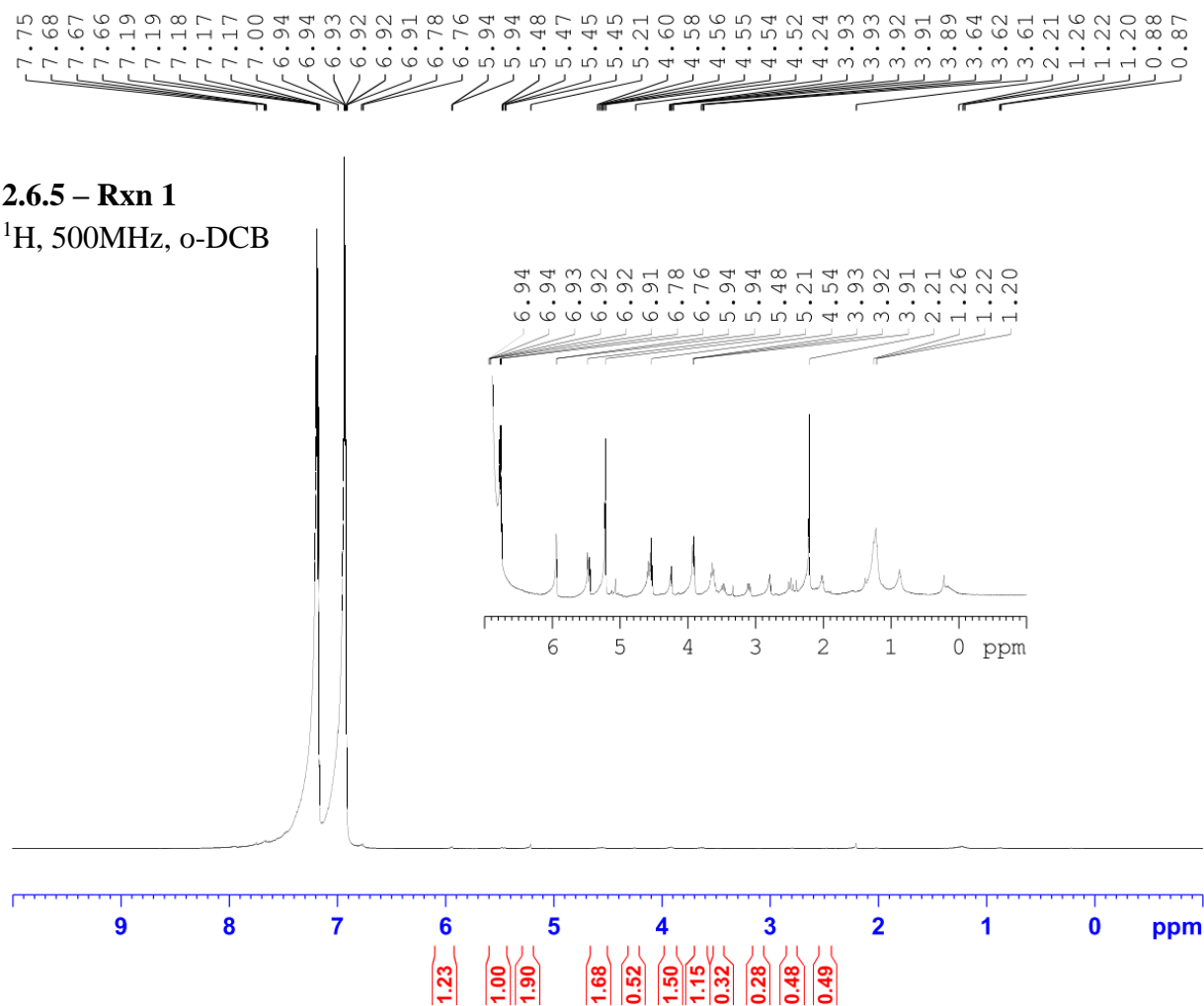
Current Data Parameters
 NAME JAW-01-008
 EXPNO 2
 PROCNO 1

F2 - Acquisition Parameters
 Date_ 20160617
 Time 13.16
 INSTRUM spect
 PROBHD 5 mm PABBO BB-
 PULPROG zg30
 TD 65536
 SOLVENT C6D6
 NS 16
 DS 2
 SWH 8012.820 Hz
 FIDRES 0.122266 Hz
 AQ 4.0894465 sec
 RG 128
 DW 62.400 usec
 DE 6.50 usec
 TE 95.6 K
 D1 1.00000000 sec
 TD0 1

===== CHANNEL f1 =====
 SF01 400.1324710 MHz
 NUC1 1H
 P1 13.75 usec
 PLW1 12.01700020 W

F2 - Processing parameters
 SI 65536
 SF 400.1300900 MHz
 WDW EM
 SSB 0
 LB 0.30 Hz
 GB 0
 PC 1.00

2.6.5 – Rxn 1
¹H, 500MHz, o-DCB

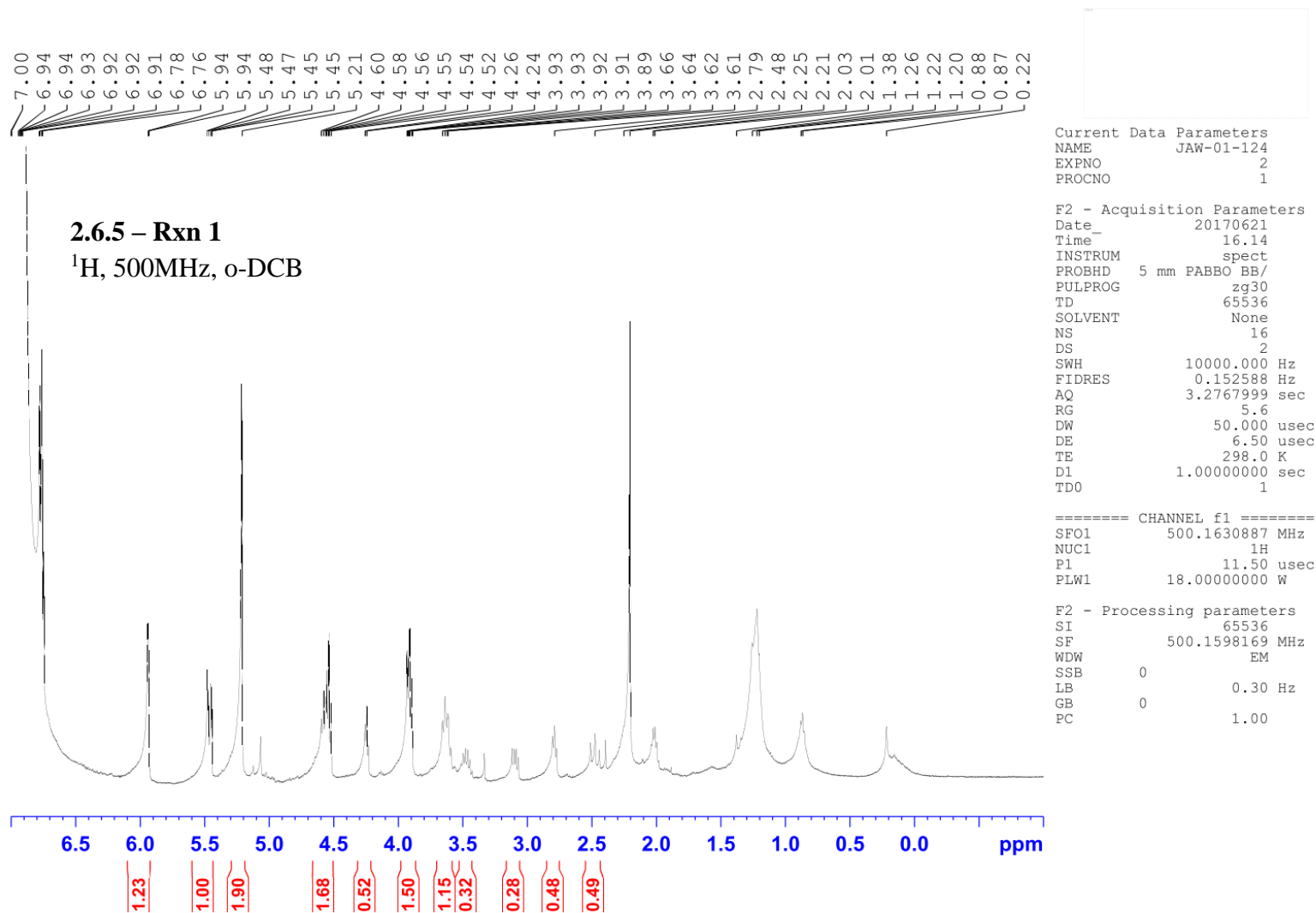


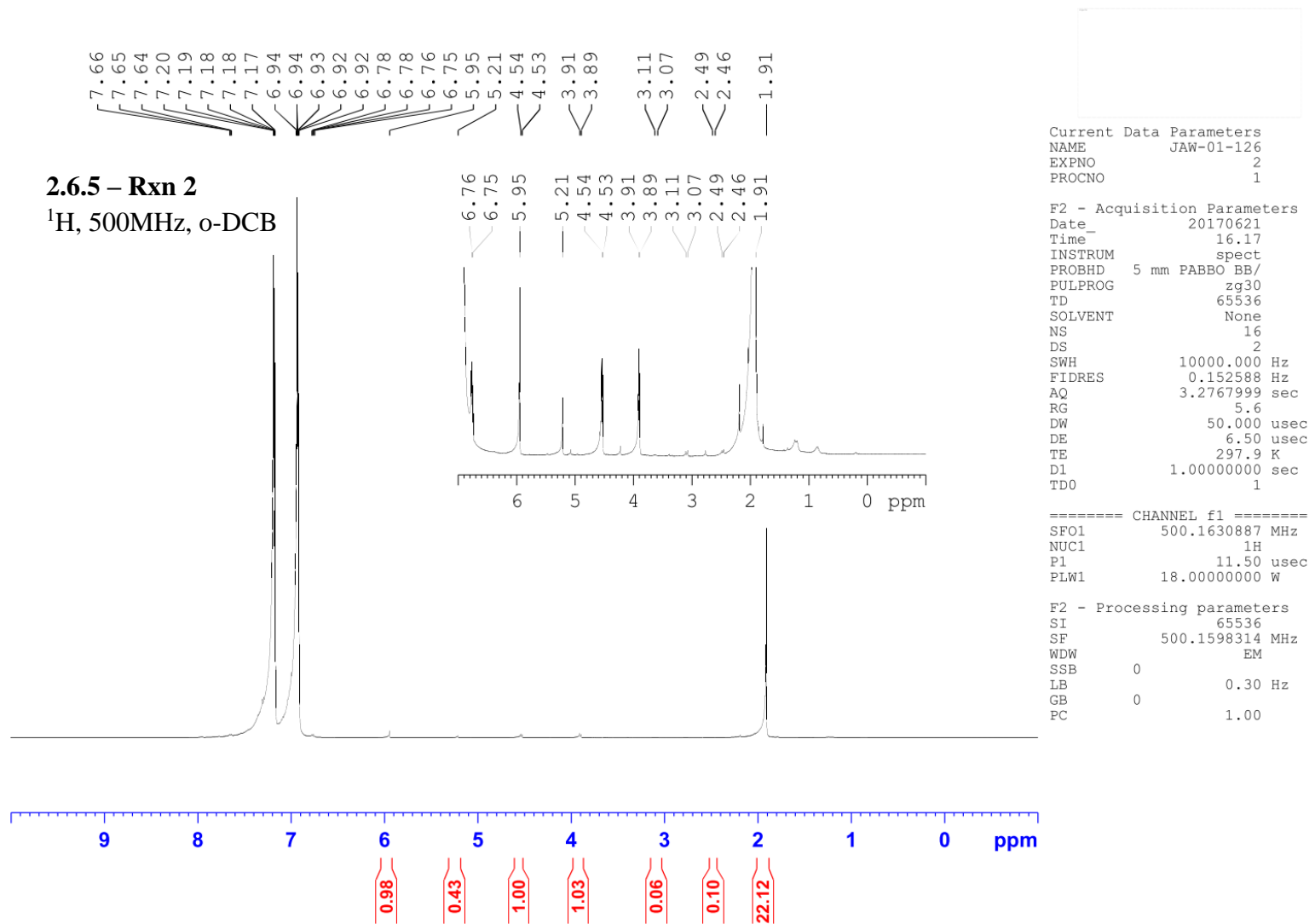
Current Data Parameters
NAME JAW-01-124
EXPNO 2
PROCNO 1

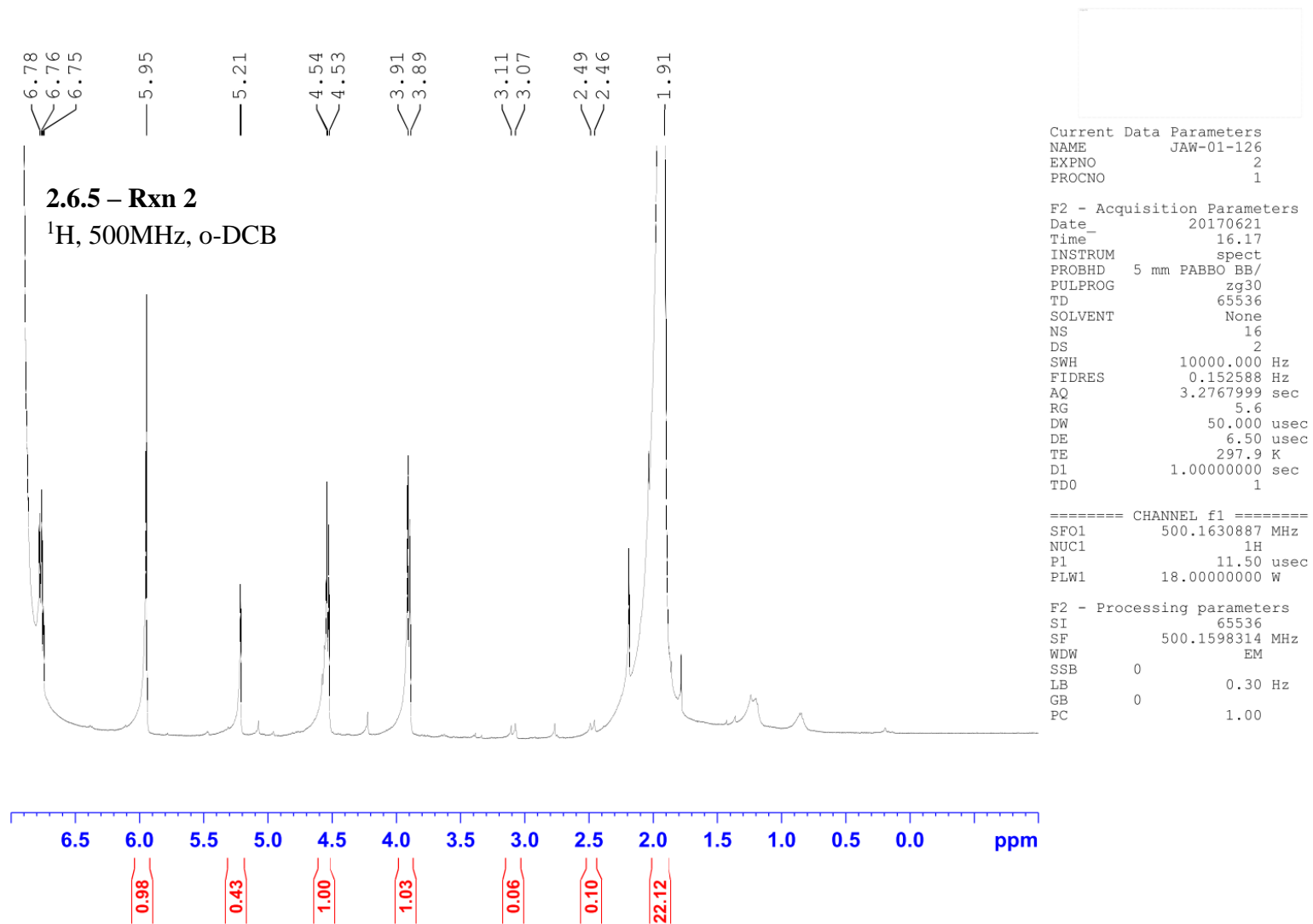
F2 - Acquisition Parameters
Date_ 20170621
Time_ 16.14
INSTRUM spect
PROBHD 5 mm PABBO BB/
PULPROG zg30
TD 65536
SOLVENT None
NS 16
DS 2
SWH 10000.000 Hz
FIDRES 0.152588 Hz
AQ 3.2767999 sec
RG 5.6
DW 50.000 usec
DE 6.50 usec
TE 298.0 K
D1 1.00000000 sec
TD0 1

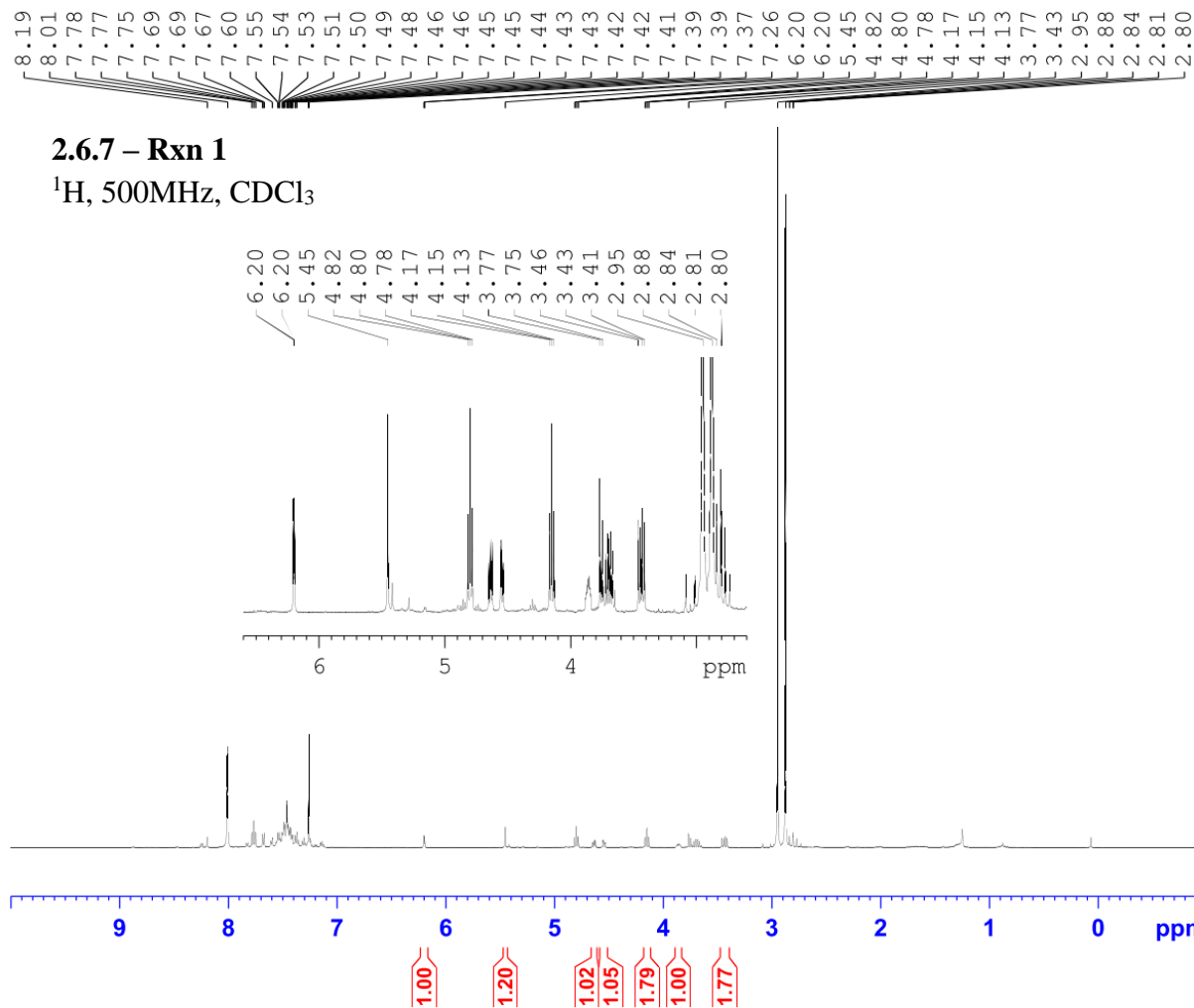
===== CHANNEL f1 =====
SF01 500.1630887 MHz
NUC1 1H
P1 11.50 usec
PLW1 18.00000000 W

F2 - Processing parameters
SI 65536
SF 500.1598169 MHz
WDW EM
SSB 0
LB 0.30 Hz
GB 0
PC 1.00







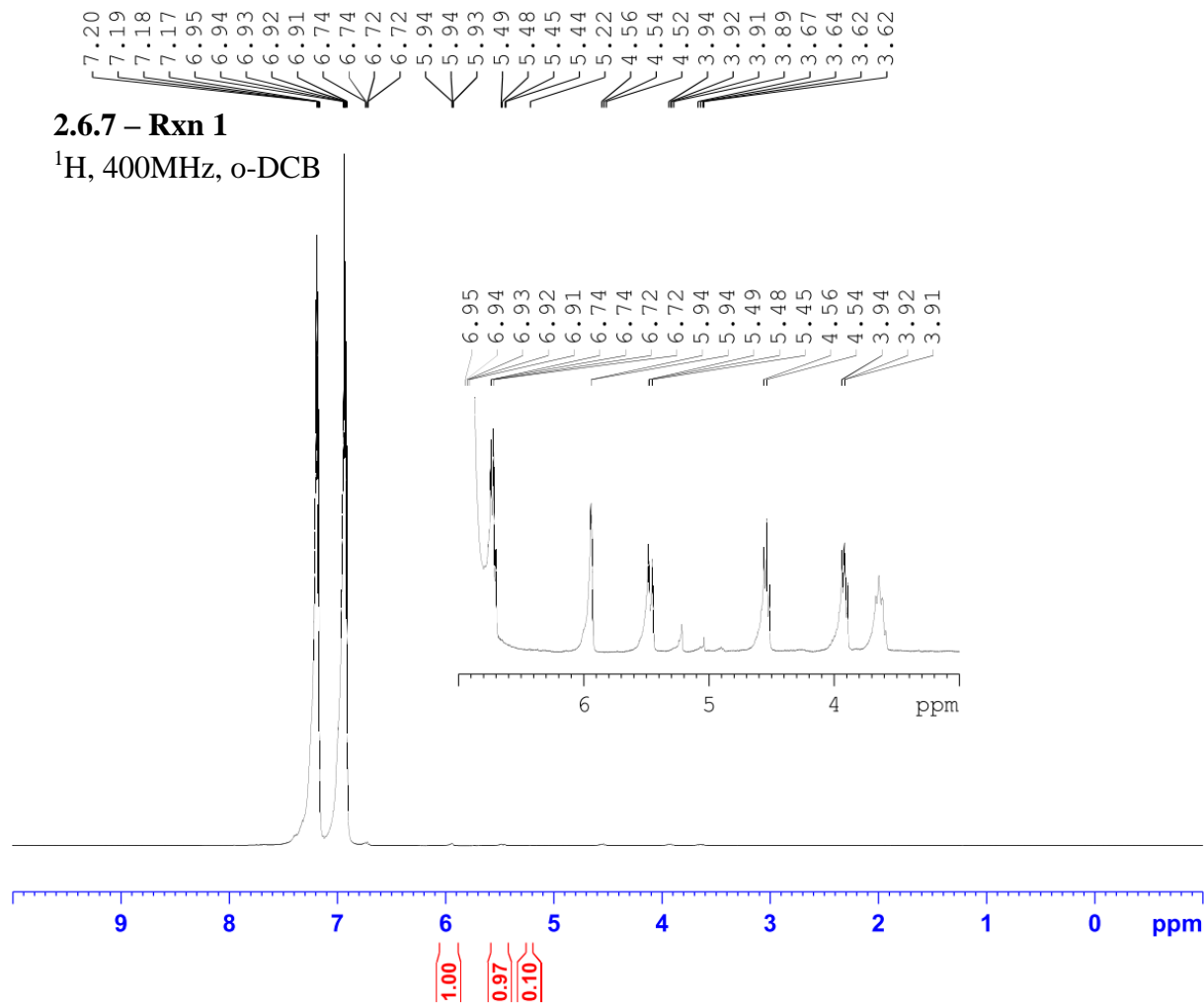


Current Data Parameters
NAME JAW-02-187
EXPNO 2
PROCNO 1

F2 - Acquisition Parameters
Date_ 20190124
Time_ 16.28
INSTRUM spect
PROBHD 5 mm PABBO BB/
PULPROG zg30
TD 65536
SOLVENT CDCl₃
NS 16
DS 2
SWH 10000.000 Hz
FIDRES 0.152588 Hz
AQ 3.2767999 sec
RG 101
DW 50.000 usec
DE 6.50 usec
TE 297.4 K
D1 1.00000000 sec
TD0 1

===== CHANNEL f1 =====
SF01 500.1630887 MHz
NUC1 1H
P1 11.50 usec
PLW1 18.00000000 W

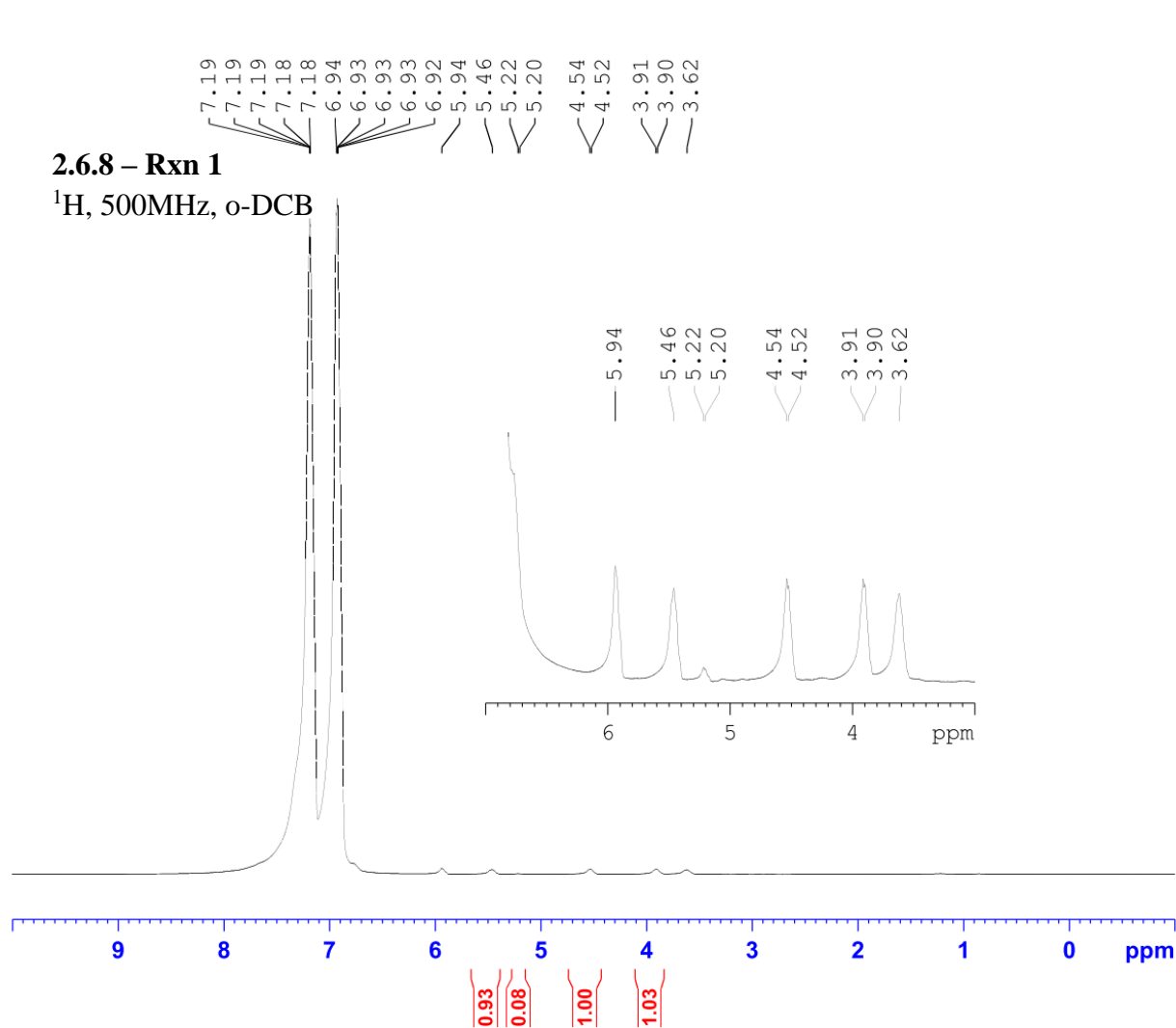
F2 - Processing parameters
SI 65536
SF 500.1600122 MHz
WDW EM
SSB 0
LB 0.30 Hz
GB 0
PC 1.00



Current Data Parameters
 NAME JAW-02-187
 EXPNO 1
 PROCNO 1

F2 - Acquisition Parameters
 Date_ 20190124
 Time_ 14.52 h
 INSTRUM spect
 PROBHD Z108618_0240 (
 PULPROG zg30
 TD 65536
 SOLVENT None
 NS 48
 DS 2
 SWH 8012.820 Hz
 FIDRES 0.244532 Hz
 AQ 4.0894465 sec
 RG 5.6
 DW 62.400 usec
 DE 6.50 usec
 TE 91.8 K
 D1 1.00000000 sec
 TD0 1
 SFO1 400.1324708 MHz
 NUC1 1H
 P0 4.83 usec
 P1 14.50 usec
 PLW1 12.00000000 W

F2 - Processing parameters
 SI 65536
 SF 400.1295236 MHz
 WDW EM
 SSB 0
 LB 0.30 Hz
 GB 0
 PC 1.00

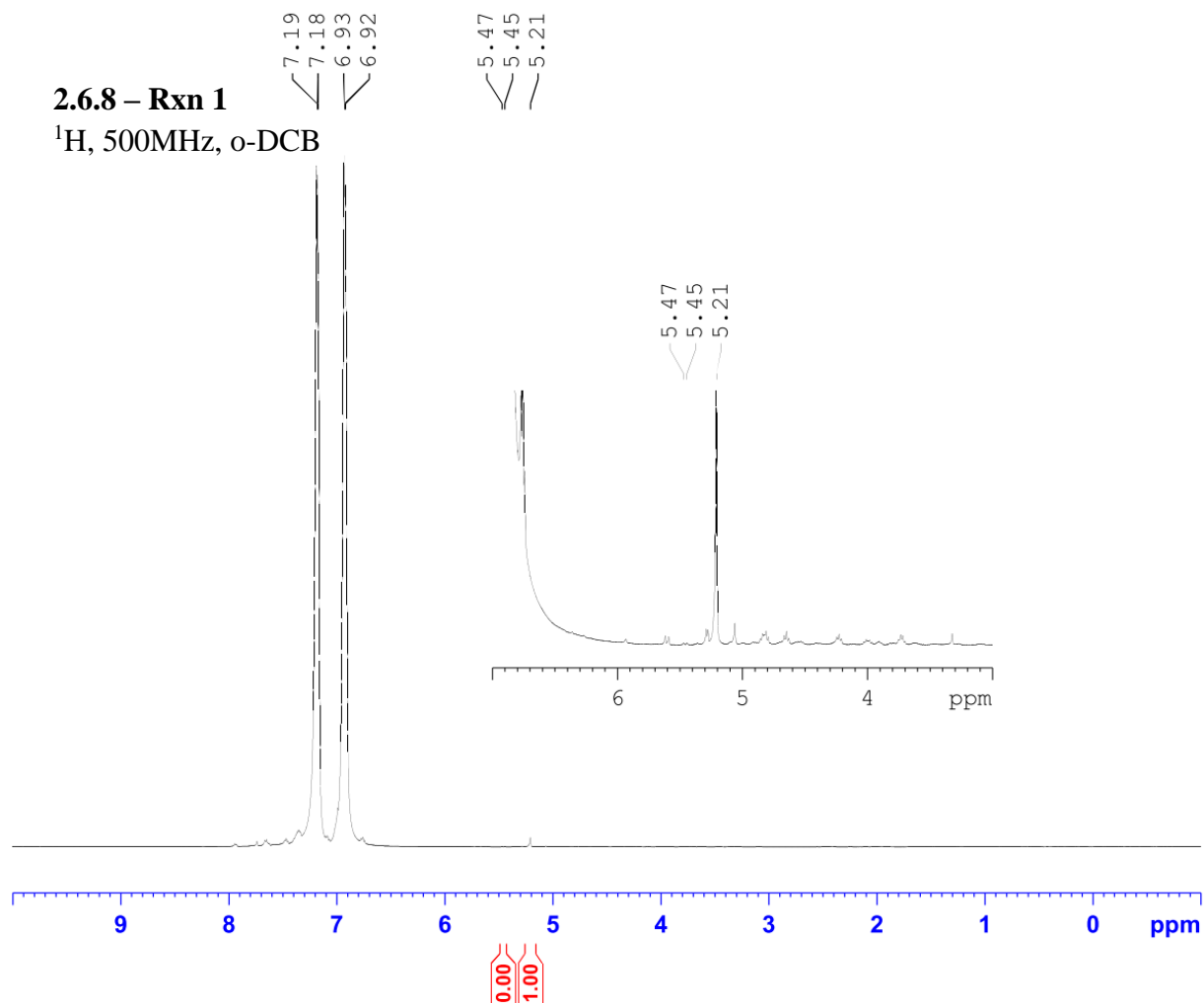


Current Data Parameters
NAME JAW-02-183
EXPNO 1
PROCNO 1

F2 - Acquisition Parameters
Date_ 20181219
Time_ 14.19
INSTRUM spect
PROBHD 5 mm PABBO BB/
PULPROG zg30
TD 65536
SOLVENT None
NS 48
DS 2
SWH 10000.000 Hz
FIDRES 0.152588 Hz
AQ 3.2767999 sec
RG 5.6
DW 50.000 usec
DE 6.50 usec
TE 297.3 K
D1 1.00000000 sec
TD0 1

===== CHANNEL f1 =====
SF01 500.1630887 MHz
NUC1 1H
P1 11.50 usec
PLW1 18.00000000 W

F2 - Processing parameters
SI 65536
SF 500.1595369 MHz
WDW EM
SSB 0
LB 0.30 Hz
GB 0
PC 1.00

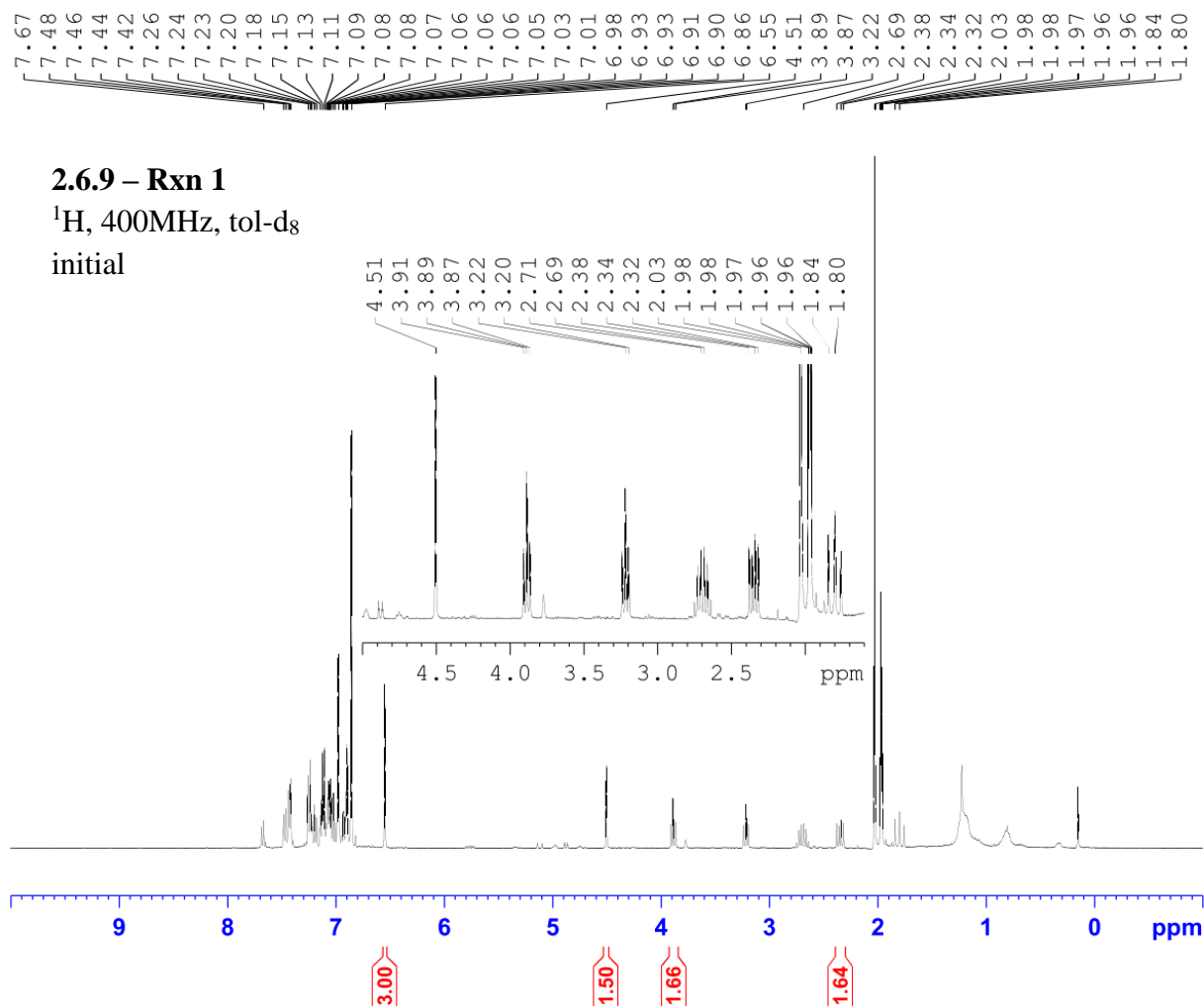


Current Data Parameters
 NAME JAW-02-183
 EXPNO 3
 PROCNO 1

F2 - Acquisition Parameters
 Date_ 20181219
 Time_ 16.58
 INSTRUM spect
 PROBHD 5 mm PABBO BB/
 PULPROG zg30
 TD 65536
 SOLVENT None
 NS 48
 DS 2
 SWH 10000.000 Hz
 FIDRES 0.152588 Hz
 AQ 3.2767999 sec
 RG 5
 DW 50.000 usec
 DE 6.50 usec
 TE 297.3 K
 D1 1.00000000 sec
 TD0 1

===== CHANNEL f1 =====
 SF01 500.1630887 MHz
 NUC1 1H
 P1 11.50 usec
 PLW1 18.00000000 W

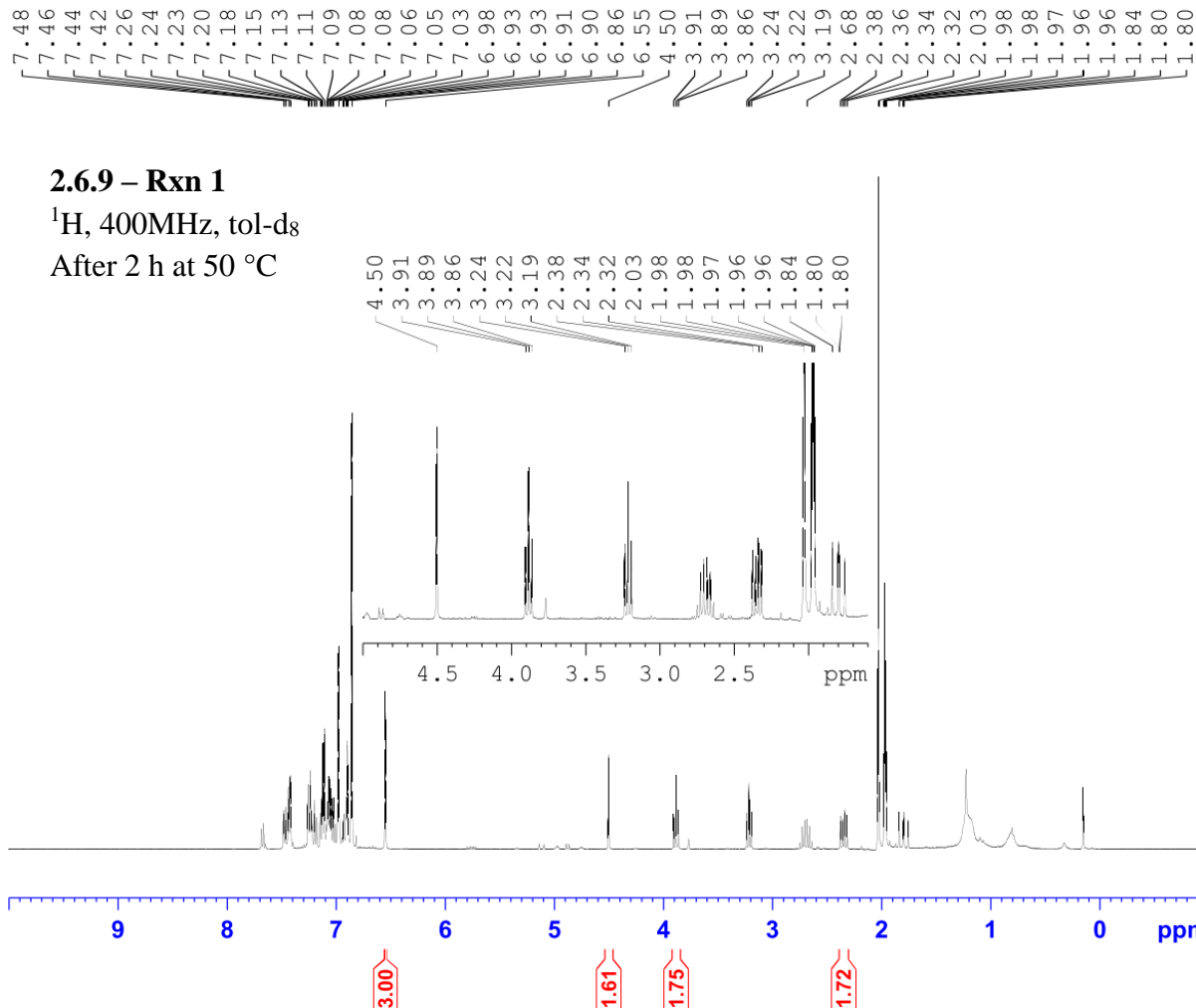
F2 - Processing parameters
 SI 65536
 SF 500.1598062 MHz
 WDW EM
 SSB 0
 LB 0.30 Hz
 GB 0
 PC 1.00



Current Data Parameters
 NAME JAW-03-097
 EXPNO 1
 PROCNO 1

F2 - Acquisition Parameters
 Date_ 20200227
 Time_ 13.36 h
 INSTRUM spect
 PROBHD z108618_0240 (z)
 PULPROG zg30
 TD 65536
 SOLVENT Tol
 NS 16
 DS 2
 SWH 8012.820 Hz
 FIDRES 0.244532 Hz
 AQ 4.0894465 sec
 RG 90.5
 DW 62.400 usec
 DE 6.50 usec
 TE 91.3 K
 D1 1.00000000 sec
 TD0 1
 SFO1 400.1324708 MHz
 NUC1 1H
 P0 4.83 usec
 P1 14.50 usec
 PLW1 12.00000000 W

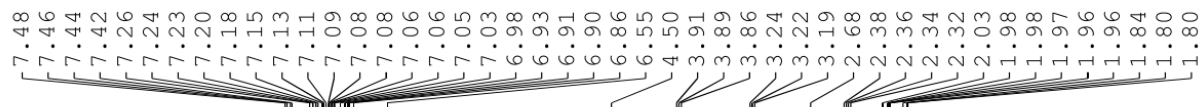
F2 - Processing parameters
 SI 65536
 SF 400.1300627 MHz
 WDW EM
 SSB 0
 LB 0.30 Hz
 GB 0
 PC 1.00



Current Data Parameters
 NAME JAW-03-097
 EXPNO 2
 PROCNO 1

F2 - Acquisition Parameters
 Date_ 20200227
 Time_ 16.18 h
 INSTRUM spect
 PROBHD Z108618_0240 (
 PULPROG zg30
 TD 65536
 SOLVENT Tol
 NS 16
 DS 2
 SWH 8012.820 Hz
 FIDRES 0.244532 Hz
 AQ 4.0894465 sec
 RG 101
 DW 62.400 usec
 DE 6.50 usec
 TE 91.5 K
 D1 1.00000000 sec
 TD0 1
 SFO1 400.1324708 MHz
 NUC1 1H
 P0 4.83 usec
 P1 14.50 usec
 PLW1 12.00000000 W

F2 - Processing parameters
 SI 65536
 SF 400.1300628 MHz
 WDW EM
 SSB 0
 LB 0.30 Hz
 GB 0
 PC 1.00



Current Data Parameters
NAME JAW-03-097
EXPNO 4
PROCNO 1

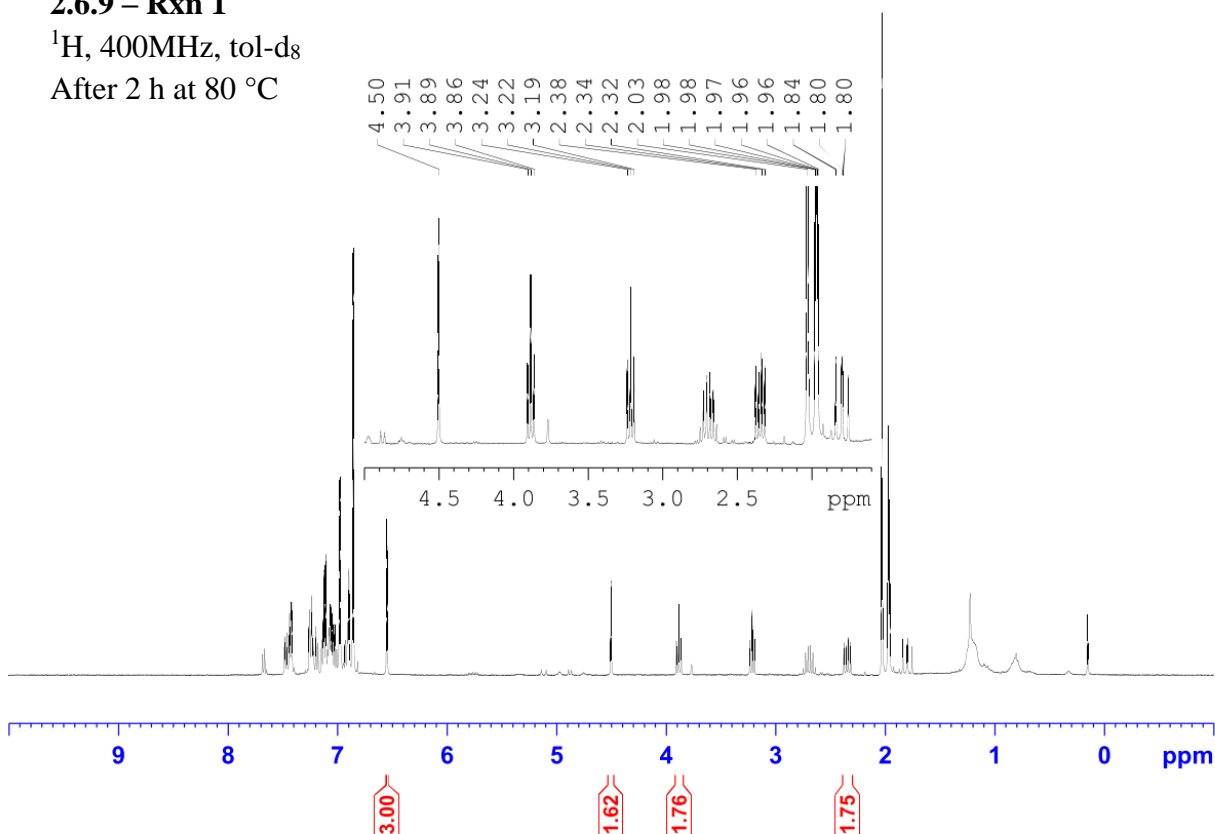
F2 - Acquisition Parameters
Date_ 20200228
Time_ 8.52 h
INSTRUM spect
PROBHD z108618_0240 (
PULPROG zg30
TD 65536
SOLVENT Tol
NS 16
DS 2
SWH 8012.820 Hz
FIDRES 0.244532 Hz
AQ 4.0894465 sec
RG 101
DW 62.400 usec
DE 6.50 usec
TE 92.2 K
D1 1.00000000 sec
TD0 1
SF01 400.1324708 MHz
NUC1 1H
P0 4.83 usec
P1 14.50 usec
PLW1 12.00000000 W

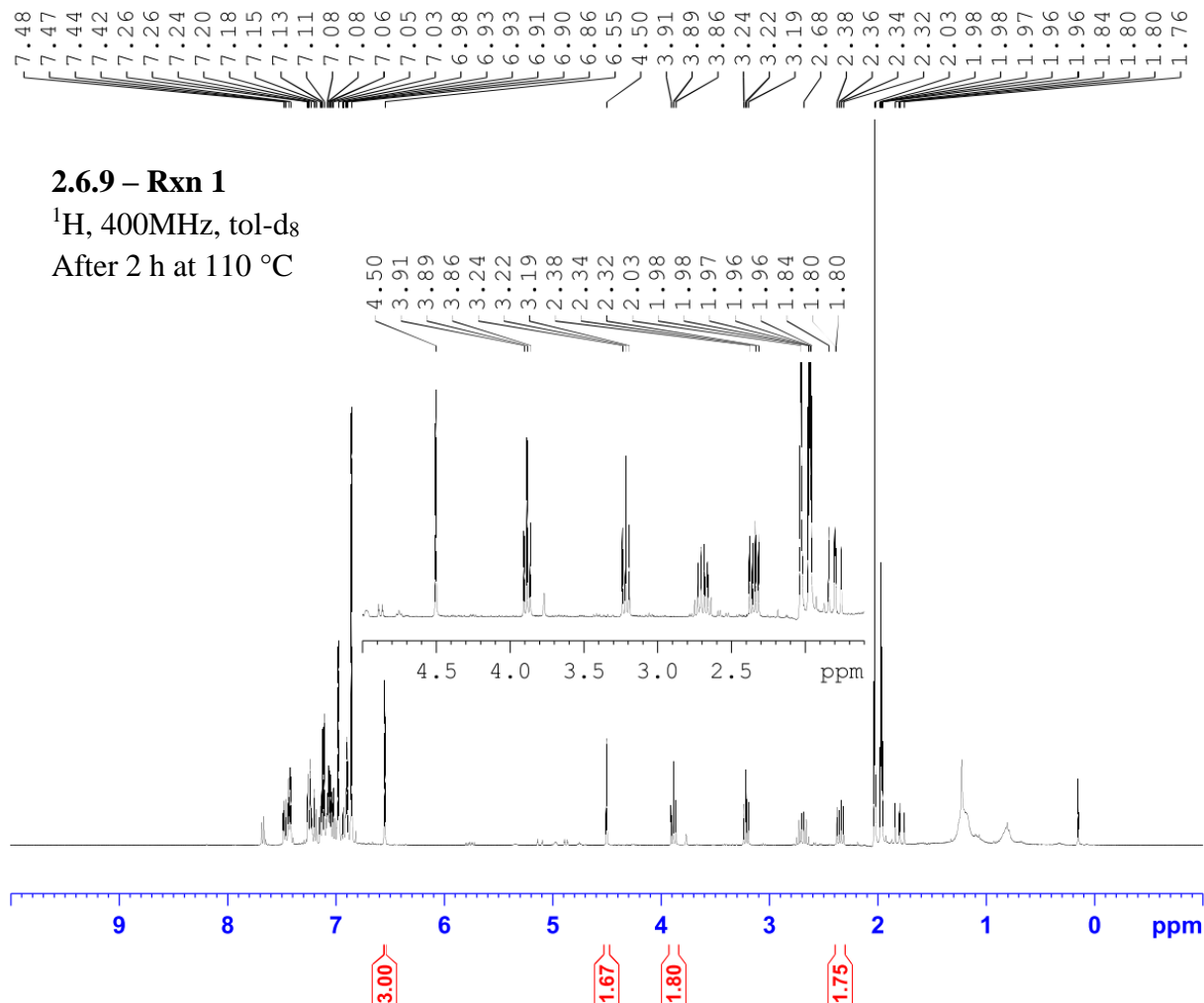
F2 - Processing parameters
SI 65536
SF 400.1300628 MHz
WDW EM
SSB 0
LB 0.30 Hz
GB 0
PC 1.00

2.6.9 – Rxn 1

¹H, 400MHz, tol-d₈

After 2 h at 80 °C





Current Data Parameters
 NAME JAW-03-097
 EXPNO 5
 PROCNO 1

F2 - Acquisition Parameters
 Date_ 20200228
 Time_ 11.35 h
 INSTRUM spect
 PROBHD z108618_0240 (zg30)
 PULPROG zg30
 TD 65536
 SOLVENT Tol
 NS 16
 DS 2
 SWH 8012.820 Hz
 FIDRES 0.244532 Hz
 AQ 4.0894465 sec
 RG 90.5
 DW 62.400 usec
 DE 6.50 usec
 TE 91.8 K
 D1 1.00000000 sec
 TD0 1
 SFO1 400.1324708 MHz
 NUC1 1H
 P0 4.83 usec
 P1 14.50 usec
 PLW1 12.00000000 W

F2 - Processing parameters
 SI 65536
 SF 400.1300628 MHz
 WDW EM
 SSB 0
 LB 0.30 Hz
 GB 0
 PC 1.00

7.48
7.46
7.44
7.42
7.26
7.24
7.23
7.20
7.18
7.15
7.13
7.11
7.09
7.08
7.06
7.05
7.03
6.98
6.93
6.91
6.90
6.86
6.55
4.50
3.91
3.89
3.87
3.24
3.22
3.19
3.32
2.03
1.98
1.97
1.96
1.96
1.84
1.84
1.80
1.80
2.38
2.36
2.34
2.32
2.03
1.98
1.97
1.96
1.96
1.84
1.84
1.80
1.80



Current Data Parameters
NAME JAW-03-097
EXPNO 6
PROCNO 1

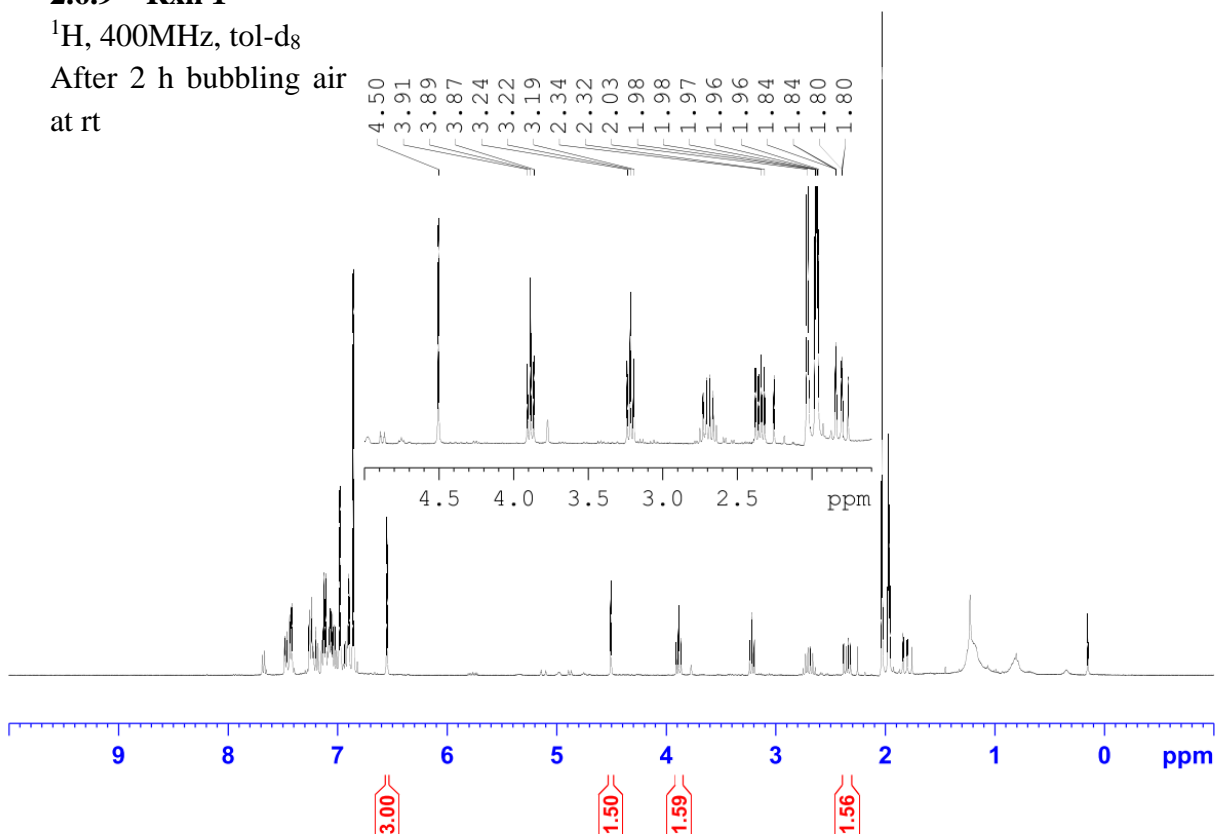
F2 - Acquisition Parameters
Date_ 20200228
Time_ 16.17 h
INSTRUM spect
PROBHD Z108618_0240 (
PULPROG zg30
TD 65536
SOLVENT Tol
NS 16
DS 2
SWH 8012.820 Hz
FIDRES 0.244532 Hz
AQ 4.0894465 sec
RG 90.5
DW 62.400 usec
DE 6.50 usec
TE 92.0 K
D1 1.00000000 sec
TD0 1
SF01 400.1324708 MHz
NUC1 1H
P0 4.83 usec
P1 14.50 usec
PLW1 12.00000000 W

F2 - Processing parameters
SI 65536
SF 400.1300627 MHz
WDW EM
SSB 0
LB 0.30 Hz
GB 0
PC 1.00

2.6.9 – Rxn 1

¹H, 400MHz, tol-d₈

After 2 h bubbling air
at rt



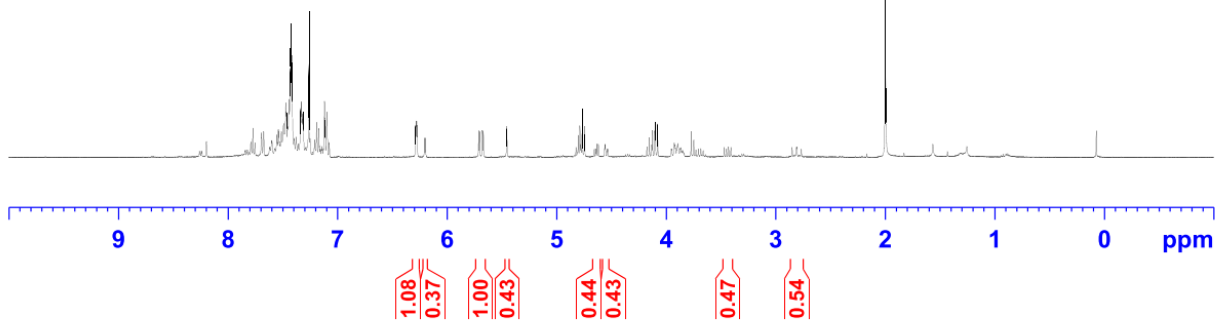
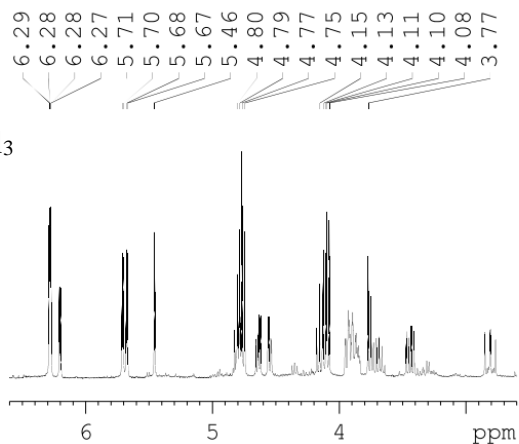


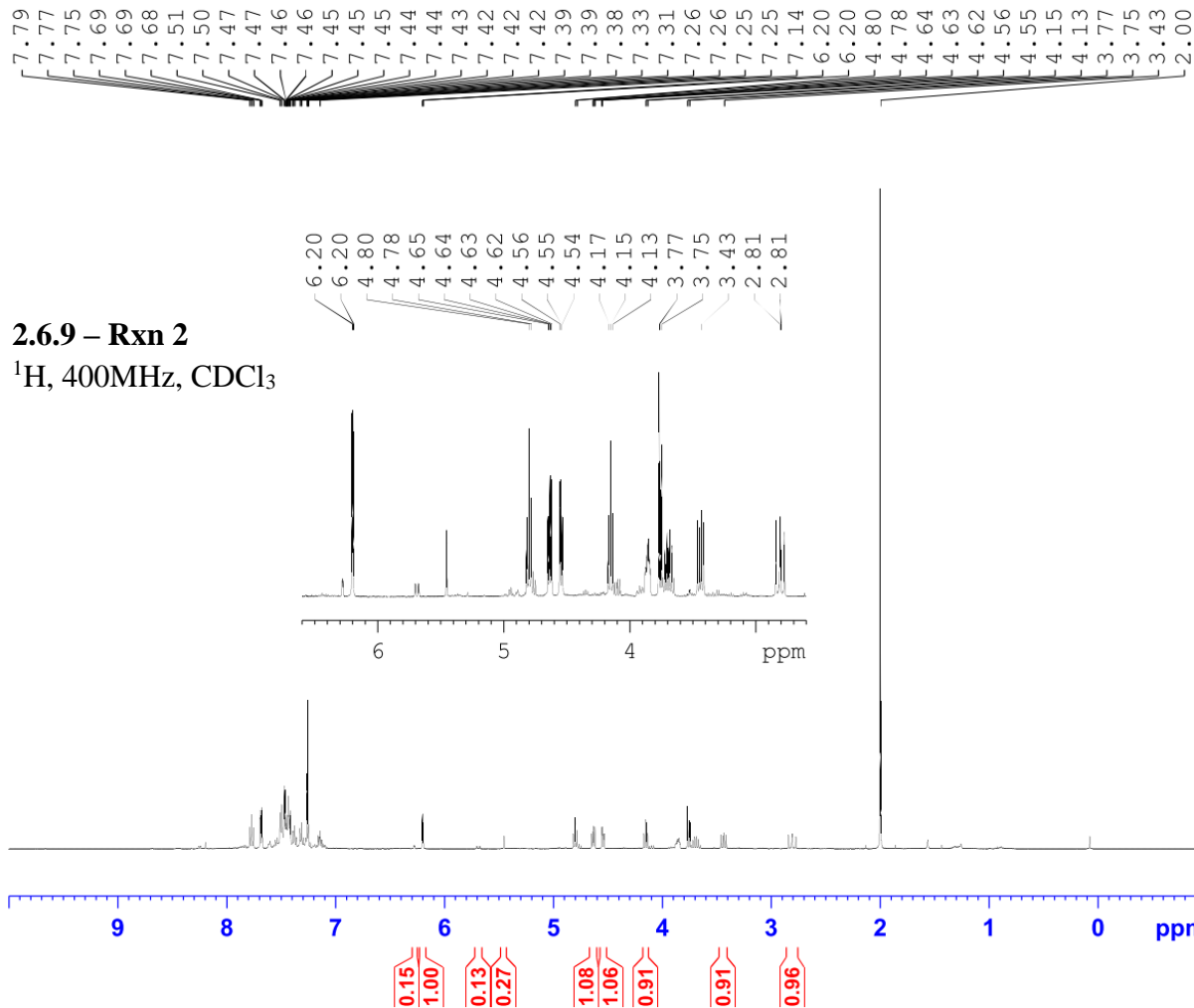
Current Data Parameters
NAME JAW-02-179
EXPNO 1
PROCNO 1

F2 - Acquisition Parameters
Date_ 20181213
Time_ 12.04 h
INSTRUM spect
PROBHD z108618_0240 (
PULPROG zg30
TD 65536
SOLVENT CDCl3
NS 16
DS 2
SWH 8012.820 Hz
FIDRES 0.244532 Hz
AQ 4.0894465 sec
RG 101
DW 62.400 usec
DE 6.50 usec
TE 90.5 K
D1 1.00000000 sec
TD0 1
SF01 400.1324708 MHz
NUC1 1H
P0 4.83 usec
P1 14.50 usec
PLW1 12.00000000 W

F2 - Processing parameters
SI 65536
SF 400.1300099 MHz
WDW EM
SSB 0
LB 0.30 Hz
GB 0
PC 1.00

2.6.9 – Rxn 1
¹H, 400MHz, CDCl₃



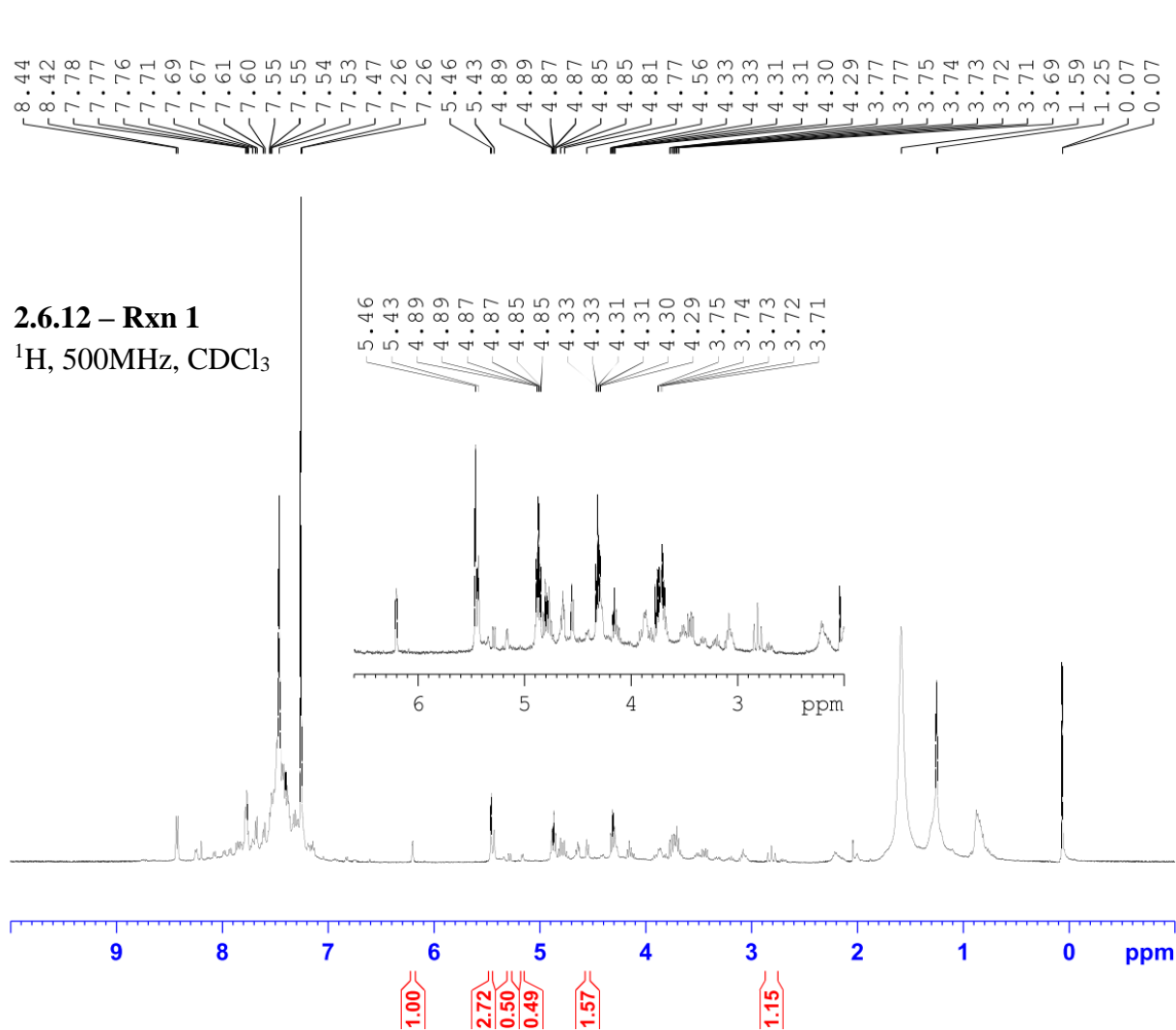


Current Data Parameters
 NAME JAW-02-179-b
 EXPNO 30
 PROCNO 1

F2 - Acquisition Parameters
 Date_ 20181213
 Time_ 15.26
 INSTRUM spect
 PROBHD 5 mm PABBO BB/
 PULPROG zg30
 TD 65536
 SOLVENT CDCl₃
 NS 16
 DS 2
 SWH 10000.000 Hz
 FIDRES 0.152588 Hz
 AQ 3.2767999 sec
 RG 101
 DW 50.000 usec
 DE 6.50 usec
 TE 297.6 K
 D1 1.00000000 sec
 TD0 1

===== CHANNEL f1 =====
 SF01 500.1630887 MHz
 NUC1 1H
 P1 11.50 usec
 PLW1 18.00000000 W

F2 - Processing parameters
 SI 65536
 SF 500.1600122 MHz
 WDW EM
 SSB 0
 LB 0.30 Hz
 GB 0
 PC 1.00

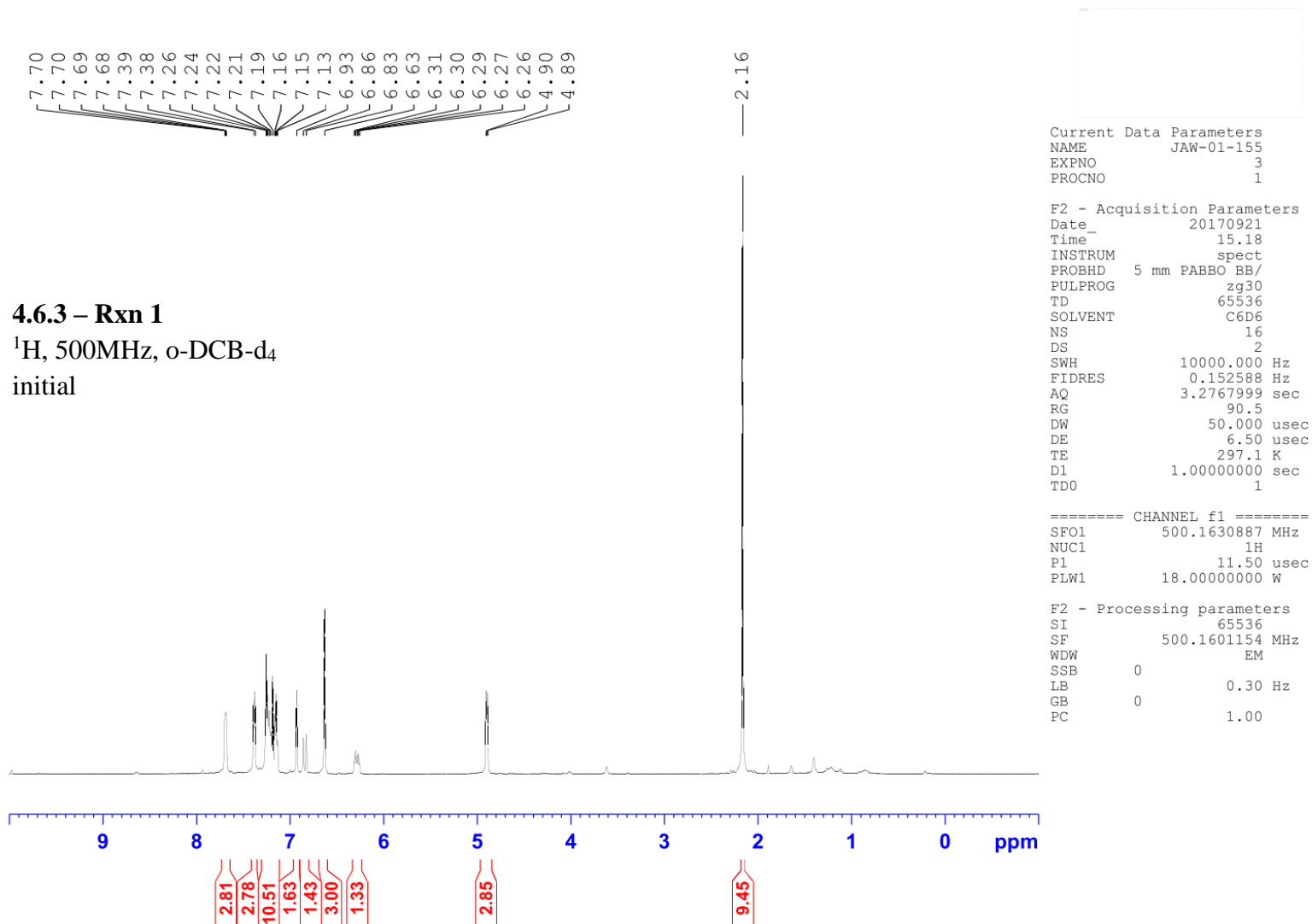


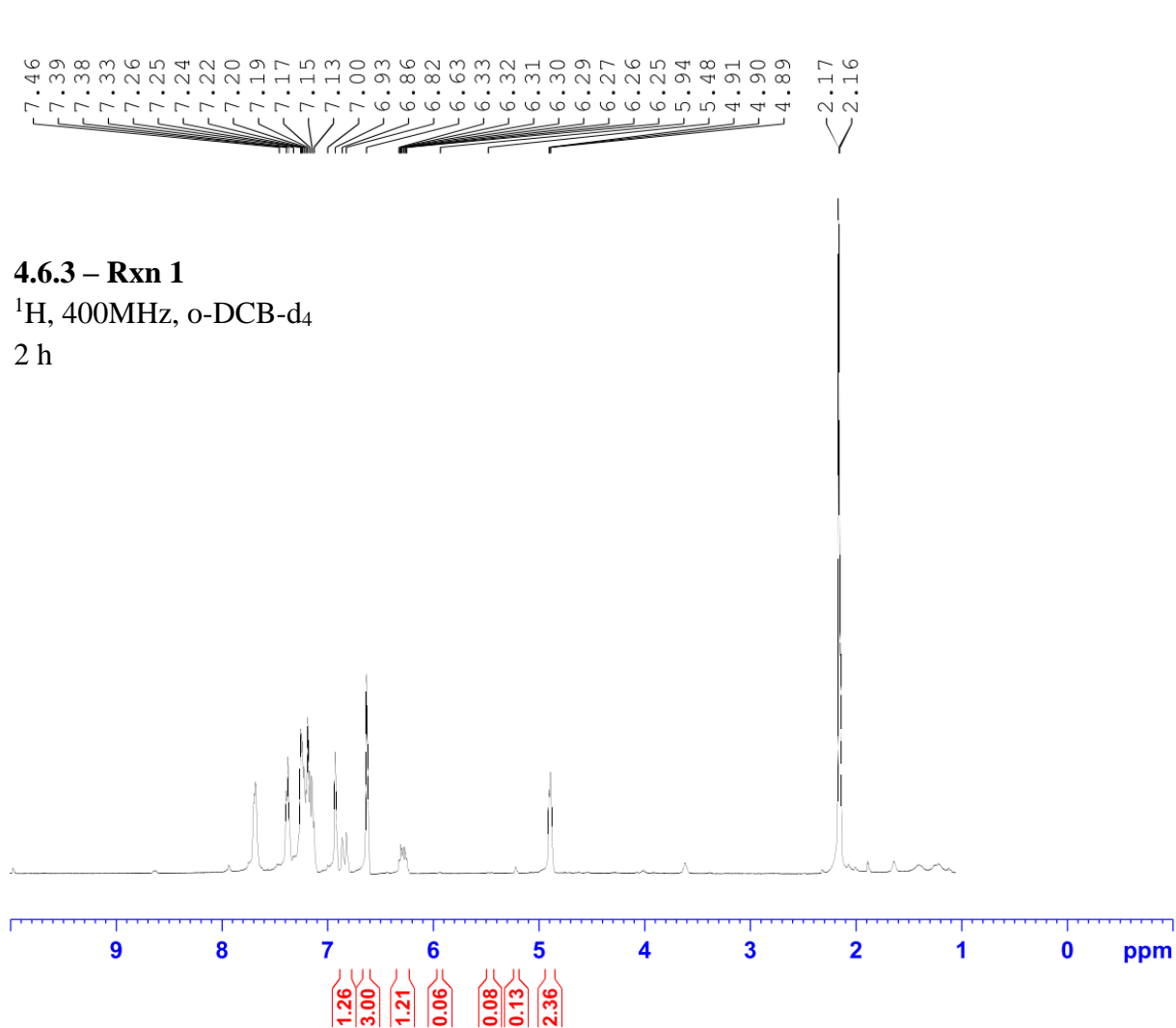
Current Data Parameters
 NAME JAW-02-110-a
 EXPNO 19
 PROCNO 1

F2 - Acquisition Parameters
 Date_ 20180828
 Time_ 14.31
 INSTRUM spect
 PROBHD 5 mm PABBO BB/
 PULPROG zg30
 TD 65536
 SOLVENT CDCl₃
 NS 32
 DS 2
 SWH 10000.000 Hz
 FIDRES 0.152588 Hz
 AQ 3.2767999 sec
 RG 203
 DW 50.000 usec
 DE 6.50 usec
 TE 295.8 K
 D1 1.00000000 sec
 TD0 1

===== CHANNEL f1 =====
 SFO1 500.1630887 MHz
 NUC1 1H
 P1 11.50 usec
 PLW1 18.00000000 W

F2 - Processing parameters
 SI 65536
 SF 500.1600133 MHz
 WDW EM
 SSB 0
 LB 0.30 Hz
 GB 0
 PC 1.00



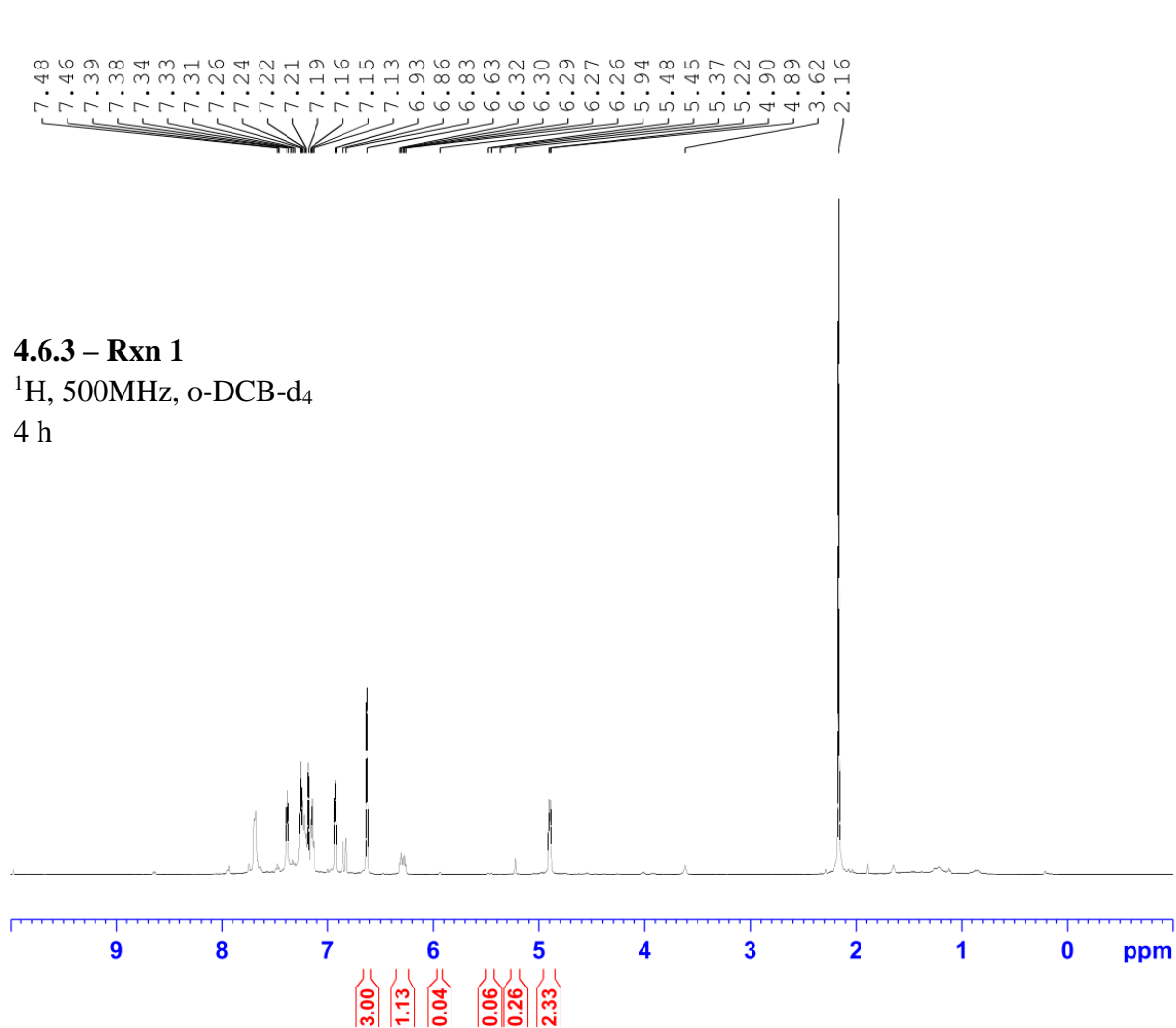


Current Data Parameters
 NAME JAW-01-155
 EXPNO 13
 PROCNO 1

F2 - Acquisition Parameters
 Date_ 20170922
 Time_ 13.23
 INSTRUM spect
 PROBHD 5 mm PADUL 13C
 PULPROG zg30
 TD 65536
 SOLVENT oC6D4Cl2
 NS 32
 DS 2
 SWH 8223.685 Hz
 FIDRES 0.125483 Hz
 AQ 3.9845889 sec
 RG 128
 DW 60.800 usec
 DE 6.50 usec
 TE 298.0 K
 D1 2.00000000 sec
 TD0 1

===== CHANNEL f1 =====
 NUC1 1H
 P1 9.31 usec
 PL1 -3.90 dB
 PL1W 21.64248466 W
 SFO1 400.2324716 MHz

F2 - Processing parameters
 SI 32768
 SF 400.2279381 MHz
 WDW EM
 SSB 0
 LB 0.30 Hz
 GB 0
 PC 1.00

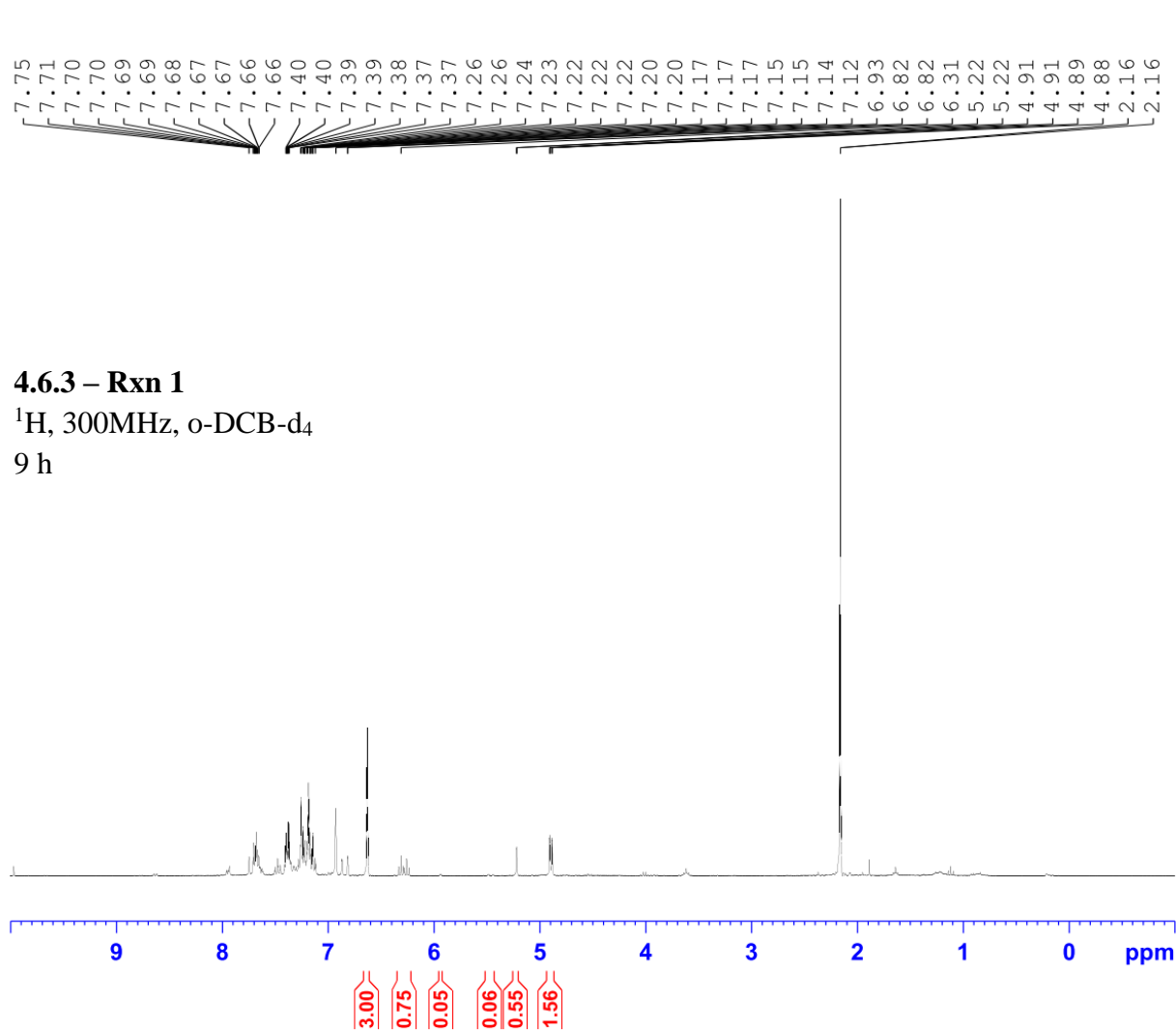


Current Data Parameters
 NAME JAW-01-155
 EXPNO 14
 PROCNO 1

F2 - Acquisition Parameters
 Date_ 20170922
 Time_ 16.57
 INSTRUM spect
 PROBHD 5 mm PABBO BB/
 PULPROG zg30
 TD 65536
 SOLVENT C6D6
 NS 32
 DS 2
 SWH 10000.000 Hz
 FIDRES 0.152588 Hz
 AQ 3.2767999 sec
 RG 90.5
 DW 50.000 usec
 DE 6.50 usec
 TE 297.1 K
 D1 1.00000000 sec
 TD0 1

===== CHANNEL f1 =====
 SF01 500.1630887 MHz
 NUC1 1H
 P1 11.50 usec
 PLW1 18.00000000 W

F2 - Processing parameters
 SI 65536
 SF 500.1599834 MHz
 WDW EM
 SSB 0
 LB 0.30 Hz
 GB 0
 PC 1.00

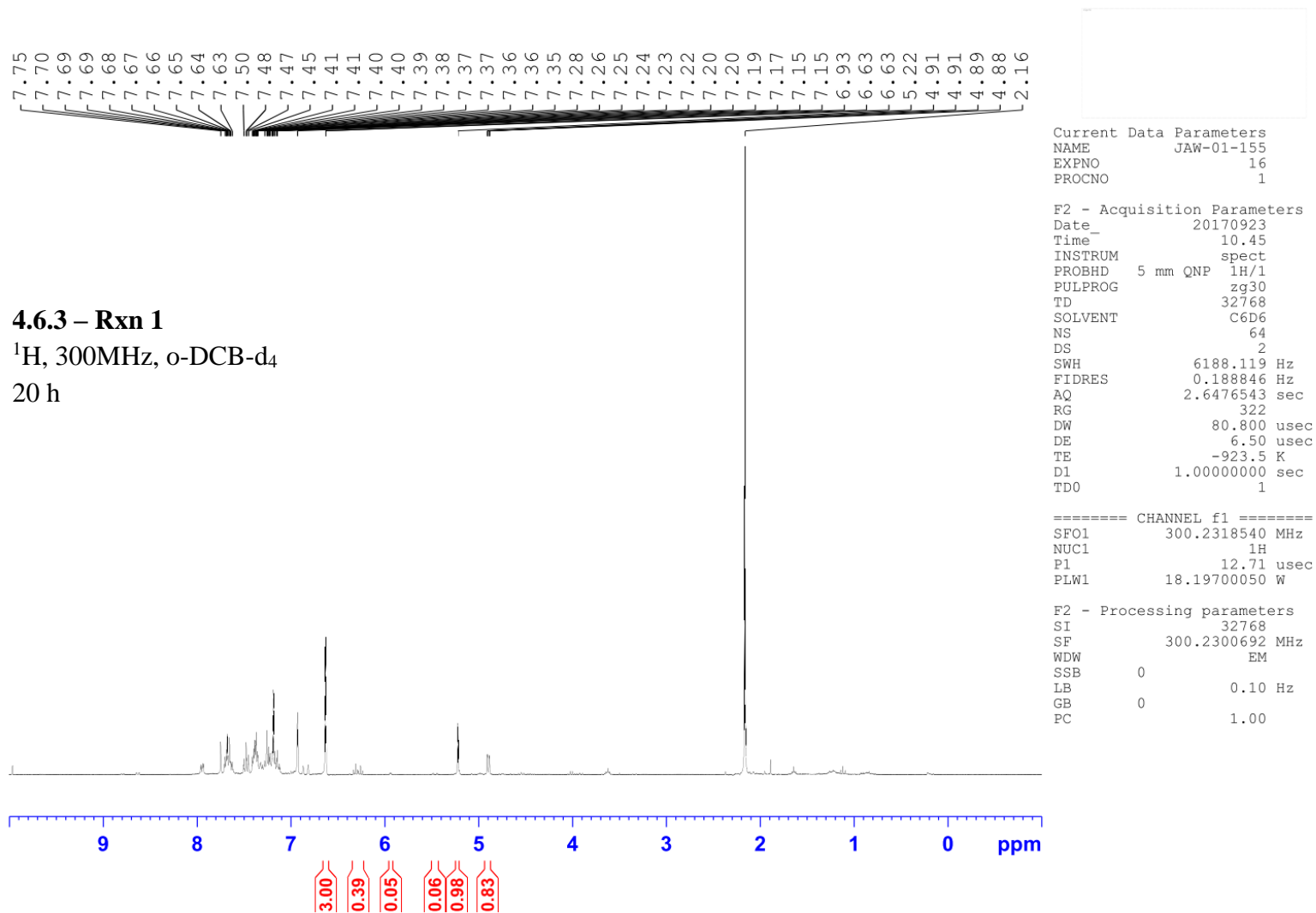


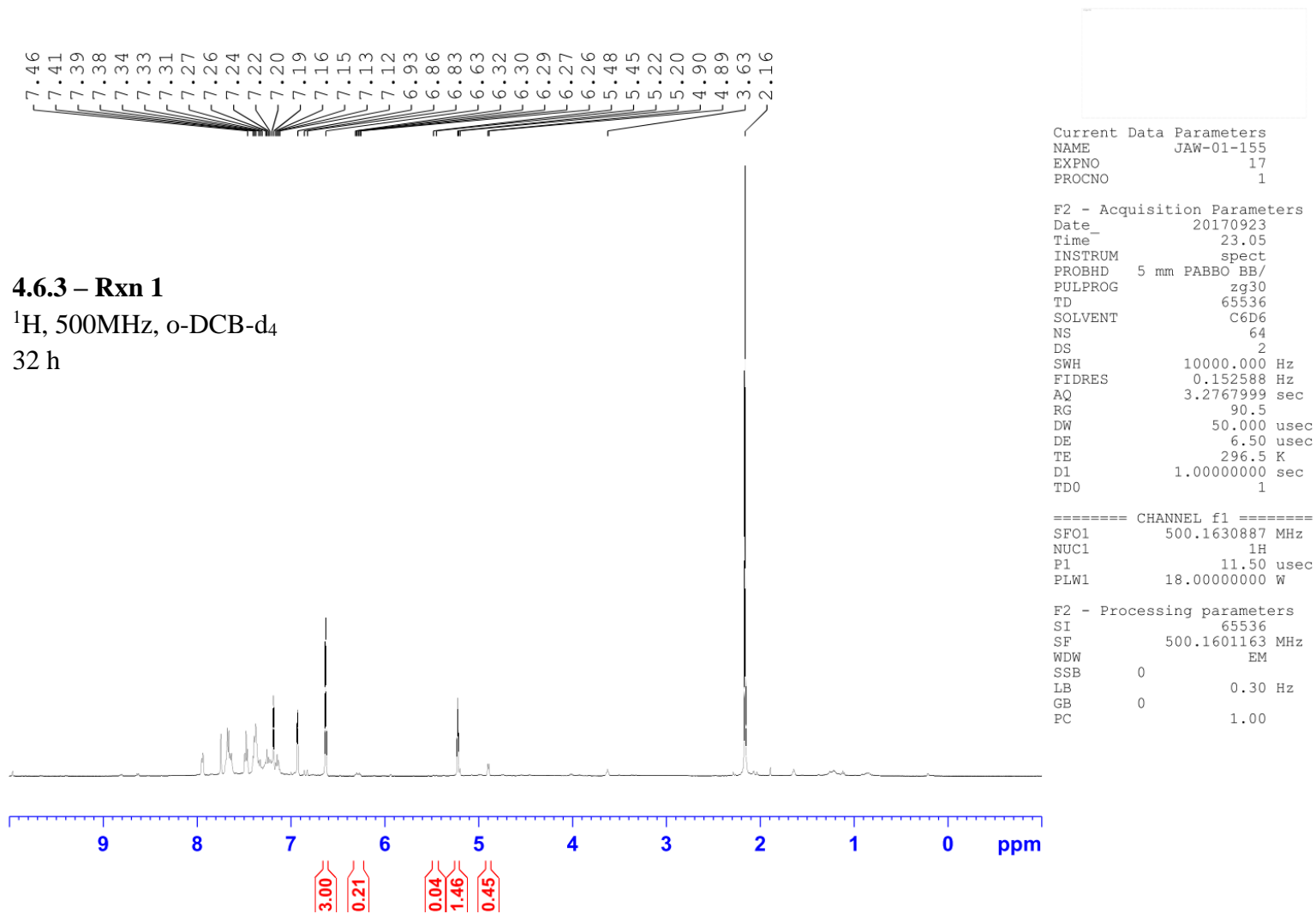
Current Data Parameters
 NAME JAW-01-155
 EXPNO 15
 PROCNO 1

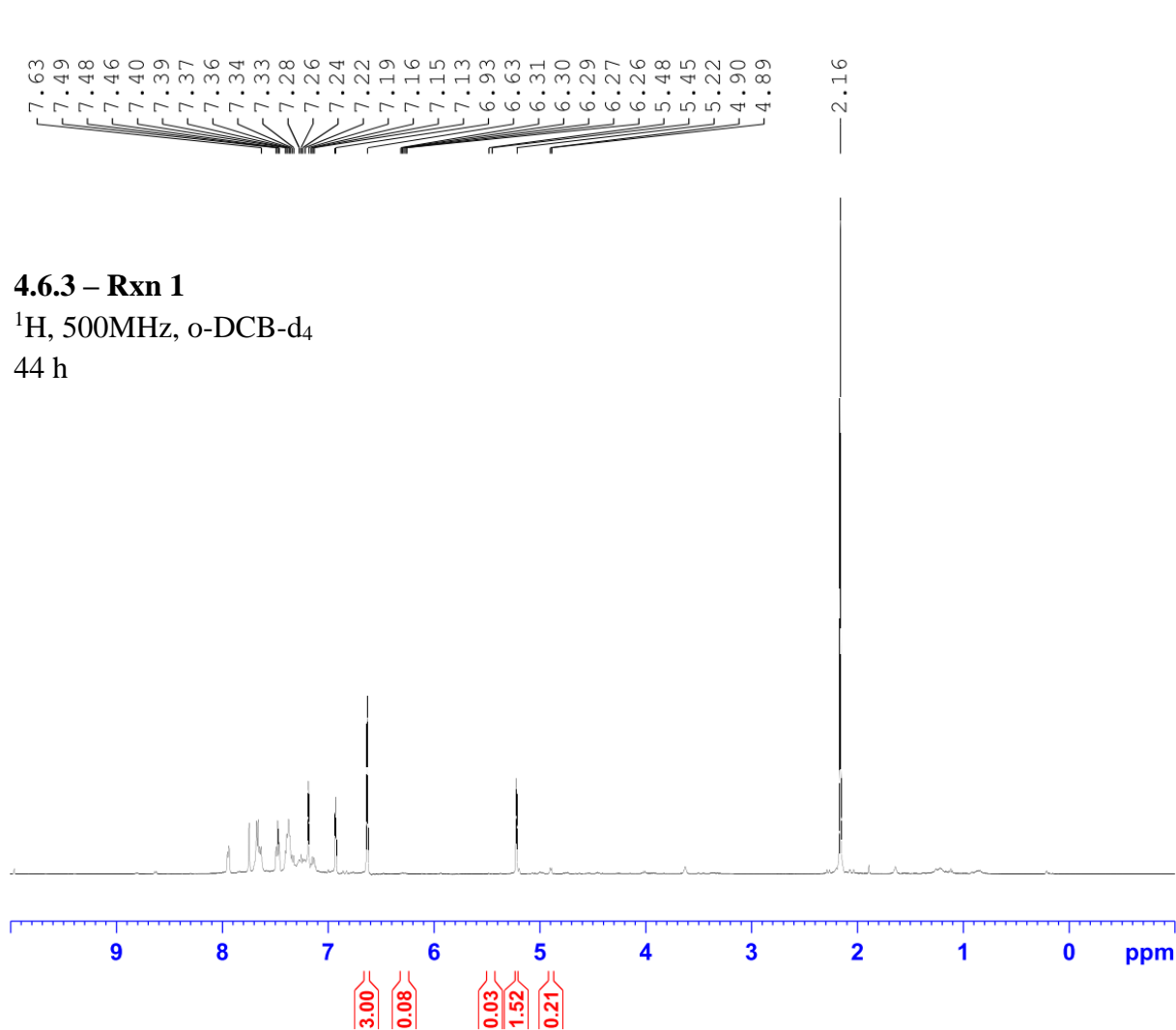
F2 - Acquisition Parameters
 Date_ 20170922
 Time_ 23.20
 INSTRUM spect
 PROBHD 5 mm QNP 1H/1
 PULPROG zg30
 TD 32768
 SOLVENT C6D6
 NS 92
 DS 2
 SWH 6188.119 Hz
 FIDRES 0.188846 Hz
 AQ 2.6476543 sec
 RG 322
 DW 80.800 usec
 DE 6.50 usec
 TE -925.2 K
 D1 1.00000000 sec
 TD0 1

===== CHANNEL f1 =====
 SF01 300.2318540 MHz
 NUC1 1H
 P1 12.71 usec
 PLW1 18.19700050 W

F2 - Processing parameters
 SI 32768
 SF 300.2300698 MHz
 WDW EM
 SSB 0
 LB 0.10 Hz
 GB 0
 PC 1.00





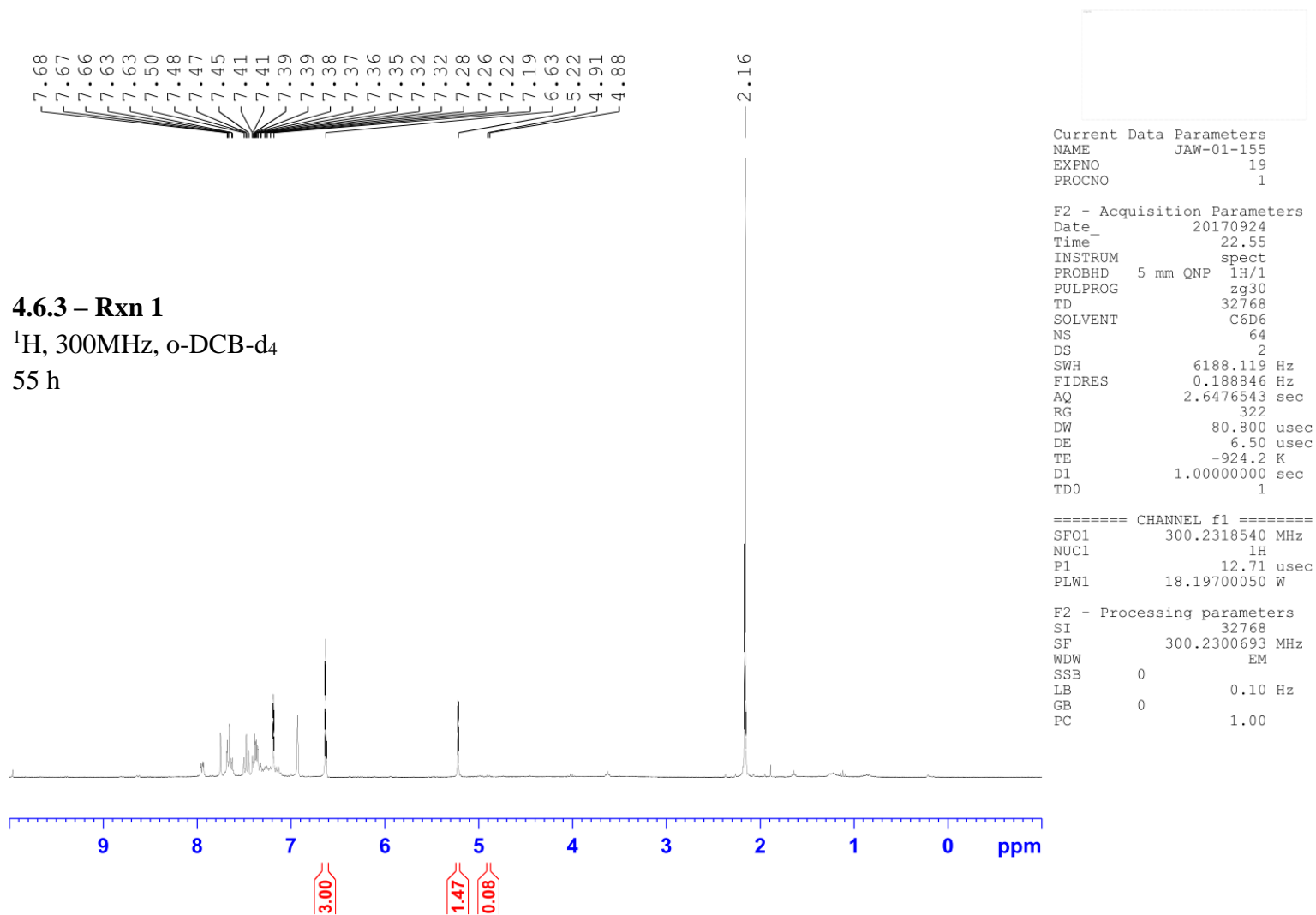


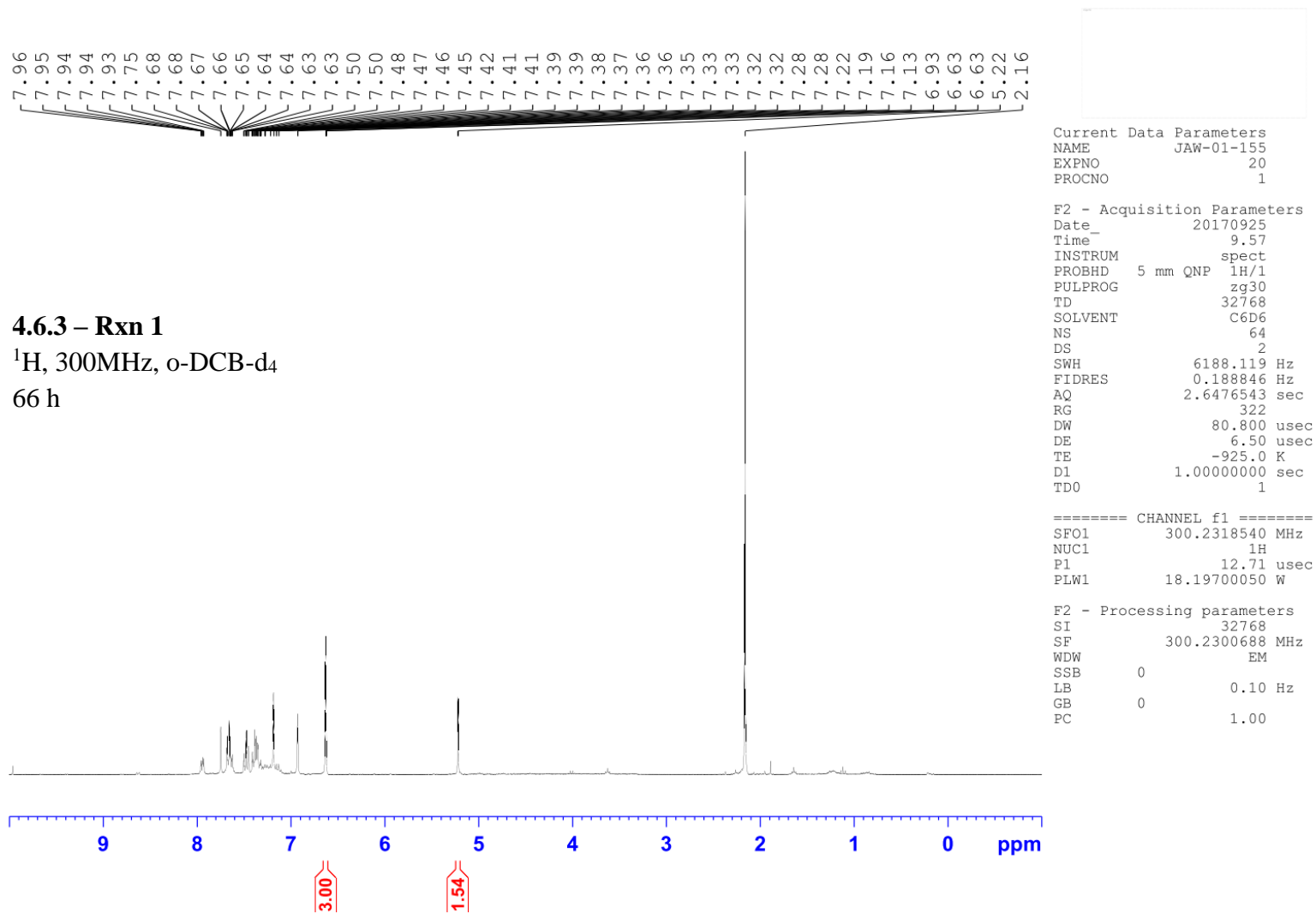
Current Data Parameters
 NAME JAW-01-155
 EXPNO 18
 PROCNO 1

F2 - Acquisition Parameters
 Date_ 20170924
 Time_ 11.04
 INSTRUM spect
 PROBHD 5 mm PABBO BB/
 PULPROG zg30
 TD 65536
 SOLVENT C6D6
 NS 64
 DS 2
 SWH 10000.000 Hz
 FIDRES 0.152588 Hz
 AQ 3.2767999 sec
 RG 90.5
 DW 50.000 usec
 DE 6.50 usec
 TE 296.6 K
 D1 1.00000000 sec
 TD0 1

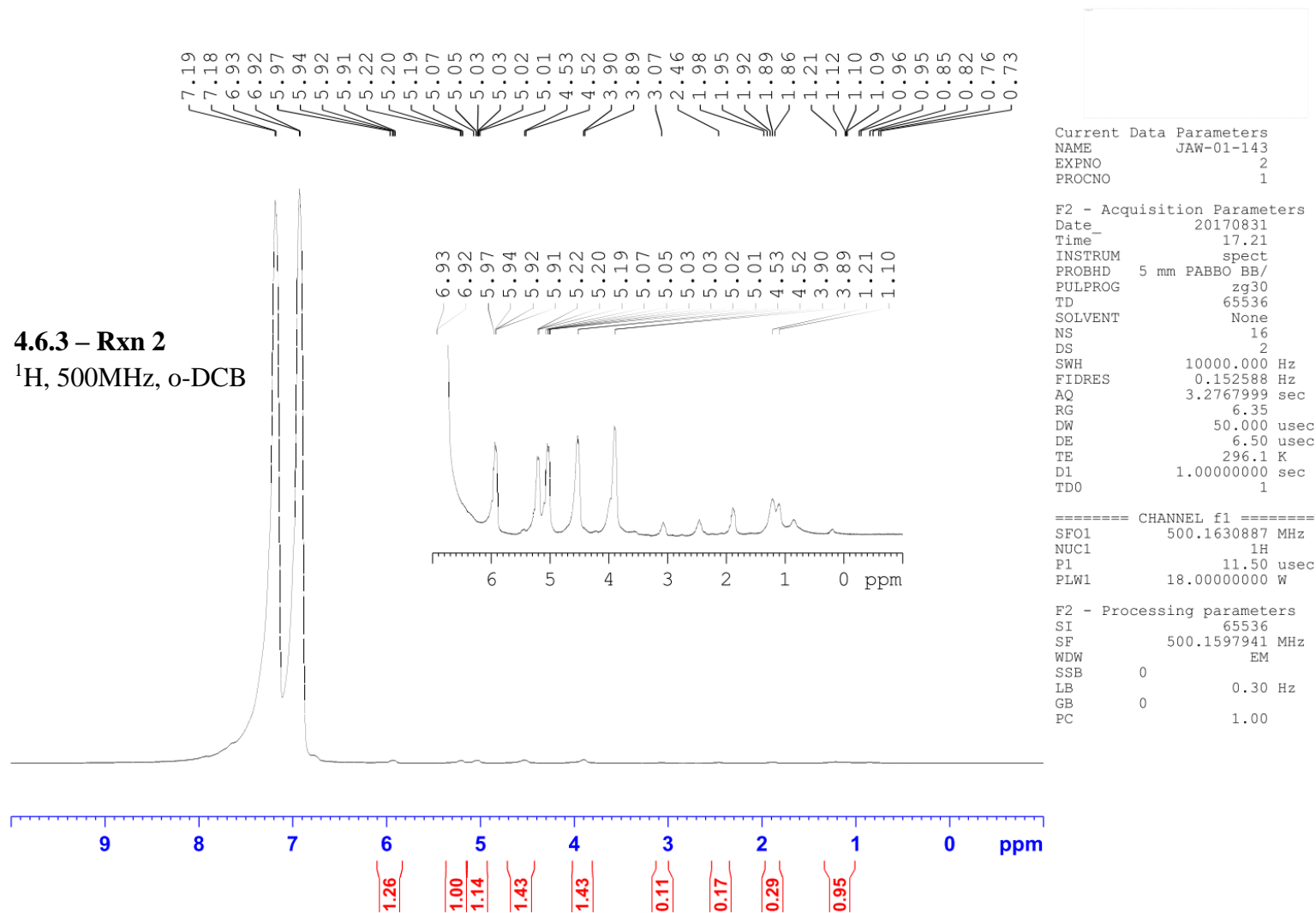
===== CHANNEL f1 =====
 SF01 500.1630887 MHz
 NUC1 1H
 P1 11.50 usec
 PLW1 18.00000000 W

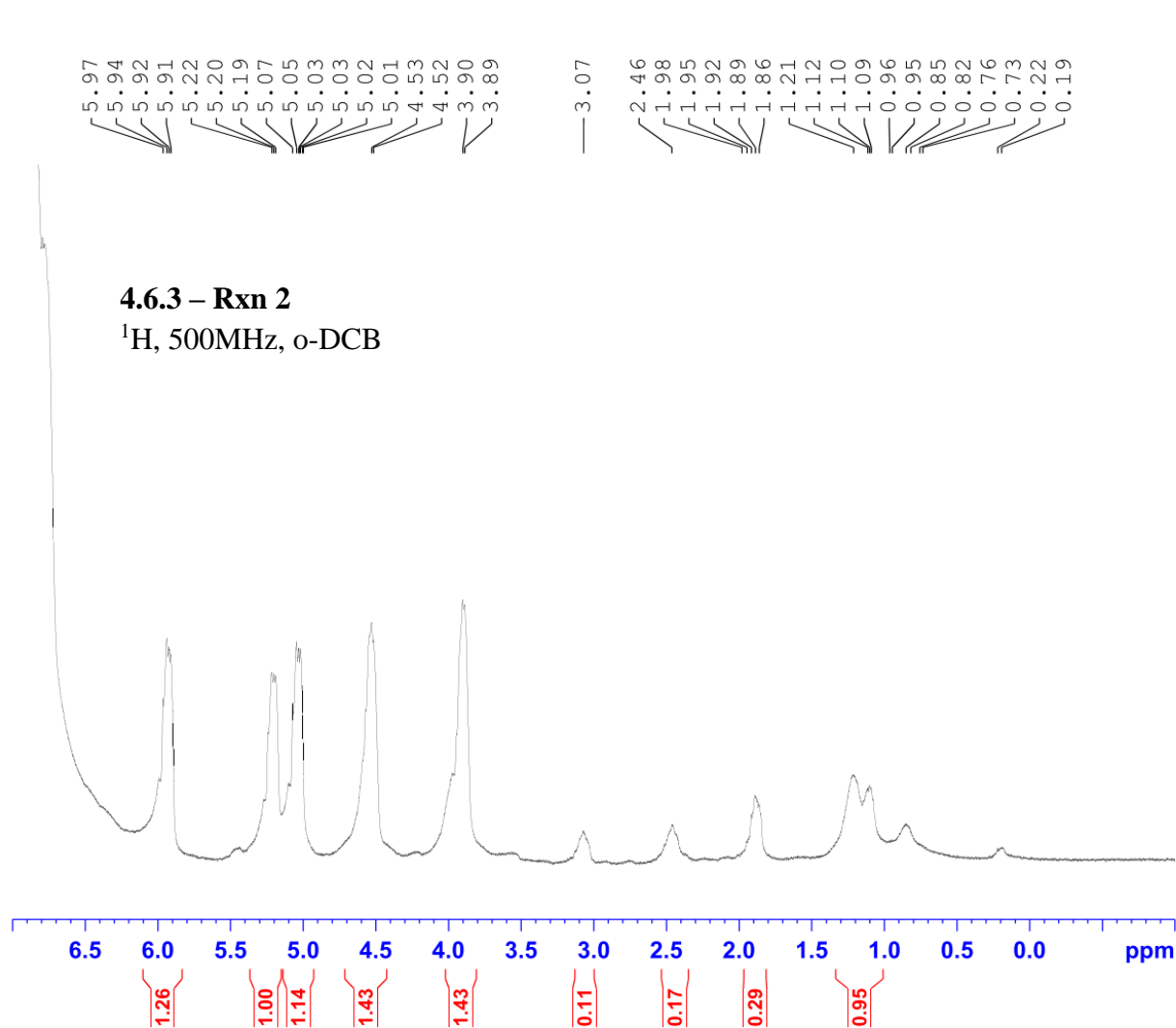
F2 - Processing parameters
 SI 65536
 SF 500.1601138 MHz
 WDW EM
 SSB 0
 LB 0.30 Hz
 GB 0
 PC 1.00





4.6.3 – Rxn 2
¹H, 500MHz, o-DCB





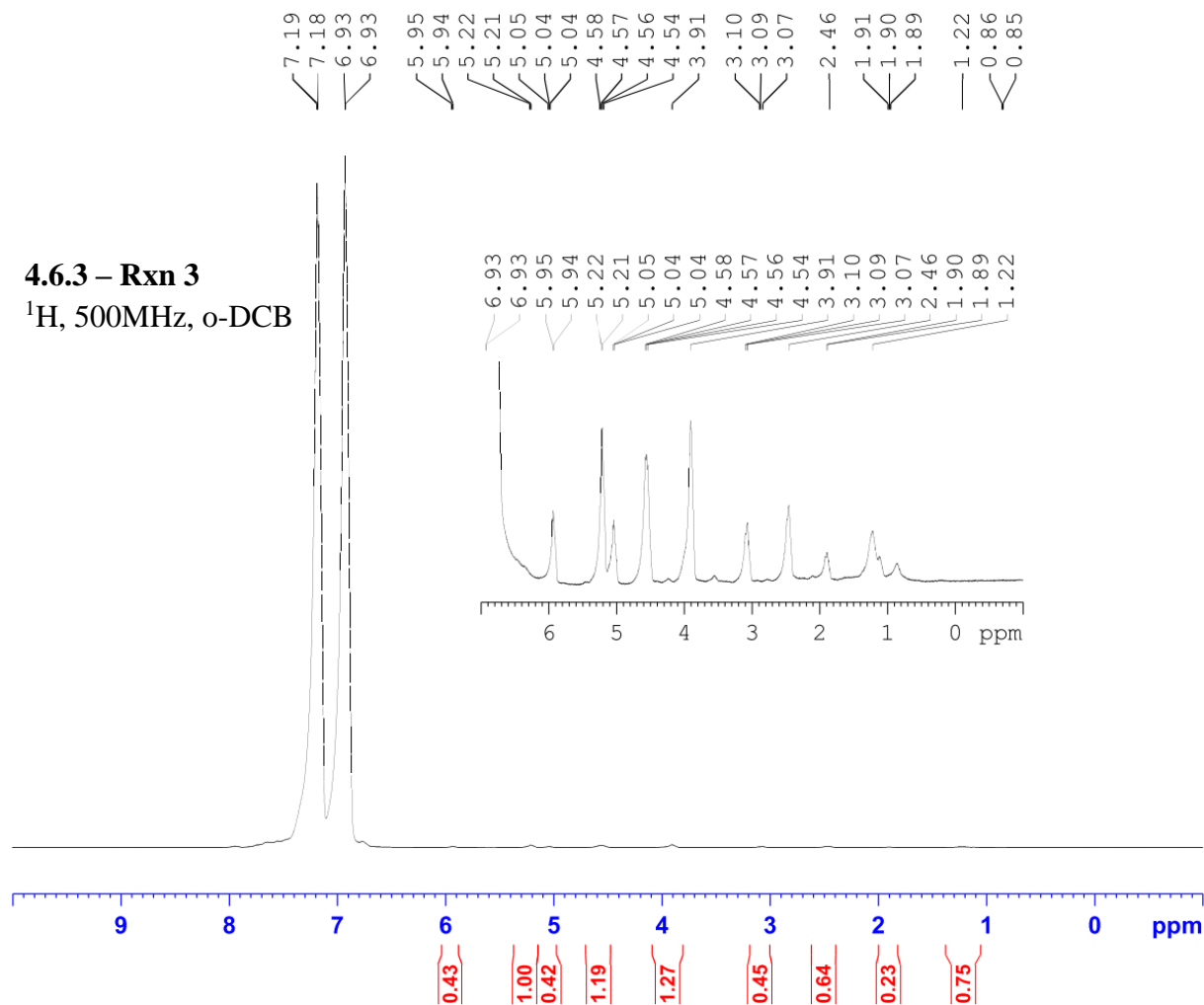
Current Data Parameters
NAME JAW-01-143
EXPNO 2
PROCNO 1

F2 - Acquisition Parameters
Date_ 20170831
Time_ 17.21
INSTRUM spect
PROBHD 5 mm PABBO BB/
PULPROG zg30
TD 65536
SOLVENT None
NS 16
DS 2
SWH 10000.000 Hz
FIDRES 0.152588 Hz
AQ 3.2767999 sec
RG 6.35
DW 50.000 usec
DE 6.50 usec
TE 296.1 K
D1 1.00000000 sec
TD0 1

===== CHANNEL f1 =====
SF01 500.1630887 MHz
NUC1 1H
P1 11.50 usec
PLW1 18.00000000 W

F2 - Processing parameters
SI 65536
SF 500.1597941 MHz
WDW EM
SSB 0
LB 0.30 Hz
GB 0
PC 1.00

4.6.3 – Rxn 3
¹H, 500MHz, o-DCB

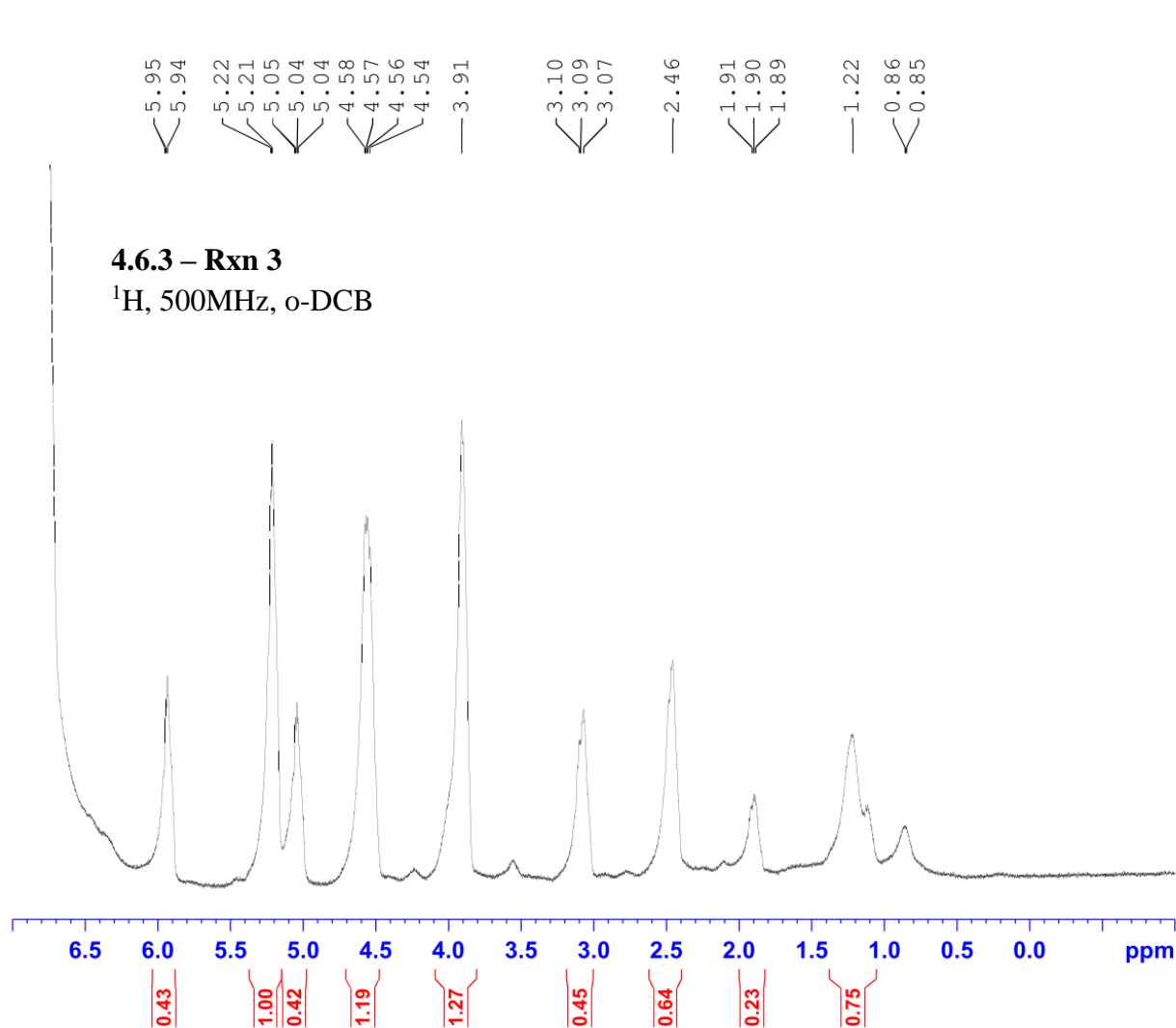


Current Data Parameters
 NAME JAW-01-144
 EXPNO 1
 PROCNO 1

F2 - Acquisition Parameters
 Date_ 20170901
 Time 14.20
 INSTRUM spect
 PROBHD 5 mm PABBO BB/
 PULPROG zg30
 TD 65536
 SOLVENT None
 NS 16
 DS 2
 SWH 10000.000 Hz
 FIDRES 0.152588 Hz
 AQ 3.2767999 sec
 RG 6.35
 DW 50.000 usec
 DE 6.50 usec
 TE 296.5 K
 D1 1.00000000 sec
 TD0 1

===== CHANNEL f1 =====
 SF01 500.1630887 MHz
 NUC1 1H
 P1 11.50 usec
 PLW1 18.00000000 W

F2 - Processing parameters
 SI 65536
 SF 500.1597306 MHz
 WDW EM
 SSB 0
 LB 0.30 Hz
 GB 0
 PC 1.00

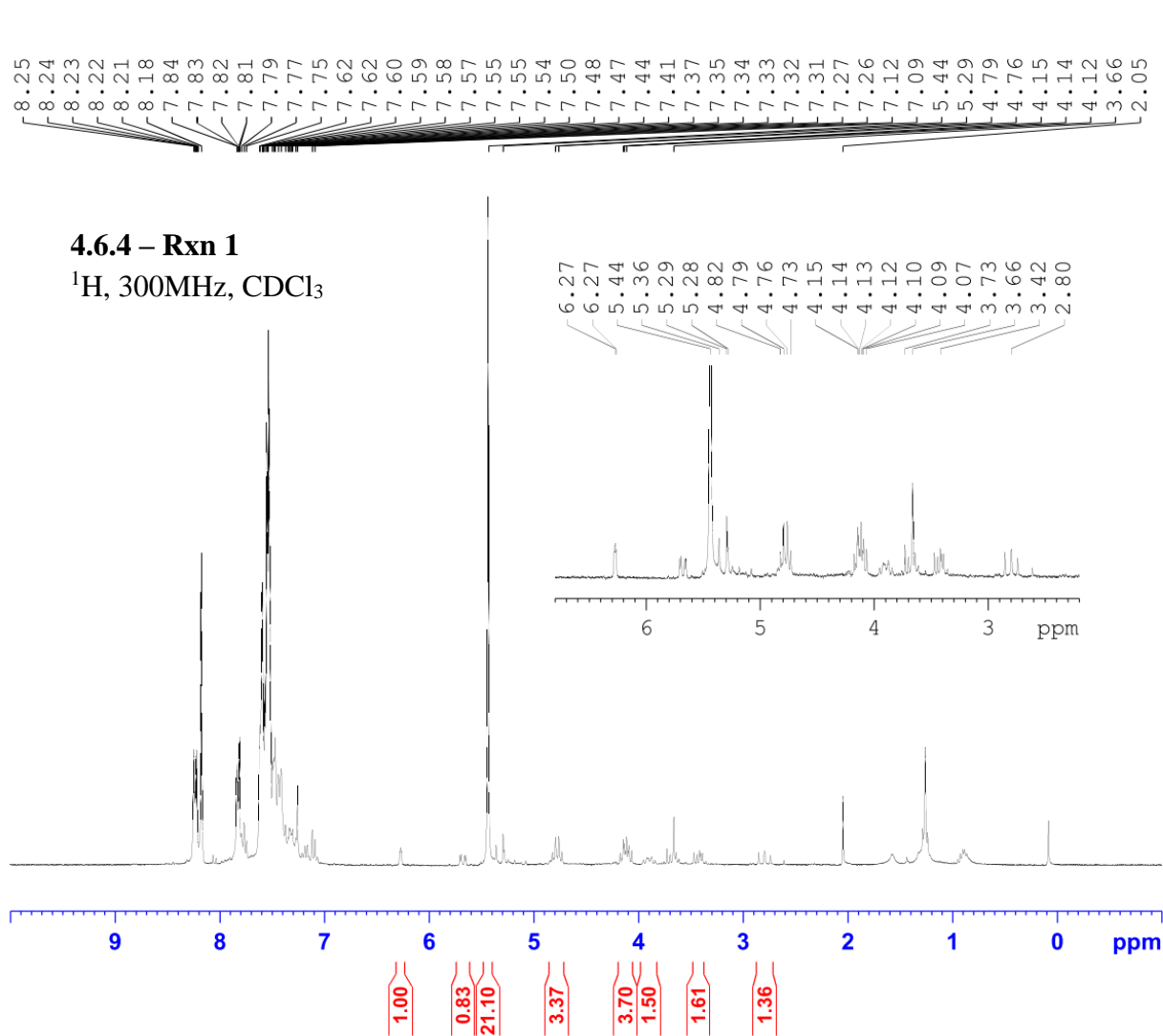


Current Data Parameters
NAME JAW-01-144
EXPNO 1
PROCNO 1

F2 - Acquisition Parameters
Date_ 20170901
Time_ 14.20
INSTRUM spect
PROBHD 5 mm PABBO BB/
PULPROG zg30
TD 65536
SOLVENT None
NS 16
DS 2
SWH 10000.000 Hz
FIDRES 0.152588 Hz
AQ 3.2767999 sec
RG 6.35
DW 50.000 usec
DE 6.50 usec
TE 296.5 K
D1 1.00000000 sec
TD0 1

===== CHANNEL f1 =====
SF01 500.1630887 MHz
NUC1 1H
P1 11.50 usec
PLW1 18.00000000 W

F2 - Processing parameters
SI 65536
SF 500.1597306 MHz
WDW EM
SSB 0
LB 0.30 Hz
GB 0
PC 1.00

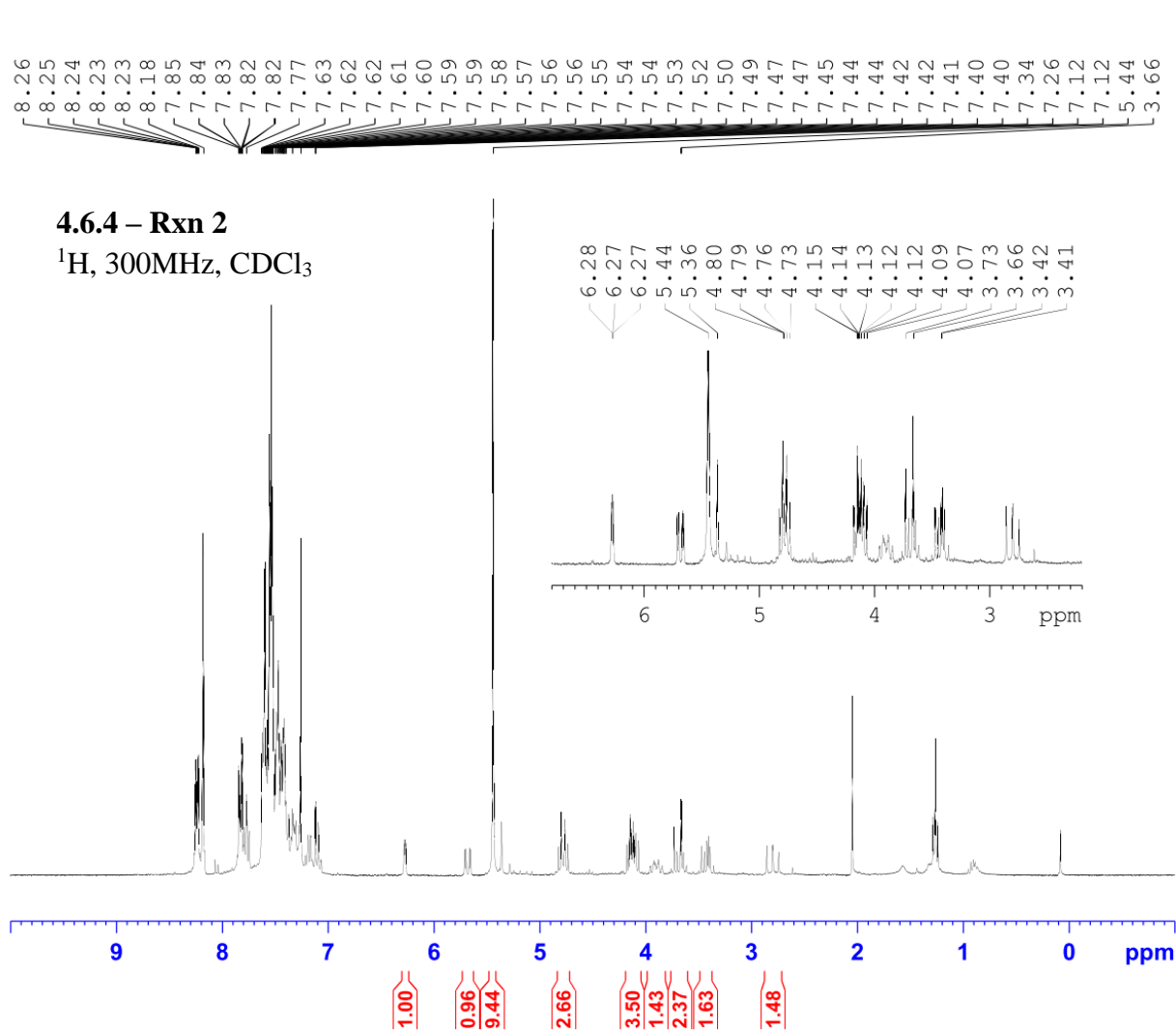


Current Data Parameters
 NAME JAW-02-160
 EXPNO 1
 PROCNO 1

F2 - Acquisition Parameters
 Date_ 20181022
 Time_ 15.40
 INSTRUM spect
 PROBHD 5 mm QNP 1H/1
 PULPROG zg30
 TD 32768
 SOLVENT CDCl3
 NS 16
 DS 2
 SWH 6188.119 Hz
 FIDRES 0.188846 Hz
 AQ 2.6476543 sec
 RG 128
 DW 80.800 usec
 DE 6.50 usec
 TE -925.3 K
 D1 1.00000000 sec
 TD0 1

===== CHANNEL f1 =====
 SF01 300.2318540 MHz
 NUC1 1H
 P1 12.71 usec
 PLW1 18.19700050 W

F2 - Processing parameters
 SI 32768
 SF 300.2300086 MHz
 WDW EM
 SSB 0
 LB 0.10 Hz
 GB 0
 PC 1.00

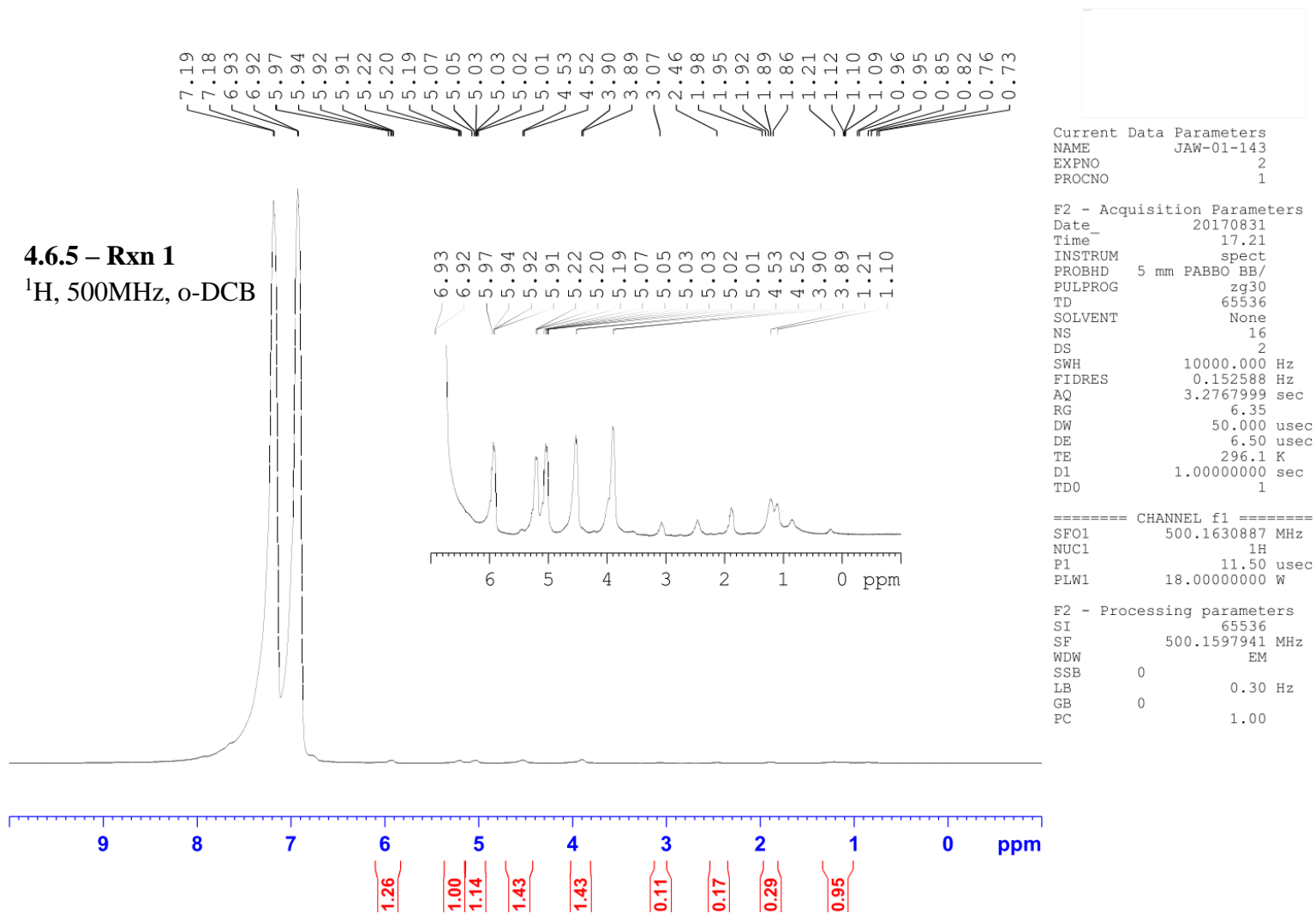


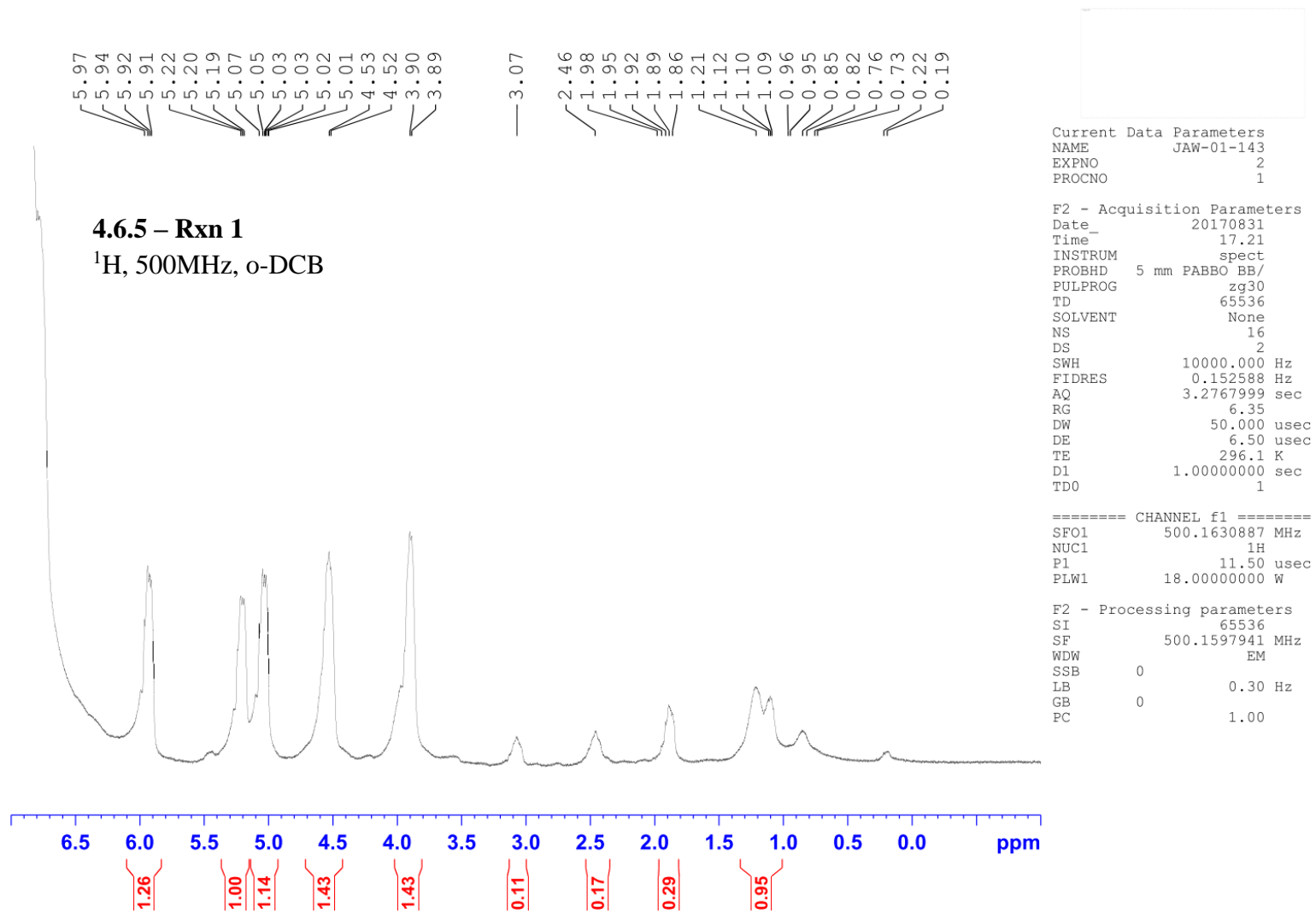
Current Data Parameters
 NAME JAW-02-161
 EXPNO 1
 PROCNO 1

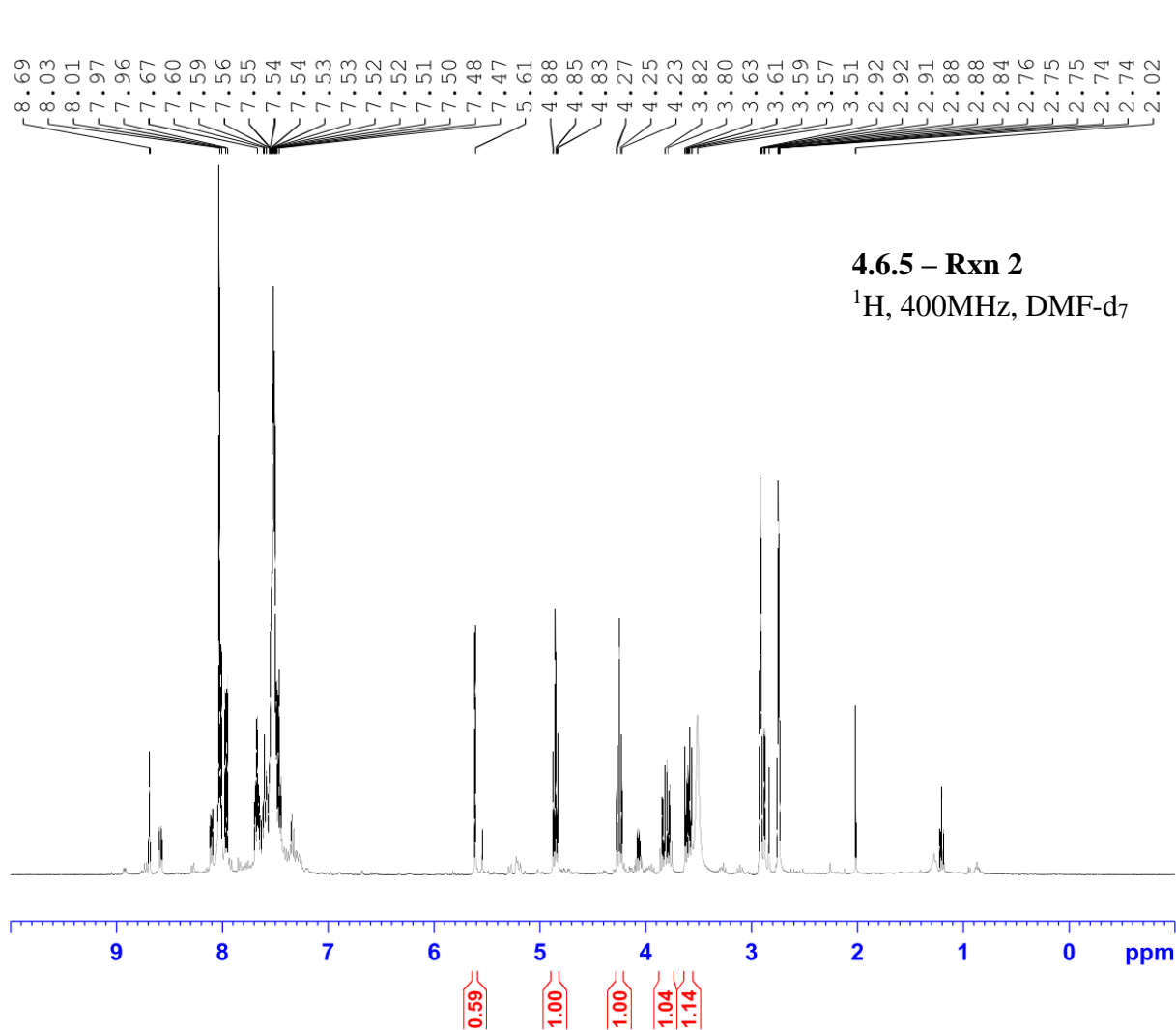
F2 - Acquisition Parameters
 Date_ 20181022
 Time_ 19.45
 INSTRUM spect
 PROBHD 5 mm QNP 1H/1
 PULPROG zg30
 TD 32768
 SOLVENT CDCl3
 NS 32
 DS 2
 SWH 6188.119 Hz
 FIDRES 0.188846 Hz
 AQ 2.6476543 sec
 RG 144
 DW 80.800 usec
 DE 6.50 usec
 TE -923.2 K
 D1 1.00000000 sec
 TD0 1

===== CHANNEL f1 =====
 SF01 300.2318540 MHz
 NUC1 1H
 P1 12.71 usec
 PLW1 18.19700050 W

F2 - Processing parameters
 SI 32768
 SF 300.2300086 MHz
 WDW EM
 SSB 0
 LB 0.10 Hz
 GB 0
 PC 1.00





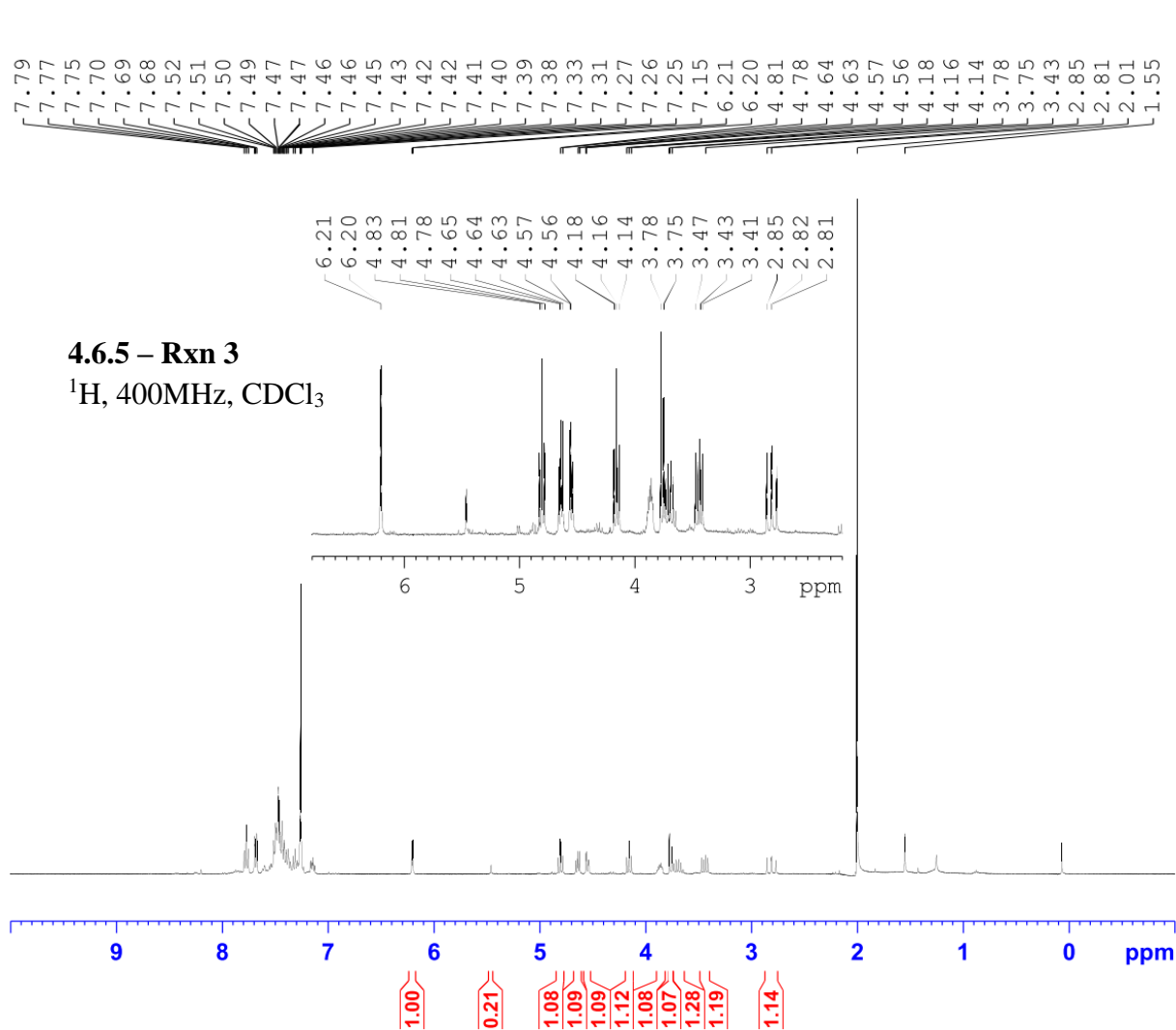


Current Data Parameters
NAME JAW-01-174
EXPNO 3
PROCNO 1

F2 - Acquisition Parameters
Date_ 20171024
Time_ 17.24
INSTRUM spect
PROBHD 5 mm PABBO BB-
PULPROG zg30
TD 65536
SOLVENT DMF
NS 16
DS 2
SWH 8012.820 Hz
FIDRES 0.122266 Hz
AQ 4.0894465 sec
RG 90.5
DW 62.400 usec
DE 6.50 usec
TE -2372.0 K
D1 1.00000000 sec
TD0 1

===== CHANNEL f1 =====
SF01 400.1324710 MHz
NUC1 1H
P1 13.75 usec
PLW1 12.01700020 W

F2 - Processing parameters
SI 65536
SF 400.1300735 MHz
WDW EM
SSB 0
LB 0.30 Hz
GB 0
PC 1.00

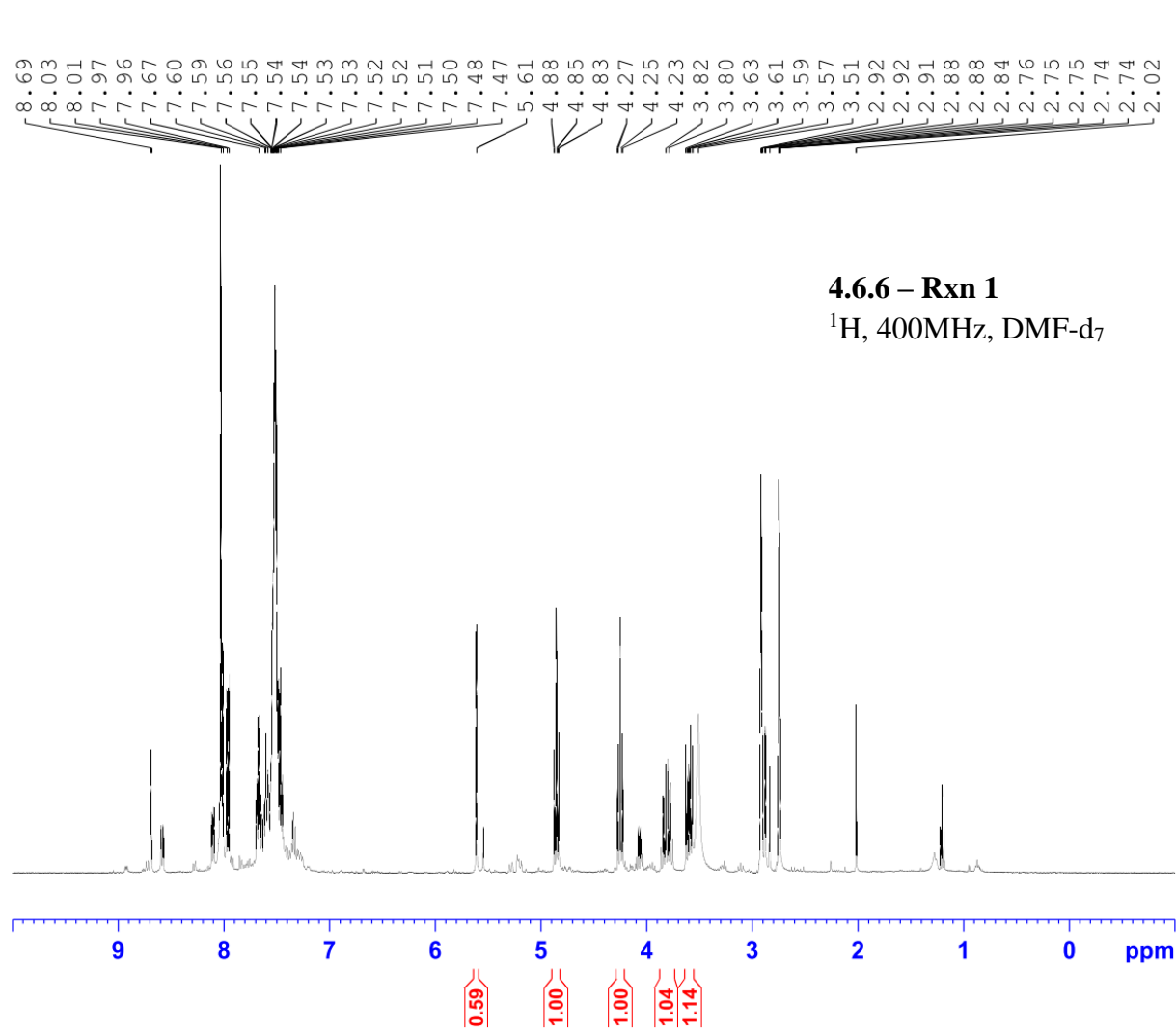


Current Data Parameters
 NAME JAW-02-035
 EXPNO 3
 PROCNO 1

F2 - Acquisition Parameters
 Date_ 20180330
 Time_ 16.02
 INSTRUM spect
 PROBHD 5 mm PABBO BB-
 PULPROG zg30
 TD 65536
 SOLVENT CDCl_3
 NS 16
 DS 2
 SWH 8012.820 Hz
 FIDRES 0.122266 Hz
 AQ 4.0894465 sec
 RG 128
 DW 62.400 usec
 DE 6.50 usec
 TE 2466.6 K
 D1 1.00000000 sec
 TD0 1

===== CHANNEL f1 =====
 SF01 400.1324710 MHz
 NUC1 ^1H
 P1 14.50 usec
 PLW1 12.01700020 W

F2 - Processing parameters
 SI 65536
 SF 400.1300101 MHz
 WDW EM
 SSB 0
 LB 0.30 Hz
 GB 0
 PC 1.00

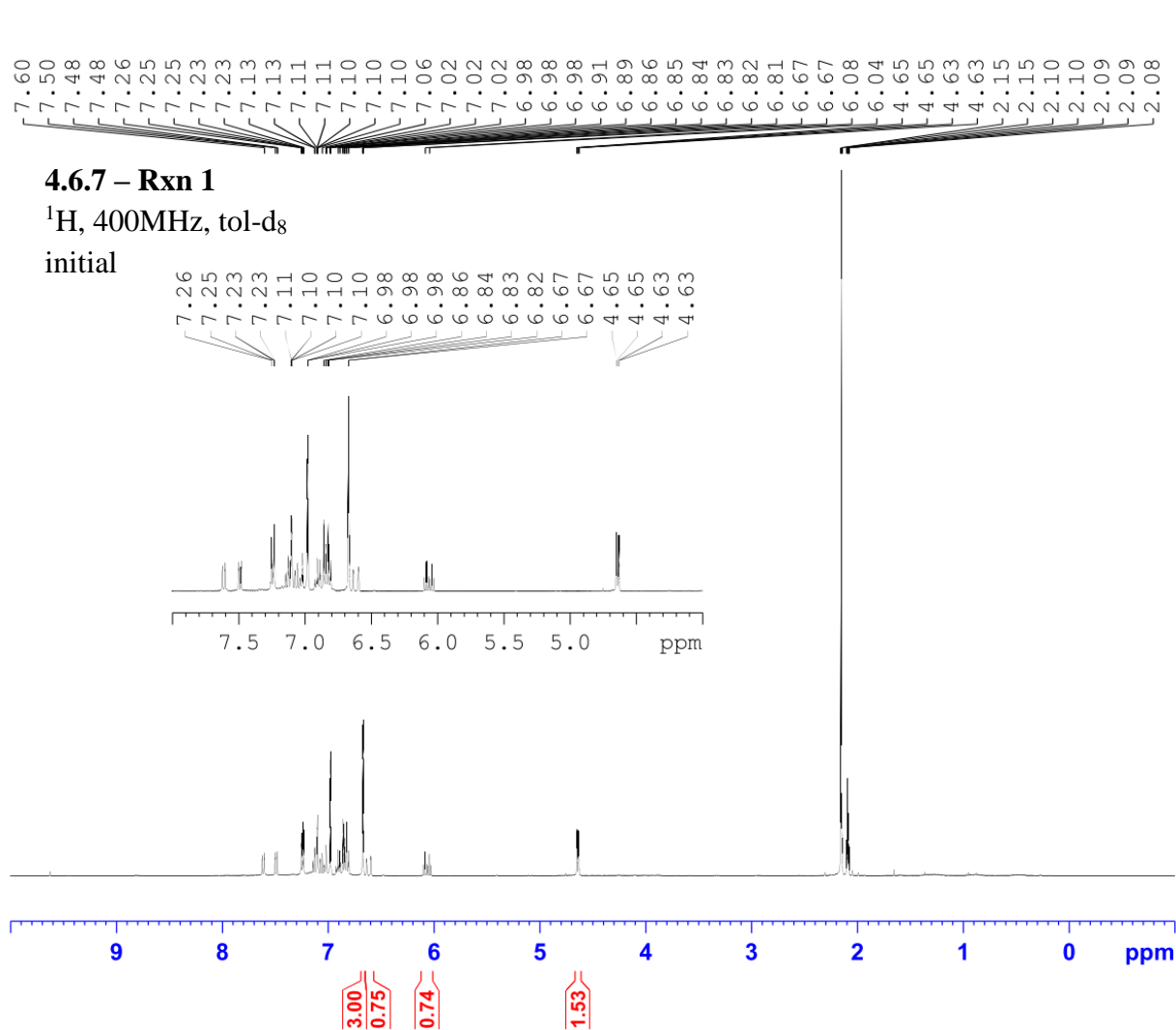


Current Data Parameters
 NAME JAW-01-174
 EXPNO 3
 PROCNO 1

F2 - Acquisition Parameters
 Date_ 20171024
 Time_ 17.24
 INSTRUM spect
 PROBHD 5 mm PABBO BB-
 PULPROG zg30
 TD 65536
 SOLVENT DMF
 NS 16
 DS 2
 SWH 8012.820 Hz
 FIDRES 0.122266 Hz
 AQ 4.0894465 sec
 RG 90.5
 DW 62.400 usec
 DE 6.50 usec
 TE -2372.0 K
 D1 1.00000000 sec
 TD0 1

===== CHANNEL f1 =====
 SF01 400.1324710 MHz
 NUC1 1H
 P1 13.75 usec
 PLW1 12.01700020 W

F2 - Processing parameters
 SI 65536
 SF 400.1300735 MHz
 WDW EM
 SSB 0
 LB 0.30 Hz
 GB 0
 PC 1.00

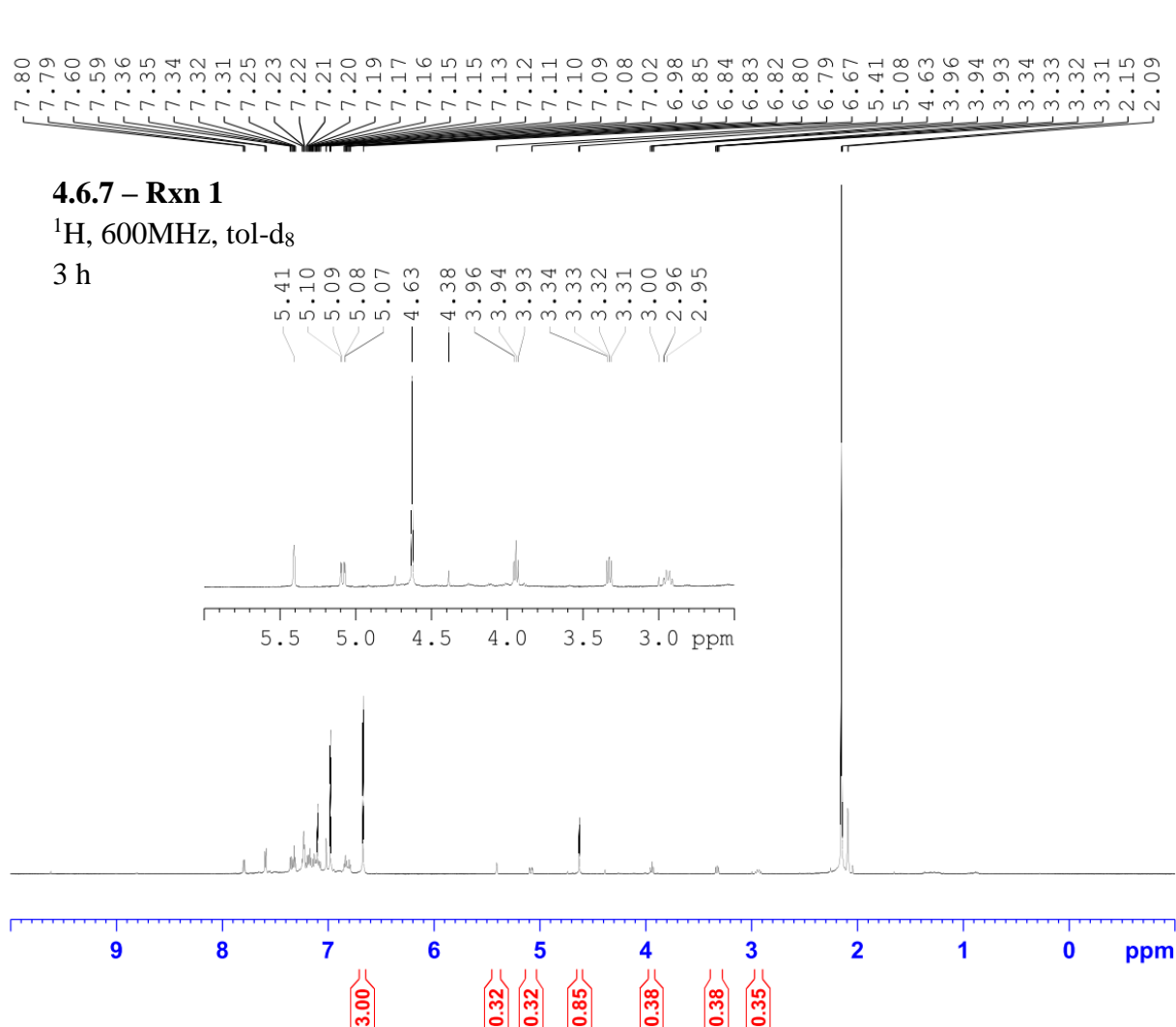


Current Data Parameters
 NAME JAW-03-070
 EXPNO 1
 PROCNO 1

F2 - Acquisition Parameters
 Date_ 20191121
 Time_ 12.20
 INSTRUM spect
 PROBHD 5 mm PADUL 13C
 PULPROG zg30
 TD 65536
 SOLVENT Tol
 NS 16
 DS 2
 SWH 8223.685 Hz
 FIDRES 0.125483 Hz
 AQ 3.9845889 sec
 RG 101
 DW 60.800 usec
 DE 6.50 usec
 TE 298.2 K
 D1 2.00000000 sec
 TD0 1

===== CHANNEL f1 =====
 NUC1 1H
 P1 9.31 usec
 PL1 -3.90 dB
 PL1W 21.64248466 W
 SFO1 400.2324716 MHz

F2 - Processing parameters
 SI 32768
 SF 400.2300165 MHz
 WDW EM
 SSB 0
 LB 0.30 Hz
 GB 0
 PC 1.00

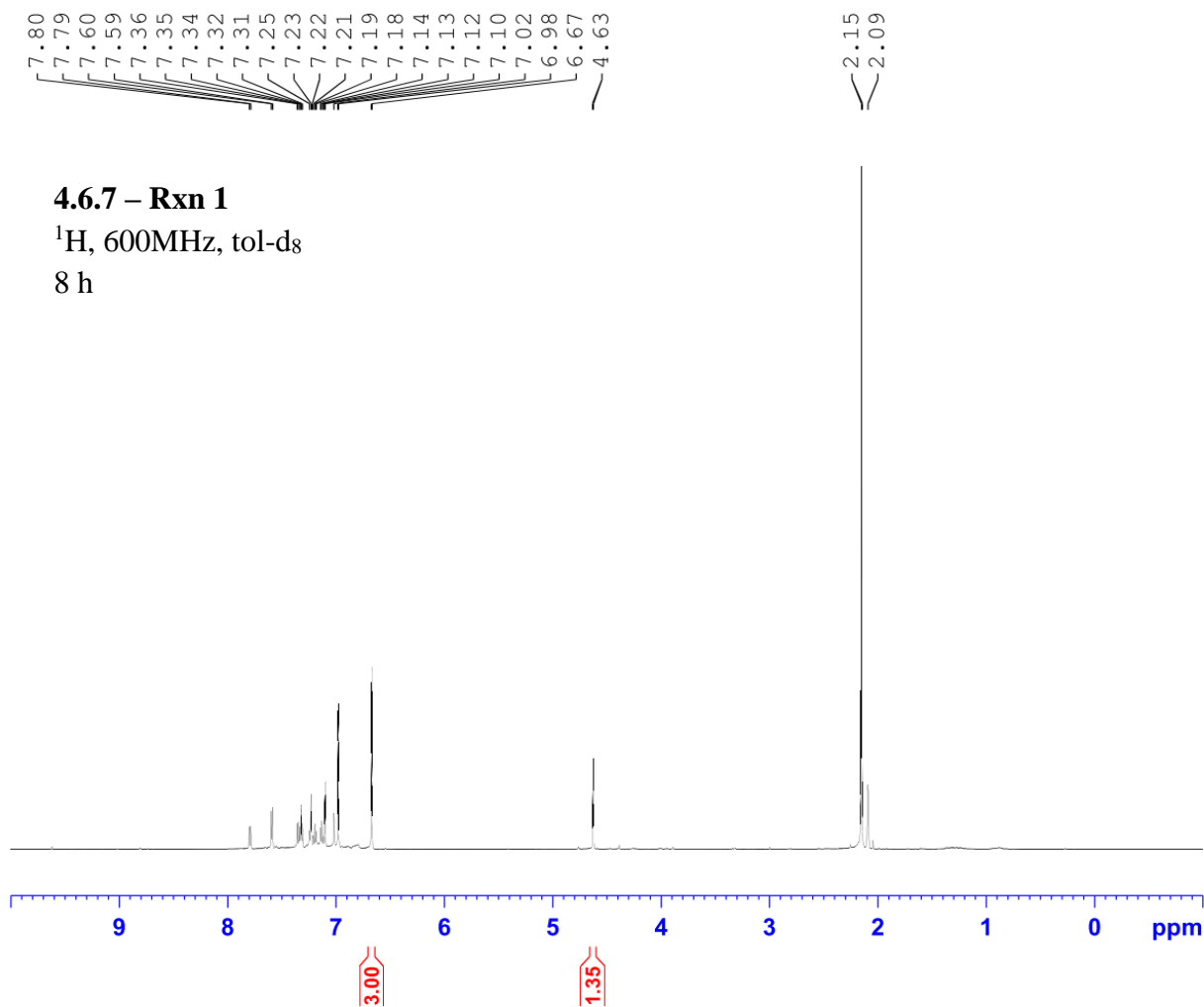


Current Data Parameters
 NAME JAW-03-070
 EXPNO 2
 PROCNO 1

F2 - Acquisition Parameters
 Date_ 20191121
 Time_ 16.37
 INSTRUM spect
 PROBHD 5 mm PABBO BB-
 PULPROG zg30
 TD 65536
 SOLVENT Tol
 NS 16
 DS 2
 SWH 12335.526 Hz
 FIDRES 0.188225 Hz
 AQ 2.6563926 sec
 RG 64
 DW 40.533 usec
 DE 6.50 usec
 TE 295.2 K
 D1 1.00000000 sec
 TD0 1

===== CHANNEL f1 =====
 NUC1 1H
 P1 10.86 usec
 PL1 -2.00 dB
 PL1W 19.70630455 W
 SFO1 600.7137096 MHz

F2 - Processing parameters
 SI 32768
 SF 600.7100223 MHz
 WDW EM
 SSB 0
 LB 0.30 Hz
 GB 0
 PC 1.00

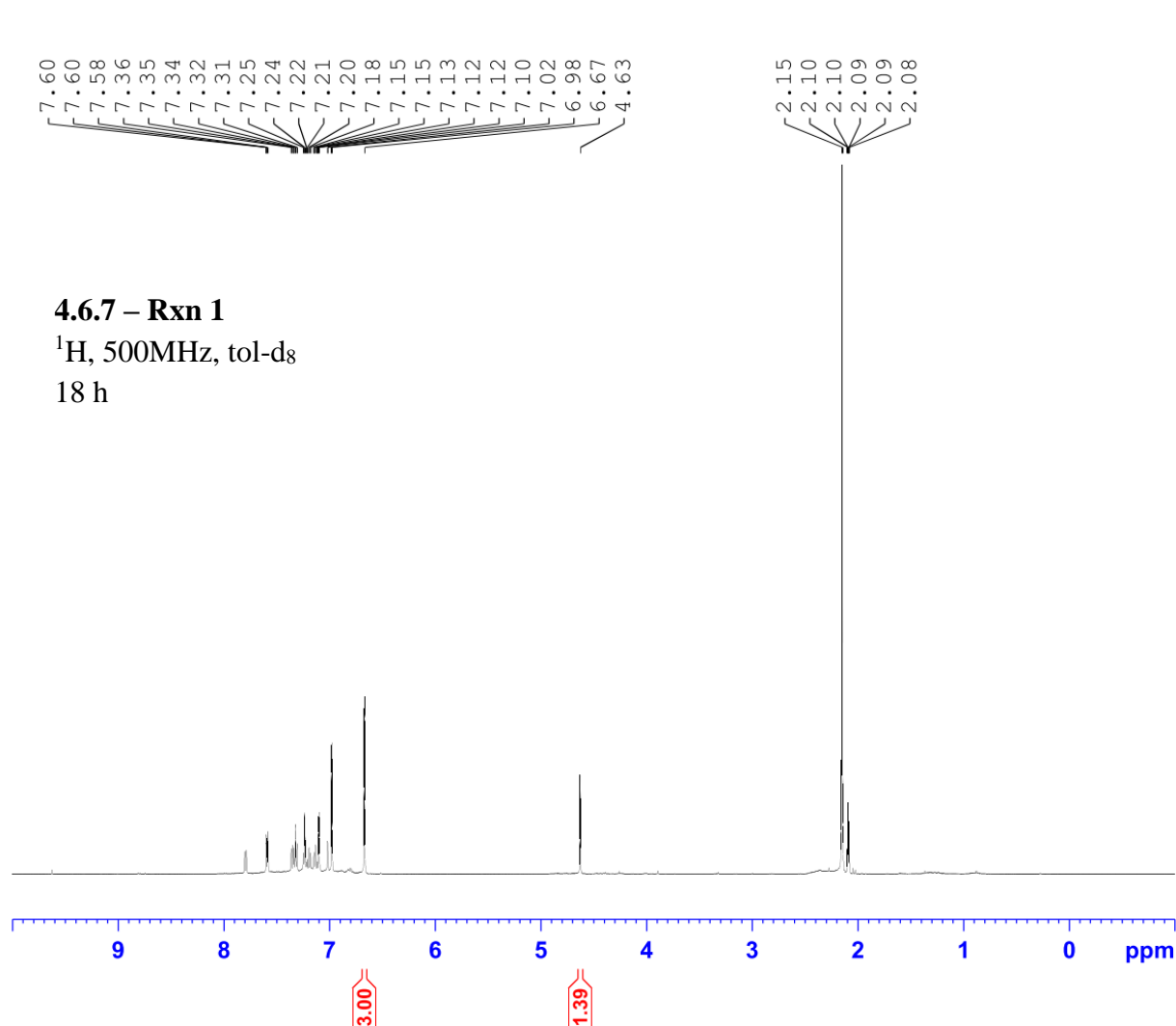


Current Data Parameters
 NAME JAW-03-070
 EXPNO 3
 PROCNO 1

F2 - Acquisition Parameters
 Date_ 20191121
 Time_ 22.05
 INSTRUM spect
 PROBHD 5 mm PABBO BB-
 PULPROG zg30
 TD 65536
 SOLVENT Tol
 NS 16
 DS 2
 SWH 12335.526 Hz
 FIDRES 0.188225 Hz
 AQ 2.6563926 sec
 RG 101
 DW 40.533 usec
 DE 6.50 usec
 TE 295.1 K
 D1 1.00000000 sec
 TD0 1

===== CHANNEL f1 =====
 NUC1 1H
 P1 10.86 usec
 PL1 -2.00 dB
 PL1W 19.70630455 W
 SFO1 600.7137096 MHz

F2 - Processing parameters
 SI 32768
 SF 600.7100224 MHz
 WDW EM
 SSB 0
 LB 0.30 Hz
 GB 0
 PC 1.00

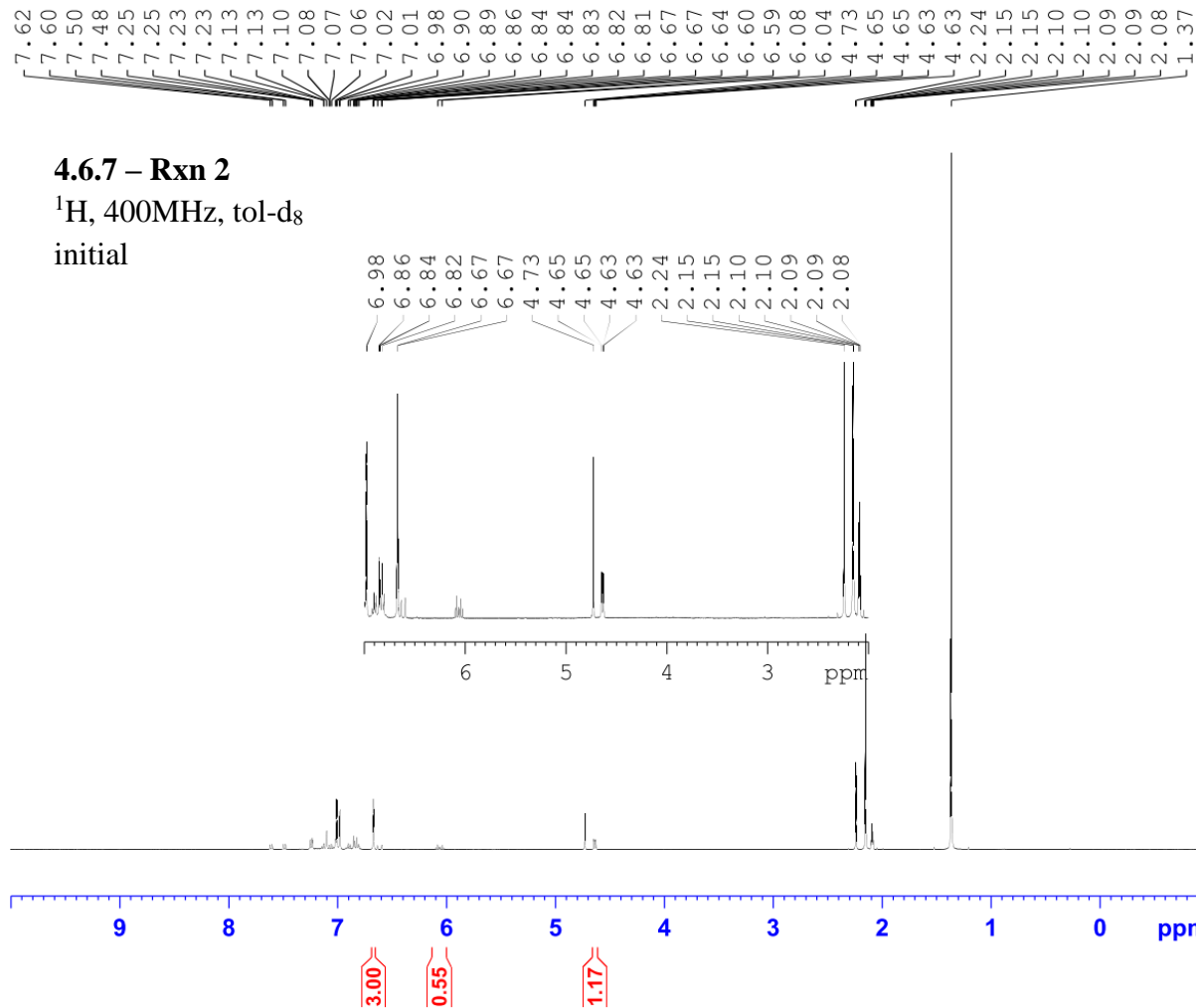


Current Data Parameters
 NAME JAW-03-070
 EXPNO 5
 PROCNO 1

F2 - Acquisition Parameters
 Date_ 20191122
 Time_ 9.29
 INSTRUM spect
 PROBHD 5 mm PABBO BB/
 PULPROG zg30
 TD 65536
 SOLVENT Tol
 NS 16
 DS 2
 SWH 10000.000 Hz
 FIDRES 0.152588 Hz
 AQ 3.2767999 sec
 RG 80.6
 DW 50.000 usec
 DE 6.50 usec
 TE 297.2 K
 D1 1.00000000 sec
 TD0 1

===== CHANNEL f1 =====
 SF01 500.1630887 MHz
 NUC1 1H
 P1 11.50 usec
 PLW1 18.00000000 W

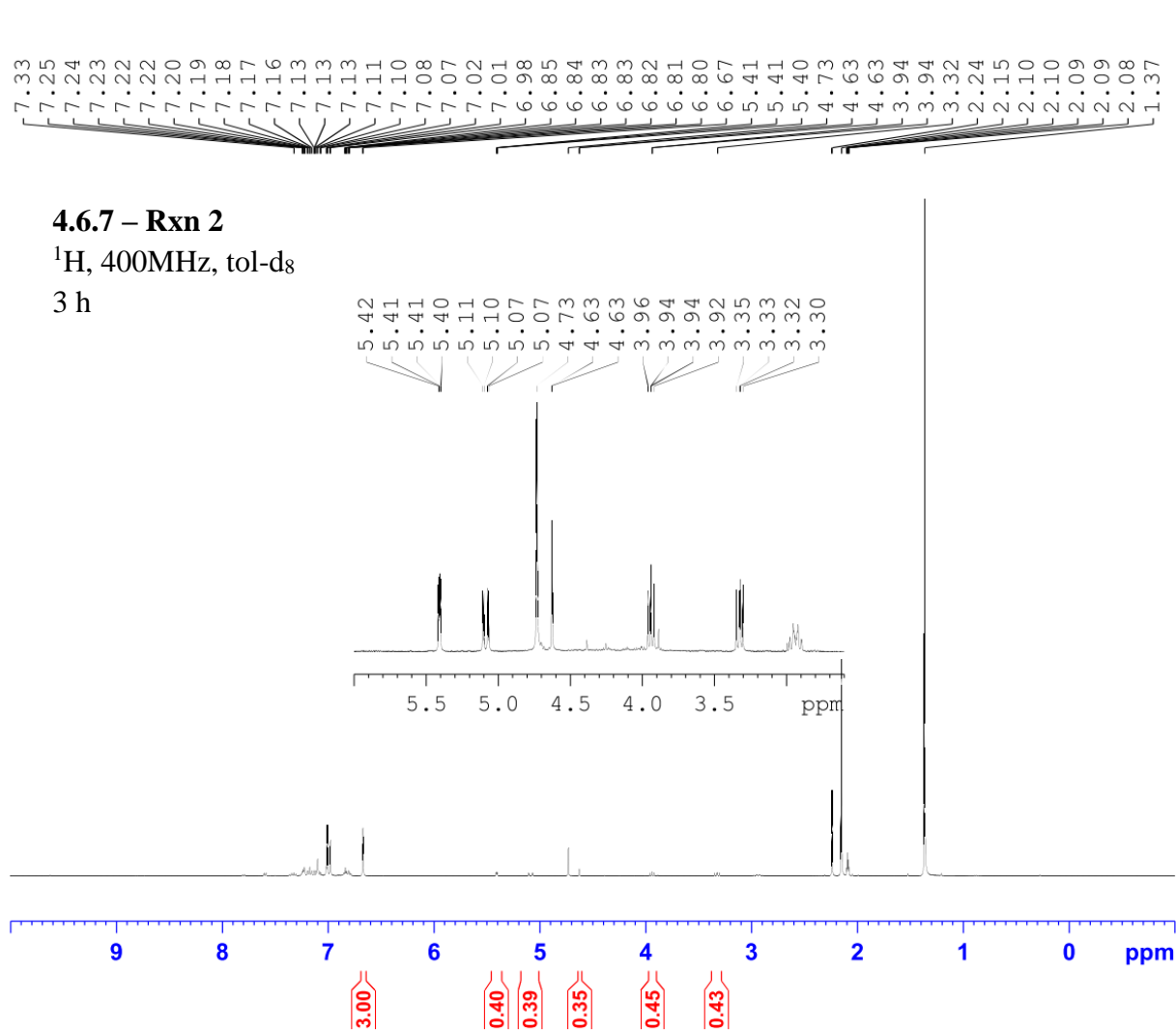
F2 - Processing parameters
 SI 65536
 SF 500.1600172 MHz
 WDW EM
 SSB 0
 LB 0.30 Hz
 GB 0
 PC 1.00



Current Data Parameters
 NAME JAW-03-078
 EXPNO 1
 PROCNO 1

F2 - Acquisition Parameters
 Date_ 20191230
 Time_ 13.40 h
 INSTRUM spect
 PROBHD Z108618_0240 (
 PULPROG zg30
 TD 65536
 SOLVENT Tol
 NS 16
 DS 2
 SWH 8012.820 Hz
 FIDRES 0.244532 Hz
 AQ 4.0894465 sec
 RG 57
 DW 62.400 usec
 DE 6.50 usec
 TE 91.1 K
 D1 1.00000000 sec
 TD0 1
 SFO1 400.1324708 MHz
 NUC1 1H
 P0 4.83 usec
 P1 14.50 usec
 PLW1 12.00000000 W

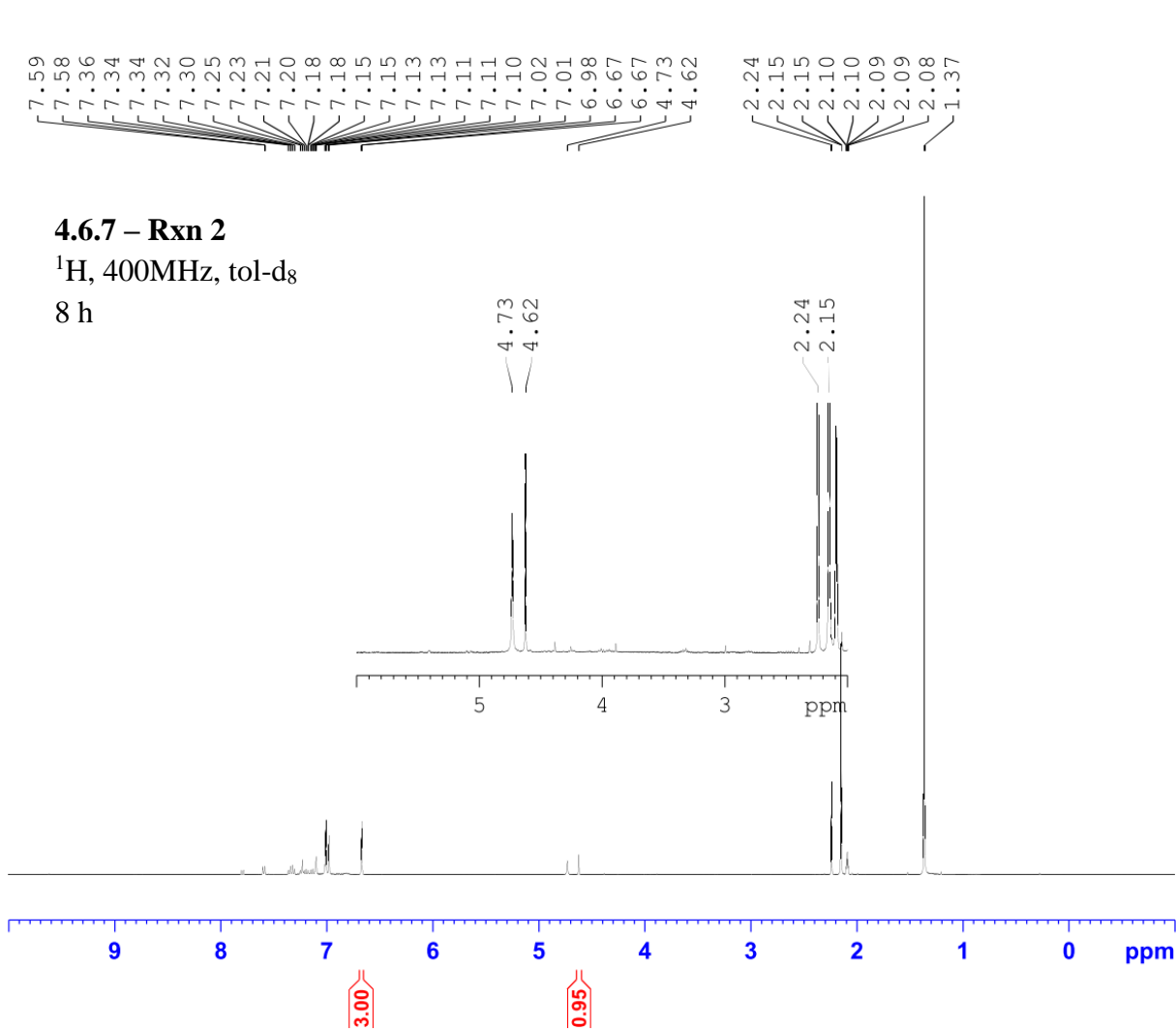
F2 - Processing parameters
 SI 65536
 SF 400.1300139 MHz
 WDW EM
 SSB 0
 LB 0.30 Hz
 GB 0
 PC 1.00



Current Data Parameters
 NAME JAW-03-078
 EXPNO 2
 PROCNO 1

F2 - Acquisition Parameters
 Date_ 20191230
 Time_ 17.39 h
 INSTRUM spect
 PROBHD Z108618_0240 (
 PULPROG zg30
 TD 65536
 SOLVENT Tol
 NS 16
 DS 2
 SWH 8012.820 Hz
 FIDRES 0.244532 Hz
 AQ 4.0894465 sec
 RG 57
 DW 62.400 usec
 DE 6.50 usec
 TE 89.7 K
 D1 1.00000000 sec
 TD0 1
 SFO1 400.1324708 MHz
 NUC1 1H
 P0 4.83 usec
 P1 14.50 usec
 PLW1 12.00000000 W

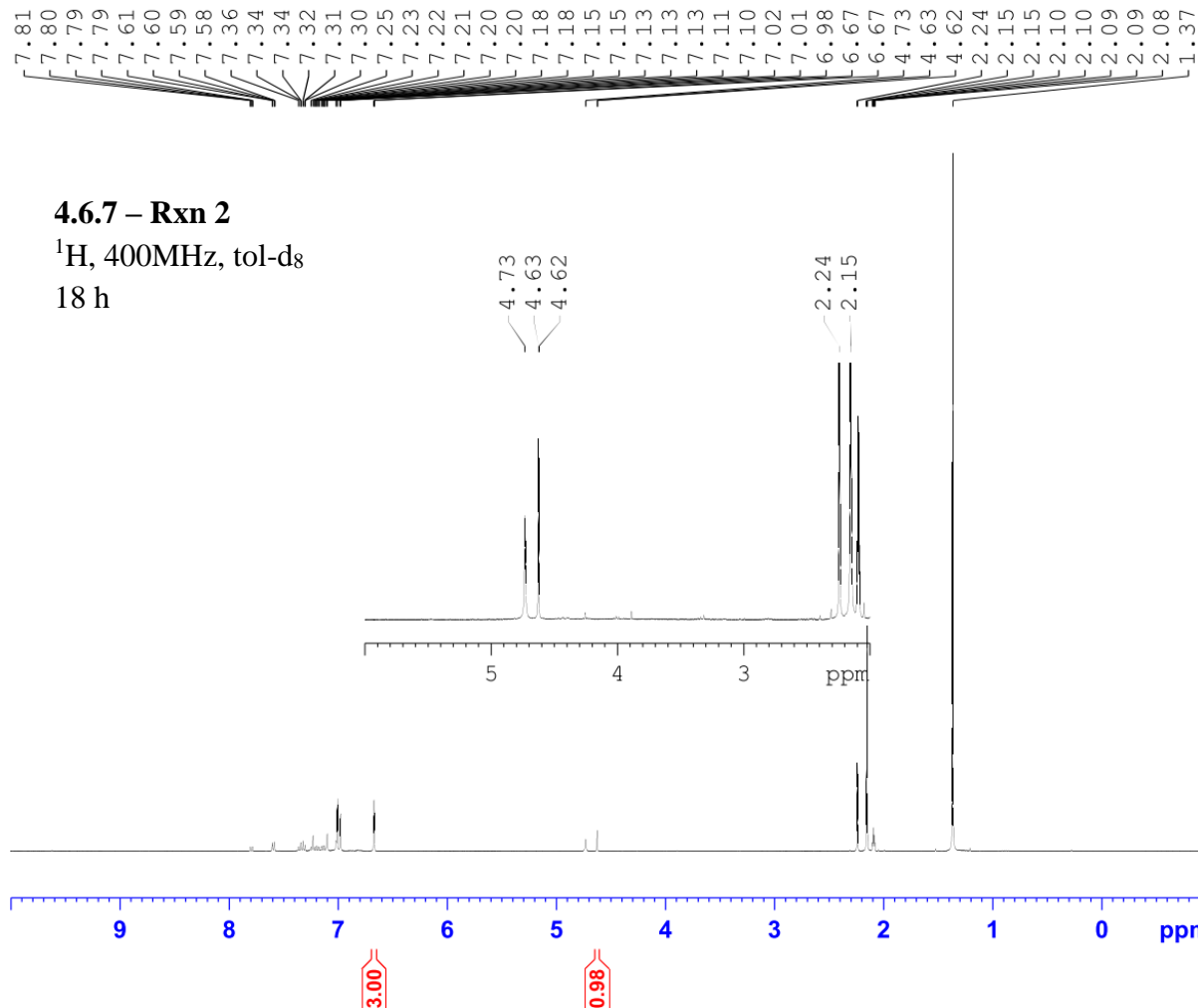
F2 - Processing parameters
 SI 65536
 SF 400.1300140 MHz
 WDW EM
 SSB 0
 LB 0.30 Hz
 GB 0
 PC 1.00



Current Data Parameters
 NAME JAW-03-078
 EXPNO 3
 PROCNO 1

F2 - Acquisition Parameters
 Date_ 20191230
 Time_ 23.21 h
 INSTRUM spect
 PROBHD Z108618_0240 (
 PULPROG zg30
 TD 65536
 SOLVENT Tol
 NS 16
 DS 2
 SWH 8012.820 Hz
 FIDRES 0.244532 Hz
 AQ 4.0894465 sec
 RG 64
 DW 62.400 usec
 DE 6.50 usec
 TE 90.4 K
 D1 1.00000000 sec
 TD0 1
 SF01 400.1324708 MHz
 NUC1 1H
 P0 4.83 usec
 P1 14.50 usec
 PLW1 12.00000000 W

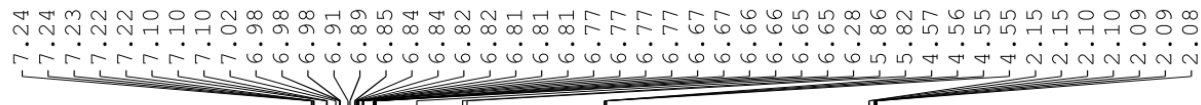
F2 - Processing parameters
 SI 65536
 SF 400.1300141 MHz
 WDW EM
 SSB 0
 LB 0.30 Hz
 GB 0
 PC 1.00



Current Data Parameters
 NAME JAW-03-078
 EXPNO 4
 PROCNO 1

F2 - Acquisition Parameters
 Date_ 20191231
 Time_ 10.51 h
 INSTRUM spect
 PROBHD Z108618_0240 (
 PULPROG zg30
 TD 65536
 SOLVENT Tol
 NS 16
 DS 2
 SWH 8012.820 Hz
 FIDRES 0.244532 Hz
 AQ 4.0894465 sec
 RG 57
 DW 62.400 usec
 DE 6.50 usec
 TE 91.3 K
 D1 1.00000000 sec
 TD0 1
 SF01 400.1324708 MHz
 NUC1 1H
 P0 4.83 usec
 P1 14.50 usec
 PLW1 12.00000000 W

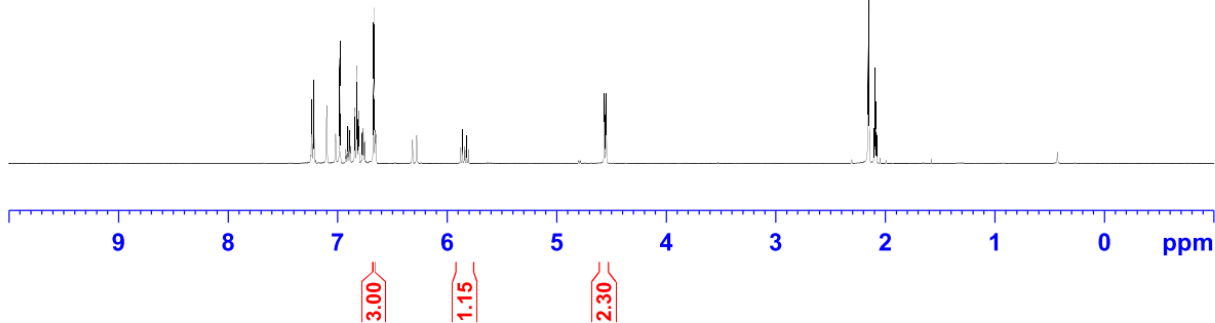
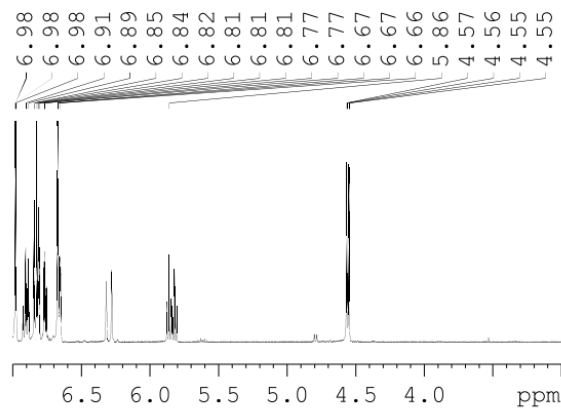
F2 - Processing parameters
 SI 65536
 SF 400.1300141 MHz
 WDW EM
 SSB 0
 LB 0.30 Hz
 GB 0
 PC 1.00



4.6.7 – Rxn 3

¹H, 400MHz, tol-d₈

initial

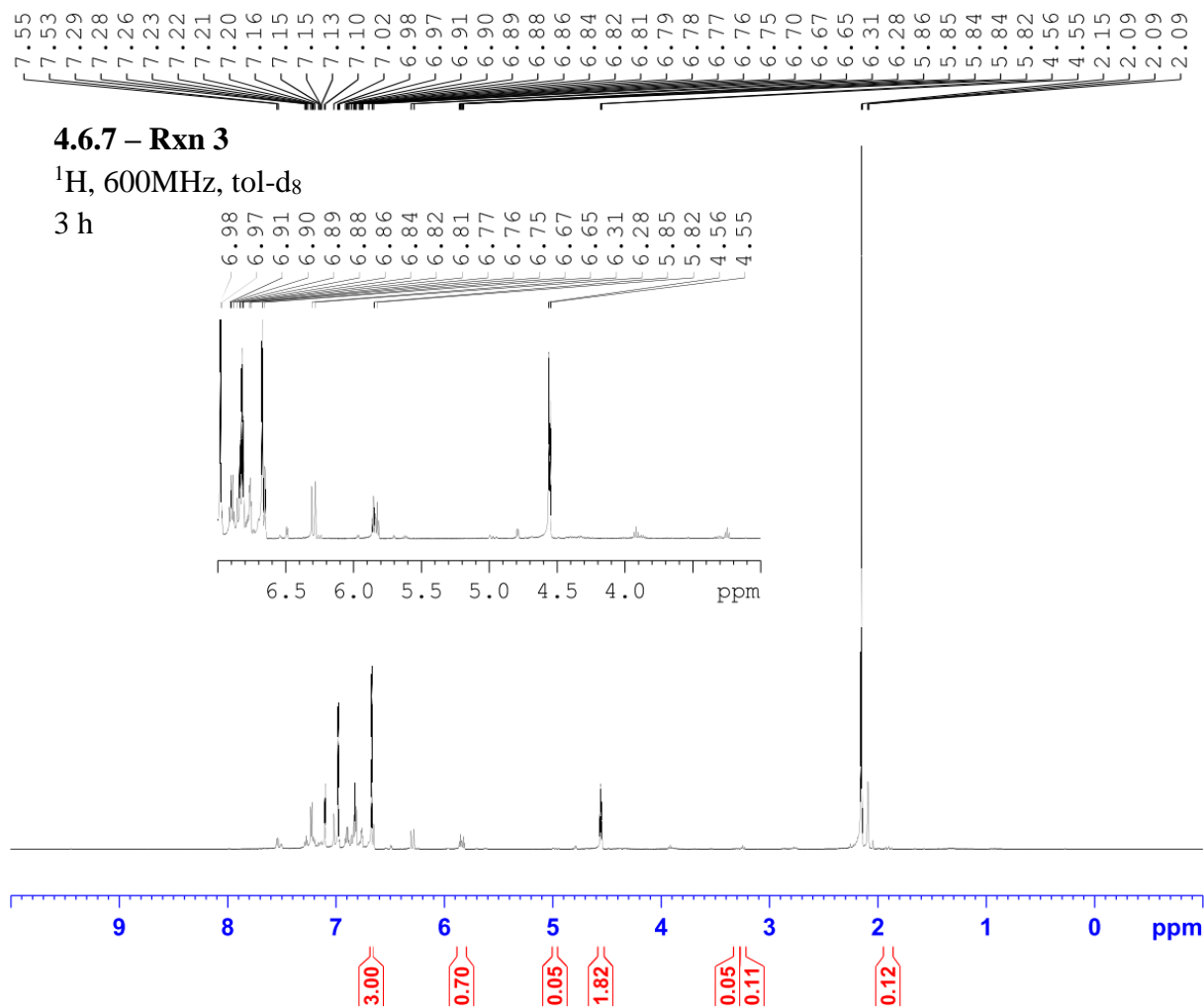


Current Data Parameters
NAME JAW-03-072
EXPNO 1
PROCNO 1

F2 - Acquisition Parameters
Date_ 20191121
Time_ 12.34
INSTRUM spect
PROBHD 5 mm PADUL 13C
PULPROG zg30
TD 65536
SOLVENT Tol
NS 16
DS 2
SWH 8223.685 Hz
FIDRES 0.125483 Hz
AQ 3.9845889 sec
RG 114
DW 60.800 usec
DE 6.50 usec
TE 298.2 K
D1 2.00000000 sec
TD0 1

===== CHANNEL f1 =====
NUC1 1H
P1 9.31 usec
PL1 -3.90 dB
PL1W 21.64248466 W
SFO1 400.2324716 MHz

F2 - Processing parameters
SI 32768
SF 400.2300165 MHz
WDW EM
SSB 0
LB 0.30 Hz
GB 0
PC 1.00

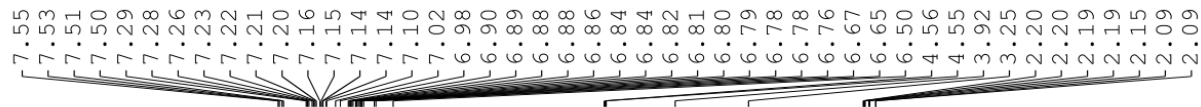


Current Data Parameters
 NAME JAW-03-072
 EXPNO 2
 PROCNO 1

F2 - Acquisition Parameters
 Date_ 20191121
 Time_ 16.12
 INSTRUM spect
 PROBHD 5 mm PABBO BB-
 PULPROG zg30
 TD 65536
 SOLVENT Tol
 NS 16
 DS 2
 SWH 12335.526 Hz
 FIDRES 0.188225 Hz
 AQ 2.6563926 sec
 RG 101
 DW 40.533 usec
 DE 6.50 usec
 TE 295.2 K
 D1 1.00000000 sec
 TD0 1

===== CHANNEL f1 =====
 NUC1 1H
 P1 10.86 usec
 PL1 -2.00 dB
 PL1W 19.70630455 W
 SFO1 600.7137096 MHz

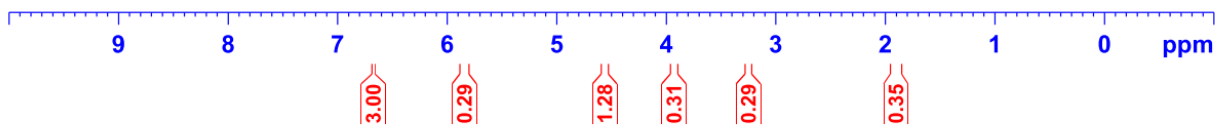
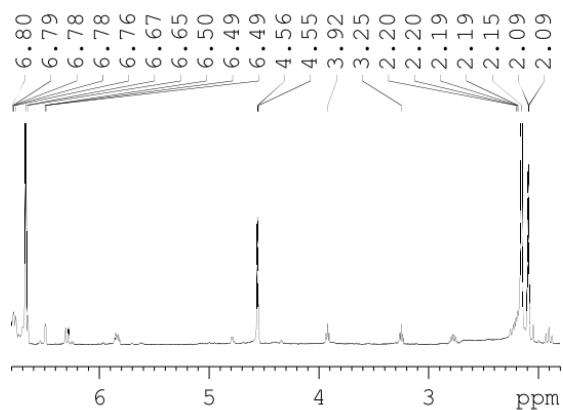
F2 - Processing parameters
 SI 32768
 SF 600.7100218 MHz
 WDW EM
 SSB 0
 LB 0.30 Hz
 GB 0
 PC 1.00



4.6.7 – Rxn 3

¹H, 600MHz, tol-d₈

8 h

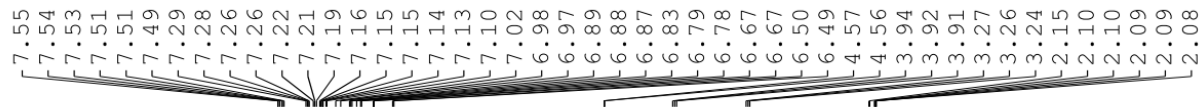


Current Data Parameters
NAME JAW-03-072
EXPNO 4
PROCNO 1

F2 - Acquisition Parameters
Date_ 20191121
Time_ 22.29
INSTRUM spect
PROBHD 5 mm PABBO BB-
PULPROG zg30
TD 65536
SOLVENT Tol
NS 16
DS 2
SWH 12335.526 Hz
FIDRES 0.188225 Hz
AQ 2.6563926 sec
RG 101
DW 40.533 usec
DE 6.50 usec
TE 295.2 K
D1 1.00000000 sec
TD0 1

===== CHANNEL f1 =====
NUC1 1H
P1 10.86 usec
PL1 -2.00 dB
PL1W 19.70630455 W
SFO1 600.7137096 MHz

F2 - Processing parameters
SI 32768
SF 600.7100233 MHz
WDW EM
SSB 0
LB 0.30 Hz
GB 0
PC 1.00



Current Data Parameters
NAME JAW-03-072
EXPNO 5
PROCNO 1

F2 - Acquisition Parameters
Date_ 20191122
Time_ 9.50
INSTRUM spect
PROBHD 5 mm PABBO BB/
PULPROG zg30
TD 65536
SOLVENT Tol
NS 16
DS 2
SWH 10000.000 Hz
FIDRES 0.152588 Hz
AQ 3.2767999 sec
RG 80.6
DW 50.000 usec
DE 6.50 usec
TE 297.2 K
D1 1.00000000 sec
TD0 1

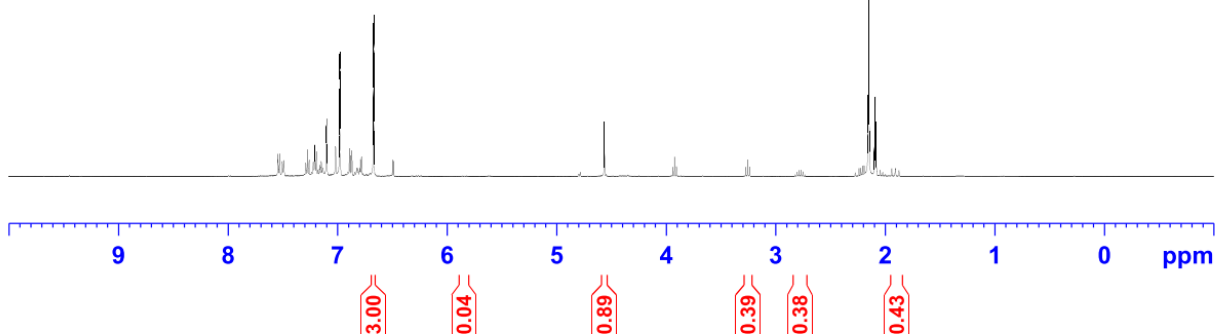
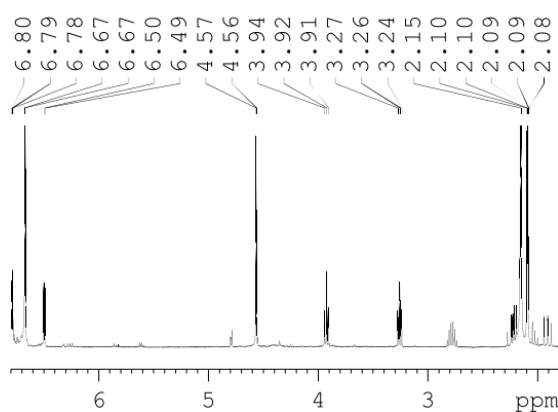
===== CHANNEL f1 =====
SF01 500.1630887 MHz
NUC1 1H
P1 11.50 usec
PLW1 18.00000000 W

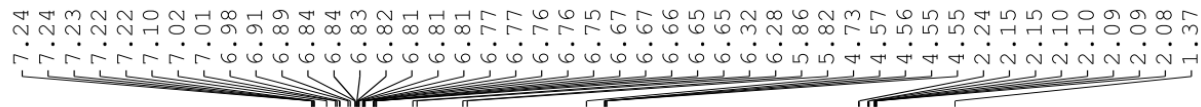
F2 - Processing parameters
SI 65536
SF 500.1600174 MHz
WDW EM
SSB 0
LB 0.30 Hz
GB 0
PC 1.00

4.6.7 – Rxn 3

¹H, 500MHz, tol-d₈

18 h

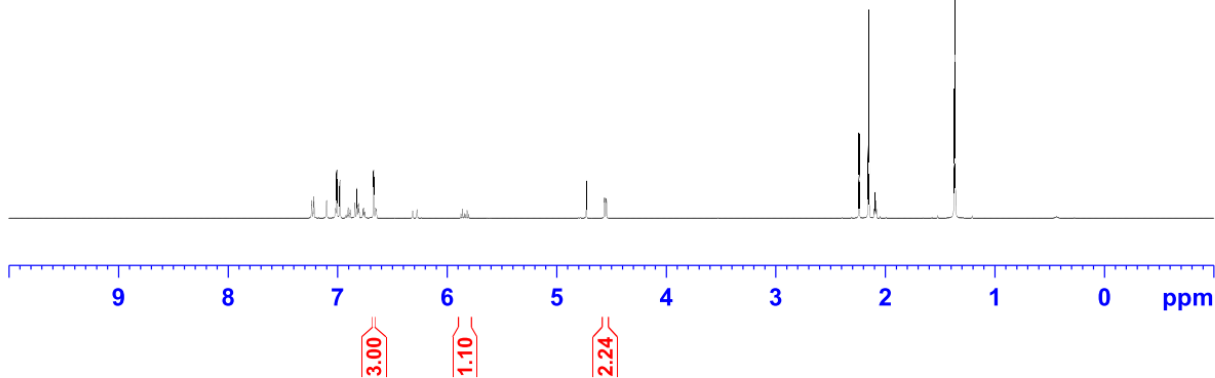
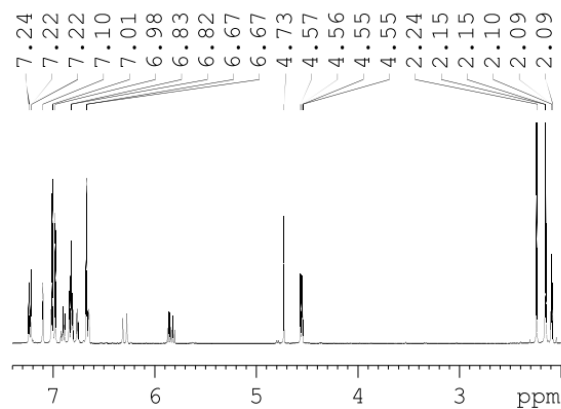




4.6.7 – Rxn 4

¹H, 400MHz, tol-d₈

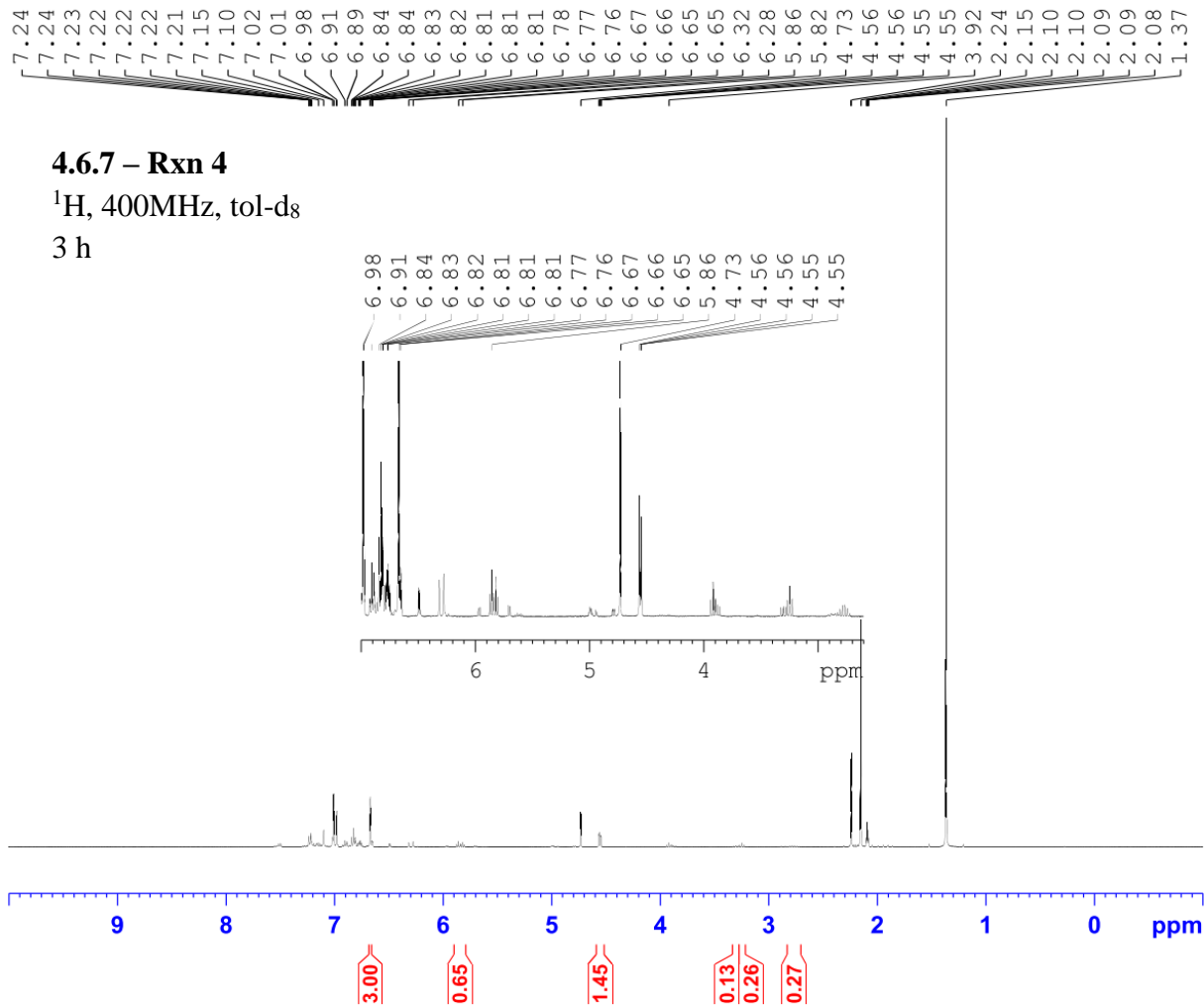
initial



Current Data Parameters
NAME JAW-03-080
EXPNO 1
PROCNO 1

F2 - Acquisition Parameters
Date_ 20191230
Time_ 13.49 h
INSTRUM spect
PROBHD Z108618_0240 (
PULPROG zg30
TD 65536
SOLVENT Tol
NS 16
DS 2
SWH 8012.820 Hz
FIDRES 0.244532 Hz
AQ 4.0894465 sec
RG 57
DW 62.400 usec
DE 6.50 usec
TE 90.6 K
D1 1.00000000 sec
TD0 1
SF01 400.1324708 MHz
NUC1 1H
P0 4.83 usec
P1 14.50 usec
PLW1 12.00000000 W

F2 - Processing parameters
SI 65536
SF 400.1300139 MHz
WDW EM
SSB 0
LB 0.30 Hz
GB 0
PC 1.00



Current Data Parameters
 NAME JAW-03-080
 EXPNO 2
 PROCNO 1

F2 - Acquisition Parameters
 Date_ 20191230
 Time_ 17.26 h
 INSTRUM spect
 PROBHD Z108618_0240 (
 PULPROG zg30
 TD 65536
 SOLVENT Tol
 NS 16
 DS 2
 SWH 8012.820 Hz
 FIDRES 0.244532 Hz
 AQ 4.0894465 sec
 RG 57
 DW 62.400 usec
 DE 6.50 usec
 TE 89.9 K
 D1 1.00000000 sec
 TD0 1
 SFO1 400.1324708 MHz
 NUC1 1H
 P0 4.83 usec
 P1 14.50 usec
 PLW1 12.00000000 W

F2 - Processing parameters
 SI 65536
 SF 400.1300140 MHz
 WDW EM
 SSB 0
 LB 0.30 Hz
 GB 0
 PC 1.00

7.51
7.51
7.49
7.24
7.23
7.22
7.22
7.21
7.19
7.17
7.15
7.10
7.02
7.01
6.98
6.97
6.89
6.83
6.82
6.81
6.79
6.78
6.67
6.67
6.50
6.49
4.73
4.56
4.56
4.55
4.55
3.94
3.92
3.90
3.27
3.25
3.23
2.24
2.15
2.15
2.10
2.10
2.09
2.09
2.08
2.08
1.37



Current Data Parameters
NAME JAW-03-080
EXPNO 3
PROCNO 1

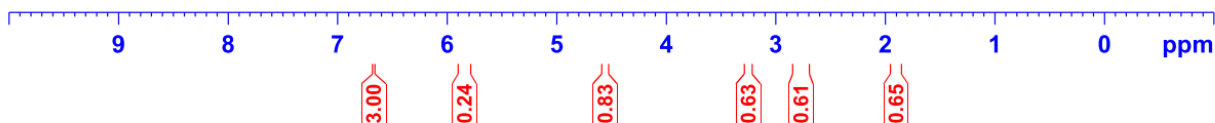
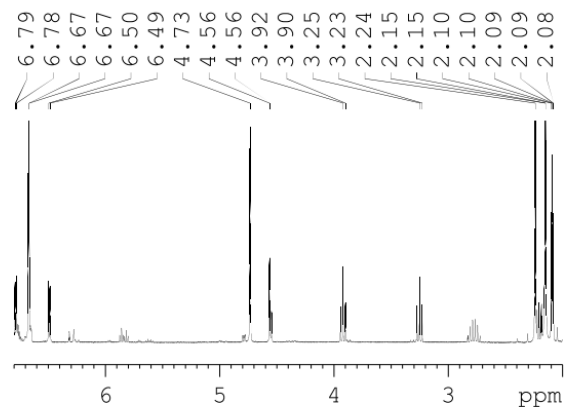
F2 - Acquisition Parameters
Date_ 20191230
Time_ 23.42 h
INSTRUM spect
PROBHD z108618_0240 (
PULPROG zg30
TD 65536
SOLVENT Tol
NS 16
DS 2
SWH 8012.820 Hz
FIDRES 0.244532 Hz
AQ 4.0894465 sec
RG 57
DW 62.400 usec
DE 6.50 usec
TE 90.2 K
D1 1.00000000 sec
TD0 1
SF01 400.1324708 MHz
NUC1 1H
P0 4.83 usec
P1 14.50 usec
PLW1 12.00000000 W

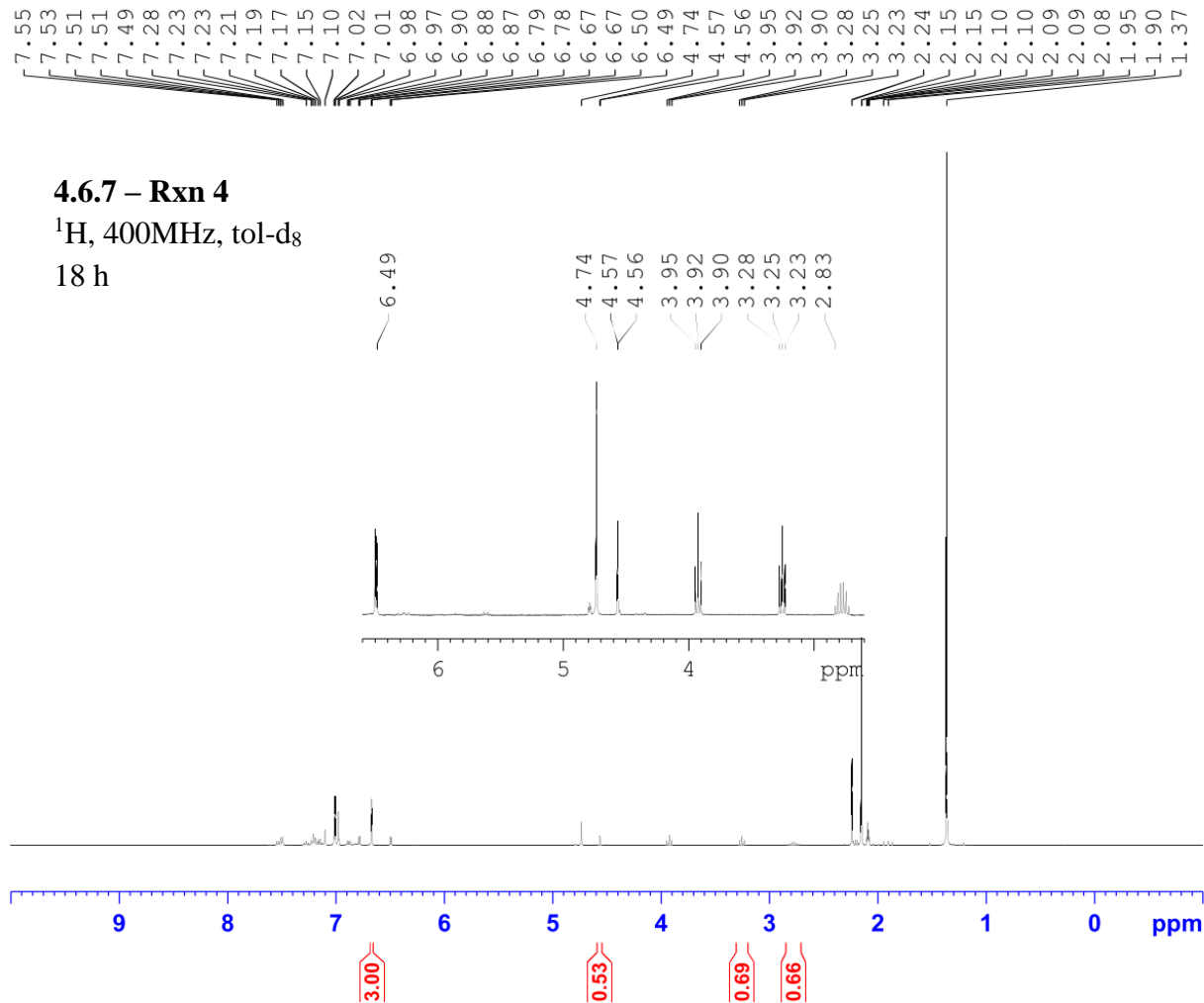
F2 - Processing parameters
SI 65536
SF 400.1300140 MHz
WDW EM
SSB 0
LB 0.30 Hz
GB 0
PC 1.00

4.6.7 - Rxn 4

¹H, 400MHz, tol-d₈

8 h

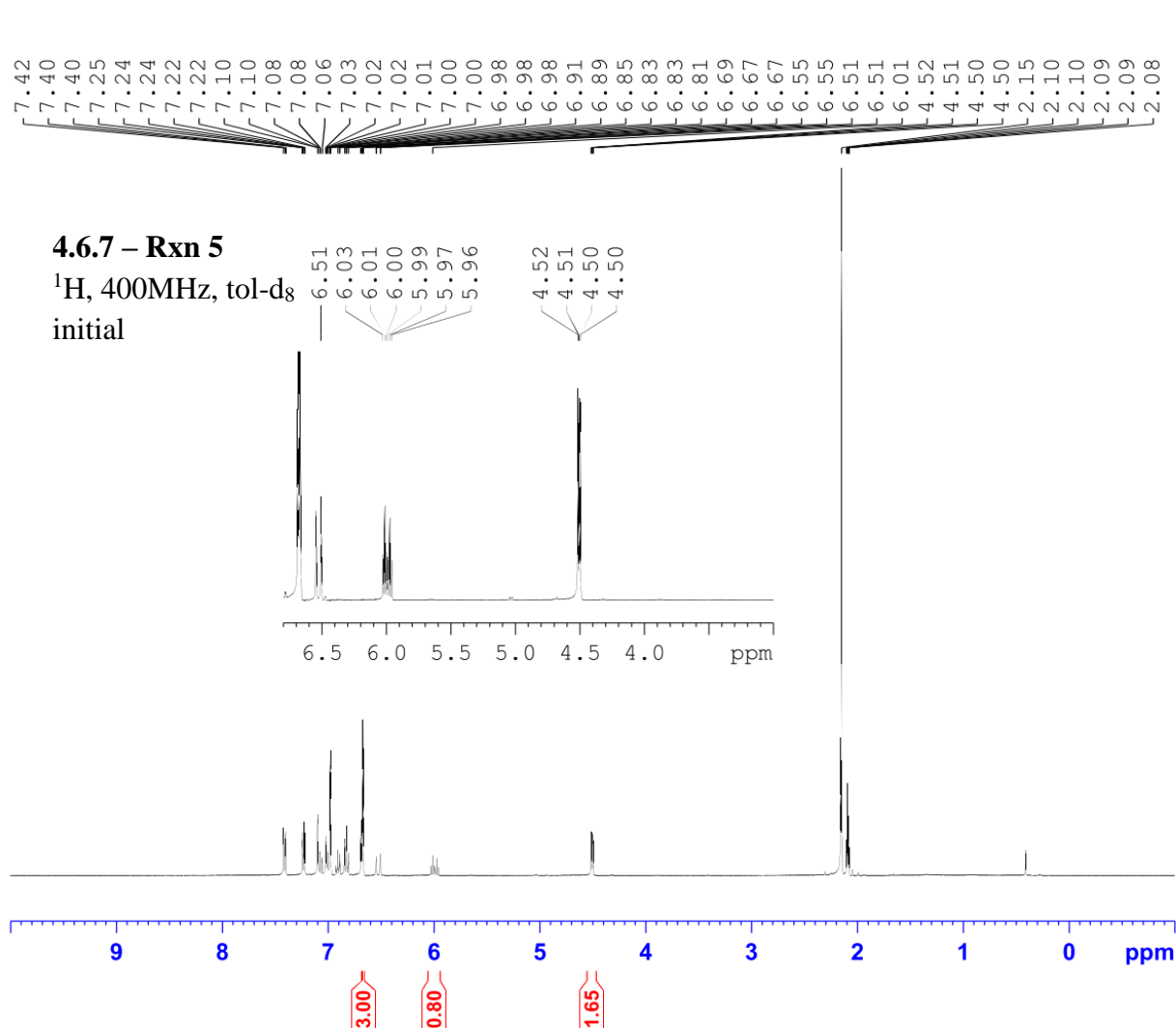




Current Data Parameters
 NAME JAW-03-080
 EXPNO 4
 PROCNO 1

F2 - Acquisition Parameters
 Date_ 20191231
 Time_ 11.09 h
 INSTRUM spect
 PROBHD Z108618_0240 (
 PULPROG zg30
 TD 65536
 SOLVENT Tol
 NS 16
 DS 2
 SWH 8012.820 Hz
 FIDRES 0.244532 Hz
 AQ 4.0894465 sec
 RG 57
 DW 62.400 usec
 DE 6.50 usec
 TE 91.1 K
 D1 1.00000000 sec
 TD0 1
 SFO1 400.1324708 MHz
 NUC1 1H
 P0 4.83 usec
 P1 14.50 usec
 PLW1 12.00000000 W

F2 - Processing parameters
 SI 65536
 SF 400.1300140 MHz
 WDW EM
 SSB 0
 LB 0.30 Hz
 GB 0
 PC 1.00

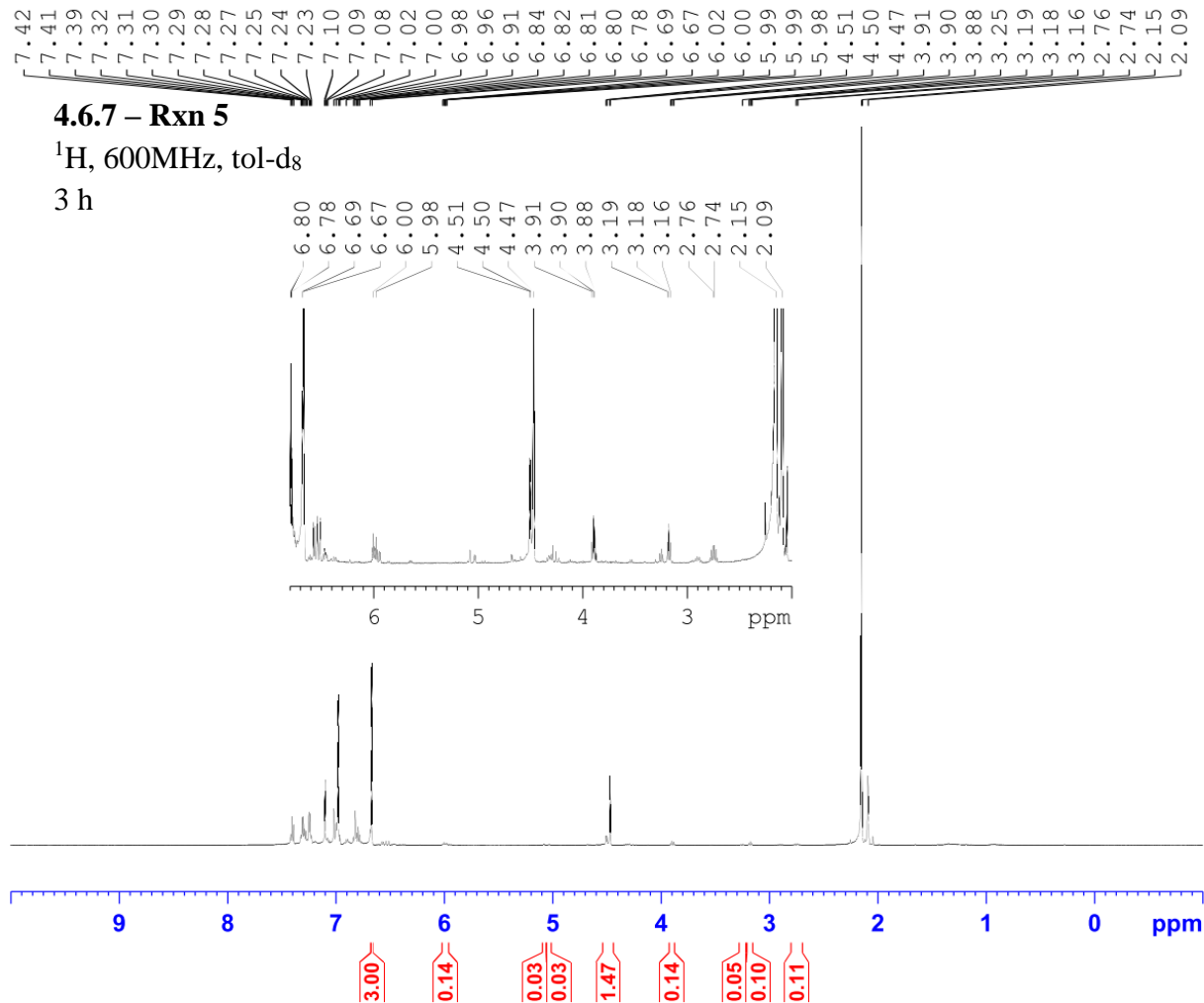


Current Data Parameters
 NAME JAW-03-071
 EXPNO 1
 PROCNO 1

F2 - Acquisition Parameters
 Date_ 20191121
 Time_ 12.28
 INSTRUM spect
 PROBHD 5 mm PADUL 13C
 PULPROG zg30
 TD 65536
 SOLVENT Tol
 NS 16
 DS 2
 SWH 8223.685 Hz
 FIDRES 0.125483 Hz
 AQ 3.9845889 sec
 RG 114
 DW 60.800 usec
 DE 6.50 usec
 TE 298.2 K
 D1 2.00000000 sec
 TD0 1

===== CHANNEL f1 =====
 NUC1 1H
 P1 9.31 usec
 PL1 -3.90 dB
 PL1W 21.64248466 W
 SFO1 400.2324716 MHz

F2 - Processing parameters
 SI 32768
 SF 400.2300166 MHz
 WDW EM
 SSB 0
 LB 0.30 Hz
 GB 0
 PC 1.00

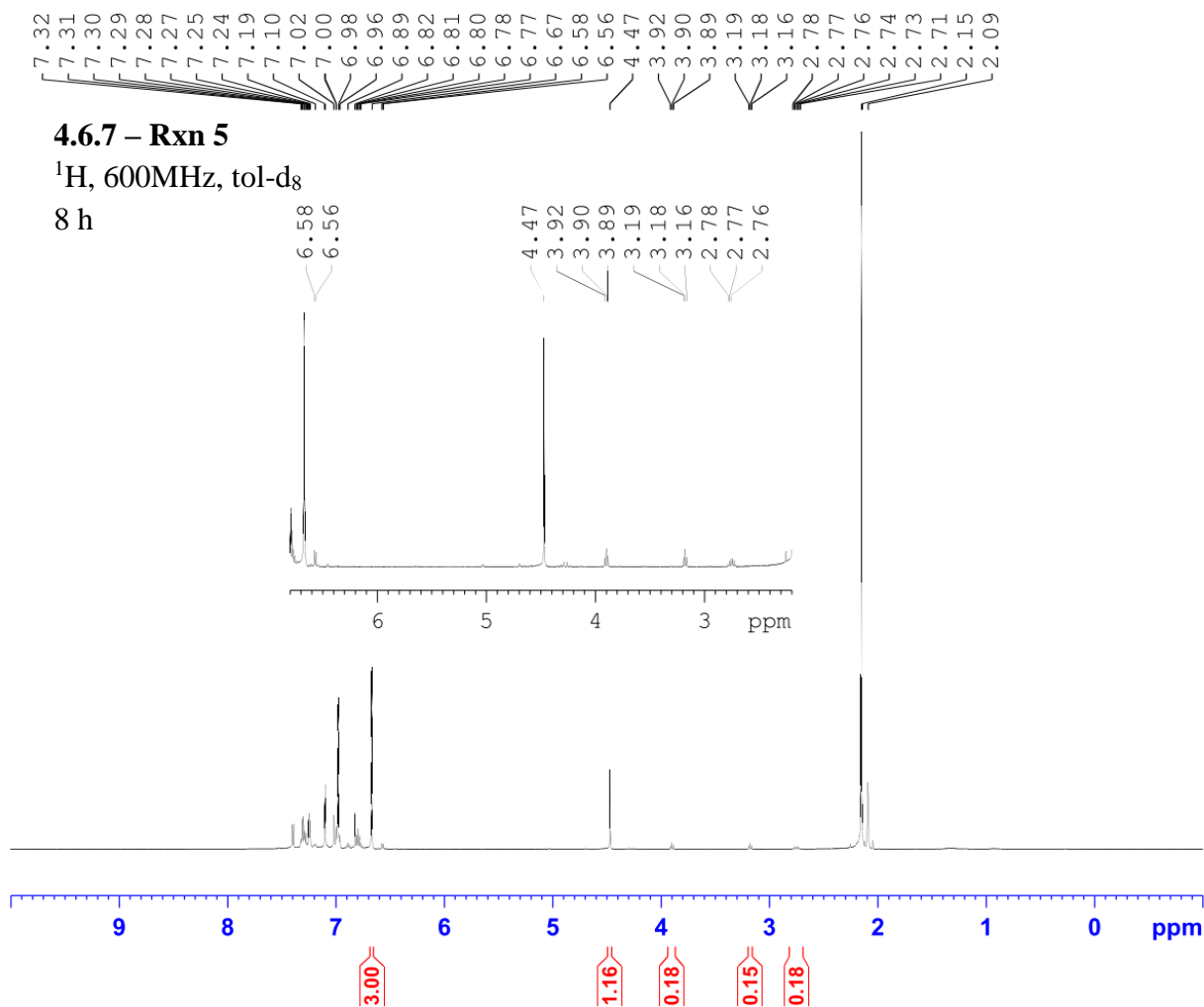


Current Data Parameters
 NAME JAW-03-071
 EXPNO 2
 PROCNO 1

F2 - Acquisition Parameters
 Date_ 20191121
 Time_ 16.06
 INSTRUM spect
 PROBHD 5 mm PABBO BB-
 PULPROG zg30
 TD 65536
 SOLVENT Tol
 NS 16
 DS 2
 SWH 12335.526 Hz
 FIDRES 0.188225 Hz
 AQ 2.6563926 sec
 RG 71.8
 DW 40.533 usec
 DE 6.50 usec
 TE 295.2 K
 D1 1.00000000 sec
 TD0 1

===== CHANNEL f1 =====
 NUC1 1H
 P1 10.86 usec
 PL1 -2.00 dB
 PL1W 19.70630455 W
 SFO1 600.7137096 MHz

F2 - Processing parameters
 SI 32768
 SF 600.7100220 MHz
 WDW EM
 SSB 0
 LB 0.30 Hz
 GB 0
 PC 1.00

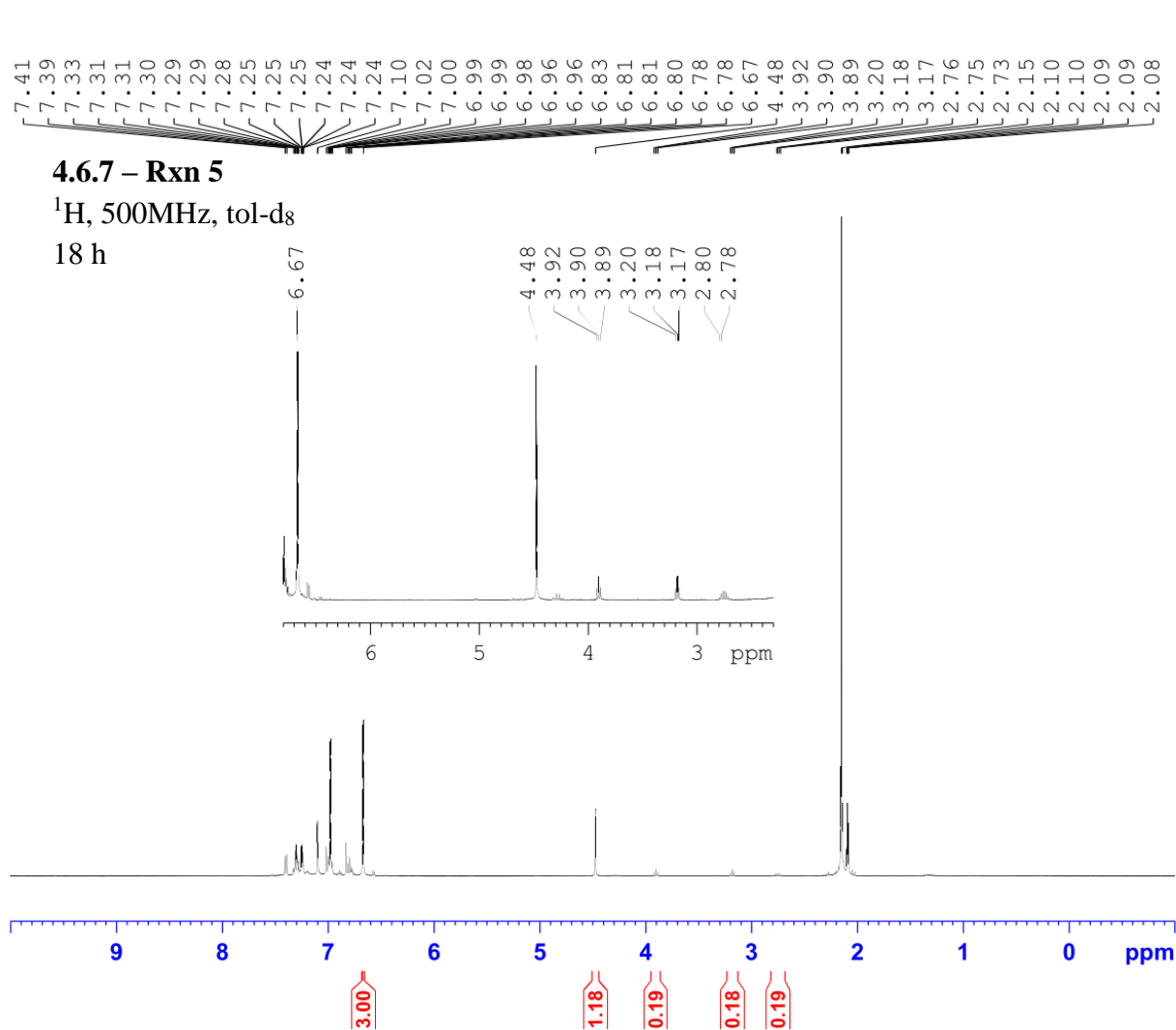


Current Data Parameters
 NAME JAW-03-071
 EXPNO 3
 PROCNO 1

F2 - Acquisition Parameters
 Date_ 20191121
 Time_ 22.16
 INSTRUM spect
 PROBHD 5 mm PABBO BB-
 PULPROG zg30
 TD 65536
 SOLVENT Tol
 NS 16
 DS 2
 SWH 12335.526 Hz
 FIDRES 0.188225 Hz
 AQ 2.6563926 sec
 RG 71.8
 DW 40.533 usec
 DE 6.50 usec
 TE 295.1 K
 D1 1.00000000 sec
 TD0 1

===== CHANNEL f1 =====
 NUC1 1H
 P1 10.86 usec
 PL1 -2.00 dB
 PL1W 19.70630455 W
 SFO1 600.7137096 MHz

F2 - Processing parameters
 SI 32768
 SF 600.7100217 MHz
 WDW EM
 SSB 0
 LB 0.30 Hz
 GB 0
 PC 1.00

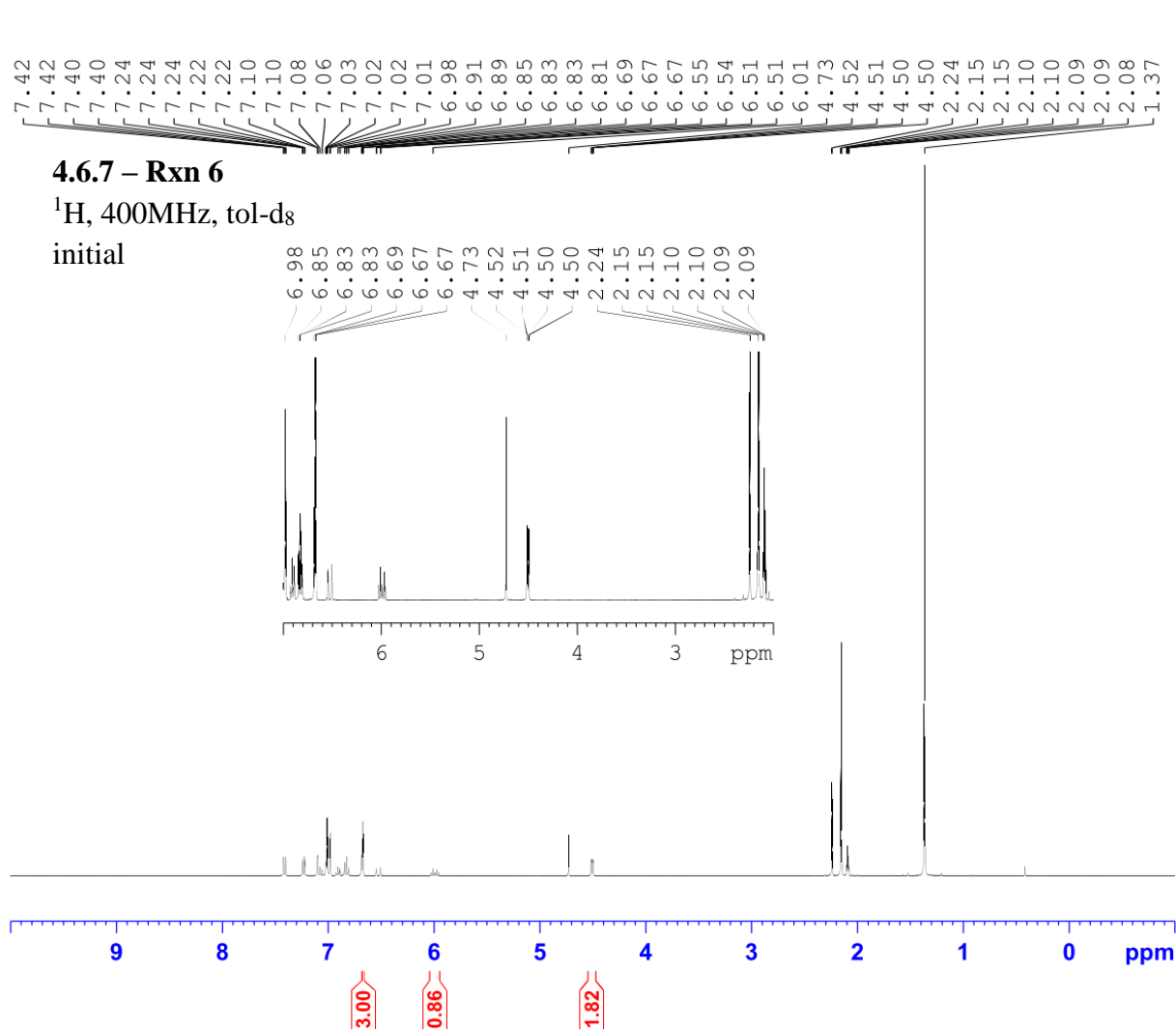


Current Data Parameters
 NAME JAW-03-071
 EXPNO 5
 PROCNO 1

F2 - Acquisition Parameters
 Date_ 20191122
 Time_ 9.40
 INSTRUM spect
 PROBHD 5 mm PABBO BB/
 PULPROG zg30
 TD 65536
 SOLVENT Tol
 NS 16
 DS 2
 SWH 10000.000 Hz
 FIDRES 0.152588 Hz
 AQ 3.2767999 sec
 RG 90.5
 DW 50.000 usec
 DE 6.50 usec
 TE 297.2 K
 D1 1.00000000 sec
 TD0 1

===== CHANNEL f1 =====
 SF01 500.1630887 MHz
 NUC1 1H
 P1 11.50 usec
 PLW1 18.00000000 W

F2 - Processing parameters
 SI 65536
 SF 500.1600174 MHz
 WDW EM
 SSB 0
 LB 0.30 Hz
 GB 0
 PC 1.00



Current Data Parameters
 NAME JAW-03-079
 EXPNO 1
 PROCNO 1

F2 - Acquisition Parameters
 Date_ 20191230
 Time_ 14.08 h
 INSTRUM spect
 PROBHD z108618_0240 (
 PULPROG zg30
 TD 65536
 SOLVENT Tol
 NS 16
 DS 2
 SWH 8012.820 Hz
 FIDRES 0.244532 Hz
 AQ 4.0894465 sec
 RG 64
 DW 62.400 usec
 DE 6.50 usec
 TE 90.3 K
 D1 1.00000000 sec
 TD0 1
 SF01 400.1324708 MHz
 NUC1 1H
 P0 4.83 usec
 P1 14.50 usec
 PLW1 12.00000000 W

F2 - Processing parameters
 SI 65536
 SF 400.1300139 MHz
 WDW EM
 SSB 0
 LB 0.30 Hz
 GB 0
 PC 1.00

7.32
7.30
7.29
7.26
7.25
7.24
7.23
7.10
7.09
7.02
7.00
6.98
6.89
6.87
6.83
6.78
6.77
6.67
6.67
6.47
6.47
5.95
5.93
5.09
5.08
5.08
5.08
4.73
4.48
4.47
3.91
3.89
3.89
3.87
3.28
3.25
3.25
3.23
3.23
2.24
2.15
2.15
2.10
2.10
2.09
2.09
2.08



Current Data Parameters
NAME JAW-03-079
EXPNO 2
PROCNO 1

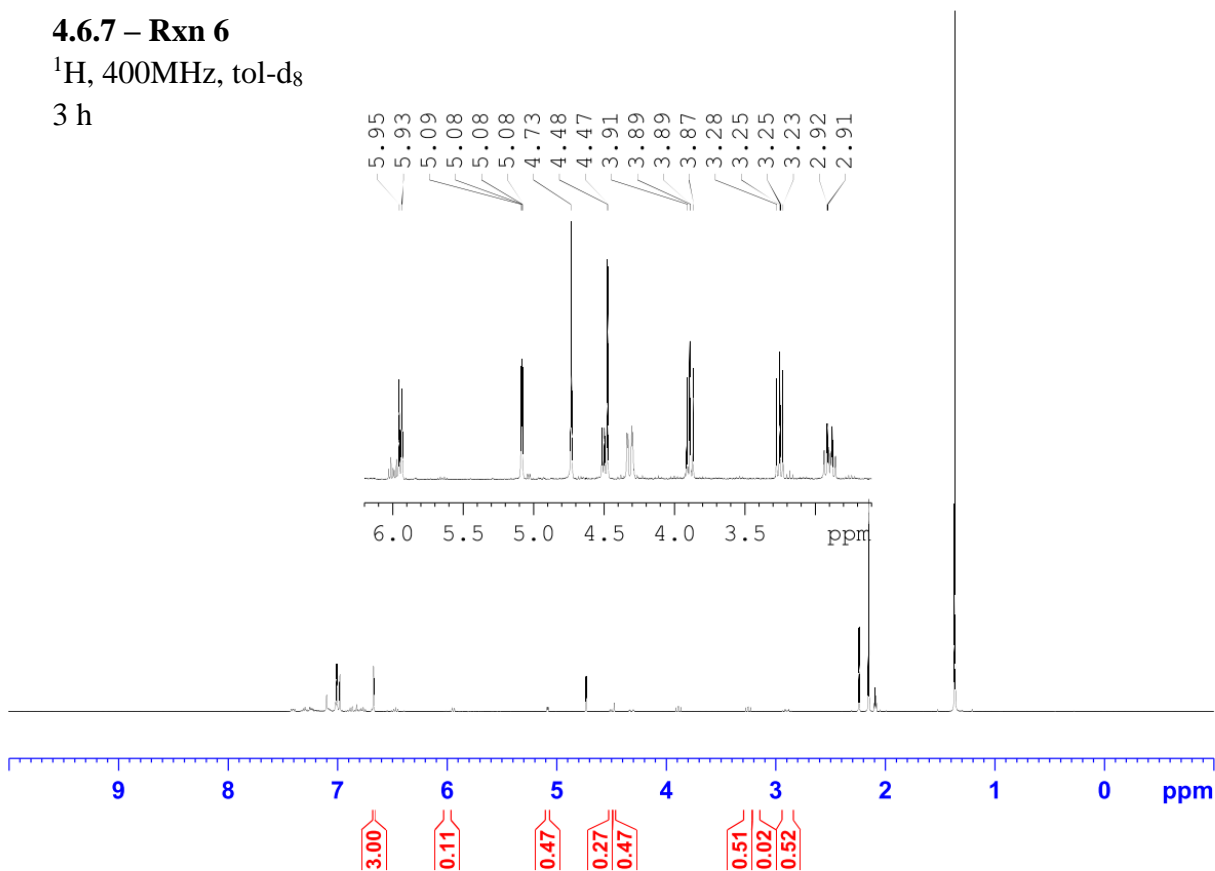
F2 - Acquisition Parameters
Date_ 20191230
Time_ 17.14 h
INSTRUM spect
PROBHD Z108618_0240 (
PULPROG zg30
TD 65536
SOLVENT Tol
NS 16
DS 2
SWH 8012.820 Hz
FIDRES 0.244532 Hz
AQ 4.0894465 sec
RG 64
DW 62.400 usec
DE 6.50 usec
TE 90.3 K
D1 1.00000000 sec
TD0 1
SF01 400.1324708 MHz
NUC1 1H
P0 4.83 usec
P1 14.50 usec
PLW1 12.00000000 W

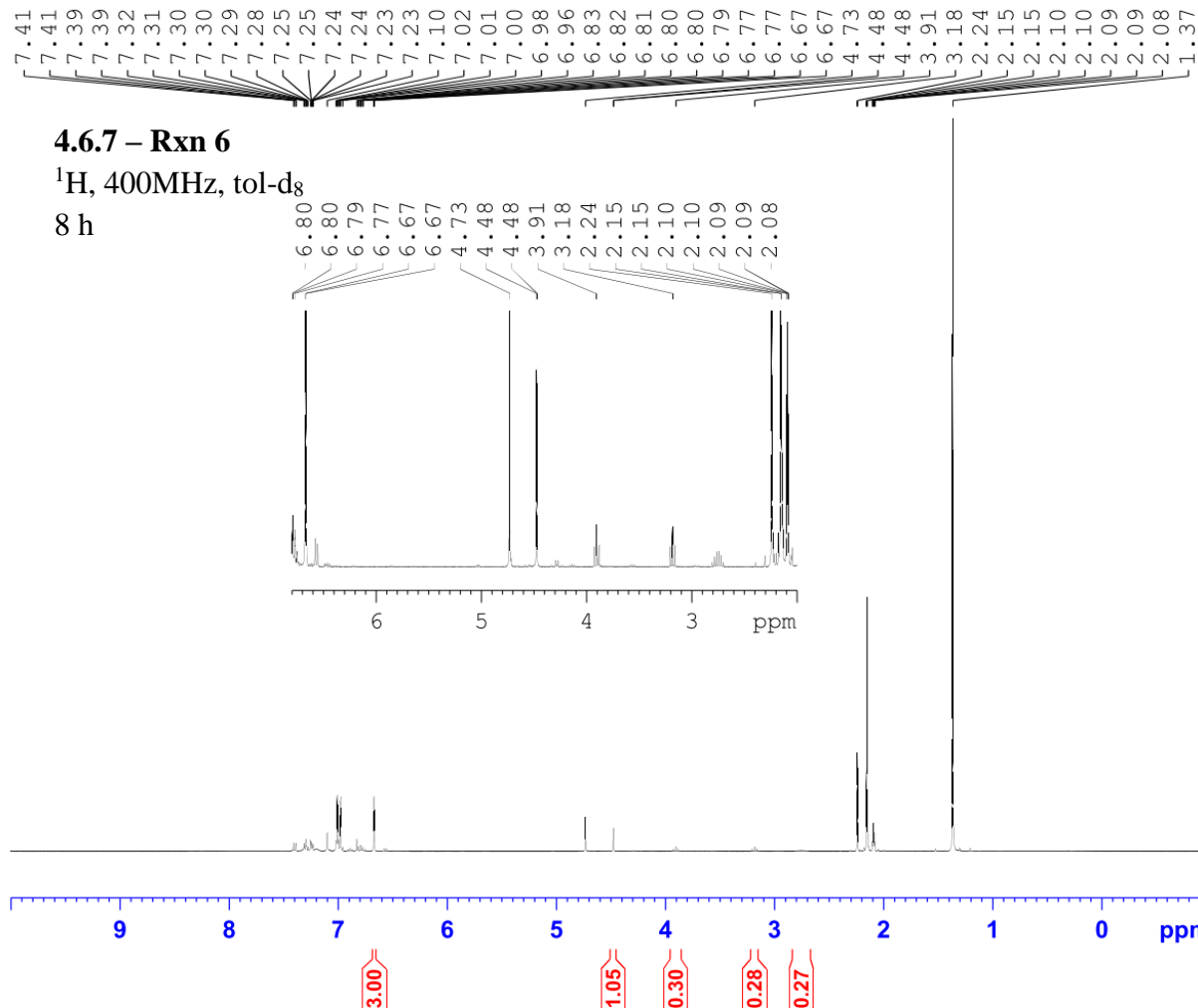
F2 - Processing parameters
SI 65536
SF 400.1300141 MHz
WDW EM
SSB 0
LB 0.30 Hz
GB 0
PC 1.00

4.6.7 – Rxn 6

¹H, 400MHz, tol-d₈

3 h

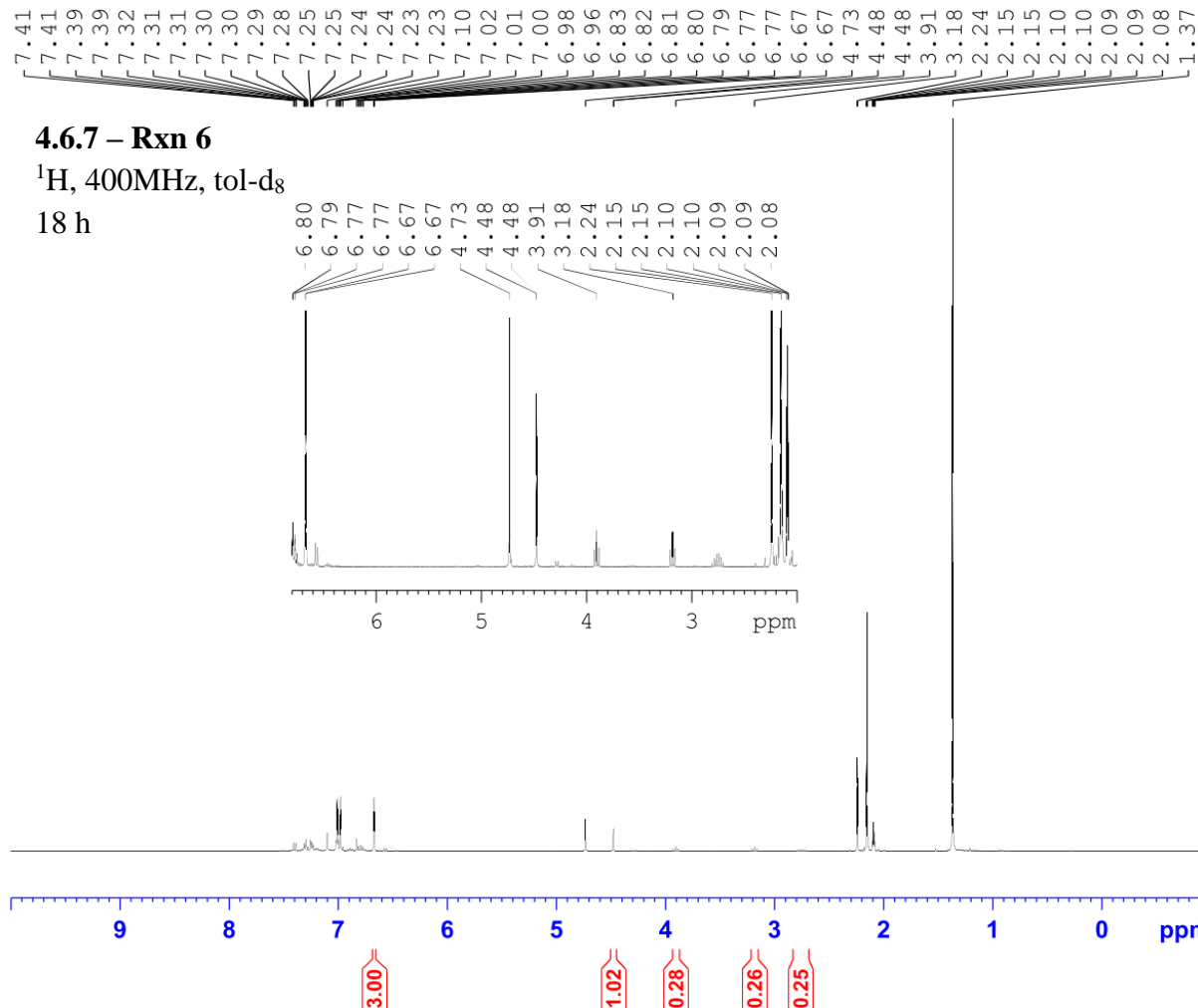




Current Data Parameters
 NAME JAW-03-079
 EXPNO 3
 PROCNO 1

F2 - Acquisition Parameters
 Date_ 20191230
 Time_ 23.29 h
 INSTRUM spect
 PROBHD Z108618_0240 (
 PULPROG zg30
 TD 65536
 SOLVENT Tol
 NS 16
 DS 2
 SWH 8012.820 Hz
 FIDRES 0.244532 Hz
 AQ 4.0894465 sec
 RG 64
 DW 62.400 usec
 DE 6.50 usec
 TE 90.2 K
 D1 1.00000000 sec
 TD0 1
 SFO1 400.1324708 MHz
 NUC1 1H
 P0 4.83 usec
 P1 14.50 usec
 PLW1 12.00000000 W

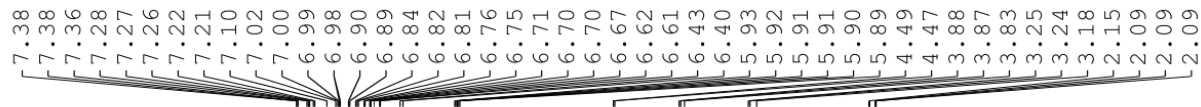
F2 - Processing parameters
 SI 65536
 SF 400.1300139 MHz
 WDW EM
 SSB 0
 LB 0.30 Hz
 GB 0
 PC 1.00



Current Data Parameters
 NAME JAW-03-079
 EXPNO 4
 PROCNO 1

F2 - Acquisition Parameters
 Date_ 20191231
 Time_ 10.59 h
 INSTRUM spect
 PROBHD z108618_0240 (
 PULPROG zg30
 TD 65536
 SOLVENT Tol
 NS 16
 DS 2
 SWH 8012.820 Hz
 FIDRES 0.244532 Hz
 AQ 4.0894465 sec
 RG 64
 DW 62.400 usec
 DE 6.50 usec
 TE 91.3 K
 D1 1.00000000 sec
 TD0 1
 SF01 400.1324708 MHz
 NUC1 1H
 P0 4.83 usec
 P1 14.50 usec
 PLW1 12.00000000 W

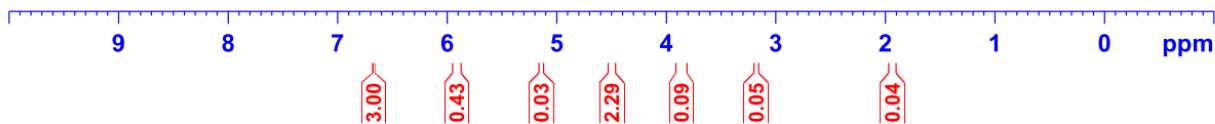
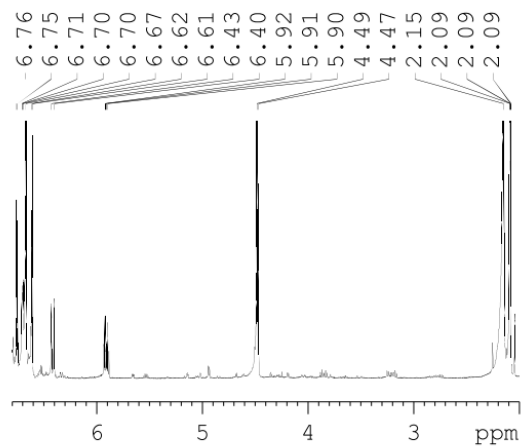
F2 - Processing parameters
 SI 65536
 SF 400.1300138 MHz
 WDW EM
 SSB 0
 LB 0.30 Hz
 GB 0
 PC 1.00



4.6.7 – Rxn 7

¹H, 600MHz, tol-d₈

3 h

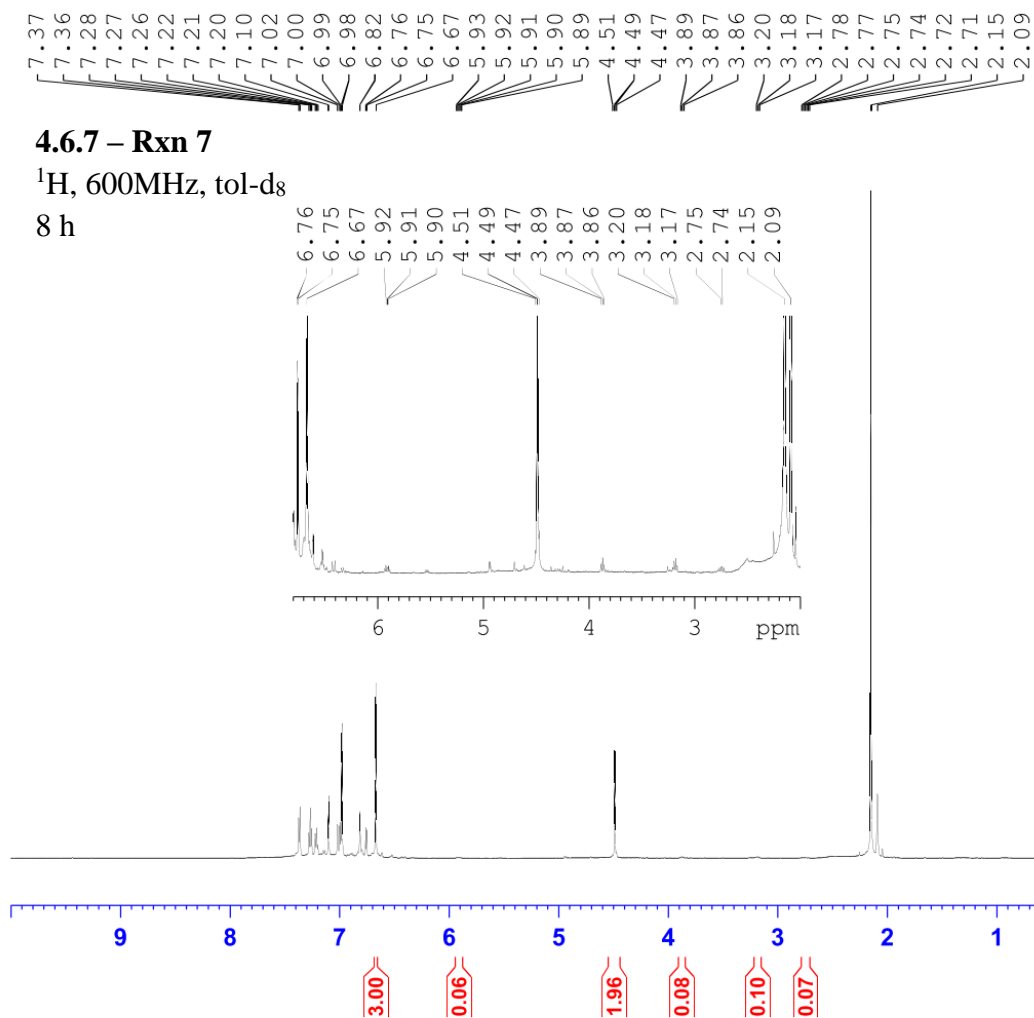


Current Data Parameters
NAME JAW-03-073
EXPNO 2
PROCNO 1

F2 - Acquisition Parameters
Date_ 20191121
Time 16.21
INSTRUM spect
PROBHD 5 mm PABBO BB-
PULPROG zg30
TD 65536
SOLVENT Tol
NS 16
DS 2
SWH 12335.526 Hz
FIDRES 0.188225 Hz
AQ 2.6563926 sec
RG 101
DW 40.533 usec
DE 6.50 usec
TE 295.2 K
D1 1.00000000 sec
TD0 1

===== CHANNEL f1 =====
NUC1 1H
P1 10.86 usec
PL1 -2.00 dB
PL1W 19.70630455 W
SFO1 600.7137096 MHz

F2 - Processing parameters
SI 32768
SF 600.7100217 MHz
WDW EM
SSB 0
LB 0.30 Hz
GB 0
PC 1.00



Current Data Parameters
 NAME JAW-03-073
 EXPNO 3
 PROCNO 1

F2 - Acquisition Parameters
 Date_ 20191121
 Time_ 22.44
 INSTRUM spect
 PROBHD 5 mm PABBO BB-
 PULPROG zg30
 TD 65536
 SOLVENT Tol
 NS 16
 DS 2
 SWH 12335.526 Hz
 FIDRES 0.188225 Hz
 AQ 2.6563926 sec
 RG 101
 DW 40.533 usec
 DE 6.50 usec
 TE 295.3 K
 D1 1.00000000 sec
 TD0 1

===== CHANNEL f1 =====
 NUC1 1H
 P1 10.86 usec
 PL1 -2.00 dB
 PL1W 19.70630455 W
 SFO1 600.7137096 MHz

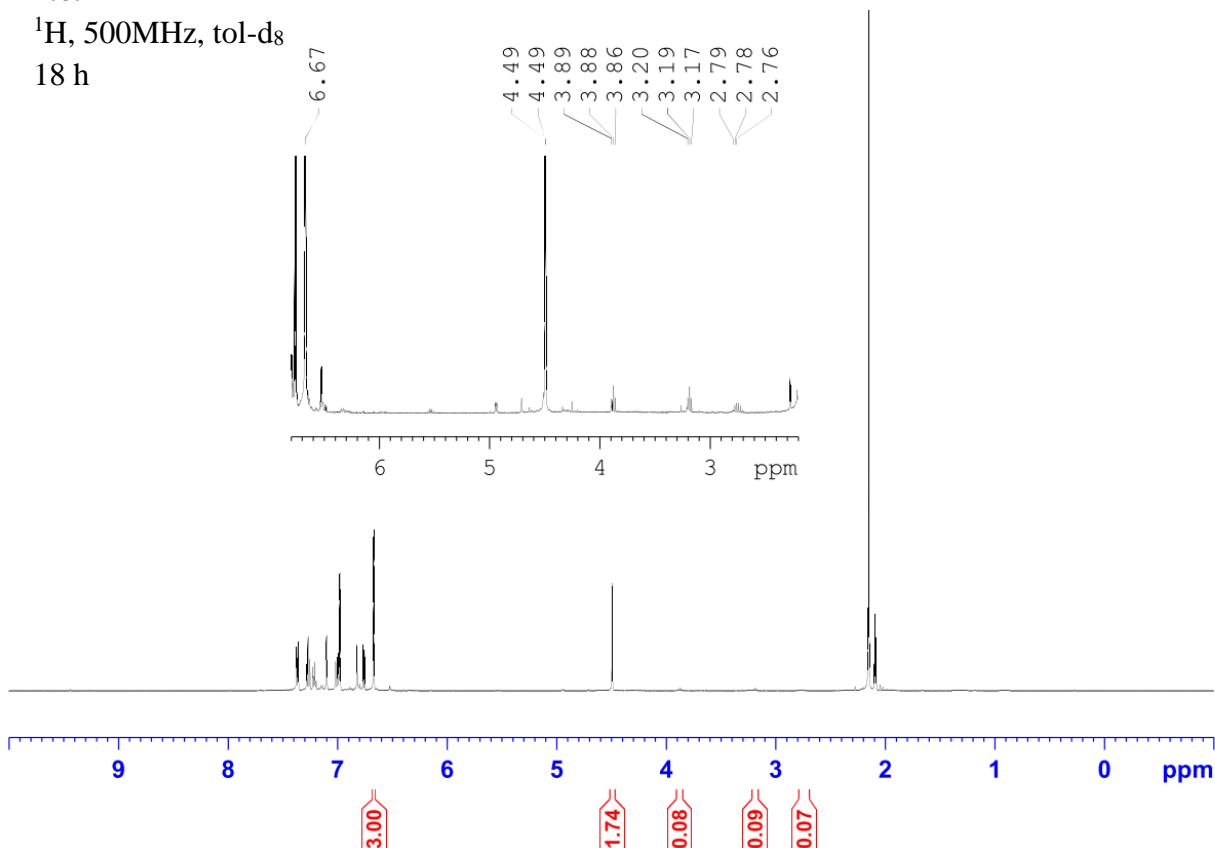
F2 - Processing parameters
 SI 32768
 SF 600.7100219 MHz
 WDW EM
 SSB 0
 LB 0.30 Hz
 GB 0
 PC 1.00

7.36
7.29
7.28
7.27
7.27
7.26
7.25
7.23
7.21
7.10
7.02
7.00
7.00
6.99
6.99
6.98
6.82
6.82
6.77
6.76
6.67
6.67
4.49
4.49
3.89
3.88
3.86
3.20
3.19
3.17
3.20
3.19
3.17
2.79
2.78
2.76
2.74
2.73
2.71
2.15
2.15
2.10
2.10
2.09
2.09
2.08

4.6.7 – Rxn 7

¹H, 500MHz, tol-d₈

18 h

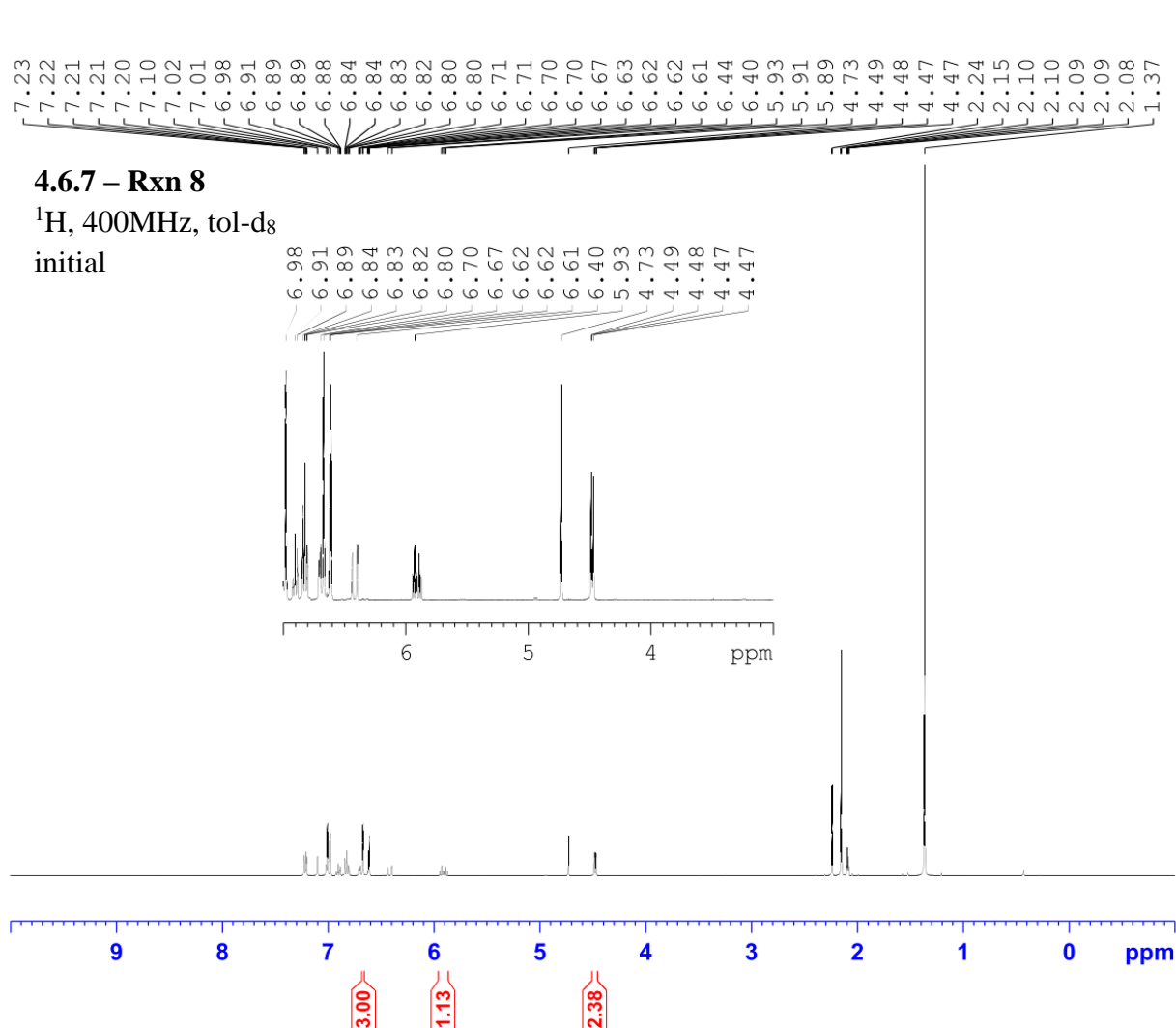


Current Data Parameters
NAME JAW-03-073
EXPNO 5
PROCNO 1

F2 - Acquisition Parameters
Date_ 20191122
Time_ 10.00
INSTRUM spect
PROBHD 5 mm PABBO BB/
PULPROG zg30
TD 65536
SOLVENT Tol
NS 16
DS 2
SWH 10000.000 Hz
FIDRES 0.152588 Hz
AQ 3.2767999 sec
RG 80.6
DW 50.000 usec
DE 6.50 usec
TE 297.3 K
D1 1.00000000 sec
TD0 1

===== CHANNEL f1 =====
SF01 500.1630887 MHz
NUC1 1H
P1 11.50 usec
PLW1 18.00000000 W

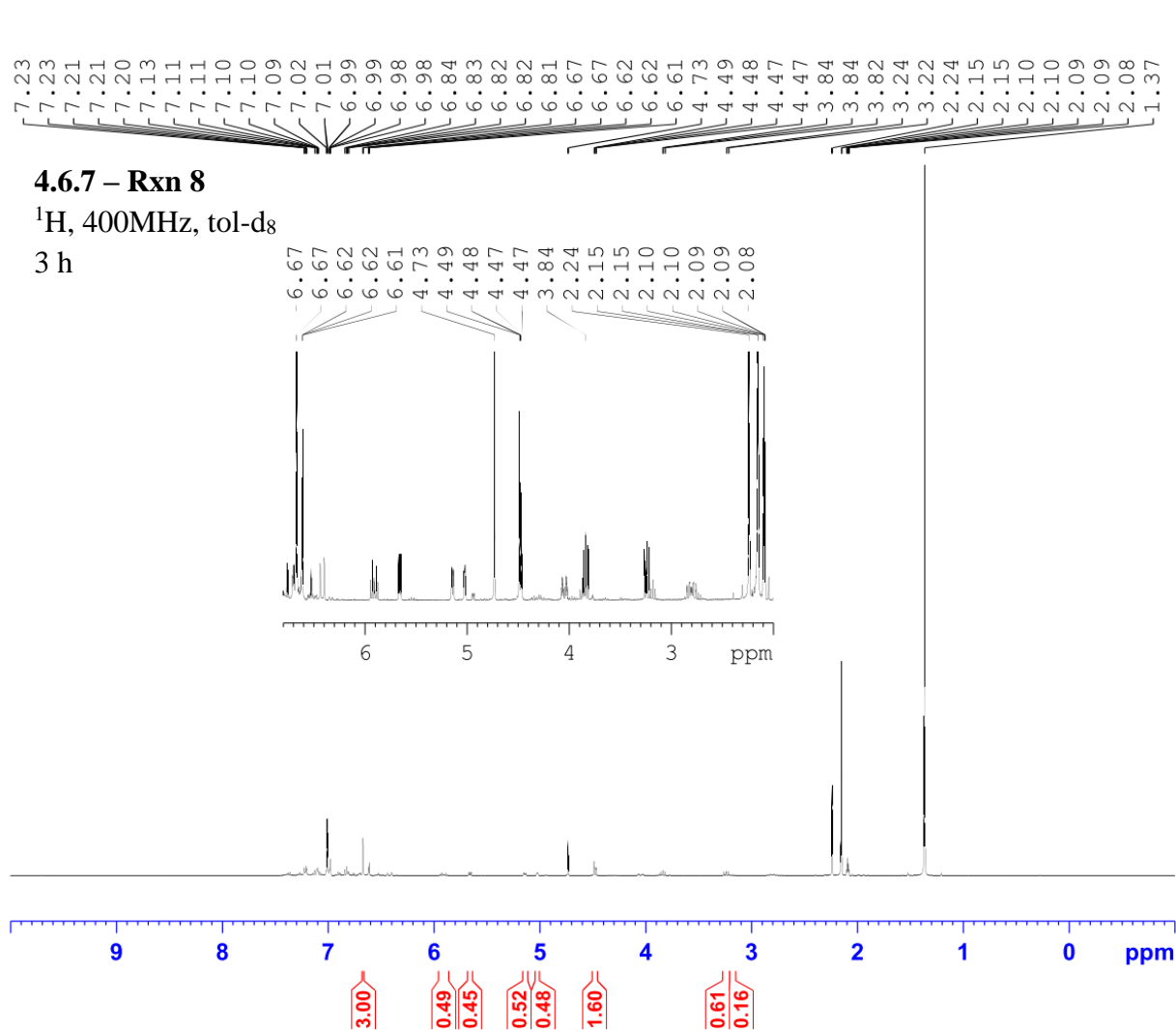
F2 - Processing parameters
SI 65536
SF 500.1600176 MHz
WDW EM
SSB 0
LB 0.30 Hz
GB 0
PC 1.00



Current Data Parameters
 NAME JAW-03-081
 EXPNO 1
 PROCNO 1

F2 - Acquisition Parameters
 Date_ 20191230
 Time_ 13.58 h
 INSTRUM spect
 PROBHD Z108618_0240 (
 PULPROG zg30
 TD 65536
 SOLVENT Tol
 NS 16
 DS 2
 SWH 8012.820 Hz
 FIDRES 0.244532 Hz
 AQ 4.0894465 sec
 RG 57
 DW 62.400 usec
 DE 6.50 usec
 TE 90.2 K
 D1 1.00000000 sec
 TD0 1
 SF01 400.1324708 MHz
 NUC1 1H
 P0 4.83 usec
 P1 14.50 usec
 PLW1 12.00000000 W

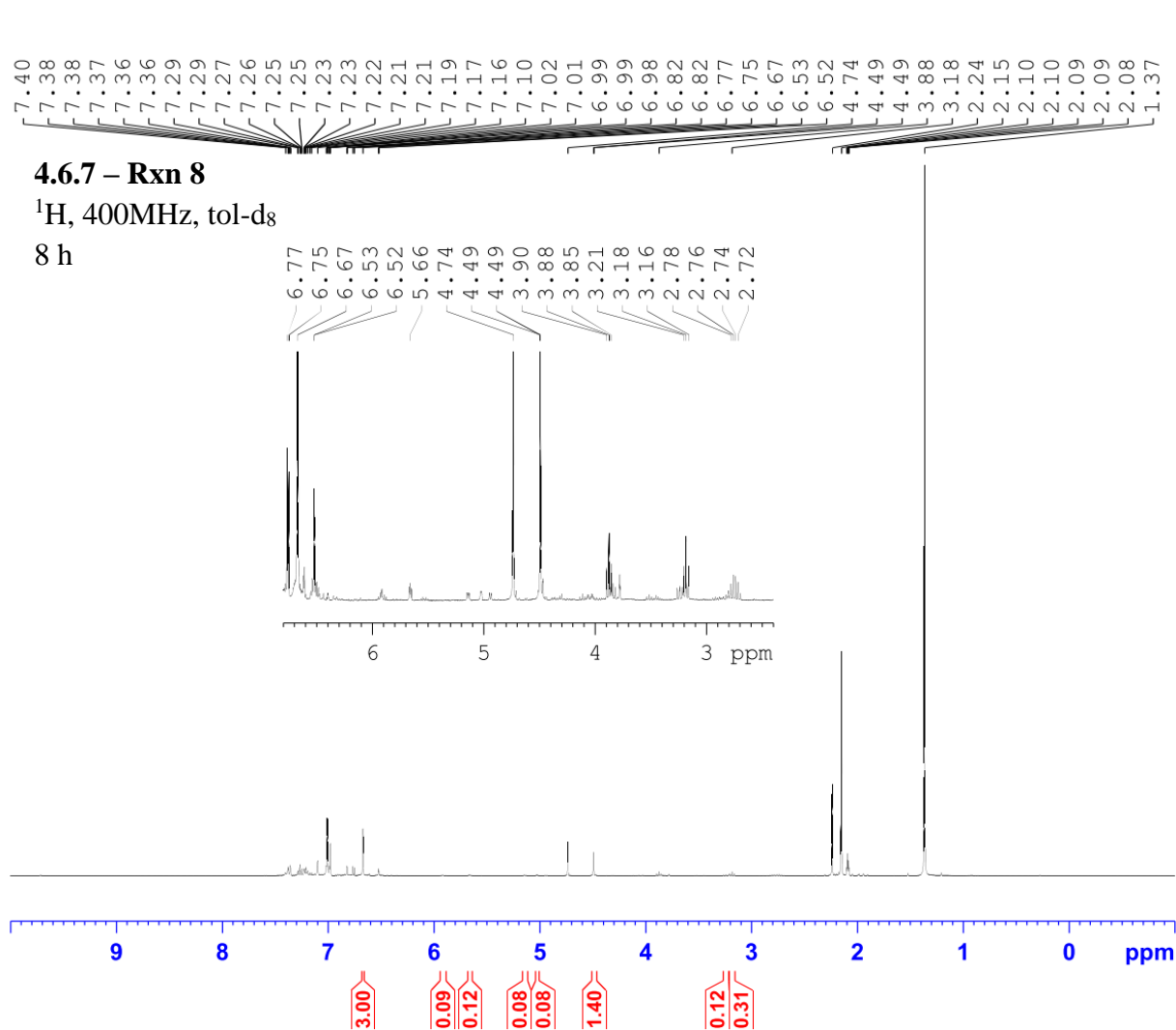
F2 - Processing parameters
 SI 65536
 SF 400.1300139 MHz
 WDW EM
 SSB 0
 LB 0.30 Hz
 GB 0
 PC 1.00



Current Data Parameters
 NAME JAW-03-081
 EXPNO 2
 PROCNO 1

F2 - Acquisition Parameters
 Date_ 20191230
 Time_ 17.48 h
 INSTRUM spect
 PROBHD Z108618_0240 (
 PULPROG zg30
 TD 65536
 SOLVENT Tol
 NS 16
 DS 2
 SWH 8012.820 Hz
 FIDRES 0.244532 Hz
 AQ 4.0894465 sec
 RG 57
 DW 62.400 usec
 DE 6.50 usec
 TE 90.1 K
 D1 1.00000000 sec
 TD0 1
 SFO1 400.1324708 MHz
 NUC1 1H
 P0 4.83 usec
 P1 14.50 usec
 PLW1 12.00000000 W

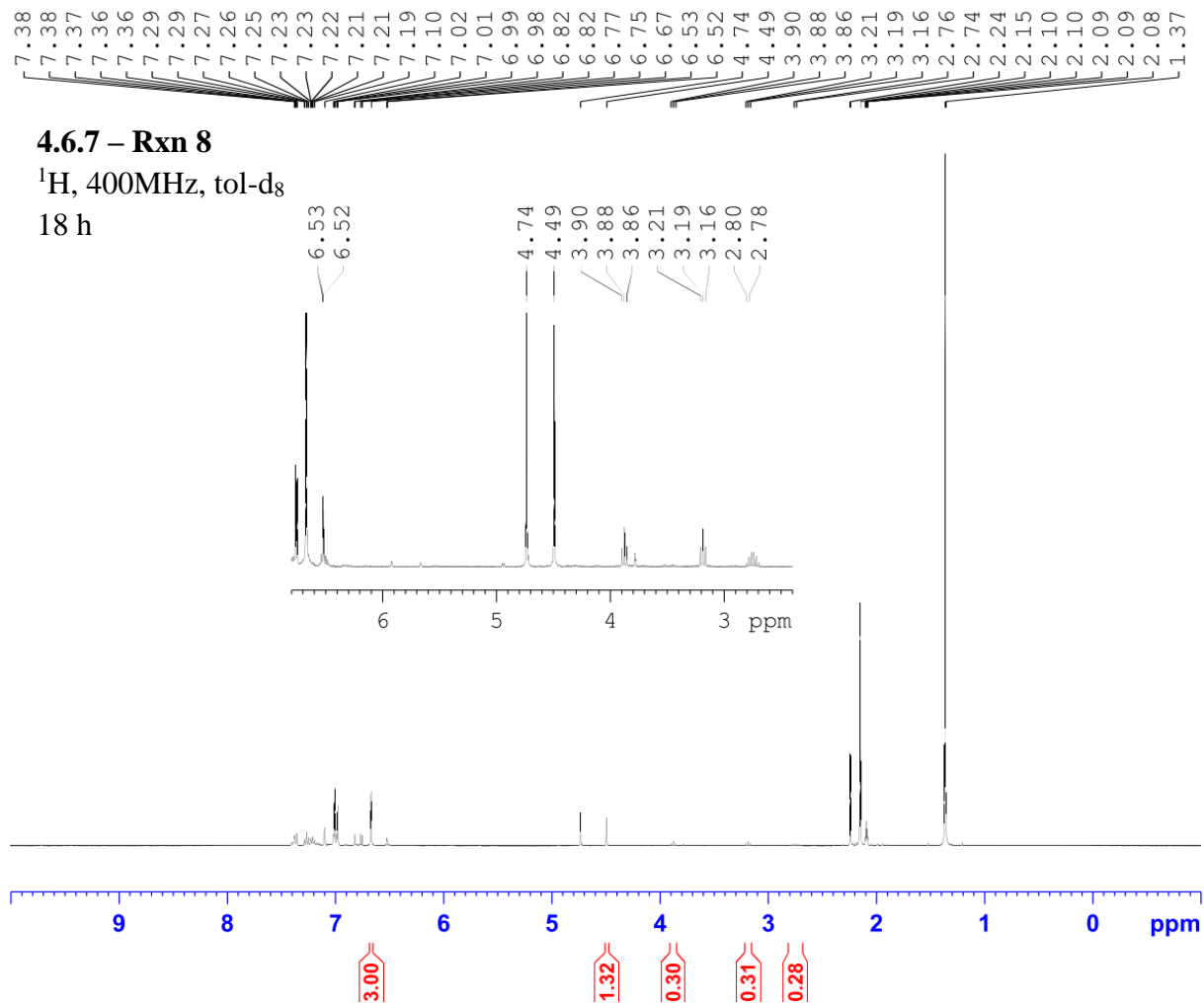
F2 - Processing parameters
 SI 65536
 SF 400.1300143 MHz
 WDW EM
 SSB 0
 LB 0.30 Hz
 GB 0
 PC 1.00



Current Data Parameters
 NAME JAW-03-081
 EXPNO 3
 PROCNO 1

F2 - Acquisition Parameters
 Date_ 20191230
 Time_ 23.54 h
 INSTRUM spect
 PROBHD z108618_0240 (
 PULPROG zg30
 TD 65536
 SOLVENT Tol
 NS 16
 DS 2
 SWH 8012.820 Hz
 FIDRES 0.244532 Hz
 AQ 4.0894465 sec
 RG 57
 DW 62.400 usec
 DE 6.50 usec
 TE 90.2 K
 D1 1.00000000 sec
 TD0 1
 SFO1 400.1324708 MHz
 NUC1 1H
 P0 4.83 usec
 P1 14.50 usec
 PLW1 12.00000000 W

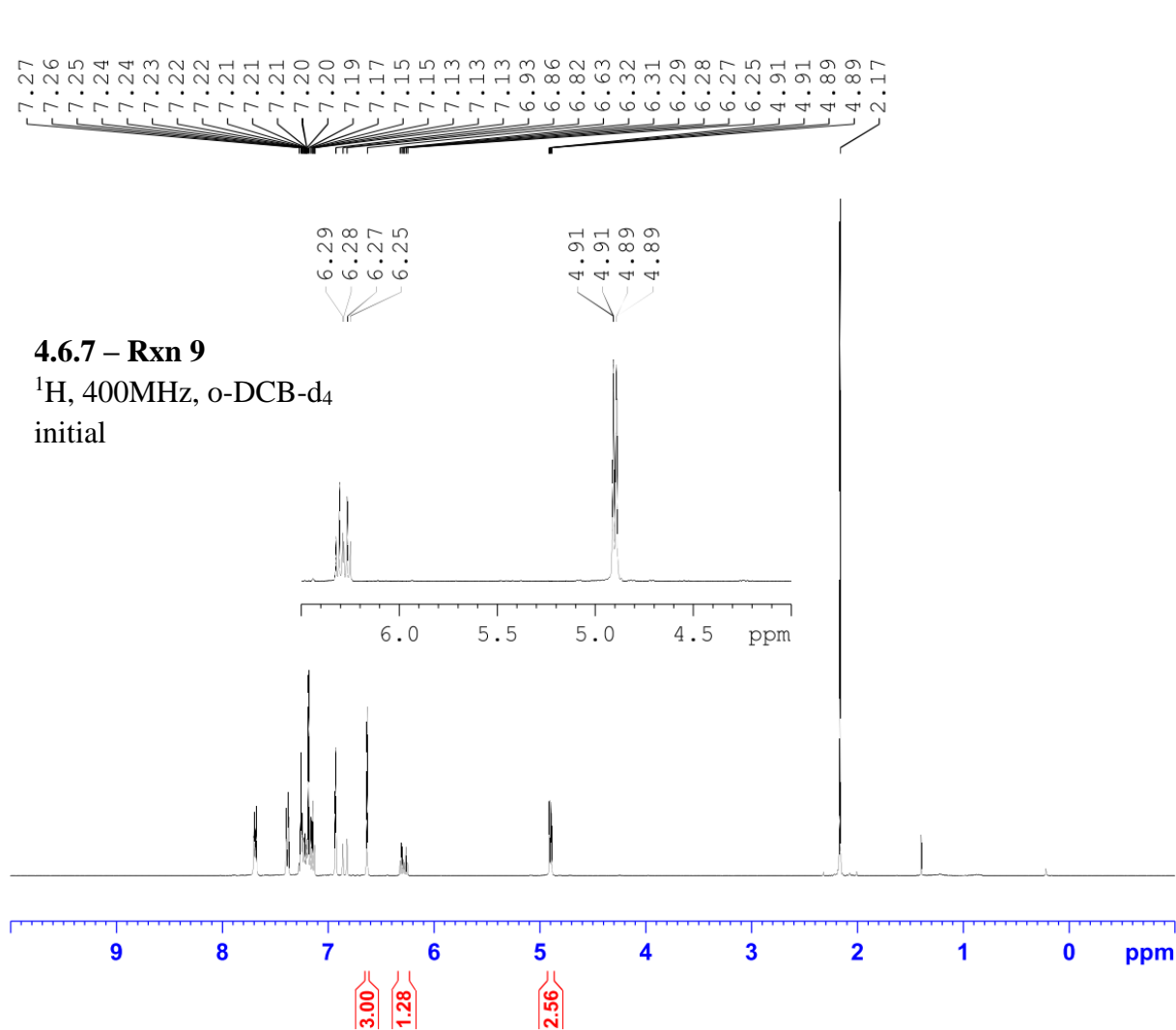
F2 - Processing parameters
 SI 65536
 SF 400.1300141 MHz
 WDW EM
 SSB 0
 LB 0.30 Hz
 GB 0
 PC 1.00



Current Data Parameters
 NAME JAW-03-081
 EXPNO 4
 PROCNO 1

F2 - Acquisition Parameters
 Date_ 20191231
 Time_ 11.23 h
 INSTRUM spect
 PROBHD Z108618_0240 (
 PULPROG zg30
 TD 65536
 SOLVENT Tol
 NS 16
 DS 2
 SWH 8012.820 Hz
 FIDRES 0.244532 Hz
 AQ 4.0894465 sec
 RG 57
 DW 62.400 usec
 DE 6.50 usec
 TE 91.3 K
 D1 1.00000000 sec
 TD0 1
 SFO1 400.1324708 MHz
 NUC1 1H
 P0 4.83 usec
 P1 14.50 usec
 PLW1 12.00000000 W

F2 - Processing parameters
 SI 65536
 SF 400.1300139 MHz
 WDW EM
 SSB 0
 LB 0.30 Hz
 GB 0
 PC 1.00

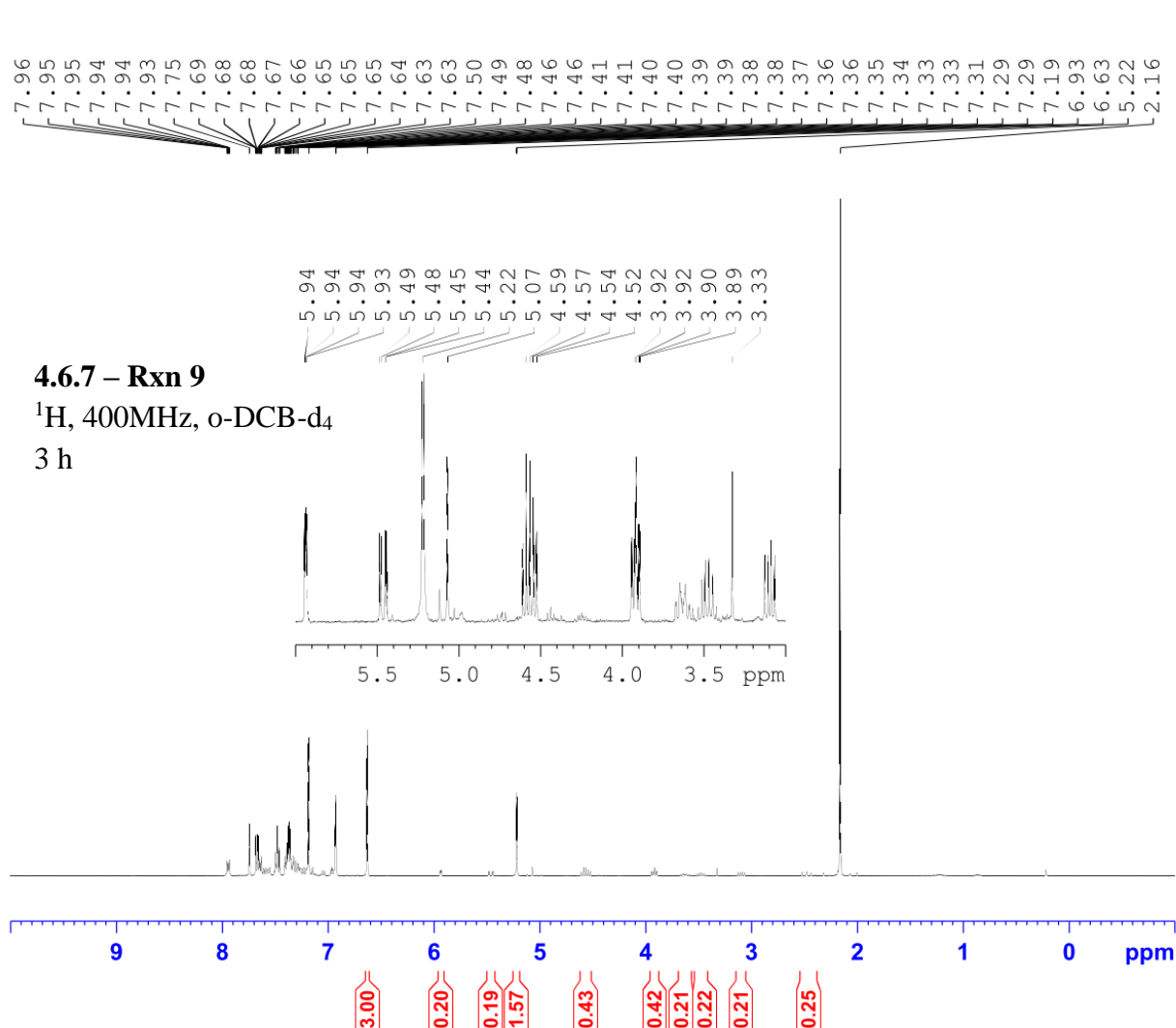


Current Data Parameters
 NAME JAW-03-109
 EXPNO 5
 PROCNO 1

F2 - Acquisition Parameters
 Date_ 20210419
 Time_ 9.36
 INSTRUM spect
 PROBHD 5 mm PADUL 13C
 PULPROG zg30
 TD 65536
 SOLVENT oC6D4Cl2
 NS 16
 DS 2
 SWH 8223.685 Hz
 FIDRES 0.125483 Hz
 AQ 3.9845889 sec
 RG 114
 DW 60.800 usec
 DE 6.50 usec
 TE 295.1 K
 D1 2.00000000 sec
 TD0 1

===== CHANNEL f1 =====
 NUC1 1H
 P1 9.31 usec
 PL1 -3.90 dB
 PL1W 21.64248466 W
 SFO1 400.2324716 MHz

F2 - Processing parameters
 SI 32768
 SF 400.2300667 MHz
 WDW EM
 SSB 0
 LB 0.30 Hz
 GB 0
 PC 1.00

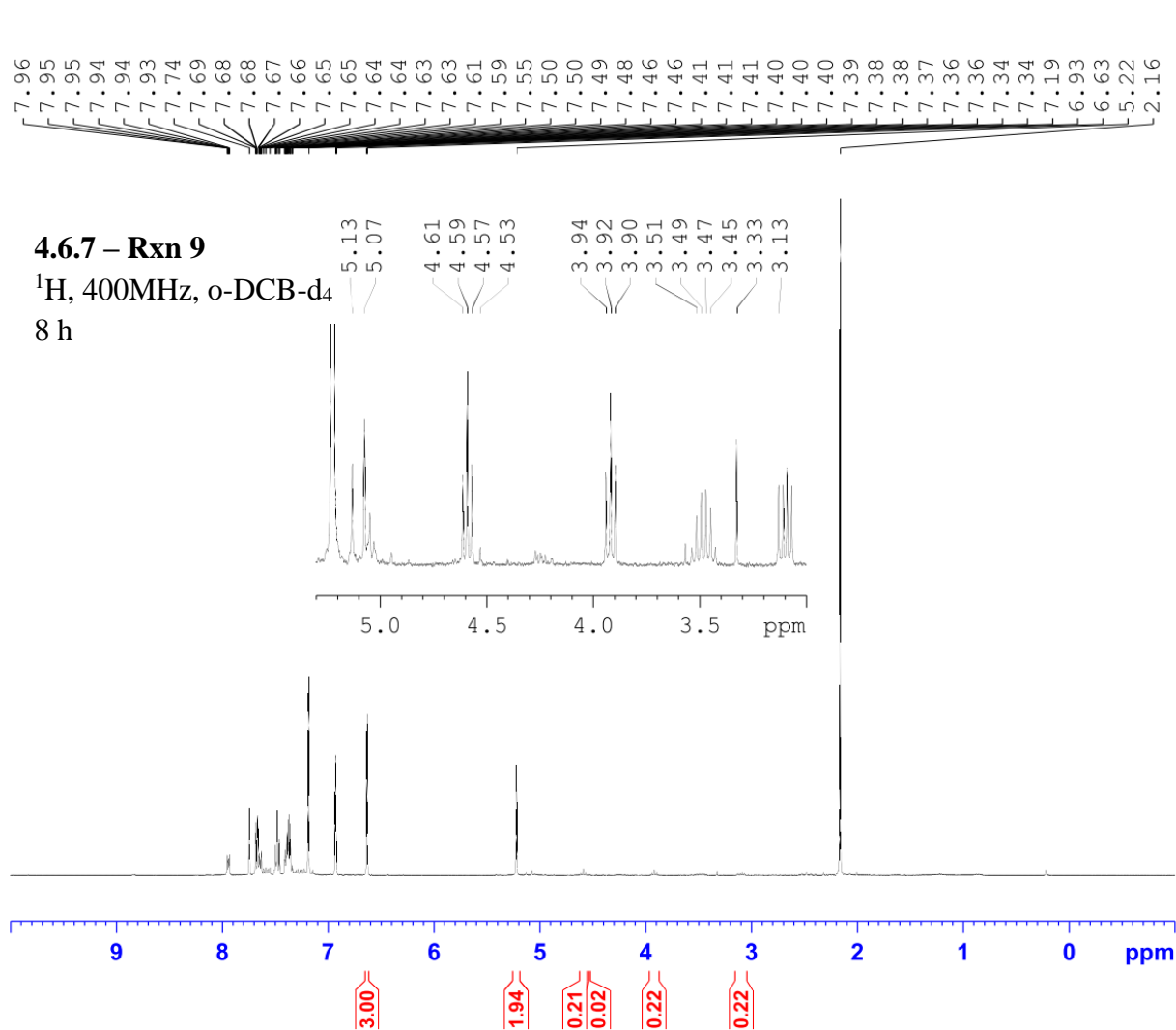


Current Data Parameters
 NAME JAW-03-109
 EXPNO 6
 PROCNO 1

F2 - Acquisition Parameters
 Date_ 20210419
 Time_ 12.55
 INSTRUM spect
 PROBHD 5 mm PADUL 13C
 PULPROG zg30
 TD 65536
 SOLVENT oC6D4Cl2
 NS 16
 DS 2
 SWH 8223.685 Hz
 FIDRES 0.125483 Hz
 AQ 3.9845889 sec
 RG 114
 DW 60.800 usec
 DE 6.50 usec
 TE 295.1 K
 D1 2.00000000 sec
 TD0 1

===== CHANNEL f1 =====
 NUC1 1H
 P1 9.31 usec
 PL1 -3.90 dB
 PL1W 21.64248466 W
 SF01 400.2324716 MHz

F2 - Processing parameters
 SI 32768
 SF 400.2299657 MHz
 WDW EM
 SSB 0
 LB 0.30 Hz
 GB 0
 PC 1.00

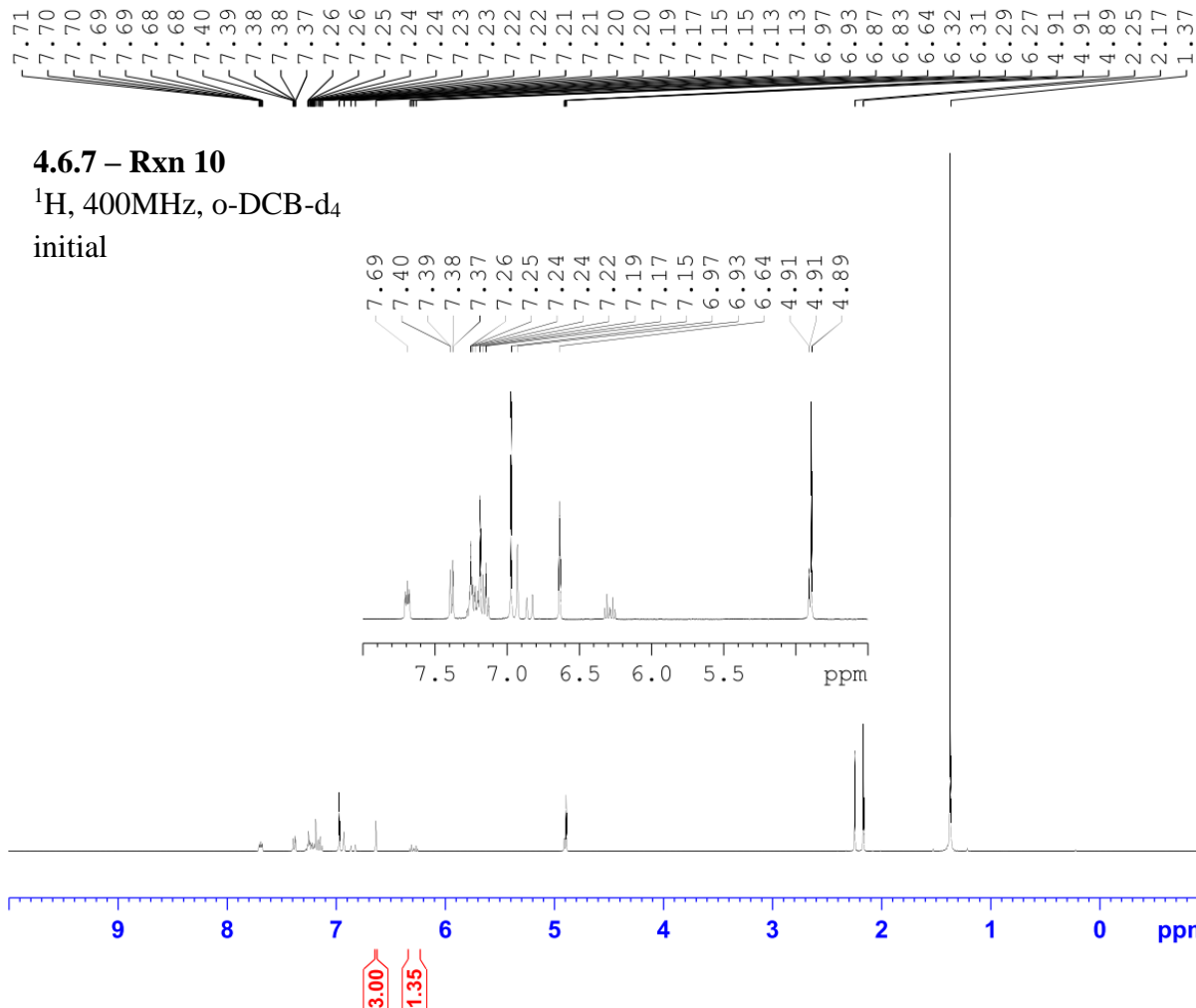


Current Data Parameters
 NAME JAW-03-109
 EXPNO 7
 PROCNO 1

F2 - Acquisition Parameters
 Date_ 20210419
 Time_ 22.30
 INSTRUM spect
 PROBHD 5 mm PADUL 13C
 PULPROG zg30
 TD 65536
 SOLVENT oC6D4Cl2
 NS 16
 DS 2
 SWH 8223.685 Hz
 FIDRES 0.125483 Hz
 AQ 3.9845889 sec
 RG 114
 DW 60.800 usec
 DE 6.50 usec
 TE 295.4 K
 D1 2.00000000 sec
 TD0 1

===== CHANNEL f1 =====
 NUC1 1H
 P1 9.31 usec
 PL1 -3.90 dB
 PL1W 21.64248466 W
 SFO1 400.2324716 MHz

F2 - Processing parameters
 SI 32768
 SF 400.2300665 MHz
 WDW EM
 SSB 0
 LB 0.30 Hz
 GB 0
 PC 1.00

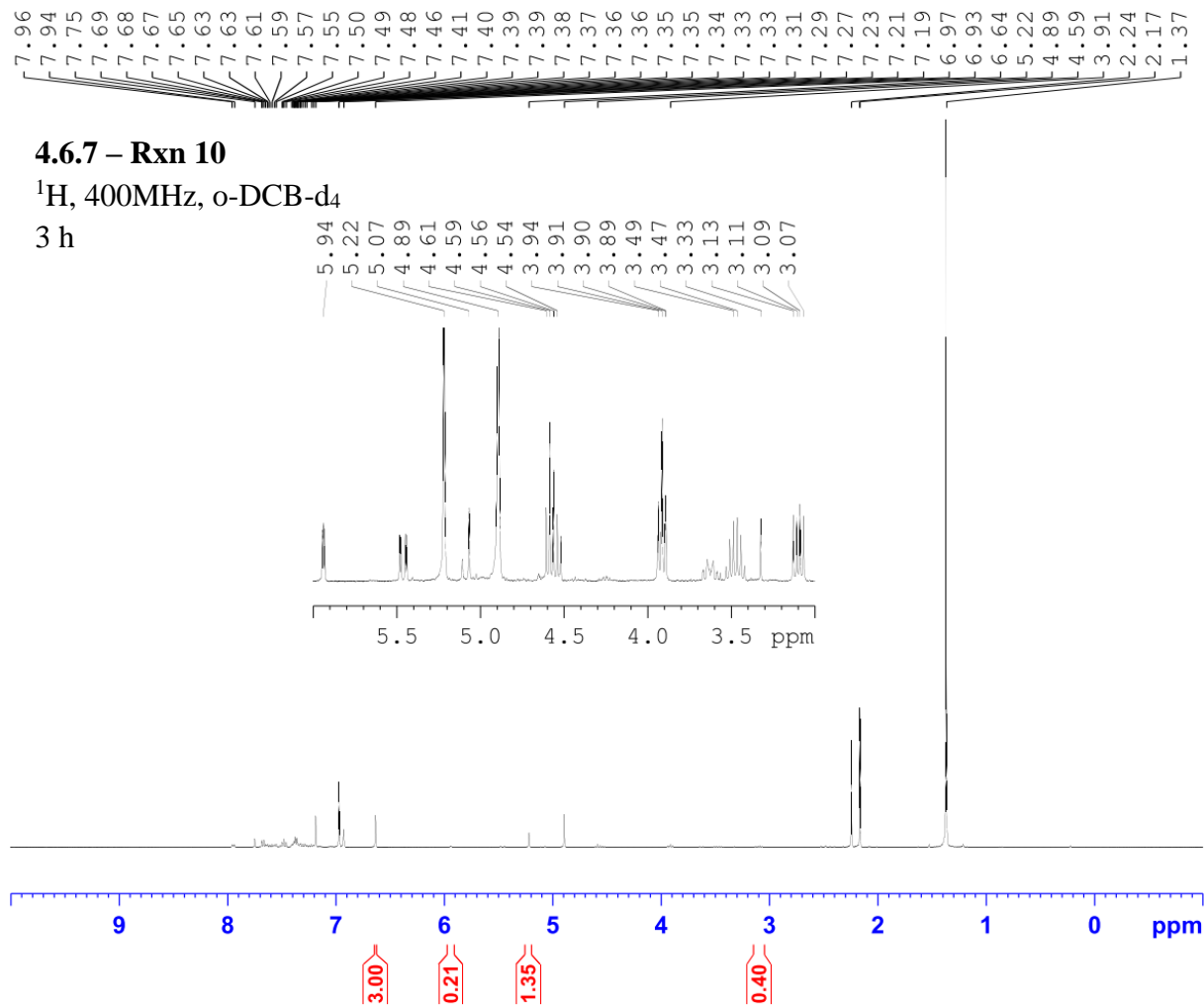


Current Data Parameters
 NAME JAW-03-110
 EXPNO 1
 PROCNO 1

F2 - Acquisition Parameters
 Date_ 20210421
 Time_ 9.47
 INSTRUM spect
 PROBHD 5 mm PADUL 13C
 PULPROG zg30
 TD 65536
 SOLVENT oC6D4Cl2
 NS 16
 DS 2
 SWH 8223.685 Hz
 FIDRES 0.125483 Hz
 AQ 3.9845889 sec
 RG 71.8
 DW 60.800 usec
 DE 6.50 usec
 TE 295.0 K
 D1 2.00000000 sec
 TD0 1

===== CHANNEL f1 =====
 NUC1 1H
 P1 9.31 usec
 PL1 -3.90 dB
 PL1W 21.64248466 W
 SFO1 400.2324716 MHz

F2 - Processing parameters
 SI 32768
 SF 400.2299650 MHz
 WDW EM
 SSB 0
 LB 0.30 Hz
 GB 0
 PC 1.00

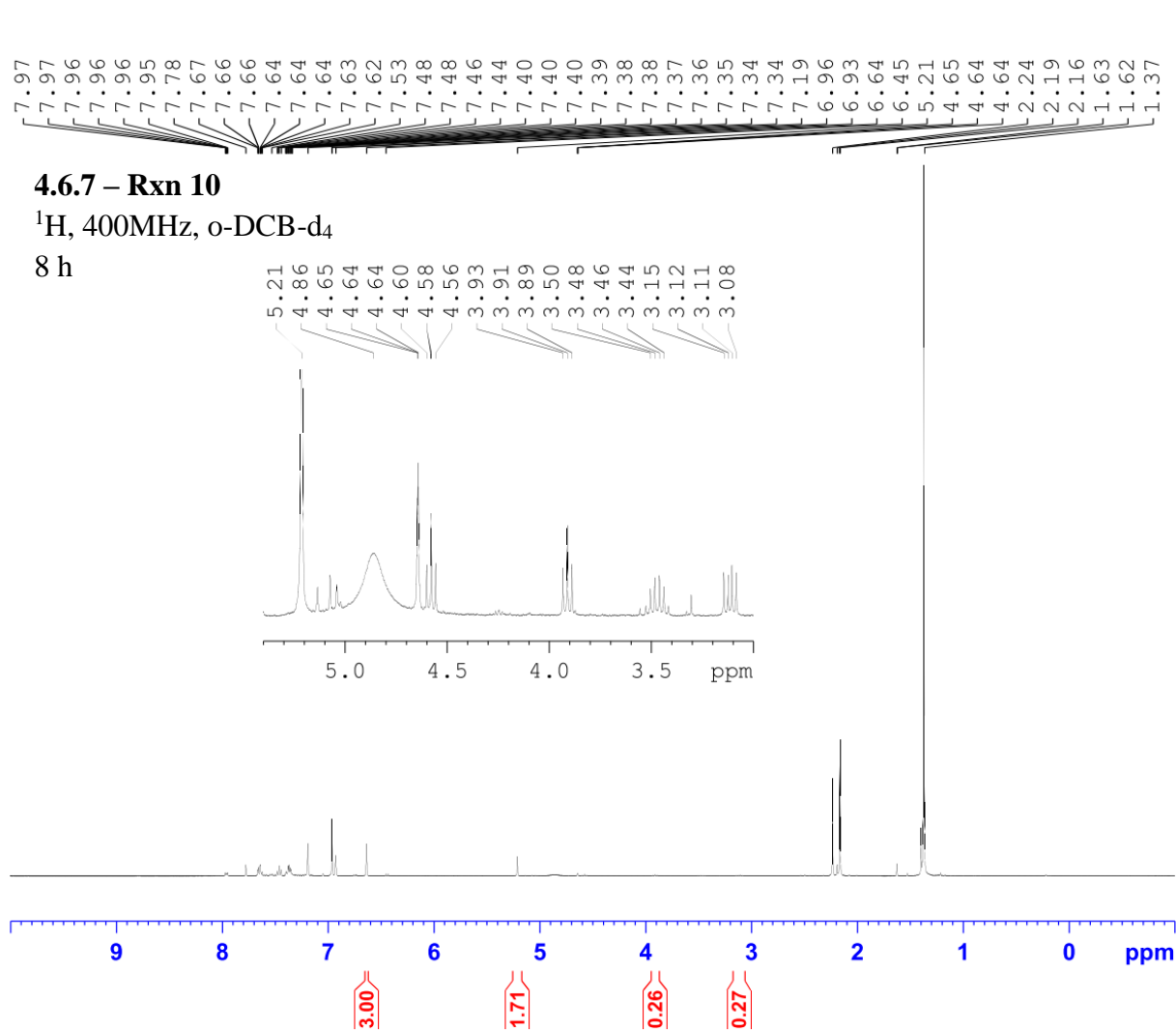


Current Data Parameters
 NAME JAW-03-110
 EXPNO 2
 PROCNO 1

F2 - Acquisition Parameters
 Date_ 20210421
 Time_ 13.01
 INSTRUM spect
 PROBHD 5 mm PADUL 13C
 PULPROG zg30
 TD 65536
 SOLVENT oC6D4Cl2
 NS 16
 DS 2
 SWH 8223.685 Hz
 FIDRES 0.125483 Hz
 AQ 3.9845889 sec
 RG 71.8
 DW 60.800 usec
 DE 6.50 usec
 TE 295.1 K
 D1 2.00000000 sec
 TD0 1

===== CHANNEL f1 =====
 NUC1 1H
 P1 9.31 usec
 PL1 -3.90 dB
 PL1W 21.64248466 W
 SFO1 400.2324716 MHz

F2 - Processing parameters
 SI 32768
 SF 400.2299652 MHz
 WDW EM
 SSB 0
 LB 0.30 Hz
 GB 0
 PC 1.00



Current Data Parameters
 NAME JAW-03-110
 EXPNO 3
 PROCNO 1

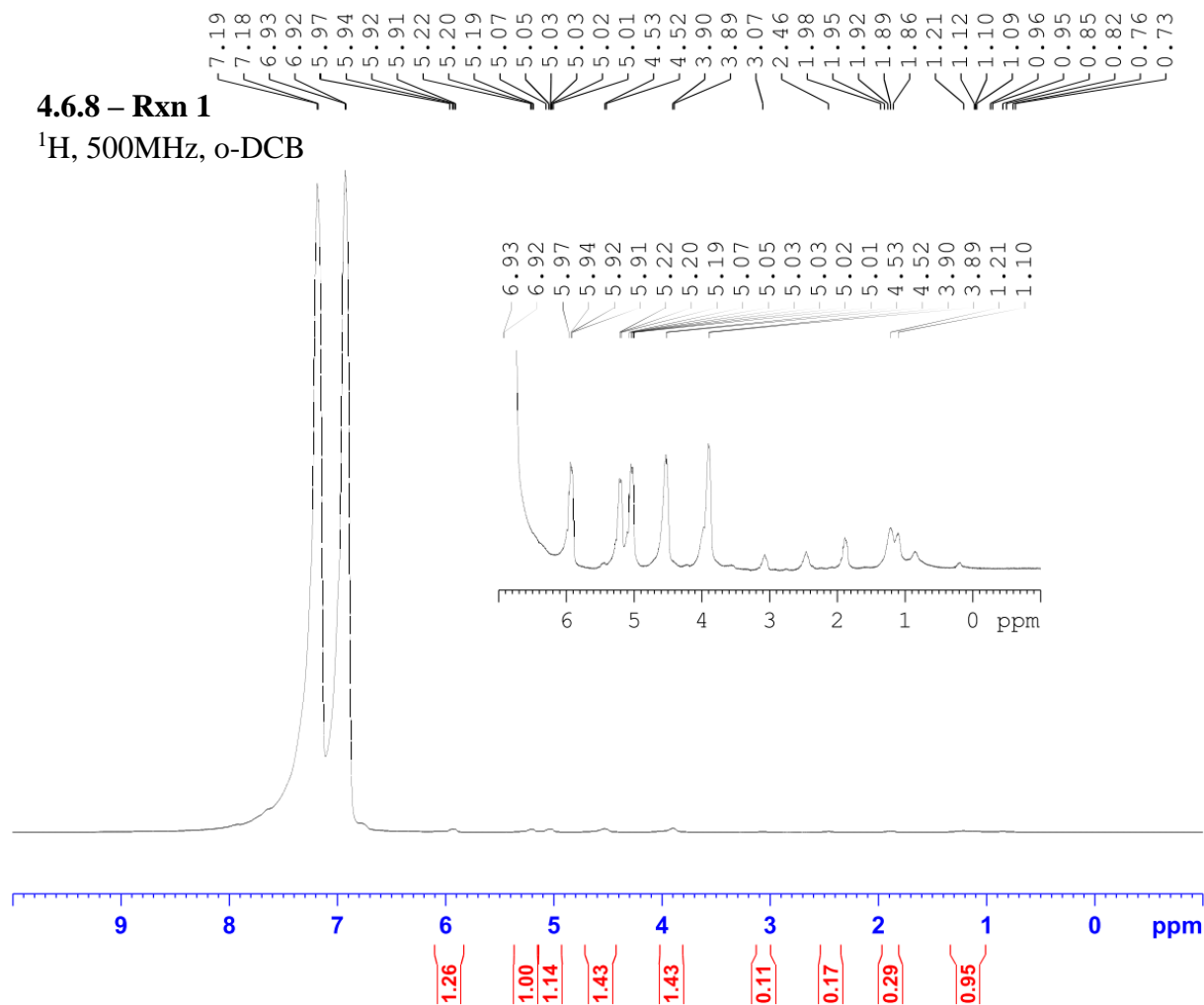
F2 - Acquisition Parameters
 Date_ 20210422
 Time_ 8.04
 INSTRUM spect
 PROBHD 5 mm PADUL 13C
 PULPROG zg30
 TD 65536
 SOLVENT oC6D4Cl2
 NS 16
 DS 2
 SWH 8223.685 Hz
 FIDRES 0.125483 Hz
 AQ 3.9845889 sec
 RG 71.8
 DW 60.800 usec
 DE 6.50 usec
 TE 312.2 K
 D1 2.00000000 sec
 TD0 1

===== CHANNEL f1 =====
 NUC1 1H
 P1 9.31 usec
 PL1 -3.90 dB
 PL1W 21.64248466 W
 SFO1 400.2324716 MHz

F2 - Processing parameters
 SI 32768
 SF 400.2299629 MHz
 WDW EM
 SSB 0
 LB 0.30 Hz
 GB 0
 PC 1.00

4.6.8 – Rxn 1

¹H, 500MHz, o-DCB

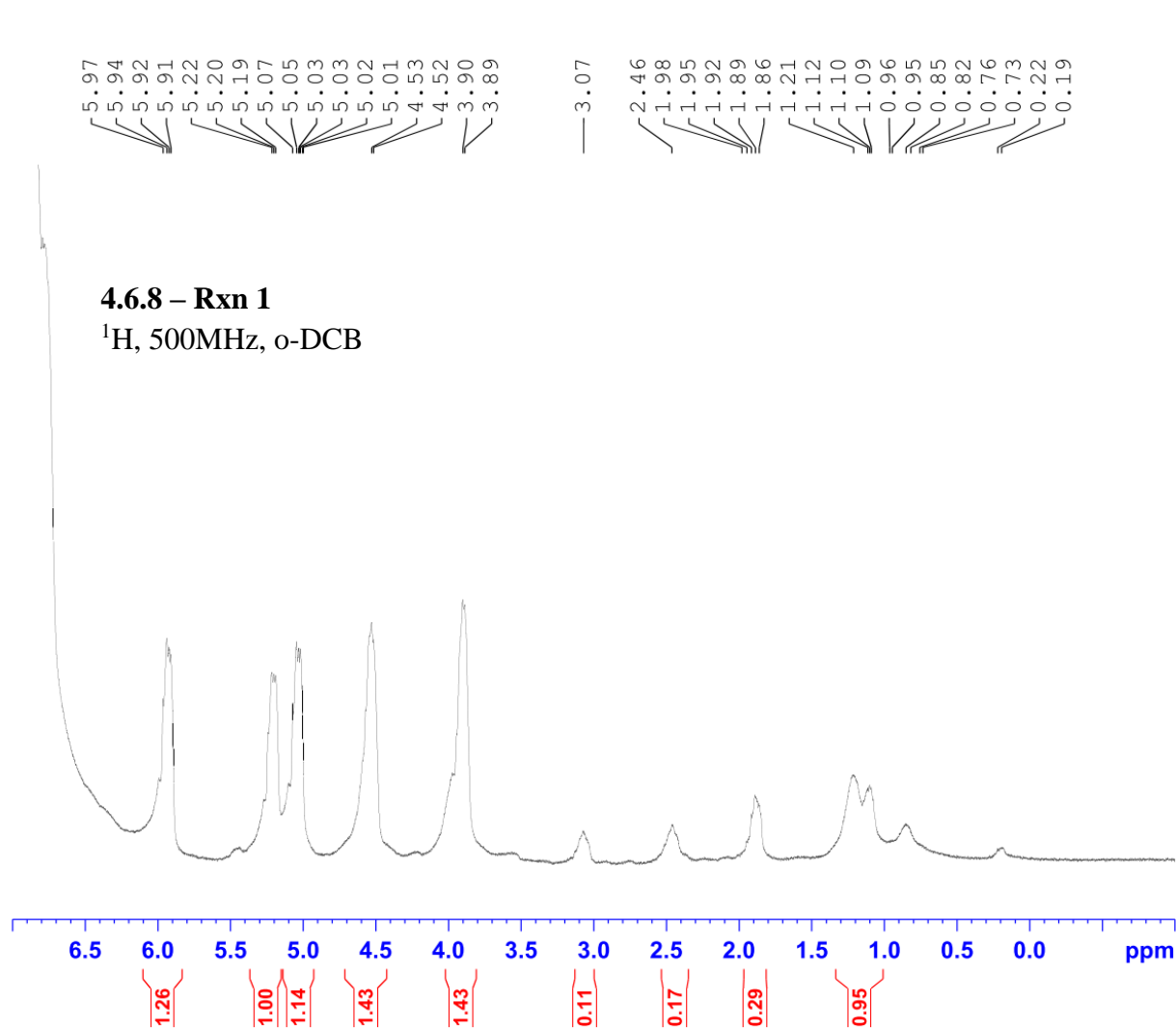


Current Data Parameters
NAME JAW-01-143
EXPNO 2
PROCNO 1

F2 - Acquisition Parameters
Date_ 20170831
Time_ 17.21
INSTRUM spect
PROBHD 5 mm PABBO BB/
PULPROG zg30
TD 65536
SOLVENT None
NS 16
DS 2
SWH 10000.000 Hz
FIDRES 0.152588 Hz
AQ 3.2767999 sec
RG 6.35
DW 50.000 usec
DE 6.50 usec
TE 296.1 K
D1 1.00000000 sec
TD0 1

===== CHANNEL f1 =====
SF01 500.1630887 MHz
NUC1 1H
P1 11.50 usec
PLW1 18.00000000 W

F2 - Processing parameters
SI 65536
SF 500.1597941 MHz
WDW EM
SSB 0
LB 0.30 Hz
GB 0
PC 1.00

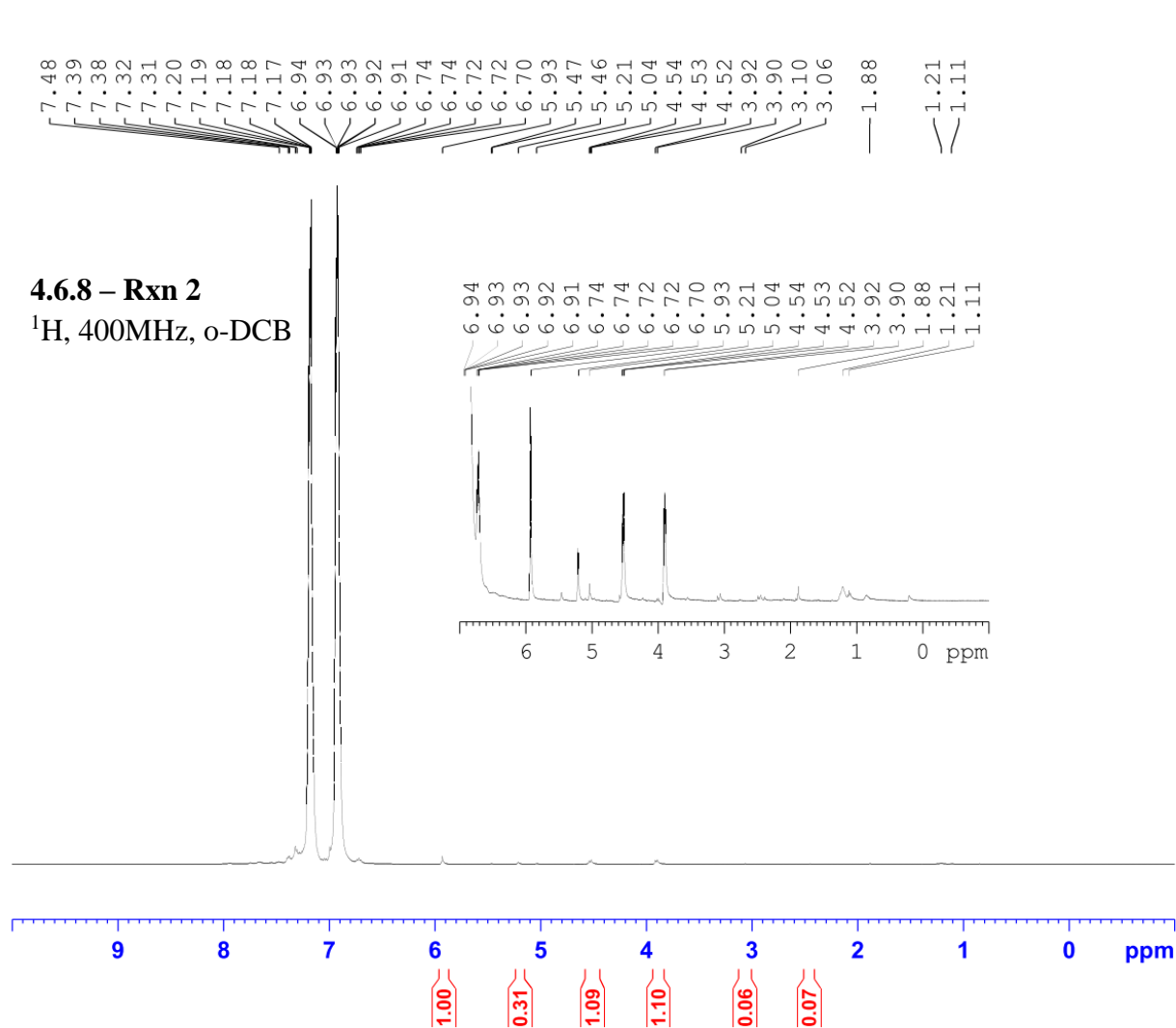


Current Data Parameters
NAME JAW-01-143
EXPNO 2
PROCNO 1

F2 - Acquisition Parameters
Date_ 20170831
Time_ 17.21
INSTRUM spect
PROBHD 5 mm PABBO BB/
PULPROG zg30
TD 65536
SOLVENT None
NS 16
DS 2
SWH 10000.000 Hz
FIDRES 0.152588 Hz
AQ 3.2767999 sec
RG 6.35
DW 50.000 usec
DE 6.50 usec
TE 296.1 K
D1 1.00000000 sec
TD0 1

===== CHANNEL f1 =====
SF01 500.1630887 MHz
NUC1 1H
P1 11.50 usec
PLW1 18.00000000 W

F2 - Processing parameters
SI 65536
SF 500.1597941 MHz
WDW EM
SSB 0
LB 0.30 Hz
GB 0
PC 1.00

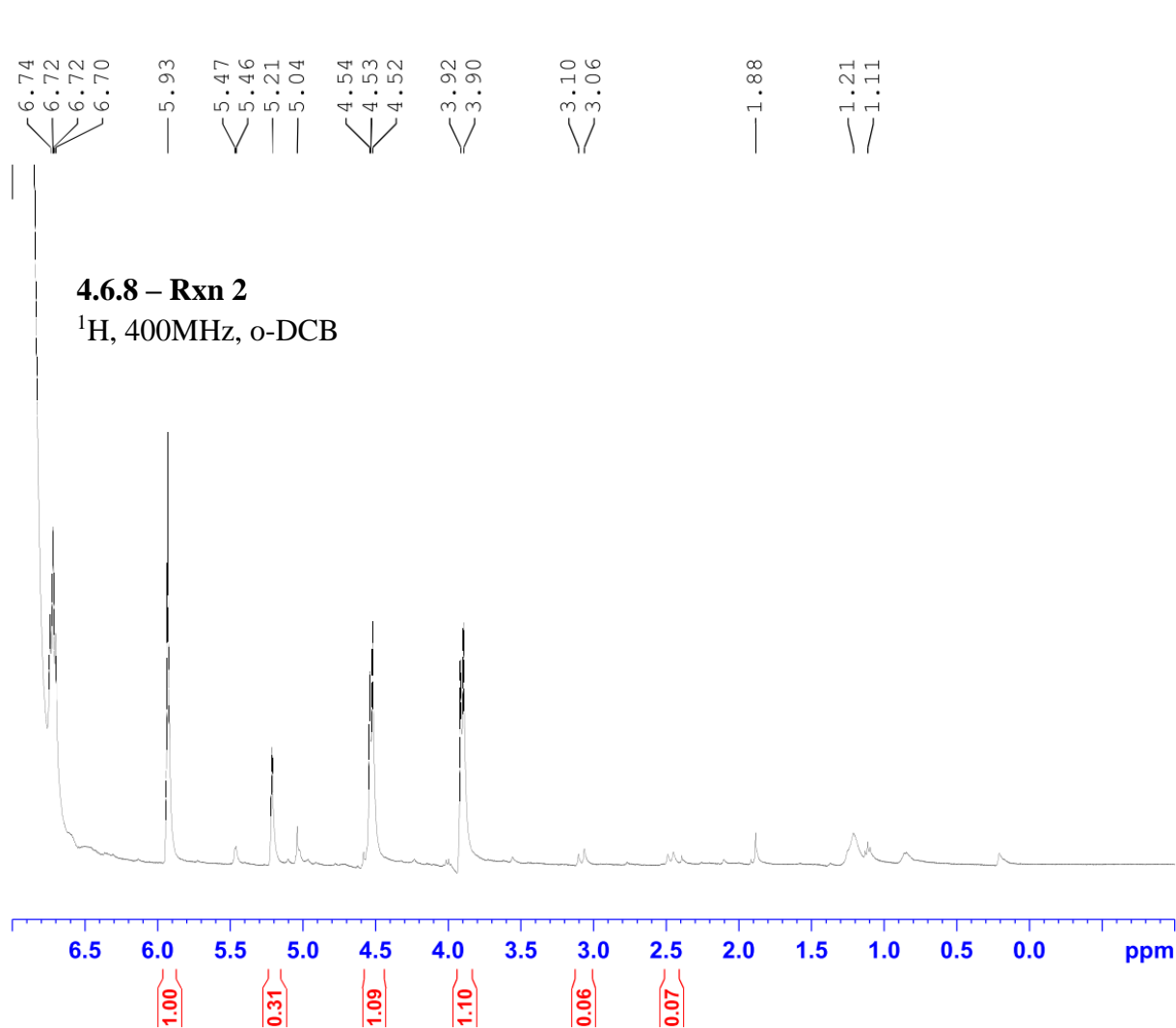


Current Data Parameters
NAME JAW-01-149
EXPNO 1
PROCNO 1

F2 - Acquisition Parameters
Date_ 20170913
Time 14.02
INSTRUM spect
PROBHD 5 mm PABBO BB-
PULPROG zg30
TD 65536
SOLVENT CDCl3
NS 32
DS 2
SWH 8012.820 Hz
FIDRES 0.122266 Hz
AQ 4.0894465 sec
RG 6.35
DW 62.400 usec
DE 6.50 usec
TE 3030.7 K
D1 1.00000000 sec
TD0 1

===== CHANNEL f1 =====
SF01 400.1324710 MHz
NUC1 1H
P1 13.75 usec
PLW1 12.01700020 W

F2 - Processing parameters
SI 65536
SF 400.1305116 MHz
WDW EM
SSB 0
LB 0.30 Hz
GB 0
PC 1.00

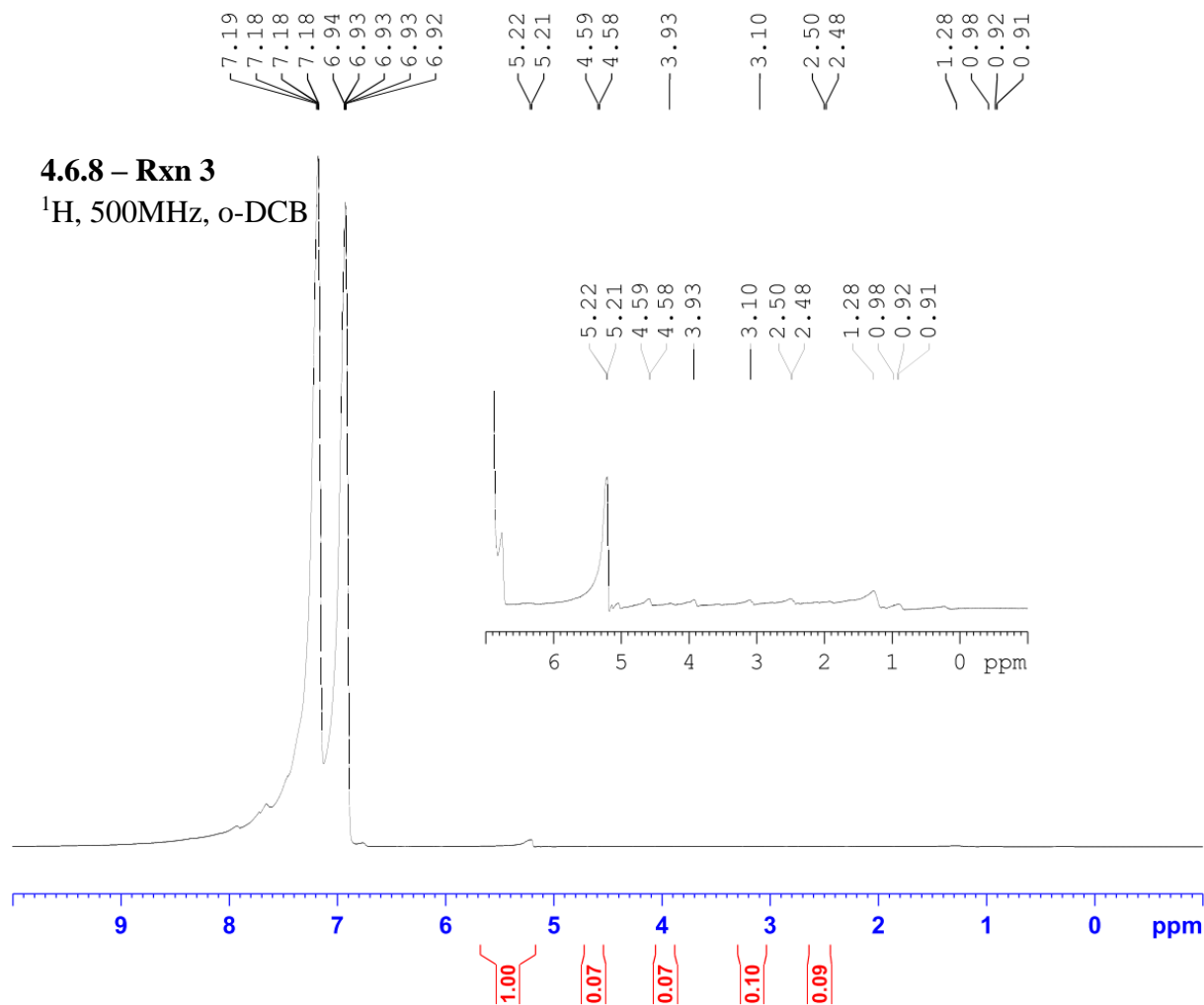


Current Data Parameters
 NAME JAW-01-149
 EXPNO 1
 PROCNO 1

F2 - Acquisition Parameters
 Date_ 20170913
 Time_ 14.02
 INSTRUM spect
 PROBHD 5 mm PABBO BB-
 PULPROG zg30
 TD 65536
 SOLVENT CDC13
 NS 32
 DS 2
 SWH 8012.820 Hz
 FIDRES 0.122266 Hz
 AQ 4.0894465 sec
 RG 6.35
 DW 62.400 usec
 DE 6.50 usec
 TE 3030.7 K
 D1 1.00000000 sec
 TD0 1

===== CHANNEL f1 =====
 SF01 400.1324710 MHz
 NUC1 1H
 P1 13.75 usec
 PLW1 12.01700020 W

F2 - Processing parameters
 SI 65536
 SF 400.1305116 MHz
 WDW EM
 SSB 0
 LB 0.30 Hz
 GB 0
 PC 1.00

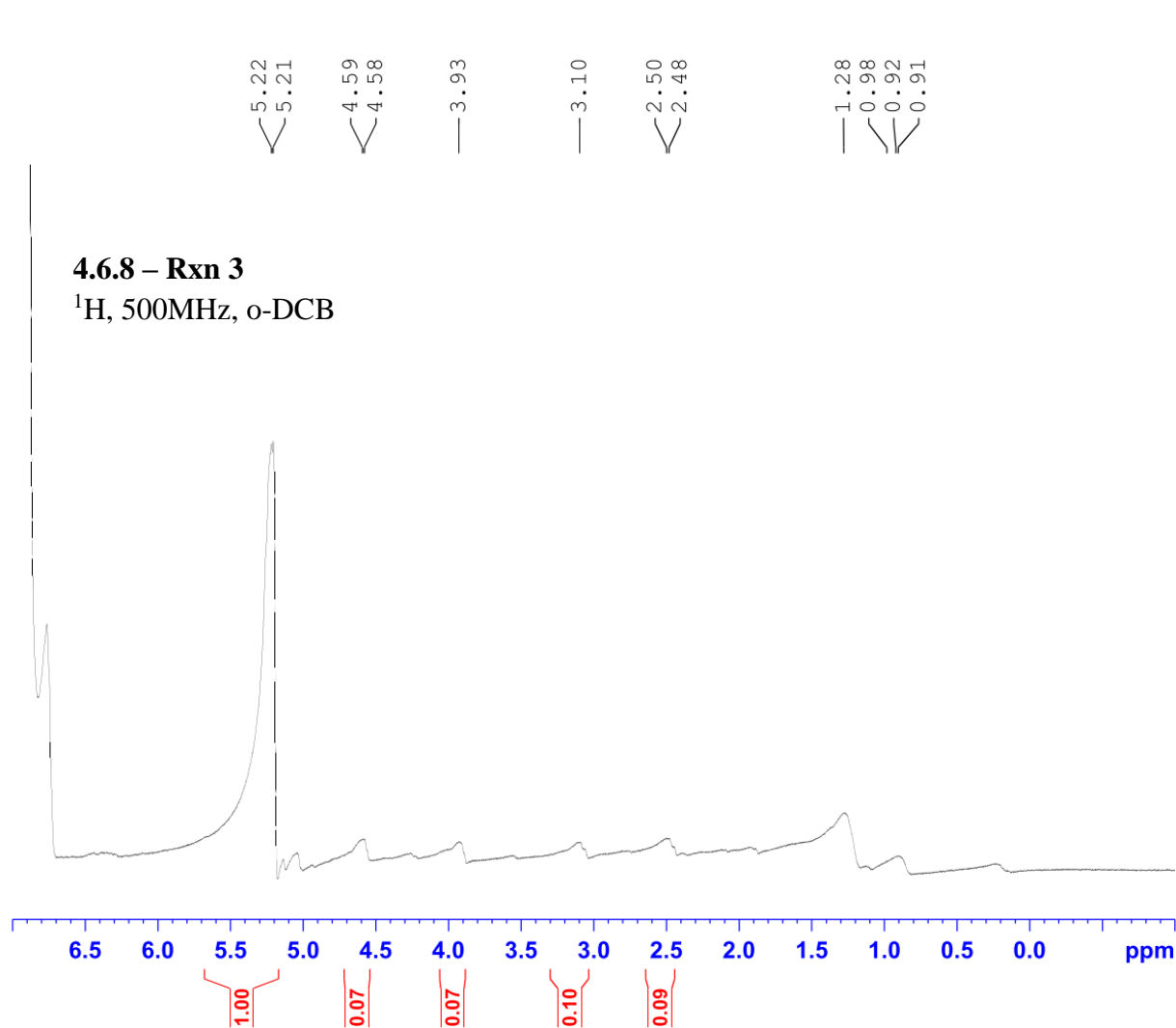


Current Data Parameters
NAME JAW-01-150
EXPNO 1
PROCNO 1

F2 - Acquisition Parameters
Date_ 20170914
Time_ 16.41
INSTRUM spect
PROBHD 5 mm PABBO BB/
PULPROG zg30
TD 65536
SOLVENT None
NS 32
DS 2
SWH 10000.000 Hz
FIDRES 0.152588 Hz
AQ 3.2767999 sec
RG 5.6
DW 50.000 usec
DE 6.50 usec
TE 296.2 K
D1 1.00000000 sec
TD0 1

===== CHANNEL f1 =====
SF01 500.1630887 MHz
NUC1 1H
P1 11.50 usec
PLW1 18.00000000 W

F2 - Processing parameters
SI 65536
SF 500.1597985 MHz
WDW EM
SSB 0
LB 0.30 Hz
GB 0
PC 1.00

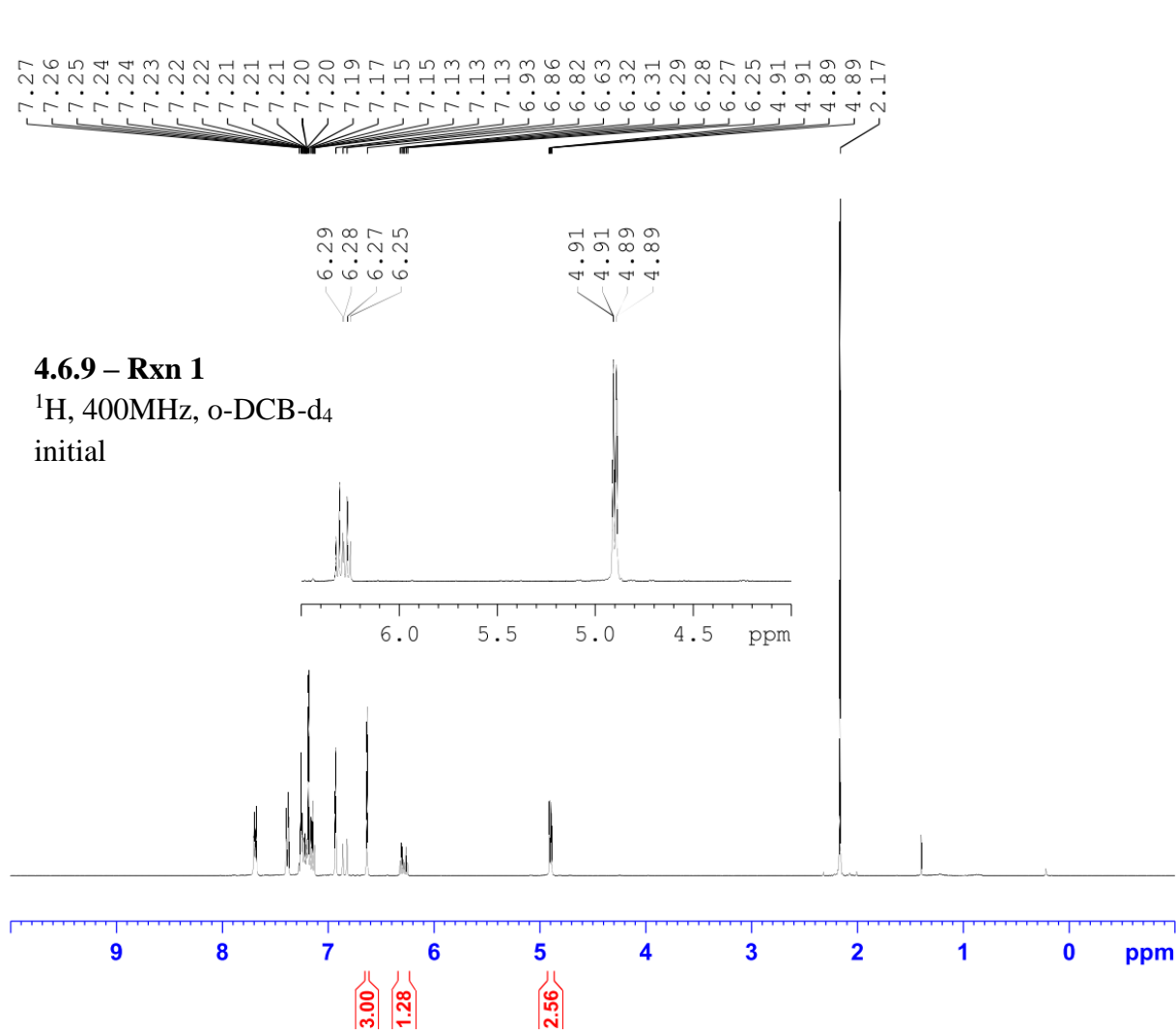


Current Data Parameters
NAME JAW-01-150
EXPNO 1
PROCNO 1

F2 - Acquisition Parameters
Date_ 20170914
Time_ 16.41
INSTRUM spect
PROBHD 5 mm PABBO BB/
PULPROG zg30
TD 65536
SOLVENT None
NS 32
DS 2
SWH 10000.000 Hz
FIDRES 0.152588 Hz
AQ 3.2767999 sec
RG 5.6
DW 50.000 usec
DE 6.50 usec
TE 296.2 K
D1 1.00000000 sec
TD0 1

===== CHANNEL f1 =====
SF01 500.1630887 MHz
NUC1 1H
P1 11.50 usec
PLW1 18.00000000 W

F2 - Processing parameters
SI 65536
SF 500.1597985 MHz
WDW EM
SSB 0
LB 0.30 Hz
GB 0
PC 1.00

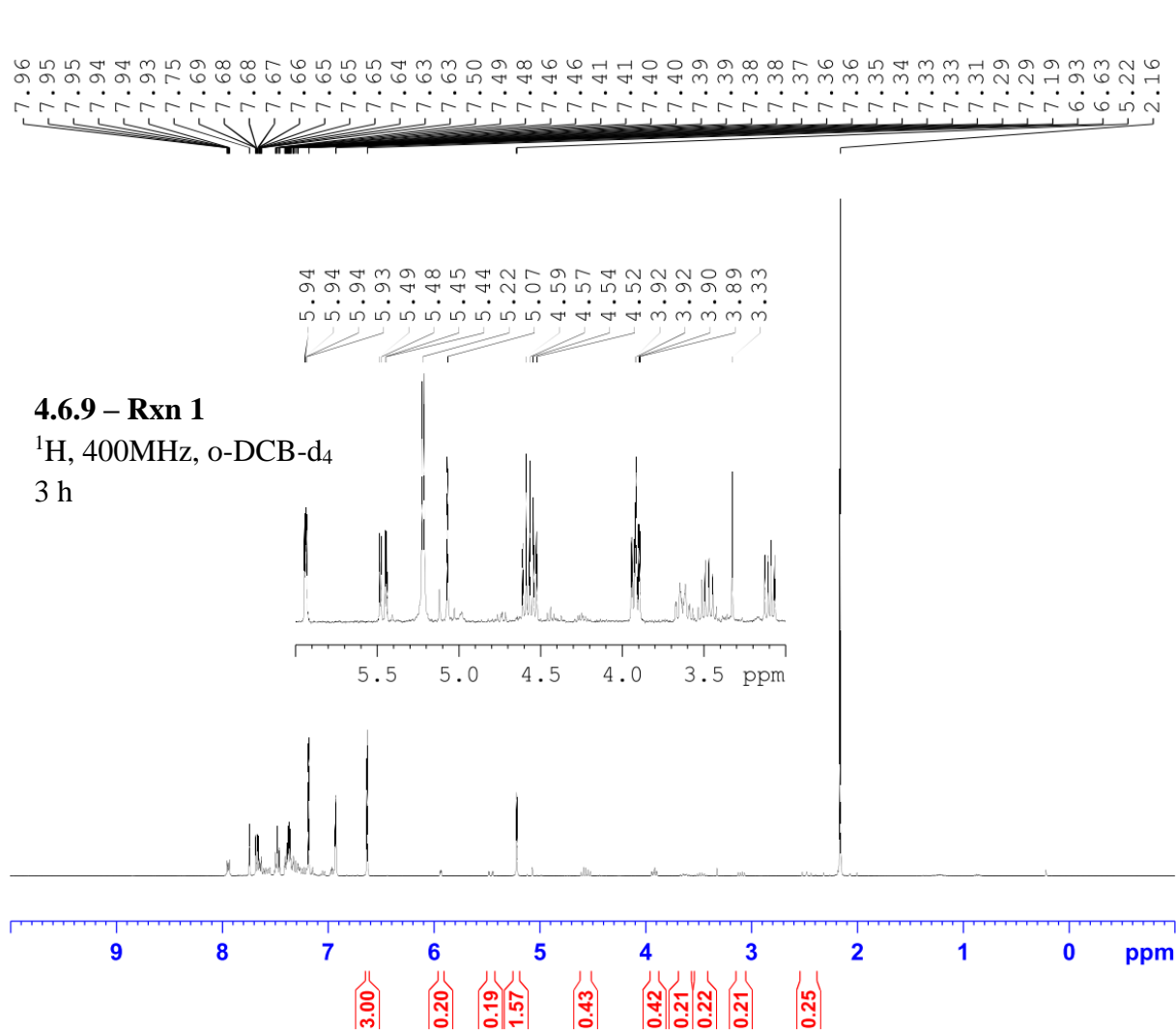


Current Data Parameters
 NAME JAW-03-109
 EXPNO 5
 PROCNO 1

F2 - Acquisition Parameters
 Date_ 20210419
 Time_ 9.36
 INSTRUM spect
 PROBHD 5 mm PADUL 13C
 PULPROG zg30
 TD 65536
 SOLVENT oC6D4Cl2
 NS 16
 DS 2
 SWH 8223.685 Hz
 FIDRES 0.125483 Hz
 AQ 3.9845889 sec
 RG 114
 DW 60.800 usec
 DE 6.50 usec
 TE 295.1 K
 D1 2.00000000 sec
 TD0 1

===== CHANNEL f1 =====
 NUC1 1H
 P1 9.31 usec
 PL1 -3.90 dB
 PL1W 21.64248466 W
 SFO1 400.2324716 MHz

F2 - Processing parameters
 SI 32768
 SF 400.2300667 MHz
 WDW EM
 SSB 0
 LB 0.30 Hz
 GB 0
 PC 1.00

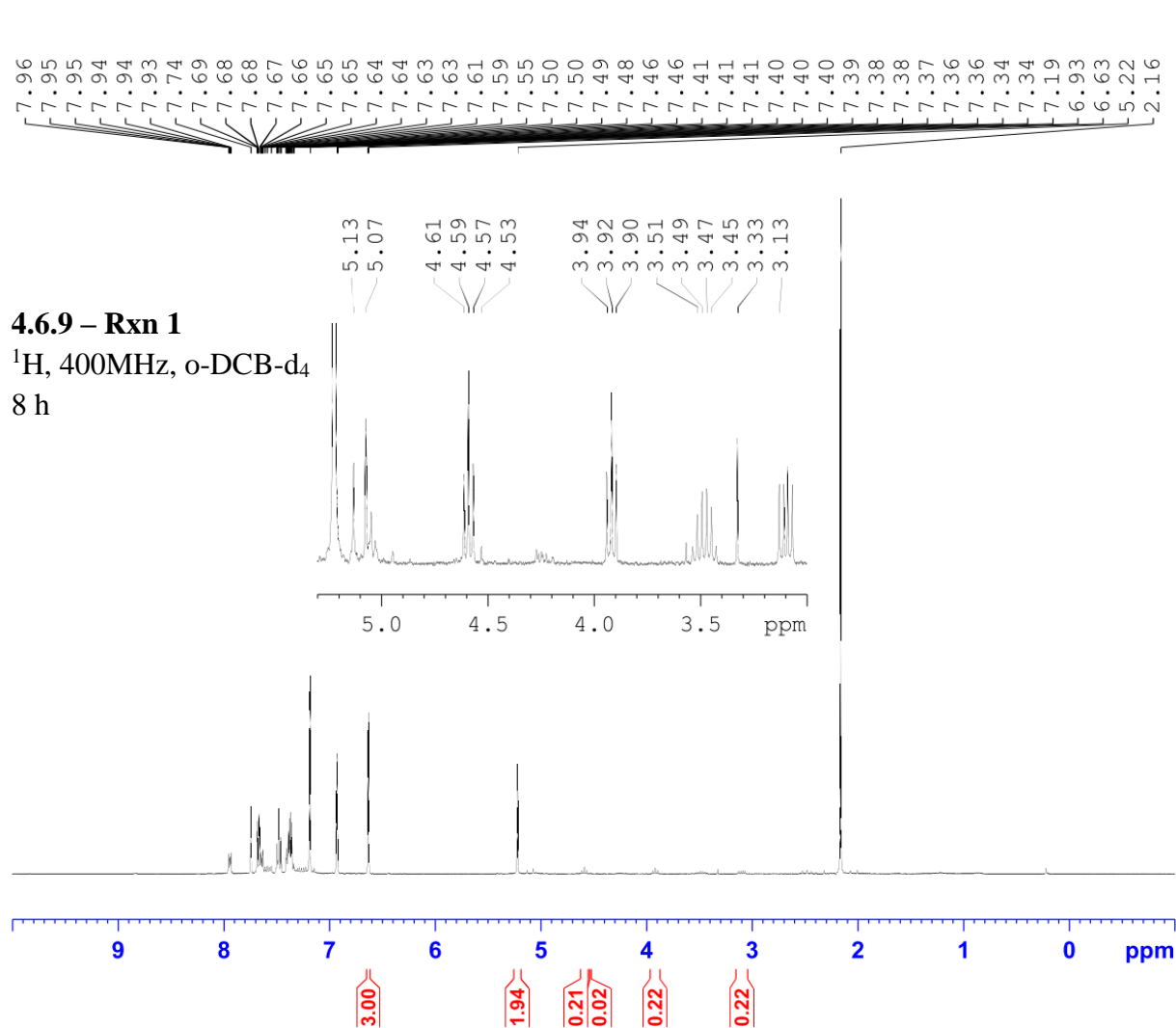


Current Data Parameters
 NAME JAW-03-109
 EXPNO 6
 PROCNO 1

F2 - Acquisition Parameters
 Date_ 20210419
 Time_ 12.55
 INSTRUM spect
 PROBHD 5 mm PADUL 13C
 PULPROG zg30
 TD 65536
 SOLVENT oC6D4Cl2
 NS 16
 DS 2
 SWH 8223.685 Hz
 FIDRES 0.125483 Hz
 AQ 3.9845889 sec
 RG 114
 DW 60.800 usec
 DE 6.50 usec
 TE 295.1 K
 D1 2.00000000 sec
 TD0 1

===== CHANNEL f1 =====
 NUC1 1H
 P1 9.31 usec
 PL1 -3.90 dB
 PL1W 21.64248466 W
 SFO1 400.2324716 MHz

F2 - Processing parameters
 SI 32768
 SF 400.2299657 MHz
 WDW EM
 SSB 0
 LB 0.30 Hz
 GB 0
 PC 1.00

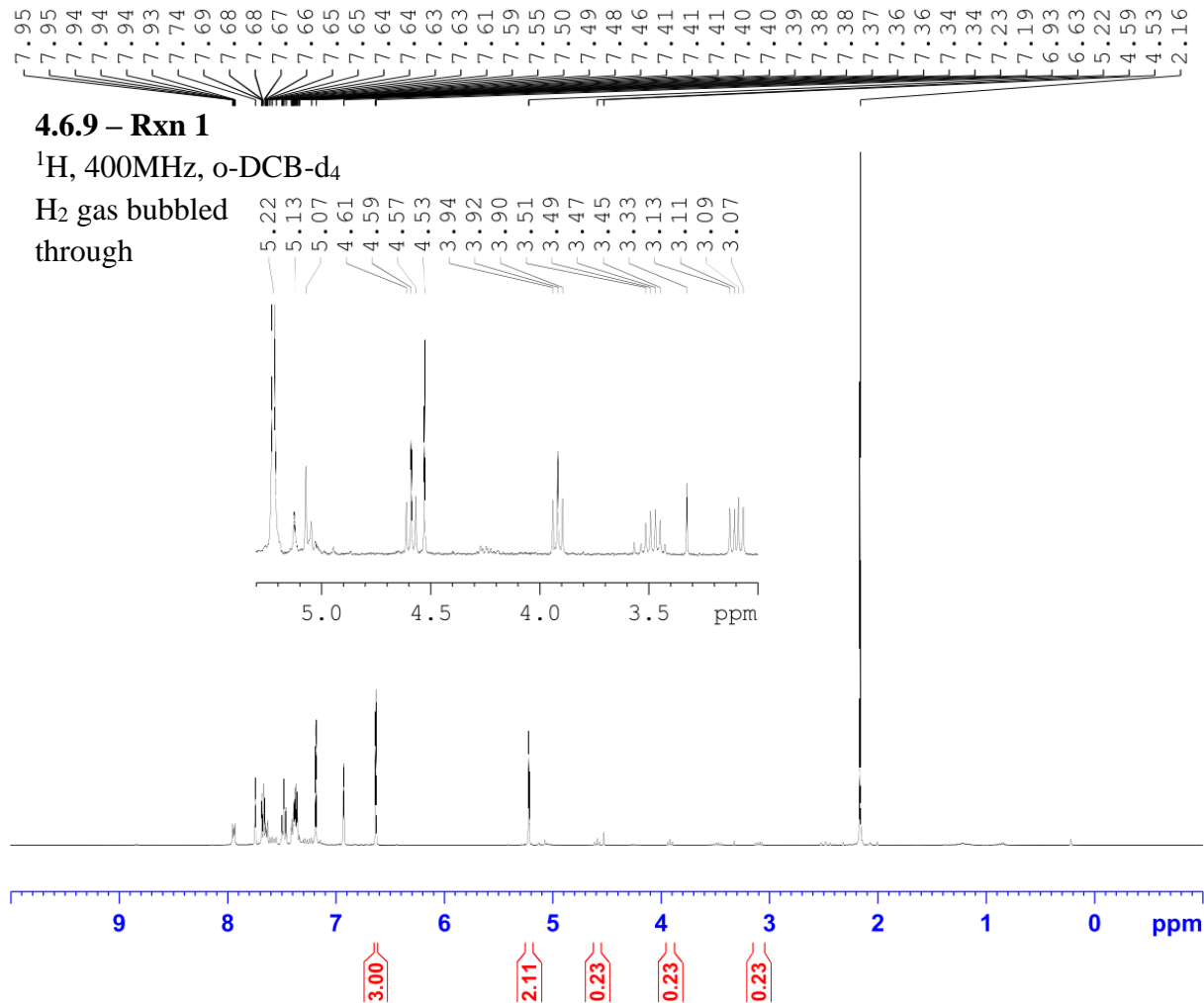


Current Data Parameters
 NAME JAW-03-109
 EXPNO 7
 PROCNO 1

F2 - Acquisition Parameters
 Date_ 20210419
 Time_ 22.30
 INSTRUM spect
 PROBHD 5 mm PADUL 13C
 PULPROG zg30
 TD 65536
 SOLVENT oC6D4Cl2
 NS 16
 DS 2
 SWH 8223.685 Hz
 FIDRES 0.125483 Hz
 AQ 3.9845889 sec
 RG 114
 DW 60.800 usec
 DE 6.50 usec
 TE 295.4 K
 D1 2.00000000 sec
 TD0 1

===== CHANNEL f1 =====
 NUC1 1H
 P1 9.31 usec
 PL1 -3.90 dB
 PL1W 21.64248466 W
 SFO1 400.2324716 MHz

F2 - Processing parameters
 SI 32768
 SF 400.2300665 MHz
 WDW EM
 SSB 0
 LB 0.30 Hz
 GB 0
 PC 1.00

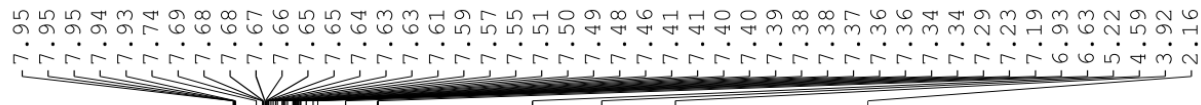


Current Data Parameters
NAME JAW-03-109
EXPNO 8
PROCNO 1

F2 - Acquisition Parameters
Date_ 20210419
Time_ 22.46
INSTRUM spect
PROBHD 5 mm PADUL 13C
PULPROG zg30
TD 65536
SOLVENT oC6D4Cl2
NS 16
DS 2
SWH 8223.685 Hz
FIDRES 0.125483 Hz
AQ 3.9845889 sec
RG 114
DW 60.800 usec
DE 6.50 usec
TE 295.3 K
D1 2.00000000 sec
TD0 1

===== CHANNEL f1 =====
NUC1 1H
P1 9.31 usec
PL1 -3.90 dB
PL1W 21.64248466 W
SFO1 400.2324716 MHz

F2 - Processing parameters
SI 32768
SF 400.2300666 MHz
WDW EM
SSB 0
LB 0.30 Hz
GB 0
PC 1.00



Current Data Parameters
 NAME JAW-03-109
 EXPNO 9
 PROCNO 1

F2 - Acquisition Parameters
 Date_ 20210419
 Time_ 23.00
 INSTRUM spect
 PROBHD 5 mm PADUL 13C
 PULPROG zg30
 TD 65536
 SOLVENT oC6D4Cl2
 NS 16
 DS 2
 SWH 8223.685 Hz
 FIDRES 0.125483 Hz
 AQ 3.9845889 sec
 RG 114
 DW 60.800 usec
 DE 6.50 usec
 TE 295.2 K
 D1 2.00000000 sec
 TD0 1

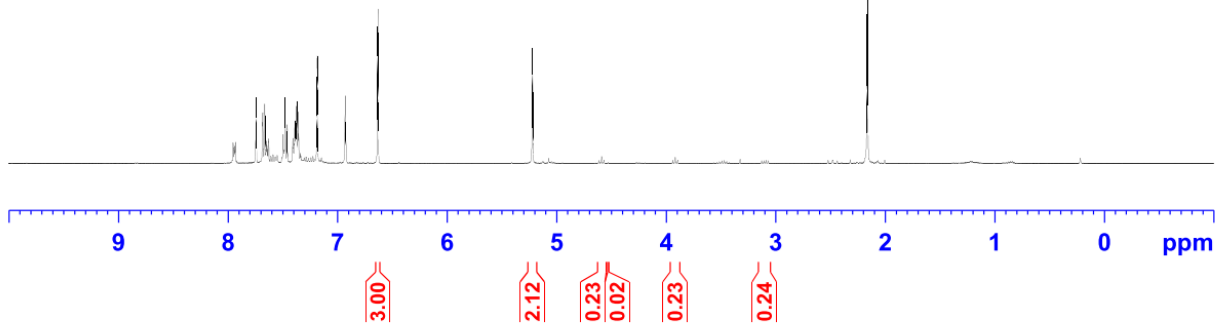
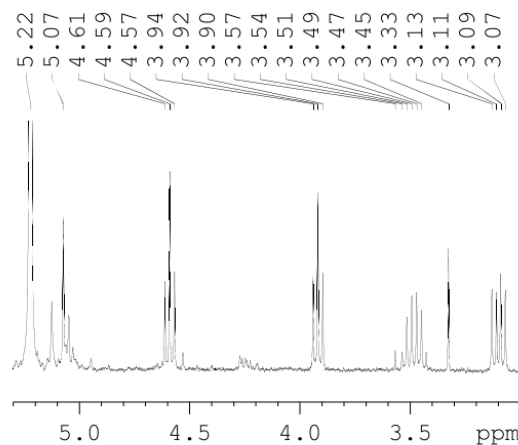
===== CHANNEL f1 =====
 NUC1 1H
 P1 9.31 usec
 PL1 -3.90 dB
 PL1W 21.64248466 W
 SFO1 400.2324716 MHz

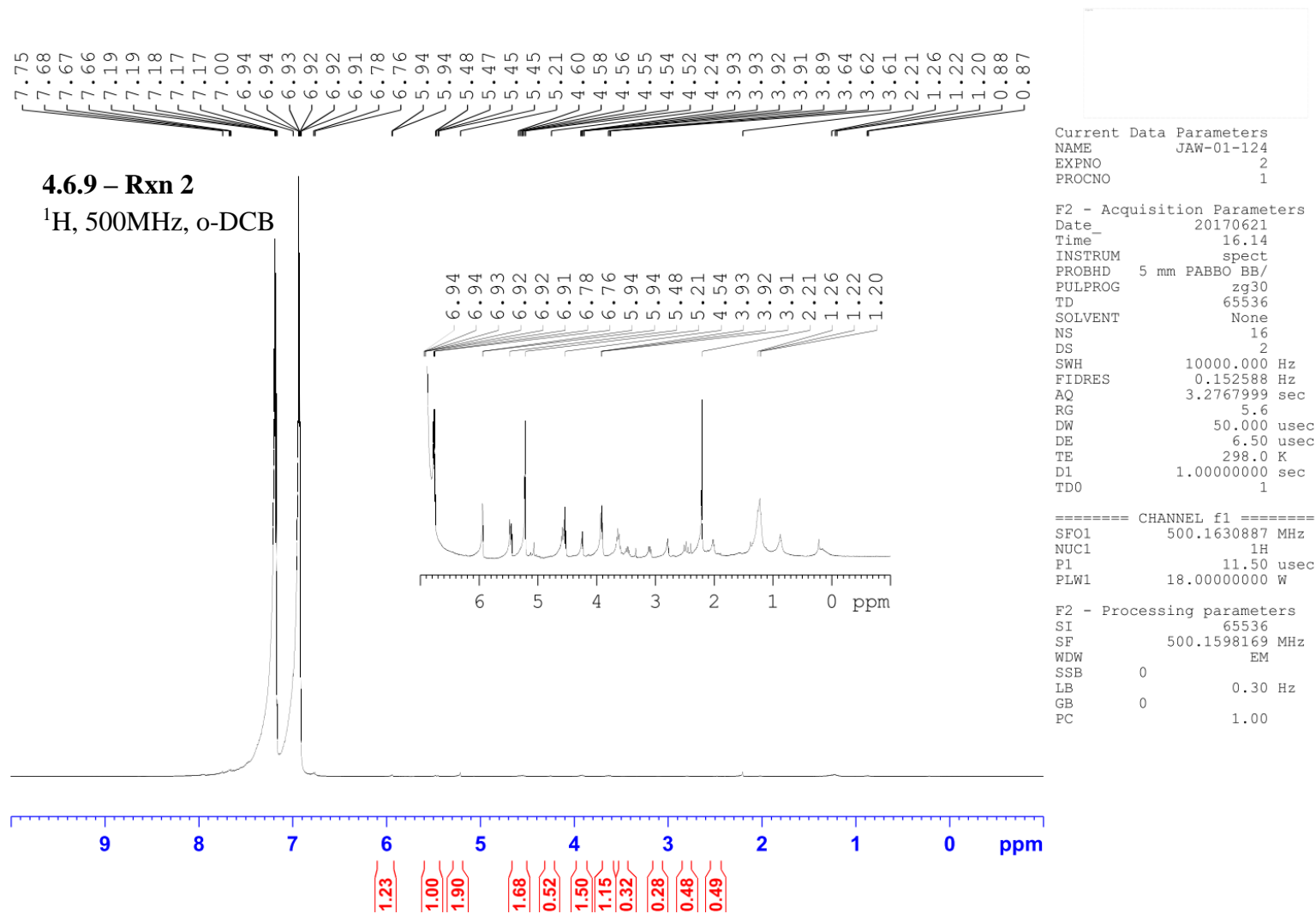
F2 - Processing parameters
 SI 32768
 SF 400.2300667 MHz
 WDW EM
 SSB 0
 LB 0.30 Hz
 GB 0
 PC 1.00

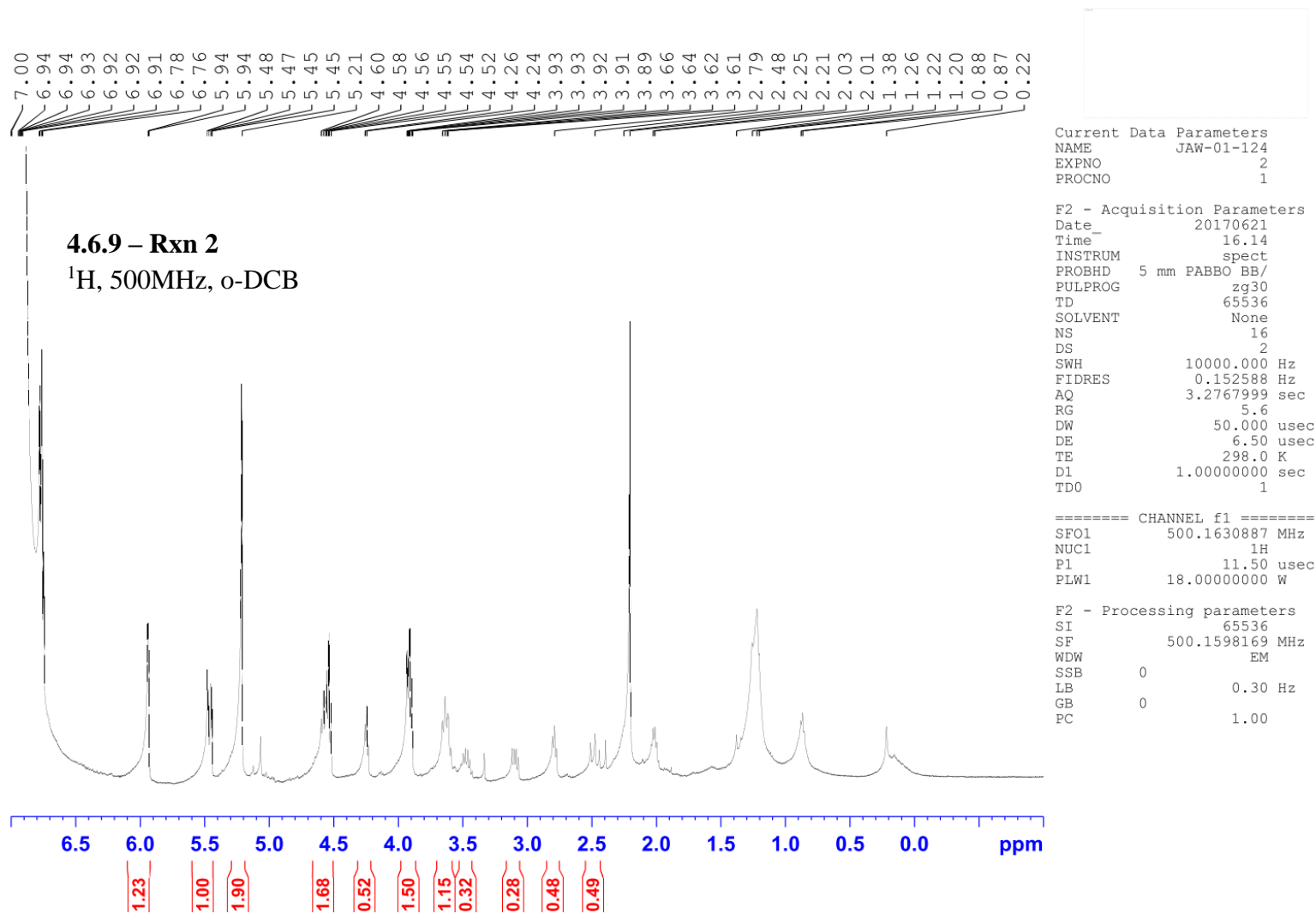
4.6.9 - Rxn 1

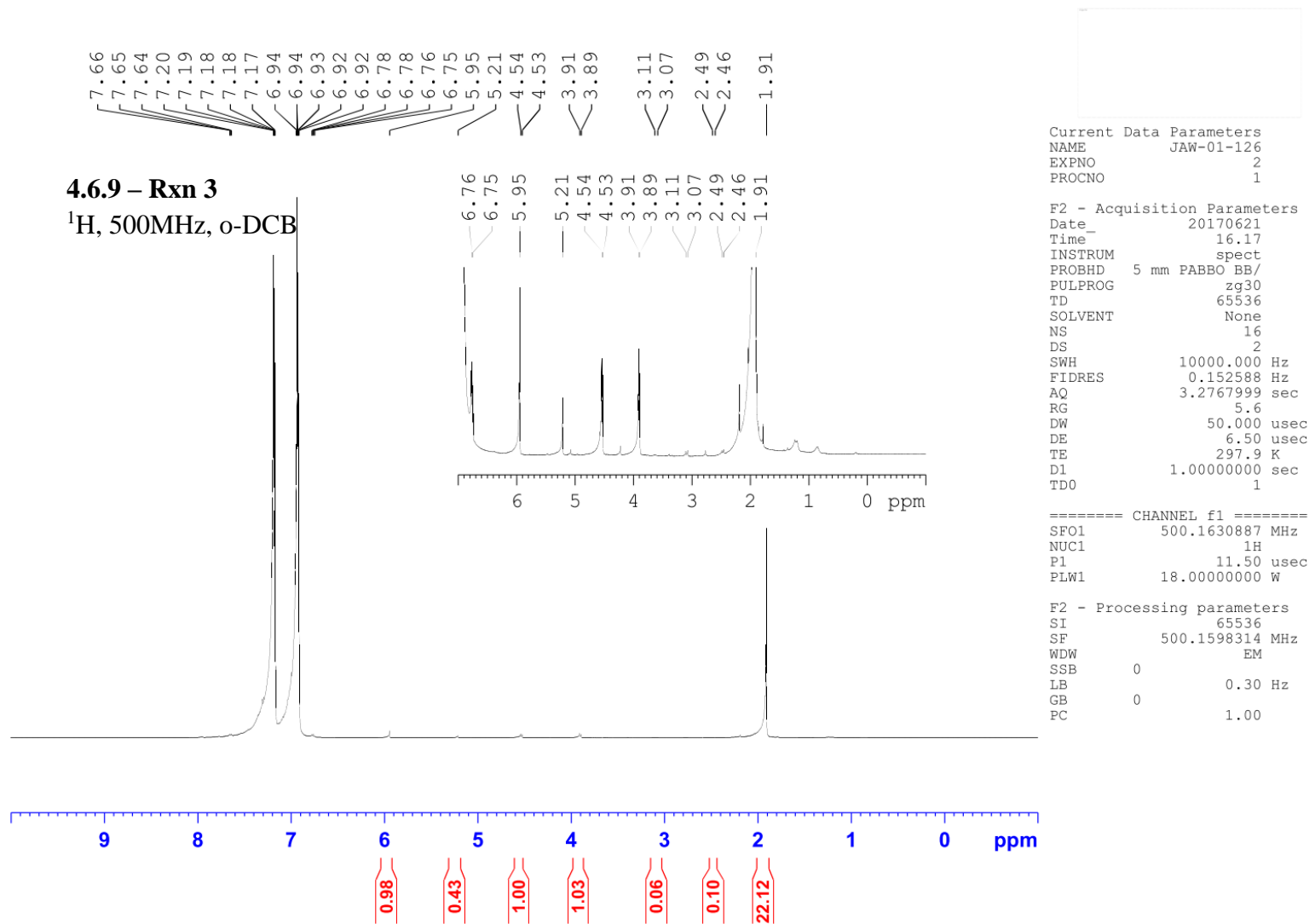
¹H, 400MHz, o-DCB-d₄

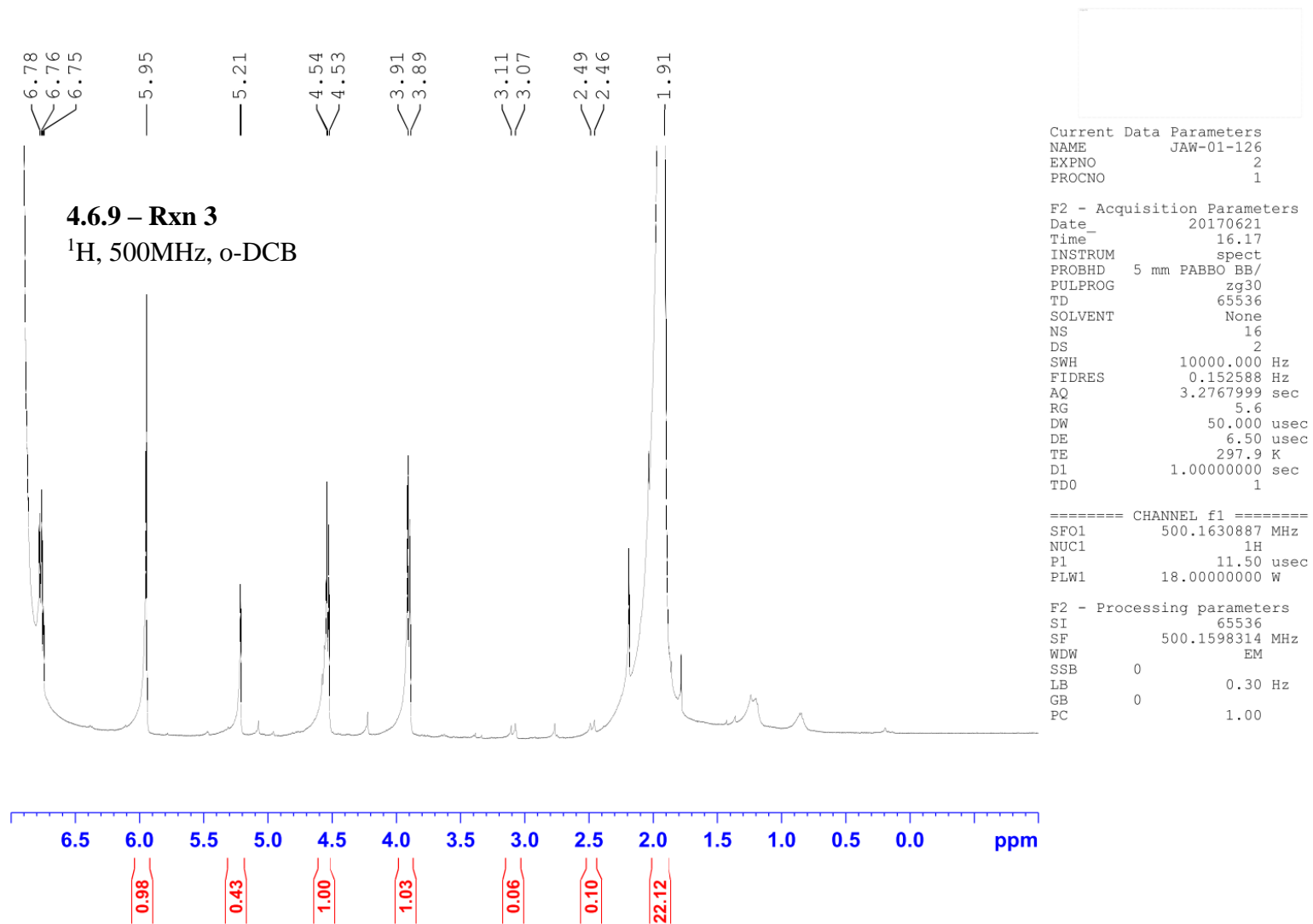
Ar gas bubbled
 through

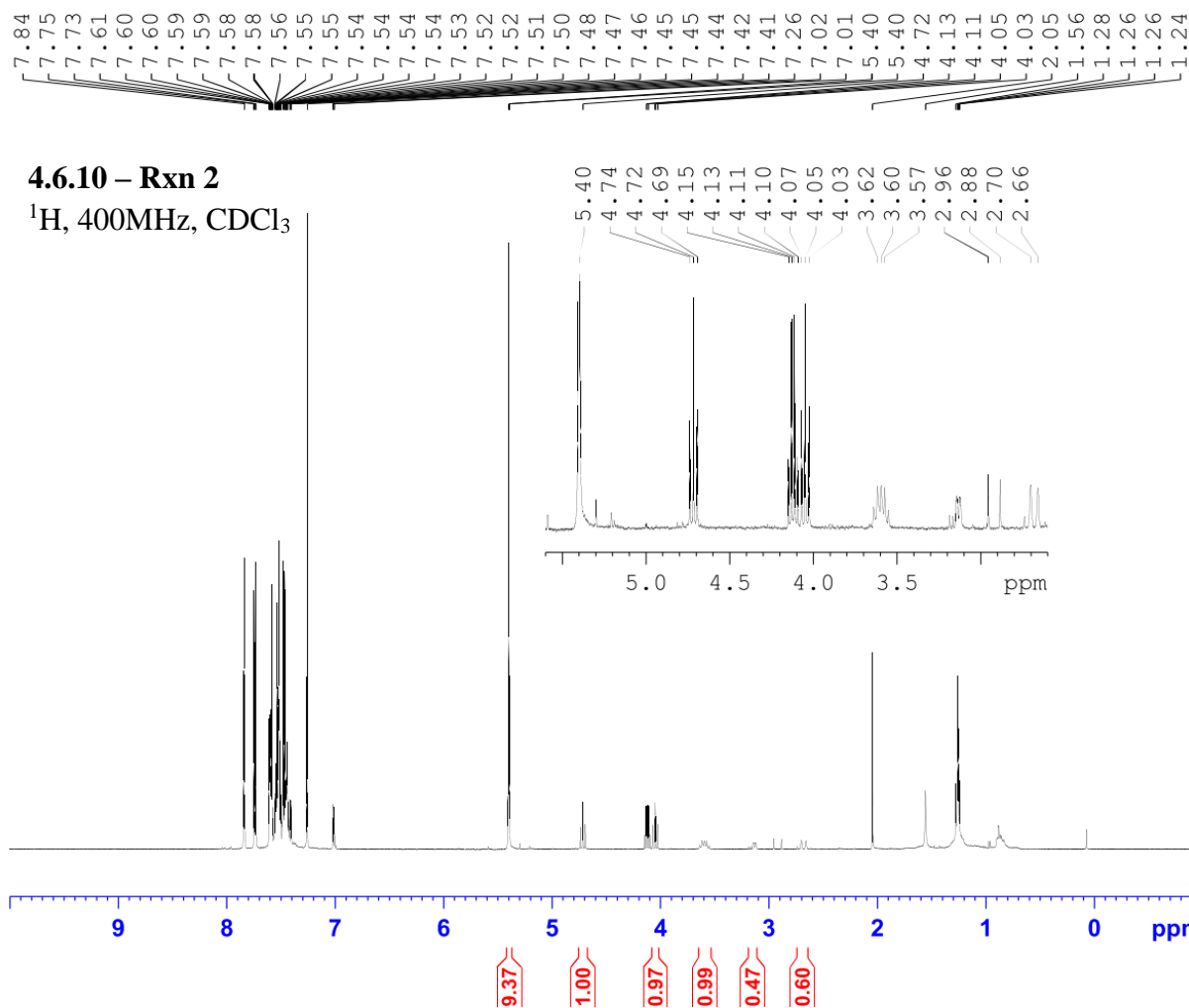










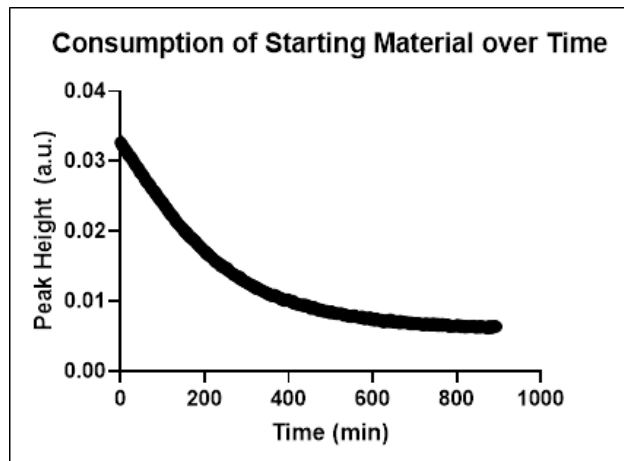


Current Data Parameters
 NAME JAW-03-091-b
 EXPNO 1
 PROCNO 1

F2 - Acquisition Parameters
 Date_ 20200125
 Time_ 14.14 h
 INSTRUM spect
 PROBHD Z108618_0240 (
 PULPROG zg30
 TD 65536
 SOLVENT CDCl₃
 NS 16
 DS 2
 SWH 8012.820 Hz
 FIDRES 0.244532 Hz
 AQ 4.0894465 sec
 RG 128
 DW 62.400 usec
 DE 6.50 usec
 TE 90.9 K
 D1 1.00000000 sec
 TD0 1
 SF01 400.1324708 MHz
 NUC1 1H
 P0 4.83 usec
 P1 14.50 usec
 PLW1 12.00000000 W

F2 - Processing parameters
 SI 65536
 SF 400.1300098 MHz
 WDW EM
 SSB 0
 LB 0.30 Hz
 GB 0
 PC 1.00

Appendix C ReactIR Data Output



Appendix Figure C.1. 1st order exponential decay of

1.50 at 77 °C

One phase decay

Best-fit values

Y0	0.03376
Plateau	0.005563
K	0.004494
Half Life	154.2
Tau	222.5
Span	0.02819
95% CI (profile likelihood)	
Y0	0.03366 to 0.03385
	0.005508 to
Plateau	0.005618
	0.004458 to
K	0.004530
Half Life	153.0 to 155.5
Tau	220.8 to 224.3
Goodness of Fit	
Degrees of Freedom	445
R squared	0.9989
Sum of Squares	2.63E-05
Sy.x	0.000243
Constraints	
K	K > 0

Number of points

of X values

Y values analyzed

448

448

Time (min)	Peak at 1280 cm ⁻¹ (a.u.)
0.00	0.032722
2.00	0.03245
4.00	0.032253
6.00	0.032155
8.00	0.031902
10.00	0.031571
12.00	0.031564
14.00	0.031489
16.00	0.031219
18.00	0.030895
20.00	0.030791
22.00	0.030669
24.00	0.030673
26.00	0.030347
28.00	0.030256
30.00	0.030093
32.00	0.029786
34.00	0.029609
36.00	0.029368
38.00	0.029304
40.00	0.029074
42.00	0.028955
44.00	0.028845
46.00	0.028394
48.00	0.028365
50.00	0.028201
52.00	0.028152
54.00	0.027877

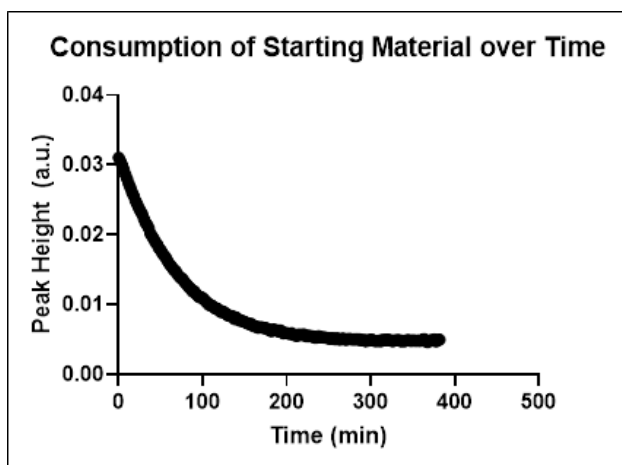
56.00	0.027773	146.00	0.020566
58.00	0.027425	148.00	0.020451
60.00	0.027183	150.00	0.020196
62.00	0.027141	152.00	0.019963
64.00	0.026852	154.00	0.019791
66.00	0.026869	156.03	0.019923
68.00	0.026757	158.00	0.01981
70.00	0.02657	160.00	0.019524
72.00	0.02629	162.00	0.019291
74.00	0.026002	164.00	0.019325
76.00	0.025977	166.00	0.019086
78.00	0.025886	168.00	0.019166
80.00	0.025762	170.00	0.018986
82.00	0.025407	172.00	0.018797
84.00	0.025473	174.05	0.018749
86.00	0.025106	176.00	0.018684
88.00	0.024981	178.00	0.018608
90.00	0.024806	180.00	0.01828
92.00	0.024654	182.00	0.018167
94.00	0.024579	184.00	0.018141
96.00	0.02427	186.00	0.017993
98.00	0.024223	188.00	0.017856
100.00	0.024181	190.00	0.017728
102.00	0.023927	192.00	0.017643
104.03	0.023725	194.00	0.017486
106.00	0.023534	196.00	0.017354
108.00	0.023368	198.00	0.017281
110.00	0.023291	200.00	0.017145
112.00	0.022954	202.00	0.016899
114.00	0.022939	204.00	0.017012
116.00	0.022691	206.00	0.016687
118.00	0.022462	208.00	0.016823
120.00	0.022429	210.05	0.016614
122.00	0.022253	212.00	0.016459
124.00	0.022156	214.00	0.016365
126.00	0.022051	216.00	0.016415
128.00	0.021865	218.00	0.016232
130.00	0.021458	220.05	0.016063
132.00	0.021459	222.00	0.015945
134.05	0.021361	224.00	0.015684
136.00	0.0211	226.00	0.015746
138.00	0.02098	228.00	0.015706
140.00	0.020878	230.00	0.015477
142.00	0.020706	232.00	0.015351
144.00	0.020515	234.00	0.015451

236.00	0.015356	326.00	0.011752
238.00	0.015032	328.00	0.011771
240.00	0.015209	330.00	0.011799
242.00	0.014961	332.00	0.011729
244.00	0.014941	334.00	0.01156
246.00	0.014883	336.00	0.011644
248.00	0.014795	338.00	0.011411
250.00	0.014597	340.00	0.01137
252.00	0.014516	342.00	0.011426
254.00	0.014762	344.05	0.011363
256.00	0.014466	346.00	0.011367
258.00	0.014293	348.00	0.011092
260.00	0.014233	350.00	0.01114
262.00	0.01421	352.00	0.010993
264.00	0.014038	354.00	0.011003
266.00	0.013902	356.00	0.010977
268.00	0.01378	358.00	0.010789
270.00	0.01385	360.00	0.01082
272.00	0.013676	362.00	0.010872
274.00	0.013665	364.00	0.010836
276.00	0.013559	366.00	0.010904
278.00	0.013593	368.00	0.010767
280.00	0.01338	370.00	0.010642
282.00	0.013277	372.00	0.010757
284.00	0.013492	374.00	0.010587
286.00	0.013072	376.00	0.010552
288.00	0.013197	378.00	0.010506
290.00	0.01309	380.00	0.010453
292.00	0.013016	382.00	0.010247
294.00	0.012826	384.00	0.010299
296.03	0.012867	386.00	0.01035
298.00	0.012699	388.02	0.010141
300.00	0.012728	390.03	0.010047
302.00	0.012647	392.00	0.010217
304.00	0.012521	394.00	0.010171
306.00	0.012453	396.00	0.010267
308.00	0.012376	398.00	0.010264
310.00	0.01235	400.00	0.010113
312.00	0.012252	402.00	0.010092
314.02	0.01227	404.00	0.009947
316.00	0.012057	406.00	0.009912
318.00	0.012091	408.00	0.009894
320.00	0.012084	410.00	0.010048
322.00	0.011831	412.00	0.009694
324.00	0.011955	414.00	0.009753

416.02	0.009607	506.00	0.008366
418.00	0.009604	508.00	0.0083
420.00	0.00964	510.00	0.008283
422.00	0.009564	512.00	0.008264
424.00	0.009507	514.00	0.008196
426.00	0.009653	516.00	0.008232
428.00	0.009463	518.00	0.008209
430.00	0.009436	520.00	0.008199
432.00	0.009372	522.00	0.008162
434.00	0.009359	524.00	0.008238
436.00	0.009501	526.00	0.008167
438.00	0.009386	528.00	0.00817
440.00	0.0093	530.05	0.008134
442.00	0.009493	532.00	0.007947
444.00	0.009247	534.00	0.00804
446.00	0.009211	536.00	0.008099
448.00	0.009329	538.00	0.008
450.00	0.009143	540.00	0.007925
452.00	0.008936	542.00	0.007979
454.00	0.008991	544.00	0.00777
456.00	0.009015	546.00	0.00793
458.00	0.009042	548.00	0.00791
460.00	0.009152	550.00	0.007796
462.00	0.009008	552.00	0.007894
464.00	0.009009	554.00	0.007877
466.00	0.008868	556.00	0.007985
468.00	0.008749	558.00	0.007904
470.00	0.008805	560.00	0.007765
472.00	0.008674	562.00	0.007749
474.00	0.008845	564.00	0.007744
476.00	0.008692	566.00	0.0077
478.00	0.008698	568.00	0.007668
480.00	0.008722	570.05	0.007691
482.00	0.008526	572.00	0.007704
484.00	0.008618	574.00	0.007819
486.00	0.008691	576.00	0.00768
488.00	0.008563	578.00	0.007605
490.00	0.008611	580.00	0.007453
492.00	0.008574	582.00	0.007544
494.00	0.008408	584.00	0.007587
496.00	0.008435	586.00	0.007693
498.00	0.008311	588.00	0.007621
500.00	0.00843	590.00	0.007499
502.00	0.00855	592.00	0.007425
504.00	0.008341	594.00	0.007684

596.00	0.007351	686.00	0.006855
598.00	0.007486	688.00	0.006929
600.00	0.007315	690.00	0.006715
602.00	0.007447	692.00	0.006954
604.00	0.007438	694.00	0.006896
606.00	0.007244	696.00	0.006771
608.00	0.007504	698.00	0.006713
610.00	0.007459	700.00	0.006834
612.00	0.007315	702.00	0.006819
614.00	0.007292	704.00	0.006888
616.00	0.007235	706.00	0.006801
618.00	0.007283	708.00	0.006709
620.00	0.007366	710.00	0.006858
622.00	0.007125	712.00	0.006799
624.00	0.007199	714.00	0.006758
626.00	0.007022	716.05	0.006794
628.05	0.007063	718.00	0.006599
630.03	0.007219	720.00	0.006707
632.00	0.007278	722.00	0.006615
634.00	0.007213	724.00	0.006657
636.00	0.007187	726.00	0.006808
638.00	0.007041	728.02	0.006635
640.00	0.007136	730.00	0.006718
642.00	0.007381	732.00	0.006657
644.00	0.007267	734.00	0.006779
646.00	0.00717	736.00	0.006779
648.00	0.007018	738.00	0.006556
650.00	0.007024	740.00	0.00666
652.00	0.007183	742.00	0.006638
654.00	0.006962	744.00	0.006818
656.00	0.006993	746.00	0.006658
658.00	0.007107	748.00	0.006572
660.00	0.006948	750.00	0.00661
662.00	0.006888	752.00	0.006694
664.00	0.006914	754.00	0.006797
666.00	0.007167	756.00	0.006475
668.00	0.006883	758.00	0.006571
670.03	0.007048	760.00	0.006626
672.00	0.006998	762.00	0.006596
674.00	0.006903	764.00	0.00651
676.05	0.006987	766.00	0.006748
678.00	0.007013	768.00	0.006516
680.00	0.006871	770.00	0.006582
682.00	0.006942	772.00	0.006567
684.00	0.006911	774.00	0.006563

776.00	0.006593	866.00	0.006348
778.00	0.006648	868.00	0.006295
780.00	0.006558	870.00	0.006214
782.00	0.006342	872.00	0.006218
784.00	0.006529	874.00	0.006119
786.00	0.00659	876.00	0.006417
788.00	0.006423	878.00	0.006176
790.00	0.006437	880.00	0.006416
792.00	0.006432	882.00	0.006413
794.00	0.006432	884.00	0.00632
796.00	0.006375	886.00	0.006231
798.00	0.006499	888.00	0.006341
800.00	0.006556	890.00	0.006437
802.00	0.00645	892.00	0.006358
804.00	0.006589	894.00	0.006375
806.00	0.006672		
808.00	0.0064		
810.00	0.006301		
812.00	0.00652		
814.00	0.00642		
816.00	0.006356		
818.00	0.006435		
820.00	0.006254		
822.00	0.006371		
824.00	0.006424		
826.00	0.006355		
828.05	0.006316		
830.00	0.006431		
832.00	0.006499		
834.00	0.006371		
836.00	0.006386		
838.00	0.006343		
840.00	0.006473		
842.00	0.006311		
844.00	0.006262		
846.00	0.006393		
848.00	0.006247		
850.02	0.006308		
852.00	0.006315		
854.00	0.00629		
856.05	0.006451		
858.00	0.006234		
860.00	0.006389		
862.00	0.006424		
864.00	0.006359		



Appendix Figure C.2. 1st order exponential decay of

1.50 at 86 °C

One phase decay

Best-fit values

Y0	0.03177
Plateau	0.004558
K	0.01466
Half Life	47.28
Tau	68.21
Span	0.02722

95% CI (profile likelihood)

Y0	0.03167 to 0.03187
	0.004521 to
Plateau	0.004594
K	0.01456 to 0.01476
Half Life	46.95 to 47.61
Tau	67.73 to 68.69

Goodness of Fit

Degrees of Freedom	189
R squared	0.9995
Sum of Squares	4.01E-06
Sy.x	0.000146

Constraints

K	K > 0
---	-------

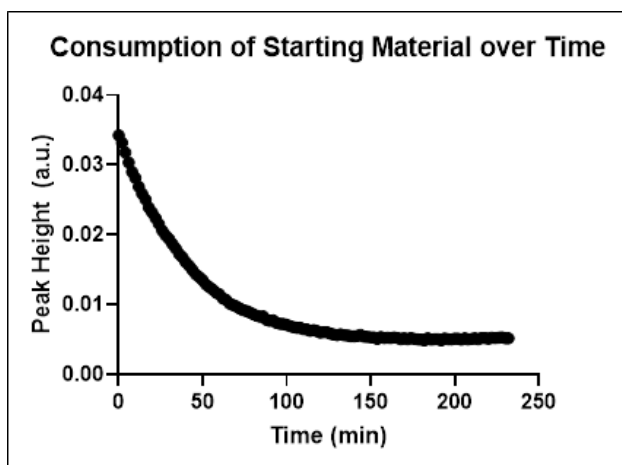
Number of points

# of X values	192
# Y values analyzed	192

Time (min)	Peak at 1280 cm ⁻¹ (a.u.)
0.00	0.031035
2.00	0.030557
4.03	0.030033
6.00	0.029388
8.00	0.028667
10.00	0.02801
12.00	0.027309
14.00	0.026761
16.00	0.02608
18.00	0.025594
20.00	0.024872
22.00	0.024389
24.00	0.023834
26.00	0.023392
28.00	0.022983
30.00	0.022267
32.00	0.021731
34.00	0.021401
36.00	0.020912
38.00	0.020136
40.00	0.019742
42.00	0.019346
44.00	0.018898
46.00	0.018662
48.05	0.018098
50.00	0.017825
52.00	0.017356
54.00	0.017052
56.00	0.016767
58.00	0.016322
60.00	0.015886
62.00	0.015591
64.00	0.015279
66.00	0.014909
68.00	0.014831
70.00	0.014329
72.00	0.014064
74.05	0.013794
76.00	0.013704
78.00	0.013306
80.00	0.013001
82.00	0.01275

84.00	0.012403	174.00	0.006613
86.00	0.012267	176.00	0.0066
88.00	0.011886	178.00	0.006455
90.00	0.011915	180.00	0.006281
92.00	0.011552	182.00	0.006186
94.00	0.011288	184.00	0.00644
96.00	0.011066	186.00	0.006343
98.00	0.011081	188.00	0.00631
100.00	0.010966	190.00	0.006144
102.00	0.010674	192.00	0.00632
104.03	0.010373	194.00	0.00618
106.00	0.01024	196.00	0.00587
108.00	0.009901	198.00	0.005906
110.00	0.00993	200.00	0.005924
112.00	0.009788	202.00	0.005841
114.03	0.009526	204.00	0.005821
116.00	0.009402	206.00	0.005924
118.03	0.009412	208.00	0.005655
120.00	0.009081	210.00	0.005629
122.00	0.008929	212.00	0.005523
124.00	0.009031	214.00	0.005733
126.00	0.008887	216.00	0.005643
128.00	0.008679	218.00	0.005656
130.00	0.008461	220.00	0.005734
132.00	0.008394	222.00	0.005558
134.00	0.008397	224.03	0.005452
136.00	0.00831	226.00	0.005554
138.00	0.007902	228.05	0.005464
140.00	0.008152	230.00	0.005469
142.00	0.00793	232.00	0.00534
144.03	0.007709	234.00	0.005258
146.00	0.007707	236.00	0.005299
148.00	0.007603	238.00	0.0055
150.00	0.00751	240.00	0.005306
152.00	0.007391	242.00	0.005323
154.00	0.007295	244.03	0.005285
156.00	0.007192	246.00	0.00528
158.00	0.007256	248.00	0.005208
160.00	0.006932	250.00	0.005169
162.00	0.006911	252.00	0.005068
164.00	0.006859	254.00	0.005185
166.00	0.006667	256.00	0.005148
168.00	0.006734	258.05	0.005024
170.00	0.006754	260.00	0.005192
172.00	0.00669	262.00	0.005017

264.02	0.004999	354.00	0.004852
266.00	0.005123	356.00	0.004814
268.00	0.005129	358.00	0.004857
270.00	0.004944	360.00	0.004802
272.00	0.005034	362.00	0.005
274.00	0.005042	364.03	0.005043
276.00	0.005098	366.00	0.004726
278.00	0.004974	368.00	0.004607
280.00	0.005017	370.00	0.004818
282.00	0.005051	372.00	0.004903
284.03	0.00498	374.00	0.004843
286.00	0.005042	376.00	0.005033
288.00	0.004929	378.00	0.004717
290.00	0.004873	380.00	0.004909
292.00	0.004955	382.00	0.004985
294.03	0.00474		
296.00	0.00489		
298.00	0.004855		
300.00	0.004968		
302.00	0.004964		
304.00	0.004816		
306.00	0.004773		
308.00	0.00479		
310.00	0.004849		
312.00	0.004734		
314.00	0.004963		
316.00	0.004873		
318.00	0.004943		
320.00	0.004994		
322.00	0.004883		
324.00	0.004886		
326.00	0.004747		
328.00	0.00485		
330.00	0.004893		
332.00	0.004899		
334.03	0.004928		
336.00	0.00474		
338.00	0.004828		
340.00	0.00475		
342.00	0.004844		
344.00	0.004925		
346.00	0.004887		
348.00	0.004774		
350.00	0.004873		
352.00	0.004823		



Appendix Figure C.3. 1st order exponential decay of

1.50 at 94 °C

One phase decay

Best-fit values

Y0 0.03477

Plateau 0.004734

K 0.02497

Half Life 27.76

Tau 40.05

Span 0.03004

95% CI (profile likelihood)

Y0 0.03459 to 0.03496
0.004667 to

Plateau 0.004801

K 0.02467 to 0.02527

Half Life 27.43 to 28.10

Tau 39.58 to 40.53

Goodness of Fit

Degrees of Freedom 114

R squared 0.9992

Sum of Squares 5.31E-06

Sy.x 0.000216

Constraints

K K > 0

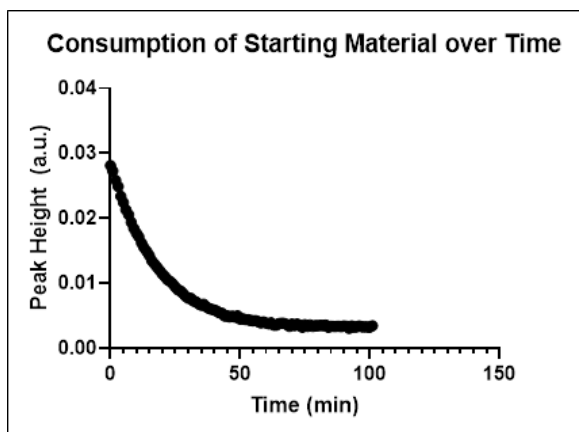
Number of points

of X values 117

Y values analyzed 117

Time (min)	Peak at 1280 cm ⁻¹ (a.u.)
0.00	0.034248
1.98	0.033186
4.00	0.031772
6.03	0.03035
8.00	0.029015
9.98	0.028162
12.00	0.026884
14.00	0.025893
15.98	0.025039
18.00	0.023881
19.98	0.023171
22.00	0.022385
24.00	0.021557
25.98	0.020585
28.00	0.019932
29.98	0.019433
32.00	0.018673
34.02	0.018048
35.98	0.017259
38.00	0.0168
39.98	0.016093
42.00	0.015552
44.00	0.01494
45.98	0.014317
48.00	0.013942
49.98	0.013515
52.00	0.012875
54.00	0.012504
55.98	0.012152
58.00	0.011704
59.98	0.011479
62.00	0.010891
63.98	0.0107
66.00	0.010164
68.00	0.009959
69.98	0.009765
72.00	0.009464
73.98	0.0092
76.00	0.00909
78.00	0.008889

79.98	0.008662	169.98	0.005173
82.00	0.008428	171.98	0.005045
83.98	0.008283	174.00	0.00521
86.00	0.008307	175.98	0.005081
88.00	0.007818	178.00	0.005001
89.98	0.007676	180.00	0.004997
92.00	0.00774	181.98	0.004882
93.98	0.007369	184.00	0.005169
96.00	0.007254	185.98	0.004977
98.00	0.007208	188.00	0.005041
99.98	0.007124	190.00	0.005048
102.00	0.00692	191.98	0.00487
103.98	0.006772	194.00	0.005134
106.00	0.006694	196.03	0.005042
108.00	0.006684	197.98	0.005009
109.98	0.006499	200.00	0.005133
112.00	0.006455	201.98	0.005116
113.98	0.00624	204.00	0.004987
115.98	0.006352	206.00	0.005192
118.00	0.006215	207.98	0.005028
119.98	0.00599	210.00	0.005082
122.00	0.006034	211.98	0.005176
124.00	0.006057	214.00	0.005059
125.98	0.005848	216.00	0.00522
128.00	0.005703	217.98	0.005213
130.00	0.005621	220.00	0.005108
131.98	0.005747	221.98	0.005234
134.00	0.005618	223.98	0.005201
135.98	0.005593	226.00	0.005264
137.98	0.005496	227.98	0.005328
140.00	0.005463	230.00	0.005169
141.98	0.005514	232.00	0.00517
144.00	0.005646		
146.00	0.005433		
147.98	0.005376		
150.00	0.005312		
152.00	0.005281		
153.98	0.005091		
156.00	0.005357		
157.98	0.005219		
160.00	0.005245		
162.00	0.005221		
164.02	0.005278		
165.98	0.005215		
168.00	0.005043		



Appendix Figure C.4. 1st order exponential decay of

1.50 at 108 °C

One phase decay

Best-fit values

Y0 0.0286

Plateau 0.003099

K 0.05587

Half Life 12.41

Tau 17.9

Span 0.0255

95% CI (profile likelihood)

Y0 0.02847 to 0.02873

0.003051 to

Plateau 0.003147

K 0.05532 to 0.05643

Half Life 12.28 to 12.53

Tau 17.72 to 18.08

Goodness of Fit

Degrees of Freedom 99

R squared 0.9995

Sum of Squares 1.96E-06

Sy.x 0.000141

Constraints

K K > 0

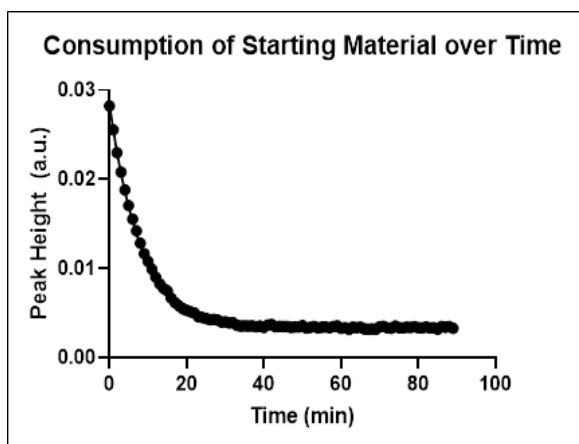
Number of points

of X values 102

Y values analyzed 102

Time (min)	Peak at 1280 cm ⁻¹ (a.u.)
0.00	0.028111
0.98	0.027245
2.03	0.025865
3.02	0.024898
4.02	0.023385
5.00	0.022425
5.98	0.021302
7.03	0.020561
8.03	0.019393
9.00	0.018437
10.00	0.0177
10.98	0.017149
12.00	0.01619
12.98	0.015489
14.00	0.014883
15.00	0.014237
15.98	0.013473
17.03	0.01294
18.00	0.012446
19.00	0.011945
20.00	0.011428
21.00	0.011025
21.98	0.010561
23.00	0.010291
24.00	0.00993
25.00	0.00942
26.00	0.008984
27.00	0.008805
27.98	0.00845
29.00	0.007968
30.00	0.007667
31.00	0.007692
32.00	0.007245
32.98	0.007144
34.00	0.006803
35.00	0.006614
35.98	0.006796
37.00	0.006348
38.00	0.006121
39.00	0.005997
40.02	0.005886
41.00	0.005721

41.98	0.005442	87.00	0.003366
43.00	0.005393	88.00	0.003373
44.00	0.004962	89.00	0.003332
45.00	0.004969	89.98	0.003426
45.98	0.004814	91.05	0.003377
47.03	0.004945	92.03	0.003063
48.03	0.004798	93.02	0.003422
49.00	0.004973	94.02	0.003264
49.98	0.0045	95.00	0.003267
51.00	0.004528	95.98	0.003416
51.98	0.004428	97.00	0.003285
53.00	0.004379	98.00	0.003279
54.00	0.004268	99.00	0.003274
54.98	0.004215	99.98	0.003203
56.00	0.004235	101.00	0.003445
57.00	0.004087		
58.00	0.003895		
59.00	0.004057		
59.98	0.003871		
61.00	0.003739		
61.98	0.003913		
63.00	0.003551		
64.00	0.003546		
64.98	0.003783		
66.00	0.003844		
67.03	0.003813		
68.00	0.003644		
69.00	0.00336		
70.03	0.003705		
71.02	0.003485		
72.02	0.003729		
73.02	0.00348		
74.00	0.003228		
74.98	0.003627		
76.00	0.003351		
76.98	0.003586		
78.00	0.003343		
79.00	0.003474		
79.98	0.00346		
81.00	0.003522		
82.02	0.003493		
83.00	0.00356		
84.00	0.00322		
85.00	0.003394		
86.00	0.003343		



Appendix Figure C.5. 1st order exponential decay of

1.50 at 119 °C

One phase decay

Best-fit values

Y0 0.0285

Plateau 0.003339

K 0.1234

Half Life 5.619

Tau 8.107

Span 0.02516

95% CI (profile likelihood)

Y0 0.02835 to 0.02866

0.003306 to

Plateau 0.003372

K 0.1221 to 0.1246

Half Life 5.561 to 5.677

Tau 8.023 to 8.191

Goodness of Fit

Degrees of

Freedom 87

R squared 0.9994

Sum of Squares 1.35E-06

Sy.x 0.000125

Constraints

K K > 0

Number of points

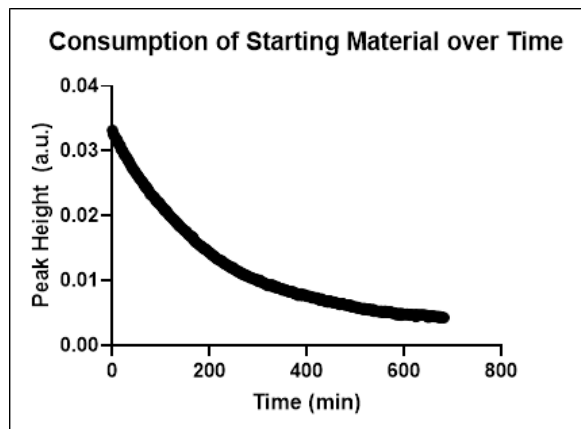
of X values 90

Y values
analyzed 90

Time (min)	Peak at 1279 cm ⁻¹ (a.u.)
0.00	0.028225
1.00	0.025561
1.98	0.022977
3.00	0.02081
4.00	0.018812
4.98	0.017063
6.00	0.015545
7.00	0.014214
8.00	0.012829
9.00	0.011662
10.00	0.010789
11.00	0.00992
11.98	0.009033
13.00	0.008295
14.00	0.007773
15.00	0.007498
15.98	0.006684
17.00	0.00617
18.00	0.005802
19.00	0.005489
19.98	0.00532
21.00	0.005131
22.00	0.005011
23.00	0.004581
23.98	0.004521
25.00	0.004393
26.00	0.004258
27.00	0.004285
28.00	0.004209
29.00	0.003982
30.00	0.004024
31.00	0.003888
32.00	0.003901
33.00	0.003619
34.00	0.003531
35.00	0.00355
36.00	0.003548
37.00	0.003568
38.00	0.003467
38.98	0.003525

40.00	0.003392	85.00	0.003181
41.00	0.003654	86.00	0.003482
42.00	0.003706	87.00	0.003404
42.98	0.003458	87.98	0.003493
44.00	0.003505	89.00	0.003286
45.00	0.003499		
46.00	0.003478		
47.00	0.00339		
47.98	0.003444		
49.00	0.003446		
50.00	0.003582		
51.00	0.00331		
51.98	0.00339		
53.00	0.003481		
54.00	0.003349		
55.00	0.003424		
55.98	0.003437		
57.03	0.003366		
58.00	0.003482		
59.00	0.003558		
59.98	0.003295		
61.00	0.003355		
62.00	0.00315		
63.00	0.003421		
63.98	0.003352		
65.00	0.003409		
66.00	0.003213		
66.98	0.003194		
68.00	0.003222		
69.00	0.003176		
70.00	0.003452		
70.98	0.003524		
72.00	0.003345		
73.05	0.003292		
74.00	0.003542		
74.98	0.003368		
76.00	0.003338		
77.00	0.003424		
78.00	0.003396		
79.00	0.003453		
80.00	0.003364		
81.00	0.003348		
82.00	0.003432		
83.00	0.003339		
83.98	0.003373		

2.7 76 °C



Appendix Figure C.6. 1st order exponential decay of

2.7 at 76 °C

One phase decay

Best-fit values

Y0	0.03299
Plateau	0.003348
K	0.004941
Half Life	140.3
Tau	202.4
Span	0.02964
95% CI (profile likelihood)	
Y0	0.03293 to 0.03304
	0.003303 to
Plateau	0.003393
	0.004914 to
K	0.004967
Half Life	139.5 to 141.1
Tau	201.3 to 203.5
Goodness of Fit	
Degrees of Freedom	339
R squared	0.9997
Sum of Squares	6.12E-06
Sy.x	0.000134
Constraints	
K	K > 0

Number of points

# of X values	342
# Y values analyzed	342

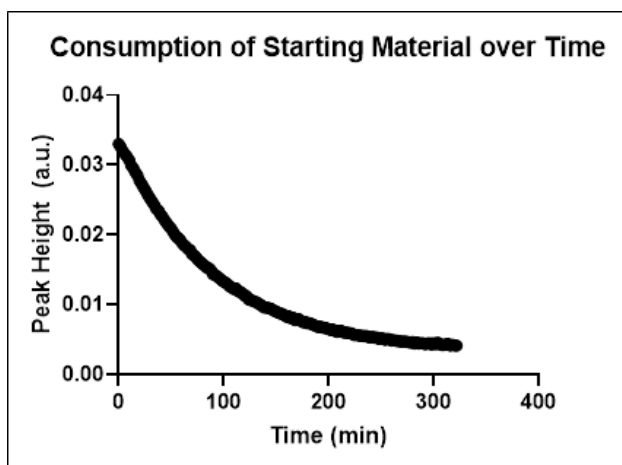
Time (min)	Peak at 1284 cm ⁻¹ (a.u.)
0.00	0.033199
2.00	0.032622
3.98	0.032326
6.00	0.032122
7.98	0.031736
10.00	0.031715
11.98	0.031259
14.00	0.030996
16.00	0.030836
17.98	0.030265
20.00	0.030113
21.98	0.029902
24.00	0.029465
25.98	0.029321
27.98	0.029146
30.03	0.028961
31.98	0.028549
34.00	0.028458
35.98	0.028082
38.00	0.027804
39.98	0.027531
42.00	0.027218
44.00	0.02711
45.98	0.026845
48.00	0.026624
49.98	0.026429
52.00	0.026195
54.00	0.026028
56.00	0.025695
57.98	0.025649
60.03	0.025391
62.00	0.025255
64.00	0.02491
66.00	0.024711
67.98	0.024427
70.00	0.024497
71.98	0.024174
74.00	0.023998

75.98	0.023712	166.00	0.016671
78.00	0.023292	167.98	0.016212
79.98	0.023342	170.03	0.016064
82.00	0.023101	171.98	0.015919
84.00	0.022921	174.00	0.015825
85.98	0.022905	176.00	0.015669
88.03	0.022556	177.98	0.015697
89.98	0.022267	180.00	0.015419
92.00	0.02228	182.03	0.015344
93.98	0.021996	184.00	0.015239
96.00	0.022064	185.98	0.015017
98.00	0.021858	188.00	0.014983
99.98	0.021577	190.00	0.014933
102.00	0.021458	191.98	0.014778
103.98	0.021232	194.00	0.014738
106.00	0.020971	195.98	0.014592
107.98	0.020773	198.00	0.014378
110.00	0.020868	199.98	0.014315
111.98	0.02065	202.00	0.014265
114.00	0.020375	203.98	0.014049
116.00	0.020225	206.03	0.013884
118.00	0.019967	207.98	0.013773
120.00	0.019848	210.03	0.013763
121.98	0.019809	212.00	0.013588
124.00	0.019544	213.98	0.013383
125.98	0.019466	216.00	0.01333
128.00	0.019316	217.98	0.013265
130.02	0.019015	220.00	0.013167
132.00	0.01893	222.00	0.013111
134.00	0.018875	223.98	0.012997
135.98	0.018547	226.00	0.013008
138.00	0.018417	227.98	0.012712
139.98	0.018305	230.00	0.01273
142.00	0.018138	231.98	0.012598
143.98	0.018172	234.00	0.012465
146.00	0.017899	235.98	0.01241
148.00	0.017691	237.98	0.0123
150.00	0.017657	240.03	0.012266
152.00	0.017598	241.98	0.012044
153.98	0.017359	244.00	0.012092
156.00	0.017085	245.98	0.01192
158.03	0.017006	248.00	0.01202
160.00	0.016961	250.00	0.011854
161.98	0.016709	251.98	0.011654
163.98	0.016774	254.00	0.011612

255.98	0.011626	346.00	0.008725
258.00	0.011357	348.00	0.008754
259.98	0.011356	349.98	0.008557
262.00	0.011375	352.00	0.008659
263.98	0.011111	354.00	0.008563
266.00	0.011005	355.98	0.008575
268.00	0.011045	358.00	0.008476
269.98	0.011018	359.98	0.008399
272.00	0.010856	362.05	0.008304
273.98	0.010768	364.00	0.008248
276.00	0.010821	365.98	0.008301
278.00	0.010654	367.98	0.008316
279.98	0.010696	370.00	0.008272
282.00	0.010552	371.98	0.008257
283.98	0.01041	374.00	0.007983
286.00	0.010434	376.00	0.008075
288.00	0.010382	378.00	0.007987
289.98	0.010304	380.03	0.007962
292.05	0.010216	382.00	0.007707
293.98	0.010186	383.98	0.007827
296.00	0.010192	385.98	0.007851
298.03	0.009988	388.00	0.007948
299.98	0.009966	389.98	0.007681
302.00	0.00984	391.98	0.007793
303.98	0.01004	394.00	0.007826
306.00	0.0098	395.98	0.007777
307.98	0.009744	398.03	0.007694
310.00	0.009695	400.00	0.007538
312.00	0.009662	401.98	0.007515
313.98	0.009517	404.00	0.007583
316.00	0.009353	405.98	0.007556
317.98	0.009433	407.98	0.007556
320.00	0.009205	410.00	0.007364
322.00	0.009275	411.98	0.007442
323.98	0.00928	414.00	0.007355
326.00	0.009218	416.00	0.007301
328.00	0.009347	417.98	0.007285
329.98	0.009069	420.00	0.007362
332.00	0.009204	421.98	0.007203
333.98	0.00904	423.98	0.007142
336.00	0.008897	426.03	0.006977
338.00	0.009054	428.00	0.007014
339.98	0.008937	430.00	0.007185
342.00	0.008858	431.98	0.006967
343.98	0.00884	433.98	0.006926

436.00	0.00691	526.00	0.005484
437.98	0.006833	527.98	0.00563
440.00	0.006827	530.00	0.00552
442.00	0.006728	532.00	0.005426
443.98	0.006719	533.98	0.00542
446.00	0.006884	536.00	0.005557
447.98	0.006798	537.98	0.005261
450.03	0.006792	539.98	0.005364
452.00	0.006628	542.00	0.00529
453.98	0.006654	543.98	0.005332
456.00	0.006697	546.00	0.00526
457.98	0.006564	548.05	0.005205
460.00	0.00658	549.98	0.005207
462.00	0.006485	552.00	0.005287
463.98	0.006436	553.98	0.005264
466.00	0.006398	555.98	0.005096
467.98	0.006326	558.00	0.005166
470.00	0.006345	559.98	0.005244
472.03	0.006362	562.00	0.005235
473.98	0.006437	564.00	0.005116
476.00	0.006311	566.03	0.00517
477.98	0.006291	568.00	0.005098
480.00	0.006205	569.98	0.005027
481.98	0.006279	571.98	0.005211
484.00	0.006237	574.00	0.005049
485.98	0.006132	575.98	0.00498
488.00	0.006094	577.98	0.005023
490.05	0.00622	580.00	0.005013
491.98	0.005999	581.98	0.004882
494.00	0.005919	584.00	0.004707
495.98	0.005951	586.00	0.004694
498.00	0.005911	587.98	0.004908
500.00	0.005903	589.98	0.004697
502.03	0.005779	592.00	0.004915
504.00	0.005886	593.98	0.004642
505.98	0.005829	596.03	0.004872
507.98	0.005724	598.00	0.004811
510.00	0.005754	599.98	0.004849
511.98	0.005704	601.98	0.004753
514.00	0.005577	604.00	0.004772
516.00	0.005577	605.98	0.004809
517.98	0.00573	607.98	0.004868
520.03	0.005511	610.00	0.004739
521.98	0.005486	611.98	0.004645
523.98	0.005561	613.98	0.004761

616.00	0.00471
617.98	0.004703
619.98	0.004634
622.00	0.004713
623.98	0.004444
626.00	0.004751
628.00	0.004579
629.98	0.004625
632.00	0.004713
634.00	0.004659
635.98	0.004669
638.00	0.004667
640.00	0.004672
641.98	0.004613
644.00	0.004688
645.98	0.004551
648.00	0.004387
650.00	0.004598
651.98	0.004371
653.98	0.004466
656.00	0.004567
657.98	0.004503
660.03	0.004515
662.00	0.004453
663.98	0.004425
666.03	0.004499
668.00	0.004375
669.98	0.004383
672.00	0.004451
673.98	0.004291
675.98	0.004381
678.00	0.004359
679.98	0.004228
682.00	0.00429



Appendix Figure C.7. 1st order exponential decay of

2.7 at 85 °C

One phase decay

Best-fit values

Y0 0.03369

Plateau 0.003168

K 0.011

Half Life 63.04

Tau 90.94

Span 0.03052

95% CI (profile likelihood)

Y0 0.03361 to 0.03377

0.003112 to

Plateau 0.003223

K 0.01092 to 0.01107

Half Life 62.62 to 63.46

Tau 90.34 to 91.55

Goodness of Fit

Degrees of Freedom 159

R squared 0.9998

Sum of Squares 2.39E-06

Sy.x 0.000123

Constraints

K K > 0

Number of points

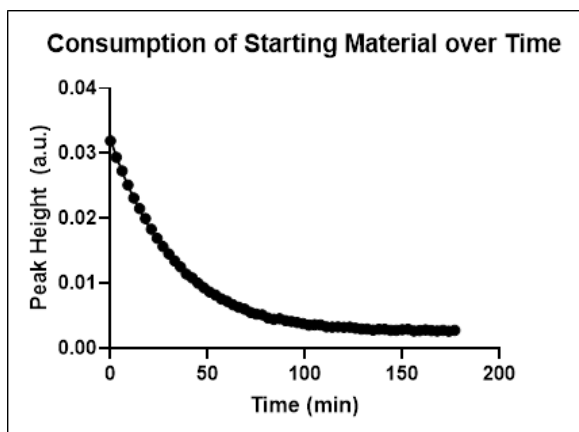
of X values 162

Y values analyzed 162

Time (min)	Peak at 1283 cm ⁻¹ (a.u.)
0.00	0.033009
1.98	0.032598
3.98	0.03201
5.98	0.03157
7.98	0.031221
10.03	0.030691
11.98	0.029961
13.98	0.029536
15.98	0.028947
17.98	0.028504
19.98	0.027753
22.00	0.027252
23.98	0.026743
25.98	0.026264
27.98	0.025693
29.98	0.025231
31.98	0.024761
33.98	0.024282
35.98	0.023732
38.00	0.023436
39.98	0.022905
41.98	0.022546
44.00	0.02201
45.98	0.021666
47.98	0.021204
49.98	0.020921
51.98	0.020405
53.98	0.019936
55.98	0.019585
57.98	0.01943
59.98	0.018936
61.98	0.018547
63.98	0.018334
66.00	0.017936
68.03	0.017825
69.98	0.017233
71.98	0.017099
73.98	0.016758
75.98	0.016345
78.02	0.016074

79.98	0.015815	169.98	0.007931
82.00	0.015592	171.98	0.007913
83.98	0.015288	173.98	0.007601
86.00	0.015208	175.98	0.007464
88.00	0.01487	177.98	0.007527
89.98	0.014345	179.98	0.007328
92.00	0.014228	181.98	0.007338
93.98	0.01404	183.98	0.007202
95.98	0.013779	185.98	0.007053
98.03	0.013518	187.98	0.006966
99.98	0.013291	189.98	0.006786
101.98	0.013134	192.00	0.006849
103.98	0.012922	193.98	0.006723
105.98	0.012577	195.98	0.006698
107.98	0.012456	197.98	0.006622
109.98	0.01221	199.98	0.006488
111.98	0.012305	202.03	0.006348
114.00	0.01189	203.98	0.00645
115.98	0.011804	205.98	0.006261
117.98	0.011606	207.98	0.006089
119.98	0.011282	209.98	0.006215
121.98	0.0112	211.98	0.006235
123.98	0.010728	213.98	0.006016
125.98	0.010636	215.98	0.006017
127.98	0.010535	217.98	0.005951
129.98	0.010408	219.98	0.005904
132.00	0.010268	221.98	0.005886
133.98	0.010036	223.98	0.00565
135.98	0.009926	225.98	0.005661
138.00	0.009623	228.02	0.005623
139.98	0.009575	229.98	0.005544
141.98	0.009565	231.98	0.005505
143.98	0.009461	233.98	0.005479
145.98	0.009339	235.98	0.005501
147.98	0.009117	237.98	0.005351
150.00	0.009011	239.98	0.005284
152.00	0.008816	242.05	0.005369
153.98	0.00875	243.98	0.005261
155.98	0.00866	245.98	0.005288
157.98	0.008486	247.98	0.005082
159.98	0.008264	249.98	0.005176
161.98	0.008349	251.98	0.005134
163.98	0.008037	253.98	0.004963
165.98	0.008157	255.98	0.005094
167.98	0.007787	257.98	0.005061

259.98	0.004851
261.98	0.004932
263.98	0.004803
265.98	0.004802
268.00	0.004723
269.98	0.004684
271.98	0.00471
274.00	0.004675
275.98	0.004602
278.00	0.004539
279.98	0.004641
281.98	0.004408
283.98	0.004597
285.98	0.004419
287.98	0.004482
290.00	0.004436
291.98	0.004304
293.98	0.004408
295.98	0.004497
297.98	0.004292
299.98	0.004489
301.98	0.004303
303.98	0.004541
306.00	0.00432
307.98	0.004209
309.98	0.004231
311.98	0.004314
313.98	0.004342
315.98	0.004127
317.98	0.004253
320.00	0.004161
321.98	0.004106



Appendix Figure C.8. 1st order exponential decay of

2.7 at 95 °C

One phase decay

Best-fit values

Y0	0.03221
Plateau	0.002406
K	0.03037
Half Life	22.82
Tau	32.92
Span	0.02981

95% CI (profile likelihood)

Y0	0.03206 to 0.03237
	0.002343 to
Plateau	0.002468
K	0.03005 to 0.03070
Half Life	22.58 to 23.06
Tau	32.58 to 33.27

Goodness of Fit

Degrees of Freedom	57
R squared	0.9997
Sum of Squares	1.04E-06
Sy.x	0.000135

Constraints

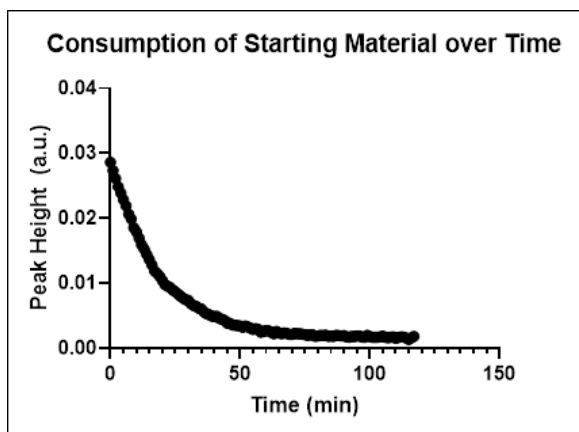
K	K > 0
---	-------

Number of points

# of X values	60
# Y values analyzed	60

Time (min)	Peak at 1282 cm ⁻¹ (a.u.)
0.00	0.031919
3.00	0.029384
6.00	0.027284
9.05	0.025112
12.00	0.023126
15.00	0.021493
18.00	0.019935
21.02	0.018321
24.00	0.016911
27.00	0.015649
30.00	0.014522
33.00	0.01344
36.00	0.012512
39.00	0.011429
42.00	0.010803
45.00	0.010028
48.00	0.009333
51.00	0.008663
54.02	0.00817
57.00	0.007591
60.00	0.007202
63.00	0.006693
66.00	0.006286
69.00	0.006001
72.00	0.005512
75.00	0.005254
78.02	0.00515
81.00	0.00466
84.02	0.004436
87.00	0.004542
90.00	0.004252
93.00	0.004111
96.00	0.003964
99.00	0.003792
102.00	0.003562
105.02	0.00363
108.00	0.003588
111.02	0.00328
114.00	0.003253
117.00	0.003287
120.00	0.003231
123.00	0.003257

126.00	0.003068
129.00	0.002956
132.00	0.002952
135.00	0.00279
138.00	0.002904
141.00	0.002908
144.02	0.002753
147.00	0.002752
150.00	0.002846
153.00	0.002901
156.00	0.002661
159.00	0.002708
162.00	0.002821
165.00	0.002708
168.00	0.002645
171.02	0.002765
174.00	0.00263
177.00	0.002749



Appendix Figure C.9. 1st order exponential decay of

2.7 at 108 °C

One phase decay

Best-fit values

Y0 0.02904

Plateau 0.001611

K 0.05423

Half Life 12.78

Tau 18.44

Span 0.02743

95% CI (profile likelihood)

Y0 0.02887 to 0.02922
0.001554 to

Plateau 0.001668

K 0.05359 to 0.05489

Half Life 12.63 to 12.93

Tau 18.22 to 18.66

Goodness of Fit

Degrees of Freedom 115

R squared 0.9991

Sum of Squares 4.36E-06

Sy.x 0.000195

Constraints

K K > 0

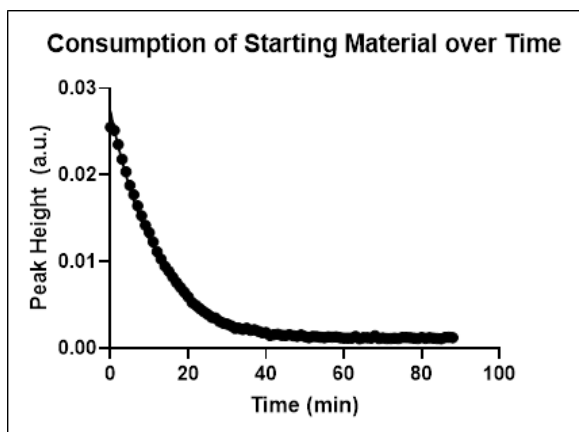
Number of points

of X values 118

Y values analyzed 118

Time (min)	Peak at 1281 cm ⁻¹ (a.u.)
0.00	0.028602
1.00	0.027335
2.00	0.026118
3.00	0.024847
4.00	0.023897
5.00	0.022861
6.00	0.021923
7.00	0.020644
8.00	0.019895
9.00	0.018544
10.02	0.01792
11.00	0.01696
12.00	0.0159
13.00	0.015234
14.02	0.014409
15.00	0.013616
16.05	0.012824
17.00	0.011898
18.00	0.011503
19.00	0.011062
20.00	0.010412
21.00	0.009796
22.00	0.009564
23.00	0.009362
24.00	0.008965
25.00	0.008715
26.00	0.008336
27.00	0.008
28.00	0.007724
29.00	0.007464
30.00	0.007378
31.00	0.006843
32.00	0.006584
33.00	0.006466
34.00	0.006138
35.00	0.006064
36.00	0.005577
37.00	0.005305
38.00	0.005179
39.02	0.004944
40.00	0.004882
41.00	0.004914

42.00	0.004591	87.00	0.001974
43.00	0.004444	88.00	0.001942
44.00	0.00427	89.00	0.00188
45.00	0.003839	90.00	0.001964
46.00	0.003838	91.00	0.001759
47.00	0.003588	92.00	0.001678
48.00	0.003527	93.00	0.001829
49.00	0.003468	94.00	0.00179
50.00	0.003428	95.00	0.001882
51.00	0.003228	96.00	0.001891
52.00	0.003409	97.00	0.001728
53.00	0.003281	98.00	0.001696
54.00	0.003069	99.00	0.001972
55.00	0.002869	100.00	0.001793
56.00	0.003011	101.00	0.001697
57.00	0.002899	102.00	0.001667
58.00	0.002447	103.00	0.001694
59.00	0.00259	104.00	0.001743
60.00	0.002729	105.00	0.001843
61.00	0.002696	106.00	0.001683
62.00	0.002457	107.00	0.00162
63.00	0.002229	108.00	0.001668
64.00	0.002577	109.00	0.001755
65.00	0.002365	110.00	0.001528
66.02	0.002201	111.00	0.001634
67.02	0.002358	112.00	0.001744
68.00	0.002277	113.00	0.001731
69.00	0.002111	114.00	0.001567
70.00	0.00211	115.00	0.001341
71.02	0.002299	116.00	0.001588
72.02	0.002225	117.00	0.00181
73.00	0.002233		
74.00	0.002164		
75.00	0.002075		
76.00	0.001979		
77.00	0.00204		
78.00	0.002037		
79.00	0.001829		
80.00	0.001879		
81.00	0.001989		
82.00	0.001961		
83.00	0.002001		
84.00	0.001822		
85.00	0.00188		
86.00	0.00181		



Appendix Figure C.10. 1st order exponential decay
of **2.7** at 113 °C

One phase decay

Best-fit values

Y0 0.02738

Plateau 0.000936

K 0.0817

Half Life 8.484

Tau 12.24

Span 0.02644

95% CI (profile likelihood)

Y0 0.02700 to 0.02776
0.0008268 to

Plateau 0.001044

K 0.07968 to 0.08377

Half Life 8.275 to 8.699

Tau 11.94 to 12.55

Goodness of Fit

Degrees of Freedom 86

R squared 0.9968

Sum of Squares 1.08E-05

Sy.x 0.000354

Constraints

K K > 0

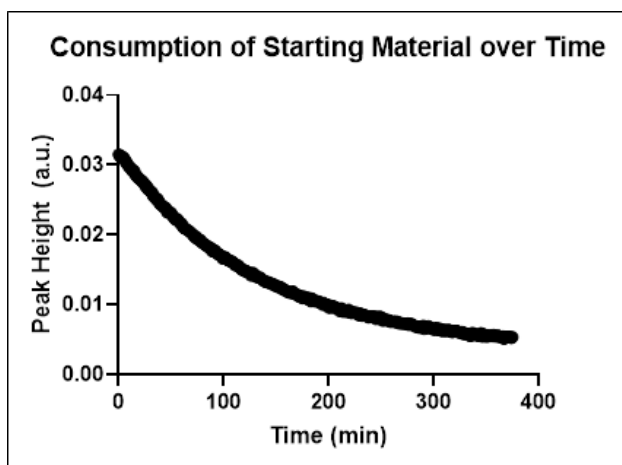
Number of points

of X values 89

Y values analyzed 89

Time (min)	Peak at 1282 cm ⁻¹ (a.u.)
0.00	0.025508
1.00	0.025143
2.00	0.02351
3.02	0.021824
4.00	0.020361
5.00	0.018793
6.00	0.017703
7.00	0.01644
8.00	0.015294
9.00	0.014181
10.00	0.013328
11.00	0.012251
12.00	0.011137
13.03	0.010283
14.02	0.009464
15.00	0.008881
16.00	0.0082
17.00	0.007555
18.02	0.007011
19.00	0.006471
20.00	0.005905
21.03	0.005254
22.00	0.004937
23.00	0.004571
24.00	0.004219
25.00	0.003912
26.00	0.003556
27.00	0.003483
28.00	0.003077
29.00	0.002893
30.00	0.002776
31.00	0.002581
32.00	0.002291
33.00	0.002315
34.00	0.002157
35.00	0.00231
36.02	0.00205
37.00	0.002137
38.00	0.001968
39.00	0.00178
40.02	0.001804
41.00	0.001469

42.00	0.00157	87.00	0.001253
43.00	0.001606	88.00	0.001208
44.00	0.001488		
45.00	0.001468		
46.00	0.001558		
47.00	0.001447		
48.00	0.001352		
49.02	0.001549		
50.00	0.001344		
51.00	0.00121		
52.00	0.001358		
53.02	0.001344		
54.00	0.001251		
55.00	0.001222		
56.00	0.00131		
57.00	0.001284		
58.02	0.00131		
59.00	0.001202		
60.00	0.001164		
61.00	0.001164		
62.02	0.001173		
63.00	0.001353		
64.00	0.001075		
65.00	0.001214		
66.02	0.001201		
67.00	0.001161		
68.00	0.001438		
69.00	0.001105		
70.02	0.001181		
71.00	0.001115		
72.00	0.001106		
73.00	0.001156		
74.00	0.001106		
75.00	0.001245		
76.00	0.001244		
77.00	0.001223		
78.00	0.001164		
79.00	0.00111		
80.00	0.001235		
81.00	0.001125		
82.00	0.001223		
83.00	0.001169		
84.00	0.001113		
85.00	0.001096		
86.00	0.001238		



Appendix Figure C.11. 1st order exponential decay
of **1.59** at 88 °C

One phase decay

Best-fit values

Y0 0.03187

Plateau 0.003693

K 0.007641

Half Life 90.71

Tau 130.9

Span 0.02818

95% CI (profile likelihood)

Y0 0.03182 to 0.03192
0.003638 to

Plateau 0.003747
0.007596 to

K 0.007687

Half Life 90.17 to 91.26

Tau 130.1 to 131.7

Goodness of Fit

Degrees of

Freedom 373

R squared 0.9997

Sum of Squares 6.62E-06

Sy.x 0.000133

Constraints

K K > 0

Number of points

of X values 376

Y values
analyzed 376

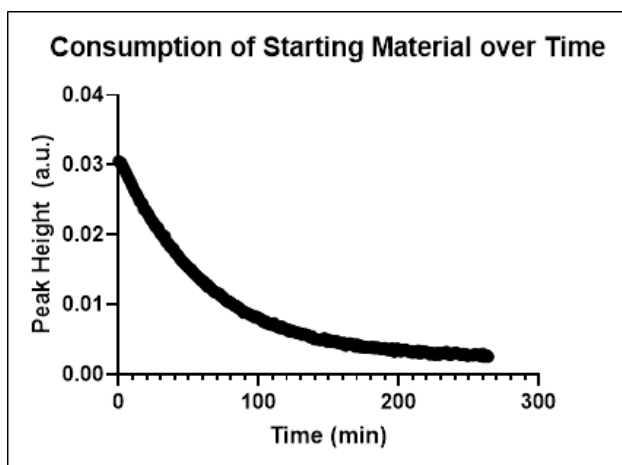
Time (min)	Peak at 1282 cm ⁻¹ (a.u.)
0.00	0.031504
1.00	0.03125
2.00	0.031245
3.02	0.031238
4.00	0.031081
5.00	0.031005
6.00	0.030752
7.00	0.030319
8.00	0.030284
9.00	0.02996
10.00	0.029698
11.00	0.029615
12.00	0.029526
13.00	0.02912
14.00	0.029186
15.00	0.029127
16.00	0.02854
17.00	0.028504
18.00	0.028173
19.00	0.028193
20.00	0.027951
21.00	0.027843
22.00	0.027692
23.00	0.027655
24.00	0.027303
25.00	0.027297
26.00	0.026828
27.00	0.026955
28.00	0.02649
29.00	0.02651
30.00	0.026235
31.00	0.026088
32.00	0.026042
33.00	0.025524
34.00	0.025442
35.05	0.025241
36.00	0.025029
37.00	0.025168
38.00	0.024837
39.00	0.024465

40.00	0.024379	85.00	0.018254
41.00	0.024216	86.00	0.0182
42.00	0.02413	87.02	0.018053
43.00	0.023904	88.00	0.018112
44.00	0.023893	89.00	0.017643
45.00	0.023855	90.00	0.017629
46.00	0.023228	91.00	0.017782
47.05	0.023234	92.00	0.017702
48.00	0.02314	93.00	0.017581
49.00	0.023123	94.00	0.01726
50.00	0.023153	95.00	0.017219
51.00	0.022815	96.00	0.017193
52.00	0.022541	97.00	0.017064
53.00	0.022393	98.00	0.016921
54.00	0.02216	99.00	0.016593
55.00	0.022217	100.00	0.016835
56.00	0.022254	101.00	0.016697
57.00	0.021968	102.00	0.016755
58.05	0.021776	103.00	0.016513
59.00	0.021537	104.00	0.016361
60.00	0.02162	105.00	0.016314
61.00	0.021193	106.00	0.016227
62.00	0.020953	107.00	0.016209
63.00	0.020993	108.00	0.016182
64.00	0.02078	109.00	0.015948
65.00	0.020877	110.00	0.015949
66.00	0.020662	111.00	0.015626
67.00	0.0205	112.00	0.015639
68.00	0.020413	113.00	0.015686
69.00	0.020437	114.00	0.01561
70.00	0.020152	115.00	0.015357
71.00	0.019913	116.00	0.015252
72.00	0.019775	117.00	0.015027
73.00	0.019588	118.00	0.015054
74.00	0.019708	119.00	0.014882
75.00	0.019381	120.00	0.014871
76.00	0.019287	121.00	0.014701
77.00	0.019193	122.00	0.014785
78.00	0.019238	123.00	0.014662
79.00	0.018904	124.00	0.01457
80.00	0.018826	125.00	0.014555
81.00	0.01878	126.00	0.01416
82.00	0.018579	127.00	0.014315
83.00	0.018542	128.02	0.014542
84.02	0.018466	129.00	0.014236

130.00	0.014237	175.00	0.010925
131.00	0.014002	176.00	0.011181
132.00	0.013886	177.00	0.011047
133.00	0.013785	178.00	0.010999
134.00	0.01385	179.00	0.01087
135.00	0.013896	180.00	0.010765
136.00	0.013652	181.03	0.010994
137.00	0.013662	182.00	0.010794
138.00	0.013397	183.00	0.010496
139.03	0.013429	184.00	0.010874
140.00	0.013213	185.00	0.010506
141.00	0.013322	186.00	0.010646
142.00	0.013179	187.00	0.010443
143.00	0.013212	188.00	0.010484
144.00	0.013038	189.03	0.010464
145.00	0.013079	190.00	0.010499
146.02	0.012872	191.00	0.010358
147.00	0.01299	192.05	0.010292
148.00	0.012823	193.00	0.010228
149.00	0.012793	194.00	0.00998
150.00	0.012594	195.00	0.010285
151.00	0.012672	196.00	0.010019
152.00	0.012559	197.00	0.010026
153.02	0.01247	198.00	0.009979
154.00	0.01247	199.00	0.010002
155.00	0.012451	200.00	0.009554
156.00	0.012166	201.00	0.009749
157.00	0.012217	202.00	0.009574
158.00	0.012147	203.02	0.009806
159.00	0.012024	204.00	0.009599
160.00	0.011846	205.00	0.009745
161.00	0.011903	206.00	0.009586
162.00	0.011718	207.00	0.009557
163.00	0.01184	208.00	0.009487
164.00	0.011658	209.00	0.00941
165.00	0.011694	210.00	0.009067
166.00	0.011882	211.00	0.009365
167.00	0.011565	212.00	0.009479
168.00	0.011495	213.00	0.009322
169.00	0.011425	214.00	0.008959
170.00	0.011435	215.00	0.009082
171.00	0.011249	216.00	0.00918
172.00	0.011127	217.00	0.009141
173.00	0.01118	218.00	0.008916
174.00	0.011182	219.00	0.009269

220.00	0.008952	265.00	0.007547
221.00	0.008811	266.00	0.007366
222.00	0.008771	267.00	0.007499
223.00	0.008906	268.00	0.007283
224.00	0.00881	269.02	0.007188
225.00	0.008735	270.00	0.007282
226.00	0.008868	271.00	0.007311
227.00	0.008752	272.00	0.007269
228.00	0.008664	273.00	0.007267
229.00	0.008434	274.00	0.007223
230.00	0.008737	275.00	0.007304
231.00	0.008499	276.00	0.007083
232.00	0.00838	277.00	0.00719
233.00	0.00854	278.00	0.007205
234.00	0.008443	279.00	0.007226
235.00	0.008452	280.00	0.007096
236.00	0.008367	281.00	0.006984
237.00	0.008302	282.00	0.006858
238.00	0.00816	283.00	0.006913
239.00	0.008253	284.00	0.006812
240.00	0.008214	285.00	0.006815
241.00	0.008356	286.00	0.006694
242.00	0.008311	287.00	0.006868
243.00	0.008227	288.00	0.006754
244.02	0.008257	289.00	0.00669
245.00	0.007904	290.00	0.006976
246.00	0.008255	291.00	0.006501
247.00	0.008105	292.00	0.006801
248.00	0.007986	293.00	0.006784
249.00	0.008276	294.00	0.006603
250.00	0.008149	295.00	0.006931
251.00	0.00773	296.00	0.006645
252.00	0.008001	297.02	0.006678
253.00	0.007717	298.00	0.006591
254.00	0.007812	299.03	0.00656
255.00	0.007818	300.00	0.006382
256.00	0.007732	301.00	0.006342
257.00	0.007793	302.00	0.006663
258.00	0.007681	303.00	0.006529
259.00	0.007507	304.00	0.006343
260.00	0.007577	305.00	0.006586
261.00	0.00754	306.00	0.006508
262.02	0.007535	307.02	0.006395
263.00	0.007509	308.00	0.00617
264.00	0.00762	309.00	0.006355

310.00	0.006411	355.00	0.00558
311.00	0.006245	356.00	0.005448
312.00	0.006233	357.00	0.005645
313.00	0.006273	358.00	0.005491
314.00	0.006429	359.00	0.005507
315.00	0.006299	360.00	0.005433
316.00	0.006155	361.00	0.005577
317.00	0.006085	362.05	0.005428
318.00	0.00605	363.00	0.005459
319.00	0.006154	364.00	0.005353
320.00	0.006255	365.00	0.005297
321.00	0.006162	366.00	0.005443
322.00	0.006257	367.05	0.005082
323.03	0.006078	368.00	0.005298
324.00	0.005996	369.03	0.005398
325.00	0.005969	370.00	0.005374
326.00	0.006005	371.00	0.005416
327.00	0.006092	372.00	0.005355
328.00	0.005786	373.00	0.005269
329.00	0.005982	374.00	0.005232
330.00	0.005775	375.00	0.005347
331.00	0.005813		
332.00	0.005825		
333.05	0.005842		
334.00	0.005501		
335.00	0.005569		
336.00	0.005548		
337.00	0.00594		
338.02	0.005785		
339.00	0.005773		
340.00	0.005645		
341.00	0.005706		
342.00	0.005512		
343.00	0.005673		
344.00	0.005695		
345.00	0.005906		
346.00	0.00541		
347.00	0.005791		
348.00	0.005447		
349.00	0.005643		
350.00	0.005592		
351.00	0.005367		
352.00	0.005538		
353.00	0.005611		
354.02	0.005546		



Appendix Figure C.12. 1st order exponential decay
of **1.59** at 98 °C

One phase decay

Best-fit values

Y0	0.03117
Plateau	0.00225
K	0.01605
Half Life	43.18
Tau	62.3
Span	0.02892

95% CI (profile likelihood)

Y0	0.03110 to 0.03124
	0.002212 to
Plateau	0.002288
K	0.01596 to 0.01614
Half Life	42.94 to 43.43
Tau	61.95 to 62.65

Goodness of Fit

Degrees of Freedom	262
R squared	0.9997
Sum of Squares	4.83E-06
Sy.x	0.000136

Constraints

K	K > 0
---	-------

Number of points

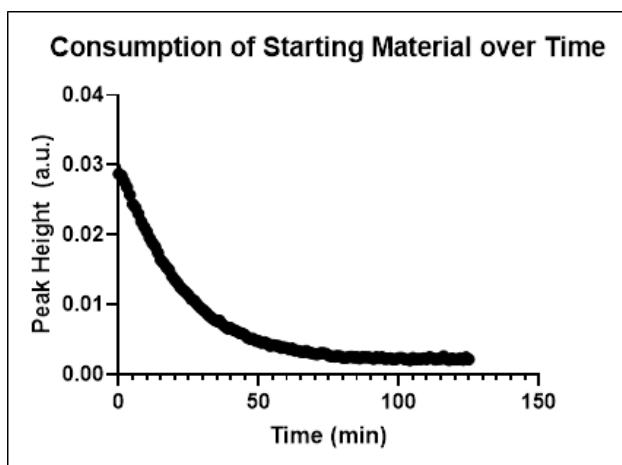
# of X values	265
# Y values analyzed	265

Time (min)	Peak at 1280 cm ⁻¹ (a.u.)
0.00	0.030556
1.00	0.030255
1.98	0.030322
3.00	0.029739
4.00	0.029364
5.00	0.028939
6.00	0.028546
7.00	0.028083
8.00	0.027759
9.00	0.027343
9.98	0.026919
11.00	0.026404
12.00	0.026025
13.00	0.025784
14.00	0.025304
15.00	0.024792
16.00	0.024678
17.00	0.024399
17.98	0.02364
19.00	0.023604
20.00	0.023238
21.00	0.023054
22.00	0.022565
23.00	0.0222
24.00	0.021931
25.00	0.021704
25.98	0.021234
27.00	0.021055
28.02	0.021054
28.98	0.020558
30.00	0.020108
31.00	0.020011
32.00	0.019605
33.00	0.019796
33.98	0.019033
35.00	0.0188
36.00	0.018643
36.98	0.018253
38.00	0.018113
39.00	0.018038

40.00	0.017555	85.00	0.009513
41.00	0.017318	86.00	0.009537
41.98	0.01719	86.98	0.00951
43.00	0.016866	88.00	0.009166
44.00	0.016543	89.00	0.008828
44.98	0.016308	89.98	0.008906
46.00	0.016082	91.00	0.008845
47.00	0.015947	92.00	0.008765
48.00	0.015666	92.98	0.008772
49.00	0.015485	94.00	0.008482
50.03	0.015236	95.00	0.008484
51.00	0.015114	95.98	0.008381
52.00	0.015019	97.00	0.008156
52.98	0.014604	98.00	0.008285
54.00	0.014488	99.00	0.008202
55.00	0.014236	100.00	0.008104
56.03	0.014031	101.00	0.007892
57.00	0.013923	102.00	0.007885
58.00	0.013568	103.00	0.007549
59.00	0.013572	104.00	0.007483
60.00	0.013235	105.00	0.0076
61.00	0.013277	106.00	0.007299
62.00	0.012931	107.00	0.007307
63.00	0.012589	107.98	0.007206
64.00	0.012784	109.00	0.007088
65.00	0.012408	110.00	0.007172
66.02	0.012333	111.00	0.007343
67.00	0.01206	112.00	0.006942
68.03	0.01181	112.98	0.006858
69.00	0.011807	114.00	0.006797
69.98	0.011754	115.00	0.006615
71.00	0.011558	115.98	0.006846
72.00	0.011599	117.00	0.00682
73.02	0.01119	118.00	0.006561
74.00	0.011162	118.98	0.006443
75.00	0.010979	120.00	0.006483
75.98	0.010709	121.00	0.006419
77.00	0.010547	121.98	0.006133
78.00	0.010356	123.00	0.006318
79.00	0.010458	124.00	0.006068
80.00	0.010285	125.00	0.006147
81.00	0.010062	126.00	0.006085
82.00	0.009952	127.00	0.005935
83.00	0.009819	128.00	0.005903
84.00	0.009817	129.00	0.005923

130.00	0.005871	175.00	0.003834
131.00	0.005656	176.00	0.003961
132.00	0.005732	177.02	0.003836
133.00	0.005731	177.98	0.003856
134.00	0.005718	179.00	0.00389
135.00	0.005605	180.00	0.003775
136.00	0.005373	181.00	0.003917
137.02	0.005357	182.00	0.003851
138.00	0.005477	183.00	0.003712
138.98	0.005192	184.00	0.003896
140.00	0.005011	185.00	0.003776
141.00	0.005036	186.00	0.00382
141.98	0.004919	187.00	0.003653
143.00	0.004981	188.00	0.003707
144.00	0.004916	189.00	0.003735
145.00	0.005054	190.00	0.003771
145.98	0.004986	191.00	0.003638
147.00	0.005187	192.00	0.003474
148.00	0.004817	193.00	0.003517
149.00	0.004689	194.00	0.00358
150.00	0.004939	195.00	0.003753
151.00	0.004829	196.00	0.003361
152.00	0.004661	197.00	0.003259
153.00	0.004824	198.00	0.003527
154.00	0.004738	199.00	0.003707
155.00	0.004585	200.05	0.00349
156.00	0.004757	201.00	0.003315
157.00	0.004526	202.00	0.003316
158.00	0.004522	203.00	0.003418
159.00	0.004392	204.00	0.003536
160.00	0.00448	205.00	0.00354
161.00	0.004501	206.02	0.003431
162.00	0.004102	207.00	0.003254
163.00	0.004209	207.98	0.003247
164.00	0.004347	209.00	0.00336
165.00	0.004438	210.00	0.003096
166.00	0.00425	210.98	0.003264
167.00	0.004303	212.00	0.003249
168.00	0.004233	213.00	0.003164
169.00	0.003953	214.00	0.003412
170.00	0.00429	214.98	0.003017
171.00	0.004238	216.00	0.003301
172.00	0.003913	217.00	0.003075
173.00	0.004095	218.02	0.003245
174.00	0.003974	219.00	0.003247

220.00	0.003202
221.00	0.003122
222.00	0.002864
223.00	0.003027
224.00	0.003086
225.00	0.002879
226.00	0.002786
227.03	0.003018
228.00	0.003078
229.00	0.002828
229.98	0.002865
231.00	0.003097
231.98	0.003007
233.00	0.002948
234.00	0.003247
235.00	0.002955
236.05	0.002853
237.00	0.002771
238.00	0.002984
239.00	0.002944
240.00	0.003085
241.00	0.003121
242.00	0.002934
243.00	0.002963
244.00	0.002812
245.00	0.002814
245.98	0.002941
247.00	0.002911
248.05	0.002868
249.00	0.00265
250.00	0.002701
250.98	0.002811
252.00	0.00277
253.00	0.002679
254.00	0.002851
255.00	0.002895
256.00	0.002786
257.00	0.002788
258.00	0.002605
259.00	0.002766
260.00	0.002993
261.00	0.002533
261.98	0.002722
263.00	0.002712
263.98	0.002532



Appendix Figure C.13. 1st order exponential decay
of **1.59** at 109 °C

One phase decay

Best-fit values

Y0	0.03019
Plateau	0.001863
K	0.04444
Half Life	15.6
Tau	22.5
Span	0.02832

95% CI (profile likelihood)

Y0	0.02998 to 0.03039
	0.001788 to
Plateau	0.001938
K	0.04383 to 0.04505
Half Life	15.39 to 15.82
Tau	22.20 to 22.82

Goodness of Fit

Degrees of Freedom	123
R squared	0.9988
Sum of Squares	7.24E-06
Sy.x	0.000243

Constraints

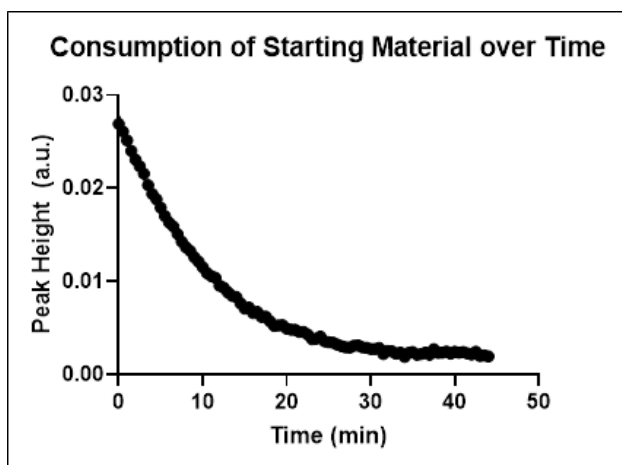
K	K > 0
---	-------

Number of points

# of X values	126
# Y values analyzed	126

Time (min)	Peak at 1281 cm ⁻¹ (a.u.)
0.00	0.028714
1.00	0.028493
2.00	0.027616
3.00	0.026768
4.00	0.025716
5.00	0.024385
6.00	0.023897
7.00	0.023004
8.02	0.02193
9.00	0.021179
10.00	0.020473
11.00	0.019551
12.00	0.018843
13.00	0.018305
14.00	0.017431
15.00	0.016394
16.00	0.015946
17.00	0.015399
18.00	0.014961
19.00	0.014088
20.00	0.013554
21.00	0.013094
22.00	0.012471
23.00	0.012097
24.00	0.01176
25.00	0.011323
26.00	0.010749
27.03	0.010576
28.00	0.010041
29.00	0.009629
30.00	0.009269
31.00	0.008939
32.00	0.008528
33.00	0.008135
34.00	0.007841
35.00	0.007607
36.00	0.007704
37.00	0.00719
38.00	0.006858
39.00	0.006547

40.00	0.00666	85.00	0.002476
41.00	0.006349	86.00	0.002291
42.00	0.006202	87.00	0.002474
43.00	0.005952	88.00	0.002435
44.00	0.005886	89.00	0.002448
45.00	0.005682	90.00	0.002381
46.00	0.005237	91.00	0.002212
47.00	0.005084	92.00	0.002468
48.00	0.005105	93.00	0.002306
49.00	0.004782	94.00	0.002469
50.00	0.004785	95.00	0.002212
51.00	0.004533	96.00	0.002239
52.00	0.004623	97.00	0.002315
53.00	0.004458	98.00	0.002142
54.00	0.004095	99.00	0.002167
55.00	0.00423	100.00	0.002364
56.00	0.004105	101.00	0.002374
57.00	0.004082	102.00	0.00219
58.00	0.003784	103.00	0.002147
59.00	0.003877	104.00	0.002027
60.00	0.003775	105.00	0.002367
61.05	0.0036	106.00	0.002157
62.00	0.003708	107.00	0.002214
63.00	0.003398	108.00	0.002168
64.00	0.003393	109.00	0.002301
65.00	0.003241	110.00	0.002191
66.00	0.003231	111.00	0.002492
67.00	0.003394	112.00	0.002301
68.00	0.003106	113.00	0.002106
69.00	0.003051	114.00	0.002234
70.00	0.002921	115.00	0.002218
71.00	0.002891	116.00	0.002612
72.00	0.003065	117.00	0.002219
73.00	0.003063	118.00	0.00205
74.00	0.002987	119.00	0.002287
75.00	0.002672	120.00	0.002156
76.00	0.002585	121.00	0.002143
77.00	0.002548	122.00	0.002305
78.00	0.002644	123.00	0.002089
79.00	0.002633	124.00	0.002445
80.00	0.002398	125.00	0.002149
81.00	0.002392		
82.00	0.002444		
83.00	0.002565		
84.00	0.002416		



Appendix Figure C.14. 1st order exponential decay
of **1.59** at 121 °C

One phase decay

Best-fit values

Y0 0.02781

Plateau 0.001448

K 0.09781

Half Life 7.087

Tau 10.22

Span 0.02636

95% CI (profile likelihood)

Y0 0.02755 to 0.02807

0.001309 to

Plateau 0.001584

K 0.09565 to 0.09999

Half Life 6.932 to 7.247

Tau 10.00 to 10.45

Goodness of Fit

Degrees of Freedom 86

R squared 0.9982

Sum of Squares 7.32E-06

Sy.x 0.000292

Constraints

K K > 0

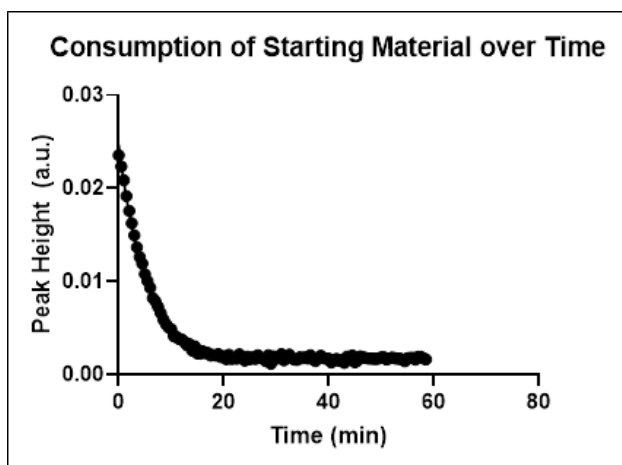
Number of points

of X values 89

Y values analyzed 89

Time (min)	Peak at 1280 cm ⁻¹ (a.u.)
0.00	0.026924
0.50	0.026095
1.00	0.025125
1.50	0.024022
2.00	0.023069
2.50	0.022365
3.00	0.021563
3.50	0.020341
4.00	0.019378
4.50	0.018806
5.00	0.017912
5.50	0.017023
6.00	0.016307
6.50	0.015899
7.00	0.015087
7.50	0.014255
8.00	0.013666
8.50	0.013252
9.02	0.012587
9.50	0.012114
10.00	0.011511
10.50	0.010878
11.00	0.010569
11.50	0.010383
12.00	0.009526
12.50	0.009319
13.00	0.008801
13.50	0.008427
14.00	0.008324
14.50	0.007632
15.00	0.007052
15.50	0.007184
16.00	0.006593
16.50	0.006702
17.00	0.006199
17.50	0.006204
18.00	0.005706
18.50	0.005201
19.00	0.00525
19.50	0.005287

20.00	0.004907	42.50	0.002443
20.50	0.004804	43.00	0.00199
21.00	0.004792	43.50	0.002027
21.50	0.004571	44.00	0.001926
22.00	0.00457		
22.50	0.004278		
23.00	0.003781		
23.50	0.003828		
24.00	0.004057		
24.50	0.003561		
25.00	0.003459		
25.50	0.003411		
26.00	0.003202		
26.50	0.003049		
27.00	0.002924		
27.50	0.002879		
28.00	0.003097		
28.50	0.003111		
29.00	0.002918		
29.50	0.002854		
30.00	0.002742		
30.50	0.00274		
31.00	0.002847		
31.50	0.002195		
32.00	0.002524		
32.50	0.002496		
33.00	0.002236		
33.53	0.00233		
34.03	0.001878		
34.52	0.002311		
34.98	0.002415		
35.50	0.002108		
36.00	0.002176		
36.50	0.002342		
37.00	0.002123		
37.50	0.002721		
38.00	0.002317		
38.50	0.002333		
39.00	0.00247		
39.50	0.002247		
40.00	0.002439		
40.50	0.002337		
41.00	0.002413		
41.50	0.002254		
42.00	0.002145		



Appendix Figure C.15. 1st order exponential decay
of **1.59** at 132 °C

One phase decay

Best-fit values

Y0	0.0247
Plateau	0.00161
K	0.1922
Half Life	3.607
Tau	5.203
Span	0.02309

95% CI (profile likelihood)

Y0	0.02438 to 0.02501
	0.001546 to
Plateau	0.001673
K	0.1880 to 0.1965
Half Life	3.528 to 3.687
Tau	5.090 to 5.319

Goodness of Fit

Degrees of Freedom	115
R squared	0.9964
Sum of Squares	9.14E-06
Sy.x	0.000282

Constraints

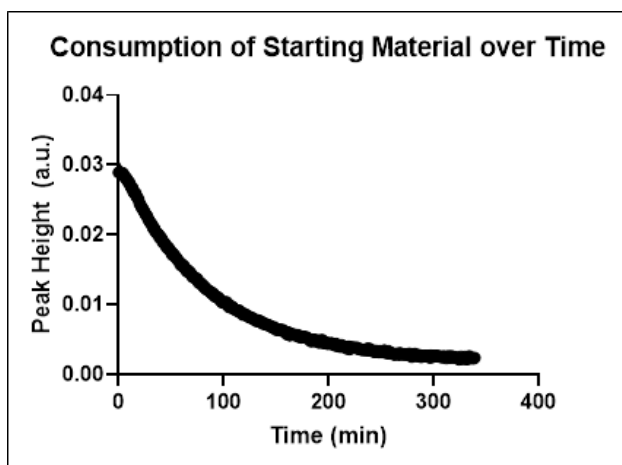
K	K > 0
---	-------

Number of points

# of X values	118
# Y values analyzed	118

Time (min)	Peak at 1278 cm ⁻¹ (a.u.)
0.00	0.023538
0.50	0.02234
1.00	0.020874
1.50	0.019154
2.00	0.017555
2.50	0.016225
3.00	0.01493
3.50	0.013653
4.00	0.01261
4.50	0.011902
5.00	0.010783
5.50	0.010039
6.00	0.009313
6.50	0.008212
7.00	0.007868
7.50	0.007276
8.00	0.006578
8.50	0.005908
9.00	0.005417
9.50	0.005062
10.00	0.004872
10.50	0.004124
11.03	0.00403
11.50	0.003822
12.00	0.003758
12.50	0.003505
13.00	0.003142
13.50	0.003273
14.00	0.002571
14.50	0.003006
15.00	0.002271
15.50	0.00223
16.00	0.00249
16.50	0.002282
17.02	0.002303
17.52	0.002035
18.02	0.002083
18.50	0.002036
19.00	0.002185
19.50	0.001867

20.00	0.001945	42.50	0.001545
20.52	0.001649	43.00	0.001227
21.00	0.002124	43.50	0.001906
21.50	0.001659	44.00	0.001647
22.00	0.001726	44.50	0.002046
22.50	0.001677	45.00	0.001312
23.00	0.00215	45.50	0.001495
23.50	0.001863	46.00	0.001949
24.00	0.00149	46.50	0.001842
24.50	0.001901	47.00	0.001795
25.00	0.001636	47.50	0.001711
25.50	0.001843	48.00	0.001723
26.00	0.001671	48.50	0.001688
26.50	0.002074	49.00	0.001656
27.00	0.001817	49.50	0.001719
27.50	0.001699	50.00	0.001843
28.00	0.001446	50.50	0.001834
28.50	0.002064	51.00	0.001616
29.00	0.001139	51.50	0.0017
29.50	0.001933	52.00	0.0018
30.00	0.001693	52.50	0.00177
30.50	0.001761	53.00	0.001692
31.00	0.002176	53.50	0.001713
31.50	0.001502	54.00	0.001581
32.00	0.001785	54.50	0.00141
32.50	0.002141	55.00	0.001731
33.00	0.001726	55.50	0.001783
33.50	0.001592	56.00	0.00178
34.00	0.001556	56.50	0.001583
34.52	0.001828	57.00	0.001884
35.00	0.001748	57.52	0.00189
35.50	0.001836	58.02	0.001741
36.00	0.001711	58.52	0.001607
36.50	0.002061		
37.00	0.001644		
37.50	0.001432		
38.00	0.001786		
38.50	0.002002		
39.00	0.001771		
39.50	0.00168		
40.00	0.001694		
40.50	0.001282		
41.00	0.001524		
41.50	0.001651		
42.00	0.001472		



Appendix Figure C.16. 1st order exponential decay
of **2.5** at 73 °C

One phase decay

Best-fit values

Y0	0.03032
Plateau	0.001773
K	0.0119
Half Life	58.24
Tau	84.02
Span	0.02855

95% CI (profile likelihood)

Y0	0.03024 to 0.03040
	0.001728 to
Plateau	0.001818
K	0.01182 to 0.01198
Half Life	57.86 to 58.62
Tau	83.48 to 84.57

Goodness of Fit

Degrees of Freedom	337
R squared	0.9995
Sum of Squares	9.81E-06
Sy.x	0.000171

Constraints

K	K > 0
---	-------

Number of points

# of X values	340
# Y values analyzed	340

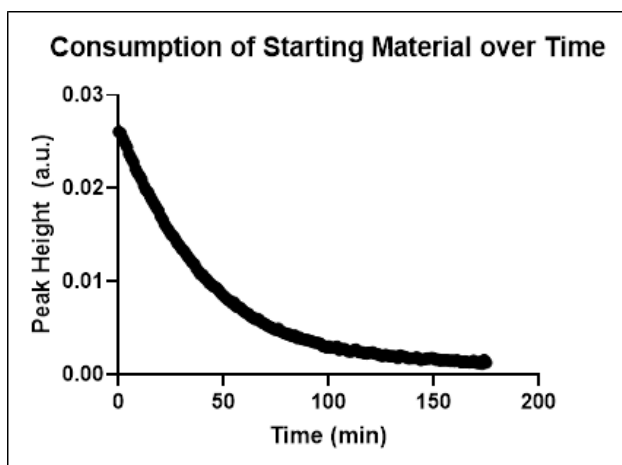
Time (min)	Peak at 1284 cm ⁻¹ (a.u.)
0.00	0.028924
1.00	0.028987
2.00	0.028907
3.00	0.028734
4.00	0.028824
5.02	0.028524
6.00	0.028188
7.00	0.028174
8.00	0.027901
9.00	0.027584
10.00	0.027516
11.00	0.02713
12.02	0.026757
13.02	0.026773
14.02	0.026156
15.05	0.025994
16.00	0.025993
17.00	0.025476
18.02	0.025279
19.00	0.025006
20.00	0.024444
21.00	0.024229
22.00	0.023857
23.00	0.023707
24.00	0.023427
25.02	0.023123
26.00	0.022842
27.00	0.02272
28.00	0.022283
29.00	0.022038
30.00	0.021763
31.02	0.021621
32.00	0.021351
33.00	0.020923
34.03	0.020904
35.03	0.020448
36.00	0.02031
37.00	0.020159
38.02	0.020042
39.03	0.019594

40.02	0.019644	85.02	0.012143
41.00	0.01941	86.00	0.011948
42.00	0.018921	87.00	0.011895
43.00	0.018913	88.05	0.011668
44.02	0.018736	89.02	0.0116
45.00	0.018416	90.02	0.011611
46.00	0.018108	91.00	0.011286
47.00	0.018226	92.00	0.011118
48.00	0.017988	93.05	0.011229
49.00	0.017723	94.00	0.011077
50.00	0.017504	95.02	0.010968
51.02	0.01713	96.00	0.010797
52.00	0.017286	97.00	0.010652
53.00	0.017036	98.00	0.01039
54.00	0.016813	99.00	0.010278
55.00	0.016728	100.00	0.010351
56.00	0.016382	101.00	0.010298
57.02	0.016368	102.02	0.01015
58.00	0.016085	103.00	0.010348
59.00	0.015682	104.00	0.009975
60.02	0.015792	105.00	0.009652
61.00	0.015474	106.00	0.009812
62.00	0.015582	107.00	0.009654
63.02	0.015231	108.02	0.009726
64.02	0.015016	109.00	0.009407
65.00	0.014743	110.00	0.009379
66.00	0.014925	111.00	0.009269
67.00	0.014613	112.00	0.0092
68.00	0.014602	113.00	0.009229
69.00	0.014393	114.02	0.008988
70.03	0.014002	115.00	0.009138
71.00	0.013918	116.00	0.008944
72.00	0.013942	117.00	0.008873
73.00	0.01387	118.03	0.008543
74.00	0.013637	119.00	0.008697
75.00	0.013687	120.00	0.008657
76.02	0.013157	121.02	0.008581
77.00	0.0132	122.00	0.008492
78.00	0.013059	123.00	0.008333
79.02	0.013	124.00	0.008267
80.00	0.012738	125.00	0.008163
81.00	0.012545	126.00	0.008104
82.02	0.012518	127.02	0.008071
83.00	0.012258	128.03	0.008023
84.02	0.012153	129.00	0.007977

130.00	0.007702	175.05	0.005353
131.00	0.007799	176.00	0.005423
132.00	0.007614	177.00	0.005391
133.02	0.007757	178.03	0.005307
134.02	0.007663	179.03	0.005304
135.02	0.007526	180.00	0.005103
136.00	0.00755	181.02	0.005117
137.00	0.007275	182.00	0.005043
138.00	0.007321	183.00	0.004752
139.03	0.007305	184.00	0.004767
140.03	0.00715	185.00	0.00499
141.02	0.007093	186.00	0.004977
142.00	0.007095	187.02	0.00477
143.00	0.007028	188.03	0.004742
144.05	0.006969	189.00	0.004895
145.00	0.006908	190.00	0.004865
146.00	0.00676	191.00	0.004535
147.02	0.006675	192.00	0.004627
148.00	0.006784	193.02	0.004901
149.00	0.006695	194.00	0.004916
150.00	0.006391	195.00	0.004507
151.00	0.006476	196.00	0.004579
152.00	0.006453	197.00	0.004451
153.02	0.006432	198.00	0.004551
154.00	0.006383	199.03	0.004395
155.00	0.006279	200.05	0.004414
156.02	0.006369	201.03	0.004395
157.00	0.006249	202.00	0.004472
158.02	0.006076	203.03	0.004453
159.00	0.006095	204.03	0.004261
160.02	0.005745	205.02	0.004172
161.00	0.006005	206.00	0.004149
162.00	0.005979	207.02	0.004369
163.00	0.005591	208.00	0.004078
164.00	0.005837	209.00	0.00407
165.05	0.005714	210.00	0.004116
166.00	0.00568	211.00	0.00394
167.02	0.005674	212.02	0.004201
168.00	0.005656	213.00	0.004134
169.05	0.0055	214.00	0.004052
170.05	0.00565	215.00	0.003942
171.00	0.005417	216.00	0.003918
172.00	0.005547	217.00	0.003729
173.02	0.005338	218.00	0.003936
174.00	0.005295	219.02	0.003975

220.00	0.003603	265.02	0.003051
221.00	0.00386	266.00	0.002994
222.00	0.003862	267.02	0.00282
223.05	0.003848	268.00	0.00306
224.00	0.003807	269.00	0.002982
225.02	0.00383	270.05	0.002869
226.00	0.003775	271.03	0.002906
227.00	0.003841	272.00	0.002862
228.00	0.003636	273.07	0.002928
229.02	0.003538	274.07	0.002895
230.00	0.003655	275.00	0.002902
231.00	0.003557	276.00	0.002776
232.07	0.003521	277.00	0.002969
233.02	0.00353	278.00	0.00273
234.00	0.003508	279.00	0.002531
235.05	0.003492	280.02	0.002671
236.00	0.003612	281.00	0.002872
237.02	0.003671	282.00	0.002954
238.00	0.003409	283.00	0.002788
239.02	0.003682	284.00	0.002627
240.03	0.003434	285.00	0.002716
241.00	0.003308	286.00	0.002772
242.00	0.003292	287.02	0.00269
243.00	0.003399	288.02	0.002477
244.00	0.00321	289.02	0.002585
245.05	0.003375	290.00	0.002641
246.00	0.003258	291.00	0.00261
247.02	0.003349	292.00	0.002699
248.00	0.003194	293.00	0.002569
249.05	0.003364	294.03	0.002646
250.00	0.003267	295.00	0.002606
251.00	0.003189	296.00	0.002416
252.00	0.003241	297.00	0.002716
253.02	0.003463	298.00	0.002463
254.02	0.003226	299.02	0.002608
255.00	0.003037	300.00	0.002639
256.00	0.003131	301.02	0.002521
257.00	0.003334	302.00	0.002634
258.00	0.002981	303.02	0.002688
259.02	0.003017	304.00	0.002568
260.02	0.003067	305.00	0.002476
261.00	0.00318	306.02	0.002503
262.00	0.002835	307.00	0.002568
263.00	0.002859	308.00	0.002436
264.00	0.002938	309.00	0.002509

310.02	0.002599
311.00	0.002556
312.00	0.002316
313.02	0.002504
314.00	0.002562
315.00	0.002606
316.00	0.002381
317.00	0.002576
318.00	0.002528
319.02	0.00252
320.00	0.002421
321.00	0.002393
322.00	0.002326
323.00	0.002412
324.00	0.002146
325.00	0.002279
326.02	0.002536
327.00	0.002212
328.00	0.002319
329.00	0.002419
330.03	0.002519
331.00	0.002176
332.00	0.002196
333.05	0.002437
334.02	0.002628
335.00	0.002355
336.00	0.002306
337.00	0.002296
338.00	0.002276
339.00	0.002381



Appendix Figure C.17. 1st order exponential decay
of **2.5** at 81 °C

One phase decay

Best-fit values

Y0	0.02687
Plateau	0.000859
K	0.02452
Half Life	28.27
Tau	40.78
Span	0.02601

95% CI (profile likelihood)

Y0	0.02677 to 0.02697
	0.0008063 to
Plateau	0.0009120
K	0.02431 to 0.02474
Half Life	28.02 to 28.52
Tau	40.43 to 41.14

Goodness of Fit

Degrees of Freedom	173
R squared	0.9995
Sum of Squares	4.24E-06
Sy.x	0.000157

Constraints

K	K > 0
---	-------

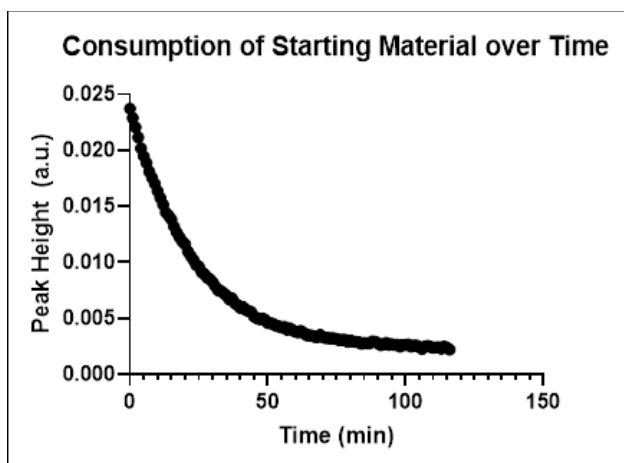
Number of points

# of X values	176
# Y values analyzed	176

Time (min)	Peak at 1284 cm ⁻¹ (a.u.)
0.00	0.026063
1.00	0.025905
2.00	0.025346
3.00	0.024838
4.00	0.024408
4.98	0.023693
6.00	0.023214
7.00	0.022796
8.00	0.022097
8.98	0.021673
10.00	0.021304
10.98	0.020942
12.00	0.020273
13.00	0.019779
14.00	0.019595
15.00	0.019105
15.98	0.018705
17.00	0.018285
18.00	0.017905
19.00	0.01757
20.00	0.016969
21.00	0.0166
21.98	0.016124
23.00	0.01573
24.00	0.015414
25.05	0.014987
25.98	0.014884
27.00	0.014521
27.98	0.014075
29.00	0.013839
30.00	0.013472
31.00	0.013302
32.00	0.012967
32.98	0.012637
34.00	0.012328
35.00	0.012017
36.00	0.011867
37.00	0.01135
38.00	0.011091
38.98	0.010743

40.00	0.010706	85.00	0.003882
41.00	0.010348	86.00	0.003982
42.00	0.010221	87.00	0.003803
43.00	0.009808	88.00	0.003755
44.00	0.009721	88.98	0.003706
44.98	0.009473	90.00	0.00372
46.00	0.009388	91.00	0.00358
47.00	0.009202	92.00	0.003558
48.00	0.008909	93.00	0.003425
49.00	0.008632	93.98	0.003417
50.00	0.008438	95.00	0.003386
50.98	0.008228	96.00	0.003304
52.00	0.007983	97.00	0.003028
53.00	0.007921	98.00	0.003022
54.00	0.007638	98.98	0.002888
55.00	0.007745	100.00	0.003017
55.98	0.007292	101.00	0.002857
57.00	0.007217	102.00	0.00285
58.02	0.007172	102.98	0.00289
59.00	0.006854	104.00	0.002979
59.98	0.006744	105.00	0.002617
61.00	0.006541	106.00	0.002732
61.98	0.006524	107.00	0.002729
63.00	0.006182	107.98	0.002707
64.00	0.006119	109.00	0.002484
65.03	0.005917	109.98	0.002457
66.00	0.005957	111.00	0.002465
66.98	0.005891	112.00	0.002635
68.00	0.005588	113.00	0.002687
69.00	0.005487	114.00	0.002442
70.00	0.005396	114.98	0.00237
71.00	0.005181	116.00	0.00239
72.00	0.005118	117.00	0.002255
72.98	0.005001	118.00	0.002234
74.00	0.00484	119.00	0.002341
75.00	0.004776	120.00	0.002321
76.00	0.004931	120.98	0.002383
76.98	0.004666	122.00	0.002243
78.00	0.004516	123.00	0.002172
79.00	0.004441	124.00	0.002142
80.00	0.004309	125.00	0.001986
81.00	0.004329	126.00	0.001978
81.98	0.004151	127.00	0.002112
83.00	0.004117	128.00	0.002021
83.98	0.004193	129.03	0.001933

130.03	0.001963	175.03	0.001255
131.02	0.001974		
132.00	0.001913		
132.98	0.001725		
134.00	0.002047		
135.00	0.001952		
136.00	0.001876		
136.98	0.001828		
138.00	0.001706		
138.98	0.001733		
140.00	0.001748		
141.00	0.001756		
142.00	0.00184		
143.00	0.001668		
143.98	0.001525		
145.00	0.001635		
146.00	0.001646		
147.00	0.001728		
148.00	0.001685		
148.98	0.00178		
150.00	0.001729		
151.00	0.001567		
152.00	0.001623		
153.00	0.001482		
153.98	0.001541		
155.00	0.001522		
156.00	0.001539		
157.00	0.001503		
158.00	0.001429		
158.98	0.001501		
160.00	0.001411		
161.00	0.001542		
162.00	0.001432		
163.00	0.001314		
163.98	0.001304		
165.00	0.001401		
166.00	0.001324		
167.00	0.001293		
168.00	0.001321		
169.05	0.001485		
170.05	0.001259		
171.03	0.001201		
172.00	0.001367		
173.00	0.001112		
174.00	0.001568		



Appendix Figure C.18. 1st order exponential decay
of 2.5 at 90 °C

One phase decay

Best-fit values

Y0 0.02381

Plateau 0.002239

K 0.04311

Half Life 16.08

Tau 23.2

Span 0.02157

95% CI (profile likelihood)

Y0 0.02372 to 0.02389

0.002203 to

Plateau 0.002275

K 0.04276 to 0.04346

Half Life 15.95 to 16.21

Tau 23.01 to 23.39

Goodness of Fit

Degrees of Freedom 114

R squared 0.9997

Sum of Squares 1.17E-06

Sy.x 0.000101

Constraints

K K > 0

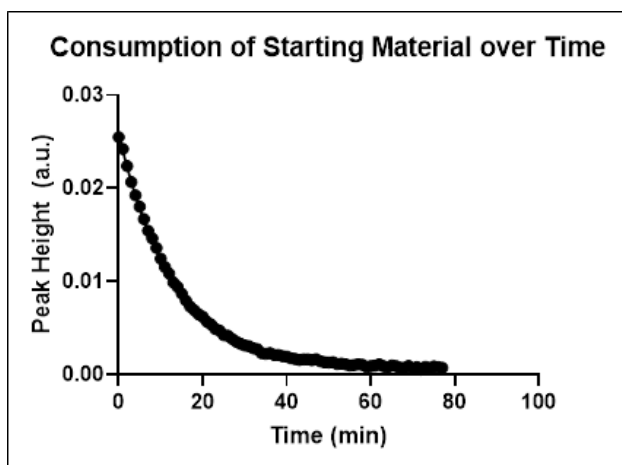
Number of points

of X values 117

Y values analyzed 117

Time (min)	Peak at 1283 cm ⁻¹ (a.u.)
0.00	0.023711
1.00	0.022877
2.00	0.022056
3.00	0.021157
4.05	0.020176
5.00	0.01947
6.02	0.018872
7.00	0.018086
8.00	0.017544
9.00	0.01702
10.00	0.016363
11.00	0.015767
12.00	0.015165
13.00	0.014443
14.02	0.014187
15.00	0.013813
16.00	0.013182
17.00	0.01266
18.00	0.012228
19.02	0.011834
20.00	0.011621
21.00	0.010968
22.00	0.010576
23.00	0.010214
24.00	0.009763
25.00	0.009641
26.00	0.009121
27.00	0.008957
28.00	0.008629
29.00	0.008498
30.00	0.008219
31.00	0.007844
32.00	0.0075
33.02	0.00742
34.00	0.007247
35.00	0.007021
36.00	0.006693
37.00	0.006789
38.00	0.006342
39.00	0.006203

40.00	0.005918	85.00	0.002778
41.00	0.006018	86.02	0.00277
42.00	0.00573	87.00	0.002752
43.00	0.005654	88.00	0.002935
44.00	0.005557	89.00	0.002892
45.00	0.005166	90.00	0.002789
46.00	0.005005	91.05	0.002591
47.00	0.004908	92.05	0.002649
48.02	0.004979	93.00	0.002811
49.00	0.004862	94.00	0.002618
50.00	0.004569	95.00	0.002674
51.00	0.00456	96.02	0.002611
52.00	0.004489	97.00	0.002639
53.02	0.00433	98.02	0.002479
54.00	0.004281	99.00	0.002621
55.00	0.004186	100.00	0.002618
56.00	0.004249	101.00	0.002646
57.05	0.003973	102.00	0.002474
58.00	0.004088	103.00	0.002545
59.00	0.003935	104.00	0.002555
60.00	0.003795	105.00	0.002429
61.00	0.003737	106.00	0.002253
62.00	0.003872	107.00	0.002471
63.02	0.003691	108.00	0.002536
64.00	0.003482	109.00	0.002443
65.00	0.003463	110.02	0.002356
66.00	0.00345	111.00	0.002388
67.02	0.003352	112.00	0.002412
68.00	0.003325	113.00	0.002277
69.00	0.00351	114.00	0.002465
70.00	0.003322	115.00	0.002361
71.00	0.003242	116.00	0.00219
72.00	0.003222		
73.02	0.003201		
74.00	0.003202		
75.00	0.003127		
76.00	0.003049		
77.03	0.003069		
78.00	0.003065		
79.00	0.002895		
80.00	0.003016		
81.00	0.002916		
82.00	0.002877		
83.00	0.002872		
84.00	0.002709		



Appendix Figure C.19. 1st order exponential decay
of **2.5** at 96 °C

One phase decay

Best-fit values

Y0	0.02592
Plateau	0.000674
K	0.0767
Half Life	9.037
Tau	13.04
Span	0.02524

95% CI (profile likelihood)

Y0	0.02579 to 0.02605
	0.0006280 to
Plateau	0.0007205
K	0.07594 to 0.07746
Half Life	8.948 to 9.128
Tau	12.91 to 13.17

Goodness of Fit

Degrees of Freedom	75
R squared	0.9996
Sum of Squares	1.12E-06
Sy.x	0.000122

Constraints

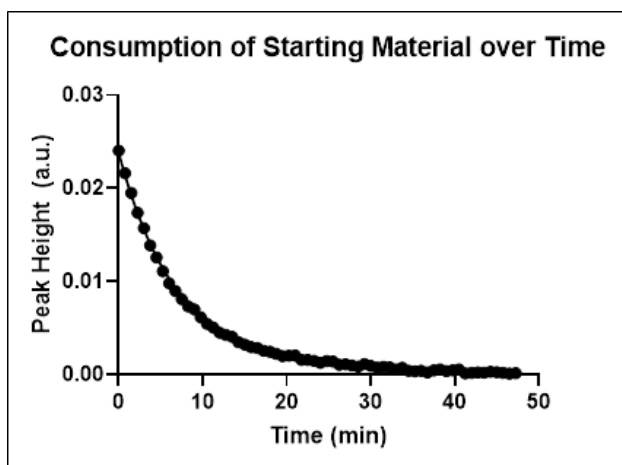
K	K > 0
---	-------

Number of points

# of X values	78
# Y values analyzed	78

Time (min)	Peak at 1284 cm ⁻¹ (a.u.)
0.00	0.025499
1.00	0.024202
2.00	0.022398
3.00	0.020664
4.00	0.019229
5.00	0.018014
6.00	0.016699
7.00	0.015436
8.00	0.014614
9.00	0.013596
10.00	0.01244
11.00	0.01154
12.00	0.010836
13.00	0.009895
14.00	0.009411
15.00	0.008691
16.00	0.007936
17.00	0.00728
18.00	0.006877
19.05	0.00646
20.03	0.006199
21.00	0.005658
22.00	0.005358
23.00	0.004892
24.00	0.004714
25.00	0.004208
26.02	0.004151
27.00	0.00382
28.00	0.003515
29.00	0.00328
30.05	0.003109
31.00	0.003036
32.00	0.002822
33.00	0.00272
34.00	0.002289
35.02	0.002223
36.02	0.002278
37.00	0.002075
38.00	0.002094
39.00	0.001962

40.00	0.001918
41.00	0.001745
42.00	0.001659
43.00	0.001573
44.00	0.001601
45.00	0.001603
46.00	0.001528
47.00	0.00163
48.05	0.001421
49.00	0.00131
50.00	0.001291
51.00	0.001313
52.00	0.001123
53.00	0.001152
54.00	0.001097
55.00	0.000953
56.02	0.001024
57.00	0.001099
58.00	0.001036
59.00	0.000824
60.03	0.00089
61.00	0.000945
62.00	0.001088
63.00	0.000894
64.00	0.000762
65.00	0.000957
66.02	0.000881
67.00	0.000701
68.00	0.000722
69.00	0.000913
70.00	0.000651
71.00	0.000799
72.00	0.000524
73.00	0.000821
74.00	0.000661
75.00	0.000868
76.02	0.000793
77.00	0.000702



Appendix Figure C.20. 1st order exponential decay
of 2.5 at 106 °C

One phase decay

Best-fit values

Y0	0.02384
Plateau	0.00042
K	0.1441
Half Life	4.811
Tau	6.94
Span	0.02342

95% CI (profile likelihood)

Y0	0.02357 to 0.02412
	0.0003323 to
Plateau	0.0005065
K	0.1409 to 0.1474
Half Life	4.704 to 4.921
Tau	6.786 to 7.099

Goodness of Fit

Degrees of Freedom	61
R squared	0.9985
Sum of Squares	3.11E-06
Sy.x	0.000226

Constraints

K	K > 0
---	-------

Number of points

# of X values	64
# Y values analyzed	64

Time (min)	Peak at 1285 cm ⁻¹ (a.u.)
0.00	0.024033
0.75	0.021623
1.50	0.019497
2.25	0.017366
3.00	0.015722
3.75	0.013856
4.50	0.012562
5.25	0.011079
6.00	0.009786
6.77	0.008965
7.50	0.008086
8.27	0.007319
9.00	0.006981
9.75	0.006125
10.50	0.005443
11.25	0.005033
12.00	0.004476
12.75	0.004249
13.50	0.004032
14.25	0.00346
15.00	0.00322
15.75	0.002941
16.50	0.002827
17.25	0.002527
18.00	0.002439
18.75	0.002213
19.50	0.001967
20.25	0.002002
21.00	0.002048
21.77	0.001558
22.50	0.001558
23.25	0.001466
24.00	0.001235
24.75	0.001425
25.50	0.001394
26.27	0.001037
27.00	0.00108
27.75	0.000971
28.50	0.00083
29.25	0.001117

30.00	0.000903	39.75	0.000431
30.75	0.000733	40.50	0.000546
31.50	0.000804	41.25	0.000124
32.25	0.000768	42.00	0.000173
33.05	0.000529	42.75	0.000221
33.75	0.000724	43.50	0.000192
34.50	0.00039	44.25	0.000298
35.25	0.000346	45.00	0.000245
36.00	0.000379	45.75	0.000155
36.75	0.000213	46.50	0.0000835
37.50	0.000433	47.25	0.000129
38.25	0.000532		
39.00	0.00037		

Bibliography

1. Jampilek, J., Heterocycles in Medicinal Chemistry. *Molecules* **2019**, *24* (21).
2. Davison, E. K.; Sperry, J., Natural Products with Heteroatom-Rich Ring Systems. *Journal of Natural Products* **2017**, *80* (11), 3060-3079.
3. Ciufolini, M. A., Synthetic studies on heterocyclic natural products. *Il Farmaco* **2005**, *60* (8), 627-641.
4. Heravi, M. M.; Ahmadi, T.; Ghavidel, M.; Heidari, B.; Hamidi, H., Recent applications of the hetero Diels–Alder reaction in the total synthesis of natural products. *RSC Advances* **2015**, *5* (123), 101999-102075.
5. Eguchi, S., Recent Progress in the Synthesis of Heterocyclic Natural Products by the Staudinger/Intramolecular aza-Wittig Reaction. *ChemInform* **2005**, *36*.
6. Lahsasni, S.; Al-Hemyari, D. A. M.; Ghabbour, H. A.; Mabkhoot, Y. N.; Aleanizy, F. S.; Alothman, A. A.; Almarhoon, Z. M., Synthesis, Characterization, and Antibacterial and Anti-Inflammatory Activities of New Pyrimidine and Thiophene Derivatives. *Journal of Chemistry* **2018**, *2018*, 8536063.
7. Shah, R.; Verma, P. K., Therapeutic importance of synthetic thiophene. *Chemistry Central Journal* **2018**, *12* (1), 137.
8. Pathania, S.; Narang, R. K.; Rawal, R. K., Role of sulphur-heterocycles in medicinal chemistry: An update. *European Journal of Medicinal Chemistry* **2019**, *180*, 486-508.
9. Keri, R. S.; Chand, K.; Budagumpi, S.; Balappa Somappa, S.; Patil, S. A.; Nagaraja, B. M., An overview of benzo[b]thiophene-based medicinal chemistry. *European Journal of Medicinal Chemistry* **2017**, *138* (Supplement C), 1002-1033.
10. Khovidhunkit, W.; Shoback, D. M., CLinical effects of raloxifene hydrochloride in women. *Annals of Internal Medicine* **1999**, *130* (5), 431-439.
11. Berger, W.; De Chandt, M. T. M.; Cairns, C. B., Zileuton: clinical implications of 5-Lipoxygenase inhibition in severe airway disease. *International Journal of Clinical Practice* **2007**, *61* (4), 663-676.
12. Croxtall, J. D.; Plosker, G. L., Sertaconazole. *Drugs* **2009**, *69* (3), 339-359.
13. Tohen, M.; Vieta, E.; Calabrese, J.; Ketter, T. A.; Sachs, G.; Bowden, C.; Mitchell, P. B.; Centorrino, F.; Risser, R.; Baker, R. W.; Evans, A. R.; Beymer, K.; Dubé, S.; Tollefson, G. D.; Breier, A., Efficacy of Olanzapine and Olanzapine-Fluoxetine

- Combination in the Treatment of Bipolar I Depression. *Archives of General Psychiatry* **2003**, *60* (11), 1079-1088.
14. Harris, A.; Arend, O.; Arend, S.; Martin, B., Effects of topical dorzolamide on retinal and retrobulbar hemodynamics. *Acta Ophthalmologica Scandinavica* **1996**, *74* (6), 569-572.
 15. Gurbel, P. A.; Tantry, U. S., Clopidogrel resistance? *Thrombosis Research* **2007**, *120* (3), 311-321.
 16. Meng, L.; Zhang, Y.; Wan, X.; Li, C.; Zhang, X.; Wang, Y.; Ke, X.; Xiao, Z.; Ding, L.; Xia, R.; Yip, H.-L.; Cao, Y.; Chen, Y., Organic and solution-processed tandem solar cells with 17.3% efficiency. *Science* **2018**, *361* (6407), 1094-1098.
 17. Di Carlo Rasi, D.; Janssen, R. A. J., Advances in Solution-Processed Multijunction Organic Solar Cells. *Advanced Materials* **2019**, *31* (10), 1806499.
 18. Chen, J.; Yang, K.; Zhou, X.; Guo, X., Ladder-Type Heteroarene-Based Organic Semiconductors. *Chemistry – An Asian Journal* **2018**, *13* (18), 2587-2600.
 19. He, D.; Zhao, F.; Jiang, L.; Wang, C., A–D–A small molecule acceptors with ladder-type arenes for organic solar cells. *Journal of Materials Chemistry A* **2018**, *6* (19), 8839-8854.
 20. Wu, J.-S.; Cheng, S.-W.; Cheng, Y.-J.; Hsu, C.-S., Donor–acceptor conjugated polymers based on multifused ladder-type arenes for organic solar cells. *Chemical Society Reviews* **2015**, *44* (5), 1113-1154.
 21. Roche, S. P.; Porco Jr., J. A., Dearomatization Strategies in the Synthesis of Complex Natural Products. *Angewandte Chemie International Edition* **2011**, *50* (18), 4068-4093.
 22. Wang, Z., Palladium-catalyzed asymmetric dearomative cyclization in natural product synthesis. *Organic & Biomolecular Chemistry* **2020**, *18* (23), 4354-4370.
 23. Zi, W.; Zuo, Z.; Ma, D., Intramolecular Dearomative Oxidative Coupling of Indoles: A Unified Strategy for the Total Synthesis of Indoline Alkaloids. *Accounts of Chemical Research* **2015**, *48* (3), 702-711.
 24. Okumura, M.; Sarlah, D., Visible-Light-Induced Dearomatizations. *European Journal of Organic Chemistry* **2020**, *2020* (10), 1259-1273.
 25. Lv, S.; Zhang, G.; Chen, J.; Gao, W., Electrochemical Dearomatization: Evolution from Chemicals to Traceless Electrons. *Advanced Synthesis & Catalysis* **2020**, *362* (3), 462-477.
 26. Zheng, L.; Hua, R., Recent Advances in Construction of Polycyclic Natural Product Scaffolds via One-Pot Reactions Involving Alkyne Annulation. *Frontiers in Chemistry* **2020**, *8*, 906.
 27. Zhuo, C.-X.; Zhang, W.; You, S.-L., Catalytic Asymmetric Dearomatization Reactions. *Angewandte Chemie International Edition* **2012**, *51* (51), 12662-12686.

28. Ding, Q.; Zhou, X.; Fan, R., Recent advances in dearomatization of heteroaromatic compounds. *Organic & Biomolecular Chemistry* **2014**, *12* (27), 4807-4815.
29. Ouyang, B.; Yu, T.; Luo, R.; Lu, G., The asymmetric Cu(ii)-indolinylnmethanol complex catalyzed Diels–Alder reaction of 2-vinylindoles with β,γ -unsaturated α -ketoesters: an efficient route to functionalized tetrahydrocarbazoles. *Organic & Biomolecular Chemistry* **2014**, *12* (24), 4172-4176.
30. Huang, Y.; Song, L.; Gong, L.; Meggers, E., Asymmetric Synthesis of Hydrocarbazoles Catalyzed by an Octahedral Chiral-at-Rhodium Lewis Acid. *Chemistry – An Asian Journal* **2015**, *10* (12), 2738-2743.
31. Harada, S.; Morikawa, T.; Nishida, A., Chiral Holmium Complex-Catalyzed Diels–Alder Reaction of Silyloxyvinylindoles: Stereoselective Synthesis of Hydrocarbazoles. *Organic Letters* **2013**, *15* (20), 5314-5317.
32. Sugiura, H.; Yamazaki, S.; Ogawa, A., Sequential Intramolecular Diels–Alder Reaction of 3-Heteroaryl-2-propenylamides of Ethenetricarboxylate. *Journal of Heterocyclic Chemistry* **2019**, *56* (9), 2592-2603.
33. Pirovano, V.; Brambilla, E.; Moretti, A.; Rizzato, S.; Abbiati, G.; Nava, D.; Rossi, E., Synthesis of Cyclohepta[b]indoles by (4 + 3) Cycloaddition of 2-Vinylindoles or 4H-Furo[3,2-b]indoles with Oxyallyl Cations. *The Journal of Organic Chemistry* **2020**, *85* (5), 3265-3276.
34. Pirovano, V.; Borri, M.; Abbiati, G.; Rizzato, S.; Rossi, E., Gold(I)-Catalyzed Enantioselective Synthesis of Tetrahydrocarbazoles through Dearomative [4+2] Cycloadditions of 3/2-Substituted 2/3-Vinylindoles. *Advanced Synthesis & Catalysis* **2017**, *359* (11), 1912-1918.
35. Pirovano, V.; Decataldo, L.; Rossi, E.; Vicente, R., Gold-catalyzed synthesis of tetrahydrocarbazole derivatives through an intermolecular cycloaddition of vinyl indoles and N-allenamides. *Chemical Communications* **2013**, *49* (34), 3594-3596.
36. Xu, G.; Chen, L.; Sun, J., Rhodium-Catalyzed Asymmetric Dearomative [4 + 3]-Cycloaddition of Vinylindoles with Vinyl diazoacetates: Access to Cyclohepta[b]indoles. *Organic Letters* **2018**, *20* (11), 3408-3412.
37. Tu, M.-S.; Chen, K.-W.; Wu, P.; Zhang, Y.-C.; Liu, X.-Q.; Shi, F., Advances in organocatalytic asymmetric reactions of vinylindoles: powerful access to enantioenriched indole derivatives. *Organic Chemistry Frontiers* **2021**.
38. Yang, X.; Zhou, Y.-H.; Yang, H.; Wang, S.-S.; Ouyang, Q.; Luo, Q.-L.; Guo, Q.-X., Asymmetric Diels–Alder Reaction of 3-Vinylindoles and Nitroolefins Promoted by Multiple Hydrogen Bonds. *Organic Letters* **2019**, *21* (4), 1161-1164.

39. Jones, S. B.; Simmons, B.; MacMillan, D. W. C., Nine-Step Enantioselective Total Synthesis of (+)-Minfiensine. *Journal of the American Chemical Society* **2009**, *131* (38), 13606-13607.
40. Zhang, M.; Duan, Y.; Li, W.; Cheng, Y.; Zhu, C., Visible-light-induced aerobic dearomative reaction of indole derivatives: access to heterocycle fused or spirocyclic indolones. *Chemical Communications* **2016**, *52* (26), 4761-4763.
41. Liu, K.; Tang, S.; Huang, P.; Lei, A., External oxidant-free electrooxidative [3 + 2] annulation between phenol and indole derivatives. *Nat Commun* **2017**, *8* (1), 775-775.
42. Mohamed, Y. A. M.; Inagaki, F.; Takahashi, R.; Mukai, C., A new procedure for the preparation of 2-vinylindoles and their [4+2] cycloaddition reaction. *Tetrahedron* **2011**, *67* (29), 5133-5141.
43. Cotterill, L. J.; Harrington, R. W.; Clegg, W.; Hall, M. J., Thermal 1,3-Trityl Migrations in Diels–Alder Domino Reactions of 1-Trityl-4-vinyl-1H-imidazoles. *The Journal of Organic Chemistry* **2010**, *75* (13), 4604-4607.
44. Bober, A. E.; Proto, J. T.; Brummond, K. M., Intramolecular Didehydro-Diels–Alder Reaction for the Synthesis of Benzo- and Dihydrobenzo-Fused Heterocycles. *Organic Letters* **2017**, *19* (7), 1500-1503.
45. Klemm, L. H.; Gopinath, K. W., Intramolecular diels-alder cyclization into the thiophene ring. *Journal of Heterocyclic Chemistry* **1965**, *2* (3), 225-227.
46. Hayakawa, K.; Yodo, M.; Ohsuki, S.; Kanematsu, K., Novel bicycloannulation via tandem vinylation and intramolecular Diels-Alder reaction of five-membered heterocycles: a new approach to construction of psoralen and azapsoralen. *Journal of the American Chemical Society* **1984**, *106* (22), 6735-6740.
47. Hajbi, Y.; Neagoie, C.; Biannic, B.; Chilloux, A.; Vedrenne, E.; Baldeyrou, B.; Bailly, C.; Mérour, J.-Y.; Rosca, S.; Routier, S.; Lansiaux, A., Synthesis and biological activities of new furo[3,4-b]carbazoles: Potential topoisomerase II inhibitors. *European Journal of Medicinal Chemistry* **2010**, *45* (11), 5428-5437.
48. Lima, H. M.; Sivappa, R.; Yousufuddin, M.; Lovely, C. J., Total Synthesis of 7'-Desmethylkealiiquinone, 4'-Desmethoxykealiiquinone, and 2-Deoxykealiiquinone. *The Journal of Organic Chemistry* **2014**, *79* (6), 2481-2490.
49. Saavedra, D. I.; Rencher, B. D.; Kwon, D.-H.; Smith, S. J.; Ess, D. H.; Andrus, M. B., Synthesis and Computational Studies Demonstrate the Utility of an Intramolecular Styryl Diels–Alder Reaction and Di-*t*-butylhydroxytoluene Assisted [1,3]-Shift to Construct Anticancer dl-Deoxypodophyllotoxin. *The Journal of Organic Chemistry* **2018**, *83* (4), 2018-2026.

50. Kocsis, L. S.; Kagalwala, H. N.; Mutto, S.; Godugu, B.; Bernhard, S.; Tantillo, D. J.; Brummond, K. M., Mechanistic Insight into the Dehydro-Diels–Alder Reaction of Styrene–Ynes. *The Journal of Organic Chemistry* **2015**, *80* (23), 11686-11698.
51. Durham, L. J.; Studebaker, J.; Perkins, M. J., Long-range coupling in the proton magnetic resonance spectra of 1,4-dihydrobenzenes. *Chemical Communications (London)* **1965**, (19), 456-457.
52. Smith, S. G.; Goodman, J. M., Assigning Stereochemistry to Single Diastereoisomers by GIAO NMR Calculation: The DP4 Probability. *Journal of the American Chemical Society* **2010**, *132* (37), 12946-12959.
53. Peng, H.; Soeller, C.; Travas-Sejdic, J., Novel Conducting Polymers for DNA Sensing. *Macromolecules* **2007**, *40* (4), 909-914.
54. Tay, D. W.; Jong, H.; Lim, Y. H.; Wu, W.; Chew, X.; Robins, E. G.; Johannes, C. W., Palladium-meta-Terarylphosphine Catalyst for the Mizoroki–Heck Reaction of (Hetero)Aryl Bromides and Functional Olefins. *The Journal of Organic Chemistry* **2015**, *80* (8), 4054-4063.
55. Yang, B.; Wang, Z.-X., Synthesis of Allylsilanes via Nickel-Catalyzed Cross-Coupling of Silicon Nucleophiles with Allyl Alcohols. *Organic Letters* **2019**, *21* (19), 7965-7969.
56. Werner, T.; Hoffmann, M.; Deshmukh, S., Phospholane-Catalyzed Wittig Reaction. *European Journal of Organic Chemistry* **2015**, *2015* (15), 3286-3295.
57. Guo, Y.; Shen, Z., Palladium-catalyzed allylic C–H oxidation under simple operation and mild conditions. *Organic & Biomolecular Chemistry* **2019**, *17* (12), 3103-3107.
58. Gronowitz, S.; Raznikiewicz, T., 3-Bromothiophene. *Organic Syntheses* **1964**, *44*, 9.
59. Paegle, E.; Belyakov, S.; Arsenyan, P., An Approach to the Selenobromination of Aryl(thienyl)alkynes: Access to 3-Bromobenzo[b]selenophenes and Selenophenothiophenes. *European Journal of Organic Chemistry* **2014**, *2014* (18), 3831-3840.
60. Dieckmann, A.; Houk, K. N., Elucidation of Strong Cooperative Effects Caused by Dispersion Interactions in a Recognition-Mediated Diels–Alder Reaction. *Journal of Chemical Theory and Computation* **2012**, *8* (12), 5064-5071.
61. Litvinov, G. G. I. V. D. K. E. A. K. L. N. P. E. A. B. D. B. K. I. A., Diels-Alder reaction between naphthalene and N-phenylmaleimide under ambient and high pressure conditions. *Arkivoc* **2005**, *2004* (12), 70-79.
62. Hendry, D. G.; Schuetzle, D., Reactions of hydroperoxy radicals. Liquid-phase oxidation of 1,4-cyclohexadiene. *Journal of the American Chemical Society* **1975**, *97* (24), 7123-7127.

63. Borden, W. T.; Hoffmann, R.; Stuyver, T.; Chen, B., Dioxygen: What Makes This Triplet Diradical Kinetically Persistent? *Journal of the American Chemical Society* **2017**, *139* (26), 9010-9018.
64. Hoye, T. R.; Eklov, B. M.; Ryba, T. D.; Voloshin, M.; Yao, L. J., No-D NMR (No-Deuterium Proton NMR) Spectroscopy: A Simple Yet Powerful Method for Analyzing Reaction and Reagent Solutions. *Org. Lett.* **2004**, *6* (6), 953-956.
65. Chen, C.-H.; Cheng, Y.-J.; Dubosc, M.; Hsieh, C.-H.; Chu, C.-C.; Hsu, C.-S., Alternating and Diblock Donor–Acceptor Conjugated Polymers Based on Diindeno[1,2-b:2',1'-d]thiophene Structure: Synthesis, Characterization, and Photovoltaic Applications. *Chemistry – An Asian Journal* **2010**, *5* (12), 2483-2492.
66. Baierweck, P.; Simmross, U.; Müllen, K., Biindenyls, Biindenylides, and Diindeno-Fused Heterocycles from Oxidative Coupling of 1- and 2-Indanone. *Chemische Berichte* **1988**, *121* (12), 2195-2200.
67. Wang, G.; Gan, Y.; Liu, Y., Nickel-Catalyzed Direct Coupling of Allylic Alcohols with Organoboron Reagents. *Chinese Journal of Chemistry* **2018**, *36* (10), 916-920.